BEILSTEIN JOURNAL OF ORGANIC CHEMISTRY

Supramolecular chemistry

Edited by Christoph A. Schalley

Imprint

Beilstein Journal of Organic Chemistry
www.bjoc.org
ISSN 1860-5397
Email: journals-support@beilstein-institut.de

The *Beilstein Journal of Organic Chemistry* is published by the Beilstein-Institut zur Förderung der Chemischen Wissenschaften.

Beilstein-Institut zur Förderung der Chemischen Wissenschaften
Trakehner Straße 7–9
60487 Frankfurt am Main
Germany
www.beilstein-institut.de

Beilstein Journal of Organic Chemistry

Thematic series on supramolecular chemistry

Christoph A. Schalley

Editorial

Open Access

Address:
Institut für Chemie und Biochemie der Freien Universität Berlin, Takustr. 3, D-14195 Berlin, Germany

Email:
Christoph A. Schalley - christoph@schalley-lab.de

Beilstein Journal of Organic Chemistry **2009,** *5,* No. 76.
doi:10.3762/bjoc.5.76

Received: 15 November 2009
Accepted: 16 November 2009
Published: 11 December 2009

Guest Editor: C. A. Schalley

"Some might say that supramolecular systems rescued physical organic chemistry. The discovery of crown ethers gave the field new recognition: molecular recognition." [1]

As the above citation from a paper by Julius Rebek and his coworkers indicates, supramolecular chemistry at its beginning gave new impetus to physical organic chemistry, which at that time had got trapped in ever more detailed kinetic studies. Early on, the nature of non-covalent interactions was of great interest. The first synthetic host-guest complexes were studied with respect to their components' ability to bind selectively to each other through weak interactions. Mostly cations were used as the guests, because they provided rather strong binding interactions due to their charge and formed quite directional bonds.

Since these first steps supramolecular chemistry has matured into a research field in its own right. A large number of concepts have been developed which increased the binding strengths due to preorganization and the chelate effect. These concepts have been successfully transferred to neutral and anionic hosts. Nowadays, multivalent interactions start to play a significant role for host-guest chemistry.

But supramolecular chemistry is much more than molecular recognition. Concepts such as templated synthesis, (hierarchical) self-assembly, and self-sorting have made supramolecular synthesis a powerful tool to construct large and complex chemical architecture from simple building blocks with an inherent program of well-designed binding sites. Based on these concepts, functional supramolecules were developed, among them molecular switches, logic gates, molecular containers, elevators, valves and springs, supramolecular catalysts and many more.

Fixing such functional supramolecules in a suitable way, for example on nanoparticles, at interfaces or in membranes can be a way to generate even novel materials with interesting macroscopic effects.

This exciting development has been accompanied by a development of new methods able to monitor the sometimes quite fast dynamics of supramolecular systems. With this, supramolecular chemistry has become fruitful also for other areas in chemistry.

It is a great pleasure to act as the editor of a thematic series on supramolecular chemistry and I would like to thank very much all contributors to this thematic series for their excellent contributions.

Christoph A. Schalley

Berlin, November 2009

Reference

1. O'Leary, B. M.; Szabo, T.; Svenstrup, N.; Schalley, C. A.; Lützen, A.; Schäfer, M.; Rebek, J., Jr. *J. Am. Chem. Soc.* **2001,** *123,* 11519–11533. doi:10.1021/ja011651d

License and Terms

Beilstein Journal of Organic Chemistry

Structural studies on encapsulation of tetrahedral and octahedral anions by a protonated octaaminocryptand cage

I. Ravikumar[1], P. S. Lakshminarayanan[1], E. Suresh[*,2] and Pradyut Ghosh[*,1]

Full Research Paper

Open Access

Address:
[1]Department of Inorganic Chemistry, Indian Association for the Cultivation of Science, 2A & 2B Raja S. C. Mullick Road, Kolkata 700 032, India, Fax: (+91) 33-2473-2805 and [2]Analytical Science Discipline, Central Salt & Marine Chemicals Research Institute, G. B. Marg, Bhavnagar 364 002, India

Email:
E. Suresh[*] - esuresh@csmcri.org; Pradyut Ghosh[*] - icpg@iacs.res.in

* Corresponding author

Keywords:
anion receptor; cryptand; molecular recognition; proton cage

Beilstein Journal of Organic Chemistry **2009,** *5,* No. 41.
doi:10.3762/bjoc.5.41

Received: 22 April 2009
Accepted: 27 August 2009
Published: 31 August 2009

Editor-in-Chief: J. Clayden

Abstract

Structural aspects of the binding of inorganic anions such as perchlorate, hydrogen sulfate, and hexafluorosilicate with the proton cage of octaaminocryptand **L**$^{\mathbf{1}}$, N($CH_2CH_2NHCH_2$-*p*-xylyl-$CH_2NHCH_2CH_2)_3$N), are examined thoroughly. Crystallographic results for a hexaprotonated perchlorate complex of **L**$^{\mathbf{1}}$, $[(H_6L^1)^{6+}(ClO_4^-)]5(ClO_4^-)\cdot 11H_2O\cdot CH_3CN$ (**1**), an octaprotonated hydrogen sulfate complex of **L**$^{\mathbf{1}}$, $[(H_8\mathbf{L}^{\mathbf{1}})^{8+}(HSO_4^-)]7(HSO_4^-)\cdot 3H_2O\cdot CH_3OH$ (**2**) and an octaprotonated fluorosilicate complex of **L**$^{\mathbf{1}}$, $[(H_8\mathbf{L}^{\mathbf{1}})^{8+}(HSiF_6^-)]3(SiF_6^{2-})\cdot(HSiF_6^-)\cdot 15H_2O$ (**3**), show encapsulation of one perchlorate, hydrogen sulfate and hexafluorosilicate, respectively inside the cage of **L**$^{\mathbf{1}}$ in their protonated states. Further, detailed structural analysis on complex **1** reveals that the hexaprotonated **L**$^{\mathbf{1}}$ encapsulates a perchlorate *via* two N–H···O and five O–H···O hydrogen bonds from protonated secondary nitrogen atoms of **L**$^{\mathbf{1}}$ and lattice water molecules, respectively. Encapsulated hydrogen sulfate in complex **2** is "glued" inside the octaprotonated cage of **L**$^{\mathbf{1}}$ *via* four N–H···O and six C–H···O hydrogen bonds whereas encapsulated $HSiF_6^-$ in complex **3** has short contacts *via* six N–H···F and three C–H···F hydrogen bonds with $[H_8\mathbf{L}^{\mathbf{1}}]^{8+}$. In the cases of complexes **2** and **3**, the cryptand **L**$^{\mathbf{1}}$ in octaprotonated state shows monotopic encapsulation of the guest and the final conformation of these receptors is spherical in nature compared to the elongated shape of hexaprotonated state of **L**$^{\mathbf{1}}$ in complex **1**.

Introduction

In recent years considerable efforts have been made in elucidating the coordination chemistry of anions because of their vital roles in biological systems [1], medicine [2], catalysis [3], and environmental issues [4]. Perchlorate is harmful to human health and has applications in defense [5], commercial and domestic purposes [6], whereas sulfate recognition is of current interest due to its biological [7] and environmental importance [8]. It has been observed that protonated amines and quaternary

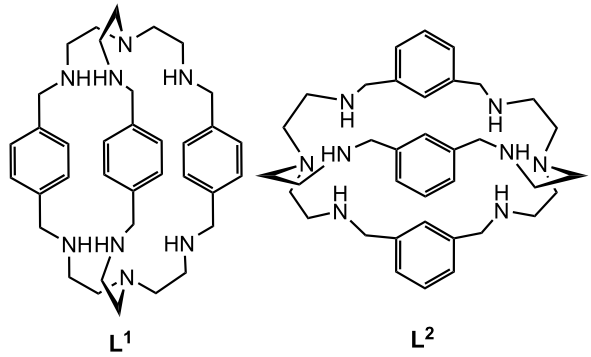

Figure 1: Octaaminocryptand with *p*-xylyl spacers $\mathbf{L^1}$, with *m*-xylyl spacers $\mathbf{L^2}$.

ammonium functions incorporated in a suitable ligand topology make them attractive receptors for anions [1-4]. Azamacropolycycles $\mathbf{L^1}$ and $\mathbf{L^2}$ (Figure 1) have shown encapsulation of different anions in their protonated states [9-22]. For example, azamacropolycycle $\mathbf{L^1}$ (Figure 1) forms a fluoride-based cascade complex [9], whilst for chloride/bromide encapsulation inside the cavity of hexaprotonated $\mathbf{L^1}$, $[H_6\mathbf{L^1}]^{6+}$ leads to both monohydrated complexes [10] and monotopic chloride/bromide complexes [11]. Protonated ligand $[H_7\mathbf{L^1}]^{7+}$ leads to monotopic encapsulation of chloride *via* hydrogen bonding with external undecameric water clusters [12] whilst iodide encapsulation has been observed in the case of $[H_8\mathbf{L^1}]^{8+}$ [13]. Whereas there are a large number of reports on halide encapsulation in different protonated states for $\mathbf{L^1}$, encapsulation of polyatomic anions such as tetrahedral (ClO_4^-, HSO_4^-, $H_2PO_4^-$), and octahedral (SiF_6^{2-}, PF_6^-) anions etc. have not been reported with this system, although planar (NO_3^-) encapsulation and binding of $H_2PO_4^-$ by $[H_6\mathbf{L^1}]^{6+}$ have been observed [14,15]. By contrast, $\mathbf{L^2}$, as host has been extensively used for oxyanion binding [16-22]. In 1995 the first structurally characterized encapsulated ClO_4^- and SiF_6^{2-} by hexaprotonated furan and pyridine analogues of $\mathbf{L^1}$, respectively were reported by Nelson et al. [23]. Very recently, Bowman-James et al. have shown encapsulation of sulfate inside the cavity of $[H_6\mathbf{L^2}]^{6+}$ [24]. Other organic receptors for perchlorate [25,26] and sulfate [27-32] have been described in the literature. Nelson et al. have reviewed the recognition of oxanions by different azacryptand hosts [33]. Steed et al. have reported a macrobicyclic azaphane receptor for halide binding through C–H···X^- and N–H···X^- interactions [34]. In this article we report solid state structural evidence of encapsulation and binding of tetrahedral oxyanions ClO_4^- and HSO_4^- as well as encapsulation of octahedral anion $HSiF_6^-$ with $\mathbf{L^1}$ in different protonated states.

Results and Discussion

Syntheses. The cryptand $\mathbf{L^1}$ was prepared on multi-gram scale and in very high yield following the modified literature procedure [13]. The key step in the scaled-up synthesis of this octaazacryptand is the condensation of tris(2-aminoethyl)amine (tren) with terephthaldehyde at 5–10 °C by the slow addition of a dry methanolic tren solution to the aldehyde also dissolved in dry methanol. Reduction of the resulting Schiff base was achieved using $NaBH_4$. Both higher temperatures (40–50 °C) and fast addition rates lead to mostly polymeric products in the scaled-up synthesis. In the case of **1**, a white precipitate is obtained after addition of perchloric acid to the methanolic solution of $\mathbf{L^1}$, which after crystallization from acetonitrile/water (1:1 v/v), gave perchlorate encapsulated in a $[H_6\mathbf{L^1}]^{6+}$ cage. Complex **2** is obtained as white solid upon reacting sulfuric acid with $\mathbf{L^1}$ in acetonitrile medium followed by crystallization from water/MeOH (1:1 v/v). Complex **3** is obtained as a white precipitate upon treating the receptor with hydrofluoric acid in methanol followed by crystallization from water. The syntheses of the complexes are all straight forward and, with the exception of complex **3**, are obtained in high yield.

Description of the Crystal Structure, $[(H_6\mathbf{L^1})^{6+}(ClO_4^-)][5(ClO_4^-)\cdot 11H_2O\cdot CH_3CN$ (**1**). Hexaprotonated cryptand cage $[H_6\mathbf{L^1}]^{6+}$ shows encapsulation of one perchlorate ion in the cavity. This represents monotopic recognition of perchlorate whereas five perchlorate counter anions, along with eleven molecules of water and one acetonitrile molecule as solvent of crystallization are present in the lattice. The ORTEP diagram of the hexaprotonated cryptand moiety with the encapsulated perchlorate is shown in Figure 2. Here the

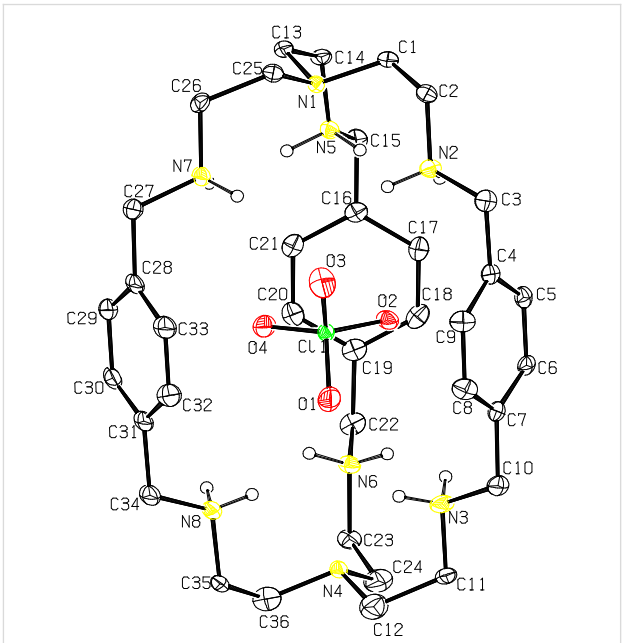

Figure 2: ORTEP diagram of the $[H_6\mathbf{L^1}]^{6+}$ with encapsulated ClO_4^- (40% probability factor for the thermal ellipsoids and hydrogen atoms attached to the protonated nitrogen atoms only are shown for clarity).

$[H_6\mathbf{L^1}]^{6+}$ moiety has an *endo-endo* conformation with a distance of 9.850 Å between the two bridgehead nitrogen atoms (N1 and N4). The window between three phenyl rings ranges from 6.815 Å to 7.126 Å (measured by the centroid of phenyl distance) with an average window of 6.993 Å indicates the elliptical nature of the perchlorate encapsulated $[H_6\mathbf{L^1}]^{6+}$ moiety (Figure 2). All the secondary amino nitrogen atoms N2, N3, N5, N6, N7 and N8, from all three strands of the cryptand moiety are protonated, which is evident by the comparatively longer C–N bond distances of these nitrogen atoms with the neighboring carbons (Table 1).

Table 1: Selected non-bonded distances (Å) of complex **1**.

N···N Distance [Å]	
N2···C2	1.494(8)
N2···C3	1.508(8)
N3···C10	1.484(9)
N3···C11	1.485(9)
N5···C14	1.502(8)
N5···C15	1.502(8)
N6···C22	1.493(8)
N6···C23	1.505(8)
N7···C26	1.489(8)
N7···C27	1.497(3)
N8···C34	1.497(8)
N8···C35	1.491(8)

The encapsulated perchlorate is involved in two N–H···O and five O–H···O hydrogen bonding interactions with the protonated amino hydrogen atoms and lattice water molecules, respectively, as depicted in Figure 3. Thus, the perchlorate oxygen O1 is involved in two weak intermolecular hydrogen bonds N–H···O with amino hydrogen atoms H3D and H8D of the protonated nitrogens (N3 and N8) of the cryptand with N···O distances of N3···O1 = 3.018(9) Å and N8···O1 = 3.146(8) Å, and N–H···O angles <N3–H3D···O1 = 118° and <N8–H8D···O1 = 137°, respectively. The lattice water molecules also play a vital role in anchoring the ClO_4^- ion inside the flexible hexaprotonated cryptand moiety. Five lattice water molecules O25, O26, O27, O28 and O29, which act as donors and are involved in strong O–H···O hydrogen bonds with the encapsulated perchlorate oxygen atoms fasten the anion inside the cryptand moiety. All of these five water molecules act as acceptors and are oriented outside the cryptand leading to

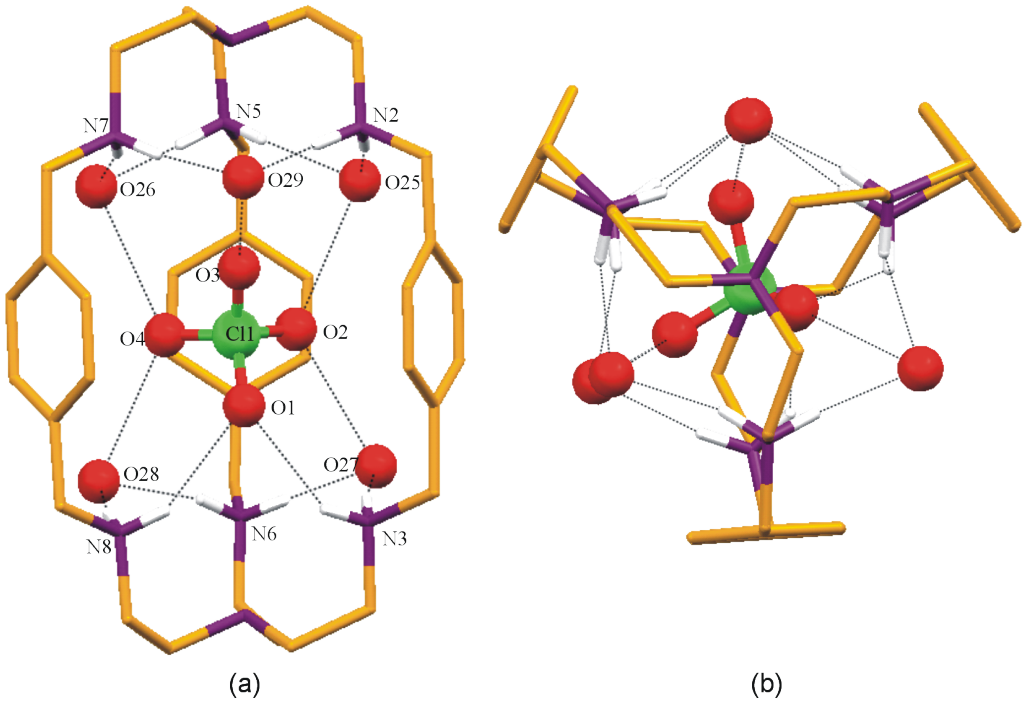

Figure 3: (a) Mercury diagram depicting the interactions of the encapsulated ClO_4^- within the $[H_6\mathbf{L^1}]^{6+}$ and the surrounding water molecules. (b) Mercury diagram depicting the interactions of the encapsulated ClO_4^- within the hexaprotonated tere-cryptand moiety and the surrounding water molecules viewed down the bridgehead nitrogen atoms. Hydrogen atoms other than acidic, external perchlorates and lattice water molecules are omitted for clarity.

good hydrogen bonding *via* N–H···O with the protonated secondary amino hydrogen atoms (Table 2).

Table 2: Selected hydrogen-bond lengths (Å) and bond angles (°) of complex **1**.

D–H···A	D–H [Å]	H···A [Å]	D···A [Å]	D–H···A [°]
N2−H2C···O25	0.92	1.90	2.818(7)	172
N5−H5C···O25	0.92	1.98	2.855(7)	159
N5–H5D···O26	0.92	1.97	2.865(7)	163
N7–H7D···O26	0.92	2.03	2.929(7)	167
N3–H3C···O27	0.92	1.96	2.869(9)	168
N6–H6D···O27	0.92	1.96	2.845(8)	179
N6–H6C···O28	0.92	1.96	2.848(7)	162
N8–H8D···O28	0.92	1.98	2.897(9)	172
N2–H2D···O29	0.92	2.04	2.909(8)	158
N7–H7C···O29	0.92	1.93	2.840(8)	170

The weaker intermolecular N–H···O hydrogen bonds between the encapsulated perchlorate oxygen O1 and the $[H_6\mathbf{L^1}]^{6+}$ moiety could be attributed to the involvement of H3D and H8D (at the protonated secondary amine sites of the cryptand) *via* strong intermolecular N–H···O hydrogen bonding with the oxygen atom (O5) of lattice perchlorate (Table 3).

Table 3: Selected hydrogen-bond lengths (Å) and bond angles (°) of complex **1**.

D–H···A	D–H [Å]	H···A [Å]	D···A [Å]	D–H···A [°]
N3−H3D···O5[a]	0.92	2.04	2.932(9)	163
N8−H8D···O5[a]	0.92	2.26	3.063(8)	146

[a] −x, −1/2+y, 1/2−z.

Even though the data were collected at 100 K, hydrogen atoms of the water molecules could not be located from the difference Fourier map, the interaction of these five water molecules are positioned near to the protonated amino nitrogen atoms *via* N–H···O hydrogen bonds. All five water molecules are further involved in strong O···O contact with the perchlorate oxygen atoms O2, O3 and O4 whereas perchlorate oxygen atom O1 binds with protonated secondary amino nitrogen atoms through two weak N–H···O hydrogen bonds which fix the ClO_4^- inside the protonated cryptand moiety. As mentioned above, O1 of the ClO_4^- is involved only in two weak N–H···O hydrogen bonds with the amino nitrogen atoms, whereas O2 makes short contact with O25 and O27 at distances of 2.815, and 2.804 Å, O3 with O29 at a distance of 2.806 Å and O4 with O26, and O28 at distances of 2.861 and 2.901 Å, respectively. In fact, water molecules act as donors to fix the anion inside the cavity. The concomitant effect of the weak N–H···O hydrogen bonds by the hexaprotonated cryptand moiety and the orientation of the water molecules surrounding the protonated secondary amine followed by their short contacts with the other ClO_4^- ions pave way for the encapsulation of ClO_4^- in the cryptand cavity. Further, in $[H_6\mathbf{L^1}]^{6+}$ moiety of **1**, the distances between any two of the secondary nitrogen atoms differ marginally in the two sets of tren cavities (N1N2N5N7) and (N3N4N6N8) (Table 4). This indicates that 3-fold symmetry about the axis passing through N1 and N4 is present in the solid state. The Cl1 of encapsulated perchlorate is sitting within the bridgehead plane (N1 and N4) and the C11 is placed closer to N4 (C11···N4 = 4.813Å) compared to the other bridgehead nitrogen N1 (C11···N1 = 5.037 Å). The distance between the bridgehead nitrogen atoms in **1** is 1.245 Å shorter than the distance observed in the free cryptand $\mathbf{L^1}$ (11.095 Å) but the distance in complex **1** is 3.364 Å longer than that of the monotopic bromide complex of $\mathbf{L^1}$ and only 0.527 Å smaller than the ditopic bromide and water in $[H_6\mathbf{L^1}]^{6+}$ complex reported recently [10, 11]. This observation suggests that depending upon guest(s), the cavity dimension of hexaprotonated $\mathbf{L^1}$ could change abruptly indicating the highly flexible nature of $\mathbf{L^1}$ in its hexaprotonated state.

Table 4: Selected non-bonded distance (Å) of complex **1**.

N···N Distance [Å]	
N2···N5	4.530
N2···N7	4.385
N5···N7	4.548
N3···N6	4.529
N3···N8	4.427
N6···N8	4.474

Description of the Crystal Structure, $[(H_8\mathbf{L^1})^{8+}(HSO_4^-)]7(HSO_4^-)\cdot 3H_2O\cdot CH_3OH$ (**2**). In this complex octaprotonated cryptand moiety acts as a cation and the eight $[HSO_4]^-$ anions present compensate the charge. Three molecules of water and one molecule of methanol are present in the lattice. The ORTEP diagram of the $[H_8\mathbf{L^1}]^{8+}$ moiety with the encapsulated HSO_4^- is depicted in Figure 4. The sulfur atom S1 of the encapsulated HSO_4^- deviates by 0.202 Å with respect to the plane containing the protonated apical nitrogen atoms N1 and N4. In solid state $[H_8\mathbf{L^1}]^{8+}$ has also an *endo-endo* conformation with a distance of 7.758 Å between two bridgehead nitrogen atoms (N1 and N4) and the window between three phenyl rings ranges from 8.099 Å to 8.403 Å (measured by the centroid of the phenyl distance) with an average window of 8.255 Å indicating the near spherical nature of the hydrogen

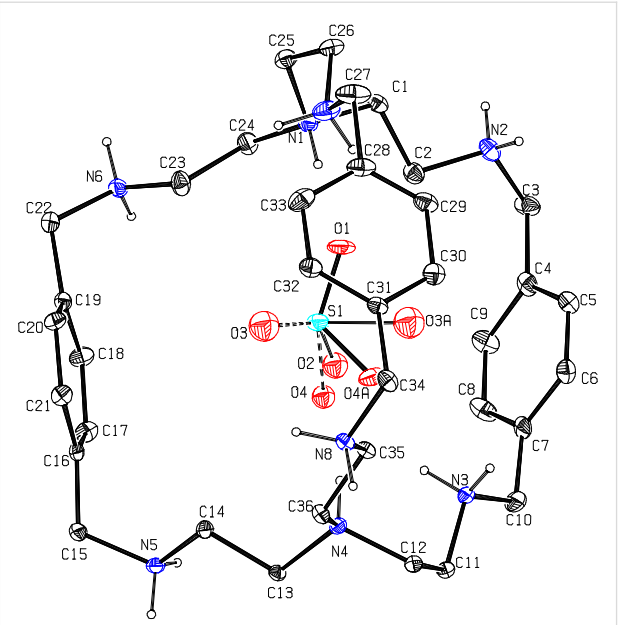

Figure 4: ORTEP diagram with atom numbering scheme depicting the octaprotonated $\mathbf{L^1}$ with disordered HSO_4^- monoanion inside the cavity (25% probability factor for the thermal ellipsoids and only hydrogen atoms attached to the amino nitrogens are shown in the figure for clarity).

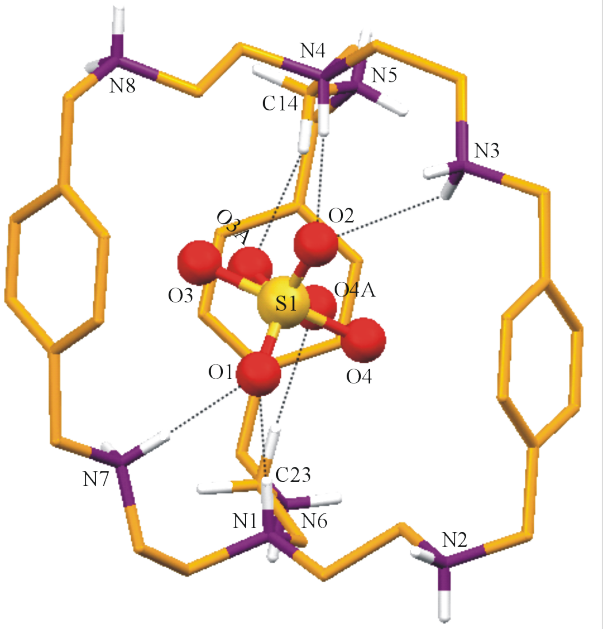

Figure 5: Mercury diagram depicting the encapsulation of disordered hydrogen sulfate in the cavity of $[H_8\mathbf{L^1}]^{8+}$ through various hydrogen bonding interactions.

sulfate encapsulated $[H_8\mathbf{L^1}]^{8+}$ moiety. The bridgehead nitrogen atoms distance in complex **2** is 2.092 Å smaller than that in complex **1** although in both cases recognition of oxyanion is monotopic in nature. This difference in complexes **1** and **2** could be due to the different degree of protonation. In fact our recent study on iodide encapsulation by $[H_8\mathbf{L^1}]^{8+}$ moiety shows that the bridgehead nitrogen distance in octaprotonated $\mathbf{L^1}$ is 6.925 Å closer to the value observed in case of **2** [13]. The relatively higher value in case of complex **2** compared with the iodide encapsulated octaprotonated $\mathbf{L^1}$ can be attributed to the polyatomic nature of HSO_4^- and flexible nature of the $[H_8\mathbf{L^1}]^{8+}$ moiety. The sulfur atom S1 of the encapsulated HSO_4^- is located at distance of 3.92 Å and 3.85 Å from N1 and N4, respectively where N4 is slightly closer to S1. In $[H_8\mathbf{L^1}]^{8+}$ the distances between any two of the secondary nitrogen atoms differ in the two sets of N4 cavities (N1N2N6N7) and (N3N4N5N8) in the cryptand (Table 5). This indicates that the 3-fold symmetry about the axis passing through N1 and N4 is lost in the solid state.

Figure 5 represents the interaction of the $[H_8\mathbf{L^1}]^{8+}$ receptor with the encapsulated disordered hydrogen sulfate. The anion is "glued" inside the receptor by two C–H···O hydrogen bonds between the methylene hydrogen atoms (H14A, H23B) with the disordered oxygen atoms O3A and O4A, respectively, and four N–H···O contacts involving the both the protonated apical hydrogen atoms (H1D, H4D) and the hydrogen atoms (H3C and H7D) of protonated secondary amino nitrogen with O1 and O2 as acceptors each make two hydrogen bonds. Details of these intermolecular contacts are given in Table 6.

Table 5: Selected non-bonded distance (Å) of complex **2**.

N···N Distance [Å]	
N2···N6	6.548
N2···N7	5.791
N6···N7	5.809
N3···N5	5.732
N3···N8	6.078
N5···N8	6.588

Table 6: Selected hydrogen-bond lengths (Å) and bond angles (°) of complex **2**.

D–H···A	D–H [Å]	H···A [Å]	D···A [Å]	D–H···A [°]
N1–H1D···O1	0.91	1.90	2.809(7)	178
N4–H4D···O2	0.91	2.02	2.896(7)	162
N3–H3C···O2	0.90	2.35	2.931(8)	123
N7–H7D···O1	0.90	2.06	2.826(10)	142
C14–H14A···O3A	0.97	2.43	3.360(2)	160
C23–H23B···O4A	0.97	2.37	3.320(17)	167

Figure 6 represents the additional interactions of the ammonium hydrogen atoms with the surrounding anions and water molecules. It is observed that with the exception of the apical amino hydrogen atoms all others are involved in N–H···O interactions with the lattice HSO_4^- or O32 of the water molecules. Thus, hydrogen atoms attached to N5 and N8 are involved in three contacts; one with water oxygen O32 and the other two with the oxygen atoms of HSO_4^- (O8, O10 for N5 and O10, O21 for N8). The rest of the ammonium hydrogen atoms are also involved in effective N–H···O contacts with the hydrogen sulfate as depicted in Figure 6.

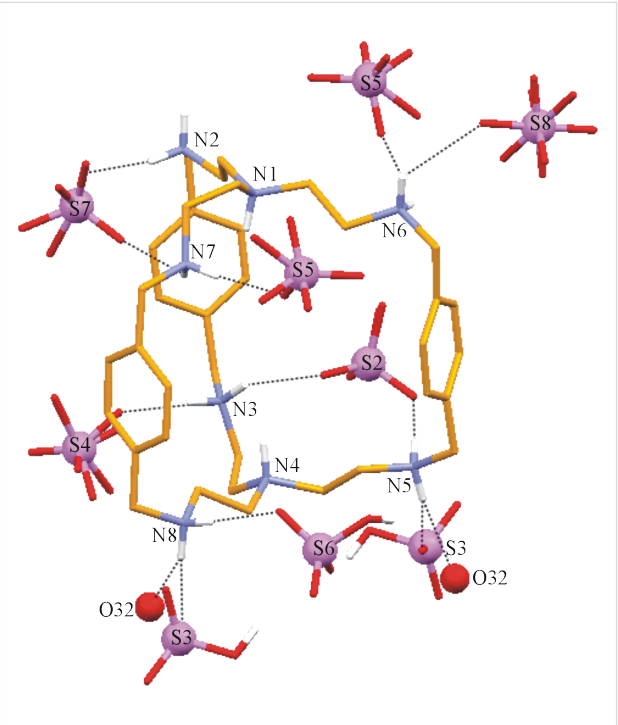

Figure 6: Interactions of the protonated amino nitrogen centers of the $[H_8\mathbf{L}^1]^{8+}$ moiety with the surrounding hydrogen sulfate and water molecules.

Description of the Crystal Structure, $[(H_8\mathbf{L}^1)^{8+}(HSiF_6^-)]3(SiF_6^{2-})\cdot(HSiF_6^-)\cdot 15H_2O$ (**3**). Silicon hexafluoride salt of $\mathbf{L}^1$ is obtained on reaction between $\mathbf{L}^1$ and HF, apparently as a result of glass corrosion. The salt $[H_8\mathbf{L}^1]^{8+}$ has three molecules of SiF_6^{2-}, and two molecules of $HSiF_6^-$ anions to compensate the charge and fifteen water molecules as solvent of crystallization. The ORTEP diagram of the octaprotonated cryptand with the encapsulated disordered $HSiF_6^-$ monoanion is depicted in Figure 7 and the various interactions of the disordered $HSiF_6^-$ monoanion with the host molecule is depicted in Figure 8. Thus, hydrogen atoms H1 and H4 attached to the apical nitrogen N1 and N4 form N–H···F hydrogen bonds (one and three) with F1 and F2A, F3, F4, respectively. Both F2A and F3 are involved in an additional N–H···F hydrogen bonding interaction with the protonated secondary amino hydrogen atoms H3D and H6D attached to N3 and N6, respectively. F1 of the disordered encapsulated $HSiF_6^-$ is involved in intermolecular C–H···F contacts with the methylenic hydrogen atom H14B, while H26B of the methylene hydrogen attached to C26 forms bifurcated weak C–H···F hydrogen bonds [35-38] with F5 and F6 in fixing the monoanion inside the cryptand moiety (Figure 8). Details of these hydrogen bonding interactions are given in Table 7. The C–N distances involving the amino nitrogen range from 1.49 to 1.53 Å clearly indicate the octa protonation of the cryptand moiety including both the apical nitrogen atoms and are well within the range of earlier reported values [13]. Protonation of the SiF_6^{2-} is clearly reflected in the case of Si1 and Si3 by the longer Si–F distances: Si(1)–F(4) = 1.725(5) Å, and Si(3)–F(14) = 1.742(6) Å, indicating that the encapsulated anion is $HSiF_6^-$. The Si1 of encapsulated $HSiF_6^-$ monoanion is slightly above by 0.89 Å from the plane involving the apical protonated nitrogen atoms with N1–Si1 distance of 3.854 Å and a N4–Si1 distance of 3.739 Å, respectively. In the solid state $[H_8\mathbf{L}^1]^{8+}$ has also an *endo-endo* conformation with a distance of 7.571 Å between the two bridgehead nitrogen atoms (N1 and N4) and the window between three phenyl rings ranges from 8.246 Å to 8.368 Å (measured by the centroid of phenyl distance) with an average window of 8.346 Å which is very close to the distances observed in complex **2** where $\mathbf{L}^1$ is also in octaprotonated state.

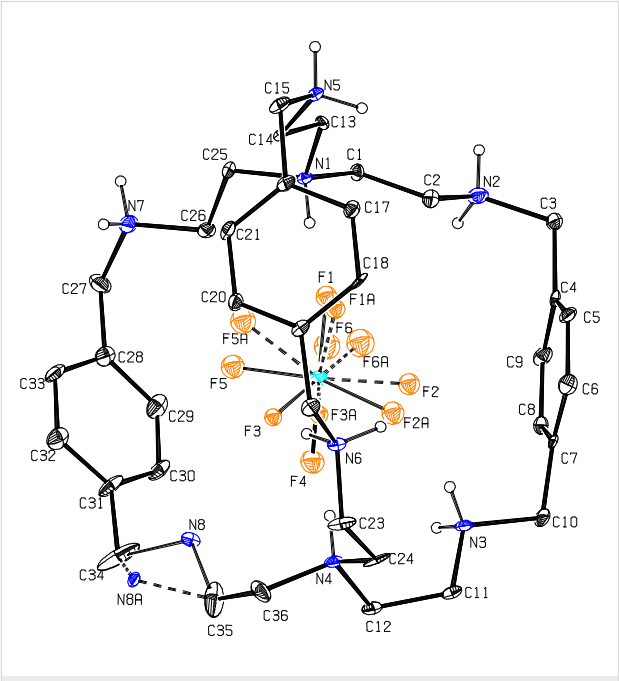

Figure 7: ORTEP diagram depicting the octaprotonated $[H_8\mathbf{L}^1]^{8+}$ moiety with the encapsulated disordered $HSiF_6^-$ monoanion with atom numbering scheme (25% probability factor for the thermal ellipsoids and only hydrogen atoms attached to the amino nitrogens are shown for clarity).

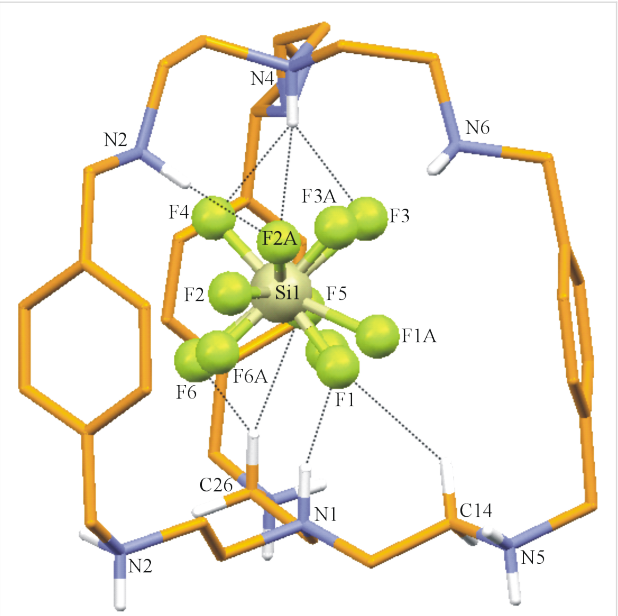

Figure 8: Mercury diagram depicting the encapsulation of the disordered $HSiF_6^-$ inside the $[H_8\mathbf{L}^1]^{8+}$ moiety along with various hydrogen bonding interactions. Only hydrogen atoms having interactions with encapsulated anion are shown for clarity.

Table 7: Selected hydrogen-bond lengths (Å) and bond angles (°) of complex **3**.

D–H···A	D–H [Å]	H···A [Å]	D···A [Å]	D–H···A [°]
N1−H···F1	0.91	1.88	2.756(9)	161
N3−H3D···F2A	0.90	1.92	2.789(11)	163
N4–H4···F2A	0.91	2.27	3.053(11)	143
N4–H4···F3	0.91	2.12	2.904(10)	143
N4–H4···F4	0.91	2.25	2.988(8)	137
N6–H6D···F3	0.90	1.86	2.726(8)	160
C14–H14B···F1	0.97	2.41	3.190(10)	137
C26–H26B···F5	0.97	2.39	3.318(14)	161
C26–H26B···F6	0.97	2.45	3.180(14)	132

Figure 9 represents the interaction of the protonated amino nitrogen atoms with the molecules surrounding the moiety. As depicted in the figure the hydrogen atoms of protonated secondary nitrogen centers are involved in strong N–H···F and N–H···O hydrogen bonds with the external anions and lattice water molecules.

Conclusions

The structural results for the interaction of polyatomic anions with the ligand $\mathbf{L}^1$ in its hexa and octa protonated states show some interesting results. The structures clearly illustrate the effect of hexaprotonation and octaprotonation on the encapsulation of different anions. Upon a higher degree of protonation

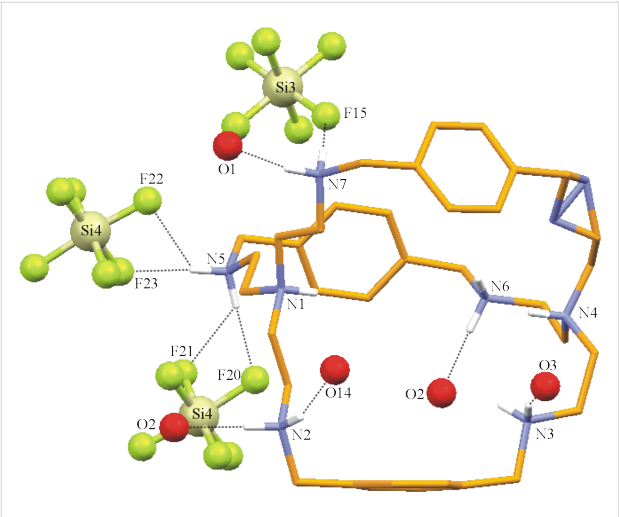

Figure 9: Mercury diagram depicting the interaction of the $[H_8\mathbf{L}^1]^{8+}$ with the surrounding molecules *via* N–H···F and N–H···O hydrogen bonds.

(hexa and octa) distribution of positive charge over the receptor increases which makes the cavity more electrophilic. Different degrees of protonation also change the overall conformation (ellipsoid and near spherical), which allows encapsulation of anions like perchlorate, hydrogen sulfate and hexafluorosilicate inside the receptor. Furthermore, these results indeed show that $\mathbf{L}^1$ is also a potential receptor for bigger polyatomic anions like perchlorate and hydrogen sulfate.

Supporting Information

Experimental procedures, characterization data and copies of spectra (^{1}H NMR and HRMS) of complexes **1**, **2**, and **3** as well as crystallographic data and tables of hydrogen bonding parameters of complexes **1**, **2**, and **3** are provided.

Supporting Information File 1

Experimental and analytical data.
[http://www.beilstein-journals.org/bjoc/content/supplementary/1860-5397-5-41-S1.doc]

Acknowledgments

P.G. gratefully acknowledges the Department of Science and Technology (DST), New Delhi, India for financial support. PSL would like to acknowledge CSIR, New Delhi, India for Senior Research Fellowship.

References

1. Bianchi, A.; Bowman-James, K.; García-España, E., Eds. *Supramolecular Chemistry of Anions;* Wiley-VCH: New York, 1997.
2. *Coord. Chem. Rev.* **2003,** *240,* 1–226.

3. Atwood, J. L.; Steed, J. W. *The Encyclopedia of Supramolecular Chemistry;* Dekker: New York, 2004.
4. *Coord. Chem. Rev.* **2006,** *250,* 2917–3244.
5. Robinson, B. H.; Williams, G. R. *Biochem. Biophys. Acta* **1970,** *216,* 63–70. doi:10.1016/0005-2728(70)90159-3
6. Kimura, E. Macrocyclic polyamines as biological cation and anion complexones – An application to calculi dissolution. In *Topics in Current Chemistry;* Springer: Berlin/Heidelberg, 1985; Vol. 128, pp 113–141.
7. He, J. H.; Quicocho, F. A. *Science* **1991,** *251,* 1479–1481. doi:10.1126/science.1900953
8. Barth, M. C.; Church, A. T. *J. Geophys. Res.* **1999,** *104,* 30231–30239. doi:10.1029/1999JD900809
9. Hossain, M. A.; Llinares, J. M.; Mason, S.; Morehouse, P.; Powell, D.; Bowman-James, K. *Angew. Chem., Int. Ed.* **2002,** *41,* 2335–2338. doi:10.1002/1521-3773(20020703)41:13<2335::AID-ANIE2335>3.0.CO;2-3
10. Hossain, M. A.; Morehouse, P.; Powell, D.; Bowman-James, K. *Inorg. Chem.* **2005,** *44,* 2143–2149. doi:10.1021/ic048937e
11. Lakshminarayanan, P. S.; Kumar, D. K.; Ghosh, P. *Inorg. Chem.* **2005,** *44,* 7540–7546. doi:10.1021/ic051191f
12. Lakshminarayanan, P. S.; Suresh, E.; Ghosh, P. *Angew. Chem., Int. Ed.* **2006,** *118,* 3891–3895. doi:10.1002/ange.200600254
13. Lakshminarayanan, P. S.; Ravikumar, I.; Suresh, E.; Ghosh, P. *Cryst. Growth Des.* **2008,** *8,* 2842–2852. doi:10.1021/cg701152v
14. Hossain, M. A.; Morehouse, P.; Powell, D.; Bowman-James, K. *Inorg. Chem.* **2005,** *44,* 2143–2149. doi:10.1021/ic048937e
15. Alcock, N. W.; Bowman-James, K.; Miler, C.; Berenguer, J. M. L. *Private Communication* **2005**.
16. Mason, S.; Llinares, J. M.; Morton, M.; Clifford, T.; Bowman-James, K. *J. Am. Chem. Soc.* **2000,** *122,* 1814–1815. doi:10.1021/ja9939800
17. Menif, R.; Reibenspies, J.; Martell, A. E. *Inorg. Chem.* **1991,** *30,* 3446–3454. doi:10.1021/ic00018a014
18. Mason, S.; Clifford, T.; Seib, L.; Kuczera, K.; Bowman-James, K. *J. Am. Chem. Soc.* **1998,** *120,* 8899–8900. doi:10.1021/ja9811593
19. Hynes, M. J.; Mauber, B.; McKee, V.; Town, R. M.; Nelson, J. *J. Chem. Soc., Dalton Trans.* **2000,** 2853–2859. doi:10.1039/b003249m
20. Maubert, B. M.; Nelson, J.; McKee, V.; Town, R. M.; Pál, I. *J. Chem. Soc., Dalton Trans.* **2001,** 1395–1397. doi:10.1039/b101832i
21. Nelson, J.; Nieuwenhuyzen, M.; Pál, I.; Town, R. M. *Chem. Commun.* **2002,** 2266–2267. doi:10.1039/b207964j
22. Farrell, D.; Gloe, K.; Gloe, K.; Goretzki, G.; McKee, V.; Nelson, J.; Nieuwenhuyzen, M.; Pál, I.; Stephan, H.; Town, R. M.; Wichmann, K. *Dalton Trans.* **2003,** 1961–1968. doi:10.1039/b210289g
23. Morgan, G.; McKee, V.; Nelson, J. *J. Chem. Soc., Chem. Commun.* **1995,** 1649–1652. doi:10.1039/C39950001649
24. Kang, S. O.; Hossain, M. A.; Powell, D.; Bowman-James, K. *Chem. Commun.* **2005,** 328–330. doi:10.1039/b411904e
25. McKee, V.; Morgan, G. G. *Acta Crystallogr.* **2003,** *C59,* o150–o152. doi:10.1107/S0108270103002580
26. Yang, L.-Z.; Jiang, L.; Feng, X.-L.; Lu, T.-B. *CrystEngComm* **2008,** *10,* 649–651. doi:10.1039/b717967g
27. Reyheller, C.; Kubik, S. *Org. Lett.* **2007,** *9,* 5271–5274. doi:10.1021/ol702386e
28. Hossain, M. A.; Llinares, J. M.; Powell, D.; Bowman-James, K. *Inorg. Chem.* **2001,** *40,* 2936–2937. doi:10.1021/ic015508x
29. Katayev, E. A.; Boev, N. V.; Khrustalev, V. N.; Ustynyuk, Y. A.; Tananaey, I. G.; Sessler, J. L. *J. Org. Chem.* **2007,** *72,* 2886–2896. doi:10.1021/jo0624849
30. Sessler, J. L.; Katayev, E.; Pantso, G. D.; Ustynyuk, Y. A. *Chem. Commun.* **2004,** 1276–1277. doi:10.1039/b403665d
31. Sessler, J. L.; Katayev, E.; Pantos, G. D.; Scherbakov, P.; Reshetova, M. D.; Khrustalev, V. N.; Lynch, V. M.; Ustynyuk, Y. A. *J. Am. Chem. Soc.* **2005,** *127,* 11442–11446. doi:10.1021/ja0522938
32. Clifford, T.; Dnaby, A.; Llinares, J. M.; Mason, S.; Alcock, N. W.; Powell, D.; Aguilar, J. A.; Garcìa-España, E.; Bowman-James, K. *Inorg. Chem.* **2001,** *40,* 4710–4720. doi:10.1021/ic010135l
33. McKee, V.; Nelson, J.; Town, R. M. *Chem. Soc. Rev.* **2003,** *32,* 309–325. doi:10.1039/b200672n
34. Ilioudis, C. A.; Tocher, D. A.; Steed, J. W. *J. Am. Chem. Soc.* **2004,** *126,* 12395–12402. doi:10.1021/ja047070g
35. Abouderbala, L. O.; Belcher, W. J.; Boutelle, M. G.; Cragg, P. J.; Steed, J. W.; Turner, D. R.; Wallace, K. J. *Proc. Natl. Acad. Sci. U. S. A.* **2002,** *99,* 5001–5006. doi:10.1073/pnas.082633299
36. Jeffery, G. A. *An Introduction to Hydrogen Bonding;* Oxford Univ. Press: Oxford, 1997.
37. Braga, D.; Grepioni, F.; Desiraju, G. R. *Chem. Rev.* **1998,** *98,* 1375–1405. doi:10.1021/cr960091b
38. Arya, P.; Channa, A.; Cragg, P. J.; Prince, P. D.; Steed, J. W. *New J. Chem.* **2002,** *4,* 440–447. doi:10.1039/b108522k

License and Terms

Beilstein Journal of Organic Chemistry

Versatile supramolecular reactivity of zinc-tetra(4-pyridyl)porphyrin in crystalline solids: Polymeric grids with zinc dichloride and hydrogen-bonded networks with mellitic acid

Sophia Lipstman and Israel Goldberg*

Full Research Paper

Open Access

Address:
School of Chemistry, Sackler Faculty of Exact Sciences, Tel Aviv University, 69978 Ramat Aviv, Tel Aviv, Israel

Email:
Israel Goldberg* - goldberg@post.tau.ac.il

* Corresponding author

Keywords:
coordination polymers; crystal engineering; hydrogen-bonded networks; porphyrin assemblies; supramolecular chemistry

Beilstein Journal of Organic Chemistry **2009,** *5,* No. 77.
doi:10.3762/bjoc.5.77

Received: 19 October 2009
Accepted: 07 December 2009
Published: 11 December 2009

Guest Editor: C. A. Schalley

Abstract

Crystal engineering studies confirm that the zinc-tetra(4-pyridyl)porphyrin building block reveals versatile supramolecular chemistry. In this work, it was found to be reactive in the assembly of both (a) a 2D polymeric array by a unique combination of self-coordination and coordination through external zinc dichloride linkers and (b) an extended heteromolecular hydrogen-bonded network with mellitic acid sustained by multiple connectivity between the component species.

Introduction

The tetra(4-pyridyl)porphyrin entity in its free-base (TPyP) as well as its metallated (MTPyP) forms has an extraordinarily rich supramolecular chemistry, playing an important role in the construction of diverse polymeric architectures. The TPyPs are readily available [1], and the tendency of the zinc-porphyrin derivative to form polymeric chains by self-coordination between the peripheral pyridyl sites of one molecule and the zinc center of an adjacent species was demonstrated nearly two decades ago [2,3]. Subsequently, it was discovered that MTPyP can not only self-assemble into 1D polymeric arrays, but can also form a robust 3D architecture with molecular sieving features [4]. The facile formation of 3D aggregates, in which the porphyrin units are inter-coordinated via exocyclic metal ion linkers (e.g., tetrahedral Cu^{I}), has also been observed [5]. The latter mode of coordination polymerization, in which the peripheral pyridyl sites of different TPyP/MTPyP moieties can be readily bridged by various metal ion connectors due to the high affinity of the pyridyl N-sites to coordinate to transition metal ions, has attracted much attention over the years, leading to the formulation of a large variety of hybrid organic–inorganic 1D ladders and ribbons, 2D nets, and 3D supramolecular constructs (representative refs [6-11]).

Moreover, a new series of MTPyP-based homomolecular coordination polymers has been reported [12-19]. In particular, supramolecular isomerism characterizes the zinc metalloporphyrin compound, which results in a range of coordination aggregates with diverse connectivity patterns [17-19]. The high propensity of the ZnTPyP moiety to exhibit various modes of self-coordination can be attributed to the binding flexibility of the zinc ion, as well as to the multiple potential ligating sites (the four pyridyl substituents) of the square-planar porphyrin framework. Thus, the zinc ion in the porphyrin core can be four-coordinate (to the four pyrrole N-sites without any axial ligation and no option for self-coordination), or, as most frequently encountered, five-coordinate (binding, in addition, one axial ligand), or six-coordinate (in an octahedral environment with two axial ligands on both sides of the porphyrin macrocycle). In the five-coordinate case, the ZnTPyP assemblies are either 1D chain-polymeric or 0D square-oligomeric, whereas in the six-coordinate case, they form either 3D honeycomb architectures or 2D square-grid networks [17-19]. Simultaneous appearance of the two coordination modes in a single homomeric assembly has also been observed, yielding in such a case ladder-type 1D polymeric ribbons [13,15].

The hydrogen-bonding capacity of TPyP and MTPyP in network formation has not been explored until recently. The porphyrin framework is characterized by a square-planar symmetry, bearing laterally diverging pyridyl sites. The latter are available for hydrogen bonding as proton acceptors with complementary components that can act as proton donors. Formulation of extended hydrogen-bonding-sustained networks requires ideally a tetradentate proton donor of similar square-planar symmetry. It has been confirmed that 1,2,4,5-benzenetetracarboxylic acid (B4CA) is perfectly suited for this purpose, as are hydrogen-bonded dimers of 1,3,5-benzenetricarboxylic acid (B3CA) [20,21]. In both cases the TPyP moiety self-assembles with the corresponding acid in appropriate solubilizing environments into 2D heteromolecular grids held together by multiple hydrogen bonding. The same applies to ZnTPyP, when the axial coordination site of the zinc ion is blocked.

In order to expand the library of the available polymeric materials and further explore the different possible modes of self-assembly, we report here on two new ZnTPyP-based structures characterized by either coordination or hydrogen-bonding networking. They represent a coordination polymer ZnTPyP·$ZnCl_2$, which crystallizes as a 1,1,2,2-tetrachloroethane (TCE) trisolvate (**I**), and a hydrogen-bonded polymeric network composed of Zn(EtOH)TPyP (where the ethanol solvent occupies and protects the axial coordination site of the zinc ion) and 1,2,3,4,5,6-benzenehexacarboxylic (mellitic) acid (1:1), which crystallizes with one molecule of *o*-dichlorobenzene and three molecules of methanol solvent (**II**). The component building blocks are shown in Scheme 1.

Results and Discussion

The coordination polymer in structure **I** was obtained by chance, while attempting to network ZnTPyP with different tetracarboxylic acids (see Experimental). It exhibits, however, a uniquely interesting connectivity scheme that combines direct and through-$ZnCl_2$ porphyrin-to-porphyrin coordination (Figure 1), a pattern not previously observed.

Crystal data for I: $C_{40}H_{24}N_8{\cdot}ZnCl_2{\cdot}3C_2H_2Cl_4$, M = 1321.82, monoclinic, space group $P2_1/c$, a = 19.1157(2) Å, b = 12.9275(2) Å, c = 21.8495(2) Å, β = 103.396(1)°, V = 5252.5(1) $Å^3$, Z = 4, D_c = 1.672 g cm^{-3}, μ(Mo Kα) = 1.67 mm^{-1}, 38848 reflections measured, 12452 unique (R_{int} = 0.045), final R = 0.065 for 8437 reflections with $I > 2\sigma(I)$ and R = 0.099 (wR = 0.200) for all data.

The zinc ion in the porphyrin core is five-coordinate with square-pyramidal environment. A given porphyrin unit is involved in two direct coordination bonds to its neighbors. One of the four peripheral pyridyl substituents links to the zinc

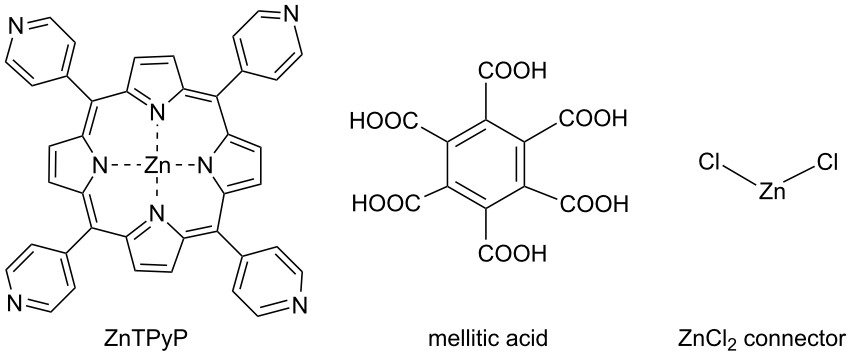

Scheme 1: Component building blocks of the supramolecular assembly in **I** and **II**.

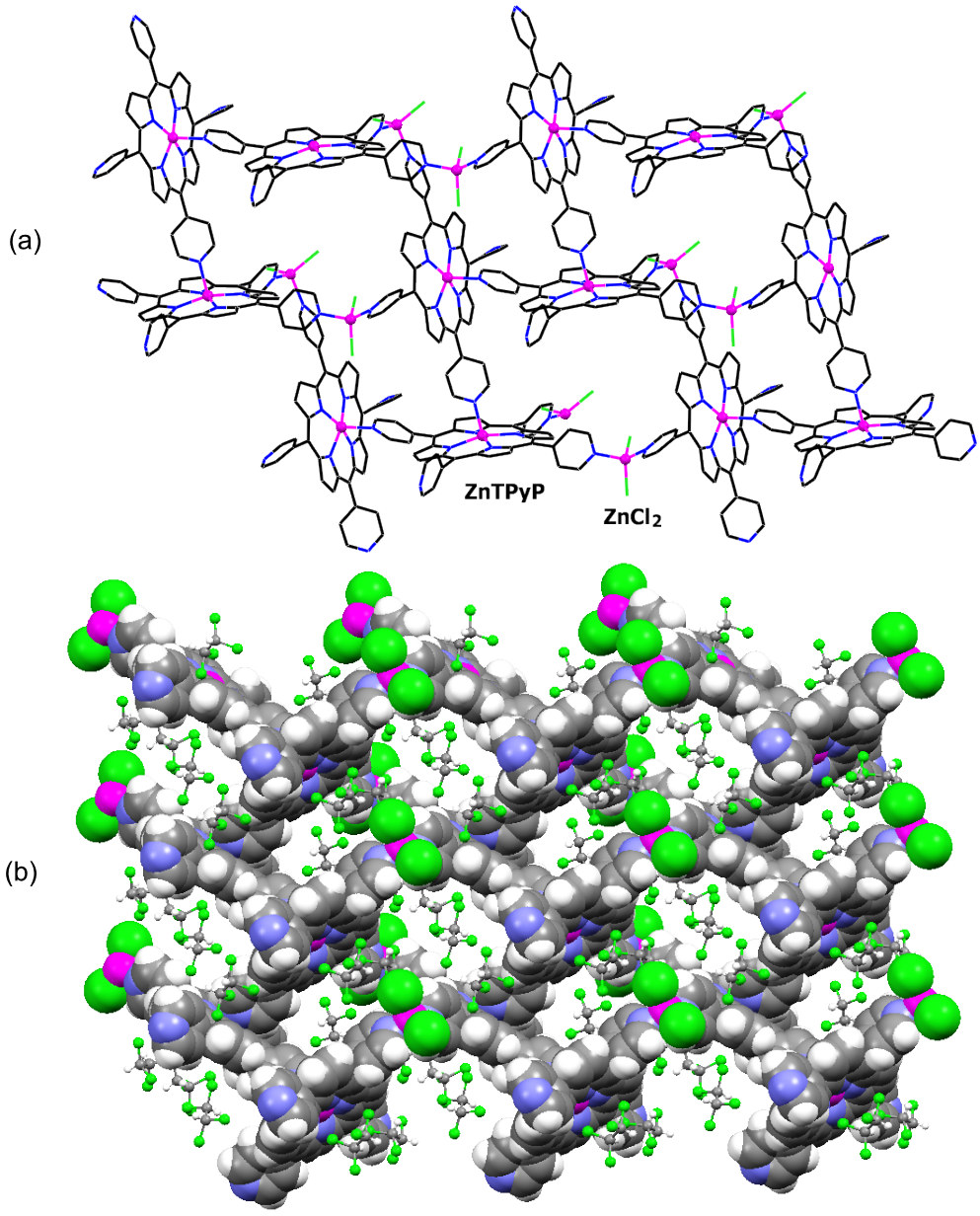

Figure 1: Fragment of the continuous coordination scheme in **I**, forming a corrugated layer that is aligned perpendicular to the *c*-axis of the crystal. (a) Wireframe presentation, with the exception of the zinc ions which are depicted as small spheres, illustrating the connectivity scheme. (b) Space-filling view of the coordination polymer. Note that the $ZnCl_2$ bridges and the non-coordinated pyridyl groups point outward from the network. The interporphyrin kinks and voids within the polymeric layer, as well as between neighboring layers, are occupied by the TCE solvent (shown as "ball-and-stick" molecules).

center of an adjacent species, while the metal ion binds to a pyridyl group of a third porphyrin unit (at Zn–N = 2.150 Å; all the $Zn–N_{pyrrole}$ bond lengths are in the range 2.066–2.075 Å). It is further coordinated to two additional porphyrins with the aid of the tetrahedral zinc dichloride connectors (at Zn–N = 2.040 and 2.046 Å), each bridging between pyridyl groups of two neighboring moieties. The fourth pyridyl group is not involved in intermolecular coordination, and is rotationally disordered in the crystal. Such a four-point per porphyrin binding model, which involves the zinc ion and three of the pyridyl groups, results in the formation of a 2D grid coordination polymer wherein neighboring porphyrins are roughly perpendicular to each other. There is a considerable resemblance between the observed connectivity and that found in the recently reported "paddle-and-wheel"-like square-grid homomolecular coordination polymer of ZnTPyP with a six-coordinate environment

around the zinc center [17,18]. The inter-coordinated assembly represents a markedly corrugated layer, which is aligned normal to the *c*-axis of the unit cell. The non-coordinated pyridyl groups and the chloride ions lie above and below the molecular surface of this layer. In the crystals the layers are stacked along the *c*-axis and partly interdigitate into one another. Molecules of the TCE crystallization solvent accommodate the interporphyrin kinks and voids within the polymeric assembly, as well as voids in the interface between adjacent layers. The formation of coordination polymers bridged by exocyclic zinc ions of tetrahedral geometry has also been observed in supramolecular materials based on the tetra(4-carboxyphenyl)porphyrin building blocks [22,23].

Based on previous findings [20,21], the ZnTPyP and mellitic acid components provide excellent building blocks for the construction of heteromolecular networks sustained by cooperative hydrogen bonding. Both have multiple laterally diverging functions, the 4-pyridyl substituents in ZnTPyP acting as proton acceptors and the carboxylic residues in mellitic acid as complementary proton donors. The heteromeric COOH···$N_{pyridyl}$ interaction results in a relatively strong hydrogen bond, which frequently directs supramolecular organization in organic crystals [24]. Preferential hydrogen bonding of ZnTPyP to the mellitic acid, over self-coordination (as in **I**), may occur only if the axial coordination ability of the central zinc ion is blocked. This can be achieved by introducing small zinc-coordinating ligands (e.g., water, MeOH, EtOH, DMF, or DMSO) into the crystallization mixture [20], as in the present case. Ideally, the use of tetracarboxylic ligand of square-planar geometry such as B4CA is best suited to optimize hydrogen-bonding interactions with the complementary tetradentate TPyP moiety [20,21]. When 1,3,5-benzenetricarboxylic acid was used in a similar reaction, it formed hydrogen-bonded dimers first by using one COOH function of each monomer to yield an entity with four free carboxylic groups to bind to the porphyrin.

Not surprisingly, therefore, when the mellitic acid was used in this study, two of its carboxylic acid functions (at positions 3 and 6 of the central benzene ring) did not interact with Zn(EtOH)TPyP, thus mimicking effectively the functionality of B4CA. The supramolecular assembly that formed in this case is depicted in Figure 2.

Crystal data for II: $C_{40}H_{24}N_8Zn{\cdot}C_2H_5OH{\cdot}C_{12}H_6O_{12}$ (crystallization solvent, X = $C_6H_4Cl_2{\cdot}3CH_3OH$, excluded due to

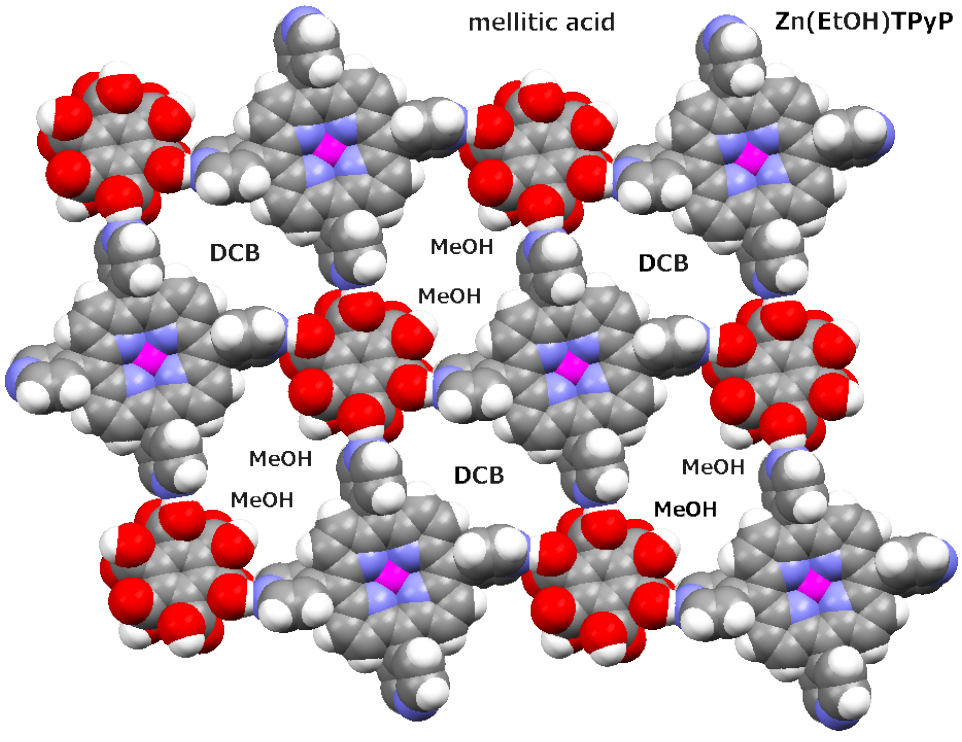

Figure 2: Space-filling representation of the hydrogen-bonded heteromolecular network in **II**. Note that every porphyrin unit is in direct hydrogen-bonding contact through its pyridyl groups with four molecules of mellitic acid and vice versa. Two of the carboxylic groups of the latter point into the intralayer voids. They are solvated in the crystal by molecules of the methanol solvent (MeOH) that occupy the adjacent voids, the alternating voids being occupied by the *o*-dichlorobenzene (DCB) solvent. These flat layers are aligned parallel to the (110) plane of the crystal. In this figure, at every porphyrin site the EtOH axial ligand is connected to the central zinc ion from below, preventing self-coordination of the ZnTPyP units (as in **I**).

disorder), M = 1070.28, triclinic, space group $P\bar{1}$, a = 11.8660(3) Å, b = 13.8803(4) Å, c = 20.4843(5) Å, α = 78.237(2)°, β = 78.185(2)°, γ = 84.288(1)°, V = 3227.1(2) Å^3, Z = 2, D_c = 1.101 g cm^{-3} and μ(Mo Kα) = 0.44 mm^{-1} (*X* excluded), 35843 reflections measured, 15151 unique (R_{int} = 0.051), final R = 0.060 for 9766 reflections with $I > 2\sigma(I)$ and R = 0.092 (wR = 0.167) for all data. Molecules of the crystallization solvent are included in a severely disordered manner within the interstitial voids of the crystal lattice (the solvent-accessible voids amount to 35.3% of the crystal volume) and cannot be modeled reliably by discrete atoms. Conventional least-squares refinement of the complete structural model resulted in $R1$ = 0.10. In the final calculations the contribution of the disordered solvent was subtracted from the diffraction data by the Squeeze procedure [25], a common practice in similar situations. The least-squares refinement converged smoothly to a lower R-value, allowing a precise determination of the hydrogen-bonded network.

Compound **II** is characterized by a 1:1 stoichiometry of the Zn(EtOH)TPyP and mellitic acid components. Every porphyrin is efficiently hydrogen bonded to four adjacent acids, and every acid is hydrogen bonded to four different porphyrins. This connectivity scheme results in a fascinating supramolecular grid sustained by such cooperative COOH···N_{py} hydrogen bonding (at N···O within 2.56–2.62 Å). The layered array thus formed has an open structure, with voids of two types lined by the two pairs of the networking components and encircled by four hydrogen bonds (Figure 2). The two "excess" carboxylic functions of the mellitic acid are solvated by the methanol solvent that protrudes into 50% of the intralayer voids. The other voids within the layered array are filled by DCB. Such neighboring layers are related to one another by inversion in an offset manner. Within the inversion-related layers the axial EtOH ligands of one layer penetrate into the voids of another layer. The concave surfaces of the five-coordinate porphyrin moieties are located on the outside of the paired layers, inducing further incorporation of crystallization solvent (MeOH) to fill this interfacial space between the paired layers, which stack effectively along the [110] axis of the crystal.

Conclusion

This study confirms the high versatility of the ZnTPyP moiety as an effective building block in the formulation of supramolecular grids. The square-planar ZnTPyP framework has diverse and multidentate binding capacities. It can self-coordinate directly via the Zn-pyridyl bonds to form 2D and 3D polymeric arrays [4,18,19]. Then, it can form supramolecular assemblies of varying dimensionality with the aid of exocyclic metal ion linkers capable of coordinating simultaneously to several neighboring ZnTPyP units [5-11]. The ZnTPyP can adopt in the above constructs either five-coordinate or six-coordinate geometries, which affects the architecture of the resulting assembly. Formation of coordination networks by combining direct porphyrin–porphyrin coordination and coordination through an external linker (as in **I**) has been demonstrated here for the first time. It has further been demonstrated that TPyP and ZnTPyP scaffolds may be used also for the formulation of supramolecular assemblies sustained by cooperative hydrogen bonding with the pyridyl substituents as excellent proton acceptors for compatible proton donating species [20,21]. In particular, the strong COOH···N_{py} interaction [24] can be harnessed to this end by reacting the tetrapyridylporphyrin with a polycarboxylic acid entity, and thus inducing cooperative hydrogen-bonding interactions in four different directions. The observed structure of compound **II** provides an attractive example of designed formulation of such heteromolecular networks. The observed modes of self-assembly are of further significance to studies of surface-based crystallizations of monolayer and multilayer hydrogen-bonded networks and metal–organic frameworks on various substrates [26,27], in the context of the design of novel molecular devices.

Experimental

The ZnTPyP, 1,4,5,8-naphthalenetetracarboxylic acid (NTCA), 1,2,3,4,5,6-benzenehexacarboxylic (mellitic) acid, 3,4,9,10-perylenetetracarboxylic acid (PTCA), as well as common laboratory solvents were procured commercially, and used without further purification. The porphyrin was treated with different acids under diverse experimental conditions in an attempt to synthesize heteromeric hydrogen-bonding networks of the interacting components. The coordination polymeric compound (**I**) was first obtained when a methanol solution of PTCA (in which ZnTPyP is sparingly soluble) was carefully layered at room temperature over a solution of ZnTPyP (0.015 mmol) in a 1:1 mixture of TCE and methanol (10 ml). Crystals appeared in the bottom solution after a few days. The same crystalline compound was obtained under reflux conditions when 0.05 mmol of ZnTPyP was reacted with 0.05 mmol of NTCA in a 1:1:1:1 solvent mixture of TCE, *o*-chlorophenol/*o*-dichlorobenzene, ethanol, and *N*,*N*-dimethylformamide (DMF). The resulting solution was refluxed for 16 h, and then cooled to room temperature and left for crystallization. X-ray quality crystals were obtained after four days. It appeared in both cases that $ZnCl_2$ was formed in situ under the acidic conditions by extracting some of the zinc ions from the metalloporphyrin. The porphyrin-mellitic acid hydrogen-bonded compound (**II**) was obtained when a methanol solution (10 ml) of mellitic acid (0.055 mmol) was carefully layered over a solution of 0.010 mmol of ZnTPyP dissolved in a 1:1 mixture (10 ml) of ethanol and *o*-dichlorobenzene. Sizeable crystals appeared after three days. The uniformity of the formed crystal-

line materials was confirmed in each case by repeated measurements of the unit cell dimensions from several randomly chosen single crystals.

The diffraction measurements were carried out on a Nonius KappaCCD diffractometer, using graphite monochromated Mo Kα radiation (λ = 0.7107 Å). The crystalline samples of the analyzed compounds were covered with a thin layer of light oil and freeze-cooled to ca. 110 K in order to minimize solvent escape, structural disorder, and thermal motion effects, and increase the precision of the results. The structures were solved by direct methods (SIR-97) and refined by full-matrix least-squares on F^2 (SHELXL-97). Intensity data were corrected for absorption effects. All non-hydrogen atoms (except of those of the disordered pyridyl group and TCE solvent in **I** and the disordered solvent in **II**) were refined anisotropically. The hydrogens were either found in difference Fourier maps or located in idealized positions, and were refined using a riding model with fixed thermal parameters [U_{ij} = 1.2 or 1.5 U_{ij} (eq.) for the atom to which they are bonded]. No phase transitions of the two crystalline compounds were detected between room temperature and 110 K. The two polymeric structure types contain sizeable voids, which are accommodated by molecules of crystallization solvent (three molecules of TCE in **I**, and one moiety of *o*-dichlorobenzene and three molecules of methanol in **II**). In **II**, the solvent species could be clearly identified in the electron-density maps but they were found to be severely disordered in the lattice and could not be reliably modeled by discrete atoms. Correspondingly, their contribution to the diffraction pattern was subtracted by the Squeeze procedure (commonly used in similar situations) [25], allowing smooth convergence of the crystallographic refinement and precise description of the hydrogen-bonded framework.

Supporting Information

Supporting information features X-ray data for compounds **I** and **II**.

Supporting Information File 1

X-ray data for compound **I**.
[http://www.beilstein-journals.org/bjoc/content/supplementary/1860-5397-5-77-S1.cif]

Supporting Information File 2

X-ray data for compound **II**.
[http://www.beilstein-journals.org/bjoc/content/supplementary/1860-5397-5-77-S2.cif]

Acknowledgement

This research was supported by The Israel Science Foundation (Grant No. 502/08).

References

1. Fleischer, E. B. *Inorg. Chem.* **1962,** *1,* 493–495. doi:10.1021/ic50003a010
2. Collins, D. M.; Hoard, J. L. *J. Am. Chem. Soc.* **1970,** *92,* 3761–3771. doi:10.1021/ja00715a038
3. Fleischer, E. B.; Shachter, A. M. *Inorg. Chem.* **1991,** *30,* 3763–3769. doi:10.1021/ic00019a038
4. Krupitsky, H.; Stein, Z.; Goldberg, I.; Strouse, C. E. *J. Inclusion Phenom. Mol. Recognit. Chem.* **1994,** *18,* 177–192. doi:10.1007/BF00705820
5. Abrahams, B. F.; Hoskins, B. F.; Michail, D. M.; Robson, R. *Nature* **1994,** *369,* 727–729. doi:10.1038/369727a0
6. Hagrman, D.; Hagrman, P. J.; Zubieta, J. *Angew. Chem., Int. Ed.* **1999,** *38,* 3165–3168. doi:10.1002/(SICI)1521-3773(19991102)38:21<3165::AID-ANIE3165>3.0.CO;2-O
7. Sharma, C. V. K.; Broker, G. A.; Huddleston, J. G.; Baldwin, J. W.; Metzger, R. M.; Rogers, R. D. *J. Am. Chem. Soc.* **1999,** *121,* 1137–1144. doi:10.1021/ja983983x
8. Barkigia, K. M.; Battioni, P.; Riou, V.; Mansuy, D.; Fajer, J. *Chem. Commun.* **2002,** 956–957. doi:10.1039/b202513m
9. Carlucci, L.; Ciani, G.; Proserpio, D. M.; Porta, F. *Angew. Chem., Int. Ed.* **2003,** *42,* 317–322. doi:10.1002/anie.200390106
10. Carlucci, L.; Ciani, G.; Proserpio, D. M.; Porta, F. *CrystEngComm* **2005,** *7,* 78–86. doi:10.1039/b417709f
11. Ohmura, T.; Usuki, A.; Fukumori, K.; Ohta, T.; Ito, M.; Tatsumi, K. *Inorg. Chem.* **2006,** *45,* 7988–7990. doi:10.1021/ic060358h
12. Lin, K.-J. *Angew. Chem., Int. Ed.* **1999,** *38,* 2730–2732. doi:10.1002/(SICI)1521-3773(19990917)38:18<2730::AID-ANIE2730>3.0.CO;2-9
13. Diskin-Posner, Y.; Patra, G. K.; Goldberg, I. *J. Chem. Soc., Dalton Trans.* **2001,** 2775–2782. doi:10.1039/b104961p
14. Pan, L.; Kelly, S.; Huang, X.; Li, J. *Chem. Commun.* **2002,** 2334–2335. doi:10.1039/b207855d
15. Ring, D. J.; Aragoni, M. C.; Champness, N. R.; Wilson, C. *CrystEngComm* **2005,** *7,* 621–623. doi:10.1039/b515083n
16. George, S.; Goldberg, I. *Acta Crystallogr., Sect. E: Struct. Rep. Online* **2005,** *61,* m1441–m1443. doi:10.1107/S1600536805018556
17. Koner, R.; Goldberg, I. *Acta Crystallogr., Sect. C: Cryst. Struct. Commun.* **2009,** *65,* m139–m142. doi:10.1107/S0108270109005691
18. Lipstman, S.; Goldberg, I. *CrystEngComm* **2010,** *12,* 52–54. doi:10.1039/b914799c
19. Seidel, R. W.; Goddard, R.; Föcker, K.; Oppel, I. M. *CrystEngComm* **2009**. doi:10.1039/b913791b Published on the Web as an advance article.
20. Koner, R.; Goldberg, I. *CrystEngComm* **2009,** *11,* 1217–1219. doi:10.1039/b906538p
21. Koner, R.; Goldberg, I. *J. Inclusion Phenom. Macrocyclic Chem.* **2009**. doi:10.1007/s10847-009-9611-0 Published on the Web as an advance article.
22. Diskin-Posner, Y.; Dahal, S.; Goldberg, I. *Chem. Commun.* **2000,** 585–586. doi:10.1039/b001189o

23. Shmilovits, M.; Vinodu, M.; Goldberg, I. *Cryst. Growth Des.* **2004,** *4,* 633–638. doi:10.1021/cg0342009
24. Aakeröy, C. B.; Beatty, A. M.; Helfrich, B. A. *J. Am. Chem. Soc.* **2002,** *124,* 14425–14432. doi:10.1021/ja027845q
25. Spek, A. L. *J. Appl. Crystallogr.* **2003,** *36,* 7–13. doi:10.1107/S0021889802022112
26. Blunt, M.; Lin, X.; Gimenez-Lopez, M. C.; Schröder, M.; Champness, N. R.; Beton, P. H. *Chem. Commun.* **2008,** 2304–2306. doi:10.1039/b801267a
27. Shi, N.; Yin, G.; Han, M.; Jiang, L.; Xu, Z. *Chem.–Eur. J.* **2008,** *14,* 6255–6259. doi:10.1002/chem.200702032

License and Terms

Beilstein Journal of Organic Chemistry

An enantiomerically pure siderophore type ligand for the diastereoselective 1 : 1 complexation of lanthanide(III) ions

Markus Albrecht*[1], Olga Osetska[1], Thomas Abel[1], Gebhard Haberhauer*[2] and Eva Ziegler[2]

Full Research Paper

Open Access

Address:
[1]Institut für Organische Chemie, RWTH Aachen University, Landoltweg 1, 52074 Aachen, Germany and [2]Institut für Organische Chemie, Universität Duisburg-Essen, Universitätsstraße 7, 45117 Essen, Germany

Email:
Markus Albrecht* - markus.albrecht@oc.rwth-aachen.de;
Gebhard Haberhauer* - gebhard.haberhauer@uni-due.de

* Corresponding author

Keywords:
CD spectroscopy; enterobactin; lanthanide; macrocycles; molecular modeling

Beilstein Journal of Organic Chemistry **2009,** *5,* No. 78.
doi:10.3762/bjoc.5.78

Received: 23 September 2009
Accepted: 24 November 2009
Published: 11 December 2009

Guest Editor: C. A. Schalley

Abstract

A facile synthesis of a highly preorganized tripodal enterobactine-type ligand **1a**-H_3 consisting of a chiral C_3-symmetric macrocyclic peptide and three tridentate 2-amido-8-hydroxyquinoline coordinating units is presented. Complex formation with various metal ions (Al^{3+}, Ga^{3+}, Fe^{3+}, La^{3+} and Eu^{3+}) was investigated by spectrophotometric methods. Only in the case of La^{3+} and Eu^{3+} were well defined 1 : 1 complexes formed. On the basis of CD spectroscopy and DFT calculations the configuration at the metal centre of the La^{3+} complex was determined to show *Λ* helicity. The coordination compounds [(**1a**)Ln] presented should be prototypes for further lanthanide(III) complexes with an enterobactine analogue binding situation.

Introduction

The availability of metal ions for biological systems is essential for growth and function. Therefore microorganisms have to develop strategies how to solubilise and take up charged ions through highly non-polar membranes [1,2].

An important class of natural products which is responsible for the uptake of iron are the siderophores [3-5]. The probably most prominent example of this class is enterobactin (Figure 1) [6-8]. It has inspired the synthesis of a wide series of non-natural compounds which are used for metal ion binding and medical purposes [9-22]. However, the efficiency of this artificial chelators to bind iron(III) excels only in few cases the one observed for enterobactin [23,24].

Enterobactin resembles the ideal raw model for the design of highly efficient metal ion receptors. It combines two different

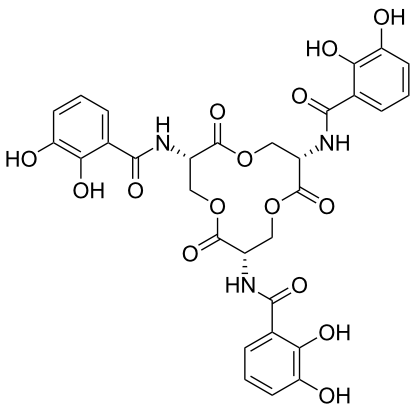

Figure 1: Structural formula of the siderophore enterobactine.

structural aspects which are important for effective binding of the metals: (i) **Chelating moieties**: Catechol is an efficient chelating moiety, which can form highly stable complexes with a series of first row transition metals. (ii) **Chirality**: The enterobactin-backbone is based on L-serine units and therefore is chiral (and enantiomerically pure). This chiral information gives all three ligand units the same spatial orientation, leading to a bowl-shape structure which is preorganized for the uptake of the metal. Here we present the synthesis of a novel tripodal ligand, which mimics some features of enterobactin, but in contrast is specific for the binding of high coordinated lanthanide(III) ions. The backbone is based on an enantiomerically pure "non-natural" peptide moiety [25], which organizes three tridenate metal binding sites in one direction [26-28]. The synthesis of the compound is facile and utilizes a multiple Claisen-rearrangement reaction as introduced by Hiratani as the keystep [29,30]. UV and CD titration experiments use the constricted chirality in the metal complex and allow the investigation of the binding of f-element cations and the determination of the selectivity towards this class of metal ions.

Results and Discussion

Synthesis of the Ligand

The preparations of the required building blocks **2** [31,32] and **3** [33] for the synthesis of the ligand **1a**-H_3 have already been described before (Scheme 1).

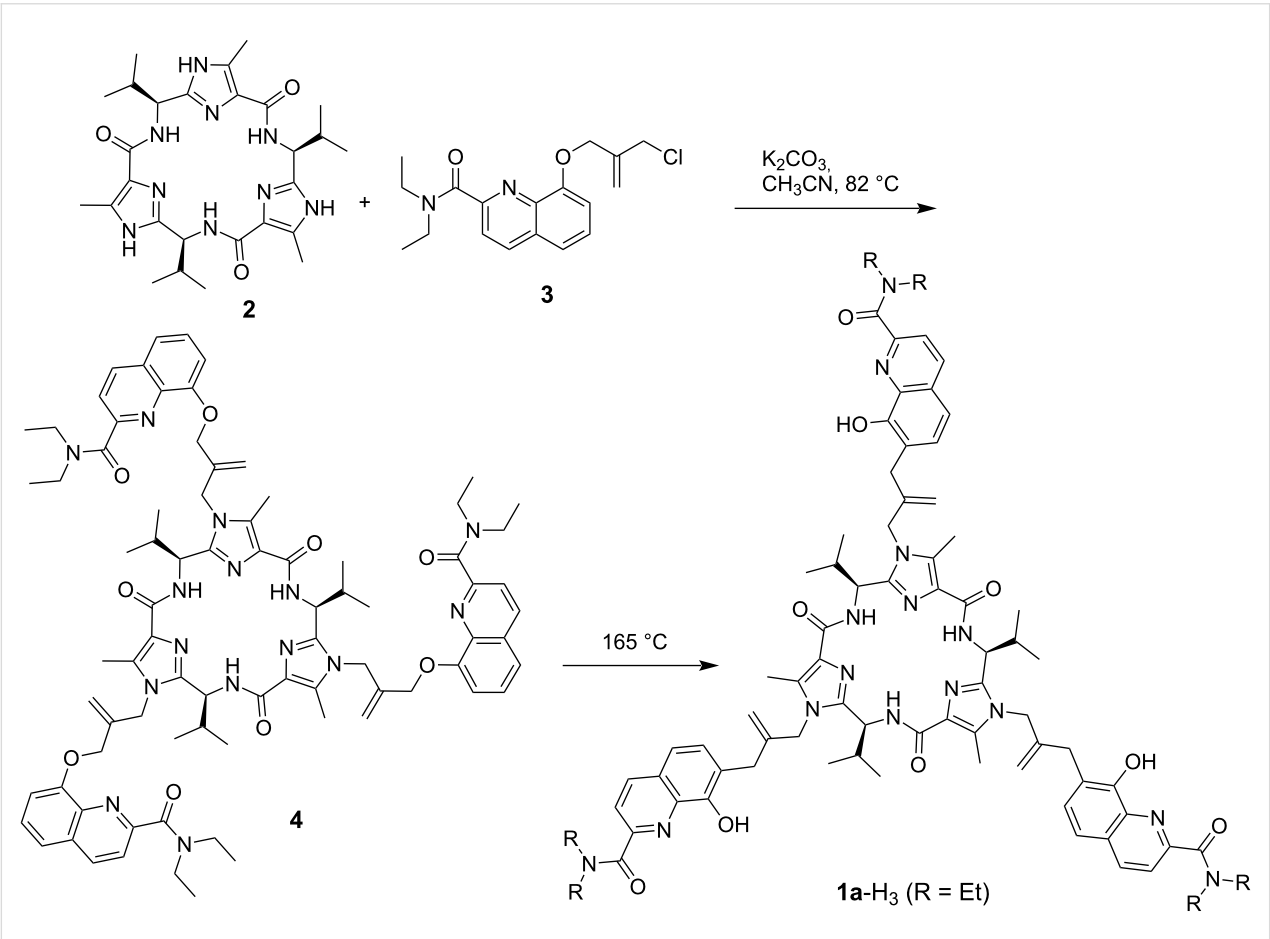

Scheme 1: Preparation of the compound **1a**-H_3 by utilization of a multiple Claisen-rearrangement.

The C_3-symmetric scaffold **2** is obtained in an eight step sequence starting from Z-protected valine and methyl 2-amino-3-oxobutanoate hydrochloride [31,32]. Compound **2** resembles the ideal platform for an enterobactine-type ligand system. It possesses a concave shape in which the three anchor points at the NH units of imidazole are orientated towards the same direction in space. The ether **3** is attached to this position by an S_N-reaction. Derivative **3** possesses a masked 8-hydroxyquinoline unit which is extended to be tridentate by addition of diethylamide to the 2-position. Recently 2-amido-8-hydoxyquinolines were shown to be good ligands for the 3 : 1 complexation of lanthanide(III)ions [34,35]. The aryl ether of **3** bears already the allylic unit for Claisen rearrangement as well as the chloride leaving group for the attachment of other units. Coupling of **2** with three equivalents of **3** results in the formation of the ligand precursor **4**. The triple Claisen rearrangement of **4** proceeds at 165 °C under inert atmosphere (N_2) within 6 hours [36]. No epimerization occurs at the chiral carbon atoms of the peptidic scaffold and the final ligand **1a**-H_3 is obtained in good yield (90%). Successive Cope rearrangement of the spacers to the 5-position of the quinoline moiety is not observed under the chosen reaction conditions.

^{1}H NMR spectra of **4** and **1a**-H_3 show pronounced differences for the resonances of the 8-hydroxyquinoline moiety and the spacer, while the signals of the backbone do not change significantly (Figure 2). Most remarkable is the disappearance of the signal of the proton in 7-position of **4** at δ = 7.06 ppm. The vinylic hydrogen atoms appear for the precursor **4** at δ = 5.29 and 4.55 ppm and are shifted in **1a**-H_3 to δ = 4.91 and 4.24 ppm. Differences are also observed for the CH_2 units of the spacer. In **4** they are both observed as multiplets around δ = 4.71 ppm, while they appear separated in **1a**-H_3 as a singlet at δ = 4.33 ppm (N–CH_2) and as a signal which is hidden under the methylene units of the diethylamide at δ = 3.56 ppm (C_{aryl}–CH_2).

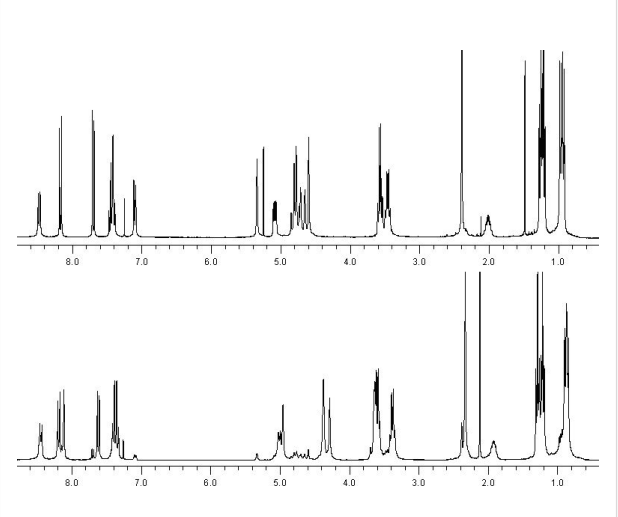

Figure 2: ^{1}H NMR spectra (300 MHz, $CDCl_3$) of the ether compound **4** (top) and the ligand **1a**-H_3 (bottom).

Coordination studies

In an orientating coordination study we reacted the ligand **1a**-H_3 on a preparative scale (30 mg) with lanthanum(III) chloride heptahydrate in the presence of potassium carbonate as base in methanol at room temperature. After four days solvent was distilled off and the residue was washed with water in order to remove potassium chloride and uncoordinated lanthanide salts. The complex was obtained in 82% yield as a red solid with elemental analysis correct for the pentahydrate of [(**1a**)La]. NMR spectroscopy of the complex did not show significant shift differences between the ligand and the complex. This could be due to the lability of the compound in solution and fast dissociation/association equilibria. However, positive ESI MS in chloroform showed the base peak at m/z = 1600.8 for $\{K[(\mathbf{1a})La]\}^+$ with correct isotopic pattern (Figure 3). Due to the already described dissociation equilibrium in solution uncoordinated ligand can be observed as well at m/z = 1464.9 $\{K(\mathbf{1a}\text{-}H_3)\}^+$.

UV and CD titration experiments

As a sensitive technique for the investigation of the complex formation of ligand **1a**-H_3 with a series of trivalent metal ions we performed UV–vis as well as CD spectroscopic titrations in methanol together with NaOH as base (10^{-4} M; Figure 4). Upon coordination of the metal ions to the ligand the transitions at the aromatic unit are influenced leading to changes in the UV–vis spectrum. In addition, metal coordination restricts the conformation at the ligand leading to a significant change of the observed CD spectra.

Small trivalent metal ions like aluminium(III), gallium(III) or iron(III) which are able to form (distorted) octahedral coordination compounds lead to UV–vis spectra which show isosbestic behaviour. However, the titration curves show more or less linear changes of the absorption (in case of iron(III) a kink is observed at 1.5–2.0 equivalents iron(III) salt added). This indicates that not a 1 : 1 but probably polymeric coordination compounds are formed.

Only titrations with lanthanum(III) or europium(III) salts show well defined reliable behaviour (Figure 5). The spectra for the two different metal ions are very similar indicating that the observed transitions are ligand-centered. CD as well as UV spectra of the titration of **1a**-H_3 with lanthanum(III) are shown in Figure 4, while Figure 5 depicts the corresponding titration curve following the absorption at 279 nm.

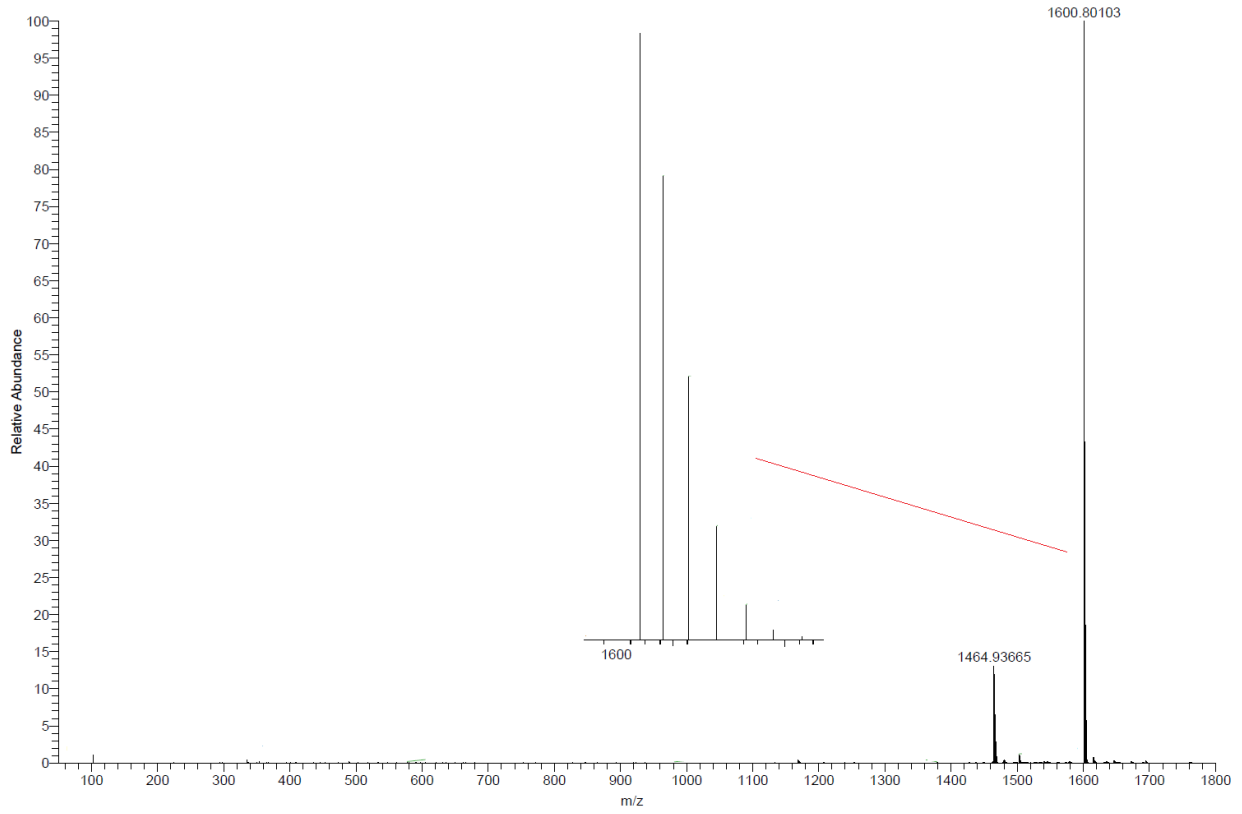

Figure 3: Positive ESI MS of [(**1a**)La] in chloroform showing the peaks of $\{K[(\mathbf{1a})La]\}^+$ (m/z = 1600.8) as well as of $\{K(\mathbf{1a}\text{-}H_3)\}^+$ (m/z = 1464.9). The inset shows the isotopic pattern of the peak at m/z = 1600.8, which corresponds to the one calculated for $\{K[(\mathbf{1a})La]\}^+$.

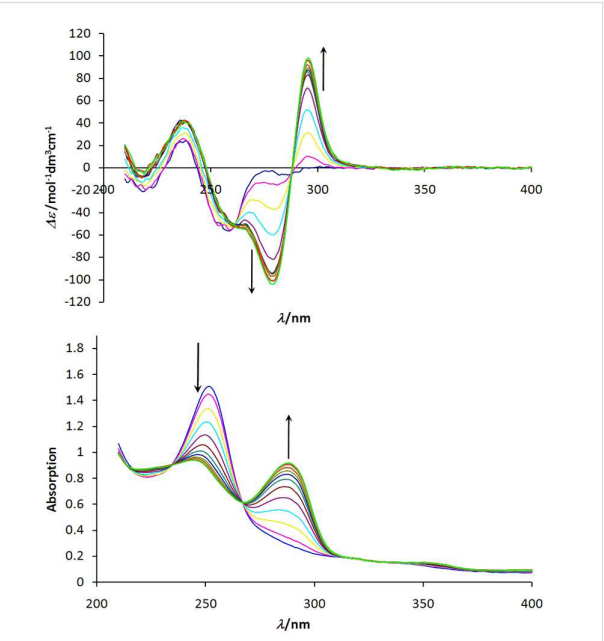

Figure 4: CD and UV absorption titration curves for complexation of ligand **1a**-H_3 with lanthanum(III)nitrate hexahydrate [**1a**-H_3] = 10^{-5}M; 10^{-4} M NaOH. Top: CD spectra; bottom: UV absorption spectra.

Analysis of the titration data reveals high binding constants for lanthanum(III) ($K_a = 8.3 \times 10^5$ M^{-1}) as well as europium(III) ($K_a = 7.8 \times 10^5$ M^{-1}) for the reaction of deprotonated ligand $\mathbf{1a}^{3-}$ with the Ln^{3+} ion to form [(**1a**)Ln] in methanol at room temperature.

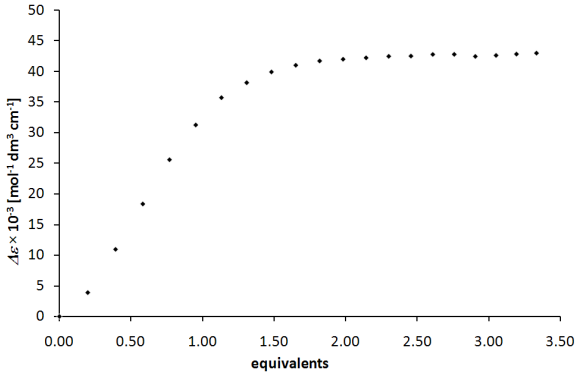

Figure 5: Titration curve observed for ligand **1a**-H_3 upon addition of lanthanum(III) nitrate hexahydrate.

Ab initio calculations

In order to determine the configuration at the metal centres of the **1a**·Ln (R = Et) complexes ab initio calculations were performed for the stereoisomers of complex **1b**·La (R = Me) [37]. The difference between **1a** and **1b** is only the substitution of the ethyl groups in **1a** by methyl groups in **1b**. This simplification reduces the number of optimization steps in the calculations and should not affect the extent of diastereoselectivity for the complex formation. In principle the C_3-symmetric **1b**·La complex can adopt four different conformations (*Λ1*, *Λ2*, *Δ1*, *Δ2*): The 8-hydroxyquinoline units can be present in two opposite helicities (*Λ* and *Δ*) and the three isobutenylidene spacers can adopt two different orientations relative to the macrocycle: the CH_2 units of the spacers point to the interior of the molecule in the case of the conformers (*Λ1*)-**1b**·La and (*Δ1*)-**1b**·La and to the exterior in the case of the conformers (*Λ2*)-**1b**·La and (*Δ2*)-**1b**·La. The structures of the complex **1b**·La were determined by geometry optimizations at DFT-level by using B3LYP/LANL2DZ.

The calculations revealed that the *Λ2* isomer is the energetically favored one (Figure 6). The energies of the other conformers were calculated to be much higher (38 kJ mol^{-1} for *Δ2*, 49 kJ mol^{-1} for *Λ1* and 52 kJ mol^{-1} for *Δ1*) relative to the *Λ2* isomer. On the basis of these high energy differences between the four diastereomers and the assumption that the enthalpy of hydrolysis does not differ significantly for the four possible helical isomers, the *Λ2* isomer should be the only C_3-symmetric isomer present in solution.

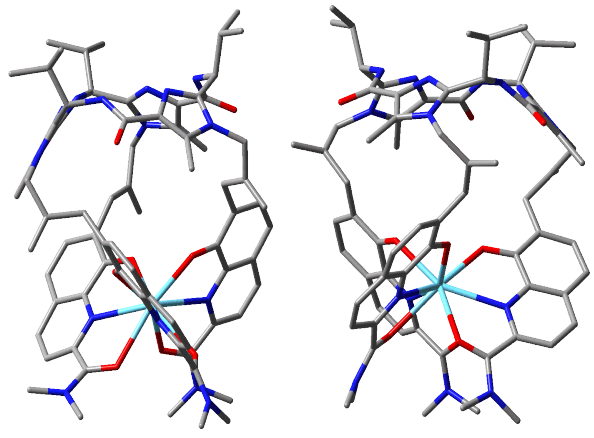

Figure 6: Molecular structures of the *Λ2* (left) and *Δ2* (right) isomers of complex **1b**·La calculated by using B3LYP/LANL2DZ. All hydrogen atoms were omitted for clarity.

As further evidence that the formation of the **1**·La complex is strictly diastereoselective the UV and CD spectra of the (*Λ2*)-**1b**·La complex were simulated on the basis of time-dependent density functional theory (TD-DFT) with the PBE1PBE functional and by employing the LANL2DZ basis set [37]. TD-DFT calculations were performed at the optimized ground-state geometry (B3LYP/LANL2DZ), calculating the energy, oscillator strength and rotatory strength for each of the 200 lowest singlet excitations. The CD spectrum was simulated by overlapping Gaussian functions for each transition where the width of the band at 1/*e* height was fixed at 0.4 eV and the resulting intensity of the combined spectrum was scaled to the experimental values (Figure 7).

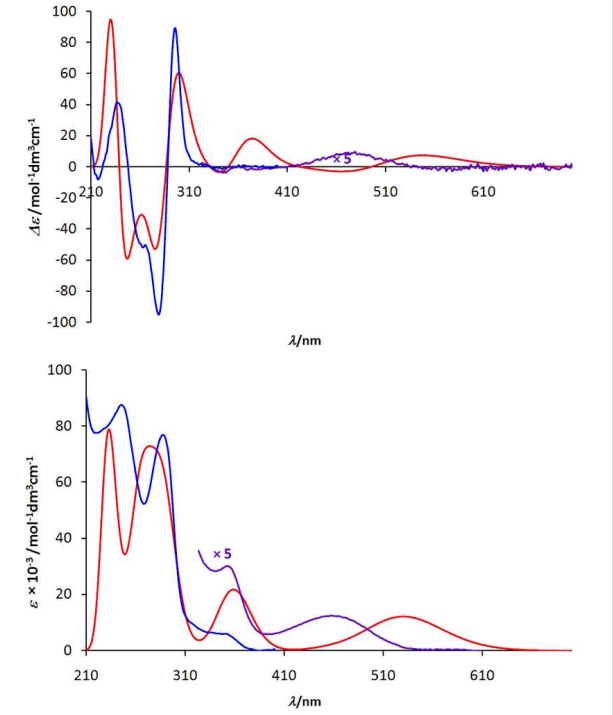

Figure 7: UV and CD spectra of the complex (*Λ*)-**1**·La. Blue and violet curve: experimentally determined spectra of (*Λ*)-**1**·La; red curve: calculated spectrum of the *Λ2* isomer of complex **1b**·La calculated at the TD-DFT-PBE1PBE/LANL2DZ level.

A comparison of the calculated spectrum with the experimentally determined one shows that the complex exhibits *Λ2* conformation in solution, too. The positive Cotton effect at 295 nm as well as the negative Cotton effect at 280 nm are found in both spectra. These effects derive from an exciton coupling [38] of the 8-hydroxyquinoline chromophore and therefore they can be used for the unambiguous determination of the helicity. Even the Cotton effects at around 350 nm are of the same sign in both spectra. However, the calculations overestimate the intensity of this excitation; this overestimation can also be found in the calculated UV spectrum. Moreover, in both spectra the excitations at higher wavelengths exhibit a positive Cotton effect. As the calculated maximum of the UV spectrum (530 nm) shows a bathochromic shift relative to the measured

UV spectrum (470 nm), the corresponding peak in the calculated CD spectrum (540 nm) is shifted to higher wavelengths relative to the experimentally measured one (480 nm).

Conclusion

We present the facile synthesis of a highly preorganized tripodal enterobactine-type ligand **1a**-H_3 consisting of the chiral C_3-symmetric backbone **2** and three tridentate 2-amido-8-hydroxyquinoline coordinating units. The ligand units can be easily attached to the backbone by an alkylation reaction followed by a triple Claisen rearrangement as described by Hiratani. In this way three new C–C bonds are formed in one reaction step and three isobutenylidene spacers are installed.

UV–vis and CD titrations show that ligand **1a**$^{3-}$ forms well defined 1:1 complexes only with lanthanide(III) ions, while smaller cations lead to an unspecific complex formation (probably oligomerization or polymerization). On the basis of ab initio calculations and CD spectroscopy we could show that the formed complex (**1a**)La exhibits exclusively *Λ* helicity.

We were able to isolate the corresponding lanthanum(III) complex as solid material and to characterize it by elemental analysis and positive ESI MS.

The coordination compounds [(**1a**)Ln] we describe should be prototypes for further lanthanide(III) complexes with an enterobactine analogue binding situation. In this context the strong complexation of lanthanide(III) ions is of interest, due to the special properties of those compounds as light emitting or magnetic materials [39].

Experimental

NMR spectra were recorded on a Varian Mercury 300 NMR spectrometer. FT-IR spectra were measured on a PerkinElmer Spektrum 100 spectrometer. Mass spectra were taken on a ThermoFisher Scientific LTQ-Orbitrap XL mass spectrometer. Elemental analyses were obtained with a Heraeus Elementar Vario EL analyser.

Synthesis and characterization of macrocyclic imidazole peptide **4**

To **2** (80 mg, 0.15 mmol) in acetonitrile (80 ml) were added anhydrous potassium carbonate (400 mg, 1.20 mmol) and **3** (200 mg, 0.62 mmol). The solution was heated and refluxed for 12 h. After cooling to room temperature the solution was stirred 12 h and afterwards concentrated to dryness. The residue was dissolved in ethyl acetate, washed with water and brine and dried with anhydrous magnesium sulfate. The solution was concentrated to dryness. The crude product was purified by column chromatography (silica gel; methylene chloride/ethyl acetate/methanol, 75:25:10; R_f = 0.37) to yield **4** as a brown solid.

Yield: 81 mg (41 %); mp 107–108 °C. ^{1}H NMR (300 MHz, $CDCl_3$): δ = 8.43 (d, *J* = 8.9 Hz, 3H), 8.13 (d, *J* = 8.9 Hz, 3H), 7.65 (d, *J* = 8.4 Hz, 3H), 7.38 (m, 6H), 7.06 (dd, *J* = 1.6/7.8 Hz, 3H), 5.29 (s, 3H), 5.04 (q, *J* = 4.6 Hz, 3H), 4.71 (m, 12H), 4.55 (s, 3H), 3.53 (q, *J* = 7.2 Hz, 6H), 3.42 (q, *J* = 7.2 Hz, 6H), 2.35 (s, 9H), 1.97 (m, 3H), 1.21 (t, *J* = 7.2 Hz, 9H), 1.17 (t, *J* = 7.2 Hz, 9H), 0.93 (d, *J* = 6.68 Hz, 9H), 0.89 (d, *J* = 6.68 Hz, 9H). IR (KBr): $\tilde{\nu}$ (cm^{-1}) = 3383 (m), 3062 (w), 2965 (m), 2933 (m), 2873 (m), 2360 (w), 1658 (vs), 1633 (vs), 1595 (s), 1462 (s), 1423 (s), 1377 (s), 1325 (m), 1254 (m), 1205 (m), 1112 (s), 990 (w), 922 (w), 846 (m), 763 (m), 633 (w). HRMS (ESI): calcd. for $C_{81}H_{99}N_{15}O_9$ $[M + Na]^+$: m/z = 1448.7642; found 1448.7639. HRMS (ESI): calcd. for $C_{81}H_{99}N_{15}O_9$ $[M + H]^+$: m/z = 1426.7823; found 1426.7808. HRMS (ESI): $[M + 2Na]^{++}$: m/z = 735.8739; found 735.8767.

Synthesis and characterization of macrocyclic imidazole peptide based tris(*N*,*N*-diethyl-8-hydroxyquinoline-2-carboxamide) **1a**-H_3

The ether **4** (0.18 g, 0.13 mmol) was placed in a Schlenk flask. The rearrangement proceeded at 165 °C under dry inert atmosphere of N_2. The dark brown residue was purified by a short silica column (EtOAc, R_f = 0.26) to furnish a bright brown solid.

Yield: 0.16 g (90 %); mp 189–196 °C. ^{1}H NMR (300 MHz, $CDCl_3$): δ = 8.40 (d, *J* = 8.7 Hz, 3H), 8.14 (d, *J* = 8.7 Hz, 3H), 8.07 (s, 3H), 7.57 (d, *J* = 8.4 Hz, 3H), 7.34 (m, 6H), 4.96 (q, *J* = 4.3 Hz, 3H), 4.91 (s, 3H), 4.33 (s, 6H), 4.24 (s, 3H), 3.56 (m, 12H), 3.33 (q, *J* = 7.0 Hz, 6H), 2.28 (s, 9H), 1.87 (m, 3H), 1.24 (t, *J* = 7.0 Hz, 9H), 1.17 (t, *J* = 7.0 Hz, 9H), 0.84 (d, *J* = 6.8 Hz, 9H), 0.81 (d, *J* = 6.8 Hz, 9H). IR (KBr): $\tilde{\nu}$ (cm^{-1}) = 3383 (m), 3083 (w), 2964 (m), 2927 (m), 2720 (w), 2283 (w), 2085 (w), 1732 (w), 1629 (vs), 1595 (vs), 1508 (vs), 1453 (vs), 1378 (m), 1321 (m), 1289 (w), 1253 (m), 1204 (s), 1139 (w), 1107 (s), 1021 (m), 992 (w), 909 (m), 848 (s), 809 (w), 774 (m), 723 (m), 662 (w). HRMS (ESI): calcd. for $C_{81}H_{99}N_{15}O_9$ $[M + Na]^+$: m/z = 1448.7619; found 1448.7637.

Synthesis and characterization of a mononuclear lanthanum(III) complex with cyclohexapeptide based tris(*N*,*N*-diethyl-8-hydroxyquinoline-2-carboxamide) [(**1a**)La]

$LaCl_3 \cdot 7\ H_2O$ (0.008g, 0.02 mmol, 1.0 equiv.) and K_2CO_3 (0.009 g, 0.06 mmol, 3.0 equiv.) in MeOH / H_2O (4 ml / 1 ml)

were added to ligand **2** (0.030 g, 0.02 mmol, 1.0 equiv.) in MeOH (10 ml). The mixture was stirred at RT for 4 days. The solution was concentrated under reduced pressure and the red coloured residue was washed with water.

Yield: 0.027 g (82%); mp 242–248 °C (dec.). Positive ESI MS (chloroform): m/z (%) = 1600.8 ($[C_{81}H_{96}N_{15}O_9LaK]^+$, 100), 1464.9 ($[C_{81}H_{99}N_{15}O_9K]^+$, 14). $C_{81}H_{96}N_{15}O_9La \cdot 5\ H_2O$: C 58.87, H 6.46, N 12.71; found: C 58.38, H 6.62, N 12.62.

To determine the thermodynamic parameters of the metal complexes all titration experiments were accomplished at room temperature by using a Jasco J-815 spectrophotometer connected to an automatic titration unit (Jasco ATS-443). For this purpose a methanolic solution containing ligand **1a**-H_3 (10^{-5} M) with NaOH (10^{-4} M) and a titrant solution containing the metal salt ([**1a**-H_3] = 10^{-5} M, $[M^{3+}] = 2 \times 10^{-4}$ M, [NaOH] = 10^{-4} M in MeOH) were prepared. The titrant solution was added in discrete steps to the solution containing ligand **1a**-H_3. After a mixing time of 2 min the spectra were recorded.

The virtual binding constants were evaluated according to Equation 1. It represents a simple association constant which involves all protonation/deprotonation and metal ion coordination steps.

$$K_{virt}^{LM} = \frac{[LM]}{\left([L]_{tot} - [LM]\right)\left([M]_{tot} - [LM]\right)} \qquad (1)$$

The virtual association constants of the complexation systems were calculated by non-linear-square fitting according to the Benesi–Hildebrand equation from the UV absorbtion data set. For a simple 1 : 1 binding model the calculations were carried out with the SigmaPlot program. Best results and lowest error could be observed at 279 nm in the case of lanthanum(III) and at 281 nm in the case of europium(III).

Acknowledgements

This work was supported by the DFG (SPP 1166) and the Fonds der Chemischen Industrie.

References

1. Raymond, K. N.; Tufano, T. P. Coordination chemistry of the siderophores and recent studies of synthetic analogues. In *The biological chemistry of iron;* Dunford, H. D.; Dolphin, D.; Raymond, K. N.; Sieker, L. D., Eds.; Reidel Publishing Co.: Dordrecht, Netherlands, 1981; pp 85–105.
2. Matzanke, B. F.; Müller-Matzanke, G.; Raymond, K. N. Siderophore-mediated iron transport. In *Iron carriers and iron proteins;* Loehr, T. M., Ed.; VCH: Weinheim, Germany, 1989; pp 1–121.
3. Steed, J. W.; Atwood, J. L. *Supramolecular Chemistry;* John Wiley & Sons: Chichester, 2000; pp 187–191.
4. Vögtle, F. *Supramolekulare Chemie;* Teubner: Stuttgart, 1992; pp 111–139.
5. Vögtle, F. *Supramolecular Chemistry;* John Wiley & Sons: Chichester, 1991; pp 84–106.
6. Isied, S. S.; Kuo, G.; Raymond, K. N. *J. Am. Chem. Soc.* **1976,** *98,* 1763–1767. doi:10.1021/ja00423a021
7. O'Brien, I. G.; Gibson, F. *Biochim. Biophys. Acta* **1970,** *215,* 393–402.
8. Pollack, J. R.; Neilands, J. B. *Biochem. Biophys. Res. Commun.* **1970,** *38,* 989–992. doi:10.1016/0006-291X(70)90819-3
9. Pintér, Á.; Haberhauer, G. *Chem.–Eur. J.* **2008,** *14,* 11061–11068. doi:10.1002/chem.200801552
10. Pluth, M. D.; Bergman, R. G.; Raymond, K. N. *J. Am. Chem. Soc.* **2007,** *129,* 11459–11467. doi:10.1021/ja072654e
11. Janser, I.; Albrecht, M.; Hunger, K.; Burk, S.; Rissanen, K. *Eur. J. Inorg. Chem.* **2006,** 244–251. doi:10.1002/ejic.200500711
12. Cai, W.; Kwok, S. W.; Taulane, J. P.; Goodman, M. *J. Am. Chem. Soc.* **2004,** *126,* 15030–15031. doi:10.1021/ja0442062
13. Albrecht, M.; Janser, I.; Runsink, J.; Raabe, G.; Weis, P.; Fröhlich, R. *Angew. Chem., Int. Ed.* **2004,** *43,* 6662–6666. doi:10.1002/anie.200453975
14. Meyer, M.; Kersting, B.; Powers, R. E.; Raymond, K. N. *Inorg. Chem.* **1997,** *36,* 5179–5191. doi:10.1021/ic970864u
15. Albrecht, M.; Fröhlich, R. *J. Am. Chem. Soc.* **1997,** *119,* 1656–1661. doi:10.1021/ja963265f
16. Kersting, B.; Meyer, M.; Powers, R. E.; Raymond, K. N. *J. Am. Chem. Soc.* **1996,** *118,* 7221–7222. doi:10.1021/ja9613522
17. Lofthagen, M.; Siegel, J. S.; Hackett, M. *Tetrahedron* **1995,** *51,* 6195–6208. doi:10.1016/0040-4020(95)00287-I
18. Tse, B.; Kishi, Y. *J. Org. Chem.* **1994,** *59,* 7807–7814. doi:10.1021/jo00104a043
19. Tse, B.; Kishi, Y. *J. Am. Chem. Soc.* **1993,** *115,* 7892–7893. doi:10.1021/ja00070a051
20. Coleman, A. W.; Lin, C. C.; Miocque, M. *Angew. Chem., Int. Ed. Engl.* **1992,** *31,* 1381–1383. doi:10.1002/anie.199213811
21. Tor, Y.; Libman, J.; Shanzer, A.; Felder, C. E.; Lifson, S. *J. Am. Chem. Soc.* **1992,** *114,* 6661–6671. doi:10.1021/ja00043a008
22. Tor, Y.; Libman, J.; Shanzer, A.; Lifson, S. *J. Am. Chem. Soc.* **1987,** *109,* 6517–6518. doi:10.1021/ja00255a050
23. Loomis, L. D.; Raymond, K. N. *Inorg. Chem.* **1991,** *30,* 906–911. doi:10.1021/ic00005a008
24. Stutte, P.; Kiggen, W.; Vögtle, F. *Tetrahedron* **1987,** *43,* 2065–2074. doi:10.1016/S0040-4020(01)86788-0
25. Haberhauer, G.; Rominger, F. *Tetrahedron Lett.* **2002,** *43,* 6335–6338. doi:10.1016/S0040-4039(02)01365-5
26. Ziegler, E.; Haberhauer, G. *Eur. J. Org. Chem.* **2009,** 3432–3438. doi:10.1002/ejoc.200900250
27. Pintér, Á.; Haberhauer, G. *Eur. J. Org. Chem.* **2008,** 2375–2387. doi:10.1002/ejoc.200701153
28. Haberhauer, G.; Oeser, T.; Rominger, F. *Chem. Commun.* **2005,** 2799–2801. doi:10.1039/b502158h
29. Hiratani, K.; Takahashi, T.; Kasuga, K.; Sugihara, H.; Fujiwara, K.; Ohashi, K. *Tetrahedron Lett.* **1995,** *36,* 5567–5570. doi:10.1016/0040-4039(95)01062-M
30. Hiratani, K.; Albrecht, M. *Chem. Soc. Rev.* **2008,** *37,* 2413–2421. doi:10.1039/b719548f
31. Haberhauer, G.; Oeser, T.; Rominger, F. *Chem.–Eur. J.* **2005,** 6718–6726. doi:10.1002/chem.200500224

32. Haberhauer, G.; Rominger, F. *Eur. J. Org. Chem.* **2003,** 3209–3218. doi:10.1002/ejoc.200300207
33. Albrecht, M.; Osetska, O.; Fröhlich, R. *Eur. J. Org. Chem.* **2007,** 4902–4908. doi:10.1002/ejoc.200700513
34. Albrecht, M.; Osetska, O.; Klankermayer, J.; Fröhlich, R.; Gumy, F.; Bünzli, J.-C. G. *Chem. Commun.* **2007,** 1834–1836. doi:10.1039/b618918k
35. Albrecht, M.; Osetska, O.; Fröhlich, R.; Bünzli, J.-C. G.; Aebischer, A.; Gumy, F.; Hamacek, J. *J. Am. Chem. Soc.* **2007,** *129,* 14178–14179. doi:10.1021/ja0768688
36. Burk, S.; Albrecht, M.; Hiratani, K. *J. Inclusion Phenom.* **2008,** *61,* 353–359. doi:10.1007/s10847-008-9429-1 (See for example.)
37. *Gaussian 03,* Revision C.02; Gaussian, Inc.: Wallingford CT, 2004. (All computations were performed with the Gaussian 03 program-package.)
38. Lightner, A. D.; Gurst, J. E. *Organic Conformational Analysis and Stereochemistry from Circular Dichroism Spectroscopy;* John Wiley & Sons: New York, 2000.
39. Binnemans, K. *Chem. Rev.* **2009,** *109,* 4283–4374. doi:10.1021/cr8003983 (See for example.)

License and Terms

Beilstein Journal of Organic Chemistry

Control of stilbene conformation and fluorescence in self-assembled capsules

Mark R. Ams[1], Dariush Ajami[1], Stephen L. Craig[2], Jye-Shane Yang[3] and Julius Rebek Jr[*1]

Full Research Paper

Open Access

Address:
[1]The Skaggs Institute for Chemical Biology and Department of Chemistry, The Scripps Research Institute, 10550 North Torrey Pines Road, La Jolla, CA 92037, U.S., Tel: 858 784 2250; Fax: 858 784 2876, [2]Department of Chemistry, Duke University, Durham, NC, 27708-0346, U.S. and [3]Department of Chemistry, National Taiwan University, No. 1. Sec. 4, Roosevelt Road, Taipei, 10617, Taiwan

Email:
Julius Rebek Jr[*] - jrebek@scripps.edu

* Corresponding author

Keywords:
molecular twisting; quenching; reversible encapsulation; self-assembly; stilbene fluorescence

Beilstein Journal of Organic Chemistry **2009,** *5,* No. 79.
doi:10.3762/bjoc.5.79

Received: 09 October 2009
Accepted: 24 November 2009
Published: 11 December 2009

Guest Editor: C. A. Schalley

Abstract

The extensively studied *trans*-stilbene molecule is known to give only weak fluorescence in solution and inside loosely-fitting synthetic capsules. However, *trans*-stilbene has been recently studied in the context of antibody interiors, where binding results in strong blue fluorescence. The present research was undertaken to understand the spatial factors that influence stilbene fluorescence. *trans*-Stilbene was encapsulated in the snug, self-assembled complex **1.1** and exhibited fluorescence quenching due to the distortion of its ground-state geometry. When the complex is elongated by incorporating glycouril spacers, *trans*-stilbene is allowed to adapt a fully coplanar arrangement and fluorescence returns.

Introduction

The fluorescence of *trans*-stilbene has been extensively researched [1], and weak fluorescence occurs in aqueous solutions or typical organic solvents. In a highly structured environment such as an antibody interior [2-4], recent studies show that nearby tryptophans can transfer electrons to the stilbene excited state and an intense blue fluorescence develops. Inside the tight-fitting capsule **1.1** [5,6] (Figure 1) where it is surrounded by 16 aromatic panels, *trans*-stilbene's fluorescence is reduced to only 2% of what is observed in bulk solution. In contrast, normal fluorescence is observed in a loose-fitting capsule [7] although the photostationary *trans*-/*cis*-isomerization equilibria are altered in the limited space [8]. Isomerization of *trans*- to *cis*-stilbene is not possible in **1.1** but little else is known about the photophysics of guests in this capsule. This research was undertaken to understand what controls the behavior of stilbenes in this and related constrained environments.

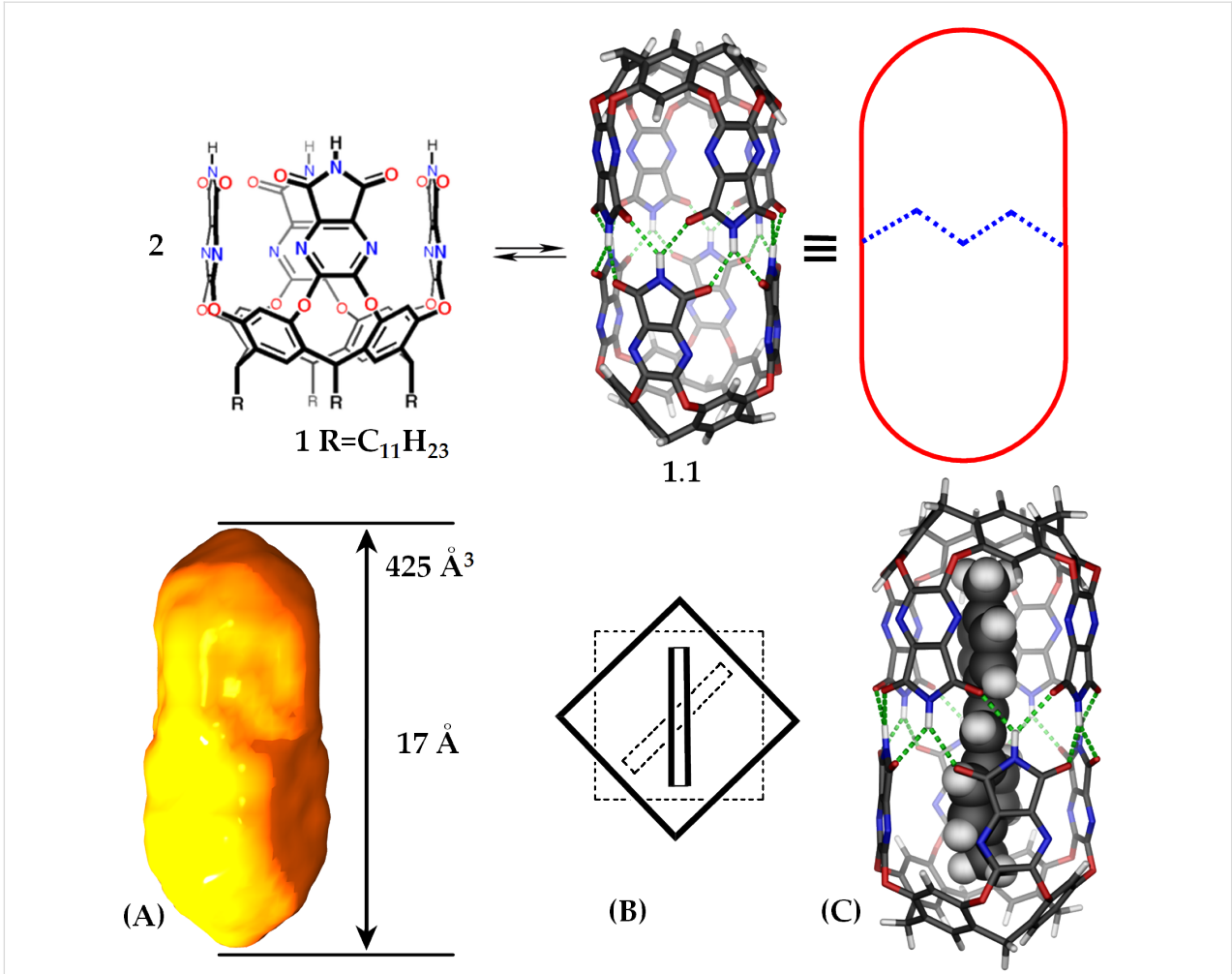

Figure 1: (Top) Tetraimide cavitand **1**, the dimeric capsule **1.1** and its cartoon representation. (Bottom) The shape of the space inside (A), a schematic view along the central axis with two aromatic guests (B) and an energy-minimized (AM1) complex of stilbene in **1.1** (C).

Results and Discussion

The space inside capsule **1.1** is defined by two pyramids comprising resorcinarenes at the ends and square prisms of the heterocyclic walls near the middle. The quenching of stilbene fluorescence may be an effect of the fixed aromatics of the resorcinarene or the heterocyclic walls, but we surmised that there was a subtler cause. As seen in the skeletal model **1.1** of the space within depicted in Figure 1A, the square prisms are twisted by about 45° along their long axes. A typical aromatic guest such as benzene fits best when it is nestled diagonally in a prism's space. Accordingly, the aromatic rings of longer molecules such as biphenyls and stilbenes cannot be coplanar in their lowest energy conformations inside **1.1.** Rather, they must be twisted by 45° or so along their rotatable internal bonds.

Among guests of **1.1**, 4,4′-dimethylstilbene (**2**) provides an excellent fit; it fills about 53% of the capsule's space and the methyl groups of the guest can access the tapered ends of the host. The homologue, 4-ethyl-4′-methylstilbene (**3**), is also encapsulated (see Supporting Information File 1 for NMR spectrum), but the slightly longer 4,4′-diethyl derivative **4** simply does not fit. Figure 2 illustrates the effect of encapsulation on **3** (assembly **6**). The fluorescence is 96% quenched when λ_{exc} = 318 nm. For comparison, the emission of the permanently twisted, *o*-substituted stilbene **5** (λ_{exc} = 300 nm) is also shown [9].

Can the fluorescence of the encapsulated stilbene be restored? When suitable guests are present, addition of glycolurils such as **7** to solutions of **1.1** generates extended capsule **1.7$_4$.1** (Figure 3) [10]. The glycolurils are arranged in a chiral manner, in either cycloenantiomer of the extended capsule. The glycolurils force the two square prisms of **1.7$_4$.1** into registry (Figure 3A). That is, the square prisms are now aligned and stilbene as well as related guests may be found either in the fully coplanar arrangement favored by extended resonance stabiliza-

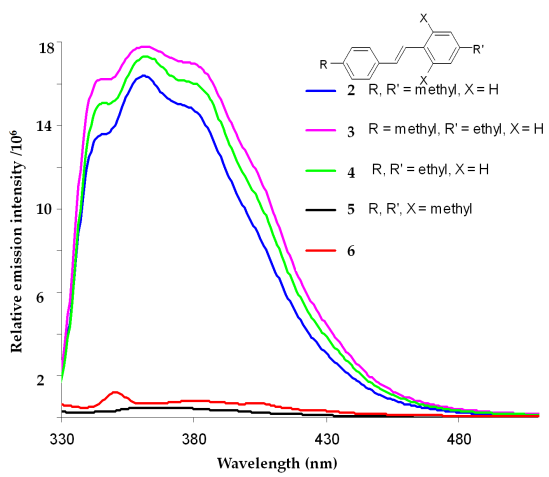

Figure 2: Room temperature fluorescence spectra at λ_{exc} = 318 nm for 10 μM mesitylene solutions of 4,4′-dimethylstilbene (**2**); 4-ethyl-4′-methylstilbene (**3**); 4,4′-diethylstilbene (**4**); 2,4,4′,6-tetramethylstilbene (**5**) and assembly **6** (λ_{exc} = 300 nm).

tion (Figure 3B) or at another minimum with a 90° dihedral angle between their aromatic rings. 4-Ethyl-4′-methylstilbene (**3**) is a guest for **1.7$_4$.1** when CD_2Cl_2 is a co-guest (see Supporting Information File 1 for NMR spectrum). In the fluorescence experiments at λ_{exc} = 318 nm, the fluorescence of 4-ethyl-4′-methylstilbene **3** and assembly **8** is restored, as shown in Figure 4. As a control experiment to test for the possibility of any fluorescence contribution from assembly **1.7$_4$.1**, the fluorescence of the complex of **1.7$_4$.1** with alkyl chain $C_{17}H_{36}$ was also investigated. No additional fluorescence was observed when $C_{17}H_{36}$ was a guest (see Supporting Information File 1 for fluorescence and NMR spectra).

Earlier we showed that it is possible to reversibly interconvert capsules **1.1** and **1.7$_4$.1**. The weakly basic glycoluril spacer is protonated by addition of gaseous HCl and precipitates in typical organic solutions. The remaining components reassemble to the original capsule **1.1** [11]. Subsequent addition of NEt_3 releases the glycoluril into solution and restores the extended capsule **1.7$_4$.1**. This was shown previously to be a fully rever-

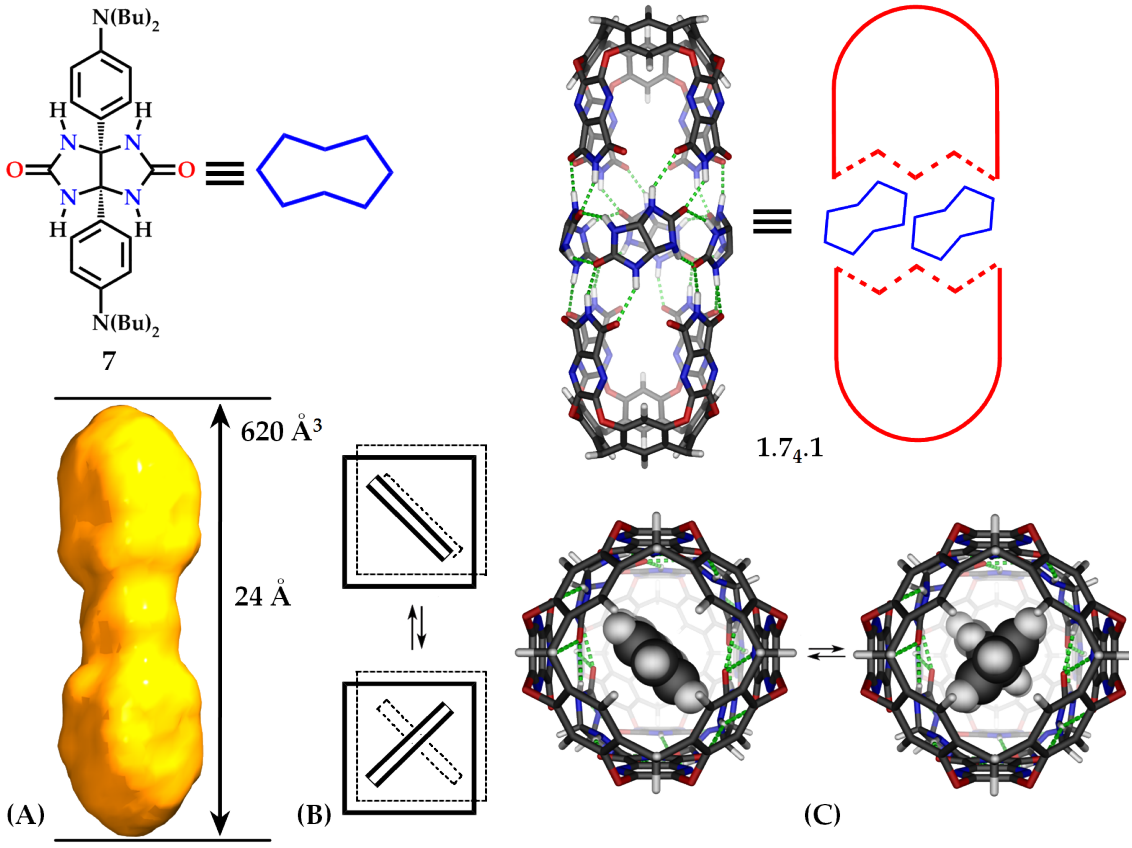

Figure 3: (Top) Glycouril **7**, the extended capsule **1.7$_4$.1**, (only one enantiomeric arrangement is shown) and its cartoon representation. The shape of the space inside (A) a schematic view along the central axis with two aromatic guests (B) and an end-on view of an energy-minimized complex of stilbene inside (C).

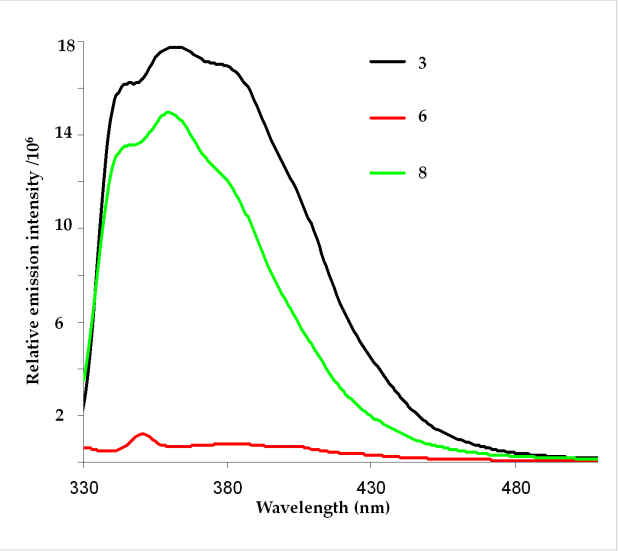

Figure 4: Room temperature emission spectra for 10 μM solutions of 4-ethyl-4′-ethylstilbene (**3**) in the capsule **1.1** (**6**) and **1.7$_4$.1** (**8**). λ_{exc} = 318 nm.

sible process with long chain alkane guests. We are currently pursuing this application with stilbenes and studying the exchange of subunits in the process [12,13].

Many fluorescent sensors have been reported in the literature [14-17], however they usually respond to chemical changes rather than purely geometrical ones. Here, self-assembly of an external host system is responsible for turning on and off stilbene fluorescence through geometrical control of the stilbene's surroundings.

Supporting Information

Supporting Information File 1

Control of stilbene conformation and fluorescence in self-assembled capsules.
[http://www.beilstein-journals.org/bjoc/content/supplementary/1860-5397-5-79-S1.pdf]

Acknowledgements

We are grateful to the National Institutes of Health and the Skaggs Institute for support. The authors would also like to recognize the help of Prof. David P. Millar and Dr. Goran Plevaljčić.

References

1. Waldeck, D. H. *Chem. Rev.* **1991,** *91,* 415–436. doi:10.1021/cr00003a007
2. Debler, E. W.; Kaufmann, F. G.; Meijler, M. M.; Heine, A.; Mee, J. M.; Plevaljčić, G.; Di Bilio, A. J.; Schultz, P. G.; Millar, D. P.; Janda, K. D.; Wilson, I. A.; Gray, H. B.; Lerner, R. A. *Science* **2008,** *319,* 1232–1235. doi:10.1126/science.1153445
3. Armitage, B. A.; Berget, P. B. *Science* **2008,** *319,* 1195–1196. doi:10.1126/science.1155093
4. Matsushita, M.; Meijler, M. M.; Wirsching, P.; Lerner, R. A.; Janda, K. D. *Org. Lett.* **2005,** *7,* 4943–4946. doi:10.1021/ol051919w
5. Heinz, T.; Rudkevich, D. M.; Rebek, J., Jr. *Angew. Chem., Int. Ed.* **1999,** *38,* 1136–1139. doi:10.1002/(SICI)1521-3773(19990419)38:8<1136::AID-ANIE1136>3.0.CO;2-I
6. Heinz, T.; Rudkevich, D. M.; Rebek, J., Jr. *Nature* **1998,** *394,* 764–766. doi:10.1038/29501
7. Natarajan, A.; Kaanumalle, L. S.; Jockusch, S.; Gibb, C. L. D.; Gibb, B. C.; Turro, N. J.; Ramamurthy, V. *J. Am. Chem. Soc.* **2007,** *129,* 4132–4133. doi:10.1021/ja070086x
8. Parthasarathy, A.; Kaanumalle, L. S.; Ramamurthy, V. *Org. Lett.* **2007,** *9,* 5059–5062. doi:10.1021/ol702322u
9. Gegiou, D.; Muszkat, K. A.; Fischer, E. *J. Am. Chem. Soc.* **1968,** *90,* 3907–3918. doi:10.1021/ja01017a002
10. Ajami, D.; Rebek, J., Jr. *J. Am. Chem. Soc.* **2006,** *128,* 5314–5315. doi:10.1021/ja060095q
11. Ajami, D.; Rebek, J., Jr. *J. Am. Chem. Soc.* **2006,** *128,* 15038–15039. doi:10.1021/ja064233n
12. Barrett, E. S.; Dale, T. J.; Rebek, J., Jr. *J. Am. Chem. Soc.* **2007,** *129,* 8818–8824. doi:10.1021/ja071774j
13. Castellano, R. K.; Craig, S. L.; Nuckolls, C.; Rebek, J., Jr. *J. Am. Chem. Soc.* **2000,** *122,* 7876–7882. doi:10.1021/ja994397m
14. Thomas, S. W., III; Joly, G. D.; Swager, T. M. *Chem. Rev.* **2007,** *107,* 1339–1386. doi:10.1021/cr0501339
15. Suksai, C.; Tuntulani, T. *Top. Curr. Chem.* **2005,** *255,* 163–198. doi:10.1007/b101166
16. Martínez-Máñez, R.; Sancenón, F. *Chem. Rev.* **2003,** *103,* 4419–4476. doi:10.1021/cr010421e
17. McQuade, D. T.; Pullen, A. E.; Swager, T. M. *Chem. Rev.* **2000,** *100,* 2537–2574. doi:10.1021/cr9801014

License and Terms

Beilstein Journal of Organic Chemistry

Self-association of an indole based guanidinium-carboxylate-zwitterion: formation of stable dimers in solution and the solid state

Carolin Rether[1], Wilhelm Sicking[1], Roland Boese[2] and Carsten Schmuck*[1]

Full Research Paper

Open Access

Address:
[1]Institute of Organic Chemistry, Faculty of Chemistry, University of Duisburg-Essen, Universitätsstraße 7, 45141 Essen, Germany and [2]Institute of Inorganic Chemistry, Faculty of Chemistry, University of Duisburg-Essen, Universitätsstraße 7, 45141 Essen, Germany

Email:
Carsten Schmuck* - carsten.schmuck@uni-due.de

* Corresponding author

Keywords:
dimerisation; molecular recognition; self-assembly; supramolecular chemistry; zwitterions

Beilstein Journal of Organic Chemistry **2010,** *6,* No. 3.
doi:10.3762/bjoc.6.3

Received: 28 October 2009
Accepted: 04 January 2010
Published: 14 January 2010

Guest Editor: C. A. Schalley

Abstract

The indole based zwitterion **2** forms stable dimers held together by H-bond assisted ion pairs. Dimerisation was confirmed in the solid state and studied in solution using dilution NMR experiments. Even though zwitterion **2** forms very stable dimers even in DMSO, their stability is lower than of an analogous pyrrole based zwitterion **1**. As revealed by the X-ray crystal structure the two binding sites in **2** cannot be planar due to steric interactions between the guanidinium group and a neighbouring aromatic CH. Hence the guanidinium moiety is twisted out of planarity from the rest of the molecule forcing the two monomers in dimer **2**·**2** to interact in a non-ideal orientation. Furthermore, the acidity of the NHs is lower than in **1** (as determined by UV-pH-titration) also leading to less efficient binding interactions.

Introduction

The vast majority of supramolecular self-assembling systems known so far form stable assemblies only in non polar solvents such as chloroform, as they mainly rely on hydrogen bonds [1-4]. The design of self-complementary molecules that assemble even in polar solvents is still a challenging task despite all the progress made in this field in recent years. The use of metal-ligand coordination and hydrophobic interactions has proven especially useful in this context [5-11]. We are interested in developing self-complementary zwitterions that from stable aggregates in polar solution based on H-bond assisted ion pair formation. A few years ago we introduced the guanidinio-carbonyl pyrrole carboxylate zwitterion **1** which forms extremely stable dimers not only in the solid state but also in polar solution [12]. In DMSO the stability is too large to evaluate with an estimated association constant of $K_{ass} > 10^{10}$ M^{-1}. Even in water dimerisation still takes place (K_{ass} = 170 M^{-1}) [13]. The

stability of the dimer **1**·**1** is significantly larger than the simple Coulomb-interactions of point charges, suggesting that indeed the formation of directed, H-bond assisted salt-bridges is crucial. Zwitterion **1** combines in a near perfect fit geometrical self-complementarity with the possibility to form two salt-bridges assisted by a network of six H-bonds. The superior stability of **1**·**1** compared to analogous zwitterions based on other aromatic scaffolds such as benzene or furan instead of pyrrole or with an amidinium cation instead of a guanidinium cation was also confirmed by DFT calculations [14]. Zwitterion **1** has thus found widespread application in the formation of self-assembled nanostructures such as vesicles or supramolecular polymers [15-17].

We have now synthesized and studied the indole based zwitterion **2**, a close analogue of **1**. In **2** the guanidinium group is not acylated as in **1** but conjugated to an aromatic ring. Compared to the parent guanidinium cation, in both cases the acidity of the NHs is significantly increased due to the −M effect of the carbonyl group or the aromatic ring, respectively, thus facilitating the formation of H-bond assisted ion pairs [18, 19]. Apart from the increased acidity of the NHs in **1** and **2**, also the geometric shape of **2** is very similar to **1** at least based on the inspection of simple models. It was therefore expected that the new zwitterion **2** might form dimers with similar stability to **1**, increasing our repertoire of self-complementary binding motifs that efficiently self-assemble in polar solution. And indeed we could show that zwitterion **2** is able to form highly stable dimers in polar solution and in the solid state as well. However, dimer **2**·**2** is significantly less stable than dimer **1**·**1**. Possible reasons for this decreased stability are discussed.

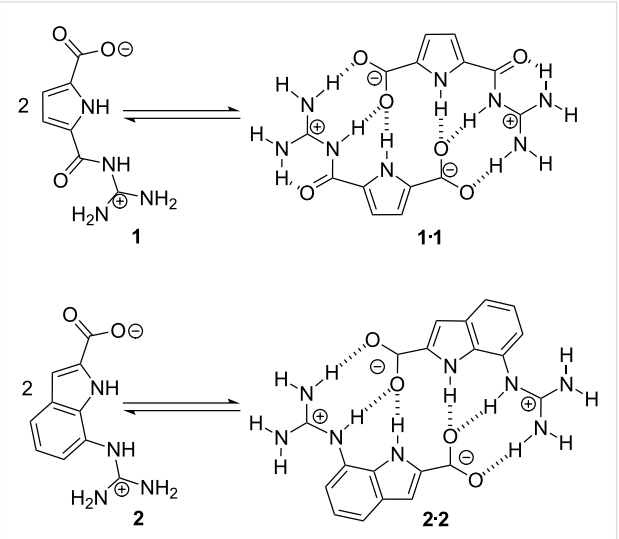

Figure 1: Self-assembly of zwitterion **1** to give dimer **1**·**1** and self-assembly of zwitterion **2** to give dimer **2**·**2** – both using the same intermolecular interactions: a pattern of six H-bonds and two salt bridges.

Results and Discussion

The indole zwitterion **2** was prepared by a four-step synthesis (Scheme 1). Commercially available 7-nitro-1*H*-indole-2-carboxylate **3** was reduced by reaction with hydrogen in the presence of Pd/C to provide the amine **4** in a yield of 98%. For the next stept, first, thiourea was *N*-Boc-protected at both amino-functions following a literature procedure [20]. Thiourea was deprotonated with sodium hydride and afterwards reacted with di-*tert*-butyl dicarbonate to give the di-Boc-protected thiourea **5** in 79% yield. The di-Boc-protected thiourea **5** was then reacted with the amine **4** in the presence of Mukaiyama's reagent [21] and triethylamine as a base, which provided **6** in a yield of 71% [22]. Deprotection of the two Boc-groups was achieved by treatment with TFA and the guanidinium salt **7** was obtained quantitatively. In the last reaction step the ethyl ester in **7** was hydrolysed with lithium hydroxide in a THF/water mixture (THF/water = 4/1). Zwitterion **2** was then obtained after adjustment of the pH to 6 with 1M HCl in a yield of 84% as a light brown crystalline solid.

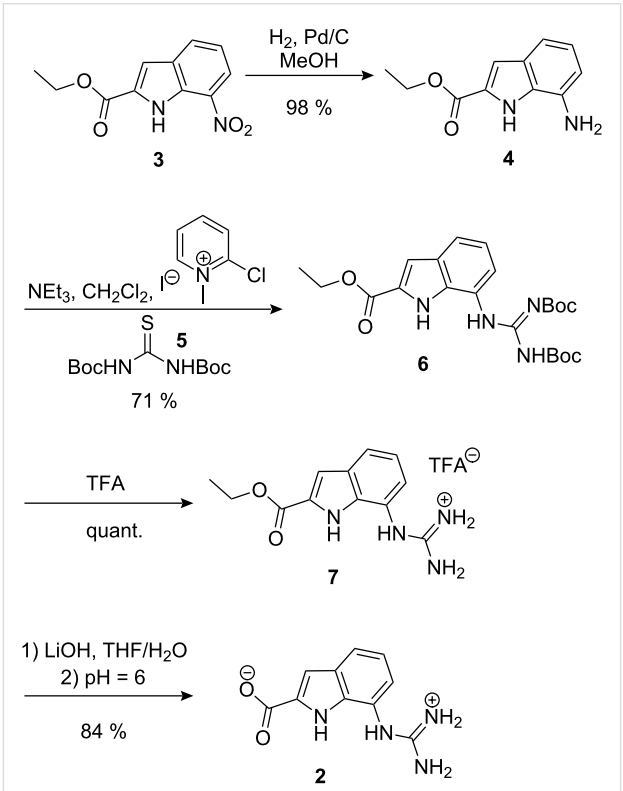

Scheme 1: Synthesis of zwitterion **2**.

For the spectroscopic characterisation and as a reference compound also the picrate salt of **2** was prepared by treating a methanolic solution of **2** with picric acid (Scheme 2). The picrate salt **2**·$\mathbf{H}^+$ was isolated in form of a yellow, crystalline solid in 89% yield.

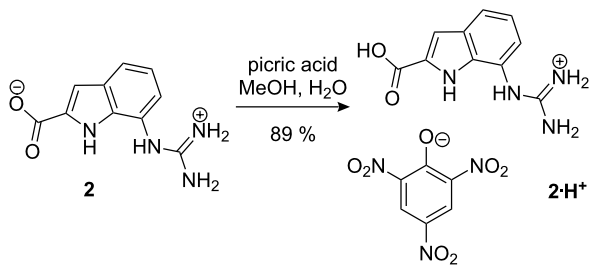

Scheme 2: Synthesis of compound **2**·$\mathbf{H}^+$.

While the picrate salt **2**·$\mathbf{H}^+$ is moderately soluble in methanol and water, the zwitterionic form of **2** is virtually insoluble in all solvents except DMSO and DMSO-containing solvent mixtures, such as DMSO–MeOH or DMSO–$CHCl_3$, so that the dimerisation studies in solution were limited to DMSO. The ^{1}H NMR spectrum (Figure 2) of the protonated zwitterion **2**·$\mathbf{H}^+$ (picrate salt in [D_6]DMSO) shows the signals expected for an aromatic guanidinium cation [23]. The four guanidinium NH_2 protons have a chemical shift of δ = 7.19, whereas the NH of the guanidinium group shows up at δ = 9.21 and the indole NH at δ = 12.06. The signals were assigned based on 2D NMR experiments.

The ^{1}H NMR spectrum of zwitterion **2** is significantly different. Especially the NH signals are shifted downfield. The indole NH is shifted downfield by 0.2 ppm and appears at δ = 12.26 and the four guanidinium NH_2 are shifted to δ = 8.00 ppm. Most significantly the NH of the guanidinium group is shifted downfield by nearly 4 ppm from δ = 9.21 to δ = 13.07 pm. A similar dramatic downfield shift was observed for the guanidinium amide NH of zwitterion **1** upon dimer formation [12,13].

Hence, the downfield shifts in the spectrum of zwitterion **2** relative to the protonated form **2**·$\mathbf{H}^+$ are most likely also due to the formation of a H-bonded ion pair which can only take place intermolecularly due to the rigidity of **2**. The similarity of the shift changes with those of zwitterion **1** suggests that dimerisation takes place.

The stability of these dimers was determined by an NMR dilution experiment. To obtain the binding constant for the dimerisation, we studied the concentration dependence of the ^{1}H NMR spectrum of **2** in a concentration range from 0.25 to 100 mM in [D_6]DMSO. The ^{1}H NMR shifts are concentration-dependent as expected for a dimerisation (Figure 3).

As the binding isotherms show (Figure 4), even at concentrations > 10 mM dimerisation is mostly complete. This suggests very large stability of the dimers even in DMSO. In agreement with this, a quantitative data analysis provided a dimerisation constant $K_{ass} > 10^5$ M^{-1}, too large to be measured accurately by NMR techniques. Similar observations were made earlier for zwitterion **1**. However, for **1** the estimated stability in DMSO was even higher. Interestingly, at higher concentrations the formation of larger aggregates also seems to occur. For example, the signal for the guanidinium NH_2 protons shows a second shift change at concentrations > 20 mM. First, the signal is shifted to lower field due to the dimerisation, and then a smaller upfield shift is observed (Figure 5). This could be indicative of a second association process in which the dimers **2**·**2** start to interact at concentration > ca. 15 mM. However, the exact nature of these larger aggregates is unclear at the moment.

We were able to determine the solid state structure of **2**. X-ray quality crystals of compound **2** were obtained by slow evapora-

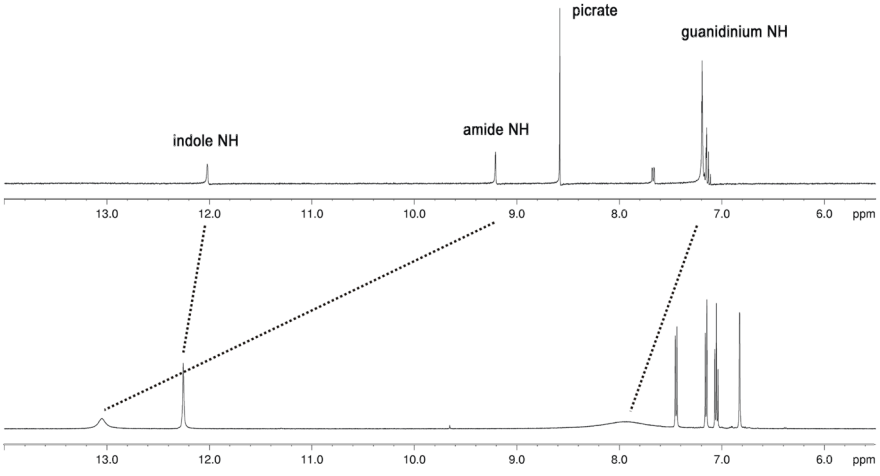

Figure 2: ^{1}H NMR spectra of zwitterion **2** (bottom) and its protonated form **2**·$\mathbf{H}^+$ (top).

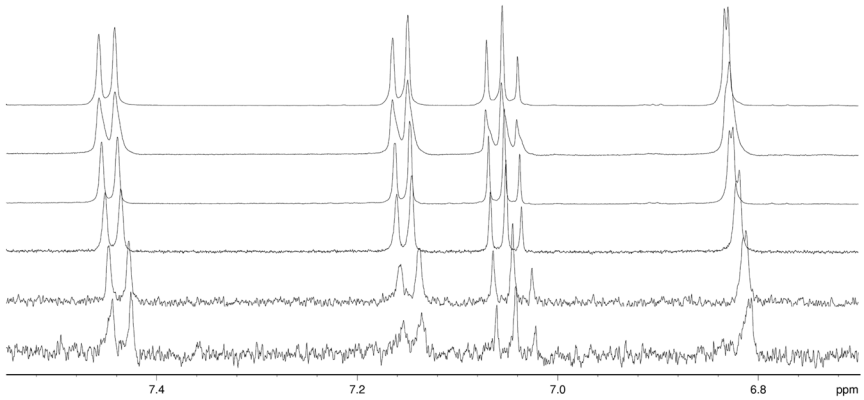

Figure 3: Part of the ^{1}H NMR spectrum of **2** in [D_6]DMSO showing the complexation-induced shifts of the indole CH protons (concentration from bottom to top: 0.4, 1, 6, 12, 25 and 50 mM).

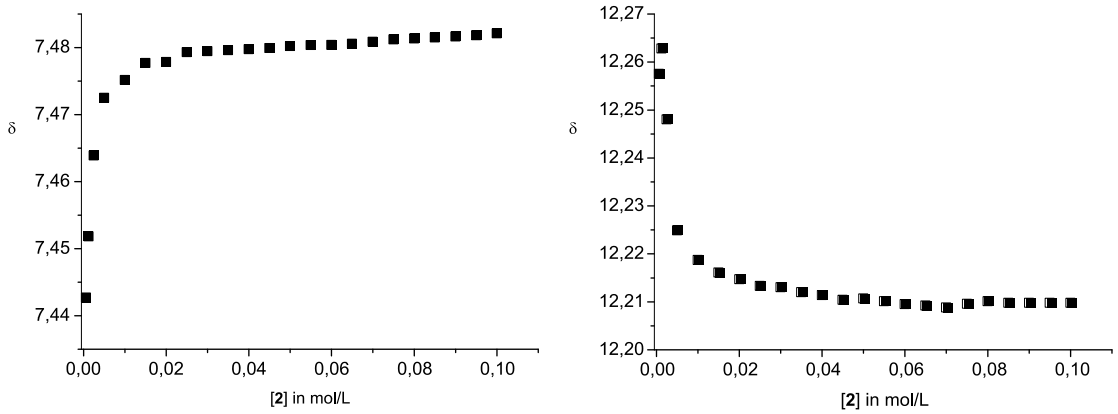

Figure 4: Representative binding isotherm of the aromatic proton d (left) and the indole NH proton (right).

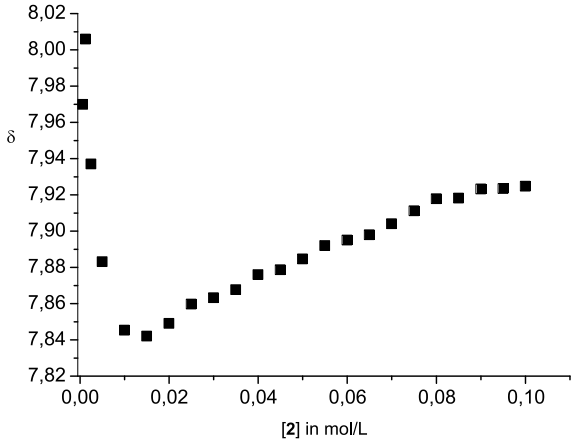

Figure 5: Binding isotherm of the guanidinium NH_2 protons.

tion of a dimethyl sulfoxide solution. X-ray crystallography confirmed the formation of head-to-tail dimers, which are held together by the formation of two salt bridges assisted by a network of six hydrogen bonds (Figure 6). The hydrogen bond distances between the aromatic N···O (2.703 Å), the guanidinium N···O (2.942 Å) and the indole N···O (2.935 Å) are all rather short.

However, the distances are larger than the corresponding distances in dimer **1**·**1**: the amide N···O (2.679 Å), the guanidinium N···O (2.854 Å), and the pyrrole N···O (2.731 Å) distances in dimer **1**·**1** are even shorter than in dimer **2**·**2**. The main difference between **1**·**1** and **2**·**2** is however that the dimers **2**·**2** are not completely planar. Zwitterion **2** itself is not planar, but the guanidinium group is twisted out of planarity by 48.75° (Figure 7). Also the two molecules within the dimer are not within the same plane but slightly offset (by 1.050 pm). This is a consequence of the twisted guanidinium group. To allow

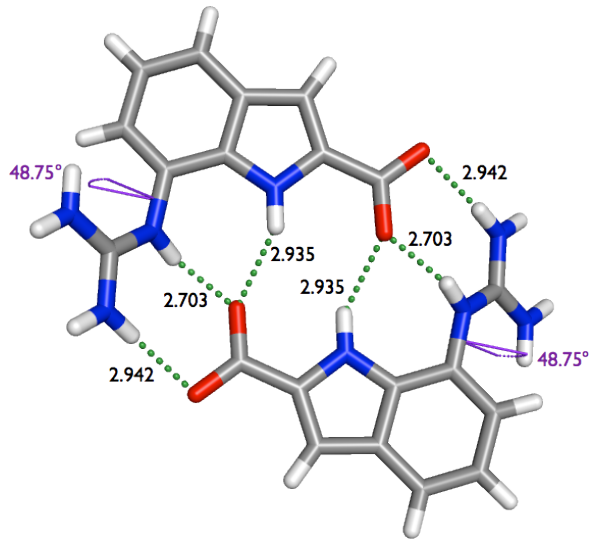

Figure 6: Crystal structure of dimer **2**·**2** with hydrogen bond distances (Å) and dihedral angles.

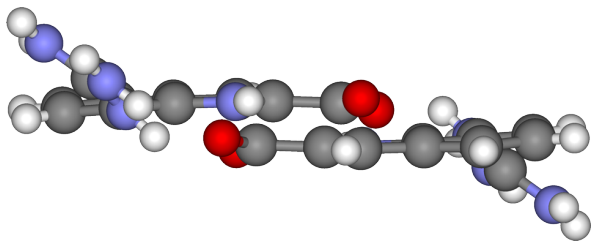

Figure 7: Side view of dimer **2**·**2** in the solid state.

optimal interaction of the carboxylate with the NHs of the guanidinium group the second molecule has to be a little bit out of plane of the first, which results in longer hydrogen bond distances for the guanidinium N···O and the indole N···O (Figure 7) and less favorable H-bond angles within the dimer (164.78° for the outer and 148.97° for the inner guanidinium NH-bonds and 141.37° for the indole NH-bond).

Within the crystal lattice the molecules of **2** are arranged in parallel planes held together most likely by aromatic stacking interactions: The centroid-centroid distance of two indoles is 3.636 Å. Furthermore, the "backside" of the out of plane twisted guanidinium cation also interacts with the carboxylate group one plane below (Figure 8). The corresponding hydrogen bond distances are 2.790 Å and 2.922 Å, respectively, and are therefore similar to the hydrogen bond distances within the dimer.

The main difference between the pyrrole zwitterion **1** and the indole zwitterion **2** is hence the non-planar, twisted structure of

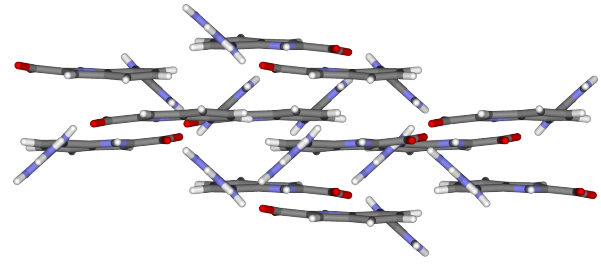

Figure 8: Part of the crystal lattice of zwitterion **2**.

the latter. This is most likely due to steric interactions with the neighboring aromatic C-H bond (Scheme 3). In the pyrrole zwitterion **1** this position is occupied by the carbonyl oxygen which forms an H-bond to the guanidinium moiety and thus actually helps to keep the molecule planar. This amide group in **1** is replaced by the aromatic benzene ring in **2**, thereby replacing an attractive H-bond with a repulsive steric interaction.

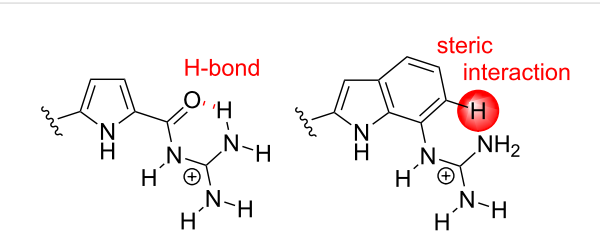

Scheme 3: An attractive H-bond in **1** (left) is replaced by a repulsive steric interaction in **2** (right).

This twisted, non-planar structure of dimer **2**·**2** is also reproduced by DFT calculations. Geometry optimizations were performed with the Gaussian03 program package using the M05-2X/6-311+G** basis set [24]. In all calculations DMSO as a solvent was included (CPCM, ε = 48) [25,26]. The optimization revealed the twisted dimer, which fits quite well to the X-ray structure. Though the calculated structure of dimer **2**·**2** is not completely symmetric like the X-ray structure, all the hydrogen bond distances, as well as the torsion angle match pretty well (Figure 9). In the solid state structure, the hydrogen bond distances between the aromatic N···O (2.703 Å), the guanidinium N···O (2.942 Å) and the indole N···O (2.935 Å) are quite short, as mentioned above. The torsion angle between the aromatic scaffold and the guanidinium group is 48.75°. The DFT calculation give an average dihedral angle of 53.57° and lead to the following averaged hydrogen bond distances: 2.738 Å (aromatic N···O), 2.931 Å (guanidinium N···O) and 2.850 (indole N···O).

Hence, the good agreement of the observed structure in the solid state and the calculated structure obtained from DFT

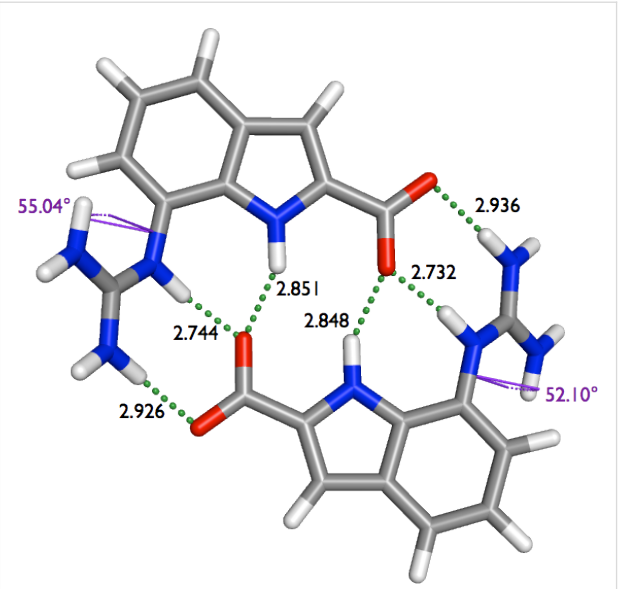

Figure 9: Energy-minimized structure for dimer **2**·**2** with hydrogen bond distances (Å) and dihedral angles.

calculations suggests that the level of theory used in these calculations describes the dimer with sufficient accuracy. We therefore also calculated the enthalpy values for the dimerisation process of zwitterion **2** and of **1**, respectively, as the experimental values were too large to measure them accurately in DMSO (as mentioned above). The calculated stability of dimer **2**·**2** is significantly lower than for the pyrrole zwitterion **1**: ΔH −54 kJ/mol and −85 kJ/mol, respectively. Hence, even though the bonding interactions in dimer **1**·**1** and **2**·**2** are temptingly similar the latter is only two third as stable as the former.

This difference in stability is most likely due to the non-ideal geometry of the H-bonded ion pairs and reflects the importance of planarity in zwitterion **1** for an effective dimerisation. Due to the twisted guanidinium groups in **2** the two monomers in dimer **2**·**2** are not in-plane, which leads to less efficient interactions. Also as mentioned above, the guanidinium group in zwitterion **2** is directly attached to the aromatic indole scaffold, whereas it is acylated in **1**. Though the overall structure looks similar, this replaces an attractive H-bond which also help to planarize zwitterion **1** by a repulsive steric interaction in **2**, which is responsible for its non-planar structure.

Furthermore, the pK_a value of the two guanidinium groups as well is an important factor for the stability of the dimers. While simple guanidinium cations as in arginine have a pK_a of 13.5, the pK_a of the acylguanidinium group in **1** was measured by UV-pH-titration to be 6.3 ± 0.1. Analysis of the pH dependent UV spectral changes was performed using the Specfit/32 software program from Spectrum Software Associates. However, the pK_a of the guanidinium group in **2** also obtained from a UV-pH-titration is significantly larger with pK_a = 10.6 ± 0.1. Hence, the lower acidity of the NHs in **2** is a second important factor leading to the overall reduced stability of dimer **2**·**2**.

Conclusion

In conclusion, we have presented the synthesis of a new indole based zwitterion **2**, a close analogue of the 5-(guanidiniocarbonyl)-1*H*-pyrrole-2-carboxylate (**1**) which we recently introduced as one of the most stable self-complementary simple molecules known so far. Both dimers rely on the same intermolecular interactions, two salt-bridges assisted by a very similar network of six H-bonds. We could show here that zwitterion **2** also self-assembles into stable dimers in the solid state and also solution (K_{ass} > 10^5 M^{-1} in DMSO). However, DFT calculations suggest that the dimers are significantly less stable than dimer **1**·**1** despite the overall similarity of the binding interactions. The calculated dimerisation enthalpy for dimer **2**·**2** is only 66% of that for dimer **1**·**1**. This is most likely due to two reasons. As the solid state structure shows, the two binding sites in **2**·**2** are not coplanar, but the guanidinium moiety is twisted out of plane of the aromatic ring. This forces the two zwitterions in the dimer also to be out of plane leading to less efficient interactions between them. Furthermore, the NHs in **2** are significantly less acidic than in **1** which also reduces the stability of H-bonded ion pairs. Hence, geometric as well as electronic fit is the important factor controlling the stability of aggregates obtained from such self-complementary molecules. Nevertheless, zwitterion **2** is an efficient self-assembling molecule. This indole guanidinium cation might also be an interesting binding motif for the recognition of oxoanions by indole based receptors [27-29], similar to our guanidiniocarbonyl pyrrole cation [30-32].

Experimental

General Remarks: Solvents were dried and distilled before use. The starting materials and reagents were used as obtained from Aldrich or Fluka. ^{1}H and ^{13}C NMR spectra were recorded with a Bruker Avance 400 spectrometer. The chemical shifts are reported relative to the deuterated solvents. The ESI-mass spectra were recorded with a Finnigan MAT 900 S spectrometer. IR spectra were recorded by measuring the Attenuated Total Reflectance (ATR). Melting points are not corrected. The pH values were measured with a Knick pH meter 766 Calimatic at 25 °C. UV spectra were measured in 10 mm rectangular cells with a Jasco V660 spectrometer.

Ethyl 7-amino-1*H*-indole-2-carboxylate (4): A mixture of ethyl 7-nitro-1*H*-indole-2-carboxylate (**3**; 200 mg, 0.85 mmol) and Pd/C (20 mg) in methanol (40 mL) was hydrogenated at ambient temperature for 1.5 h. The mixture was filtered over

Celite to remove Pd/C, and the solvent was evaporated to give the desired product **4** (170 mg, 0.83 mmol, 98%) as a colourless solid: mp 146 °C; ^{1}H NMR (400 MHz, [D$_6$]DMSO, 25 °C): δ = 1.34 (t, 3H), 4.34 (q, 2H), 5.38 (s, 2H), 6.41 (dd, 1H), 6.78-6.86 (m, 2H), 7.02 (d, 1H), 11.40 (bs, 1H) ppm; ^{13}C NMR (100 MHz, [D$_6$]DMSO, 25 °C): δ = 14.3, 60.3, 106.5, 108.1, 109.5, 121.5, 126.2, 127.3, 127.6, 134.6, 161.5; IR (KBr): ν = 3329 (s), 2996 (w), 2939 (w), 1668 (s), 1250 (s), 1215(s) cm^{-1}; HR-MS (ESI) calcd for [M+H]$^+$: 205.0972; found 205.0979.

***N*,*N*'-Di-(*tert*-butoxycarbonyl)thiourea (5):** To a stirred solution of thiourea (570 mg, 7.50 mmol) in dry tetrahydrofuran (150 mL) sodium hydride (1.35 g, 33.80 mmol, 60% in mineral oil) was added under argon atmosphere at 0 °C (ice bath). After 5 min the ice bath was removed and the mixture was stirred for additional 10 min at ambient temperature. The mixture was cooled to 0 °C again and di-*tert*-butyl dicarbonate (3.60 g, 16.50 mmol) was added. After 40 min of stirring at 0 °C the ice bath was removed and the mixture was stirred for additional 3 h at ambient temperature. The reaction was quenched by adding an aqueous saturated solution of $NaHCO_3$ (10 mL). Water (200 mL) was added and the reaction mixture was extracted with ethyl acetate (3 × 75 mL). The collected organic layers were dried over $MgSO_4$, filtered and evaporated to dryness. The white solid was purified by flash column chromatography on silica gel (hexane/ethyl acetate = 1 : 1 + 0.5% triethylamine) to give *N*,*N*'-di-(*tert*-butoxycarbonyl)thiourea (**5**, 1.63 g, 5.92 mmol, 79%) as a colourless solid: mp 130 °C; ^{1}H NMR (400 MHz, [D$_6$]DMSO, 25 °C): δ = 1.44 (s, 9H), 1.45 (s, 9H), 8.96 (s, 1H), 9.14 (s, 1H) ppm; ^{13}C NMR (100 MHz, [D$_6$]DMSO, 25 °C): δ = 27.6, 82.5, 150.5, 178.7; IR (KBr): ν = 3160 (s), 2987 (m), 2933 (m), 1767 (m), 1718 (m), 1128 (s) cm^{-1}; HR-MS (ESI) calcd for [M+H]$^+$: 277.1217; found 277.1056.

Ethyl 7-{*N*,*N*'-bis-[*tert*-(butoxycarbonyl)guanidino]}-1*H*-indole-2-carboxylate (6): To a solution of ethyl 7-amino-1*H*-indole-2-carboxylate (**4**, 130 mg, 0.65 mmol), *N*,*N*'-di-(*tert*-butoxycarbonyl)thiourea (**5**, 185 mg, 0.65 mmol) and triethylamine (0.35 mL, 2.44 mmol) in dry dichloromethane (30 mL) was added 2-chloro-1-methyl-pyridinium iodide (297 mg, 1.14 mmol) at 0° C and the mixture was stirred for 30 min. The ice bath was removed and the reaction mixture was stirred at ambient temperature for 24 h. The solvent was removed under reduced pressure, and the residue was purified by flash column chromatography on silica gel (ethyl acetate/hexane = 2:3) to give **6** (206 mg, 0.46 mmol, 71%) as a colourless solid: mp 144 °C; ^{1}H NMR (400 MHz, [D$_6$]DMSO, 25 °C): δ = 1.28 (s, 9H), 1.34 (t, 3H), 1.54 (s, 9H), 4.36 (q, 2H), 7.09 (t, 1H), 7.20 (d, 2H), 7.60 (d, 1H), 9.73 (s, 1H), 11.56 (bs, 1H), 11.95 (bs, 1H) ppm; ^{13}C NMR (100 MHz, [D$_6$]DMSO, 25 °C): δ = 14.3, 27.8, 27.8, 60.5, 78.4, 82.9, 108.4, 120.2, 120.9, 121.8, 122.8, 127.8, 128.3, 133.5, 152.0, 155.0, 161.2, 162.8; IR (KBr): ν = 3136 (w), 2974 (w), 2930 (w), 1717 (m), 1636 (m), 1360 (m) cm^{-1}; HR-MS (ESI) calcd for [M+Na]$^+$: 469.2058; found 469.2096.

2-(Ethoxycarbonyl)-1*H*-indole-7-guanidinium trifluoroacetate (7): Trifluoroacetic acid (3 mL) was added to the ethyl 7-[*N*,*N*'-bis-(*tert*-butoxycarbonyl)guanidino]-1*H*-indole-2-carboxylate (**6**, 170 mg, 0.39 mmol), and the reaction mixture was stirred at room temperature for 2 h. The excess trifluoroacetic acid was removed in vacuo to give **7** as a colourless solid (140 mg, 0.39 mmol, 100%): mp > 240 °C; ^{1}H NMR (400 MHz, [D$_6$]DMSO, 25 °C): δ = 1.35 (t, 3H), 4.36 (q, 2H), 7.13-7.26 (m, 7H), 7.69 (d, 1H), 9.29 (s, 1H), 12.11 (s, 1H) ppm; ^{13}C NMR (100 MHz, [D$_6$]DMSO, 25 °C): δ = 14.3, 60.6, 108.7, 112.0, 120.7, 121.8, 122.8, 128.3, 128.9, 133.5, 156.4, 161.1; IR (KBr): ν = 3298 (w), 3193 (w), 3101 (w), 2955 (w), 1699 (m), 1671 (s), 1255 (s) cm^{-1}; HR-MS (ESI) calcd for [M+H]$^+$: 247.1190; found 247.1215.

7-Guanidinio-1*H*-indole-2-carboxylate (2): To a solution of the trifluoroacetate salt **7** (130 mg, 0.53 mmol) in water/THF (1/4; 15 mL) $LiOH{\cdot}H_2O$ (223 mg, 5.30 mmol) was added. The reaction mixture was heated to 40 °C and stirred for 8 h. The solvent was removed under reduced pressure and the residue was dissolved in water (20 mL). The solution was acidified dropwise with hydrochloric acid (0.1 molar) until a yellow solid precipitated at a pH = 6. The solid was filtered and to remove inorganic salts again suspended in water (25 mL), some dioxane (5 mL) was added. The mixture was heated to reflux for 40 min. The residue was filtered, and washed with water and afterwards with diethyl ether. The residue was dried in vacuo to give **2** as a light brown solid (98 mg, 0.44 mmol, 84%): mp > 240 °C; ^{1}H NMR (400 MHz, [D$_6$]DMSO, 25 °C): δ = 6.82 (s, 1H), 7.05 (t, 1H), 7.15 (d, 1H), 7.43 (d, 1H), 7.99 (bs, 4H), 12.26 (bs, 1H), 13.07 (bs, 1H) ppm; ^{13}C NMR (100 MHz, [D$_6$]DMSO, 25 °C): δ = 103.4, 113.0, 118.1, 119.7, 122.0, 128.1, 129.6, 135.9, 155.9, 166.4; IR (KBr): ν = 3327 (m), 3086 (m), 3724 (m), 1397 (s), 737 (s) cm^{-1}; HR-MS (ESI) calcd for [M+H]$^+$: 219.0877; found 219.0884.

(2-Carboxy-1*H*-indole-7-yl)guanidinium picrate (2·H$^+$): To a suspension of the zwitterion **2** (20 mg, 0.09 mmol) in methanol (4 mL) a saturated solution of picric acid in water (6 mL) was added and the mixture was stirred for 24 h at ambient temperature. The picrate salt crystallized and was filtered, washed several times with methanol, and dried to provide the yellow solid **2**·H$^+$ (35 mg, 0.08 mmol, 89%): mp > 240 °C; ^{1}H NMR (400 MHz, [D$_6$]DMSO, 25 °C): δ = 7.11-7.20 (m, 8H), 7.67 (d, 1H), 8.58 (s, 2H), 9.21 (s, 1H), 12.02 (s, 1H), 13.23 (bs, 1H)

ppm; ^{13}C NMR (100 MHz, [D$_6$]DMSO, 25 °C): δ = 120.5, 124.1, 125.2, 129.1, 129.2, 141.9, 156.3, 160.9; IR (KBr): ν = 3200(w), 1674 (w), 1554 (m), 1336 (m) cm^{-1}; HR-MS (ESI) calcd for $[M+H]^+$: 219.0877; found 219.0884.

X-ray Crystallographic Data

Crystal structure of 2: $C_{10}H_{10}N_4O_2$, colourless crystals, dimensions 0.16 × 0.13 × 0.10 mm^3, measured with a Bruker D8 KAPPA series II with APEX II area detector system at 100 K; a = 12.1695 (5) Å, b = 7.1061 (3) Å, c = 12.3061 (4) Å, V = 985.45 (7) Å^3, Z = 4, ρ = 1.471 g/cm^3, space group $P2_1/n$, 7030 intensities measured (θ_{max} = 28.33°), 2458 independent ($R_{(int)}$ = 0.0279), 2061 observed, structure solution by direct methods and refinement of 145 parameters on F^2 with the Bruker software package SHELXTL Vers. 2008/4/(c) 2008, R_1 = 0.0485, ωR_2 (all data) = 0.1111, Gof = 1.053, max electron density 0.407 e Å^{-3}.

Acknowledgements

Financial support by the Deutsche Forschungsgemeinschaft and the Fonds der Chemischen Industrie is gratefully acknowledged.

References

1. Jeffrey, G. A. *An Introduction to Hydrogen Bonding;* Oxford University Press: New York, 1997.
2. Kelly, T. R.; Kim, M. H. *J. Am. Chem. Soc.* **1994,** *116,* 7072–7080. doi:10.1021/ja00095a009
3. Cook, J. L.; Hunter, C. A.; Low, C. M. R.; Perez-Velasco, A.; Vinter, J. G. *Angew. Chem.* **2007,** *119,* 3780–3783. doi:10.1002/ange.200604966
4. Cook, J. L.; Hunter, C. A.; Low, C. M. R.; Perez-Velasco, A.; Vinter, J. G. *Angew. Chem., Int. Ed.* **2007,** *46,* 3706–3709. doi:10.1002/anie.200604966
5. Leininger, S.; Olenyuk, B.; Stang, P. J. *Chem. Rev.* **2000,** *100,* 853–908. doi:10.1021/cr9601324
6. Seidel, S. R.; Stang, P. J. *Acc. Chem. Res.* **2002,** *35,* 972–983. doi:10.1021/ar010142d
7. Fujita, M.; Tominaga, M.; Hori, A.; Therrien, B. *Acc. Chem. Res.* **2005,** *38,* 369–378. doi:10.1021/ar040153h
8. Kruppa, M.; König, B. *Chem. Rev.* **2006,** *106,* 3520–3560. doi:10.1021/cr010206y
9. Nitschke, J. R.; Hutin, M.; Bernardinelli, G. *Angew. Chem., Int. Ed.* **2004,** *43,* 6724–6727. doi:10.1002/anie.200461308
10. Pluth, M. D.; Bergman, R. G.; Raymond, K. N. *J. Org. Chem.* **2008,** *73,* 7132–7136. doi:10.1021/jo800991g
11. Baram, J.; Shirman, E.; Ben-Shirit, N.; Ustinov, A.; Weissman, H.; Pinkas, I.; Wolf, S. G.; Rybtchinski, B. *J. Am. Chem. Soc.* **2008,** *130,* 14966–14967. doi:10.1021/ja807027w
12. Schmuck, C. *Eur. J. Org. Chem.* **1999,** 2397–2403. doi:10.1002/(SICI)1099-0690(199909)1999:9<2397::AID-EJOC2397>3.0.CO;2-3
13. Schmuck, C.; Wienand, W. *J. Am. Chem. Soc.* **2003,** *125,* 452–459. doi:10.1021/ja028485+
14. Schlund, S.; Schmuck, C.; Engels, B. *J. Am. Chem. Soc.* **2005,** *127,* 11115–11124. doi:10.1021/ja052536w
15. Schmuck, C.; Rehm, T.; Klein, K.; Gröhn, F. *Angew. Chem., Int. Ed.* **2007,** *46,* 1693–1697. doi:10.1002/anie.200603629
16. Schmuck, C.; Rehm, T.; Gröhn, F.; Klein, K.; Reinhold, F. *J. Am. Chem. Soc.* **2006,** *128,* 1430–1431. doi:10.1021/ja056465c
17. Gröger, G.; Stepanenko, V.; Würthner, F.; Schmuck, C. *Chem. Commun.* **2009,** 698–700. doi:10.1039/b820281h
18. Zheng, Y.-J.; Ornstein, R. L. *J. Am. Chem. Soc.* **1996,** *118,* 11237–11243. doi:10.1021/ja960041o
19. Dietrich, B.; Fyles, D. L.; Fyles, T. M.; Lehn, J.-M. *Helv. Chim. Acta* **1979,** *62,* 2763–2787. doi:10.1002/hlca.19790620827
20. Expósito, A.; Fernández-Suárez, M.; Iglesias, T.; Muñoz, L.; Riguera, R. *J. Org. Chem.* **2001,** *66,* 4206–4213. doi:10.1021/jo010076t
21. Mukaiyama, T. *Angew. Chem., Int. Ed. Engl.* **1979,** *18,* 707–721. doi:10.1002/anie.197907073
22. Sansone, F.; Dudič, M.; Donofrio, G.; Rivetti, C.; Baldini, L.; Casnati, A.; Cellai, S.; Ungaro, R. *J. Am. Chem. Soc.* **2006,** *128,* 14528–14536. doi:10.1021/ja0634425
23. Porcheddu, A.; Giacomelli, G.; Chighine, A.; Masala, S. *Org. Lett.* **2004,** *6,* 4925–4927. doi:10.1021/ol047926m
24. Zhao, Y.; Schultz, N. E.; Truhlar, D. G. *J. Chem. Theory Comput.* **2006,** *2,* 364–382. doi:10.1021/ct0502763
25. Barone, V.; Cossi, M. *J. Phys. Chem. A* **1998,** *102,* 1995–2001. doi:10.1021/jp9716997
26. Cossi, M.; Rega, N.; Scalmani, G.; Barone, V. *J. Comput. Chem.* **2003,** *24,* 669–681. doi:10.1002/jcc.10189
27. Bates, G. W.; Triyanti; Light, M. E.; Albrecht, M.; Gale, P. A. *J. Org. Chem.* **2007,** *72,* 8921–8927. doi:10.1021/jo701702p
28. Makuc, D.; Lenarčič, M.; Bates, G.; Gale, P. A.; Plavec, J. *Org. Biomol. Chem.* **2009,** *7,* 3505–3511. doi:10.1039/b908947k
29. Makuc, D.; Triyanti; Albrecht, M.; Plavec, J.; Rissanen, K.; Valkonen, A.; Schalley, C. A. *Eur. J. Org. Chem.* **2009,** 4854–4866. doi:10.1002/ejoc.200900721
30. Schmuck, C.; Geiger, L. *J. Am. Chem. Soc.* **2005,** *127,* 10486–10487. doi:10.1021/ja052699k
31. Schmuck, C.; Schwegmann, M. *J. Am. Chem. Soc.* **2005,** *127,* 3373–3379. doi:10.1021/ja0433469
32. Schmuck, C.; Bickert, V. *J. Org. Chem.* **2007,** *72,* 6832–6839. doi:10.1021/jo070981z

License and Terms

Beilstein Journal of Organic Chemistry

The subtle balance of weak supramolecular interactions: The hierarchy of halogen and hydrogen bonds in haloanilinium and halopyridinium salts

Kari Raatikainen, Massimo Cametti and Kari Rissanen*

Full Research Paper

Open Access

Address:
Nanoscience Center, Department of Chemistry, University of Jyväskylä, P.O. Box 35, 40014 Jyväskylä, Finland

Email:
Kari Rissanen* - kari.t.rissanen@jyu.fi

* Corresponding author

Keywords:
crystal engineering; halogen bonding; hydrogen bonding; supramolecular chemistry; weak interactions

Beilstein Journal of Organic Chemistry **2010,** *6,* No. 4.
doi:10.3762/bjoc.6.4

Received: 29 September 2009
Accepted: 07 January 2010
Published: 15 January 2010

Guest Editor: C. A. Schalley

Abstract

The series of haloanilinium and halopyridinium salts: 4-IPhNH$_3$Cl (**1**), 4-IPhNH$_3$Br (**5**), 4-IPhNH$_3$H$_2$PO$_4$ (**6**), 4-ClPhNH$_3$H$_2$PO$_4$ (**8**), 3-IPyBnCl (**9**), 3-IPyHCl (**10**) and 3-IPyH-5NIPA (3-iodopyridinium 5-nitroisophthalate, **13**), where hydrogen or/and halogen bonding represents the most relevant non-covalent interactions, has been prepared and characterized by single crystal X-ray diffraction. This series was further complemented by extracting some relevant crystal structures: 4-BrPhNH$_3$Cl (**2**, CCDC ref. code TAWRAL), 4-ClPhNH$_3$Cl (**3**, CURGOL), 4-FPhNH$_3$Cl (**4**, ANLCLA), 4-BrPhNH$_3$H$_2$PO$_4$, (**7**, UGISEI), 3-BrPyHCl, (**11**, CIHBAX) and 3-ClPyHCl, (**12**, VOQMUJ) from Cambridge Structural Database for sake of comparison. Based on the X-ray data it was possible to highlight the balance between non-covalent forces acting in these systems, where the relative strength of the halogen bonding C–X···A$^-$ (X = I, Br or Cl) and the ratio between the halogen and hydrogen bonds [C–X···A$^-$: D–H···A$^-$] varied across the series.

Introduction

Non-covalent interaction, such as hydrogen bonding and metal coordination represent the basic set of tools for the construction of elaborate architectures in the supramolecular chemistry of organic or metal-organic compounds [1]. In the past few years, there has been a growing interest towards the development of new types of intermolecular interactions. In particular, halogen bonding has attracted significant attention and it is considered nowadays as a promising instrument in supramolecular chemistry [2]. Halogen bonding (XB) is the non-covalent interaction involving halogen atoms as electrophilic species [3]. The first reports of these interactions, only later classified as halogen bonds, date back to the late 1960's [4]. In the following years, several X-ray studies demonstrated the existence of the short interaction distance between the halogen atom and a nucleophilic atom in a number of crystal structures [5,6]. In 1996 Allen and co-workers [7] did an extensive statistical analysis of all of the crystal structures in the Cambridge Structural Database (CSD) for carbon-bound halogen atoms (C–X where

X = F, Cl, Br or I) and nucleophilic atoms (S, O or N, in their various hybridization states). The analysis was based on intermolecular contact distances shorter than 1.26 times the sum of the van der Waals (VDW) radii of the two interacting atoms. The analysis showed that the intermolecular contacts between halogen (Cl, Br, and I but not F) atoms and nucleophilic (O and N) atoms manifest a highly directional, attractive interaction leading to contact distances clearly shorter than the sum of VDW radii [7]. They also concluded that the attractive nature of the interaction is mainly due to electrostatic effects, but polarization, charge-transfer, and dispersion contributions all play an important role, more recently confirmed also by theoretical and experimental studies [8-10].

Interactions between halogens and nucleophilic atoms were generally considered to be too weak to be used in crystal engineering, until the late '90s when G. Resnati and P. Metrangolo [11-16] made a major breakthrough in the field by exploring the use of perfluorocarbon (PFC) iodides and aliphatic amines in the formation of strong halogen–nucleophile interactions, from then systematically called "halogen bonding". In these systems, the C_{PFC}–I···N contact distances are usually around 2.8 Å corresponding to ca. 20% reduction of the sum of standard VDW radii of nitrogen (1.55 Å) and iodine (1.98 Å) [17]. The strong interaction between the highly polarized iodine and the nitrogen atom, manifested by the remarkably short interaction distance, has been shown to overcome the low affinity between hydro- and perfluorinated carbon molecules by effectively forming stable high melting co-crystals. Since then, this novel interaction has become a common tool in supramolecular chemistry, especially in crystal engineering [18,19], and lately it has widely and successfully applied in other fields of material science, such as in supramolecular separations, liquid crystals, organic semiconductors and paramagnetic materials technologies [20,21]. Recently, the important role of XBs in biological systems and its potential in drug development has also been recognized [22].

The halogen bond (XB), whose terminology emphasizes the similarity with hydrogen bonding [23] can be schematically described by Y–X···A, where X is the XB donor atom (Lewis acid, electrophilic) and A is the XB acceptor atom (Lewis base, nucleophilic) [20]. According to this definition, halogen bonding covers a vast family of non-covalent interactions, and a very wide range of interaction energies [20]. Concurrently with the development of practical applications and experimental studies on halogen bonding systems, theoretical and conceptual aspects of halogen bonding have been scrutinized in detail. Theoretical studies [24,25] of halogen bonding show that the electron density is anisotropically distributed around the covalently bound halogen atom. A region of a positive electrostatic potential is formed at the surface of the halogen atom, localized along the extension of the Y–X···A covalent bond. The existence and magnitude of this positive region, known as σ-hole [25], depends on the polarizability of the halogen atom, and by no surprise the interaction energy is found to increase in by the order Cl < Br < I [26], following the polarizability of halogen atom. The hybridization of the C–X carbon atom on the XB donor molecule has also an effect on the strength and directionality of the halogen bond. The order $C(sp^3) < C(sp^2) < C(sp)$ is generally followed [24-26] and for example haloalkynes are found to be particularly good halogen bond donors [27,28]. As seen in PFC compounds, electron withdrawing moieties present on the Y group favor the interaction. For this reason haloarenes where the aromatic ring has electron withdrawing substituents e.g. fluorines [11-16,18,19] are also excellent halogen bond donors. Iodonitrobenzene derivatives represent a less explored type of haloarenes [29,30]. In these XB systems, secondary C–I···O_2N_{Ar} halogen bonds (distances 13% shorter than the sum of standard VDW radii [17]) have been observed for iodonitrobenzenes themselves [31,32] or in co-crystals of iodo- and nitrobenzenes [29,30]. In our recent studies [33], we have shown that 1-iodo-3,5-dinitrobenzene forms surprisingly strong C–I···N halogen bonds (23% shorter than the sum of standard VDW radii [17]) with 1,4-diazabicyclo[2.2.2]octane (DABCO).

One of the main challenges in supramolecular chemistry and crystal engineering is to identify the hierarchies of non-covalent interactions in order to develop efficient synthetic strategies for attaining advanced supramolecular systems [1]. The structure of a supramolecular assembly in crystalline solids generally results from the balance of all intermolecular interactions in the crystal, which results from maximizing the attractive interactions and minimizing the repulsive ones, generally affording the densest of packing. When two major interactions, such as hydrogen bonding (HB) and halogen bonding (XB), are simultaneously present in a system, it is not always straightforward to predict which one of them is going to determine the overall crystal architecture. In some cases, the strength of the halogen bond interactions allows them to overrule hydrogen bonds in the hierarchy of intermolecular interactions [15,34]. Recently it has been proposed [35,36] that the hierarchy of intermolecular non-covalent interactions carefully balancing hydrogen- and halogen bonding can be affected and thus applied in rational design of supramolecular entities and crystal structures.

In this paper, we describe a number of simple haloanilinium and halopyridinium salt structures which clearly show how the balance of intermolecular interactions such as HB and XB can determine the supramolecular architectures found in the solid state (Scheme 1).

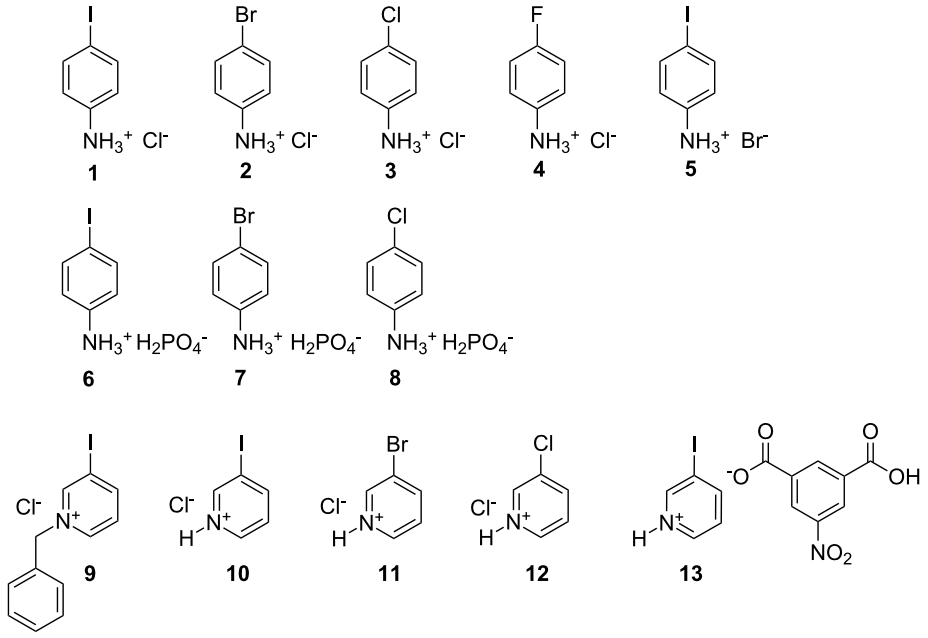

Scheme 1: The chemical structures of the salts **1–13**.

The detailed study of the seven new crystal structures, namely anilinium salts 4-IPhNH$_3$Cl (**1**), 4-IPhNH$_3$Br (**5**), 4-IPhNH$_3$H$_2$PO$_4$ (**6**), 4-ClPhNH$_3$H$_2$PO$_4$ (**8**) and corresponding pyridinium salts 3-IPyBnCl (**9**), 3-IPyHCl (**10**) and 3-IPyH-5NIPA (3-iodopyridinium 5-nitroisophthalate, **13**), complemented by the comparison with corresponding structures found in the literature, reveals the subtle balance between HB and XB in these salts. The structures of salts 4-BrPhNH$_3$Cl (**2**, CCDC ref. code TAWRAL) [37], 4-ClPhNH$_3$Cl (**3**, CURGOL) [38], 4-FPhNH$_3$Cl (**4**, ANLCLA) [39], 4-BrPhNH$_3$H$_2$PO$_4$, (**7**, UGISEI) [40], 3-BrPyHCl, (**11**, CIHBAX) [41] and 3-ClPyHCl, (**12**, VOQMUJ) [42] were extracted from the CSD [43] in order to obtain the full homogeneous series.

Results and Discussion

In addition to the exact measurement of C–X···A contact distances, we also calculated the relative XB distances **R** (Equation 1), following the definition of Lommerse et al., [7] where standard VDW radii of interacting atoms were taken into account to bring interaction distances into the standardized scale.

$$\mathbf{R} = \frac{d}{r_{\mathrm{X}} + r_{\mathrm{D}}} \qquad (1)$$

Here, d is X···D distance and r_{X} and r_{D} (or r_{ion}) are standard VDW radii of the involved atoms (or ions) (r_{Cl^-} = 1.81 Å, r_{Cl} = 1.75 Å, r_{Br} = 1.85, r_{Br^-} = 1.96 Å, r_{I} = 1.98, r_{O} = 1.52) [17,44]. In addition to the relative XB distances **R**, the ratio of the most relevant interactions, that are the charge assisted hydrogen and halogen bonds, were taken into the consideration. The ratio (D^+–H···) : (Y–I···), namely hydrogen bonding and halogen bonding, donor sites in haloanilinium halides is 3 : 1, whereas in H_2PO_4 salts it is 5 : 1. In halopyridinium salts corresponding ratio of donor sites vary from a solely halogen bonding (0 : 1) system to a 2 : 1 ratio in **13**.

Halogen and hydrogen bonding in 4-IPhNH$_3$Cl (1), 4-BrPhNH$_3$Cl (2), 4-ClPhNH$_3$Cl (3) and 4-FPhNH$_3$Cl (4)

The first four structures (**1–4**) form a series of haloanilinium chlorides (Scheme 1) carefully chosen to probe the effect of the halogen substituent on the balance of HB and XB in these systems.

X-ray-quality crystals of **1** were obtained by crystallization of 4-iodoaniline from ethanol–HCl solution (Figure 1a). The halogen bond I···Cl$^-$ is about 10% shorter than the sum of standard VDW radii of the interacting atoms (3.79 Å) [17,44], definitely weaker than in the classical PFC-I···N systems [11-16]. The crystal packing reveals a pattern of complementary donor and acceptor sites for three N^+–H···Cl$^-$ hydrogen bonds, which in addition to one I···Cl$^-$ mentioned above, creates a distorted tetrahedral coordination sphere around the Cl$^-$ anion (Figure 1a). The N^+–H···Cl$^-$ hydrogen bonds are situated on the *a,b*-plane forming 2D hexagonal network (Figure 1b). The iodobenzene moieties, perpendicular to the hydrogen bond network, are segregated between these HB layers, with the

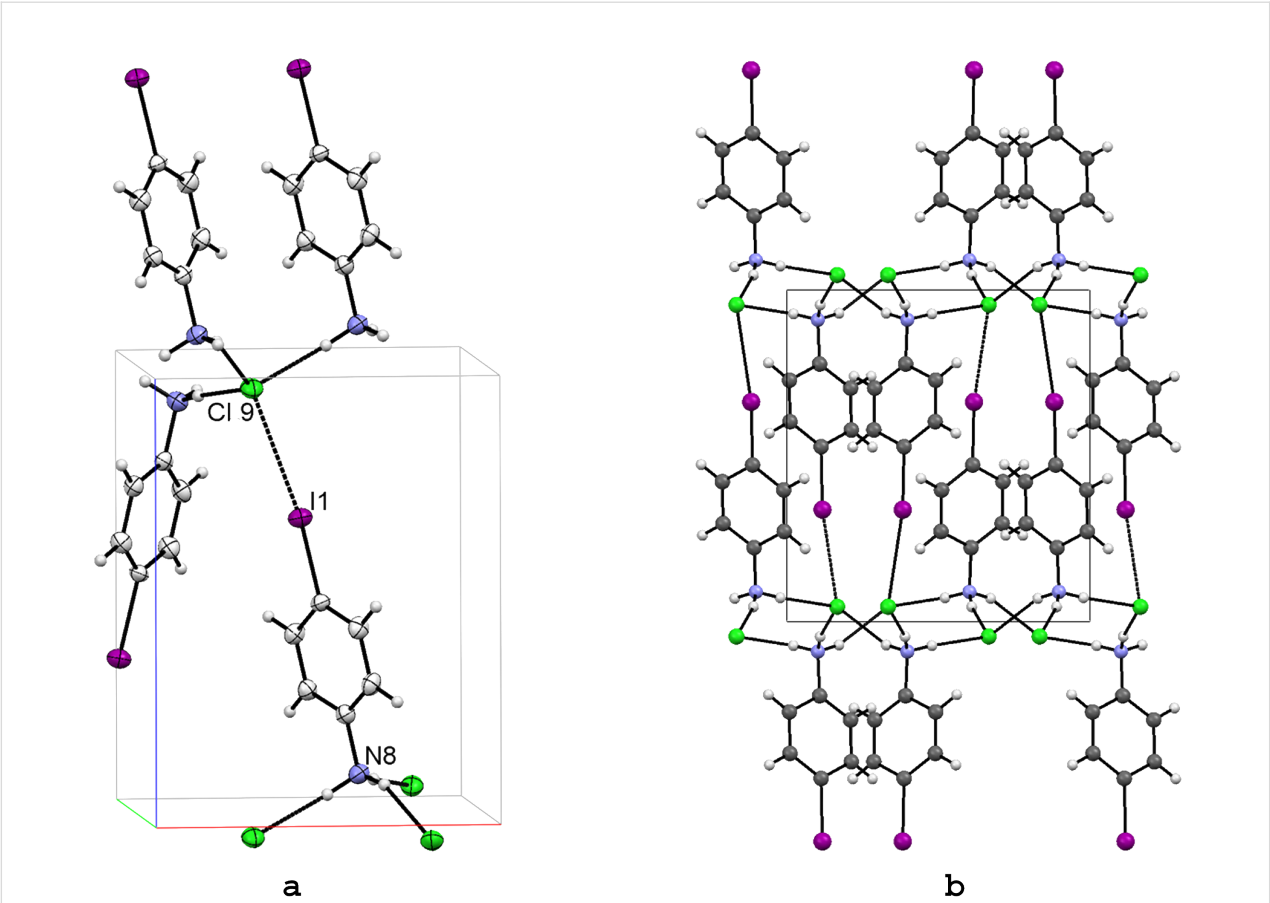

Figure 1: X-ray structure of 4-IPhNH$_3$Cl (**1**) with numbering for selected atoms (a) and the packing scheme viewed down the *a* axis (b). Thermal ellipsoids are shown at the 50% probability level. Hydrogen and halogen bonds are shown in dotted lines.

halogen bonding acting as an anchor to the fourth coordination site of the Cl anion, to further stabilize the structure in direction of the *c* axis.

To gain more information about the effect of the halogen (X) identity on C–X···Cl$^-$ halogen bonding distances, the structure of 4-IPhNH$_3$Cl (**1**) was compared with a series of *p*-substituted bromo- (**2**), chloro- (**3**), and fluoroanilinium chlorides (**4**) published previously. Based on these previous experimental and theoretical studies [24-26], halogen bond strength was expected to vary from a clearly non-existent F···Cl$^-$ interaction to most attractive I···Cl$^-$ interaction. Comparing these analogous structures, where instead the charge assisted hydrogen bond network is kept constant, the relative strength and role of halogen bond in crystal architecture can be evaluated. In this respect, the variation of the size of the VDW radii of the halogen atom was considered to have a minor effect in the present context. In all these crystals, the structurally similar charge-assisted hydrogen bond network is the main structural feature, which determines the overall orientation of the molecules [see packing of 4-IPhNH$_3$Cl (**1**) in Figure 1b]. Halogen bonding is evident only in the structure of 4-IPhNH$_3$Cl (**1**; Figure 2a), but weak halogen bonding Br···Cl$^-$ is observed in 4-BrPhNH$_3$Cl (**2**, TAWRAL [39]; Figure 2b) as well.

In 4-ClPhNH$_3$Cl (**3**, CURGOL [39]; Figure 2c), distance Cl···Cl$^-$ is slightly longer than Br···Cl$^-$ and the sum of VDW radii [17,44]. However, the structures of 4-BrPhNH$_3$Cl (**2**) and 4-ClPhNH$_3$Cl (**3**) are isomorphous. The measured X···Cl$^-$ distances, angles and other pertinent structural data are given in Table 1. At variance with the other members of the series, the structure of fluoro-substituted anilinium chloride **4** [39] is completely different (Figure 2d) and does not show similar hydrogen bonding and no halogen bonding and thus it was excluded from Table 1.

This difference can be explained by the fact that, instead, the fluorine substituent forms weak F···H hydrogen bonds with aryl hydrogens (Figure 2d). It is also interesting to note that the intermolecular interaction pattern in 4-IPhNH$_3$Cl (**1**) differs

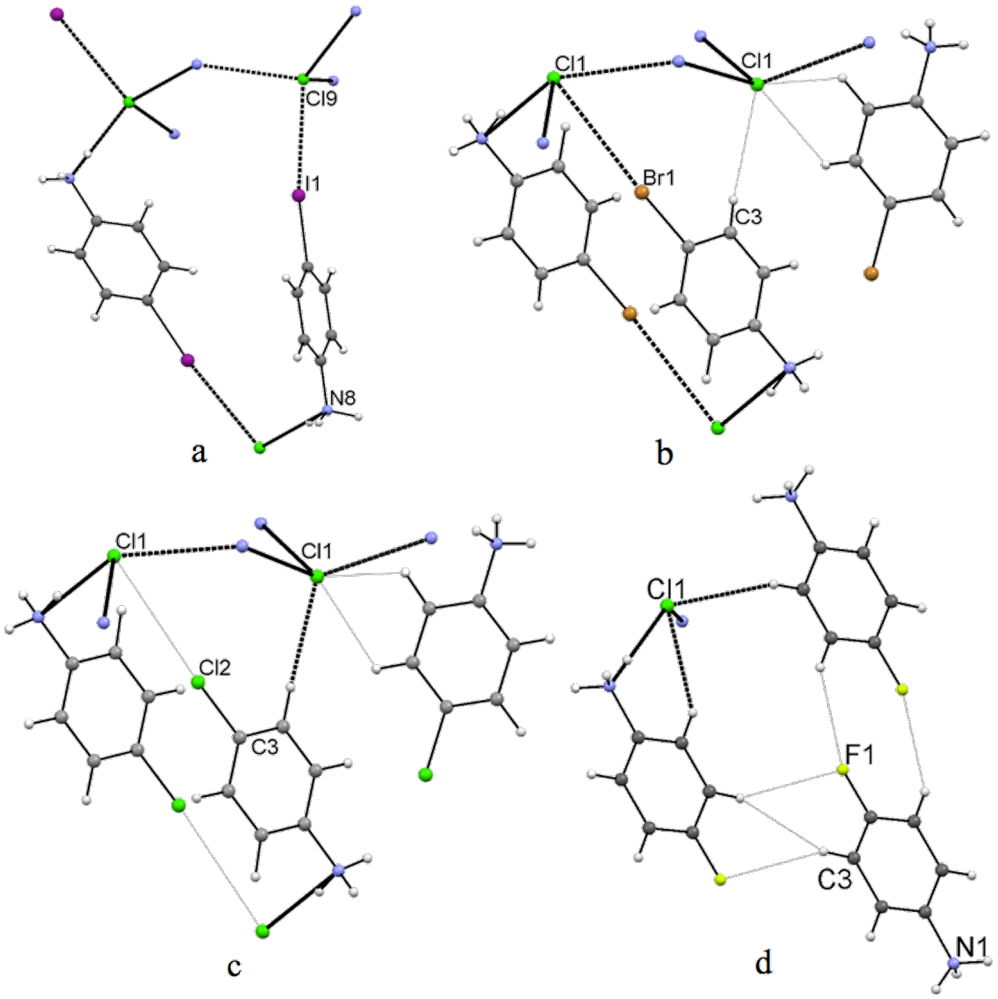

Figure 2: Interaction contacts in 4-IPhNH$_3$Cl (**1**; a), 4-BrPhNH$_3$Cl (**2**; b), 4-ClPhNH$_3$Cl (**3**; c) and 4-FPhNH$_3$Cl (**4**; d). Dotted lines represent the hydrogen and halogen interactions, where the shorter (stronger) contact distances are shown in bold lines and the longer (weaker) with narrow lines.

Table 1: Relevant C–X, hydrogen bond and halogen bond lengths and angles in **1**–**3**.

	C–X [Å] [X]	X···Cl$^-$ [Å] [Cl$^-$] [**R**]*	C–X···Cl$^-$ [°]	Cl$^-$···H–N$_a$ [Å]	N$_a$···Cl$^-$···N$_b$
4-IPhNH$_3$Cl, **1**	2.102 [I1]	3.405 [Cl9] [0.90]	169.8°	3.049	108.8°
				3.092	117.1°
				3.103	110.6°
4-BrPhNH$_3$Cl, **2** (TAWRAL [37])	1.892 [Br1]	3.587 [Cl1] [0.98]	165.9°	3.135	87.3°
				3.161	139.2°
				3.143	106.8°
4-ClPhNH$_3$Cl, **3** (CURGOL [38])	1.741 [Cl2]	3.635 [Cl1] [1.02]	166.6°	3.135	85.8°
				3.157	138.5°
				3.115	106.9°

* **R** = $d/(r_X + r_D)$, see Equation 1.

from the isomorphic chloro- and bromo-derivates **2** and **3** and is explained by the existing, though quite weak, I···Cl^- halogen bond.

Detailed inspection of the structures **1**–**4** revealed that non-covalent tetrahedral coordination of Cl^- by three charge-assisted hydrogen bonds and one halogen bond exists only in structure of *p*-iodo salt **1** (Figure 2a), resulting in a more linear C–I···Cl^- interaction angle, which is consistent with the shorter XB distance. Also the HB distances are shorter. When compared to the *p*-bromo and *p*-chloro structures **2** and **3** (Figure 2b and Figure 2c), the weaker halogen bonding tendency reverts the orientation of the benzene moiety to a closed dimer motif. As a conclusion, the C–Br···Cl^- and C–Cl···Cl^- interactions in **2** and **3** are not comparable to the halogen bond in **1**, but can be considered as intermediate structures between the truly halogen bonded **1** and the only hydrogen bonded **4**. When the polarizability of the halogen atom is increased (I > Br > Cl > F), thus increasing the effect of the halogen bond, the changed balance of the intermolecular interactions will influence the spatial organization of the adjacent molecules leading to a different crystal architecture. The strong charge-assisted hydrogen bonding clearly overrules the weaker halogen bonding and is the major cause for the crystal packing.

Halogen and hydrogen bonding in 4-IPhNH$_3$Br (5)

Exchanging the chlorine counter anion for bromine was expected to give weaker halogen bond interactions due to the lower nucleophilicity of the bromine anion, but also hydrogen bonding distances and coordination were expected to be different. Crystallization from ethanol–HBr solution resulted in crystals of **5** in which the asymmetric unit contains three molecules of *p*-iodoanilinium bromide (Figure 3a). The main structural feature of **5** is, surprisingly, the very similar overall HB motif (Figure 3b) with the one in 4-IPhNH$_3$Cl (**1**; Figure 1a), despite the clearly different coordination around the Br anion (Figure 3a). The 4-IPhNH$_3$Br (**5**) displays quite long I···Br^- XB distances, shown in Table 2, being only slightly shorter than the sum of VDW. The weaker interactions, i.e. the longer I···Br^- distances, manifest the lower nucleophilicity of the Br anion. Even though the I···Br^- distances are relatively long, the quite linear C-I···Br^- bond angle supports the presence of weak XB interaction, clearly weaker that in the corresponding anilinium chloride **1**.

Halogen and hydrogen bonding in 4-IPhNH$_3$H$_2$PO$_4$ (6), 4-BrPhNH$_3$H$_2$PO$_4$ (7) and 4-ClPhNH$_3$H$_2$PO$_4$ (8)

The balance between the halogen bonding and hydrogen bonding in anilinium salts can be also modulated by the exchange of the spherical halide anions with tetrahedral anions such as dihydrogenphosphate. In addition, $H_2PO_4^-$ ion offers two OH groups providing two additional hydrogen bond donor sites differing from the corresponding anilinium halides, thus the interaction type ratio (D^+–H···) : (C–I···) in **6** is 5 : 1. As the dihydrogenphosphate anion is a stronger hydrogen bond acceptor that the halide anions (Cl^-, Br^- or I^-), it was interesting to study whether the weak halogen bonding observed in the anilinium halide salts **1** and **2** would be completely overruled by the dihydrogenphosphate anion or not. Crystals of 4-IPhNH$_3$H$_2$PO$_4$ (**6**) were obtained from a methanol–phos-

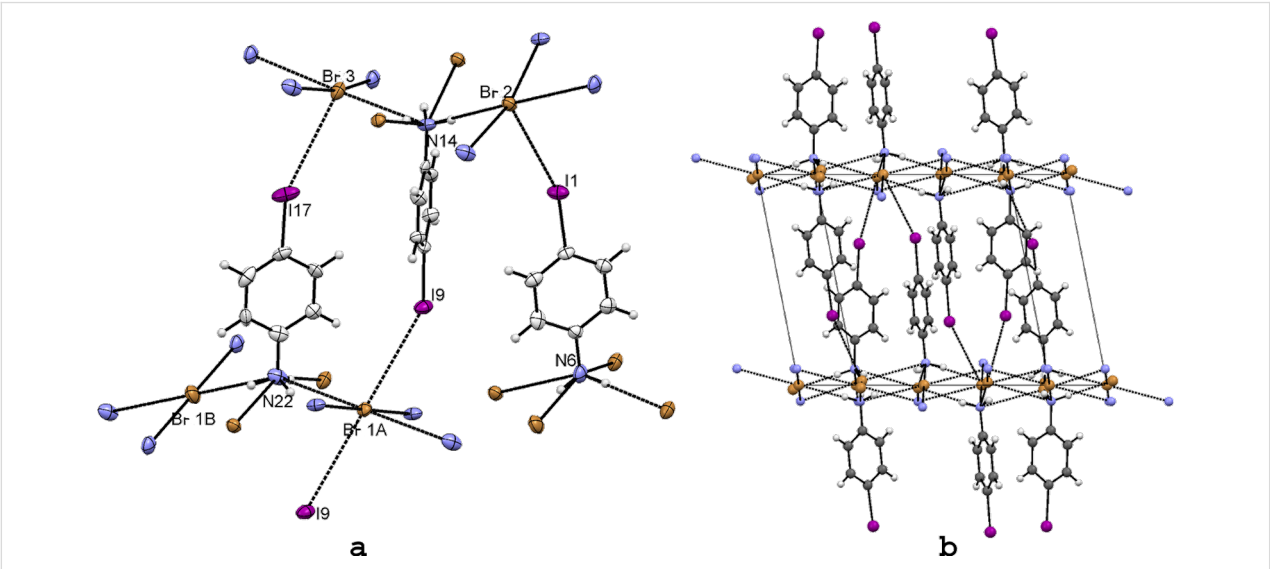

Figure 3: X-ray structure of 4-IPhNH$_3$Br (**5**) with selected numbering scheme (a) and the packing scheme viewed down the *a* axis (b). Thermal ellipsoids are drawn at the 50% probability level. Hydrogen and halogen bonds are shown in dotted lines.

Table 2: Relevant covalent bond, hydrogen bond and halogen bond lengths and angles in **5**.

	C–I [Å] [I]	X···Br⁻ [Å] [Br⁻] [**R**]*	C–X···Br⁻	Br⁻···H–N_a [Br···N] [Å]	N_b···Br⁻···N_a
4-IPhNH$_3$Br, **5**	2.102 [I1]	3.704 [Br2] [0.94]	158.4°	3.265 [Br2···N14]	87.3° [N22··Br2···N14]
				3.408 [Br2···N22]	92.3° [N6···Br2···N22]
				3.347 [Br2···N6]	90.8° [N14···Br2···N6]
				3.441 [Br2···N14]	89.8° [N14···Br2···N14]
	2.083 [I17]	3.834 [Br3] [0.97]	154.1°	3.257 [Br3···N6]	81.7° [N22···Br3···N6]
				3.294 [Br3···N22]	96.0° [N14···Br3···N22]
				3.333 [Br3···N14]	93.6° [N6···Br3···N14]
				3.269 [Br3···N6]	88.5° [N6···Br3···N6]
	2.087 [I9]	3.893 [Br1A] [0.99]	148.5°	3.310 [Br1A···N22]	86.2° [N14···Br1A···N22]
				3.430 [Br1A···N14]	93.8° [N22···Br1A···N14]
		[Br1B]		3.219 [Br1B···N22]	82.6° [N6···Br1B···N22]
				3.269 [Br1B···N6]	97.4° [N22···Br1B···N6]

* **R** = $d/(r_X + r_D)$, see Equation 1.

phoric acid solution of 4-iodoaniline by slow evaporation. The asymmetric unit of **6** is depicted in Figure 4a. The hydrogen bonding pattern consists of three N–H···O and two O–H···O interactions, as expected. Hence the H_2PO_4 anions and H_3N^+ moieties are H-bonded together forming a 2D layer of strong hydrogen bonds. The layers are perpendicular to the crystallographic *c* axis and the spacing between the layers is about 13 Å. Aromatic moieties are segregated between these layers, thus the overall crystal packing (Figure 4b) is very similar to the haloanilinium halides (Figure 1 and Figure 3). Unexpectedly, a quite strong I1···O12 halogen bond with **R** = 0.93 is formed between the iodine atoms and one of the O atoms in the dihydrogenphosphate anion. The XB angle C–I1···O12 is ~ 160°, which is consistent with the halogen bonds seen in 4-IPhNH$_3$Br (**5**), 4-BrPhNH$_3$Cl (**2**) and 4-ClPhNH$_3$Cl (**3**) structures.

Hydrogen bonding clearly dominates the crystal packing of 4-IPhNH$_3$H$_2$PO$_4$ (**6**). Yet the most nucleophilic oxygen atom in the dihydrogenphosphate anion acts as a halogen bond acceptor towards the moderately polarized iodine atom. The relative strength of the halogen bonding can be tuned by changing the polarizability of the halogen atom as manifested by the anilinium salts discussed above. Thus, substitution of the iodine atom for bromine, as in 4-BrPhNH$_3$H$_2$PO$_4$ (**7**, UGISEI [40]) was expected to show longer XB interaction distances due to the lower polarizability of the bromine atom [24-26]. In **7**, the XB distance Br···O is 3.348 Å, with **R** = 0.99 (Table 3), thus reflecting the weaker or nearly non-existent interaction. In spite of the slight differences in the halogen bonding interactions the crystal structures of **6** and **7** are isomorphic. This feature indicates that the weak halogen bonding observed in **6** is not able to overrule the strong hydrogen bonding induced by the dihydrogenphosphate, as in the case of the chloride (a weaker hydrogen bonding donor) in the structure of **1**. To prove that indeed the **R** = 0.99 in **7** does not represent halogen bonding interactions, we crystallized *p*-chloroaniline from ethanol–phosphoric acid solution to get the crystal structure of the corresponding 4-ClPhNH$_3$H$_2$PO$_4$ (**8**). As expected, the **R** = 1.00 in **8** and the structure is isomorphic with **6** and **7**. Table 3 shows that due to the strong and governing hydrogen bonding by the dihydrogenphosphate the X···O distances and C–X···O contact angles do not show the trend observed in the haloanilinium chlorides (**1**–**3**).

Halogen bonding in 3-IPyBnCl (9)

One additional way to polarize the halogen atom is to attach it into a charged aromatic ring, as in the pyridinium moiety where the positive charge is delocalized over the aromatic ring inducing a stronger polarizing effect to the halogen substituent. By no surprise, short halogen bond interactions are characteristic in halopyridinium salts [45-47]. Depending on the structure of the pyridinium moiety, namely protonated N^+–H or *N*-alkylated N^+–R, the hydrogen bonding interactions between the molecular components can be influenced. The protonated pyridinium is a very strong hydrogen bond donor whereas the *N*-alkylated pyridinium is not. Thus the ratio of [N^+–H···] and [C–I···], HB and XB, donor sites is 0 : 1 [N^+–R] or 1 : 1 [N^+–H]. To override the hydrogen bond contribution we first focused our attention on *N*-benzylpyridinium salts, which should completely suppress the strong hydrogen bond interactions and give space to strong XB interaction instead if an iodine substituent would sit on the aromatic ring. Therefore, we prepared *N*-benzyl-3-iodopyridinium chloride (**9**) by nucleophilic substitution reaction of 3-iodopyridine with (chloromethyl)benzene (the synthesic details will be reported else-

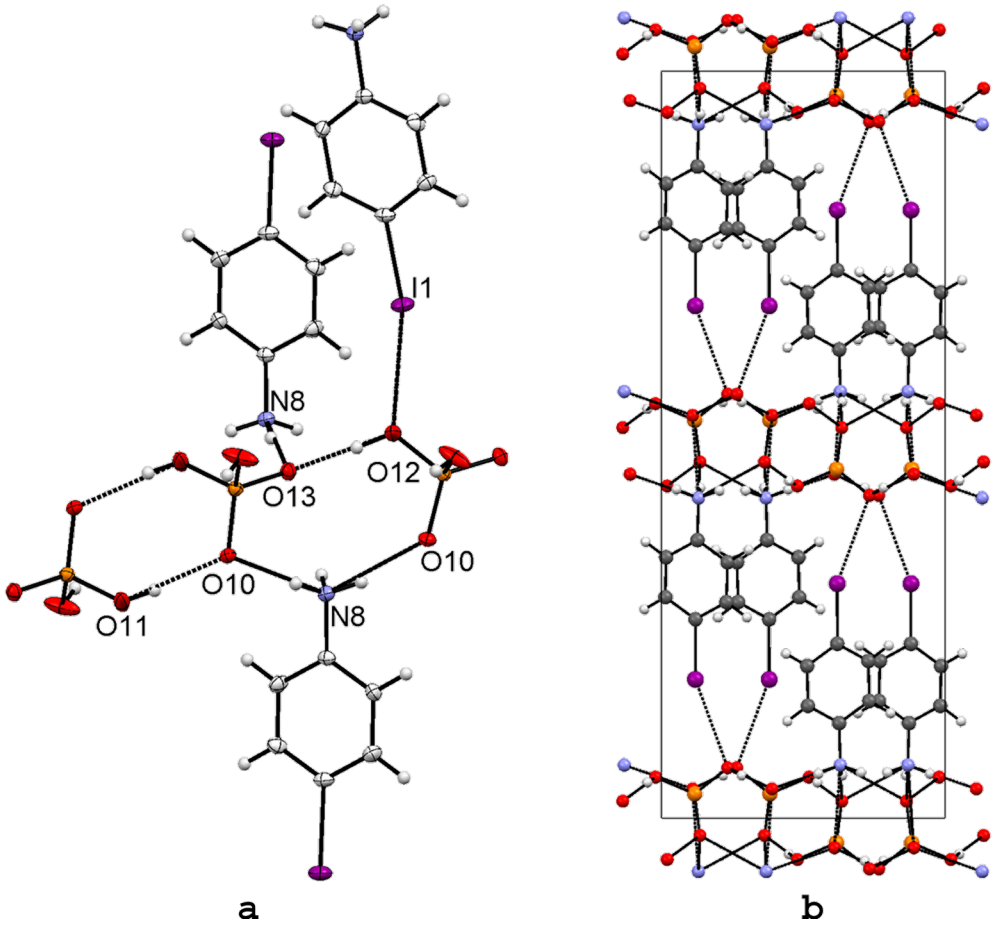

Figure 4: X-ray structure of 4-IPhNH$_3$H$_2$PO$_4$ (**6**) with selected numbering scheme of the asymmetric unit and the packing scheme viewed down the *a* axis (b). Thermal ellipsoids are drawn at the 50% probability level. Hydrogen and halogen bonds are shown in dotted lines.

Table 3: Relevant covalent bond, hydrogen bond and halogen bond lengths and angles in **6**–**8**.

	C–X [Å] [X]	X···O [Å] [O] [**R**]*	C–X···O	D–H···O [D]	D–H···O [O]
4-IPhNH$_3$H$_2$PO$_4$, **6**	1.892 [I1]	3.262 [O12] [0.93]	159.5°	2.930 Å [N8]	165.8° [O10]
				2.860 Å [N8]	173.9° [O10]
				2.707 Å [N8]	173.7° [O13]
				2.598 Å [O11]	155.6° [O10]
				2.533 Å [O12]	160.3° [O13]
4-BrPhNH$_3$H$_2$PO$_4$, **7** (UGISEI, [40])	1.902 [Br1]	3.348 [O1] [0.99]	157.2°	2.951 Å	
				2.873 Å	
				2.701 Å	
				2.582 Å	
				2.540 Å	
4-ClPhNH$_3$H$_2$PO$_4$, **8**	1.742 [Cl1]	3.260 [O2] [1.00]	156.9°	2.920 Å [N8]	164.7° [O10]
				2.844 Å [N8]	175.4° [O10]
				2.678 Å [N8]	174.7° [O13]
				2.590 Å [O11]	161.4° [O10]
				2.534 Å [O12]	158.8° [O13]

* **R** = $d/(r_X + r_D)$, see Equation 1. D represents the hydrogen bond donor atom.

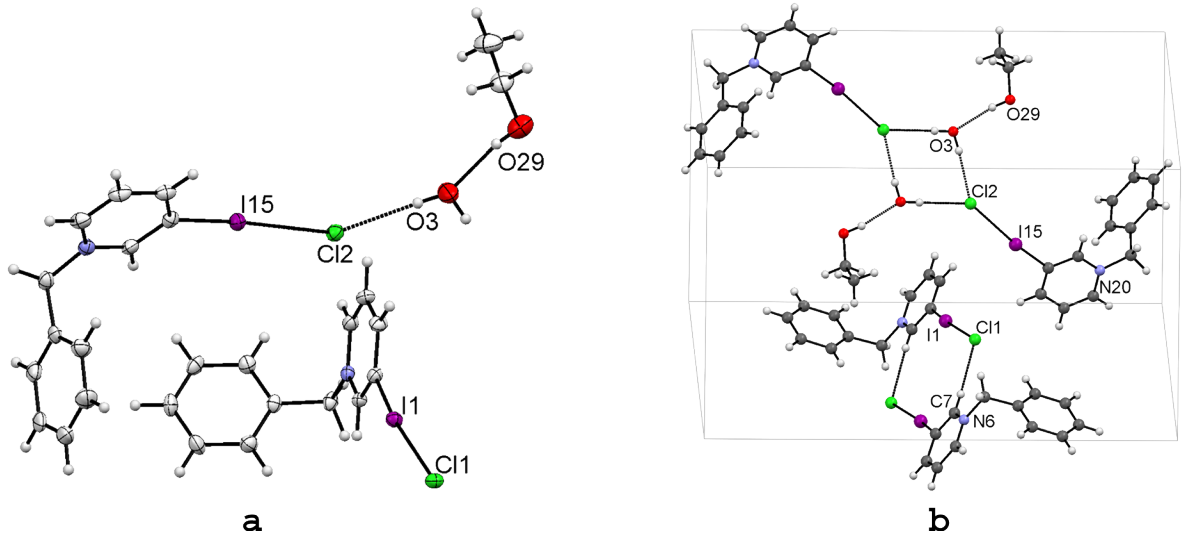

Figure 5: X-ray structure of 3-IPyBnCl (**9**) with the selected numbering scheme of the asymmetric unit (a) and selected packing scheme viewed down the *a* axis (b). Thermal ellipsoids are drawn at the 50% probability level. Hydrogen and halogen bonds are shown in dotted lines.

where). Slow evaporation of a moist ethanol solution gave an X-ray-quality crystal of **9**. The asymmetric unit contains two molecules of *N*-benzyl-3-iodopyridinium chloride, a water molecule and an ethanol solvent molecule (Figure 5a). The electron withdrawing effect of *N*-benzylpyridinium cation gives rise to short halogen bonds, where the **R** = 0.83 and **R** = 0.85 for I1···Cl1 and I15···Cl2, respectively (Table 4). The short halogen bond distances are consistent with the linearity of C–I1···Cl1 and C–I15···Cl2 angles [174.1(1)° and 174.6(1)°, respectively].

Since the alkylation on the N atom prevents any hydrogen bond interactions with pyridine, the packing is predominantly driven by halogen bonds. As shown in Figure 5b, two independent and structurally different interaction motifs are present in the crystal lattice. The first is a dimeric motif with two symmetry equivalent *N*-benzyl-3-iodopyridinium chloride moieties coordinating through XB and weak HB, C–I1···$Cl1^-$···H–C7, interactions (Figure 5b, below). In the other motif (Figure 5b, top), the chlorine anion coordinates the pyridinium ions and water with XB, C–I15···$Cl2^-$, and HB, $Cl2^-$···H–O3, interactions. The water molecule [O3] bridges the chloride [Cl2] anions creating a parallelogram-shaped hydrogen bonded dimer. In addition, O3 forms another hydrogen bond with a solvent ethanol molecule. Interestingly, of the two independent halogen bonds (C–I1···Cl1 and C–I15···Cl2), the latter displays a slightly longer contact distance (Table 4), and this is due to the involvement the chloride atom in a second interaction, a hydrogen bond with a water molecule, which consequently weakens its I15···Cl2 interaction.

Table 4: Relevant covalent bond, hydrogen bond and halogen bond lengths and angles in **9**–**12**.

	C–X [Å] [X]	X···Cl^- [Å] [Cl^-] [**R**]*	C–X···Cl^-	Cl^-···H–N [Å]	N–H···Cl^-
3-IPyBnCl, **9**	2.101 [I1]	3.151 [Cl1] [0.83]	174.1°	–	–
	2.099 [I15]	3.223 [Cl2] [0.85]	174.6°	–	–
3-IPyHCl, **10**	2.096 [I1]	3.189 [Cl1] [0.84]	174.3°	3.035	163.0°
	2.114 [I8]	3.170 [Cl4] [0.84]	179.7°	3.058	146.0°
	2.105 [I15]	3.141 [Cl1] [0.83]	177.3°	3.044	149.4°
	2.096 [I22]	3.227 [Cl4] [0.85]	173.8°	3.024	164.9°
3-BrPyHCl, **11** (CIHBAX [41])	1.890 [Br1]	3.359 [Cl1] [0.89]	162.2°	2.995	152.9°
3-ClPyHCl, **12** (VOQMUJ [42])	1.727 [Cl1]	3.479 [Cl2] [0.92]	156.1°	2.993	169.4°

* **R** = $d/(r_X + r_D)$, see Equation 1.

Halogen and hydrogen bonding in 3-IPyHCl (10) 3-BrPyHCl (11) and 3-ClPyHCl (12)

As in all above studied salts **1**–**9**, similar type X···Cl interactions are also possible in 3-iodo-, 3-bromo- and 3-chloropyridinium chlorides (**10**–**12**). However, as the pyridinium cation is obtained by protonation of the pyridine nitrogen, the very strong hydrogen bond donor [N^+–H···] moiety is envisaged to disrupt or severely hinder the strong halogen bonding interactions manifested in the non-HB pyridinium salt **9**. Slow diffusion of ethyl acetate into the ethanol solution of 3-iodopyridinium chloride gave an X-ray-quality crystal of **10**. The asymmetric unit contains four molecules of 3-iodopyridinium chloride and one molecule solvent ethanol (Figure 6a). As in 3-IPyBnCl (**9**), the electron withdrawing effect of pyridinium cation in **10** gives rise to four short C–I···Cl^- halogen bonds, from which the shortest, in I15···Cl1, **R** = 0.83, is the same as in the non-HB salt **9**. The XB distances and angles are very similar as in **9** (Table 4), thus halogen bonding is not weakened even the presence of strong charge-assisted hydrogen bond, N^+–H···Cl^-. This can be explained by the segregation of the XB and HB interactions. In fact, two of the four chloride anions [Cl1 and Cl4] are engaged only with the halogen bonding (one of them in addition of O29–H···Cl4 [3.213 Å, 173.7°] interaction to the solvent ethanol) while the others [Cl2 and Cl3] only in the change-assisted hydrogen bonding (Figure 6a).

The asymmetric unit thus forms a XB and HB assisted cyclic structure, where two of Cl^- anions are bonded between the four iodine donors by forming nearly linear I1···Cl1···I15 (~175°) and I8···Cl4···I22 (~172°) halogen bonds. Two remaining Cl^- anions are hydrogen bonded through N13–H···Cl2···H–N6 (~102°) and N18–H···Cl3···H–N25 (~103°) interactions.

In crystal lattice these structures forms planar layers, which are packed on top of each other as in Figure 6b shows. Additional information about the relative strength of the halogen bonding in halopyridinium halides was evaluated by analysing the corresponding bromide and chloride salts. Substituting iodine with bromine or chlorine, reducing the polarizability of halogen substituent, was envisaged to show a gradual elongation of X···Cl^- contact distance [24-26]. Thus the structures 3-IPyBnCl (**9**) and 3-IPyHCl (**10**) were compared with the previously published 3-BrPyHCl (**11**, CIHBAX) [41] and 3-ClPyHCl (**12**, VOQMUJ) [42]. Relevant covalent bond, hydrogen bond and halogen bond lengths and angles are depicted in Table 4.

The salts 3-IPyHCl (**10**), 3-BrPyHCl (**11**) and 3-ClPyHCl (**12**) form a series of halopyridinium chlorides where only the size and polarizability of the halogen atom differ. The charge-assisted hydrogen bond network remains the same, but the halogen bond interaction strength should vary. Surprisingly, the X-ray structures of **10**–**12** are not polymorphs, in contrast what would be predicted from the series of haloanilinium chlorides (**2**, **3**) or haloanilinium dihydrogenphosphates (**6**, **7** and **8**). The salts **11** and **12** crystallize in a triclinic space group *P*-1 and unit cell volumes are nearly equal, but the cell parameters are clearly different, viz. a = 5.7350(6) Å, b = 7.1716(6), c = 8.4760(8) Å, α = 73.365(6)°, β = 77.773(6)°, γ = 83.912(6)° for **11** and a = 4.7691(10) Å, b = 7. 744(2) Å, c = 9.153(2) Å, α = 84.26(3)°, β = 76.91(3)°, γ = 86.06(3)° for **12**, thus these are isostructural. Hydrogen bond lengths and angles are comparable and therefore the differences in the cell parameters could be explained by differences in halogen bond distances, angles and the size of the halogen atom (Table 4).

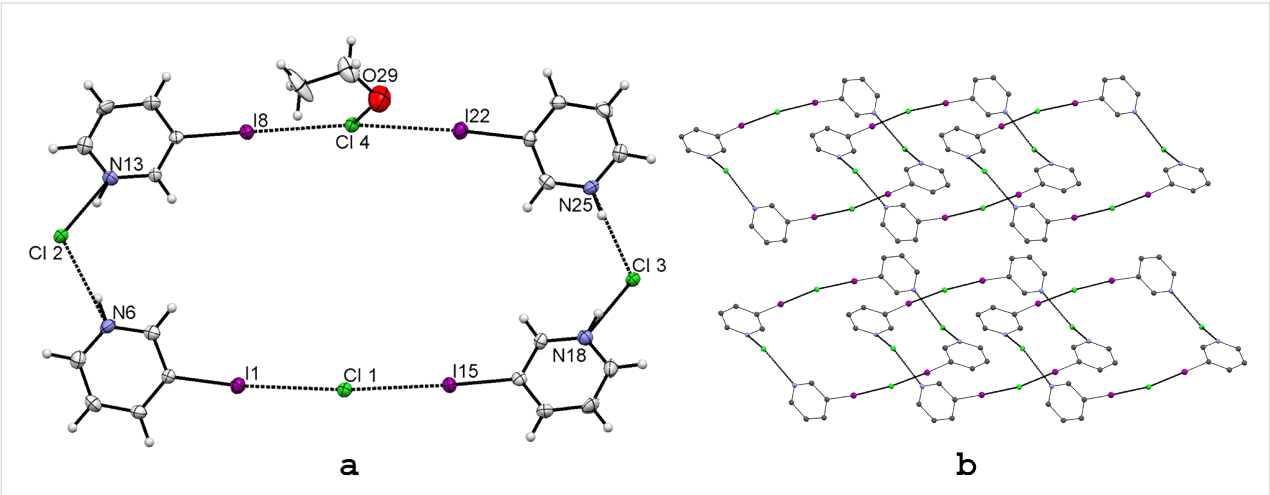

Figure 6: X-ray structure of 3-IPyHCl (**10**) with the selected numbering scheme of the asymmetric unit (a) and packing scheme viewed down the crystallographic *c* axis (b). Thermal ellipsoids are drawn at the 50% probability level. Hydrogen and halogen bonds are shown in dotted lines.

Halogen and hydrogen bonding in 3-IPyH-5-NIPA (13)

To compare the spherical and tetrahedral anions with varying HB strength to a planar strong HB anion, we selected 5-nitroisophthalic acid as a strong planar HB donor and studied its effect on the XB interactions. The 5-nitroisophthalate differs from halides by providing two hydrogen bond donors with different HB strength, thus the ratio [D^+–H···] : [C–I···] interaction sites in **13** is 2 : 1. In addition to the disturbance in the HB interactions, the nitro groups were expected to form competing halogen bond acceptor sites as demonstrated in our previous study on co-crystals of 1-iodo-3,5-dinitrobenzene and DABCO (1,4-diazabicyclo[2.2.2]octane) [33]. Thus, we prepared X-ray quality crystals of **13** from an ethyl acetate solution of 3-iodopyridine and 5-nitroisophthalic acid in 2 : 1 molar ratio. Despite the stoichiometry employed in the crystallization experiments only 1 : 1 salts was obtained (Figure 7). A strong halogen bond is formed between the iodine atom and one of the carboxylate's oxygens, **R** = 0.86 for I1···O8 XB distance. The planar 5-nitroisophthalate anion as a bridging moiety shows in addition to strong HB and moderately strong XB also C–H···O hydrogen bonds (Figure 7b).

Conclusion

Among the haloanilinium salts **1**–**5** the C–I···Cl^- type halogen bonding occurred only in **1**, where despite the presence of three strong N–H···Cl^- hydrogen bonds, it had a significant effect on the observed supramolecular architecture. The gradual diminishing of the C–X···Cl^- interaction upon changing the identity of the halogen substituent caused clearly visible changes to occur. The absence of halogen bonding contribution in structures **2** and **3** rendered them isomorphic, while the fluorine analogue **4** had a completely different structure with weak C–F···H interactions. The corresponding bromide **5** had remarkable similarities with the chloride **1** in the charge-assisted hydrogen bonding network, yet due to the weaker halogen bonding its role in the intermolecular interactions was not easily established. The occurrence of strong hydrogen bonding, as in the isomorphic haloanilinium dihydrogenphosphates **6**–**8**, limits the role of the halogen bond, which in these cases does not affect the supramolecular architecture. From these examples it seems apparent that only a strong type of halogen bond could successfully compete with strong hydrogen bonds. This is confirmed by the halopyridinium salts **9**–**13** which clearly represented the strongest halogen bonding in the studied series. While *N*-benzyl-3-iodopyridinium chloride (**9**) can be considered as a reference system where only halogen bonded existed, structures **10**–**13** manifested supramolecular architectures where simultaneous strong halogen and hydrogen bonding co-existed. They display interesting structural and crystal lattice variations from cyclic to planar XB–HB sheet structure in **13**, showing that the balance between HB and XB interactions indeed determines the solid state architectures in these systems.

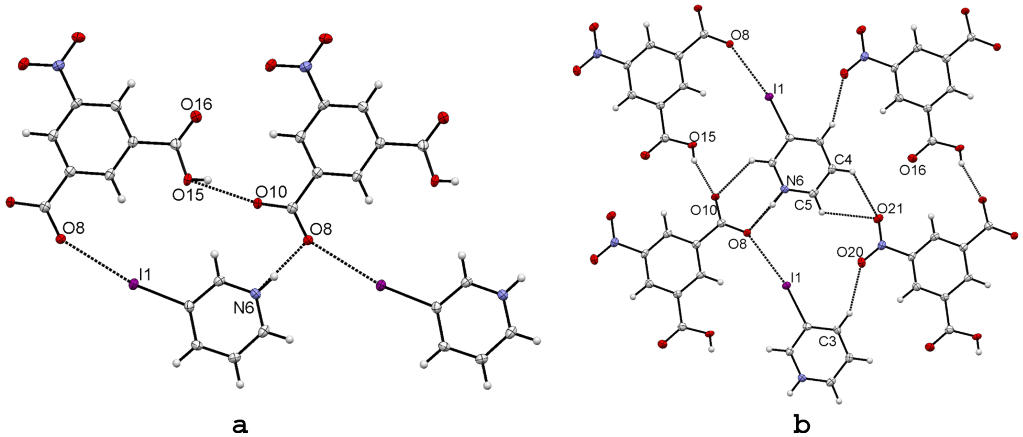

Figure 7: X-ray structure of 3-IPyH-5-NIPA (**13**) with selected numbering scheme of the asymmetric unit (a). A selected part of the packing is shown on (b). Thermal ellipsoids are drawn at the 50% probability level. Hydrogen and halogen bonds are shown in dotted lines. The contact distances and angles are; [I1···O8] 2.999(2) Å and 170.0(1)°, [N6–H···O8 $x_{1,\ y+1,\ z}$] 2.625(3) Å and 175(3)°, [O15–H···O10] 2.586(2) Å and 154(4)°.

Supporting Information

Supporting Information File 1

Experimental procedures and crystallographic data tables
[http://www.beilstein-journals.org/bjoc/content/supplementary/1860-5397-6-4-S1.pdf]

Supporting Information File 2

CIF data for compounds **1**, **5**, **6**, **8**, **9**, **10** and **13**
[http://www.beilstein-journals.org/bjoc/content/supplementary/1860-5397-6-4-S2.cif]

Acknowledgements

The authors gratefully acknowledge the Academy of Finland (KRi: proj. no. 212588) and The National Graduate School of Organic Chemistry and Chemical Biology (KRa) for financial support.

References

1. Lehn, J.-M. *Supramolecular Chemistry: Concepts and Perspectives;* VCH: Weinheim, 1995.
2. Metrangolo, P.; Resnati, G. *Science* **2008,** *321,* 918–919. doi:10.1126/science.1162215
3. Rissanen, K. *CrystEngComm* **2008,** *10,* 1107–1113. doi:10.1039/b803329n
4. Bent, H. A. *Chem. Rev.* **1968,** *68,* 587–648. doi:10.1021/cr60255a003
5. Murray-Rust, P.; Motherwell, W. D. S. *J. Am. Chem. Soc.* **1979,** *101,* 4374–4376. doi:10.1021/ja00509a056
6. Ramasubbu, N.; Parthasarathy, R.; Murray-Rust, P. *J. Am. Chem. Soc.* **1986,** *108,* 4308–4314. doi:10.1021/ja00275a012
7. Lommerse, J. P. M.; Stone, A. J.; Taylor, R.; Allen, F. H. *J. Am. Chem. Soc.* **1996,** *118,* 3108–3116. doi:10.1021/ja953281x
8. Wang, W.; Hobza, P. *J. Phys. Chem. A* **2008,** *112,* 4114–4119. doi:10.1021/jp710992h
9. Zou, J.-W.; Jiang, Y.-J.; Guo, M.; Hu, G.-X.; Zhang, B.; Liu, H.-C.; Yu, Q. S. *Chem.–Eur. J.* **2005,** *11,* 740–751. doi:10.1002/chem.200400504
10. Ananthavel, S. P.; Manoharan, M. *Chem. Phys.* **2001,** *269,* 49–57. doi:10.1016/S0301-0104(01)00363-9
11. Amico, V.; Meille, S. V.; Corradi, E.; Messina, M. T.; Resnati, G. *J. Am. Chem. Soc.* **1998,** *120,* 8261–8262. doi:10.1021/ja9810686
12. Metrangolo, P.; Resnati, G. *Chem.–Eur. J.* **2001,** *7,* 2511–2519. doi:10.1002/1521-3765(20010618)7:12<2511::AID-CHEM25110>3.0.CO;2-T
13. Walsh, R. B.; Padgett, C. W.; Metrangolo, P.; Resnati, G.; Hanks, T. W.; Pennington, W. T. *Cryst. Growth Des.* **2001,** *1,* 165–175. doi:10.1021/cg005540m
14. Cardillo, P.; Corradi, E.; Lunghi, A.; Meille, S. V.; Messina, M. T.; Metrangolo, P.; Resnati, G. *Tetrahedron* **2000,** *56,* 5535–5550. doi:10.1016/S0040-4020(00)00476-2
15. Corradi, E.; Meille, S. V.; Messina, M. T.; Metrangolo, P.; Resnati, G. *Angew. Chem.* **2000,** *112,* 1852–1856. doi:10.1002/(SICI)1521-3757(20000515)112:10<1852::AID-ANGE1852>3.0.CO;2-7
Angew. Chem., Int. Ed. **2000**, *39*, 1782–1786. doi:10.1002/(SICI)1521-3773(20000515)39:10<1782::AID-ANIE1782>3.0.CO;2-5
16. Corradi, E.; Meille, S. V.; Messina, M. T.; Metrangolo, P.; Resnati, G. *Tetrahedron Lett.* **1999,** *40,* 7519–7523. doi:10.1016/S0040-4039(99)01479-3
17. Bondi, A. *J. Phys. Chem.* **1964,** *68,* 441–451. doi:10.1021/j100785a001
18. Metrangolo, P.; Neukirch, H.; Pilati, T.; Resnati, G. *Acc. Chem. Res.* **2005,** *38,* 386–395. doi:10.1021/ar0400995
19. Raatikainen, K.; Huuskonen, J.; Lahtinen, M.; Metrangolo, P.; Rissanen, K. *Chem. Commun.* **2009,** 2160–2162. doi:10.1039/b901473j
20. Metrangolo, P.; Carcenac, Y.; Lahtinen, M.; Pilati, T.; Rissanen, K.; Vij, A.; Resnati, G. *Science* **2009,** *323,* 1461–1464. doi:10.1126/science.1168679
21. Fourmigué, M. *Curr. Opin. Solid State Mater. Sci.* **2009,** *13,* 36–45. doi:10.1016/j.cossms.2009.05.001
22. Lu, Y.; Shi, T.; Wang, Y.; Yang, H.; Yan, X.; Luo, X.; Jiang, H.; Zhu, W. *J. Med. Chem.* **2009,** *52,* 2854–2862. doi:10.1021/jm9000133
23. Metrangolo, P.; Pilati, T.; Resnati, G. *CrystEngComm* **2006,** *8,* 946–947. doi:10.1039/b610454a
24. Politzer, P.; Lane, P.; Concha, M. C.; Ma, Y.; Murray, J. S. *J. Mol. Model.* **2007,** *13,* 305–311. doi:10.1007/s00894-006-0154-7
25. Clark, T.; Hennemann, M.; Murray, J. S.; Politzer, P. *J. Mol. Model.* **2007,** *13,* 291–296. doi:10.1007/s00894-006-0130-2
26. Awwadi, F. F.; Willett, R. D.; Peterson, K. A.; Twamley, B. *Chem.–Eur. J.* **2006,** *12,* 8952–8960. doi:10.1002/chem.200600523
27. Bouchmella, K.; Boury, B.; Dutremez, S. G.; van der Lee, A. *Chem.–Eur. J.* **2007,** *13,* 6130–6138. doi:10.1002/chem.200601508
28. Sun, A.; Lauher, J. W.; Goroff, N. S. *Science* **2006,** *312,* 1030–1034. doi:10.1126/science.1124621
29. Saha, B. K.; Nangia, A.; Jaskólski, M. *CrystEngComm* **2005,** *7,* 355–358. doi:10.1039/b501693b
30. Allen, F. H.; Goud, B. S.; Hoy, V. J.; Howard, J. A. K.; Desiraju, G. R. *J. Chem. Soc., Chem. Commun.* **1994,** *23,* 2729–2730. doi:10.1039/C39940002729
31. Thaimattam, R.; Sharma, C. V. K.; Clearfield, A.; Desiraju, G. R. *Cryst. Growth Des.* **2001,** *1,* 103–106. doi:10.1021/cg010286z
32. Weiss, R.; Schwab, O.; Hampel, F. *Chem.–Eur. J.* **1999,** *5,* 968–974. doi:10.1002/(SICI)1521-3765(19990301)5:3<968::AID-CHEM968>3.0.CO;2-L
33. Raatikainen, K.; Rissanen, K. *CrystEngComm* **2009,** *11,* 750–752. doi:10.1039/b821085n
34. Valerio, G.; Raos, G.; Meille, S. V.; Metrangolo, P.; Resnati, G. *J. Phys. Chem. A* **2000,** *104,* 1617–1620. doi:10.1021/jp993415j
35. Mínguez Espallargas, M. G.; Zordan, F.; Arroyo Marín, L.; Adams, H.; Shankland, K.; van de Streek, J.; Brammer, L. *Chem.–Eur. J.* **2009,** *15,* 7554–7568. doi:10.1002/chem.200900410
36. Aakeröy, C. B.; Fasulo, M.; Schultheiss, N.; Desper, J.; Moore, C. *J. Am. Chem. Soc.* **2007,** *129,* 13772–13773. doi:10.1021/ja073201c
37. Portalone, G. *Acta Crystallogr., Sect. E* **2005,** *61,* o3083–o3085. doi:10.1107/S160053680502595X
38. Ploug-Sørensen, G.; Andersen, E. K. *Acta Crystallogr., Sect. C* **1985,** *41,* 613–615. doi:10.1107/S0108270185004838

39. Colapietro, M.; Domenicano, A.; Marciante, C.; Portalone, G. *Acta Crystallogr., Sect. B* **1981,** *37,* 387–394. doi:10.1107/S0567740881003075
40. Zhang, B.-G.; Gou, S.-H.; Duan, C.-Y.; You, X.-Z. *Wuhan Daxue Xuebao, Ziran Kexueban* **2001,** *47,* 425–427.
41. Awwadi, F. F.; Willett, R. D.; Peterson, K. A.; Twamley, B. *J. Phys. Chem. A* **2007,** *111,* 2319–2328. doi:10.1021/jp0660684
42. Freytag, M.; Jones, P. G. *Z. Naturforsch., B: Chem. Sci.* **2001,** *56,* 889–896.
43. *Cambridge Structural Database,* version 5.30, the Feb 2009 update; The Cambridge Crystallographic Data Centre: Cambridge, UK, 2009.
44. Shannon, R. D. *Acta Crystallogr., Sect. A* **1976,** *32,* 751–767. doi:10.1107/S0567739476001551
45. Kuhn, N.; Abu-Rayyan, A.; Eichele, K.; Schwarz, S.; Steimann, M. *Inorg. Chim. Acta* **2004,** *357,* 1799–1804. doi:10.1016/j.ica.2003.10.038
46. Logothetis, T. A.; Meyer, F.; Metrangolo, P.; Pilati, T.; Resnati, G. *New J. Chem.* **2004,** *28,* 760–763. doi:10.1039/b401421a
47. Freytag, M.; Jones, P. G.; Ahrens, B.; Fischer, A. K. *New J. Chem.* **1999,** *23,* 1137–1139. doi:10.1039/a906356k

License and Terms

Beilstein Journal of Organic Chemistry

Synthesis and binding studies of two new macrocyclic receptors for the stereoselective recognition of dipeptides

Ana Maria Castilla[1], M. Morgan Conn[2,3] and Pablo Ballester[*1,4]

Full Research Paper

Open Access

Address:
[1]Institute of Chemical Research of Catalonia (ICIQ), Avgda. Països Catalans 16, 43007 Tarragona, Spain, [2]Amherst College, Amherst, MA 01002, USA, [3]now at PTC Therapeutics, Inc., 100 Corporate Court, South Plainfield, NJ 07080, USA and [4]Catalan Institution for Research and Advanced Studies (ICREA), Passeig Lluís Companys, 23, 08018 Barcelona, Spain

Email:
Pablo Ballester[*] - pballester@iciq.es

* Corresponding author

Keywords:
dipeptides; host–guest; macrocyclic; molecular recognition; receptors; stereoselective

Beilstein Journal of Organic Chemistry **2010,** *6,* No. 5.
doi:10.3762/bjoc.6.5

Received: 22 September 2009
Accepted: 06 January 2010
Published: 19 January 2010

Guest Editor: C. A. Schalley

Abstract

We present here the design, synthesis, and analysis of a series of receptors for peptide ligands inspired by the hydrogen-bonding pattern of protein β-sheets. The receptors themselves can be regarded as strands 1 and 3 of a three-stranded β-sheet, with cross-linking between the chains through the 4-position of adjacent phenylalanine residues. We also report on the conformational equilibria of these receptors in solution as well as on their tendency to dimerize. ^{1}H NMR titration experiments are used to quantify the dimerization constants, as well as the association constant values of the 1:1 complexes formed between the receptors and a series of diamides and dipeptides. The receptors show moderate levels of selectivity in the molecular recognition of the hydrogen-bonding pattern present in the diamide series, selecting the α-amino acid-related hydrogen-bonding functionality. Only one of the two cyclic receptors shows modest signs of enantioselectivity and moderate diastereoselectivity in the recognition of the enantiomers and diastereoisomers of the Ala-Ala dipeptide ($\Delta\Delta G^0_1$ (DD-DL) = −1.08 kcal/mol and $\Delta\Delta G^0_1$ (DD-LD) = −0.89 kcal/mol). Surprisingly, the linear synthetic precursors show higher levels of stereoselectivity than their cyclic counterparts.

Introduction

Manipulation of protein–protein interactions is gaining interest as they are known to play a critical role in important biological processes such as the normal function of cellular/organelle structure, immune response, enzyme inhibitors, signal transduction, and apoptosis. Rational protein surface recognition poses a challenging test to our actual knowledge of molecular design. Nevertheless, its practice and developments will provide a better understanding of protein–protein interactions. Interest-

ingly, in molecule-based disease therapy, the disruption of protein–protein interactions by small molecules constitutes an alternative approach to the classical active-site enzyme inhibition design. One of the strategies employed for binding protein surfaces relies on the use of arrays of synthetic receptors originally designed for the recognition of oligopeptides. Consequently, the selective recognition of oligopeptides represents an intermediate step toward the recognition of protein surfaces [1]. The studies of host–guest complexes as model systems of peptide–peptide interactions are of particular interest because they may provide insight into the structural basis of the high size/shape specificities and enantioselectivities exhibited by the complex protein–protein recognition processes that occur in biology. Moreover, short oligopeptides are themselves worthwhile targets for recognition and their conformational flexibility represents an added challenge to achieve selective binding. The preparation of synthetic receptors for the selective binding of short oligopeptides has potential applications in the development of diagnostic sensors, separation techniques, and therapeutic agents.

With respect to this latter point, there is a significant interest in the advance of receptors that selectively bind the D-Ala-D-Ala dipeptide, the common target for the vancomycin antibiotics. This group of antibiotics is active against certain aerobic and anaerobic Gram-positive bacteria, and has been used for many years as treatment of last resort in clinical wards [2-4]. However, vancomycin resistance has recently been identified among clinical isolates of several Gram-positive species [5-8]. Therefore, although many examples already exist in the literature [9,10], the design and synthesis of new synthetic receptors for this dipeptide is still a relevant endeavor not only in terms of understanding the interactions that take place during vancomycin action, but also because the structures of the most efficient receptors prepared might be useful as scaffolds for future antibiotics.

Herein, we report the design and synthesis of two new macrocyclic receptors, **1** and **2**, conceived for the binding of dipeptides, in particular for the selective recognition of D-Ala-D-Ala. We also report on the studies performed using these two macrocyclic receptors, as well as their linear precursors, in the molecular recognition of a series of dipeptides and diamides with diverse hydrogen-bonding patterns. We rationalize the observed modulation of their binding affinity as a function of the hydrogen-bonding pattern exhibited by the target molecule. We also describe the levels of stereoselectivity displayed by these receptors in the recognition of the diastereoisomers and enantioisomers of Ala-Ala dipeptide. We explain the differences observed in their binding abilities as a function of conformational rigidity (macrocyclic vs linear receptors).

Results and Discussion

Design of the synthetic receptors: general considerations

The design of the receptors described in this article is based on the interactions that occur in the β-sheets commonly found in the secondary structure of many biologically relevant proteins. We start from a schematic termolecular complex mimicking a three-stranded β-sheet in which the central strand corresponds to the target guest peptide and the two outer strands constitute the structure of the host (Figure 1). In this design, we employ some of the properties of the β-sheet structure – the convergence of hydrogen-bonding patterns and the presence of exposed side chains. It is worth mentioning that the β-sheet structure has already been used as the inspirational binding motif for the preparation of other synthetic receptors for peptides [11-16]. However, we believe that our design includes

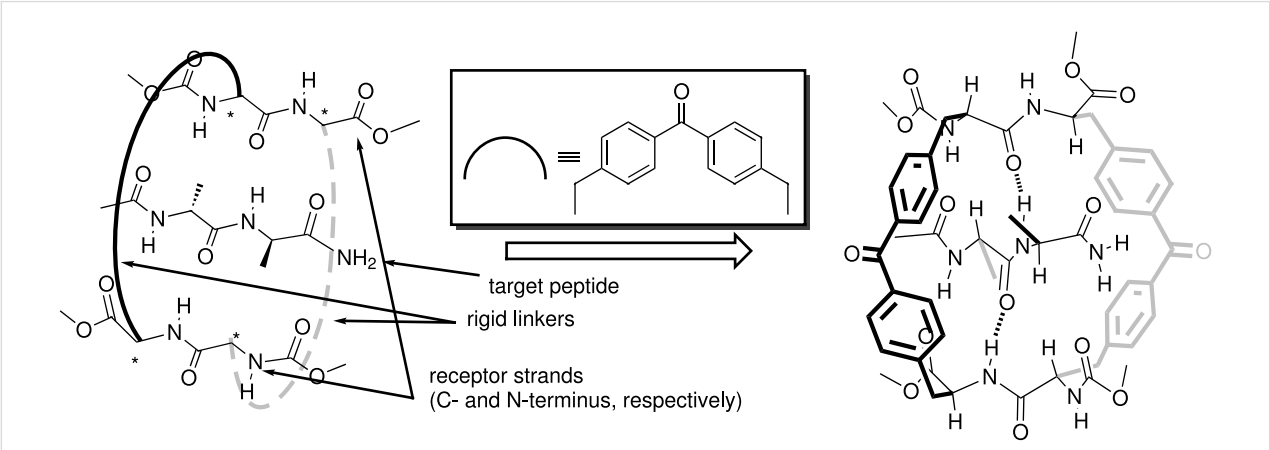

Figure 1: Schematic representation of the design of a host–guest complex based on antiparallel β-sheet geometry. *The presence of a stereogenic center.

some novelties. To reduce the conformational flexibility and confer a certain degree of preorganization to this type of receptor, the use of one or two linkers connecting the two peptide strands is mandatory. The principal difference with respect to previous designs of β-sheet-based synthetic receptors is that the connection between the two peptide strands, used as the receptor's binding sites, emerges from their side chains and not from their C- or N-terminus. In our final design, we propose the introduction of two linkers connecting the two peptide strands affording, a macrocyclic structure. In doing so, we expect that the molecular recognition properties of the designed receptor will also benefit from the *macrocyclic effect* [17-20]. Simple molecular modeling studies [21] revealed that a benzophenone unit would be ideally suited to span the gap between two methyl side chains emerging from alanyl residues of the outer strands in the three-stranded β-sheet complex (Figure 1).

In proteins, adjacent β-strands can form hydrogen bonds in antiparallel, parallel, or mixed arrangements. In an antiparallel arrangement, the successive β-strands alternate directions so that the N-termini of two adjacent strands are at opposite ends. In a parallel arrangement, all of the N-termini of successive strands are oriented in the same direction [22]. In contrast, successive strands in a mixed-mode arrangement may be parallel or antiparallel to each other. To examine the influence of the relative orientation of the two receptor strands on their binding abilities, we conceived and synthesized two analogous receptors mimicking these two types of arrangements present in the β-sheet structure (Figure 2). The outer peptide strands of receptor **1** are arranged antiparallel to each other ("antiparallel receptor"). That is, the stereogenic center of the C-terminus of one strand is covalently connected to the stereogenic center of the N-terminus of the other strand. Receptor **1** is anticipated to form a mixed-mode sheet structure with an included peptide ligand. Conversely, the two outer strands of receptor **2** are oriented parallel to each other ("parallel receptor"), such that the covalent connections between strands join similar stereogenic centers, C-terminus with C-terminus and N-terminus with

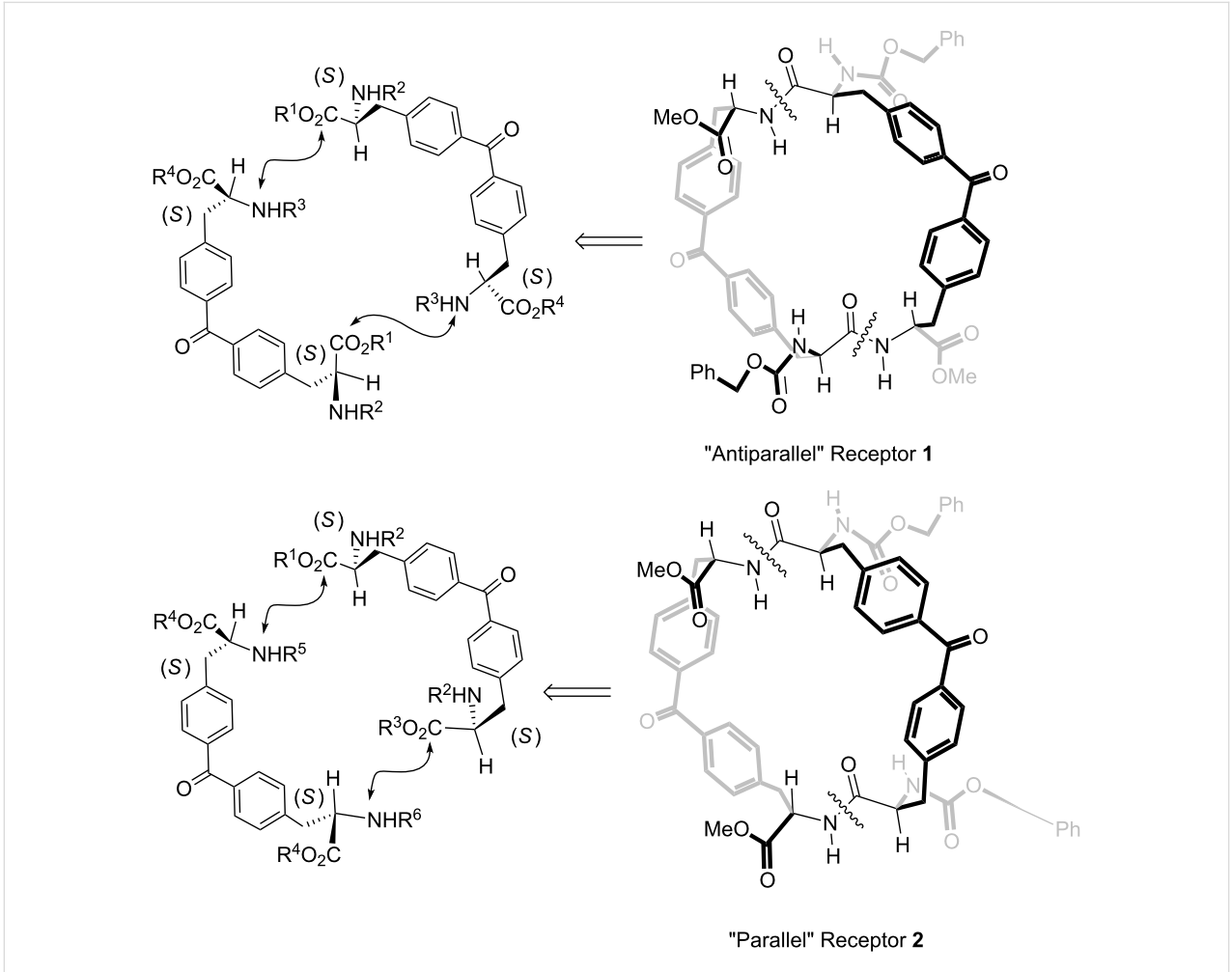

Figure 2: Molecular structures of the two designed receptors **1** and **2** having different relative orientations of the peptide strands.

N-terminus. Receptor **2** is anticipated to form an antiparallel sheet structure with the included peptide ligand. This change in connectivity does not involve any inversion of the stereogenic centers but only a modification in the sequence of peptide-coupling reactions that yield the cyclic structure, and will be explained below.

The exploration of the conformational space of both macrocycles, using molecular modeling, indicated the existence of a built-in cavity. These studies also suggested that the reduced conformational flexibility of the receptors avoids the complete collapse of the cavity through the formation of intramolecular hydrogen bonds. Moreover, we were able to minimize structures for the complexes formed between both receptors and *n*-C_6H_{13}CO-D-Ala-D-Ala-NH_2 in which the dipeptide is threaded through the macrocycle (Figure 3). In these minimized structures, the hydrogen-bonding groups of the receptor converge toward the center of the macrocycle. The macrocycle is large enough to accommodate the threading dipeptide without incurring any substantial steric clashes. We also observed appropriate complementarity between the hydrogen-bonding groups of substrate and receptor (Figure 3). The analysis of the structures of the minimized complexes revealed that they are stabilized by the formation of the same number of hydrogen bonds, that is, five. The hypothesized "*endo*" structure for the complexes of **1** and **2** with *n*-C_6H_{13}CO-D-Ala-D-Ala-NH_2, in which the ligands thread through the receptor's macrocycle, also allows for the possibility of binding short amino acid sequences not necessarily located on the edges of larger peptides.

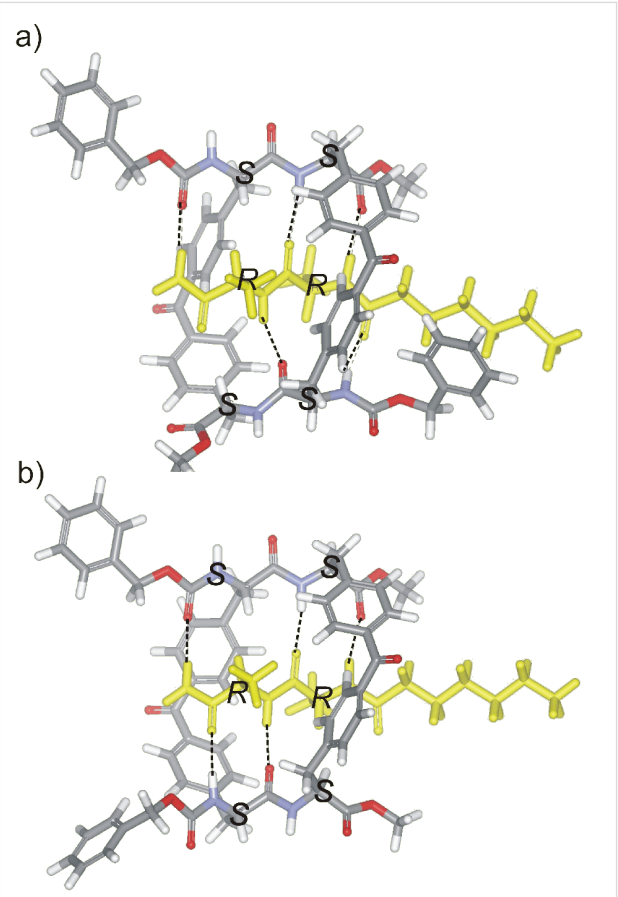

Figure 3: CAChe minimized structures for the "*endo*" complexes formed between receptors **1** (a) and **2** (b) and the *n*-C_6H_{13}CO-D-Ala-D-Ala-NH_2 dipeptide. The absolute configuration of the stereogenic centers are indicated with a capital letter. Five intermolecular hydrogen bonds are also shown as black dashed lines.

Other considerations, apart from preventing intramolecular hydrogen bond formation, related to the use of bis(alanyl)benzophenone rigid linkers include: a) to avoid steric clashes between the methyl groups of the target peptide and the benzophenone linking chains, the stereogenic centers in the linkers must have the (*S*) configuration, opposite to that of the bound peptide (*R*); b) the benzophenone aromatic ring will also provide a hydrophobic pocket for the neighboring side chains of the target peptide, and may promote the formation of additional CH–π and π–π intermolecular interactions. The pleat of the bound D-Ala-D-Ala peptide is inverted because of the unnatural stereochemistry and the resulting complex is not exactly a β-sheet. Attaching the linking groups in the side chains leaves the ends of the receptor strands open, allowing the introduction of additional interactions between the receptor and the chain of a larger peptide.

As schematically depicted in Figure 2, we planned that both receptors could be obtained through cyclic dimerization, through the formation of two peptide bonds, of two *S*,*S*-bis(alanyl)benzophenone units **3**. In turn, the synthesis of the protected *S*,*S*-bis(alanyl)benzophenone units **3** could be easily achieved by means of Stille carbonylative cross-coupling reactions of two adequately bisprotected *S*-phenylalanine derivatives, iodo-aryl **4** and trimethylstannyl-aryl **5**, following experimental procedures described in recent literature reports [23].

Synthesis

The synthetic strategy designed for the construction of receptors **1** and **2** involves the use of a carbonylative cross-coupling reaction between two aryl derivatives (iodo-aryl **4** and trimethylstannyl-aryl **5**) to prepare 4,4'-bis(alanyl)benzophenones **3**, followed by macrocyclization of two molecular units of **3**. The macrocyclization reaction of two 4,4'-bis(alanyl)benzophenones **3** will be promoted by the sequential and regioselective formation of two peptide bonds between them, the first one through an intermolecular reaction and the second one intramolecularly, affording the desired macrocyclic structures **1** and **2**. The main dissimilarity between the two synthetic

strategies resides in the type of functional groups that each 4,4'-bis(alanyl)benzophenone **3** supplies to the macrocyclization reaction. Thus, for the synthesis of antiparallel receptor **1** each benzophenone unit will provide, in an alternative way, one carboxylic and one amino function to the final macrocyclic skeleton. Conversely, for the synthesis of antiparallel receptor **2**, one benzophenone unit will donate its two carboxylic acid functions while the other will participate with its two amino groups. To achieve the regioselective control demanded in the macrocyclization reactions, a precise selection of the orthogonal protecting groups to be included in the bis-amino acid functionalities of the benzophenone derivatives **3** is needed. The starting material for both synthetic routes is 4-iodo-L-phenylalanine (**6**). We prepared **6** in multigram scale starting from commercial L-phenylalanine (**7**) by following a described procedure [24] consisting in the iodination of **7** in acetic acid solution in the presence of I_2, $NaIO_3$, and sulfuric acid (Scheme 1). We obtained (*S*)-**6** in enantiomerically pure form in 50% yield. Since we plan to assemble the 4,4'-bis(alanyl)benzophenones **3** by a Stille carbonylative cross-coupling reaction, the required trimethylstannyl derivatives **5** should be easily prepared from adequately diprotected phenylalanine iodides **4** (Scheme 1).

The mild reaction conditions used in the carbonylative cross-coupling permit the use of common protecting groups of peptide synthesis [24]. This characteristic of the carbonylative cross-coupling reaction allowed us to achieve the differential protection of the two amino acid moieties present in the 4,4'-bis(alanyl)benzophenones **3** by protecting separately the functional groups in the reaction partners, **4** and **5**, before attempting the cross-coupling. We prepared a single orthogonally protected benzophenone **3a** for the synthesis of the antiparallel macrocycle **1**. In contrast, the synthesis of parallel receptor **2** called for the preparation of two differently protected bis(alanyl)benzophenone units, **3b** and **3c**. All iodo-phenyl derivatives **4** were prepared in high yields using standard procedures (Scheme 1). Thus, 4-iodo-L-phenylalanine **6** (I-Phe) was converted into the methyl ester hydrochloride by treatment with thionyl chloride in methanol followed by acylation of the amino group with *tert*-butyl dicarbonate to yield Boc-I-Phe-OMe, **4a**. Iodo-L-phenylalanine **6** was acylated under Schotten–Baumann conditions with benzyl chloroformate to obtain the N-protected amino acid Cbz-I-Phe. This compound was esterified with 2-(trimethylsilyl)ethanol using DCC as coupling agent, providing Cbz-I-Phe-TMSE, **4c**. In a different reaction, Cbz-I-Phe was treated with 4-nitrobenzyl bromide and triethylamine to afford Cbz-I-Phe-PNB, **4b** [25]. Finally, **6** was treated with Fmoc hydroxysuccinimide (Fmoc-OSu) [26-29] to obtain the Fmoc N-protected amino acid that was subsequently esterified with diazomethane affording Fmoc-I-Phe-OMe, **4d**.

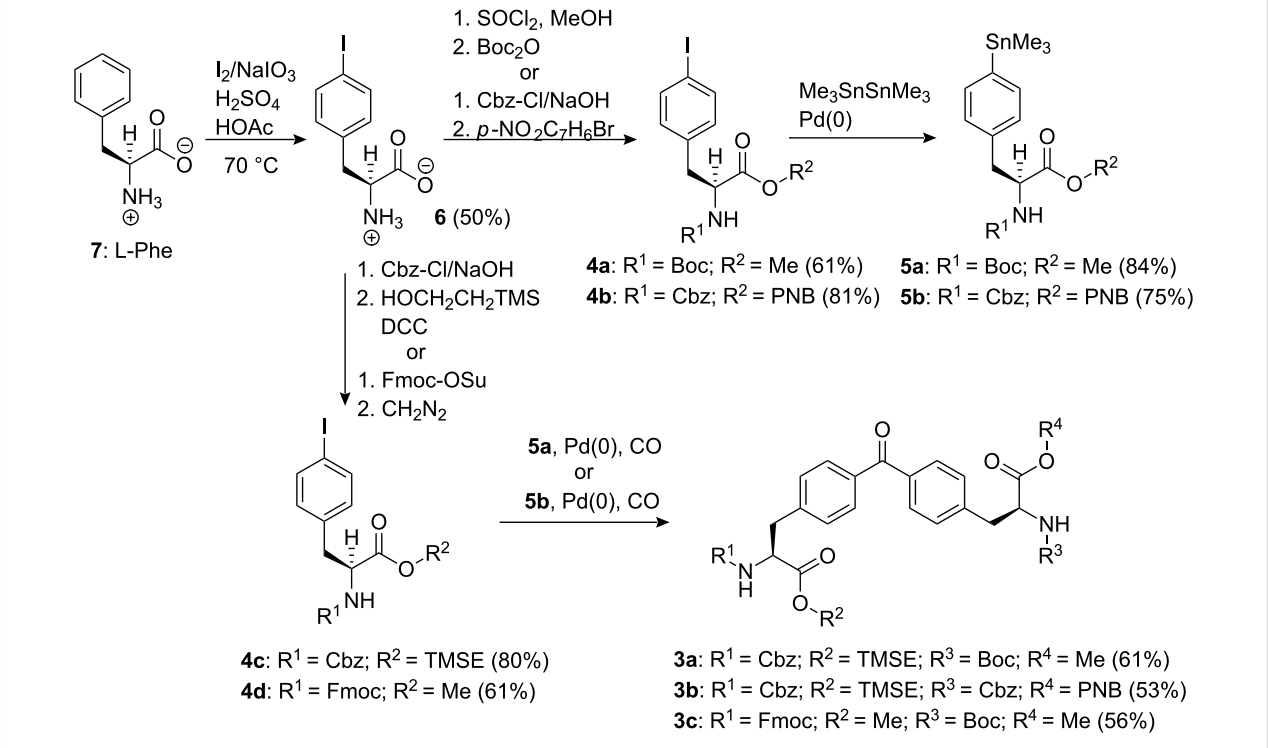

Scheme 1: Synthesis of tetraprotected bis(alanyl)benzophenones **3** from L-phenylalanine **7**.

The diprotected aryl iodides, **4a** and **4b**, were converted uneventfully to the corresponding diprotected aryl trimethylstannane derivatives, **5a** and **5b**, by reaction with hexamethylditin catalyzed by Pd(0) under inert atmosphere. The organostannanes **5** showed signs of decomposition with time, and they were freshly prepared just before being used in the cross-coupling reaction.

The 4,4'-bis(alanyl)benzophenones **3** were prepared in an orthogonally protected form by carbonylative coupling between diprotected iodo-aryl derivatives **4** and diprotected aryl trimethylstannanes **5**, using the experimental conditions described by Morera and Ortar for similar substrates [23]. The reactions were performed at 90 °C under atmospheric CO pressure in the presence of $PdCl_2/PPh_3$, proceeding smoothly to give derivatives **3** with isolated yields, after column chromatography, in the range of 53–61%. This complete synthetic sequence is reminiscent of the work of Lei et al. for the preparation of phosphinate bis-amino acids [24]. This convergent route allows the installation of diverse and differentiable functionality in a small molecule like **3**.

The sequential peptide coupling of two units of 4,4'-bis(alanyl)benzophenones **3a** should lead to the construction of the designed macrocyclic bis-dipeptide receptor **1**. Benzophenone **3a** was converted into the carboxylic acid **8** by treatment with tetrabutylammonium fluoride [25] (Scheme 2). In a separate reaction, **3a** was treated with trifluoroacetic acid to remove the Boc group and produce the trifluoroacetic salt of amine **9** [25]. Both deprotection reactions proceeded uneventfully in almost quantitative yields. The PNB group in **3b** was removed using a mixture of $SnCl_2$ and phenol in acid media and the Fmoc [30] in **3c** using piperidine to obtain **10** and **11**, respectively (Scheme 2).

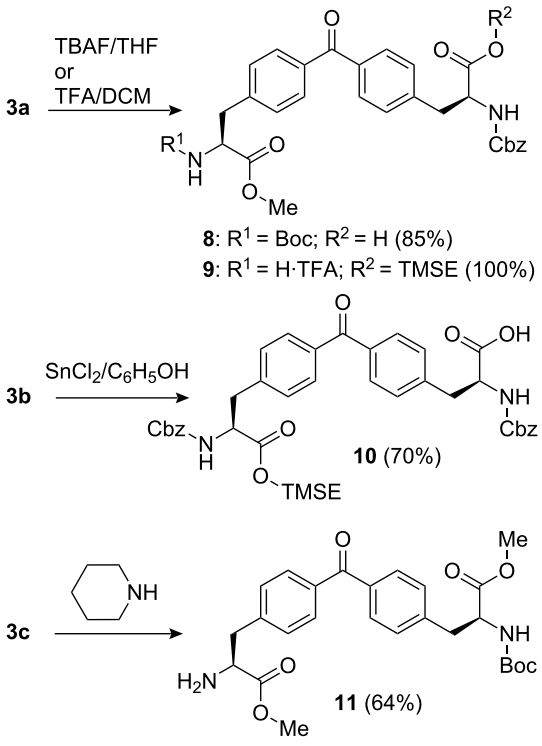

Scheme 2: Deprotection reactions of bis(alanyl)benzophenone units **3**.

Next, we carried out intermolecular peptide-coupling reactions between **8** and **9**, as well as between **10** and **11** to obtain the linear tetrapeptides **12** and **13**, direct precursors of receptors **1** and **2**, respectively. The best results for the coupling reactions were obtained when using a combination of HATU/NMM [31, 32] in DMF at room temperature (Scheme 3). The analysis of the crude reaction mixtures by HPLC and ^{1}H NMR spectroscopy revealed that both tetrapeptides, **12** and **13**, were obtained as mixtures of two diastereoisomers. Most likely, the stereogenic center in the α-position with respect to the carboxylic group undergoing activation during peptide coupling was partially epimerized. The all-*S* diastereoisomers, (*S*)-**12** and (*S*)-**13**, were the major products detected in the crude reaction mixture. They were isolated as pure compounds using preparative reverse-phase HPLC and fully characterized by a complete set of high-resolution spectra.

However, the subsequent sequence of reactions directed toward the macrocyclic receptors utilized, as starting material, the diastereomeric mixture of **12** or **13** obtained by flash chromatography purification of the reaction crude. The deprotections of the diastereoisomeric mixtures were carried out using standard methods. First, we used fluoride to cleave the TMSE group, and subsequently, we removed the Boc group by the action of TFA. We obtained the bis-deprotected tetrapeptides **15** and **17** in high yield (70–80%).

The macrocyclization reactions of the linear tetrapeptides, **15** and **17**, were carried out under high-dilution conditions. Using a syringe pump and under inert atmosphere, a DMF solution of the corresponding linear tetrapeptide was added dropwise, over a period of 12 h, to a stirred DMF solution containing the coupling agent and the base. The purification of the crude macrocyclization reactions using flash chromatography afforded the expected macrocyclic products in acceptable yields but as complex mixtures of diastereoisomers. HPLC–MS analysis of the isolated fraction showed the presence of four different peaks in the chromatogram producing ions with molecular mass value corresponding to the expected cyclic structure. We tentatively assigned the two major peaks to cyclic diastereoisomers formed during the intramolecular peptide-coupling reaction of the all-*S* linear tetrapeptide. As discussed above, one of the two diastereoisomers is probably the outcome of the epimerization reac-

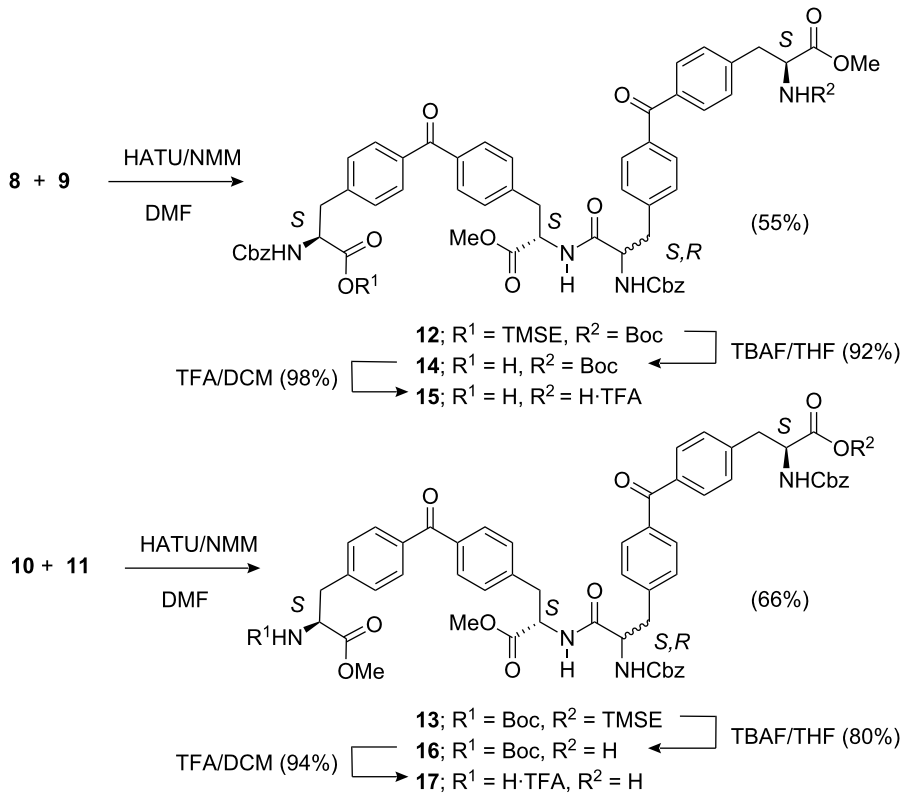

Scheme 3: Synthesis of the linear tetrapeptides **15** and **17** as mixtures of diastereoisomers.

tion experienced by the stereogenic center in the α-position with respect to the carboxylic group undergoing activation. Likewise, the two minor peaks should correspond to cyclic diastereoisomers formed from macrocyclization and concomitant epimerization reactions experienced by the minor linear tetrapeptide *S*,*S*,*S*,*R* also incorporated into the starting material. Figure 4b depicts the HPLC chromatogram obtained from the analysis of the purified fraction containing the mixture of diastereoisomers of receptor **1**. Using normal-phase preparative HPLC, we isolated the two major products of the macrocyclization reaction of **15** as pure compounds. The structures of the isolated products were assigned by means of standard spectroscopic techniques and symmetry considerations to cyclic diastereoisomers of receptor **1**. Furthermore, the structure of the major product of the cyclization of **15** was also characterized in the solid state by X-ray diffraction and proved to be the desired all-*S* antiparallel cyclic receptor **1**. The results obtained in the macrocyclization of tetrapeptide **17** were completely analogous. The all-*S* diastereoisomer corresponds to macrocyclic receptor **2**, and was the major product isolated from the purification of the reaction mixture using normal-phase preparative HPLC. Receptor **2** was fully characterized by means of standard spectroscopic techniques.

Initially, we used HBTU/NMM [25,33,34] for activation of the intramolecular peptide bond formation. We observed considerable epimerization at the stereogenic α-carbon. We assessed the coupling reaction using different coupling methods, HATU/NMM [35] and PyAOP/DIEA [36], and found that although the overall reaction yields were independent of the coupling method, the epimerization diminished substantially when the PyAOP/DIEA [35,36] combination was used (Figure 5c).

Conformational studies

The ^{1}H NMR spectra of chloroform-*d* solutions of the diastereomerically pure all-*S* cyclic receptors **1** and **2**, as well as those of their linear tetraprotected precursors, **15** and **17**, were temperature-dependent (Figure 6). We attribute this temperature dependence to the existence of conformational equilibria that are in a slow chemical exchange regime with respect to the NMR time scale, i.e., the rotation of the C–N single bond in the carbamate protecting groups [37,38].

Upon increasing the temperature of chloroform-*d* solutions of **1**, **2**, **15**, and **17**, the proton signals became sharper and well defined, which is indicative that the chemical exchange due to the conformational equilibria has been accelerated. Conversely, cooling the samples slows down the rate of the chemical

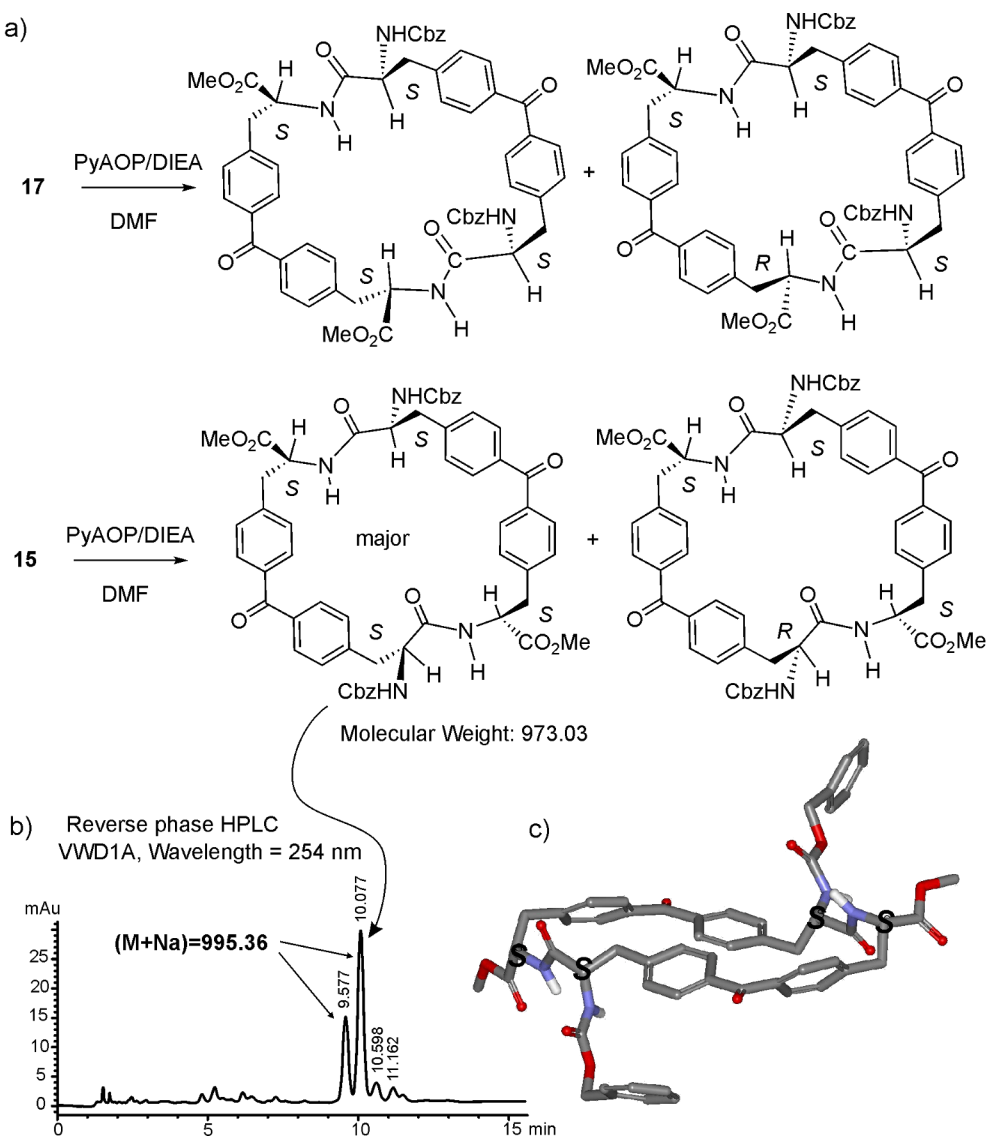

Figure 4: a) Molecular structures of the two major diastereoisomers of the cyclic receptors obtained from the intramolecular coupling reactions of **15** and **17**. b) HPLC chromatogram of the purified fraction containing the mixture of diastereoisomers of **1**. c) X-ray structure of the receptor **1**.

exchange. Thus, at low temperature, we observed the appearance of new proton signals that were assigned to different conformations. We observed another general trend in the variable-temperature ^{1}H NMR spectra, that is, as the temperature was lowered, the NH signals shifted downfield. This behavior suggested that the cyclic and acyclic peptides may dimerize or oligomerize in chloroform solution through the formation of intermolecular NH···O hydrogen bonds. We have already observed the formation of intermolecular hydrogen bonds in the solid-state structure of receptor **1** (Figure 7).

Before undertaking the study of the binding and molecular recognition properties of the receptor series, and due to their tendency to aggregate in solution, we quantified their dimerization constants in chloroform. The calculation of the dimerization constants relies on the chemical shift changes observed for certain proton signals of the receptors when their ^{1}H NMR spectra are acquired at different concentrations. In particular, the receptors' NH signals shift downfield when the concentration of the solution is increased, indicating the formation of aggregates in the solution that are stabilized through hydrogen bonding. The observed chemical shifts for the NH signals were analyzed mathematically using the HypNMR software and a simple theoretical dimerization binding model [39,40]. We obtained a good fit between the experimental and theoretical data. Additional conclusions can be drawn from the data presented in Table 1. Macrocyclic receptors **1** and **2** show greater tendency to dimerize than their linear precursors.

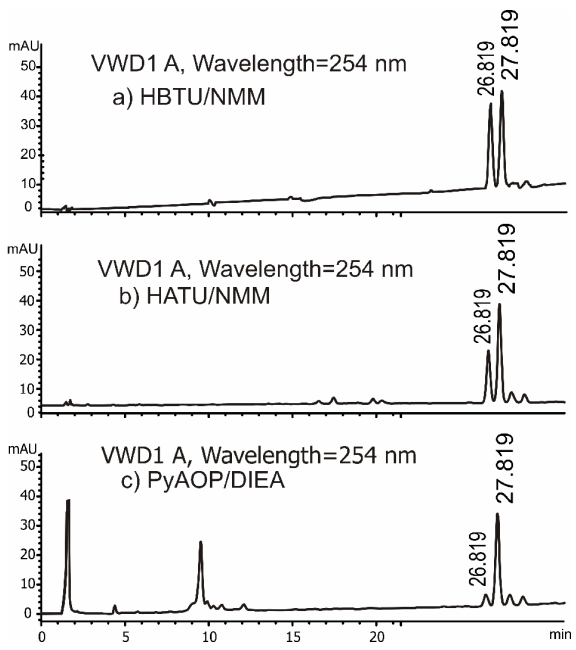

Figure 5: Reverse-phase HPLC chromatograms of the purified fraction obtained from macrocyclization reactions yielding **1** using different coupling agents. The all-*S* cyclic receptor **1** has a retention time of t_r = 26.8 min, and is the major component in the three analyzed mixtures. The peak with retention time of t_r = 27.8 min corresponds to the *R*,*R*,*R*,*S*-**1** diastereoisomer.

A stronger dimerization tendency for the antiparallel cyclic receptor **1** also becomes apparent.

We used a wide range of guest molecular structures to examine the molecular recognition properties of receptors **1**, **2**, **15**, and **17** (Figure 8). We selected a series of diamides to evaluate the effect that the hydrogen-bonding pattern produces in the

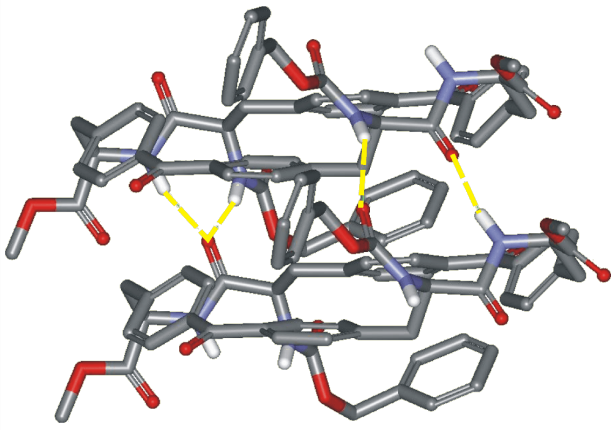

Figure 7: Small fraction of the columnar arrangement observed in solid-state packing of receptor **1**. Two adjacent molecules of **1** interact through the establishment of four hydrogen bonds (yellow dashed lines). For clarity nonpolar hydrogen atoms are omitted.

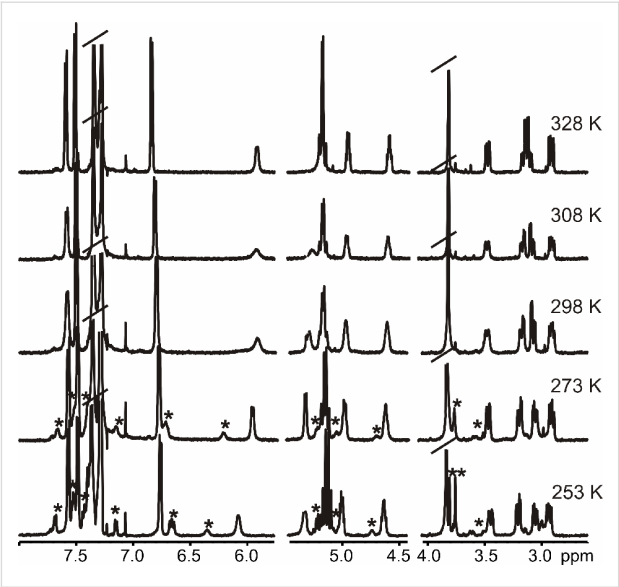

Figure 6: Variable-temperature ^{1}H NMR experiments of **1** in chloroform-*d* solution. The proton signals that appeared at low temperature are marked with an asterisk.

binding affinity. We also investigated the molecular recognition properties of the receptor series with a set of dipeptides. The effect of the size of the amino acid substituents in the dipeptide series (Ala-Ala vs L-Phe-L-Phe) was investigated to shed some light on the geometry of the complexes formed with the cyclic receptors. Finally, the stereoselective recognition properties of the receptors were derived from their binding interactions with the four diastereoisomers of Ala-Ala.

The molecular structures of all selected guests have several hydrogen-bonding groups, making them natural candidates to dimerize in solution. Therefore, before studying the interactions of these guests with the receptors, we studied their dimerization behavior in chloroform solution. Using the same methodology described above for the receptors, we calculated the dimerization constants of all guest molecules. The values obtained are summarized in Table 2. With an additional amide group with respect to diamides, the dipeptide dimers can be stabilized by a higher number of hydrogen bonds. The value of

Table 1: Calculated dimerization constant values for the receptor series.

Receptors	K_d (M^{-1})[a]
1	112
2	60
15	27
17	48

[a]Values determined in chloroform-*d* solution at 298 K using ^{1}H NMR dilution experiments. All values are associated with at least a 10% error.

the dimerization constant of the diamide of fumaric acid stands out from the rest, likely due to the higher conformational rigidity of this compound (preorganization). Figure 9 depicts the ^{1}H NMR spectra acquired in the variable-concentration experiments used for the calculation of the dimerization constant of fumaramide. The NH proton signals experience a significant downfield shift on increasing the concentration of fumaramide.

Having determined the dimerization tendency of host and guest molecules, we initiated the study of the molecular recognition properties of the receptors toward the different guests. All binding constants were determined using ^{1}H NMR titration experiments. As an example, Figure 10a shows a series of spectra acquired during the titration of receptor **2** with *n*-C_6H_{13}-D-Ala-D-Ala-NH_2. We monitored the chemical shift changes experienced by the NH proton signals of the receptor and of the guest when a 1 mM chloroform-*d* solution of the receptor is treated with incremental amounts of the guest. The titration data were fitted to a theoretical binding model considering the exclusive formation of a 1:1 complex, and the existence of dimeric aggregates of both the receptor and the guest. Figure 10b depicts the experimental data of the titration fitted to the theoretical binding isotherm derived from the above-mentioned theoretical model. The values of the calculated stability constants for the 1:1 complexes are summarized in Table 3 and Table 4.

The analysis of the tabulated data allowed us to draw several conclusions (Table 3 and Table 4). The macrocyclic receptors

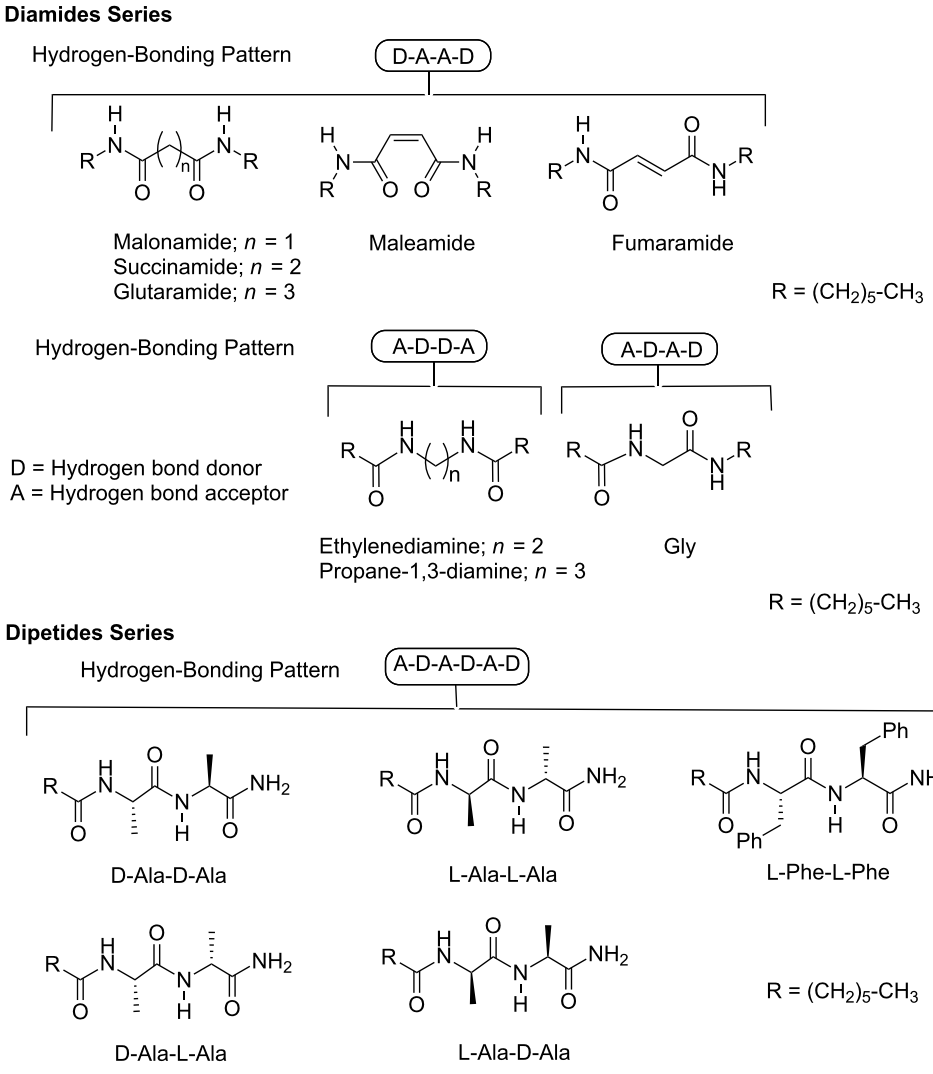

Figure 8: Molecular structures of the guests used in the binding experiments.

Table 2: Dimerization constant values calculated for the guests used in this study.

Diamides of	K_d (M^{-1})[a]	Dipeptides	K_d (M^{-1})[a]
Succinic acid	66	D-Ala-D-Ala	370
Malonic acid	11	L-Ala-L-Ala	346
Ethylenediamine	44	D-Ala-L-Ala	331
Propane-1,3-diamine	44	L-Ala-D-Ala	316
Glutaric acid	<10	L-Phe-L-Phe	346
Maleic acid	31		
Fumaric acid	478		
Gly	22		

[a]Values determined in chloroform-*d* solution at 298 K using ^{1}H NMR dilution experiments. All values are associated with at least a 10% error.

do not show any affinity for the complexation of diamides in which the two amide groups are spanned by three methylene groups (glutaramide and propane-1,3-diamine). However, these receptors do form complexes with the rest of diamides showing certain degree of selectivity in response to the hydrogen-bonding pattern (Table 3). The antiparallel macrocycle **1** exhibits a moderate preference for the hydrogen-bonding pattern DAAD (D = hydrogen bond donor, A = hydrogen bond acceptor) instead of ADAD when just one methylene group spans the two amide groups ($\Delta\Delta G^0$ (malonamide-Gly) = −0.96 kcal/mol). In contrast, parallel receptor **2** effectively discriminates in favor of the hydrogen-bonding pattern ADDA when two methylene groups span the amide groups ($\Delta\Delta G^0$ (ethylenediamine-succinamide) = −2.35 kcal/mol). The calculated stability constants are, in general, lower than the values expected for a complex that can be stabilized by an array of not adjacent four hydrogen bonds in chloroform solution ($K \approx 10^4$ M^{-1}). The stability constant values determined for the complexes formed by both cyclic receptors and fumaramide are more consistent with our estimate. Most likely, the high thermodynamic stability calculated for the complexes of fumaramide

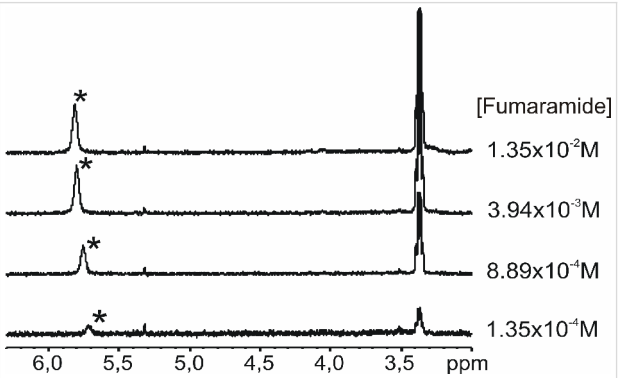

Figure 9: Selected region of the variable-concentration ^{1}H NMR spectra acquired using chloroform-*d* solutions of fumaramide. The signal of the NH proton is marked with an asterisk.

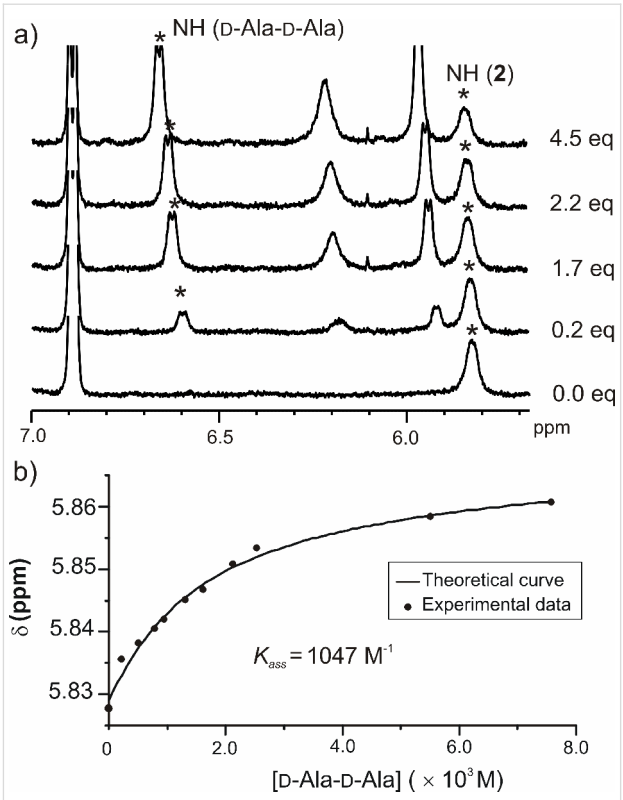

Figure 10: a) Selected region of a series ^{1}H NMR spectra acquired during titration of receptor **2** with *n*-C_6H_{13}-D-Ala-D-Ala-NH_2; b) fit of the experimental data of the titration to the theoretical binding isotherm of the formation of a complex with 1:1 stoichiometry.

in comparison with the rest of diamides resides in the reduced conformational flexibility of the substrate ($\Delta\Delta G^0_{\mathbf{1}}$ (fumaramide-succinamide) = −2.46 kcal/mol and $\Delta\Delta G^0_{\mathbf{2}}$ (fumaramide-succinamide) = −2.79 kcal/mol). When the association constant values obtained for the DAAD hydrogen-bonding pattern are compared, it becomes evident that both cyclic receptors exhibited a marked preference for the diamides in which the NH–CO groups are separated by just one methylene group ($\Delta\Delta G^0_{\mathbf{1}}$ (malonamide-succinamide) = −1.56 kcal/mol and $\Delta\Delta G^0_{\mathbf{2}}$ (malonamide-succinamide) = −1.01 kcal/mol).

Not surprisingly, the binding affinities calculated for the cyclic and acyclic receptors toward the dipeptide series were higher than those for the diamides. Dipeptides have an additional amide hydrogen-bonding group. The degree of stereoselectivity displayed by the cyclic and acyclic receptors was low (two possible binding geometries for the complexes formed between the macrocyclic receptors and *n*-C_6H_{13}-L-Phe-L-Phe-NH_2 are shown in Figure 11).

The cyclic antiparallel receptor **1** showed reduced signs of enantioselectivity and moderate diastereoselectivity in the recognition of the enantiomers and diastereoisomers of the Ala-

Table 3: Binding constants (K_{ass}) and free energies of complexation ($-\Delta G^0$ at 298 K) of the 1:1 complexes formed between the cyclic receptors **1** and **2** and the different guests used in this study.

Cyclic receptors	"Antiparallel" K_{ass}[a] (M^{-1})	Receptor 1 $-\Delta G^0$ (kcal/mol)	"Parallel" K_{ass}[a] (M^{-1})	Receptor 2 $-\Delta G^0$ (kcal/mol)
Guests (DAAD)[b]				
Malonamide ($1CH_2$)	1380	4.2	398	3.5
Succinamide ($2CH_2$)	100	2.7	72	2.5
Glutaramide ($3CH_2$)	<5	<1	<5	<1
Maleamide (2CH)	692	3.8	–[c]	–[c]
Fumaramide (2CH)	6309	5.1	7940	5.3
Guests (ADDA)[b]				
Ethylenediamine ($2CH_2$)	123	2.8	3800	4.8
Propane-1,3-diamine ($3CH_2$)	<5	<1	<5	<1
Guest (ADAD)[b]				
Gly ($1CH_2$)	275	3.3	457	3.6
Guests (ADADAD)[b]				
D-Ala-D-Ala	6606	5.2	1047	4.1
L-Ala-L-Ala	3311	4.8	912	4.0
D-Ala-L-Ala	1047	4.1	1148	4.2
L-Ala-D-Ala	1445	4.3	759	3.9
L-Phe-L-Phe	5012	5.0	2089	4.5

[a]All values are associated with at least a 10% error. [b]Hydrogen-bonding pattern; D = donor, A = acceptor. [c]Not calculated.

Ala dipeptide ($\Delta\Delta G^0_{\mathbf{1}}$ (DD-DL) = −1.08 kcal/mol and $\Delta\Delta G^0_{\mathbf{1}}$ (DD-LD) = −0.89 kcal/mol). The parallel receptor **2** showed neither enantio- nor diastereoselectivity in the recognition of the same substrates (Table 3). The difference in free energy measured for the complexes of **2** with the four diastereoisomers of Ala-Ala was in the order of 0.3 kcal/mol.

Table 4: Binding constants (K_{ass}) and free energies of complexation ($-\Delta G^0$ at 298 K) of the 1:1 complexes formed between the acyclic receptors **15** and **17** and the different guests used in this study.

Acyclic receptors	"Antiparallel" K_{ass}[a] (M^{-1})	**15** $-\Delta G^0$ (kcal/mol)	"Parallel" K_{ass}[a] (M^{-1})	**17** $-\Delta G^0$ (kcal/mol)
Guests (DAAD)[b]				
Malonamide ($1CH_2$)	104	2.7	91	2.6
Succinamide ($2CH_2$)	<5	<1.0	158	2.9
Glutaramide ($3CH_2$)	–[c]	–[c]	126	2.8
Maleamide (2CH)	95	2.6	–[c]	–[c]
Fumaramide (2CH)	973	4.0	7413	5.2
Guests (ADDA)[b]				
Ethylenediamine ($2CH_2$)	446	3.6	33	2.0
Propane-1,3-diamine ($3CH_2$)	78	2.5	–[c]	–[c]
Guest (ADAD)[b]				
Gly ($1CH_2$)	158	2.9	417	3.5
Guests (ADADAD)[b]				
D-Ala-D-Ala	6309	5.2	8318	5.3
L-Ala-L-Ala	1202	4.2	4365	4.9
D-Ala-L-Ala	436	3.6	190	3.1
L-Ala-D-Ala	794	3.9	436	3.6
L-Phe-L-Phe	–[c]	–[c]	–[c]	–[c]

[a]All values are associated with at least a 10% error. [b]Hydrogen-bonding pattern; D = donor, A = acceptor. [c]Not calculated.

We also investigated the complexation affinity of the cyclic receptors toward *n*-C_6H_{13}-L-Phe-L-Phe-NH_2, with the aim of gaining some information about the geometry of the complex. Molecular modeling suggested that although the formation of an *endo*-complex in which *n*-C_6H_{13}-L-Phe-L-Phe-NH_2 is threaded through the macrocyclic ring of the receptor is plausible, the steric clashes detected between the dipeptide side chains and the benzophenone linking units should significantly reduce the binding affinity of the cyclic receptors for this substrate or even favor the formation of an alternative complex with *exo*-geometry. Unexpectedly, the stability constant values that we calculated for the 1:1 complexes of the cyclic receptors and *n*-C_6H_{13}-L-Phe-L-Phe-NH_2 were higher than those for any of the complexes with Ala-Ala (Table 3). Probably, additional intermolecular interactions between the receptors and the phenyl side chains are responsible for the increase in affinity.

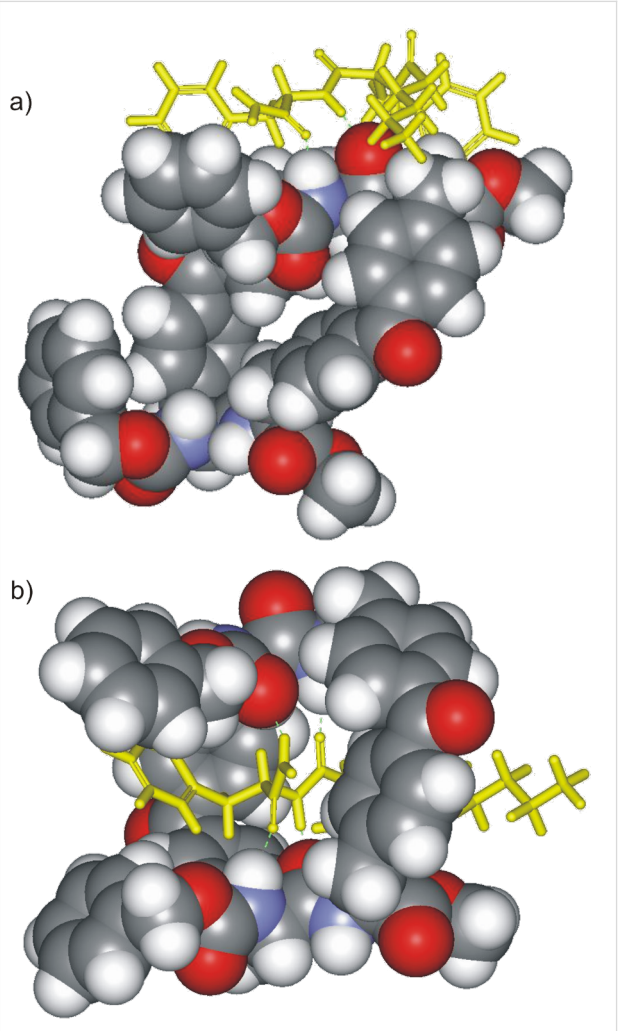

Figure 11: CAChe minimized structures for two possible binding geometries, a) *exo* and b) *endo* complexes formed between receptor **1** and *n*-C_6H_{13}-L-Phe-L-Phe-NH_2. The macrocyclic receptor is shown as CPK model and the dipeptide in yellow stick representation.

The low stereoselectivity exhibited by the cyclic receptors, together with the lack of selectivity for the size of the amino acid side chain, encourages us to propose that the geometry of the 1:1 complex is, most likely, *exo*-cyclic. In other words, the dipeptide is not threaded through the cyclophane skeleton of the receptor but bound externally. This hypothesis is also supported by the fact that we were unable to observe upfield shifts in any of the protons of the dipeptide during the binding experiments. The inclusion of the dipeptide in the aromatic cavity of the receptor should produce the shielding of some of its protons due to the anisotropic magnetic current produced by the aromatic rings.

The linear receptors **15** and **17** seem to be more promiscuous in the interaction with the diamides (Table 4). In general the binding affinities are low, except for the fumaramide. The linear receptor **17** shows moderate selectivity for the hydrogen-bonding pattern DAAD instead of ADAD when $n = 2$ ($\Delta\Delta G^0$ (succinamide-ethylenediamine) = −0.92 kcal/mol) but selects the hydrogen-bonding pattern ADAD when $n = 1$ ($\Delta\Delta G^0$ (Gly-malonamide) = −0.90 kcal/mol).

Surprisingly, linear receptors **15** and **17** exhibited higher levels of stereoselectivity than their cyclic counterparts (Table 4). Receptor **15** displayed the highest enantioselectivity we have measured in the molecular recognition of the D-Ala-D-Ala dipeptide ($\Delta\Delta G^0_{\mathbf{15}}$ (DD-LL) = −1 kcal/mol) and an acceptable level of diastereoselectivity ($\Delta\Delta G^0_{\mathbf{15}}$ (DD-DL) = −1.60 kcal/mol). Even higher values of diastereoselectivity were obtained when studying the interaction between the linear receptor **17** and Ala-Ala diastereomers ($\Delta\Delta G^0_{\mathbf{17}}$ (DD-DL) = −2.18 kcal/mol and $\Delta\Delta G^0_{\mathbf{17}}$ (DD-LD) = −1.70 kcal/mol). We attribute the surprising and superior stereoselectivity measured for the linear receptors to their higher conformational flexibility compared with the cyclic analogs. This enhanced conformational flexibility allows them to adopt a more effective binding conformation for the sensing of the substrate's chirality.

Conclusion

We have designed two macrocyclic receptors for the stereoselective recognition of dipeptides on the basis of the interactions that occur in the β-sheets commonly found in the secondary structure of many biologically relevant proteins. The geometry of the putative complex used in the design of the receptors implies the threading of the dipeptide guest through the macrocyclic skeleton of the receptor. The two designed macrocycles, **1** and **2**, have been synthesized and fully characterized. One of the key synthetic steps, which is common to both synthetic routes, consists in the use of a Stille carbonylative cross-coupling reaction that affords orthogonally tetraprotected 4,4'-bis(alanyl)benzophenone units in good to acceptable yields.

Sequential deprotection reactions combined with the formation of two consecutive amide bonds between two units of 4,4'-bis(alanyl)benzophenone produced the macrocyclic receptors in low yield. Notwithstanding the epimerization reactions observed in the formation of the peptide bonds of the macrocyclic structures, both receptors have been isolated as single diastereoisomers. The molecular structure of receptor **1** has been confirmed by single-crystal X-ray diffraction analysis. Although molecular modeling suggested that the cyclic receptors can adopt a conformation with a cavity size large enough to include a peptidic substrate, the X-ray structure obtained for antiparallel receptor **1** shows the collapse of the designed cavity. Although crystal packing may contribute to this conformational change to some degree, the solid-state structure of **1** suggests that the optimal conformation for binding is probably not the lowest-energy conformation. The prepared macrocyclic receptors **1** and **2** as well as their acyclic tetraprotected precursors **15** and **17** show a moderate tendency to aggregate in chloroform solution. Dilution studies carried out at room temperature show that the variation in chemical shift fits a simple theoretical dimerization model, although higher order aggregation cannot be ruled out. Using ^{1}H NMR titration experiments we have determined the association constant values of the 1:1 complexes formed between receptors **1**, **2**, **15**, and **17** and a series of diamides and dipeptides. We have observed that each receptor shows different selectivities in the recognition of the hydrogen-bonding patterns present in the diamide series as well as of the number of methylene groups used to separate the two amide functions. However, when the association constant values obtained for the DAAD hydrogen-bonding pattern are compared, it becomes clear that both cyclic receptors exhibited a marked preference for the diamides in which the NH–CO groups are separated by just one methylene group. It is worth noting that a single methylene unit was used as the spacer for the diamide guest used in the receptors' design. We also investigated the stereoselective recognition properties of the synthesized receptors using the four diastereoisomers of the Ala-Ala dipeptide as guests. The low stereoselectivity displayed by the cyclic receptors, together with their insensitivity to the size of the amino acid chain of the dipeptide guest, allows us to propose that the topology of the 1:1 complexes is not a pseudorotaxane as initially proposed in our design. Most likely, the guests, dipeptides and diamides, bind to the hydrogen-bonding groups that are directed toward the exterior of the aromatic cavity. If macrocyclization results in the receptor adopting a low-energy conformation different from that envisioned in the modeled structures, then preorganization will have created an additional energetic barrier to *endo*-complexation. Finally, the affinity and surprising stereoselectivity exhibited by the linear receptors **15** and **17** are very difficult to rationalize with an *endo*-complex geometry.

We conclude with the caveat that the analysis here pre-supposes that the receptors respond to different ligands with similar binding modes. Due to the complexity of the system, we have not attempted to analyze the possibility that multiple binding modes – *exo*-binding, *endo*-binding – all operate simultaneously and to varying degrees depending on the ligand.

Supporting Information

Supporting information features experimental procedures, characterization data, NMR spectra of selected compounds and crystallographic data for the solid-state structure of **1**.

Supporting Information File 1

Synthesis and binding studies of two new macrocyclic receptors for the stereoselective recognition of dipeptides
[http://www.beilstein-journals.org/bjoc/content/supplementary/1860-5397-6-5-S1.doc]

Supporting Information File 2

CIF for the solid-state structure of **1**
[http://www.beilstein-journals.org/bjoc/content/supplementary/1860-5397-6-5-S2.cif]

Acknowledgements

We thank DGPYTC, Ministerio de Ciencia e Innovación (CTQ2008-00222/BQU, Consolider Ingenio 2010 Grant CSD2006-0003), ICIQ Foundation, and Generalitat de Catalunya (Grant 2009SGR686) for generous financial support.

References

1. Peczuh, M. W.; Hamilton, A. D. *Chem. Rev.* **2000,** *100,* 2479–2494. doi:10.1021/cr9900026
2. Neu, H. C. *Science* **1992,** *257,* 1064–1073. doi:10.1126/science.257.5073.1064
3. Gold, H. S. *Clin. Infect. Dis.* **2001,** *33,* 210–219. doi:10.1086/321815
4. Williams, D. H.; Bardsley, B. *Angew. Chem., Int. Ed.* **1999,** *38,* 1172–1193. doi:10.1002/(SICI)1521-3773(19990503)38:9<1172::AID-ANIE1172>3.0.CO;2-C
5. Uttley, A. H. C.; Collins, C. H.; Naidoo, J.; George, R. C. *Lancet* **1988,** *331,* 57–58. doi:10.1016/S0140-6736(88)91037-9
6. Woodford, N.; Johnson, A. P.; Morrison, D.; Speller, D. C. *Clin. Microbiol. Rev.* **1995,** *8,* 585–615.
7. Hiramatsu, K.; Hanaki, H.; Ino, T.; Yabuta, K.; Oguri, T.; Tenover, F. C. *J. Antimicrob. Chemother.* **1997,** *40,* 135–136. doi:10.1093/jac/40.1.135
8. Roderich, D. S. *ChemBioChem* **2002,** *3,* 295–298. doi:10.1002/1439-7633(20020402)3:4<295::AID-CBIC295>3.0.CO;2-G
9. Chamorro, C.; Liskamp, R. M. J. *Tetrahedron* **2004,** *60,* 11145–11157. doi:10.1016/j.tet.2004.08.074
10. Xu, R.; Greiveldinger, G.; Marenus, L. E.; Cooper, A.; Ellman, J. A. *J. Am. Chem. Soc.* **1999,** *121,* 4898–4899. doi:10.1021/ja990240i

11. Davies, M.; Bonnat, M.; Guillier, F.; Kilburn, J. D.; Bradley, M. *J. Org. Chem.* **1998,** *63,* 8696–8703. doi:10.1021/jo981741+
12. Jeong, K. S.; Muehldorf, A. V.; Rebek, J., Jr. *J. Am. Chem. Soc.* **1990,** *112,* 6144–6145. doi:10.1021/ja00172a049
13. LaBrenz, S. R.; Kelly, J. W. *J. Am. Chem. Soc.* **1995,** *117,* 1655–1656. doi:10.1021/ja00110a029
14. Schmuck, C.; Geiger, L. *J. Am. Chem. Soc.* **2004,** *126,* 8898–8899. doi:10.1021/ja048587v
15. Yoon, S. S.; Georgiadis, T. M.; Still, W. C. *Tetrahedron Lett.* **1993,** *34,* 6697–6700. doi:10.1016/S0040-4039(00)61678-7
16. Yoon, S. S.; Still, W. C. *J. Am. Chem. Soc.* **1993,** *115,* 823–824. doi:10.1021/ja00055a083
17. Cabbiness, D. K.; Margerum, D. W. *J. Am. Chem. Soc.* **1969,** *91,* 6540–6541. doi:10.1021/ja01051a091
18. Hinz, F. P.; Margerum, D. W. *J. Am. Chem. Soc.* **1974,** *96,* 4993–4994. doi:10.1021/ja00822a050
19. Hinz, F. P.; Margerum, D. W. *Inorg. Chem.* **1974,** *13,* 2941–2949. doi:10.1021/ic50142a032
20. Izatt, R. M.; Bradshaw, J. S.; Nielsen, S. A.; Lamb, J. D.; Christensen, J. J.; Sen, D. *Chem. Rev.* **1985,** *85,* 271–339. doi:10.1021/cr00068a003
21. *CAChe WorkSytem Pro,* Version 6.1.12.33; Fujitsu Limited..
22. Levin, S.; Nowick, J. S. *J. Am. Chem. Soc.* **2007,** *129,* 13043–13048. doi:10.1021/ja073391r
23. Morera, E.; Ortar, G. *Bioorg. Med. Chem. Lett.* **2000,** *10,* 1815–1818. doi:10.1016/S0960-894X(00)00344-9
24. Lei, H.; Stoakes, M. S.; Herath, K. P. B.; Lee, J.; Schwabacher, A. W. *J. Org. Chem.* **1994,** *59,* 4206–4210. doi:10.1021/jo00094a036
25. Schwarz, H.; Arakawa, K. *J. Am. Chem. Soc.* **1959,** *81,* 5691–5695. doi:10.1021/ja01530a041
26. Paquet, A. *Can. J. Chem.* **1982,** *60,* 976–980. doi:10.1139/v82-146
27. Sigler, G. F.; Fuller, W. D.; Chaturvedi, N. C.; Goodman, M.; Verlander, M. *Biopolymers* **1983,** *22,* 2157–2162. doi:10.1002/bip.360221002
28. Milton, R. C. d. L.; Becker, E.; Milton, S. C. F.; Baxter, J. E. H.; Elsworth, J. F. *Int. J. Pept. Protein Res.* **1987,** *30,* 431–432.
29. Lapatsanis, L.; Milias, G.; Froussios, K.; Kolovos, M. *Synthesis* **1983,** 671–673. doi:10.1055/s-1983-30468
30. Zajdel, P.; Subra, G.; Bojarski, A. J.; Duszyńska, B.; Tatarczyńska, E.; Nikiforuk, A.; Chojnacka-Wójcik, E.; Pawłowski, M.; Martinez, J. *Bioorg. Med. Chem.* **2007,** *15,* 2907–2919. doi:10.1016/j.bmc.2007.02.018
31. Carpino, L. A.; Chao, H. G.; Ghassemi, S.; Mansour, E. M. E.; Riemer, C.; Warrass, R.; Sadat-Aalaee, D.; Truran, G. A.; Imazumi, H.; El-Faham, A.; Ionescu, D.; Ismail, M.; Kowaleski, T. L.; Han, C. H.; Wenschuh, H.; Beyermann, M.; Bienert, M.; Shroff, H.; Albericio, F.; Triolo, S. A.; Sole, N. A.; Kates, S. A. *J. Org. Chem.* **1995,** *60,* 7718–7719. doi:10.1021/jo00129a005
32. Carpino, L. A. *J. Am. Chem. Soc.* **1993,** *115,* 4397–4398. doi:10.1021/ja00063a082
33. Dourtoglou, V.; Ziegler, J.-C.; Gross, B. *Tetrahedron Lett.* **1978,** *19,* 1269–1272. doi:10.1016/0040-4039(78)80103-8
34. Dourtoglou, V.; Gross, B.; Lambropoulou, V.; Zioudrou, C. *Synthesis* **1984,** 572–574. doi:10.1055/s-1984-30895
35. Carpino, L. A.; El-Faham, A. *Tetrahedron* **1999,** *55,* 6813–6830. doi:10.1016/S0040-4020(99)00344-0
36. Carpino, L. A.; El-Faham, A.; Albericio, F. *Tetrahedron Lett.* **1994,** *35,* 2279–2282. doi:10.1016/0040-4039(94)85198-0
37. Lauvergnat, D.; Hiberty, P. C. *J. Am. Chem. Soc.* **1997,** *119,* 9478–9482. doi:10.1021/ja9639426
38. Marcovici-Mizrahi, D.; Gottlieb, H. E.; Marks, V.; Nudelman, A. *J. Org. Chem.* **1996,** *61,* 8402–8406. doi:10.1021/jo961446u
39. Frassineti, C.; Ghelli, S.; Gans, P.; Sabatini, A.; Moruzzi, M. S.; Vacca, A. *Anal. Biochem.* **1995,** *231,* 374–382. doi:10.1006/abio.1995.9984
40. Reniero, F.; Guillou, C.; Frassineti, C.; Ghelli, S. *Anal. Biochem.* **2003,** *319,* 179–194. doi:10.1016/S0003-2697(03)00300-2

License and Terms

Beilstein Journal of Organic Chemistry

Recognition properties of receptors consisting of imidazole and indole recognition units towards carbohydrates

Monika Mazik* and André Hartmann

Full Research Paper

Open Access

Address:
Institut für Organische Chemie der Technischen Universität Braunschweig, Hagenring 30, 38106 Braunschweig, Germany, Tel.: +495313915266, Fax: +495313918185

Email:
Monika Mazik* - m.mazik@tu-bs.de

* Corresponding author

Keywords:
carbohydrates; hydrogen bonds; molecular recognition; receptors; supramolecular chemistry

Beilstein Journal of Organic Chemistry **2010,** *6,* No. 9.
doi:10.3762/bjoc.6.9

Received: 30 September 2009
Accepted: 19 January 2010
Published: 02 February 2010

Guest Editor: C. A. Schalley

Abstract

Compounds **4** and **5**, including both 4(5)-substituted imidazole or 3-substituted indole units as the entities used in nature, and 2-aminopyridine group as a heterocyclic analogue of the asparagine/glutamine primary amide side chain, were prepared and their binding properties towards carbohydrates were studied. The design of these receptors was inspired by the binding motifs observed in the crystal structures of protein–carbohydrate complexes. ^{1}H NMR spectroscopic titrations in competitive and non-competitive media as well as binding studies in two-phase systems, such as dissolution of solid carbohydrates in apolar media, revealed both highly effective recognition of neutral carbohydrates and interesting binding preferences of these acyclic compounds. Compared to the previously described acyclic receptors, compounds **4** and **5** showed significantly increased binding affinity towards β-galactoside. Both receptors display high β- vs. α-anomer binding preferences in the recognition of glycosides. It has been shown that both hydrogen bonding and interactions of the carbohydrate CH units with the aromatic rings of the receptors contribute to the stabilization of the receptor–carbohydrate complexes. The molecular modeling calculations, synthesis and binding properties of **4** and **5** towards selected carbohydrates are described and compared with those of the previously described receptors.

Introduction

Analysis of the binding motifs found in the crystal structures of protein–carbohydrate complexes [1-5] provides much of the inspiration for the design of artificial carbohydrate receptors which use noncovalent interactions for sugar binding [6-18]. Such receptors provide valuable model systems to study the underlying principles of carbohydrate-based molecular recognition processes and might serve as a basis for the development of new therapeutic agents (for example, anti-infective agents) or saccharide sensors [19-26]. Our previous studies showed that mimicking the binding motifs observed in the crystal structures of protein–carbohydrate complexes by using natural recognition groups or their analogues [27-45] represents an effective

strategy for designing carbohydrate receptors. Among other things the crystal structures of protein–carbohydrate complexes revealed that the imidazole and indole groups of His and Trp respectively are able to participate in both hydrogen bonding and stacking interactions with the sugar ring. It should be noted that packing of an aromatic ring of the protein against a sugar is observed in most carbohydrate–binding proteins [1-5]. Such packing arrangements and the hydrogen bonding motifs shown in Figure 1 have inspired the design of receptors **1** and **2** (see Figure 2), including both 4(5)-substituted imidazole or 3-substituted indole units as the entities used in nature, and 2-aminopyridine groups as heterocyclic analogues of the asparagine/glutamine primary amide side chains (in analogy to the binding motif shown in Figure 1a) [31]. The compounds **1** and **2** were established as highly effective receptors for mono- and disaccharides and shown to display remarkable β- vs. α-anomer selectivity in the recognition of glucopyranosides, as well as a binding preference for β-glucopyranoside vs. β-galactopyranoside. It has been shown that both hydrogen bonding and interactions of the carbohydrate CH units with the aromatic rings of the receptors contribute to the stabilization of the receptor–carbohydrate complexes. Compounds **1** and **2** were shown to be more powerful carbohydrate receptors than the symmetrical aminopyridine-based receptor **3**.

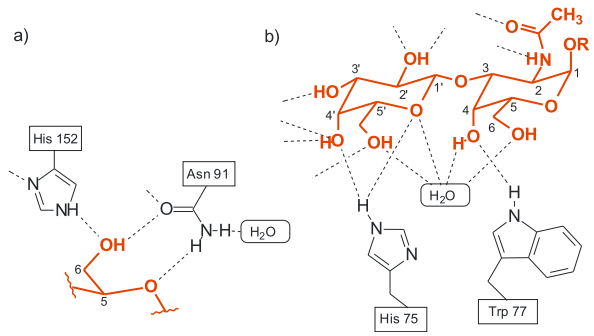

Figure 1: Examples of hydrogen bonds in the complex of a) galactose-binding protein with D-glucose [3], b) *Amaranthus caudatus* agglutinin with Galβ3GalNAc [1].

We were interested to see whether compounds **4** and **5** (see Figure 2), which consist of two imidazole or indole groups and one 2-aminopyridine unit, would be more effective with mono- and disaccharide substrates. Herein, we describe the synthesis, molecular modeling calculations and the binding properties of the compounds **4** and **5**. To compare the binding properties of the new compounds with those of the previously published receptors, octyl β-D-glucopyranoside (**6a**), methyl β-D-glucopyranoside (**6b**), octyl α-D-glucopyranoside (**7a**), methyl α-D-glucopyranoside (**7b**), octyl β-D-galactopyranoside (**8a**), methyl β-D-galactopyranoside (**8b**), methyl α-D-galactopyranoside (**9**),

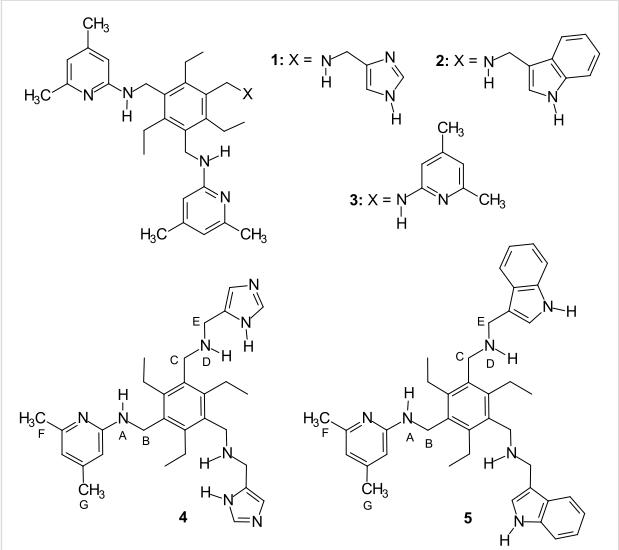

Figure 2: Structures of receptors **1**–**5**.

methyl α-D-mannopyranoside (**10**) and dodecyl β-D-maltoside (**11**) were selected as substrates for the binding experiments (see Figure 3). ^{1}H NMR spectroscopic titrations in competitive and non-competitive media as well as binding studies in two-phase systems, such as dissolution of solid carbohydrates in apolar media, revealed highly effective recognition of neutral carbohydrates and interesting binding preferences of these acyclic receptors.

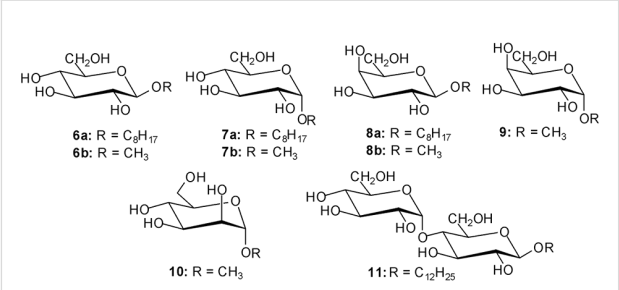

Figure 3: Structures of sugars investigated in this study.

Results and Discussion

Synthesis of the receptors

The basis for the synthesis of compounds **4** and **5** was 1,3-bis(aminomethyl)-5-[(4,6-dimethylpyridin-2-yl)aminomethyl]-2,4,6- triethylbenzene (**17**). The synthesis of compound **17** is described in reference [27]. The reaction of **17** with the corresponding carbaldehyde, such as 4(5)-imidazole-carbaldehyde (**18**) [46] or 3-indole-carbaldehyde (**19**), provided the corresponding imines **20** and **21**, which were further reduced with sodium borohydride. The synthesis of receptors **4** and **5** is summarized in Scheme 1.

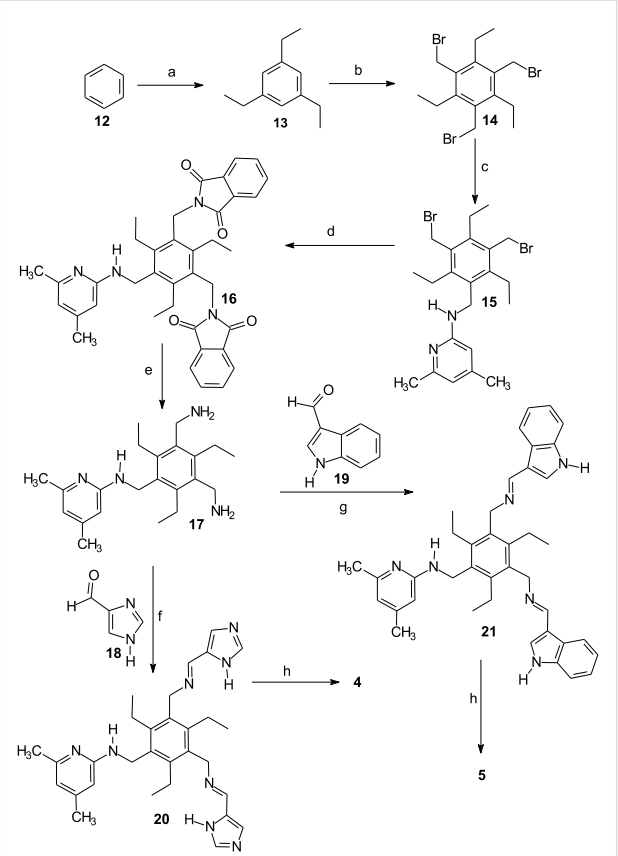

Scheme 1: Reaction conditions: a) $AlCl_3$, CH_3CH_2Br, 0 °C to r. t., 12 h (85%) [47]; b) 33% HBr in CH_3COOH, $ZnBr_2$, $(CH_2O)_n$, 90 °C, 16.5 h (94%); c) 2 equiv of 2-amino-4,6-dimethylpyridine, CH_3CN/THF, K_2CO_3, r. t., 3 d (20%); d) potassium phthalimide, dimethyl sulfoxide, 95 °C, 8 h, (57%); e) hydrazine hydrate, ethanol/toluene, reflux, 19.5 h, KOH (43%) [27]; f) 4 equiv of 4(5)-imidazole-carbaldehyde (**18**), CH_3OH, 3 d; g) 4 equiv of 3-indole-carbaldehyde (**19**) CH_3OH, 3 d; h) 8 equiv of $NaBH_4$, 0 °C to r. t., 12 h (78% of **4**, 92% of **5**).

Binding studies in two-phase systems: liquid-solid extractions

The dissolution of solid carbohydrates in apolar media provides valuable means of studying carbohydrate recognition by organic-soluble receptors (for examples of receptors which are able to dissolve solid carbohydrates in apolar media, see references [6,27,41,43,48-50]). Extractions of sugars **6b**, **7b**, **8b**, **9** and **10** from the solid state into a $CDCl_3$ solution of receptor **4** or **5** (1 mM) provided evidence for strong complexation of β-glucoside **6b** and β-galactoside **8b**. The extraction of solid methyl α-glucoside **7b**, α-galactoside **9** and α-mannoside **10** into a $CDCl_3$ solution of receptor **4** or **5** indicated a weaker binding of these sugars than that of **6b** and **8b** (see Table 1). The extraction experiments indicated that the imidazole-based receptor **4** is a more powerful carbohydrate receptor than the indole-based compound **5**. Receptor **4** was able to dissolve about 1 equiv of β-glucoside **6b** and β-galactoside **8b**, 0.5 equiv of α-glucoside **7b** and about 0.2 equiv of α-galactoside **9**. In the case of receptor **5** only about 0.7 equiv of β-glucoside **6b** and β-galactoside **8b** could be detected in the solution (see Table 1). Regarding **4** and **5**, the extractability decreased in the sequence β-glucoside **6b** ~ β-galactoside **8b** > α-glucoside **7b** > α-galactoside **9** > α-mannoside **10** (see Table 1; control experiments were performed in the absence of the receptor). The preference of **4** and **5** for β- vs. α-glucoside (**6b** vs. **7b**) as well as for β- vs. α-galactoside (**8b** vs. **9**) indicated by liquid–solid extractions was further confirmed by ^{1}H NMR spectroscopic titrations (see below). Compared to the previously studied receptors **1**–**3**, the extraction experiments indicated a significantly higher level of affinity of **4** and **5** towards β-galactoside. It should also be noted that the selectivities observed for **4** and **5** are quite different to those of the recently described phenanthroline/aminopyridine-based receptors **22** and **23** (see Figure 4) [27,29], which show a strong preference for α-glucoside and α-galactoside vs. the β-anomers. Thus, depending on the nature of the recognition units used as building blocks for the acyclic structures, effective carbohydrate receptors with different binding selectivities could be obtained. However, the exact prediction of the binding selectivity still represents an unsolved problem.

Table 1: Solubilization of sugars in $CDCl_3$ by receptor **4** and **5** (1 mM solution).

Sugar	Sugar/**4**[a]	Sugar/**5**[a]
β-D-glucoside **6b**	0.98	0.72
α-D-glucoside **7b**	0.50	0.19
β-D-galactoside **8b**	0.95	0.74
α-D-galactoside **9**	0.20	0.09
α-D-mannoside **10**	0.11	0.04

[a]Molar ratios sugar/receptor occurring in solution (the ^{1}H NMR signals of the corresponding sugar were integrated with respect to the receptor's signals to provide the sugar–receptor ratio; control experiments were performed in the absence of the receptor).

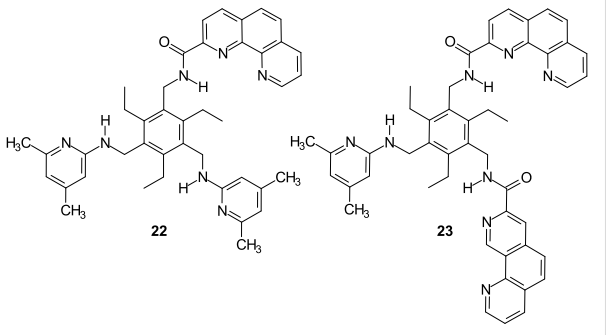

Figure 4: Structures of the recently described phenanthroline/aminopyridine-based receptors showing α- vs. β-anomer binding preferences in the recognition of glycosides [27,29].

Binding studies in homogeneous solution

The interactions of the receptors and carbohydrates were investigated by ^{1}H NMR spectroscopic titrations in $CDCl_3$ and DMSO-d_6/$CDCl_3$ mixtures. The stoichiometry of the receptor–sugar complexes was determined by mole ratio plots [51,52] and by the curve-fitting analysis of the titration data [53].

The ^{1}H NMR titration experiments [54] with octyl β-glucoside **6a**, α-glucoside **7a**, β-galactoside **8a** and methyl α-galactoside **9** were carried out by adding increasing amounts of sugar to a solution of receptor **4** or **5**. In addition, inverse titrations were performed in which the concentration of the sugar was held constant and that of the receptor was varied. The complexation between receptors **4** or **5** and the monosaccharides was evidenced by several changes in the NMR spectra (for examples, see Table 2 and Figure 5a and Figure 5b). The addition of the monosaccharides **6a**, **7a** or **8a** to a $CDCl_3$ solution of receptors **4** or **5** caused significant downfield shift of the amine NH^A signal (for labeling, see Figure 2), downfield shift and strong broadening of the NH^D signal as well as changes of the chemical shifts of the $CH_3^{F,G}$, $CH_2^{B,C,E}$, pyridine CH and imidazole or indole CH resonances of **4** or **5** (see Table 2). The signal due to the indole NH of **5** shifted downfield by 0.20–0.40 ppm. The complexation-induced chemical shifts of the NH^A, indole-NH, CH_2^B, $CH_3^{F,G}$ and the aromatic CH protons were monitored for the determination of the binding constants, which are summarized in Table 3. Binding studies with β-glucoside **6a** and β-galactoside **8a** showed the interactions of receptors **4** and **5** with these monosaccharides to be much more favorable than those with the α-anomers **7a** and **9**.

The curve fitting of the titration data for **4** and β-glucoside **6a** suggested the existence of 1:1 and 2:1 receptor–sugar complexes in $CDCl_3$ solutions with a stronger association constant for 1:1 binding and a weaker association constant for the 2:1 receptor–sugar complex (this model was further supported by the mole ratio plots). The binding constants, however, were too large to be accurately determined by the NMR spectroscopic method ($K_{11} > 10^5$ and $K_{21} \sim 10^4$ M^{-1}; see Table 3; for a review discussing the limitations of the NMR method, see ref. [55]). After the addition of 5% DMSO-d_6 the binding constants for **4•6a** were determined to be 35000 (K_{11}) and 1000 M^{-1} (K_{12}). Thus, the affinity of **4** significantly decreases as solvent polarity increases (the addition of dimethyl sulfoxide also caused the change of the binding model; for a discussion on solvent effects in carbohydrate binding by synthetic receptors, see ref. [56]).

The interactions between the β-glucoside **6a** and the indole-based receptor **5** in $CDCl_3$ were shown to be strong but less favorable than those with the receptor **4**. The best fit of the titration data was obtained with the "mixed" 1:1 and 1:2 receptor–sugar binding model. The association constants for **5•6a** were found to be 45900 (K_{11}) and 730 M^{-1} (K_{12}).

The interactions between β-glucopyranoside **6a** and receptors **4** and **5** were also investigated on the basis of inverse titrations in which the concentration of sugar **6a** was held constant and that of receptor **4** or **5** was varied. During the titration of **6a** with **4** or **5** the signals due to the OH protons of **6a** shifted downfield with strong broadening and became almost indistinguishable from the base line after the addition of only 0.1 equiv of the receptor, indicating important contribution of the OH groups of **6a** to the complex formation. Furthermore, the addition of **4** or **5** to a $CDCl_3$ solution of β-glucoside **6a** caused significant upfield shift of the CH signals of **6a**, indicating the participation of the sugar CH units in the formation of the CH···π interactions with the aromatic rings of the receptor (for discussions on the importance of carbohydrate–aromatic interactions, see

Table 2: Change in chemical shift[a] observed during ^{1}H NMR titrations of receptor **4** or **5** with sugar **6a**, **7a**, **8a** or **11** in $CDCl_3$.

Receptor–sugar complex	Δδ[a] [ppm]
4•6a	NH^A: 2.01; CH_2^B: −0.17; imidazole-CH's: 0.06, 0.08; CH_3^F: −0.07
4•7a	NH^A: 1.17; CH_2^B: −0.15; imidazole-CH's: 0.05, 0.06; CH_3^F: −0.05
4•8a	NH^A: 0.79; CH_2^B: −0.12; CH_2^E: −0.11; imidazole-CH's: 0.11, 0.08; CH_3^F: −0.10; CH_3^G: 0.05
4•11	NH^A: 0.80; CH_2^B: −0.19; CH_2^C: −0.09; imidazole-CH's: 0.09, 0.04; CH_3^F: −0.06; CH_3^G: 0.03
5•6a	NH^A: 2.06; indole-NH: 0.20; CH_2^B: −0.18; CH_2^E: −0.06; CH_3^F: −0.07; CH_3^G: 0.04
5•7a	NH^A: 1.50; indole-NH: 0.17; CH_2^B: −0.18; CH_2^C: −0.06; CH_3^F: −0.06
5•8a	NH^A: 1.15; indole-NH: 0.27; CH_2^B: −0.15; CH_2^C: 0.06; CH_2^E: −0.11; pyr-CH's: −0.01, 0.11; CH_3^F: −0.09; CH_3^G: 0.06
5•11	NH^A: 1.80; indole-NH: 0.40; CH_2^B: −0.20; CH_3^F: −0.06; CH_3^G: 0.04

[a]Largest change in chemical shift observed during the titration for receptor signals (the concentration of receptor was kept constant and that of sugar varied).
[b](−) Δδ = upfield shift.

Table 3: Association constants[a,b] for receptors **1**–**6** and carbohydrates **6a**, **7a**, **8a**, **9** and **11**.

Host–guest complex	Solvent	K_{11} [M^{-1}]	K_{21}[c] or K_{12}[d] [M^{-1}]	$\beta_{21} = K_{11}K_{21}$ or $\beta_{12} = K_{11}K_{12}$ [M^{-2}]
4•6a	$CDCl_3$	$>10^5$; [g]	[g]	
	5% DMSO-d_6/$CDCl_3$	35000	1000; [d]	3.50×10^7
4•7a	$CDCl_3$	7450	1150; [d]	8.56×10^6
4•8a	$CDCl_3$	$>10^5$; [g]	[g]	
	5% DMSO-d_6/$CDCl_3$	40700	800; [d]	3.25×10^7
4•9	5% DMSO-d_6/$CDCl_3$	700		
4•11	$CDCl_3$	$>10^5$; [g]	[g]	
	5% DMSO-d_6/$CDCl_3$	12000	3000; [c]	3.60×10^7
5•6a	$CDCl_3$	45900	730; [d]	3.35×10^7
5•7a	$CDCl_3$	1280	250; [d]	3.20×10^5
5•8a	$CDCl_3$	38000	1100; [d]	4.18×10^7
5•11	$CDCl_3$	$>10^5$; [g]	[g]	
	5% DMSO-d_6/$CDCl_3$	42000		
1•6a[e]	$CDCl_3$	191730	8560; [c]	1.64×10^9
1•7a[e]	$CDCl_3$	3160	1540; [d]	4.86×10^6
1•8a[e]	$CDCl_3$	3320	300; [d]	9.96×10^5
1•11[e]	$CDCl_3$	205760	8670; [c]	1.78×10^9
2•6a[e]	$CDCl_3$	156100	10360; [c]	1.62×10^9
2•7a[e]	$CDCl_3$	2820	350; [d]	9.87×10^5
2•8a[e]	$CDCl_3$	7470	1100; [d]	8.25×10^6
2•11[e]	$CDCl_3$	182690	14840; [c]	2.71×10^9
3•6a[f]	$CDCl_3$	48630	1320; [d]	6.42×10^7
3•7a[f]	$CDCl_3$	1310		
3•8a[f]	$CDCl_3$	3070	470; [d]	1.35×10^6

[a]Average K_a values from multiple titrations in $CDCl_3$.
[b]Errors in K_a are less than 10%.
[c]K_{21} corresponds to 2:1 receptor–sugar association constant.
[d]K_{12} corresponds to 1:2 receptor–sugar association constant.
[e]Results from ref. [31].
[f]Results from ref. [41].
[g]Hostest program indicated "mixed" 1:1 and 2:1 receptor-sugar binding model with $K_{11}>10^5$ and $K_{21} \sim 10^4$; however, the binding constants were too large to be accurately determined by the NMR method.

refs. [57-63]; for examples of CH-π interactions in the crystal structures of the complexes formed between artificial receptors and carbohydrates, see ref. [40]). Among the CH signals, the signal due to the 2-CH proton of **6a** showed the largest shift (1.78 and 1.62 ppm for the titration with **4** and **5**, respectively). In both cases, **6a•4** and **6a•5**, the best fit of the titration data was obtained with the "mixed" 1:1 and 1:2 sugar–receptor binding model. Thus, the inverse titrations fully confirmed the binding model determined through the titrations of **4** or **5** with sugar **6a**. The association constants obtained on the basis of these titrations are identical within the limits of uncertainty to those determined from titrations where the role of receptor and substrate was reversed.

Similar to **4•6a**, the best fit of the titration data for receptor **4** and β-galactoside **8a** was obtained with the "mixed" 1:1 and 2:1 receptor–sugar binding model. However, the binding constants were again too large to be accurately determined by the NMR spectroscopic method (see Table 3). Studies performed in 5% DMSO-d_6 in $CDCl_3$ revealed that K_{11} = 40700 M^{-1} and K_{12} = 800 M^{-1}. The titration experiments with β-galactoside **8a** clearly showed that receptor **5** is less effective towards this monosaccharide than the imidazole-based receptor **4** but much more effective than the previously described receptors **1**–**3**. The motions of the signals of **5** were consistent with 1:1 and 1:2 receptor–sugar binding and could be analyzed to give association constants of 38000 (K_{11}) and 1100 M^{-1} (K_{12}). Compared to receptors **1**–**3** [31,41], receptors **4** and **5** showed a significant-

ly higher binding affinity towards the β-galactoside **8a**. The differences in the complexation abilities of receptors **1**/**3** and **4**/**5** towards β-galactoside **8a** are clearly visible in the comparison of the chemical shifts of the signals of the four receptors after the addition of β-galactoside **8a** (illustrated in parts a–d of Figure 5 for the pyridine CH_3 signals).

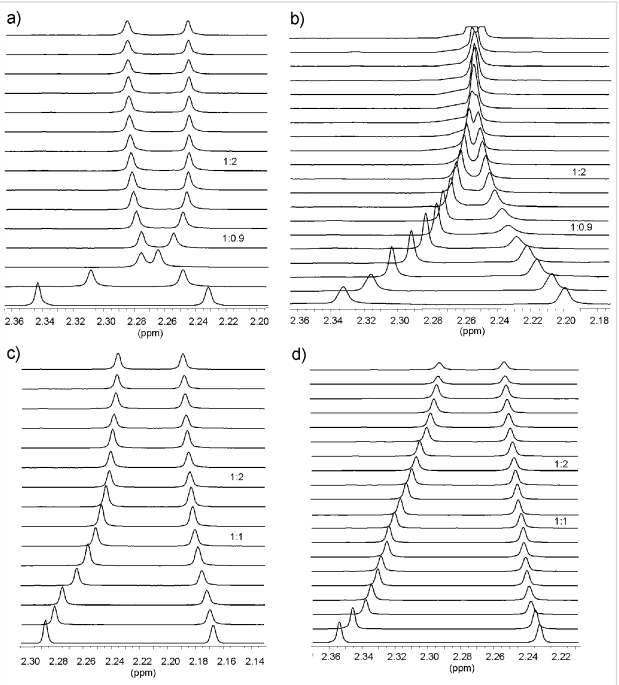

Figure 5: Partial ^{1}H NMR spectra (400 MHz; $CDCl_3$) of receptor **4** (a), **5** (b), **1** (c), and **3** (d) before (bottom) and after the addition of β-galactoside **8a**. Shown are chemical shifts of the pyridine CH_3 resonances of the corresponding receptor. [**4**] = 0.89 mM, equiv of **8a**: 0.00–4.65; [**5**] = 0.90 mM, equiv of **8a**: 00–4.52; [**1**] = 0.95 mM, equiv of **8a**: 0.00–4.26; [**3**] = 0.90 mM, equiv of **8a**: 0.00–5.20.

Our previous studies showed compounds **1**–**3** to be highly effective receptors for β-maltoside **11** [28,31]. This disaccharide [64] is almost insoluble in $CDCl_3$ but could be solubilized in this solvent in the presence of the corresponding receptor. Similar solubility behavior of **11**, indicating favorable interactions between the binding partners, could be observed in the presence of compounds **4** and **5**. Thus, the receptor in $CDCl_3$ was titrated with a solution of maltoside dissolved in the same receptor solution. The complexation between **4** or **5** and the disaccharide **11** was evidenced by several changes in the NMR spectra (for example, see Table 2 and Figure 6). The saturation occurred after the addition of about 0.7 equiv of **11**. Both the curve fitting of the titration data and and the mole ratio plots suggested the existence of 1:1 and 2:1 receptor–sugar complexes in the chloroform solution (with stronger association constant for 1:1 binding and a weaker association constant for 2:1 receptor–sugar complex). In both cases, **4**•**11** and **5**•**11**, the binding constants in $CDCl_3$ were too large to be accurately determined by the NMR spectroscopic method (see Table 3). After the addition of DMSO-d_6 a substantial fall in the binding affinity was observed. Studies that were performed with **4** and **11** in 5% DMSO-d_6 in $CDCl_3$ revealed K_{11} = 12000 M^{-1} and K_{21} = 3000 M^{-1}, those performed with **5** and **11** indicated the formation of complexes with 1:1 receptor–sugar stoichiometry with K_{11} = 42000 M^{-1}.

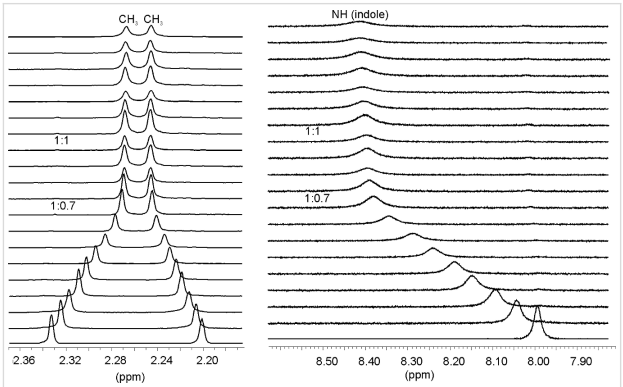

Figure 6: Partial ^{1}H NMR spectra (400 MHz, $CDCl_3$) of **5** after addition of (from bottom to top) 0.00–1.63 equiv of β-maltoside **11** ([**5**] = 0.96 mM). Shown are chemical shifts of the pyridine CH_3 and indole NH signals of receptor **5**.

Molecular modeling

The formation of hydrogen bonds and CH···π interactions between the binding partners was also suggested by molecular modeling calculations. For example, molecular modeling suggested that all OH groups and the ring oxygen atom of the bound β-galactoside **8b** in the complex **4**•**8b** are involved in the formation of hydrogen bonds (see Table 4 and Figure 7a and Figure 8). In addition, interactions of sugar C-H units with the central phenyl ring of **4** (see Table 4) were shown to provide additional stabilization of the complex. Furthermore, the molecular modeling calculations indicated that within the 2:1 receptor–sugar complex the two receptor molecules almost completely enclose the sugar, leading to involvement of all sugar hydroxyl groups in interactions with the two receptor molecules (see Table 4 and Figure 7b). The OH groups are involved in the formation of cooperative hydrogen bonds which result from the simultaneous participation of a sugar OH as donor and acceptor of hydrogen bonds. The phenyl units of the both receptors stack on the sugar ring and both sides of the pyranose ring are involved in CH···π interactions (see Table 4 and Figure 7b).

Conclusion

The analysis of the binding motifs which are observed in the crystal structures of protein-carbohydrate complexes has influenced the design of receptors **4** and **5**, including two 4(5)-substituted imidazole or 3-substituted indole units as well as an

Table 4: Examples of noncovalent interactions indicated by molecular modeling calculations[a] for the complexes formed between receptor **4** and sugar **8a** or **8b**.

1:1 receptor–sugar complex[b]	2:1 receptor–sugar complex[b,c]	1:2 receptor–sugar complex[d]
imidazole-NH···OH-2	(I) imidazole-NH···OH-2	imidazole-NH···OH-6
HN^D···HO-2	(I) HN^D···HO-2	HN^D···HO-6
NH^D···O-CH_3	(I) NH^D···O-CH_3	NH^D···OH-4
imidazole-NH···OH-3	(I) imidazole-NH···OH-3	imidazole-NH···OH-4
HN^D···HO-3	(I) HN^D···HO-3	pyridine-N···HO-2
NH^D···OH-4	(I) NH^D···OH-4	NH^A···OC_8H_{17}
phenyl···HO-4	(I) pyridine-N···HO-6	phenyl···HO-4
pyridine-N···HO-6	(I) NH^A···O-ring	phenyl···HCH-6
NH^A···O-ring	(I) phenyl···HO-4; (I) phenyl···HC-2	pyridine-N···HC-2[e]
phenyl···HC-2	(II) imidazole-NH···OH-6; (II) NH^D···OH-6	pyridine-CH_3···OH-4[e]
	(II) NH^A···OH-3	3-HO···HO-2[f]
	(II) phenyl···HC-1	3-OH···OH-3[f]
	(II) phenyl···HC-3; (II) phenyl···HC-5	

[a]MacroModel V.8.5, OPLS-AA force field, MCMM, 50000 steps.
[b]Complex with sugar **8b**.
[c]I and II: two receptors in the 2:1 receptor–sugar complex; for labeling see Figure 2.
[d]Complex with sugar **8a**.
[e]Interaction with the second sugar.
[f]Sugar–sugar interaction.

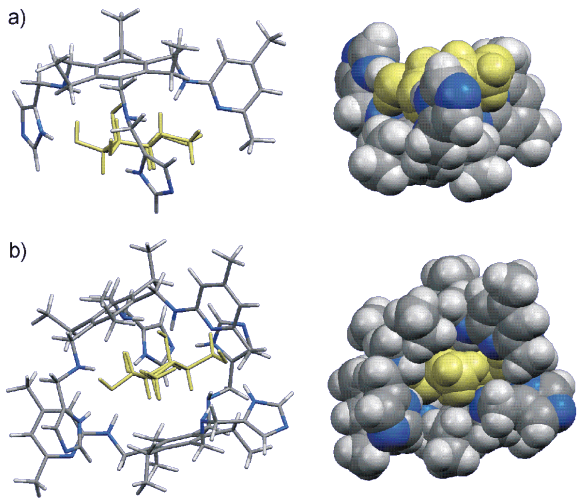

Figure 7: Energy-minimized structure of the 1:1 a) and 2:1 complex b) formed between receptor **4** and β-galactoside **8b** (different representations). MacroModel V.8.5, OPLS-AA force field, MCMM, 50000 steps. Color code: receptor C, grey; receptor N, blue; sugar molecule, yellow.

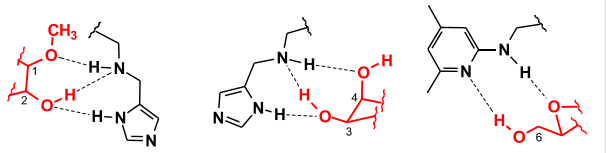

Figure 8: Examples of hydrogen bonding motifs indicated by molecular modeling studies in the 1:1 complex between receptor **4** and β-galactoside **8b** (MacroModel V.8.5, OPLS-AA force field, MCMM, 50000 steps).

aminopyridine-based recognition group. The compounds **4** and **5** were established as highly effective receptors for neutral carbohydrates and were shown to display a significantly higher level of affinity towards β-galactoside than the previously described acyclic receptors. Both receptors were shown to display high β- vs. α-anomer binding preferences in the recognition of glycosides. The binding properties of **4** and **5** were studied on the base of ^{1}H NMR spectroscopic titrations in $CDCl_3$ and DMSO-d_6/$CDCl_3$ mixtures as well as binding studies in two-phase systems, such as dissolution of solid carbohydrates in apolar media. The imidazole-based receptor **4** was found to be a more powerful monosaccharide receptor than the indole-based compound **5** and the previously described receptors **1**–**3**. Compared to **1** and **2**, incorporating only one imidazole or indole recognition unit, receptor **5** showed increased affinity to β-galactoside but decreased affinity to β-glucoside. The binding affinity of **1**–**5** towards β-galactoside **8a** and β-glucoside **6a** increases in the sequence **3** ~ **1** < **2** < **5** < **4** and **3** ~ **5** < **1** ~ **2** < **4**, respectively. It is remarkable that the strong enhancement of the binding affinity of **4** and **5** towards β-galactoside was achieved through a relatively simple variation of the receptor structure. In contrast to **4** and **5**, the previously described phenanthroline/aminopyridine-based receptors **22** and **23** were shown to display a high binding affinity towards α-galactoside as well as a strong α- vs. β-anomer

binding preference. Thus, depending on the nature of the recognition units incorporated into the acyclic receptor structure, effective carbohydrate receptors with different binding preferences can be generated. However, the exact prediction of the binding preference still represents an unsolved problem and remains an important goal for future research.

Experimental section

Analytical TLC was carried out on silica gel 60 F_{254} plates employing chloroform/methanol mixtures as the mobile phase. Melting points are uncorrected. Sugars **6**–**11**, 4(5)-imidazole-carbaldehyde (**18**) and 3-indole-carbaldehyde (**19**) are commercially available.

General procedure for the synthesis of compounds 4 and 5: To a solution of 4(5)-imidazole-carbaldehyde (**18**) or 3-indole-carbaldehyde (**19**) (3.40 mmol) in methanol (40 mL) 1,3-bis(aminomethyl)-5-[(4,6-dimethylpyridin-2-yl)aminomethyl]-2,4,6-triethylbenzene (**17**) (0.85 mmol) dissolved in 20 mL methanol was added. The reaction mixture was stirred for 72 h. The solution was cooled to 0 °C and $NaBH_4$ (6.80 mmol) was added in portions. The reaction mixture was stirred for 1 h at 0 °C and for additionally 6 h at room temperature. The solvent was removed and the residue was taken up in chloroform/water (100 mL, 1:1). The separated organic phase was further washed with water (3×30 mL), dried over $MgSO_4$ and the solvent was removed. The crude product was purified via column chromatography [$CHCl_3$/CH_3OH (incl. 1% 7 M NH_3 in CH_3OH), 2:1 or 3:1 *v*/*v*].

1,3-Bis[(4-Imidazolyl-methyl)aminomethyl]-5-[(4,6-dimethylpyridin-2-yl)aminomethyl]-2,4,6-triethylbenzene (4). Yield: 78%; mp: 76–77 °C; ^{1}H NMR (400 MHz, $CDCl_3$, 0.9 mM): δ = 7.54 (s, 2H), 6.93 (s, 2H), 6.33 (s, 1H), 6.07 (s, 1H), 4.28 (s, 2H), 4.18 (br. s, 1H), 3.89 (s, 4H), 3.71 (s, 4H), 2.68 (q, *J* = 7.3 Hz, 4H), 2.65 (q, *J* = 7.3 Hz, 2H), 2.34 (s, 3H), 2.23 (s, 3H), 1.17 (t, *J* = 7.3 Hz, 6H), 1.09 (t, *J* = 7.3 Hz, 3H) ppm; ^{13}C NMR (100 MHz, $CDCl_3$): δ = 158.33, 156.44, 148.96, 142.75, 142.43, 135.65, 134.07, 132.41, 113.85, 103.58, 46.75, 46.05, 24.01, 22.70, 22.50, 21.11, 16.83, 16.80 ppm; HR-MS (ESI) calcd for $C_{30}H_{42}N_8Na$ $[M + Na]^+$: 537.3430, found: 537.3433; R_f = 0.10 [$CHCl_3$/CH_3OH (incl. 1% 7 M NH_3 in CH_3OH), 4:1 *v*/*v*].

1,3-Bis[(3-Indolyl-methyl)aminomethyl]-5-[(4,6-dimethylpyridin-2-yl)aminomethyl]-2,4,6-triethylbenzene (5). Yield: 92%; mp: 89–90 °C; ^{1}H NMR (400 MHz, $CDCl_3$, 0.9 mM): δ = 8.00 (s, 2H), 7.68 (d, *J* = 7.8 Hz, 2H), 7.35 (d, *J* = 8.0, 2H), 7.16–7.20 (m, 4H), 7.08–7.12 (m, 2H), 6.30 (s, 1H), 6.00 (s, 1H), 4.28 (d, *J* = 4.2 Hz, 2H), 4.09 (br. s, 1H), 4.08 (s, 4H), 3.75 (s, 4H), 2.66 (m, 6H), 2.33 (s, 3H), 2.20 (s, 3H), 1.09 (t, *J* = 7.5 Hz, 6H), 1.06 (t, *J* = 7.5 Hz, 3H) ppm; ^{13}C NMR (100 MHz, $CDCl_3$): δ = 158.28, 156.64, 148.55, 142.87, 142.49, 136.37, 134.51, 132.41, 127.16, 122.48, 122.02, 119.46, 119.00, 115.21, 113.60, 111.03, 103.55, 47.28, 45.51, 40.59, 24.20, 22.59, 22.52, 21.05, 16.77 ppm; HR-MS (ESI) calcd for $C_{40}H_{49}N_6$ $[M + H]^+$: 613.4018, found: 613.4012; R_f = 0.12 [$CHCl_3$/CH_3OH (incl. 1% 7 M NH_3 in CH_3OH) 3:1 *v*/*v*].

Acknowledgements

Financial support by the Deutsche Forschungsgemeinschaft (German Research Foundation) is gratefully acknowledged.

References

1. Lis, H.; Sharon, N. *Lectins;* Kluwer Academic Publishers: Dordrecht, The Netherlands, 2003.
2. Lis, H.; Sharon, N. *Chem. Rev.* **1998,** *98,* 637–674. doi:10.1021/cr940413g
3. Quiocho, F. A. *Pure Appl. Chem.* **1989,** *61,* 1293–1306. doi:10.1351/pac198961071293
4. Weiss, W. I.; Drickamer, K. *Annu. Rev. Biochem.* **1996,** *65,* 441–473. doi:10.1146/annurev.bi.65.070196.002301
5. Lemieux, R. U. *Chem. Soc. Rev.* **1989,** *18,* 347–374. doi:10.1039/cs9891800347
6. Davis, A. P.; James, T. D. Carbohydrate Receptors. In *Functional Synthetic Receptors;* Hamilton, A. D., Ed.; Wiley-VCH: Weinheim, Germany, 2005; pp 45–109. doi:10.1002/352760572X.ch2
   For reviews on carbohydrate recognition with artificial receptors using noncovalent interactions, see [6-9].
7. Davis, A. P.; Wareham, R. S. *Angew. Chem.* **1999,** *111,* 3161–3179. doi:10.1002/(SICI)1521-3757(19991018)111:20<3160::AID-ANGE3160>3.0.CO;2-Z
   Angew. Chem., Int. Ed. **1999**, *38*, 2979–2996. doi:10.1002/(SICI)1521-3773(19991018)38:20<2978::AID-ANIE2978>3.0.CO;2-PP
8. Walker, D. B.; Joshi, G.; Davis, A. P. *Cell. Mol. Life Sci.* **2009,** *66,* 3177–3191. doi:10.1007/s00018-009-0081-8
9. Mazik, M. *Chem. Soc. Rev.* **2009,** *38,* 935–956. doi:10.1039/b710910p
10. Ferrand, Y.; Klein, E.; Barwell, N. P.; Crump, N. P.; Jiménez-Barbero, J.; Vicent, C.; Boons, G.-J.; Ingale, S.; Davis, A. P. *Angew. Chem., Int. Ed.* **2009,** *48,* 1775–1779. doi:10.1002/anie.200804905
    For some recent examples of carbohydrate receptors operating through noncovalent interactions see [10-16] and [27-45].
11. Abe, H.; Takashima, S.; Yamamoto, T.; Inouye, M. *Chem. Commun.* **2009,** 2121–2123. doi:10.1039/b902269d
12. Abe, H.; Horii, A.; Matsumoto, S.; Shiro, M.; Inouye, M. *Org. Lett.* **2008,** *10,* 2685–2688. doi:10.1021/ol800783a
13. Palde, P. B.; Gareiss, P. C.; Miller, B. L. *J. Am. Chem. Soc.* **2008,** *130,* 9566–9573. doi:10.1021/ja802229f
14. Klein, E.; Ferrand, Y.; Auty, E. K.; Davis, A. P. *Chem. Commun.* **2007,** 2390–2392. doi:10.1039/b618776e
15. Nativi, C.; Cacciarini, M.; Francesconi, O.; Moneti, G.; Roelens, S. *Org. Lett.* **2007,** *9,* 4685–4688. doi:10.1021/ol701959r
16. Ferrand, Y.; Crump, M. P.; Davis, A. P. *Science* **2007,** *318,* 619–622. doi:10.1126/science.1148735

17. James, T. D.; Shinkai, S. *Top. Curr. Chem.* **2002,** *218,* 159–200. doi:10.1007/3-540-45010-6_6
    For reviews on boronic acid-based receptors, which use covalent interactions for sugar binding, see [17,18].
18. James, T. D.; Sandanayake, K. R. A. S.; Shinkai, S. *Angew. Chem.* **1996,** *108,* 2038–2050. doi:10.1002/ange.19961081706
    Angew. Chem., Int. Ed. **1996**, *35*, 1910–1922. doi:10.1002/anie.199619101
19. Davis, A. P. *Org. Biomol. Chem.* **2009,** *7,* 3629–3638. doi:10.1039/b909856a
20. Kubik, S. *Angew. Chem.* **2009,** *121,* 1750–1753. doi:10.1002/ange.200805497
    Angew. Chem., Int. Ed. **2009**, *48*, 1722–1725. doi:10.1002/anie.200805497
21. Mazik, M. *ChemBioChem* **2008,** *9,* 1015–1017. doi:10.1002/cbic.200800038
22. Mazik, M.; Balzarini, J. Preparation of poly(hetero)arenes as antiinfective agents. PCT Int. Appl. WO 2008113557, 2008.
23. Mazik, M. Preparation of amino-naphthyridine derivatives as antiinfective agents. PCT Int. Appl. WO 2008113558, 2008.
24. Mazik, M.; Balzarini, J. Preparation of poly(hetero)arenes as antiinfective agents. Eur. Pat. Appl. EP 1972338, 2008.
25. Mazik, M. Preparation of amino-naphthyridine derivatives as antiinfective agents. Eur. Pat. Appl. EP 1972627, 2008.
26. Boltz, K. W.; Gonzalez-Moa, M. J.; Stafford, P.; Johnston, S. A.; Svarovsky, S. A. *Analyst* **2009,** *134,* 650–652. doi:10.1039/b823156g
27. Mazik, M.; Hartmann, A.; Jones, P. G. *Chem.–Eur. J.* **2009,** *15,* 9147–9159. doi:10.1002/chem.200900664
28. Mazik, M.; Buthe, A. C. *Org. Biomol. Chem.* **2009,** *7,* 2063–2071. doi:10.1039/b901173k
29. Mazik, M.; Hartmann, A. *J. Org. Chem.* **2008,** *73,* 7444–7450. doi:10.1021/jo8005842
30. Mazik, M.; Buthe, A. C. *Org. Biomol. Chem.* **2008,** *6,* 1558–1568. doi:10.1039/b719212f
31. Mazik, M.; Kuschel, M. *Chem.–Eur. J.* **2008,** *14,* 2405–2419. doi:10.1002/chem.200701269
32. Mazik, M.; Kuschel, M. *Eur. J. Org. Chem.* **2008,** 1517–1526. doi:10.1002/ejoc.200701097
33. Mazik, M.; Buthe, A. C. *J. Org. Chem.* **2007,** *72,* 8319–8326. doi:10.1021/jo701370g
34. Mazik, M.; Cavga, H. *J. Org. Chem.* **2007,** *72,* 831–838. doi:10.1021/jo061901e
35. Mazik, M.; König, A. *Eur. J. Org. Chem.* **2007,** 3271–3276. doi:10.1002/ejoc.200700295
36. Mazik, M.; Cavga, H. *Eur. J. Org. Chem.* **2007,** 3633–3638. doi:10.1002/ejoc.200700264
37. Mazik, M.; König, A. *J. Org. Chem.* **2006,** *71,* 7854–7857. doi:10.1021/jo0610309
38. Mazik, M.; Cavga, H. *J. Org. Chem.* **2006,** *71,* 2957–2963. doi:10.1021/jo052479p
39. Mazik, M.; Kuschel, M.; Sicking, W. *Org. Lett.* **2006,** *8,* 855–858. doi:10.1021/ol052902g
40. Mazik, M.; Cavga, H.; Jones, P. G. *J. Am. Chem. Soc.* **2005,** *127,* 9045–9052. doi:10.1021/ja043037i
41. Mazik, M.; Radunz, W.; Boese, R. *J. Org. Chem.* **2004,** *69,* 7448–7462. doi:10.1021/jo048979k
42. Mazik, M.; Sicking, W. *Tetrahedron Lett.* **2004,** *45,* 3117–3121. doi:10.1016/j.tetlet.2004.02.087
43. Mazik, M.; Radunz, W.; Sicking, W. *Org. Lett.* **2002,** *4,* 4579–4582. doi:10.1021/ol0201759
44. Mazik, M.; Sicking, W. *Chem.–Eur. J.* **2001,** *7,* 664–670. doi:10.1002/1521-3765(20010202)7:3<664::AID-CHEM664>3.0.CO;2-E
45. Mazik, M.; Bandmann, H.; Sicking, W. *Angew. Chem.* **2000,** *112,* 562–565. doi:10.1002/(SICI)1521-3757(20000204)112:3<562::AID-ANGE562>3.0.CO;2-N
    Angew. Chem., Int. Ed. **2000**, *39*, 551–554. doi:10.1002/(SICI)1521-3773(20000204)39:3<551::AID-ANIE551>3.0.CO;2-7
46. Katritzky, A. R.; Pozharski, A. F. *Handbook of Heterocyclic Chemistry;* Pergamon: Amsterdam, The Neverlands, 2000; p 131.
    For a discussion on annular tautomerism of NH-imidazoles, see [46].
47. Wallace, K. J.; Hanes, R.; Anslyn, E.; Morey, J.; Kilway, K. V.; Siegel, J. *Synthesis* **2005,** 2080–2083. doi:10.1055/s-2005-869963
48. Bähr, A.; Felber, B.; Schneider, K.; Diederich, F. *Helv. Chim. Acta* **2000,** *83,* 1346–1376. doi:10.1002/1522-2675(20000705)83:7<1346::AID-HLCA1346>3.0.CO;2-3
49. Inouye, M.; Chiba, J.; Nakazumi, H. *J. Org. Chem.* **1999,** *64,* 8170–8176. doi:10.1021/jo9911138
50. Inouye, M.; Miyake, T.; Furusyo, M.; Nakazumi, H. *J. Am. Chem. Soc.* **1995,** *117,* 12416. doi:10.1021/ja00155a006
51. Schneider, H.-J.; Yatsimirsky, A. *Principles and Methods in Supramolecular Chemistry;* John Wiley & Sons: Chichester, 2000; p 148.
    For a description of the mole ratio method, see [51,52].
52. Tsukube, H.; Furuta, H.; Odani, A.; Takeda, Y.; Kudo, Y.; Inoue, Y.; Liu, Y.; Sakamoto, H.; Kimura, K. In *Comprehensive Supramolecular Chemistry;* Atwood, J.-L.; Davis, J. E. D.; MacNicol, D. D.; Vögtle, F., Eds.; Pergamon: Oxford, UK, 1996; Vol. 8, p 425.
53. Wilcox, C. S.; Glagovich, N. M. Program HOSTEST 5.6. Ph.D. Thesis, University of Pittsburgh, Pittsburgh, PA, 1994.
    Hostest program is designed to fit data to different binding models, which include both “pure” binding models, taking into consideration the formation of only one type of complex in solution (1:1, 1:2 or 2:1 receptor–substrate complex), and “mixed” binding models containing more than one type of complex in solution (for example, 1:1 and 1:2 or 1:1 and 2:1 receptor–substrate complex).
54. The binding studies were carried out in $CDCl_3$ and DMSO-d_6/$CDCl_3$ mixtures at 25 °C. $CDCl_3$ was stored over activated molecular sieves and deacidified with Al_2O_3. The titration data were analyzed by non-linear regression analysis, using the program HOSTEST 5.6 (see reference [53]). For each system at least three titrations were carried out; for each titration 15–20 samples were prepared. Dilution experiments show that the receptors do not self-aggregate in the used concentration range. Error in K_a was <10%. K_{11} corresponds to the 1:1 association constant. K_{21} corresponds to the 2:1 receptor–sugar association constant. K_{12} corresponds to the 1:2 receptor–sugar association constant. $\beta_{21} = K_{11} \times K_{21}$, $\beta_{12} = K_{11} \times K_{12}$.
55. Fielding, L. *Tetrahedron* **2000,** *56,* 6151–6170. doi:10.1016/S0040-4020(00)00492-0
56. Klein, E.; Ferrand, Y.; Barwell, N. P.; Davis, A. P. *Angew. Chem.* **2008,** *120,* 2733–2736. doi:10.1002/ange.200704733
    Angew. Chem., Int. Ed. **2008**, *47*, 2693–2696. doi:10.1002/anie.200704733
57. Tsuzuki, S.; Uchimaru, T.; Mikami, M. *J. Phys. Chem. B* **2009,** *113,* 5617–5621. doi:10.1021/jp8093726

58. Terraneo, G.; Potenza, D.; Canales, A.; Jiménez-Barbero, J.; Baldridge, K. K.; Bernardi, A. *J. Am. Chem. Soc.* **2007,** *129,* 2890–2900. doi:10.1021/ja066633g
59. Chávez, M. I.; Andreu, C.; Vidal, P.; Aboitiz, N.; Freire, F.; Groves, P.; Asensio, J. L.; Asensio, G.; Muraki, M.; Cañada, F. J.; Jiménez-Barbero, J. *Chem.–Eur. J.* **2005,** *11,* 7060–7074. doi:10.1002/chem.200500367
60. Screen, J.; Stanca-Kaposta, E. C.; Gamblin, D. P.; Liu, B.; Macleod, N. A.; Snoek, L. C.; Davis, B. G.; Simons, J. P. *Angew. Chem., Int. Ed.* **2007,** *46,* 3644–3648. doi:10.1002/anie.200605116
61. Kiehna, S. H.; Laughrey, Z. R.; Waters, M. L. *Chem. Commun.* **2007,** 4026–4028. doi:10.1039/b711431a
62. Morales, J. C.; Penadés, S. *Angew. Chem., Int. Ed.* **1998,** *37,* 654–657. doi:10.1002/(SICI)1521-3773(19980316)37:5<654::AID-ANIE654>3.0.CO;2-X
63. Raju, R. K.; Ramraj, A.; Vincent, M. A.; Hillier, I. H.; Burton, N. A. *Phys. Chem. Chem. Phys.* **2008,** *10,* 6500–6508. doi:10.1039/b809164a
64. Neidlein, U.; Diederich, F. *Chem. Commun.* **1996,** 1493–1494. doi:10.1039/cc9960001493
For examples of receptors, which show strong di- vs. monosaccharide preference, see [14,28,30,33,37,64].

License and Terms

Beilstein Journal of Organic Chemistry

Size selective recognition of small esters by a negative allosteric hemicarcerand

Holger Staats and Arne Lützen*

Full Research Paper

Open Access

Address:
University of Bonn, Kekulé-Institute of Organic Chemistry and Biochemistry, Gerhard-Domagk-Str. 1, D-53121 Bonn, Germany

Email:
Arne Lützen* - arne.luetzen@uni-bonn.de

* Corresponding author

Keywords:
allosteric receptors; 2,2′-bipyridine; hemicarcerand; molecular recognition; resorcin[4]arene

Beilstein Journal of Organic Chemistry **2010,** *6,* No. 10.
doi:10.3762/bjoc.6.10

Received: 20 October 2009
Accepted: 21 January 2010
Published: 03 February 2010

Guest Editor: C. A. Schalley

Abstract

A bis(resorcinarene) substituted 2,2′-bipyridine was found to bind weakly to small esters like ethyl acetate whereas more bulky esters were not recognized by this hemicarcerand. This size selective molecular recognition could be controlled by a negative cooperative allosteric effect: coordination of a triscarbonyl rhenium chloride fragment to the bipyridine causes a conformational rearrangement that orientates the resorcinarene moieties in different directions so that they cannot act cooperatively in the binding of the substrate.

Introduction

Nature uses allosteric effects in a very elegant manner to control numerous biochemical pathways [1]. Thus, the transfer of this principle to artificial systems is both challenging and promising to regulate supramolecular functionality [2]. The idea is to employ cooperative effects in the selective association of more than one substrate to different binding sites of a single receptor. This causes conformational rearrangements that switch on or off a function that is inherently embedded in the different parts of the molecule but which need to be specially arranged in space in order to act in an optimized cooperative fashion. Some time ago we were able to report on a heterotropic positive cooperative allosteric analogue (**1**) [3] of some well known hemicarcerands [4,5] (Scheme 1). Their recognition behaviour towards non-polar substrates could be dramatically changed upon coordination of a late transition metal ion such as silver(I) as an effector or modulator to a central 2,2′-bipyridine. This structure has proved to be an excellent allosteric centre [6-26] due to its well defined ability to switch between *syn*- and an *anti*-conformations [27]. Recently, we were able to synthesize a number of derivatives of this first example of an allosteric hemicarcerand and their metal complexes formed upon coordination to metal salts or complexes like $AgBF_4$, $CuBF_4$, $[Cuphen]BF_4$, or $[(CO)_5ReCl]$ [28]. Among these, bis(resorcin[4]arene) substituted 2,2′-bipyridine **2** is a structural isomer of **1** differing only in the substitution pattern of the central bipyridine unit: whereas in **1** the 2,2′-bipyridine is substituted in the 4,4′-position it carries the resorcinarene moieties in 4,6′-position in **2**.

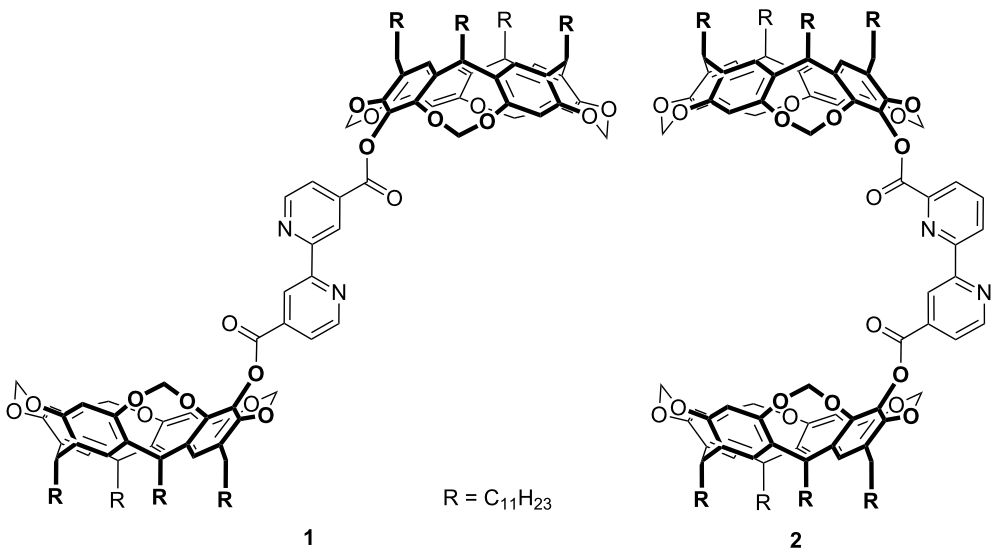

Scheme 1: Bis(resorcinarene) esters of 4,4′- and 4,6′-(2,2′-bipyridyl)dicarboxylic acid, **1** and **2**, respectively.

This, however, causes a very important difference in the receptor's function: **1** is an example of a receptor that can be controlled by a heterotropic positive allosteric effect because it has an open conformation in its non-coordinated form since the 2,2′-bipyridine adopts an *anti*-conformation which is inactive as a receptor. Therefore, it needs to be activated by the coordination of a transition metal ion in order to form the closed conformation where the two resorcinarene moieties can act together to bind to the substrate. **2**, however, can adopt a closed conformation that is ready to act as a receptor but can be transferred into an inactive open form upon coordination of a transition metal ion as an effector. Thus, **2** is designed to act as a first example for a heterotropic negative cooperative allosteric hemicarcerand whose function as a receptor can be switched off by adding a transition metal ion as an effector. In this account we present a proof of principle that this concept indeed works: **2** was found to have a weak affinity for simple esters in a size selective manner in the absence of an effector whereas it does not show any binding affinity when it is coordinated to a tris(carbonyl)rhenium chloride fragment – thus showing negative cooperative allosteric behaviour.

Results and Discussion

Molecular mechanics studies (MMFF force field, Spartan 08) indicate that **2** offers only a very small cavity surrounded by rather non-polar acetal and aryl groups for the encapsulation of a small non-polar substrate via dispersive interactions. Unfortunately, **2** is soluble only in rather non-polar solvents which, however, are reasonably good guests for **2** themselves if they are small enough to fit into the cavity. Moreover, they are also good solvents for any other non-polar substrate. Thus, we did not expect to observe high affinities in these binding studies. In order to minimize the competition of the substrates with the solvent for the encapsulation we chose to do the binding studies in mesitylene-d_{12} which seemed to be too large to fit into the cavity of **2**. We then chose to test its ability to bind to simple esters like ethyl acetate (**3**), *n*-propyl propionate (**4**), *n*-butyl butyrate (**5**), isopropyl isobutyrate (**6**), and *tert*-butyl pivalate (**7**) (Scheme 2) because esters show reasonably low polarity and can easily be obtained in different sizes and shapes.

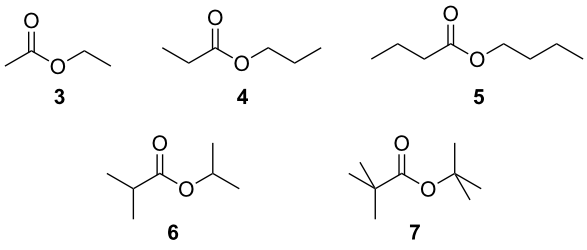

Scheme 2: Simple esters used as model substrates in this study.

With respect to the huge mass difference we decided to use an excess of guest rather than the host to get some initial qualitative information about the recognition behaviour from NMR investigations and in order to avoid solubility problems and other unspecific aggregation of **2**. Thus, in a first set of experiments 15 equivalents of the respective esters were added to a 5 mM solution of **2** in mesitylene-d_{12} in order to observe an effect for the signals of the bis(resorcinarene) host, whereas effects for the guests were only expected in case of slow guest exchange behaviour on the NMR timescale (Figure 1).

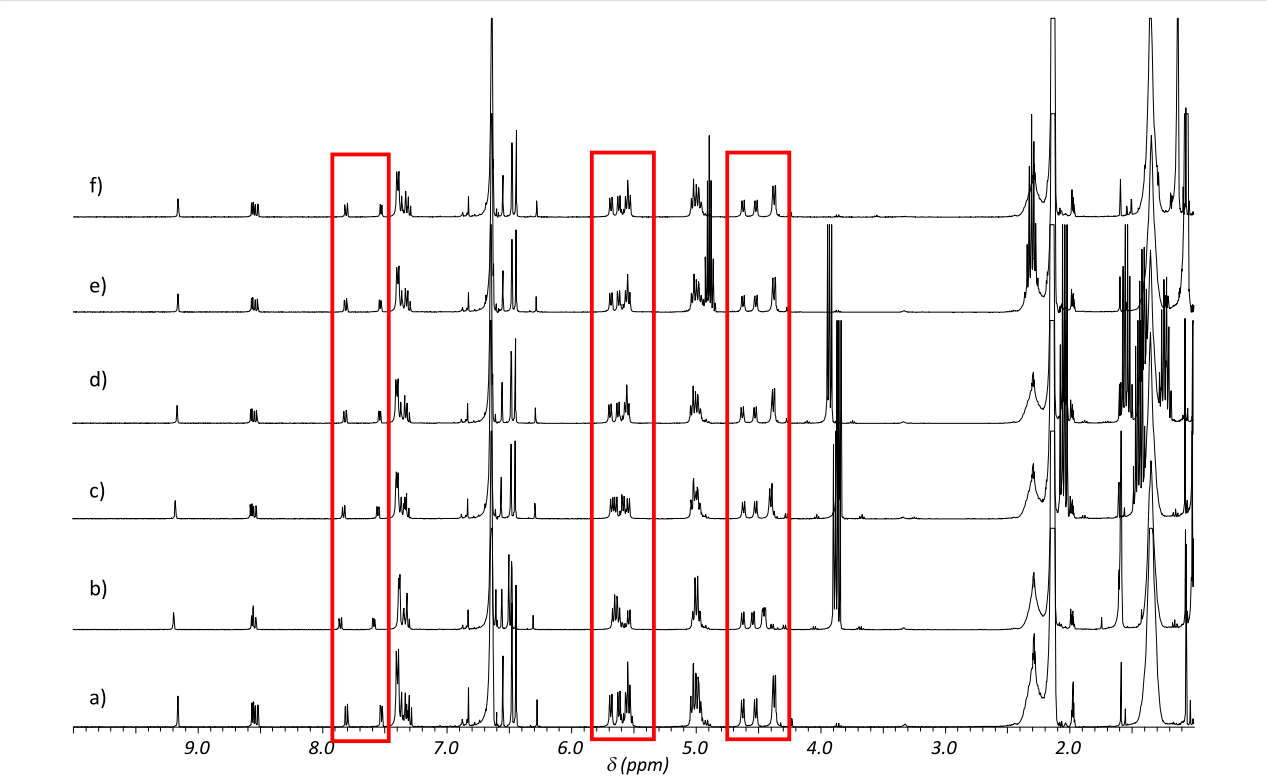

Figure 1: Qualitative binding studies of **2** and the model substrates **3**–**7**. ^{1}H NMR spectra (500.1 MHz, 298 K in mesitylene-d_{12}, c_0(**2**) = 5 mmol/L) of a) **2**, b) **2** and 15 equiv of **3**, c) **2** and 15 equiv of **4**, d) **2** and 15 equiv of **5**, e) **2** and 15 equiv of **6**, f) **2** and 15 equiv of **7**. Marked in red rectangles are the regions of the signals of the acetal and some of the bipyridine hydrogen atoms of **2**.

As expected, only the smallest esters **3** and **4** cause small but significant shifts of some of the receptor's proton signals that can be assigned to hydrogen atoms of the acetal bridges of the resorcinarenes (4.2–4.8 and 5.3–5.9 ppm) and of the bipyridine (7.5–8.0 ppm), respectively. Note that these hydrogen atoms are all located more or less inside the cavity which clearly indicates encapsulation of the esters rather than a kind of accidental binding to the receptor's convex outer surface or within the long alkyl chains in its periphery, whose signals remain almost unchanged.

The guest exchange, however, was found to be fast on the NMR time-scale since we could not detect different sets of signals for the encapsulated guest and the free guest but rather observed an averaged signal very close to the one of the free guest due to the large excess of the free substrate. Despite the large excess of the free guest this also hints at a rather low binding affinity of **2** towards the esters as expected for the reasons given above. Addition of the larger esters **5**–**7**, however, did not result in any significant shifts indicating size-selective discrimination of the different esters.

In order to evaluate this phenomenon further we performed an NMR titration to determine the association constant for the binding of the arguably best guest ethyl acetate assuming a 1:1 stoichiometry of the resulting host-guest complex (Figure 2).

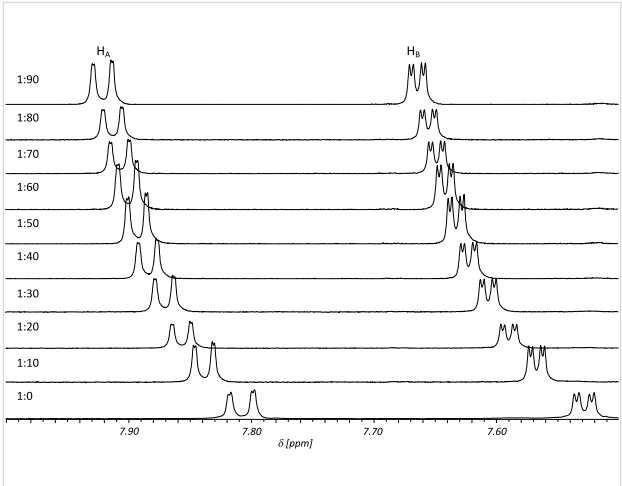

Figure 2: ^{1}H NMR titration (500.1 MHz, 298 K, c_0(**2**) = 5.3 mmol/L) of **2** with increasing amounts of ethyl acetate. H_A and H_B are both signals of protons of the 2,2′-bipyridine (see Supporting Information for further details).

Analysis of the binding isotherms by non-linear regression revealed only a small association constant of $K = 9 \pm 1\ M^{-1}$

which, however, was not unexpected given the fact that binding occurs mainly due to quite weak dispersive interactions in a rather competitive solvent (for this kind of interactions).

Having established the successful, but weak, binding in its active conformation we then examined its recognition behaviour in the presence of an effector. As demonstrated in an earlier study [28] pentacarbonylrhenium(I) chloride is able to form a stable complex [$(CO)_3$Re(**2**)Cl] that was found to be soluble in mesitylene-d_{12}. Usually, 2,2′-bipyridyl complexes of rhenium are kinetically almost inert. In this case, however, we were able to show that the rhenium can indeed be removed by adding ethylene diamine tetraacetic acid (EDTA). Thus, pentacarbonylrhenium(I) chloride seemed indeed an excellent effector here because it can be used to switch off **2** by coordination to the bipyridine and switch it on again when it is removed. When we repeated the titration with this complex we did observe some shifts of the host signals but these did not reach any saturation and the analysis of these curves did result in an association constant $K < 1\ M^{-1}$. This, however, indicates that the recognition behaviour of **2** can indeed be controlled in a heterotropic negative cooperative allosteric fashion (Scheme 3).

Having established this first example for a negative allosteric hemicarcerand we are now working on the improvement of the performance of our allosteric receptors, e.g. by using other cavitand-building blocks with deeper cavities.

Experimental

Compound **2** and its complex [$(CO)_3$Re(**2**)Cl] were prepared according to our recently published procedure [28]. Esters **3**–**7** were purchased in p.a. quality. Mesitylene-d_{12} and [$(CO)_5$ReCl] were obtained form commercial sources and used as received. NMR spectra were recorded on a Bruker DRX 500 spectrometer. ^{1}H NMR Chemical shifts are reported as δ values (ppm) relative to residual non-deuterated solvent as the internal standard.

Analysis of the binding isotherms obtained from the NMR titration experiments was done by non-linear regression methods.

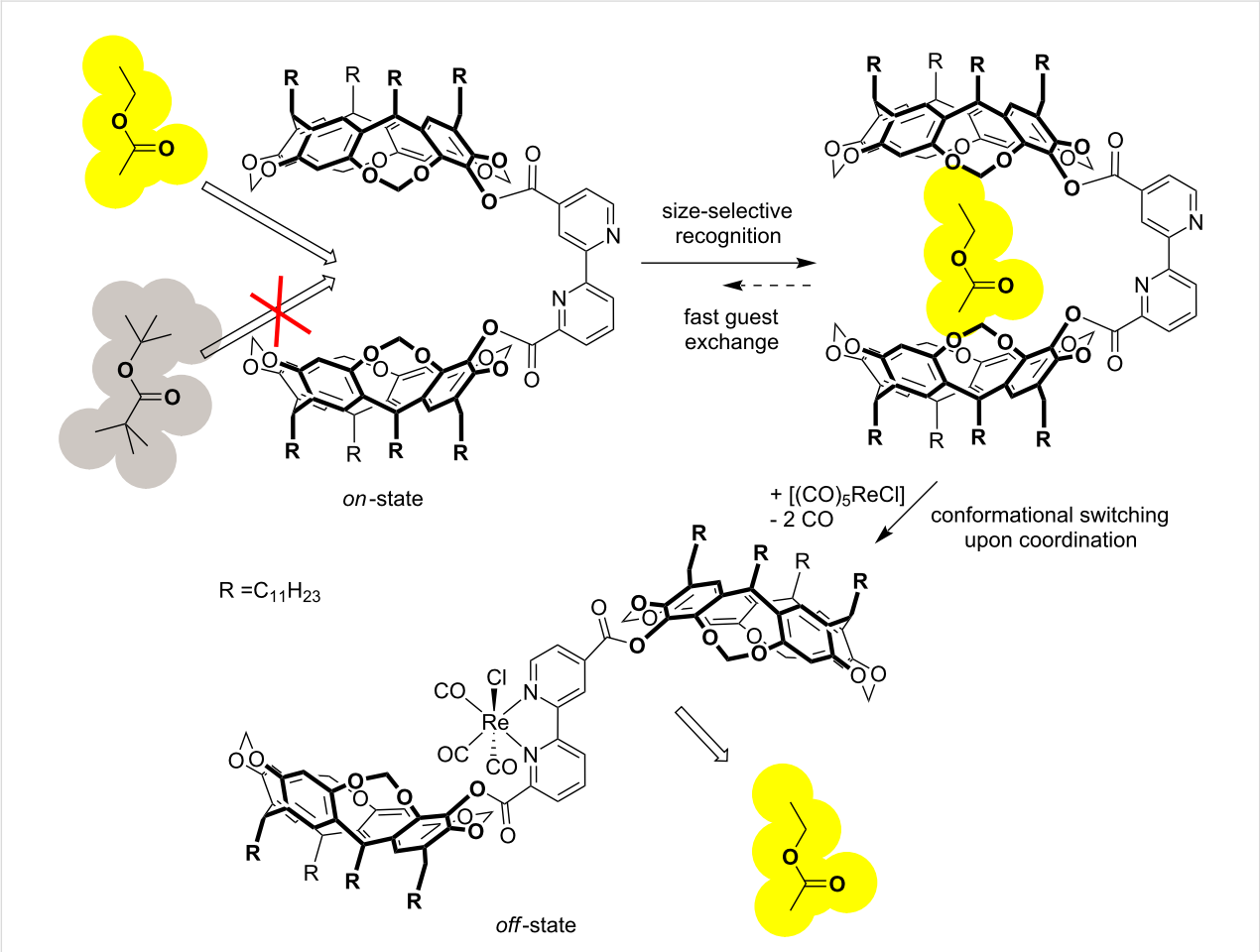

Scheme 3: Binding model of the negative cooperative allosteric behaviour of **2**.

Supporting Information

Binding isotherms obtained from the NMR titrations.

Supporting Information File 1

NMR Titrations
[http://www.beilstein-journals.org/bjoc/content/supplementary/1860-5397-6-10-S1.pdf]

Acknowledgements

Financial support from the DFG (SFB 624) is gratefully acknowledged.

References

1. Nelson, D. L.; Cox, M. M. *Lehninger Biochemie,* 3rd ed.; Springer: Berlin, 2001.
2. Kovbasyuk, L.; Krämer, R. *Chem. Rev.* **2004,** *104,* 3161–3187. doi:10.1021/cr030673a
3. Lützen, A.; Haß, O.; Bruhn, T. *Tetrahedron Lett.* **2002,** *43,* 1807–1811. doi:10.1016/S0040-4039(02)00086-2
4. Cram, D. J.; Cram, M. J. *Container Molecules and Their Guests;* Royal Society of Chemistry: Cambridge, U.K., 1994.
5. Sherman, J. C. *Tetrahedron* **1995,** *51,* 3395–3422. doi:10.1016/0040-4020(94)01072-8
6. Rebek, J., Jr.; Trend, J. E.; Wattley, R. V.; Chakravorti, S. *J. Am. Chem. Soc.* **1979,** *101,* 4333–4337. doi:10.1021/ja00509a047
7. Rebek, J., Jr.; Wattley, R. V. *J. Am. Chem. Soc.* **1980,** *102,* 4853–4854. doi:10.1021/ja00534a058
8. Rebek, J., Jr. *Acc. Chem. Res.* **1984,** *17,* 258–264. doi:10.1021/ar00103a006
9. Rebek, J., Jr.; Costello, T.; Marshall, L.; Wattley, R. V.; Gadwood, R. C.; Onan, K. *J. Am. Chem. Soc.* **1985,** *107,* 7481–7487. doi:10.1021/ja00311a043
10. Beer, P. D.; Rothin, A. S. *J. Chem. Soc., Chem. Commun.* **1988,** 52–54. doi:10.1039/C39880000052
11. Redman, J. E.; Beer, P. D.; Dent, S. W.; Drew, M. G. B. *Chem. Commun.* **1998,** 231–232. doi:10.1039/a707680k
12. Beer, P. D.; Dent, S. W. *Chem. Commun.* **1998,** 825–826. doi:10.1039/a800356d
13. Cooper, J. B.; Drew, M. G. B.; Beer, P. D. *J. Chem. Soc., Dalton Trans.* **2000,** 2721–2728. doi:10.1039/b003569f
14. Watanabe, S.; Higashi, N.; Kobayashi, M.; Hamanaka, K.; Takata, Y.; Yoshida, K. *Tetrahedron Lett.* **2000,** *41,* 4583–4586. doi:10.1016/S0040-4039(00)00635-3
15. Nakashima, K.; Shinkai, S. *Chem. Lett.* **1994,** 1267–1270. doi:10.1246/cl.1994.1267
16. Sandanayake, K. R. A. S.; James, T. D.; Shinkai, S. *Pure Appl. Chem.* **1996,** *68,* 1207–1212. doi:10.1351/pac199668061207
17. Mizuno, T.; Takeuchi, M.; Hamachi, I.; Nakashima, K.; Shinkai, S. *Chem. Commun.* **1997,** 1793–1794. doi:10.1039/a704041e
18. Mizuno, T.; Takeuchi, M.; Hamachi, I.; Nakashima, K.; Shinkai, S. *J. Chem. Soc., Perkin Trans. 2* **1998,** 2281–2288. doi:10.1039/a803382j
19. Deetz, M. J.; Smith, B. D. *Tetrahedron Lett.* **1998,** *39,* 6841–6844. doi:10.1016/S0040-4039(98)01492-0
20. Liu, Y.; Chen, Y.; Liu, S.-X.; Guan, X.-D.; Wada, T.; Inoue, Y. *Org. Lett.* **2001,** *3,* 1657–1660. doi:10.1021/ol015820a
21. Liu, Y.; Chen, Y.; Li, B.; Wada, T.; Inoue, Y. *Chem.–Eur. J.* **2001,** *7,* 2528–2535. doi:10.1002/1521-3765(20010618)7:12<2528::AID-CHEM25280>3.0.CO;2-9
22. Liu, Y.; Chen, Y.; Li, L.; Zhang, H.-Y.; Liu, S.-X.; Guan, X.-D. *J. Org. Chem.* **2001,** *66,* 8518–8527. doi:10.1021/jo0159789
23. Tomohiro, Y.; Satake, A.; Kobuke, Y. *J. Org. Chem.* **2001,** *66,* 8442–8446. doi:10.1021/jo015852b
24. Sakai, K.; Ozawa, H.; Yamada, H.; Tsubomura, T.; Hara, M.; Higuchi, A.; Haga, M.-A. *J. Chem. Soc., Dalton Trans.* **2006,** 3300–3305. doi:10.1039/b600165c
25. Plitt, P.; Gross, D. E.; Lynch, V. M.; Sessler, J. L. *Chem.–Eur. J.* **2007,** *13,* 1374–1381. doi:10.1002/chem.200601514
26. Jeffery, J. C.; Rice, C. R.; Harding, L. P.; Baylies, C. J.; Riis-Johannssen, T. *Chem.–Eur. J.* **2007,** *13,* 5256–5271. doi:10.1002/chem.200700261
27. Zahn, S.; Reckien, W.; Kirchner, B.; Staats, H.; Matthey, J.; Lützen, A. *Chem.–Eur. J.* **2009,** *15,* 2572–2580. doi:10.1002/chem.200801374
28. Staats, H.; Eggers, F.; Haß, O.; Fahrenkrug, F.; Matthey, J.; Lüning, U.; Lützen, A. *Eur. J. Org. Chem.* **2009,** 4777–4792. doi:10.1002/ejoc.200900642

License and Terms

Beilstein Journal of Organic Chemistry

Templated versus non-templated synthesis of benzo-21-crown-7 and the influence of substituents on its complexing properties

Wei Jiang and Christoph A. Schalley*

Full Research Paper

Open Access

Address:
Institut für Chemie und Biochemie, Freie Universität Berlin, Takustraße 3, 14195 Berlin, Germany

Email:
Christoph A. Schalley* - christoph@schalley-lab.de

* Corresponding author

Keywords:
benzo-21-crown-7; pseudorotaxane; self-sorting; supramolecular chemistry; template

Beilstein Journal of Organic Chemistry **2010,** *6,* No. 14.
doi:10.3762/bjoc.6.14

Received: 14 November 2009
Accepted: 16 January 2010
Published: 11 February 2010

Guest Editor: C. A. Schalley

Abstract

Two procedures for the synthesis of benzo-21-crown-7 have been explored. The [1+1] macrocyclization with KBF_4 as the template was found to be more efficient than the intramolecular macrocyclization without template. Pseudorotaxanes form with secondary ammonium ions bearing at least one alkyl chain narrow enough to slip into the crown ether. Substitution on benzo-21-crown-7 or on the secondary ammonium axle alters the binding affinity and binding mode. Compared to dibenzo-24-crown-8, the complexing properties of benzo-21-crown-7 turn out to be more susceptible to modifications at the crown periphery.

Introduction

Mechanically interlocked structures [1-4] are attractive to chemists not only because they are aesthetically appealing but also due to their potential applications in molecular machines and smart materials [5-9]. Although a few covalent templates are known [10-12], their synthesis most often makes use of non-covalent templates [13-16], for which quite a number of different binding motifs are available that make the synthesis of many diverse and complex interlocked structures possible. Among these, the threaded interaction of secondary ammonium ions with larger crown ethers is a prominent example [17-22]. Recently, Huang and co-workers reported that the macrocycle size for forming pseudorotaxane can be reduced to only 21 atoms, namely benzo-21-crown-7 [23] (**C7**; Scheme 1) and pyrido-21-crown-7 [24], which could still slip over a secondary dialkylammonium ion when one of the alkyl groups is a narrow alkyl chain. By using this binding motif, the so far smallest [2]rotaxane consisting of only 76 atoms and having a molecular weight of not more than 510 Da was synthesized by Chiu and co-workers [25]. More recently, we applied **C7** together with dibenzo-24-crown-8 (DB24C8) to the construction of a four-component self-sorting system based on the fact that **C7** cannot pass over a phenyl stopper group at the end of a dialkylammonium axle, while DB24C8 can [26]. This system was further extended to construct more complex multiply interlocked struc-

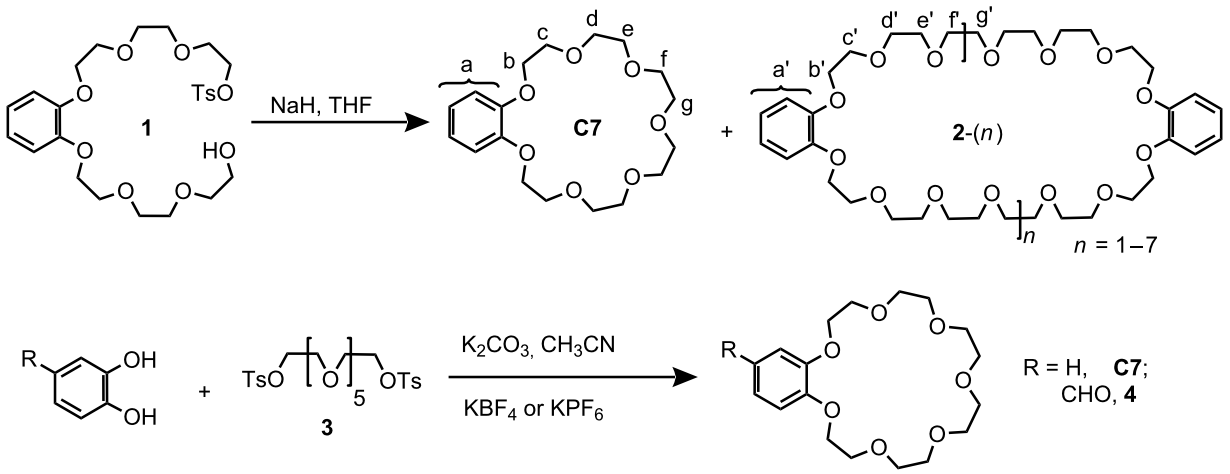

Scheme 1: Two synthetic procedures for the preparation of benzo-21-crown-7 (**C7**) and its formyl analogue **4**: Top: The non-templated macrocyclization of **1** yields a mixture of crown ethers of different sizes. Bottom: With K^+ as the template, benzo-21-crown-7 can be obtained in much better yields.

tures by using the strategy of integrative self-sorting [26,27] which ensures programmability and positional control of all distinct subunits present in the complexes. Along this line, more diverse and complex supramolecular structures could be obtained when suitable instructions are written into the structures of their components.

Modification of crown ethers and their secondary ammonium guests allows variation of their binding properties and enables them to be incorporated into more complex assemblies [28]. In this respect, benzocrown ethers are more preferable than their aliphatic analogs due to the easy-to-achieve substitution on the benzene ring. One prerequisite for the generation of more complex supramolecular architecture based on such ammonium/crown binding motifs is the efficient synthesis of the building blocks. Here we report on attempts to improve the synthesis of **C7** and the preparation of substituted derivatives. Two synthetic routes, one which utilizes a templating cation and one which does not involve a template, are compared. Finally, the effects of substituents on the crown ether binding behavior are examined to lay the basis for a more precise control over the assembly of future complex assemblies.

Results and Discussion

Synthesis of C7. Several synthetic procedures for **C7** have been explored systematically under phase-transfer conditions by Lukyanenko et al. [28]. Among them, intramolecular macrocyclization via monotosylate **1** generated in situ gives rise to the highest yield (68%). To test the efficiency of intramolecular ring closure in the absence of phase-transfer catalysis, we synthesized the monotosylate **1** which is then used in a separate macrocyclization (Scheme 1). Disappointingly, only 24% yield was achieved for the synthesis of **C7** from **1**. A second fraction of 31% turned out to be a mixture of **C7**'s bigger homologues **2**-(*n*) (*n* = 1−7) There are two reasons responsible for the relatively low yield: (i) the initial concentration (90 mM) of **1** is too high, favoring polycondensation over the intramolecular macrocyclization; (ii) the sodium ion originating from the NaH used as the base is not an appropriate template for **C7** [29]. Meanwhile, the low yield and long procedure discourage the application of intramolecular macrocylization to the synthesis of **C7**'s derivatives. Therefore, an alternative procedure with improved efficiency was sought.

The synthetic procedure with catechol and hexa(ethylene glycol) ditosylate (**3**) (Scheme 1) is advantageous since they are commercially available or easily prepared from commercially available materials. However, under phase-transfer conditions, this procedure gives **C7** in a relatively low yield (22%), which is not acceptable for synthesizing complex **C7** derivatives. Huang et al. [23] modified this procedure by introducing KPF_6 as a template, which increased the yield to 69%. Nevertheless, we found it difficult to cleanly separate the KPF_6 salt from **C7** during the reaction workup, since their complex dissolves well in organic solvents (e.g. $CDCl_3$, ethylacetate). This can be attributed to the quite high hydrophobicity of the PF_6^- anion. Instead, KBF_4 was found to be a very good template which gives a satisfying yield (70%) and could be completely removed after column chromatography. This was further supported by the application to the synthesis of **4** (yield: 62%).

Characterization of higher crown oligomers 2-(*n*). The signals in the ^{1}H NMR spectra of **2**-(*n*) (Figure 1e) appear at almost exactly the same position as those of **C7** (Figure 1c). The broadening of the signals is the only indication that the sample contains more than just **C7**. Consequently, it is difficult

to distinguish the larger oligomers from **C7** by simple ^{1}H NMR experiments. In the corresponding ESI mass spectra, the ionization efficiency is quite low. Some of the major components can be observed easily, but minor products are hard to detect. Therefore, we added charged guest **5**-H•PF_6 (Scheme 2) to the mixture to (i) detect signal shifts in the NMR spectra characteristic for the formation of complexes and (ii) to facilitate the ionization of the crown ether oligomers as ammonium complexes. This guest will furthermore provide straightforward evidence for the formation of crown ethers larger than **C7**, because the phenyl group in **5**-H•PF_6 is too bulky to thread through the cavity of **C7** [23]. Complex formation thus immediately indicates that the crown ether must have a larger cavity than **C7**. As seen in Figure 1b, the spectra of the equimolar mixture of **5**-H•PF_6 and **C7** is the simple superimposition of their individual spectra (Figure 1a,Figure 1c). However, addition of **5**-H•PF_6 to the fraction containing the larger oligomers **2**-(*n*) caused shifts of all signals for both of guest and host indicative of complex formation (Figure 1d,Figure 1e). From these experiments, we can conclude that crown ethers larger than **C7** have formed, but the composition of the fraction containing **2**-(*n*) is still not yet clear. From the structure of the starting material **1**, dibenzo-42-crown-14 (**2**-(1)) is certainly the most likely candidate, but even larger structures cannot be ruled out yet.

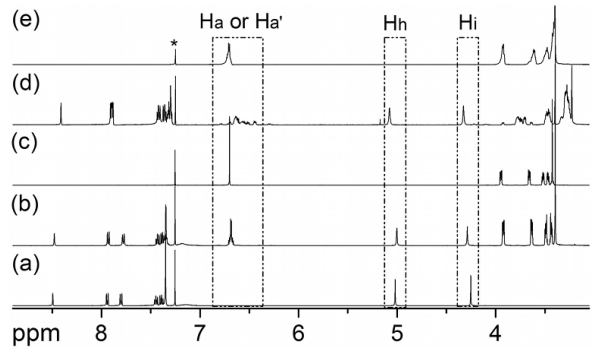

Figure 1: ^{1}H NMR spectra (500 MHz, 298 K, $CDCl_3$:CD_3CN = 2:1, 10.0 mM) of **5**-H•PF_6 (**a**), mixture of **5**-H•PF_6 and **C7** (**b**), **C7** (**c**), mixture of **5**-H•PF_6 and **2**-(*n*) (**d**), and **2**-(*n*) (**e**). Asterisk = residual undeuterated solvent.

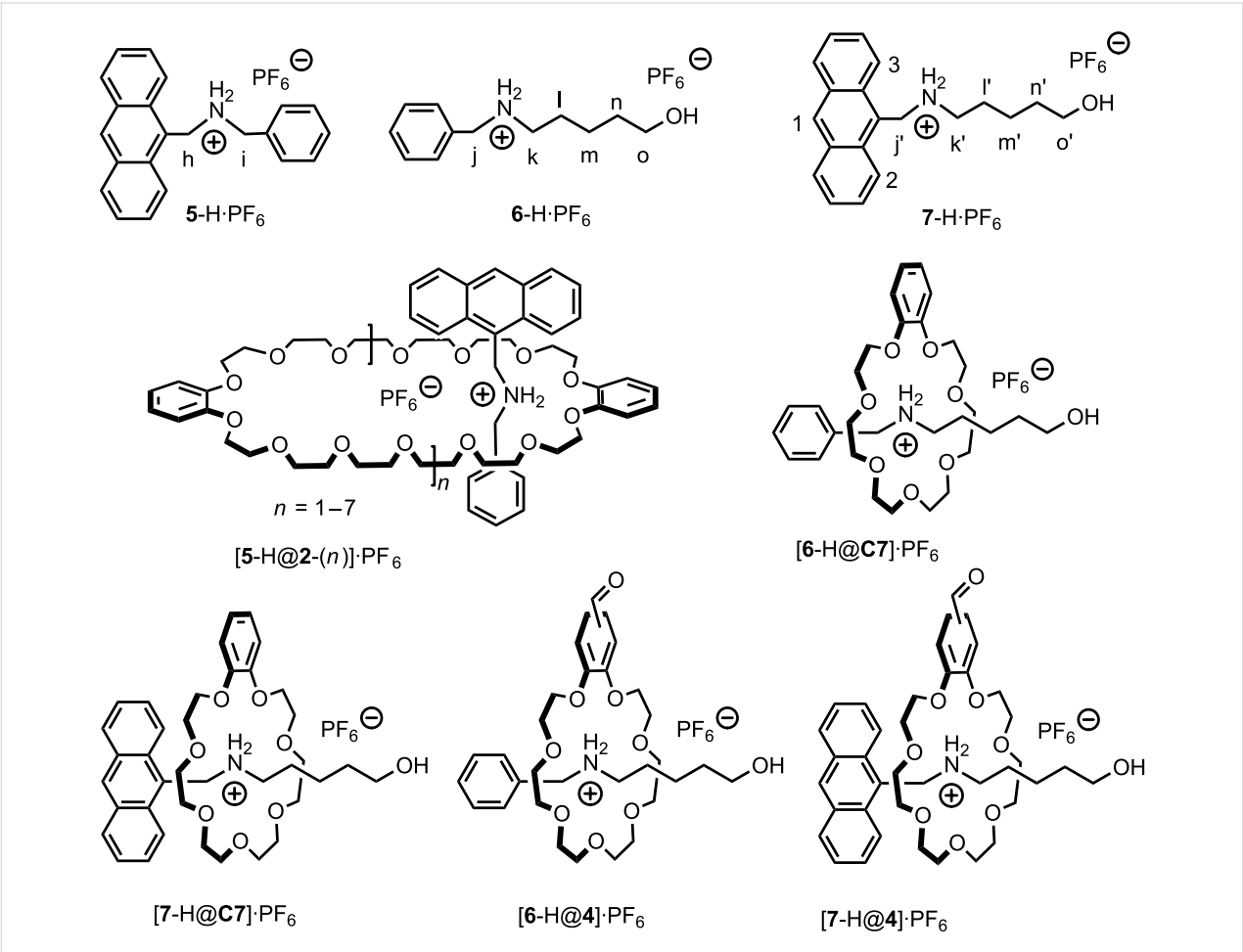

Scheme 2: Molecular structures of guests **5**-H•PF_6, **6**-H•PF_6, and **7**-H•PF_6, and their complexes with **2**-(*n*), **C7** and **4**.

To further elucidate the structure of **2**-(*n*), ESI-MS experiments were performed with the mixture of the second crown ether fraction and **5**-H•PF_6. To our surprise, a broad series of several peaks evenly spaced by a distance of Δm = 356 amu was observed in the ESI mass spectrum (Figure 2). Considering that [**5**-H]$^+$ does not simultaneously form complexes with several **C7** crown ethers, this peak distribution can only be assigned to a series of macrocycles with different sizes ranging from dibenzo-42-crown-14 (**2**-(1)) up to heptabenzo-168-crown-56 (**2**-(7)). Although the peak intensity does not necessarily reflect the solution composition quantitatively [30], the mass spectra indicate **2**-(1) − **2**-(4) to be the major components in the mixture, while the larger crown ethers are likely present only in trace amounts. Since we are focusing on **C7**, no attempt was made to separate the larger crown ethers by more sophisticated methods such as HPLC.

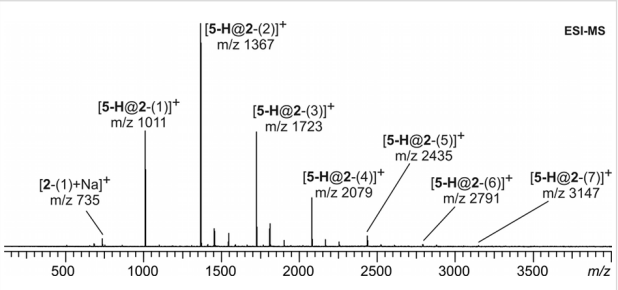

Figure 2: ESI-FTICR mass spectrum of a mixture of **5**-H•PF_6 and **2**-(*n*) in dichloromethane.

Characterization of (C7+KPF_6) formed in the KPF_6-templated synthesis of C7. The ^{1}H NMR spectrum (Figure 3c) of the **C7** product obtained from the KPF_6-templated reaction through extraction with dichloromethane (DCM) from water and column chromatography (eluent gradient: ethylacetate:methanol = 50:1 to 20:1) clearly indicates the formation of a potassium complex which even survived the column chromatography. A comparison with the spectrum of pure **C7** (Figure 3a) and a mixture of pure **C7** and KPF_6 (Figure 3b) reveals that the product obtained from the column shows similar signal shifts as compared to those of the KPF_6 complex. This is supported by ESI-MS experiments. In the ESI mass spectrum (Figure S1, Supporting Information) of (**C7**+KPF_6) sprayed from DCM, three intense peaks at *m/z* 379, 395, and 935 are observed, which can be assigned to [**C7**+Na]$^+$, [**C7**+K]$^+$ and [$\mathbf{C7}_2$+K+KPF_6]$^+$, respectively. Since no KPF_6 was added to the solution after column chromatography, the presence of the latter two signals indicated survival of the (**C7**+KPF_6) complex.

Addition of axle **5**-H•PF_6 to (**C7**+KPF_6) caused no obvious ^{1}H NMR signal changes of one of the building blocks, **5**-H•PF_6 and (**C7**+KPF_6) (Figure 4). Axle **5**-H•PF_6 is consequently not able

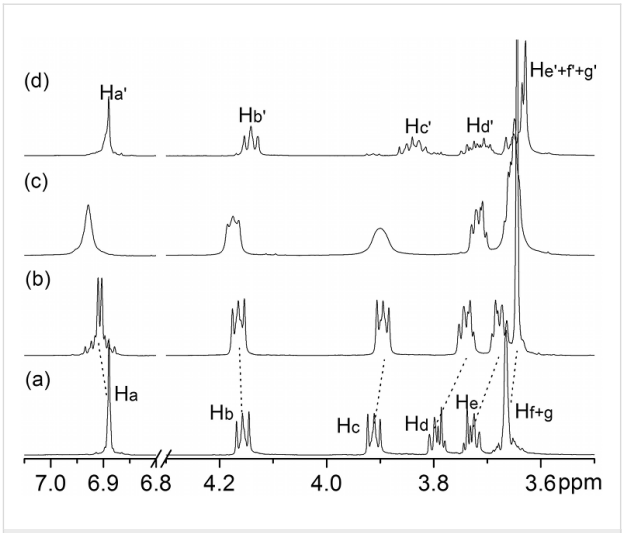

Figure 3: ^{1}H NMR spectra (500 MHz, 298 K, $CDCl_3$, 10.0 mM) of (**a**) **C7**, (**b**) **C7** in the presence of 1 eq. KPF_6, (**c**) the compound obtained after column chromatography from the KPF_6-templated reaction, and (**d**) **2**-(*n*).

to replace the potassium ion in (**C7**+KPF_6) likely because it cannot thread through the cavity.

In marked contrast, the ^{1}H NMR spectrum (Figure 4) of a mixture of **6**-H•PF_6 and (**C7**+KPF_6) shows a set of new complexation-induced signals, which appear at the same positions as those of independently generated [**6**-H@**C7**]•PF_6, suggesting that the thinner axle can thread into the crown ether to form the pseudorotaxane even in competition with the potassium ion. This conclusion is further supported by the formation of a white precipitate (KPF_6) after addition of axle **6**-H•PF_6 to the

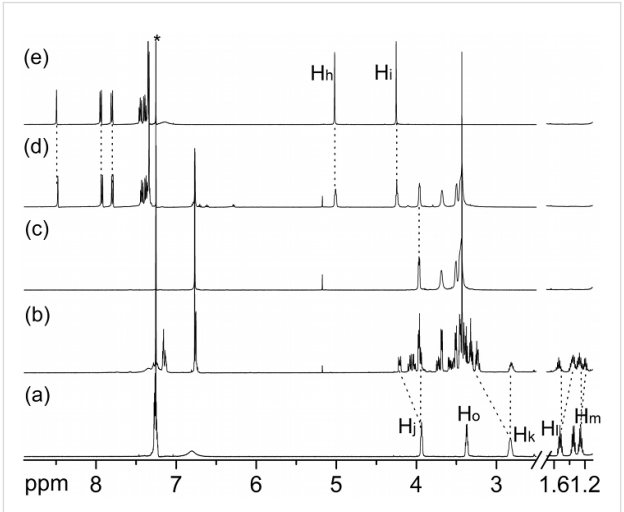

Figure 4: ^{1}H NMR spectra (500 MHz, 298 K, $CDCl_3$:CD_3CN = 2:1, 10.0 mM) of (**a**) **6**-HoPF_6, (**b**) mixture of **6**-HoPF_6 and (**C7**+KPF_6), (**c**) (**C7**+KPF_6), (**d**) mixture of **5**-HoPF_6 and (**C7**+KPF_6), (**e**) **5**-HoPF_6. Asterisk = solvent.

(**C7**+KPF_6) solution in 2:1 $CDCl_3/CD_3CN$. Furthermore, only one intense peak for [**6**-H@**C7**]$^+$ is observed in the ESI mass spectrum (Figure S2, Supporting Information). (**C7**+KPF_6) is sticky solid-like compound rather than oily product [28] as pure **C7** synthesized from **1**. The complex of (**C7**+KPF_6) could even dissolve in $CDCl_3$.

These results demonstrate the difficulties to remove KPF_6 from **C7** with a standard work-up procedure followed by column chromatography. Considering the good solubility of **C7** in water, more intense washing with water to remove the KPF_6 salt will likely reduce the yield.

Quite interestingly, the use of KBF_4 as the template during the synthesis of **C7** from catechol and **3** results in a much more easily achievable separation of uncomplexed **C7**. We speculate that the lower solubility of this salt in organic solvent helps to separate the crown ether from the salt during the extraction.

The effect of substituents on binding affinity and binding mode. The binding of axles **6**-H•PF_6 and **7**-H•PF_6 to **C7** is a slow process on the NMR time scale. Consequently, the corresponding binding constants of [**6**-H@**C7**]•PF_6, [**6**-H@**4**]•PF_6, [**7**-H@**C7**]•PF_6, and [**7**-H@**4**]•PF_6 in 2:1 $CDCl_3/CD_3CN$ solution (Figures S3–S10, Supporting Information) can easily be determined from the total host concentration and the relative integration of the separate signals for free and complexed hosts [31]. They are 17090 (±500) M^{-1}, 8000 (±270) M^{-1}, 5640 (±190) M^{-1}, and 3050 (±60) M^{-1}, respectively. The lower binding ability of **4** relative to **C7** is certainly due to the electron-withdrawing aldehyde group which decreases the electron-donating and hydrogen-bond accepting ability of the oxygen atoms on the catechol [32]. Consequently, electron-withdrawing substitution on **C7** should be avoided when aiming at strong binding between the two building blocks.

Literature reports that a change of guest from secondary dibenzylammonium hexafluorophosphate (360 M^{-1}, 1.0 mM, in acetone-d_6) [31] to the anthracenyl methyl-substituted analogue **5**-H•PF_6 (496 M^{-1}, 1.0 mM, in acetone-d_6) [26] increases the binding affinity with DB24C8, which is mainly attributed to stronger π-π stacking interactions with the larger anthracene π-system in **5**-H•PF_6.

Analogously, stronger binding of **C7** would be expected with **7**-H•PF_6 as compared to **6**-H•PF_6. Surprisingly, the binding affinities of **C7** or **4** toward anthracenyl methyl-substituted **7**-H•PF_6 turn out to be lower than to benzyl-substituted **6**-H•PF_6. There are two reasons for this remarkable difference between **C7** and the larger analogue dibenzo-24-crown-8. (i) According to related crystal structures [23-25], no π-π stacking interactions operate between hosts **C7** or **4** and guests **6**-H•PF_6 or **7**-H•PF_6. (ii) Even more important, however, are the polarized methylene groups next to the ammonium center. These groups form C-H•••O hydrogen bonds [33] with the crown ether as indicated by the quite substantial complexation-induced downfield shifts (0.25 and 0.55 ppm, respectively, observed for H_j and H_k of [**6**-H@**C7**]•PF_6 and [**6**-H@**4**]•PF_6 (Figure 5b,Figure 5c) relative to free **6**-H•PF_6. In contrast, $H_{j'}$ on **7**-H•PF_6 is observed to shift downfield by only 0.05 ppm after complexation with **C7** and undergoes hardly any shift when the axle is complexed to **4**, while $H_{k'}$ experiences a 0.76 ppm upfield shift for complexing with both hosts (Figure 5d,Figure 5e). These facts suggests that $H_{j'}$ of **7**-H•PF_6 may be only loosely involved in the C-H•••O hydrogen-bonding with **C7** or **4** due to the increased steric demand of the anthracenyl methyl group. Consequently, the symmetry and the cavity size of dibenzo-24-crown-8 are suitable to adopt to the requirements of the anthracenyl methyl group and the binding energy increases, when phenyl is replaced by anthracenyl. Instead, the cavity of **C7** is smaller and likely unable to adjust itself to the anthracenyl methyl-substituted axle. Some of the C-H•••O hydrogen bonds which can form with **6**-H•PF_6 do not form with **7**-H•PF_6 and thus weaken the complexes of the latter axle.

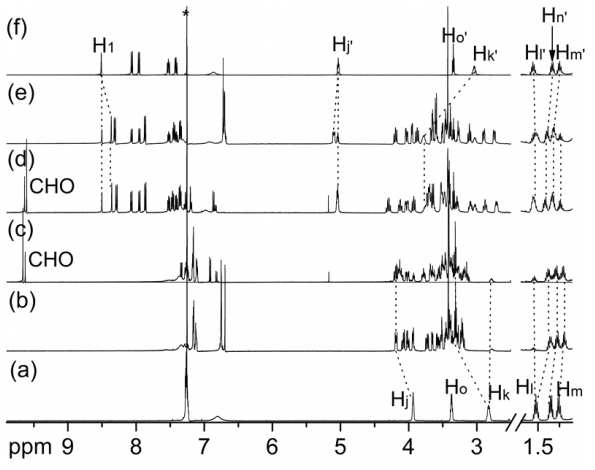

Figure 5: ^1H NMR spectra (500 MHz, 298 K, $CDCl_3$:CD_3CN = 2:1, 10.0 mM) of (**a**) **6**-H•PF_6, equimolar mixtures of (**b**) **6**-H•PF_6 and **C7**, (**c**) **6**-H•PF_6 and **4**, (**d**) **7**-H•PF_6 and **4**, and (**e**) **7**-H•PF_6 and **C7**, and (**f**) **7**-H•PF_6, Asterisk = solvent residue.

Conclusion

In summary, two procedures have been explored for the synthesis of **C7**. The one with catechol and hexa(ethylene glycol) ditosylate as starting materials and KBF_4 as template turned out to be a quite efficient synthetic pathway allowing easy introduction of a variety of substituents by choosing the appropriate catechol building block. In addition, two guests **5**-H•PF_6 and

6-H•PF_6 are found to be very useful for the characterization of **C7** and its homologues on the basis of the fact that **C7** could not pass over phenyl group. Modifications of **C7** and secondary dialkylammonium guests significantly alter the binding ability. Replacing a benzyl stopper on the axle by an anthracenyl methyl group even changes the binding mode: Formation of C-H•••O hydrogen bonds is hampered for the methylene group between the anthracene and the ammonium. Compared to DB24C8, the complexing property of **C7** is more susceptible to modification probably because the smaller macrocycle is more or less rigidified after complexation with secondary dialkylammonium, thus weakening its adjustability. This has to be taken into account if one desires to construct more complex interlocked assemblies by using **C7** and secondary dialkylammonium ions as building blocks in the future.

Experimental

General Methods. All reagents were commercially available unless explicitly stated and used without further purification. 1,2-Bis{2-[2-(2-hydroxyethoxy)ethoxy]ethoxy}benzene [34], **5**-H•PF_6 [35] and **6**-H•PF_6 [23] were synthesized according to literature procedures. Solvents were either employed as purchased or dried prior to use by usual laboratory methods. Thin-layer chromatography (TLC) was performed on aluminum sheets coated with silica gel 60/F_{254} (Merck KGaA). The plates were inspected by UV light, and if required, developed in I_2 vapor. Column chromatography was performed on silica gel 60 (Merck 40–60 nm, 230–400 mesh). ^{1}H and ^{13}C NMR spectra were recorded on Bruker ECX 400 MHz and Jeol Eclipse 500 MHz. All chemical shifts are reported in ppm with residual solvents as the internal standards, and the coupling constants (*J*) are in Hertz. The following abbreviations were used for signal multiplicities: s, singlet; d, doublet; t triplet; m, multiplet. Electrospray-ionization time-of-flight high-resolution mass spectrometry (ESI-TOF-HRMS) experiments were conducted on an Agilent 6210 ESI-TOF, Agilent Technologies and a Varian/IonSpec QFT-7 FTICR (Fourier-transform ion-cyclotron-resonance) mass spectrometer equipped with a superconducting 7 Tesla magnet and a micromass Z-spray Electrospray-ionization (ESI) ion source utilizing a stainless steel capillary with a 0.75 mm inner diameter.

2-{2-[2-(2-{2-[2-(2-Hydroxyethoxy)ethoxy]ethoxy}phenoxy)ethoxy]ethoxy}ethyl-4-methylbenzene-sulfonate (1): To a mixture of 1,2-Bis{2-[2-(2-hydroxyethoxy)ethoxy]ethoxy}benzene (5.15 g, 13.8 mmol) in THF (60 mL) and sodium hydroxide (2.2 g, 55 mmol) in H_2O (60 mL) in an ice bath was added dropwise tosyl chloride (3.2 g, 16.8 mmol) in THF (150 mL) for 2 h. The mixture was continued to stir overnight in ice bath, THF was evaporated under reduced pressure. The residue was suspended in H_2O (50 mL), extracted with CH_2Cl_2 (100 mL × 3) and then dried over anhydrous Na_2SO_4. After the solvent was removed in vacuo, the crude product was subjected to column chromatography (silica gel, eluent: ethyl acetate: hexane = 2:1) to afford a pale-yellow oil **1** (3.0 g, 41%). ^{1}H NMR (400 MHz, $CDCl_3$, 298 K): δ (ppm) = 2.42 (s, 3H), 3.58–3.62 (m, 4H), 3.64–3.75 (m, 10H), 3.80–3.88 (m, 4H), 4.12–4.17 (m, 6H), 6.89–6.91 (m, 4H), 7.31 (d, *J* = 8.0 Hz, 2H), 7.78 (d, *J* = 8.4 Hz, 2H); ^{13}C NMR (100 MHz, $CDCl_3$, 298 K): δ (ppm) = 21.7, 61.9, 68.8, 68.91, 68.94, 69.4, 69.89, 69.90, 70.5, 70.8, 70.9, 71.0, 72.6, 115.0, 121.8, 128.0, 129.9, 133.0, 144.9, 149.0; ESI-TOF-HRMS: *m/z* calcd for $[M+Na]^+$ (100%): 551.1921, found: 551.1926; *m/z* calcd for $[M+K]^+$ (20%): 567.1661, found: 567.1664.

Benzo-21-crown-7 (C7) and its homologues (2-(*n*)): The mixture of **1** (2.37 g, 4.5 mmol) and NaH (0.60 g, 25.0 mmol) in anhydrous THF (50 mL) was refluxed for 3 d. After cooling down to room temperature, water (100 mL) was added to quench the superfluous NaH. THF was removed under reduced pressure, and the residue was extract by CH_2Cl_2 (100 mL × 3). The organic phase was collected, dried over anhydrous Na_2SO_4, and concentrated in vacuo to give the crude product, which was isolated by column chromatography (silica gel, eluent: ethyl acetate/MeOH, 100:1 to 20:1) to afford **C7** [23,28] (380 mg, 24%) and **2**-(*n*) (490 mg, 31%) as yellow oil. For **C7**, ^{1}H NMR (400 MHz, $CDCl_3$, 298 K): δ (ppm) = 3.64–3.69 (m, 8H), 3.71–3.75 (m, 4H), 3.77–3.81 (m, 4H), 3.92 (t, *J* = 4.6 Hz, 4H), 4.16 (t, *J* = 4.6 Hz, 4H), 6.87–6.91 (m, 4H); ^{13}C NMR (100 MHz, $CDCl_3$, 298 K): δ (ppm) = 69.3, 69.9, 70.6, 71.07, 71.13, 71.16, 114.5, 121.6, 149.0; For **2**-(*n*), ^{1}H NMR (400 MHz, $CDCl_3$, 298 K): δ (ppm) = 3.57–3.68 (m, 12(*n*+1)H), 3.68–3.76 (m, 4(*n*+1)H), 3.79–3.87 (m, 4(*n*+1)H), 4.12–4.18 (m, 4(*n*+1)H), 6.86–6.94 (m, 4(*n*+1)H); ^{13}C NMR (100 MHz, $CDCl_3$, 298 K): δ (ppm) = 68.9, 69.0, 69.1, 69.8, 69.9, 70.6, 70.66, 70.71, 70.75, 70.87, 70.89, 70.93, 71.08, 71.14, 71.17, 114.8, 115.0, 121.6, 121.7, 149.1.

Hexa(ethylene glycol) ditosylate (3): Hexa(ethylene glycol) (5.0 g, 17.7 mol) in THF (50 mL) and sodium hydroxide (4.8 g, 120 mmol) in H_2O (50 mL) was mixed in 500 mL flask. To the mixture in an ice bath was added dropwise tosyl chloride (12 g, 63 mmol) in THF (100 mL) for 2 h. The reaction mixture was stirred for another 5 h in ice bath, and THF was then concentrated under reduced pressure. The residue was suspended in H2O (150 ml) and extracted with dichloromethane (100 mL × 3) and then dried over anhydrous Na_2SO_4. The solvent was removed in vacuo to give **3** [23] as a pale-yellow oil (10 g, 96%) which is pure enough for next step. ^{1}H NMR (400 MHz, $CDCl_3$, 298 K): δ (ppm) = 2.44 (s, 6H), 3.55–3.64 (m, 16H), 3.67 (t, *J* = 4.8 Hz, 4H), 4.14 (t, *J* = 4.8 Hz, 4H), 7.33 (d, *J* = 8.0 Hz, 2H), 7.79 (d, *J* = 8.0 Hz, 2H).

General procedure for synthesis of C7 KPF_6 or KBF_4 as template and 4 with KBF_4 as template: While stirring vigorously under argon atmosphere, a suspension of K_2CO_3 (2.07 g, 15 mmol) and KPF_6 or KBF_4 (7.5 mmol) in anhydrous CH_3CN (100 mL) was heated to reflux. To the suspension was added dropwise a solution of **3** (2.95 g, 5.0 mmol) and catechol or 3,4-dihydroxybenzaldehyde (5.0 mmol) in CH_3CN (100 mL) during 12 h. The resulting reaction mixture was stirred under reflux for another 3 d. Upon cooling down to ambient temperature, the suspension was filtered and washed with CH_2Cl_2 (100 mL). The filtrate was concentrated under vacuum. The residue was partitioned between CH_2Cl_2 (100 mL) and water (100 mL), and the aqueous phase was extracted twice by CH_2Cl_2 (50 mL). The combined organic phase was dried over anhydrous Na_2SO_4, and concentrated under reduced pressure to give the crude product, which was purified by column chromatography over silica gel (eluent: ethyl acetate/MeOH, from 50:1 to 20:1). For **C7** (with KBF_4 as template) (1.25 g, 70%), yellow oil, the ^{1}H NMR spectrum is in line with the literature [23,28] and the one synthesized from compound **1**; For **4** (1.20 g, 62%), yellow oil; ^{1}H NMR (400 MHz, $CDCl_3$, 298 K): δ (ppm) = 3.63–3.69 (m, 8H), 3.70–3.75 (m, 4H), 3.77–3.82 (m, 4H), 3.91–3.97 (m, 4H), 4.18–4.24 (m, 4H), 6.95 (d, J = 8.4 Hz, 1H), 7.38 (d, J = 1.6 Hz, 1H), 7.43 (dd, J_1 = 8.4 Hz, J_2 = 1.6 Hz, 1H), 9.82 (s, 1H); ^{13}C NMR (100 MHz, $CDCl_3$, 298 K): δ (ppm) = 69.2, 69.3, 69.5, 69.6, 70.6, 71.0, 71.05, 71.1, 71.2, 71.3, 71.4, 111.4, 112.3, 126.9, 130.3, 149.2, 154.4, 190.9; ESI-TOF-HRMS: *m/z* calcd for $[M+K]^+$ (100%): 423.1416, found: 423.1434.

5-[(Anthracen-10-yl)methylamino]pentan-1-ol (7): 9-Anthracenecarboxaldehyde (1.00 g, 4.9 mmol) and 5-aminopentan-1-ol (0.71 mL, 6.5 mmol) were refluxed for 24 h in a mixture of 90 ml of absolute ethanol and 60 ml of $CHCl_3$. After cooling down to room temperature, $NaBH_4$ (1.86 g, 49 mmol) was added and the resulting solution stirred at room temperature for another 24 h. The solvent was removed under vacuum. The resulting residue was treated with water and the compound was repeatedly extracted with CH_2Cl_2 (three times 50 ml). The organic phase was dried over anhydrous Na_2SO_4, and the solvent was evaporated to give the crude product, which was subjected to column chromatography over silica gel (eluent, CH_2Cl_2:MeOH, 100:1 to 20:1) to afford **7** [36] (1.00 g, 70%) as a yellow solid. ^{1}H NMR (400 MHz, $CDCl_3$, 298 K): δ (ppm) = 1.37–1.46 (m, 2H), 1.51–1.65 (m, 4H), 2.87 (t, J = 7.0 Hz, 2H), 3.59 (t, J = 6.4 Hz, 2H), 4.73 (s, 2H), 7.43–7.48 (m, 2H), 7.51–7.56 (m, 2H), 7.98–8.02 (m, 2H), 8.30–8.35 (m, 2H), 8.40 (s, 1H); ^{13}C NMR (100 MHz, $CDCl_3$, 298 K): δ (ppm) = 23.5, 29.7, 32.6, 45.8, 50.4, 62.8, 124.2, 125.0, 126.2, 129.3, 130.4, 131.6; ESI-TOF-HRMS: *m/z* calcd for $[M+H]^+$ (100%): 294.1852, found: 294.1858.

7-H•PF_6: To compound **7** (1.00 g, 3.41 mmol) dissolved in MeOH (30 mL) was added conc. HCl to adjust pH < 2, and the solvent was then evaporated off under reduced pressure. The residue was suspended in acetone (30 mL). Saturated aqueous NH_4PF_6 solution was added until the suspension became clear. The solvent was removed in vacuo, and water (100 mL) was added to the residue. The resulting mixture was stirred at ambient temperature overnight. The mixture was then filtered, washed with copious amounts of H_2O, and dried to give **7**-H•PF_6 as a yellow solid (1.39 g, 92%). ^{1}H NMR (400 MHz, CD_3CN, 298 K): δ (ppm) = 1.36–1.44 (m, 2H), 1.46–1.54 (m, 2H), 1.69–1.78 (m, 2H), 3.25–3.34 (m, 2H), 3.48 (t, J = 6.2 Hz, 2H), 5.23 (t, J = 6.2 Hz, 2H), 7.58–7.64 (m, 2H), 7.70–7.76 (m, 2H), 8.14–8.19 (m, 2H), 8.30–8.34 (m, 2H), 8.74 (s, 1H); ^{13}C NMR (100 MHz, CD_3CN, 298 K): δ (ppm) = 23.4, 26.2, 32.3, 44.9, 49.9, 62.0, 122.0, 124.2, 126.6, 128.6, 130.4, 131.8, 132.3; ESI-TOF-HRMS: *m/z* calcd for $[M\text{-}PF_6]^+$ (100%): 294.1852, found: 294.1852.

Supporting Information

Supporting Information File 1

NMR and MS spectra of the corresponding complexes.
[http://www.beilstein-journals.org/bjoc/content/supplementary/1860-5397-6-14-S1.pdf]

Acknowledgements

We thank the Deutsche Forschungsgemeinschaft (SFB 765) and the Fonds der Chemischen Industrie for financial support.

References

1. Sauvage, J.-P.; Dietrich-Buchecker, C. O., Eds. *Molecular Catenanes, Rotaxanes and Knots;* Wiley-VCH: Weinheim, Germany, 1999.
2. Stoddart, J. F.; Colquhoun, H. M. *Tetrahedron* **2008,** *64,* 8231–8263. doi:10.1016/j.tet.2008.06.035
3. Stoddart, J. F. *Chem. Soc. Rev.* **2009,** *38,* 1521–1529. doi:10.1039/b819336n
4. Stoddart, J. F. *Chem. Soc. Rev.* **2009,** *38,* 1802–1820. doi:10.1039/b819333a
5. Balzani, V.; Credi, A.; Raymo, F. M.; Stoddart, J. F. *Angew. Chem.* **2000,** *112,* 3484–3530. doi:10.1002/1521-3757(20001002)112:19<3484::AID-ANGE3484>3.0.CO;2-O
Angew. Chem., Int. Ed. **2000,** *39,* 3348–3391. doi:10.1002/1521-3773(20001002)39:19<3348::AID-ANIE3348>3.0.CO;2-X
6. Stoddart, J. F., Ed. Molecular Machines Special Issue In. *Acc. Chem. Res.* **2001,** *34,* 409–522.
7. Feringa, B. L., Ed. *Molecular Switches;* Wiley-VCH: Weinheim, Germany, 2001.
8. Balzani, V.; Venturi, M.; Credi, A. *Molecular Devices and Machines – A Journey into the Nano World;* Wiley-VCH: Weinheim, Germany, 2003. doi:10.1002/3527601600

9. Kay, E. R.; Leigh, D. A.; Zerbetto, F. *Angew. Chem.* **2007,** *119,* 72–196. doi:10.1002/ange.200504313
Angew. Chem., Int. Ed. **2007,** *46,* 72–191. doi:10.1002/anie.200504313
10. Schill, G.; Zollenkopf, H. *Justus Liebigs Ann. Chem.* **1969,** *721,* 53–74. doi:10.1002/jlac.19697210109
11. Hiratani, K.; Suga, J.; Nagawa, Y.; Houjou, H.; Tokuhisa, H.; Numata, M.; Watanabe, K. *Tetrahedron Lett.* **2002,** *43,* 5747–5750. doi:10.1016/S0040-4039(02)01201-7
12. Hiratani, K.; Albrecht, M. *Chem. Soc. Rev.* **2008,** *37,* 2413–2421. doi:10.1039/b719548f
13. Schalley, C. A.; Vögtle, F.; Dötz, K.-H., Eds. Templates in Chemistry I. *Top. Curr. Chem.* **2004,** *248,* 1–260. doi:10.1007/b98600
14. Schalley, C. A.; Vögtle, F.; Dötz, K.-H., Eds. Templates in Chemistry II. *Top. Curr. Chem.* **2005,** *249,* 1–349. doi:10.1007/b98632
15. Broekmann, P.; Dötz, K.-H.; Schalley, C. A., Eds. Templates in Chemistry III. *Top. Curr. Chem.* **2009,** *287,* 1–255. doi:10.1007/978-3-540-89692-0
16. Schalley, C. A.; Illigen, J. Templated Synthesis of Interlocked Molecules. In *Bottom-up Nanofabrication: Supramolecules, Self-Assemblies, and Organized Films;* Ariga, K.; Nalwa, H. S., Eds.; American Scientific Publishers: Valencia/USA, 2009.
17. Kolchinski, A. G.; Busch, D. H.; Alcock, N. W. *J. Chem. Soc., Chem. Commun.* **1995,** 1289–1291. doi:10.1039/C39950001289
18. Kolchinski, A. G.; Alcock, N. W.; Roesner, R. A.; Busch, D. H. *Chem. Commun.* **1998,** 1437–1438. doi:10.1039/a800639c
19. Gibson, H. W.; Yamaguchi, N.; Hamilton, L.; Jones, J. W. *J. Am. Chem. Soc.* **2002,** *124,* 4653–4665. doi:10.1021/ja012155s
20. Huang, F.-H.; Jones, J. W.; Gibson, H. W. *J. Org. Chem.* **2007,** *72,* 6573–6576. doi:10.1021/jo070792g
21. Wu, J.; Leung, K. C.-F.; Stoddart, J. F. *Proc. Natl. Acad. Sci. U. S. A.* **2007,** *104,* 17266–17271. doi:10.1073/pnas.0705847104
22. Wu, J.; Leung, K. C.-F.; Benítez, D.; Han, J.-Y.; Cantrill, S. J.; Fang, L.; Stoddart, J. F. *Angew. Chem.* **2008,** *120,* 7580–7584. doi:10.1002/ange.200803036
Angew. Chem., Int. Ed. **2008,** *47,* 7470–7474. doi:10.1002/anie.200803036
23. Zhang, C.-J.; Li, S.-J.; Zhang, J.-Q.; Zhu, K.-L.; Li, N.; Huang, F.-H. *Org. Lett.* **2007,** *9,* 5553–5556. doi:10.1021/ol702510c
24. Zhang, C.-J.; Zhu, K.-L.; Li, S.-J.; Zhang, J.-Q.; Wang, F.; Liu, M.; Li, N.; Huang, F.-H. *Tetrahedron Lett.* **2008,** *49,* 6917–6920. doi:10.1016/j.tetlet.2008.09.110
25. Hsu, C.-C.; Chen, N.-C.; Lai, C.-C.; Liu, Y.-H.; Peng, S.-M.; Chiu, S.-H. *Angew. Chem.* **2008,** *120,* 7585–7588. doi:10.1002/ange.200803056
Angew. Chem., Int. Ed. **2008,** *47,* 7475–7478. doi:10.1002/anie.200803056
26. Jiang, W.; Winkler, H. D. F.; Schalley, C. A. *J. Am. Chem. Soc.* **2008,** *130,* 13852–13853. doi:10.1021/ja806009d
27. Jiang, W.; Schalley, C. A. *Proc. Natl. Acad. Sci. U. S. A.* **2009,** *106,* 10425–10429. doi:10.1073/pnas.0809512106
28. Bogaschenko, T.; Basok, S.; Kulygina, C.; Lyapunov, A.; Lukyanenko, N. *Synthesis* **2002,** 2266–2270. doi:10.1055/s-2002-34853
29. Ostrowicki, A.; Koepp, E.; Vögtle, F. The “cesium effect”: Syntheses of medio- and macrocyclic compounds. *Top. Curr. Chem;* 1992; Vol. 161, pp 37–67. doi:10.1007/3-540-54348-1_7
30. Leize, E.; Jaffrezic, A.; Van Dorsselaer, A. *J. Mass Spectrom.* **1996,** *31,* 537–544. doi:10.1002/(SICI)1096-9888(199605)31:5<537::AID-JMS330>3.0.CO;2-M
31. Ashton, P. R.; Chrystal, E. J. T.; Glink, P.; Menzer, S.; Schiavo, C.; Spencer, N.; Stoddart, J. F.; Tasker, P. A.; White, A. J. P.; Williams, D. J. *Chem.–Eur. J.* **1996,** *2,* 709–728. doi:10.1002/chem.19960020616
32. Liu, Y.; Li, C.-J.; Zhang, H.-Y.; Wang, L.-H.; Li, X.-Y. *Eur. J. Org. Chem* **2007,** 4510–4516. doi:10.1002/ejoc.200700265
33. Ashton, P. R.; Campbell, P. J.; Chrystal, E. J. T.; Glink, P.; Menzer, S.; Philp, D.; Spencer, N.; Stoddart, J. F.; Tasker, P. A.; Williams, D. J. *Angew. Chem.* **1995,** *107,* 1997–2001. doi:10.1002/ange.19951071711
Angew. Chem., Int. Ed. Engl. **1995,** *34,* 1865–1869. doi:10.1002/anie.199518651
34. Jiang, W.; Han, M.; Zhang, H.-Y.; Zhang, Z.-J.; Liu, Y. *Chem.–Eur. J.* **2009,** *15,* 9938–9945. doi:10.1002/chem.200901206
35. Ashton, P. R.; Ballardini, R.; Balzani, V.; Gómez-López, M.; Lawrence, S. E.; Martínez-Díaz, M. V.; Montalti, M.; Piersanti, A.; Prodi, L.; Stoddart, J. F.; Williams, D. J. *J. Am. Chem. Soc.* **1997,** *119,* 10641–10651. doi:10.1021/ja9715760
36. Clifford, T.; Abushamleh, A.; Busch, D. H. *Proc. Natl. Acad. Sci. U. S. A.* **2002,** *99,* 4830–4836. doi:10.1073/pnas.062639799

License and Terms

Beilstein Journal of Organic Chemistry

Molecular recognition of organic ammonium ions in solution using synthetic receptors

Andreas Späth and Burkhard König*

Review

Open Access

Address:
Institut für Organische Chemie, Universität Regensburg, D-93040 Regensburg, Germany, Phone: +49-943-941-4576, Fax: +49-943-941-1717

Email:
Burkhard König* - Burkhard.Koenig@chemie.uni-regensburg.de

* Corresponding author

Keywords:
amino acids; ammonium ion; molecular recognition; synthetic receptors

Beilstein J. Org. Chem. **2010,** *6,* No. 32.
doi:10.3762/bjoc.6.32

Received: 17 January 2010
Accepted: 09 March 2010
Published: 06 April 2010

Guest Editor: C. A. Schalley

Abstract

Ammonium ions are ubiquitous in chemistry and molecular biology. Considerable efforts have been undertaken to develop synthetic receptors for their selective molecular recognition. The type of host compounds for organic ammonium ion binding span a wide range from crown ethers to calixarenes to metal complexes. Typical intermolecular interactions are hydrogen bonds, electrostatic and cation–π interactions, hydrophobic interactions or reversible covalent bond formation. In this review we discuss the different classes of synthetic receptors for organic ammonium ion recognition and illustrate the scope and limitations of each class with selected examples from the recent literature. The molecular recognition of ammonium ions in amino acids is included and the enantioselective binding of chiral ammonium ions by synthetic receptors is also covered. In our conclusion we compare the strengths and weaknesses of the different types of ammonium ion receptors which may help to select the best approach for specific applications.

Introduction

The amino group is one of the most important functional groups in molecules of biological relevance. Examples of physiologically active amines (Figure 1) are histamine (**1**), dopamine (**2**) and quaternary ammonium ions, such as acetylcholine (**3**). Amino acids have amino groups like peptides and proteins. Under physiological conditions the amino group is usually protonated as an ammonium ion.

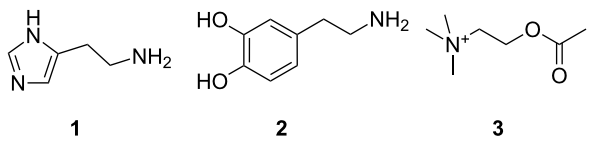

1 2 3

Figure 1: Biologically important amines and quaternary ammonium salts: histamine (**1**), dopamine (**2**) and acetylcholine (**3**).

The interaction of small ammonium ion bearing compounds with protein receptors is important for biological signal transduction processes. As in all biological regulatory processes, selectivity of recognition is of key importance for subsequent steps and cellular response. An example is the binding of histamine (**1**) to the human H_1 receptor, which results in lower blood pressure and dilatation of blood vessels or plays a primary role for allergic response [1-4]. The inhibition of biological processes is also addressed by molecular recognition involving amino acids and peptides: The antibiotic vancomycin binds selectively with its terminal lysyl-*R*-alanyl-*R*-alanine residues in bacterial cells through several hydrogen bonds [5]. Once it has bound to these particular peptides, they are no longer available for construction of the bacteria's cell wall causing their cell death.

Malfunction of dopamine-responsive neurons has been implicated in a number of disease conditions including Parkinson's disease [6]. The understanding of alkylammonium recognition in the dopamine (**2**) class of neurotransmitters is key to the development of tools to study these systems. Therefore the investigation of ammonium ion recognition is of considerable fundamental and practical interest [7,120].

Selective ligand-protein receptor binding relies typically on a number of specific interactions between two or more molecules. For the recognition of ammonium ions, three types of interactions, mostly acting simultaneously, are typically the most important:

1) Hydrogen bonds [8]

Hydrogen bonds are formed from the strongly polarized N^+–H bonds to a free electron pair of an electronegative atom (O, N, F). Crystal structures mainly show a linear arrangement of the three atoms but bifurcated hydrogen bonds can also be observed [9]. If exposed to a competing solvent, a single hydrogen bond cannot contribute much binding energy. Gas phase energies range from 22 kJ/mol (neutral hydrogen bonds between water molecules) up to 163 kJ/mol (anionic F–H–F^- complex) [10]. Quaternary ammonium ions cannot be bound by hydrogen bonds.

2) Cation–π-interaction [11]

The first experimental evidence of interactions between cations and aromatic π-systems came from Kebarle et al. who showed that binding of potassium ions to benzene and water in the gas phase is of similar energy [9,12]. Ammonium–π-interactions were experimentally investigated in detail as well as by ab initio calculations and are mainly based on electrostatic interactions. The binding energies are between 42 and 92 kJ/mol in the gas phase. The cation–π-bond is an important motif for the recognition of quaternary ammonium ions. A relevant example is the binding of acetylcholine (**3**) in biological systems [13].

3) Ion pairs and salt bridges

Coulombic interaction attracts cations and anions. In salt bridges, additional hydrogen bonds are formed [14]. A typical example of a salt bridge is the ammonium ion carboxylate ion pair. The strength of cation–anion affinity depends on the distance, the polarity of the solvent and the ionic strength. When extrapolated to zero ionic strength, most coulombic interactions are around 8 kJ/mol [15]. In aqueous medium ion pair formation is primarily driven by entropy, not directly by coulombic forces [16]. The binding energy is, in general, independent of the geometry, polarizability of the ions or the formation of a salt bridge.

In addition, the selective recognition of ammonium ions depends on steric and molecular complementarity and the preorganization [17] of interacting functional groups. As far back as 1890, Fischer suggested that enzyme–substrate interactions function like a "lock and key" between an initially empty host and a guest that exhibit molecular complementarity [18].

Today studies of non-covalent interactions, mainly by artificial model structures and receptors, have led to a far better understanding of many biological processes. Moreover, they are often the inspiration for supramolecular research, including self-assembly, mechanically-interlocked molecular architectures and molecular recognition in host–guest chemistry [19]. Analogous to biological systems, the formation and function of such supramolecular complexes occurs through a multiplicity of often difficult to differentiate non-covalent forces: Di- or polytopic receptors are used to enhance further the binding and selectivity with a binding mechanism that can be understood on the combined efforts of several non-covalent interactions such as hydrogen bonding, electrostatic interactions, hydrophobic interactions [20-22], cation–π interactions, π–π staking interactions [23,24] and steric complementarity [25]. The crucial interaction mechanisms have been comprehensively summarized [26,27]; basic rules for receptors and design have been outlined [28,29].

As in nature, molecular recognition can either be static – a complexation reaction with defined stoichiometry between a specific host and guest – or dynamic, where the binding of the first guest to the first binding site of a receptor affects the association constant of a second guest with a second binding site. Either positive allosteric binding – the first guest increases the association constant of the second guest – or negative allos-

teric binding – the first guest decreases the association constant with the second – can occur [30]. Positive allostery or co-operativity [31,32] is desireable for synthetic receptors. In most cases the host forms a cavity in which guest molecules are complexed as the "key" in the complementary binding site or an inclusion compound. This host pre-organization leads to a major enhancement of the overall energy of guest complexation. The binding is energetically favored: Both enthalpic – a less solvent accessible area leads to a less strongly solvated guest with fewer solvent-ligand bonds to break – as well as entropic – macrocycles [33] or cavities [34] being less conformationally flexible so losing fewer degrees of freedom upon complexation as a result of the reorganization energy already paid in advance in the synthesis.

In a few examples, guest molecules are enclosed on all sides by the receptor being "trapped" as in a cage forming clathrates [35]. Binding of the amino group to a planar surface of the receptor is found in metal complexes or metalla-porphyrins. The molecular environment and the solvent determine the stability of the assembly: competitive solvents building strong hydrogen bonds or having electrostatic and charge-transfer capabilities interfere with the ammonium ion binding and may even completely inhibit the complex formation. Recognition in water is especially a challenging topic of growing interest and has been recently reviewed [36].

Many types of synthetic ammonium ion receptors are available, ranging from crown ethers, calixarenes, porphyrins, cucurbiturils, cyclodextrins and cyclopeptides to tweezer ligands, sterically geared tripods and several types of metal complexes. The most important methods used for evaluating ammonium ion binding processes are direct absorption and emission measurements utilizing chromophores in the receptor or analyte molecule, displacement assays with suitable dyes, NMR titration experiments, isothermal titration calorimetry and transport through an organic phase monitored by HPLC, NMR [37,38] or UV–vis absorption [39].

Review

1. Scope and limitations of this survey

Synthetic receptors for organic ammonium ions may help to understand better the individual contributions of the different forces involved in ammonium ion binding. In addition, they are valuable tools as chemosensors for the analytical detection of drugs or biogenic amines, most of which have chiral structures. Enantiomeric recognition is an essential process in living organisms and frequently involve ammonium ion compounds, especially in enzyme–substrate interactions [40], as well as in artificial systems, e.g., in separation science [41-44] and in the design of enzyme mimetics [45-49].

In this review, we discuss the different structures of ammonium ion receptors using typical examples from the recent literature. Where available, examples of enantioselective recognition of chiral ammonium ion guests will be covered. The recognition of guanidinium ions and metal cations [50] is not included. Ion pair recognition will be discussed briefly if it is relevant for ammonium ion recognition purposes. A comprehensive review on this topic has been published by Sessler et al. [51-53]. We also discuss the substance classes that have been mostly used in organic ammonium ion recognition: crown ethers, calixarenes [54], cyclodextrins [55-57], cucurbiturils, porphyrins, phosphonate based receptors, tripodal receptors, tweezer ligands, clefts, cyclopeptides and metal complexes. We have not included rotaxanes [58-64], catenanes [58,65-68], spherands [69], cryptophanes [70-72] as well as switching devices [73-75], self assembly systems [76-84] or carcerands [85-87] because these structures are less frequently used for organic ammonium ion binding, or their binding is based on similar interactions as in the previously noted receptor classes. Comprehensive information on the recognition properties of the compounds is available in the cited literature. We will start every chapter with a short discussion of fundamental properties such as selectivity and complementarity. Beginning with structurally simple examples we will increase complexity to higher substituted moieties and combinations of recognition sites to ditopic or oligomeric receptor types of the class. Synthetic receptors bearing binding sites from different compound classes are classified by their amine recognition moiety.

We present selected results covering complexation, solvent extraction and transport of organic ammonium ions in solution, thus excluding polymer [88-92] or other solid phase [93-95] materials and gas phase measurements, without attempting to cover all available references. Representative molecules for application in ion selective electrodes (ISE) [96] are briefly discussed. Unfortunately, the scope of the review cannot cover the topic of artificial receptors for organic ammonium ions comprehensively. It is rather the intention to illustrate the scope and the limitations of a binding motif with typical examples.

2. Crown ethers

This chapter discusses recent reports on ammonium ion recognition using crown ethers and their derivatives. Firstly, the properties of the substance class is illustrated by simple examples followed by more complex crown ethers and related systems. The next part discusses molecules capable to differentiate enantiomeric ammonium ions, followed by receptors for diammonium ions, such as ditopic crown ether compounds. Finally, we discuss the simultaneous recognition of ammonium ions and a second functional group as, for example, in amino acids.

2.1. Ammonium ion binding by simple crown ethers

In his first publication, Petersen [97], who discovered the compound class and later received the Nobel Prize for it, mentioned the use of crown ethers for the recognition of ammonium ions [98]. Later, after extensive studies on *tert*-butyl ammonium thiosulfate and different crown ethers, Cram [99] and co-workers concluded that two factors are important to achieve high binding constants [100]: The principle of complementary binding sites must be fulfilled. Receptor and guest binding sites should be in close proximity – complementary geometry and fit without generating steric strain. Secondly, receptors which are suitably pre-organized for guest binding will lead to the more stable complex. Crown ether ammonium ion binding occurs by hydrogen bonding between oxygen atoms (or nitrogen, sulfur or other free electron pair in hetero crown ethers) and N^+–H bonds [101]. The cyclic arrangement leads to a pre-organization of the host [102], whereby selectivity is determined by the ring size. Primary ammonium ions are complexed with highest affinity by 18-crown-6 derivatives [9] (Figure 2).

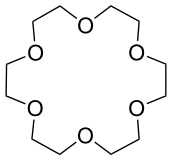

4

Figure 2: Crown ether 18-crown-6.

Table 1 summarizes exemplarily the affinity of benzyl ammonium chloride and 18-crown-6 in several solvents for comparison with other examples found in this review. The data given were determined by isothermal titration calorimetry [9].

Table 1: Binding constants of 18-crown-6 and benzyl ammonium chloride in several solvents.

Solvent	log *K*
water	1.44
methanol	4.22; 4.43[a]
isopropanol	4.14
n-octanol	3.25
dimethylformamide	2.50
dimethylsulfoxide	1.34

[a]Determined by ion-selective electrode.

These data show that crown ethers bind ammonium ions in different solvents which compete for hydrogen bonds such as dimethylsulfoxide, a very good hydrogen bond acceptor, and water, which is a poorer hydrogen bond acceptor than methanol, but very good hydrogen bond donor. Solvents competing in the intermolecular bond formation result in lower binding constants. Additionally, the binding ability is strongly affected by the polarity of the solvent [103]. The conformation of crown ethers in non-polar organic solvents reflects a "droplet of water in oil" with the lone pairs pointing to its interior in advantageous manner for ion co-ordination (Figure 3). In water, or generally speaking hydrophilic media, the lone pairs are oriented to the exterior. Upon guest co-ordination the crown ether has to be reorganized, which is energetically less favorable. Therefore, highest affinities for polar solvents are observed in methanol; in chloroform the values are even higher [104].

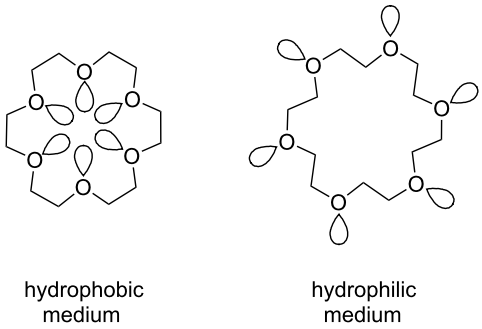

Figure 3: Conformations of 18-crown-6 (**4**) in solvents of different polarity.

Table 2 shows the effect of the crown ethers size and constitution on the binding constant in methanol. The data were determined using an ion-selective electrode.

Table 2: Binding constants of three crown ethers to benzylammonium chloride in methanol.

Crown ether	Cavity size	Guest	log *K*
12-crown-4	120–150 pm	$BnNH_3Cl$	0.80
15-crown-5	170–220 pm	$BnNH_3Cl$	2.74
18-crown-6	260–320 pm	$BnNH_3Cl$	4.43

Depending on the ratio of the crown ether ring size [103] and the diameter of the cation complex, different 1:1 topologies are observed reflecting differently strong co-ordination and complex stability (Figure 4) [105,106].

The ionic diameter of an ammonium ion is 286 pm, very similar to potassium ions with 266 pm. Important is, that ammonium ions prefer a tetrahedral and potassium ions need an octahedral co-ordination for strong binding. By reducing the co-ordination

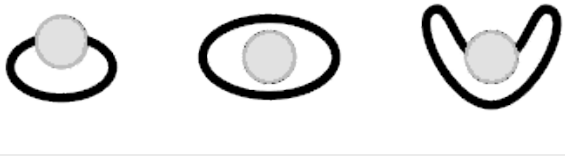

Figure 4: Binding topologies of the ammonium ion depending on the crown ring size.

points (see **7b**) [107] or changing the co-ordination sphere, the selectivity of a coronand system can be directed towards ammonium ion binding.

18-Crown-6 type structures typically show the highest affinity for primary ammonium ions, while secondary ammonium ions prefer larger crown ethers [108]. The secondary ammonium ion slips through the crown ether ring forming "pseudorotaxane" like structures (Figure 5).

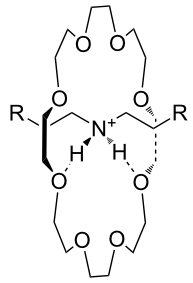

5

Figure 5: A "pseudorotaxane" structure consisting of 24-crown-8 and a secondary ammonium ion (**5**); R = Ph.

The structural variability of crown ethers is very large. This allows varying the ring size, introducing substituents and changing the donor sites from oxygen atoms, to nitrogen (aza-crowns) or sulfur, or phosphorus or arsenic atoms. Crown ether oxygen atoms as the donor site prefer harder cations of main group elements as guests, while crown ethers with sulphur atoms at the donor site are particularly suitable for the complexation of softer transition metals, e.g. Ag^{+}, Cu^{2+}, Hg^{2+} [109].

Important heterocrowns (Figure 6) are macrocycles such as cyclens (**6**) and cyclams (**7**), which show excellent complexation properties towards transition metal ions [110]. Special classes of crown ethers are pyridino crowns (**9**), with one or more oxygen atoms replaced by pyridino moieties in the polyether chain, or azacrown ethers **8**, with a certain number of nitrogen atoms instead of oxygen in the macrocycle.

A combination of both, triaza crown ether, with alternating nitrogen and oxygen atoms in the ring (**8b**), can be employed to enhance the selectivity for ammonium ions in comparison to potassium ions. It provides a sufficient number of binding sites for ammonium ions, but fewer for potassium ions compared to 18-crown-6 (Figure 7). The interaction is particularly advantageous when the number of complementary binding sites is maximal (**10b**).

Azacrown ethers with an additional side arm attached on the nitrogen of the macrocyclic ring may have, compared to the related parent crown ether, enhanced cation-binding. Crown ethers with linear or branched heteroatom-containing podand arms – depending on the connection point either *N*-pivot or

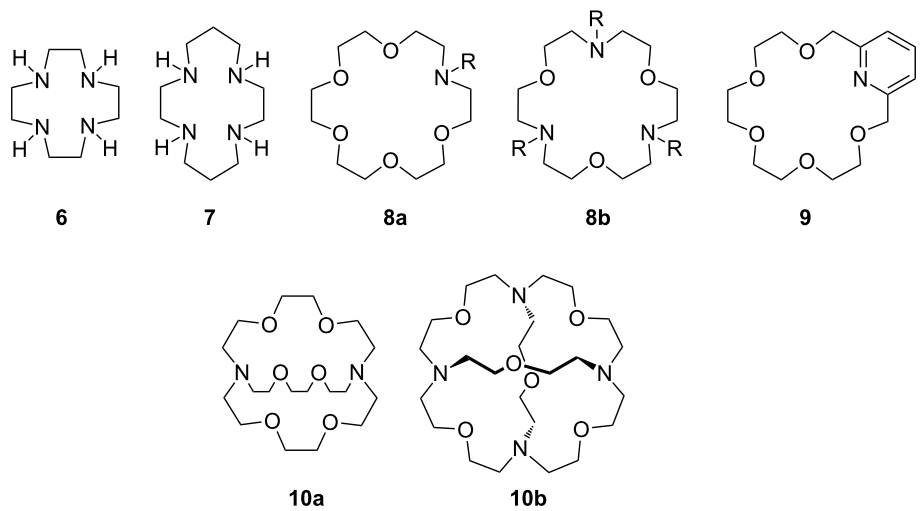

6 **7** **8a** **8b** **9**

10a **10b**

Figure 6: Typical examples of azacrown ethers, cryptands and related aza macrocycles.

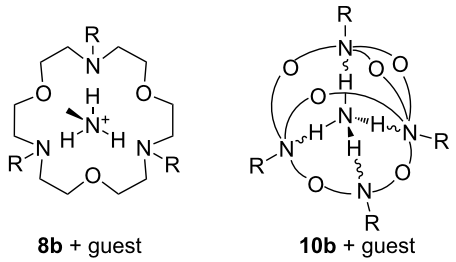

Figure 7: Binding of ammonium to azacrown ethers and cryptands [111-113].

C-pivot lariat ethers – exhibit increased guest specificity [106,114]. This argument holds for polyether compounds with two podand arms, bibraccial lariat ethers. Bridging the ring with the arm leads to cryptands, bicyclic (**10a**) or polycyclic (**10b**) crown ethers [115]. If the moiety is "tricyclic closed" via the two nitrogen atoms, the resulting cryptand **10a** permits cation encapsulation [116] (Figure 7). On inclusion in the cavity of the cryptand, the guest is shielded by three or more polyether bridges. As a result of this encapsulation, cryptands form more stable complexes than coronands ($K_a = 10^6$ for NH_4^+ in methanol at 25 °C). In addition, solution thermodynamics of amino acids with **4** and **10a** confirm these facts [117].

Macrotricyclic cryptand **10b** exhibits a substantial enhancement in ammonium vs. potassium ion selectivity in comparison to crown and azacrown ethers, as determined by both calorimetric [104] and NMR studies [118]. The high selectivity over potassium ions has been attributed to the tetrahedral binding site geometry that favors complexation of the tetrahedral ammonium ion over that of the spherically symmetrical potassium ion, underlining the particular importance of hydrogen bonding and symmetry considerations in the design of ammonium ion recognition sites. Differences between these types of ligands also show up in the kinetics of complex formation. The conformationally rigid cryptands complex slower than coronands and these in turn are slower than the flexible podands. In contrast to crown ethers, the three dimensional cryptands display peak selectivity in cation binding. The cavities are more rigid and unable to adapt to bind cations that are too small or too large for the cavity.

The large body of published work on crown ether synthesis [119] and crown ether ammonium ion binding [120] cannot be covered comprehensively in this review, and therefore we refer the reader to recent overviews. Very recent publications of cryptands for ammonium ion recognition are rare. Crown ethers and azacrowns are widely used, and we will therefore focus on these two moieties. An excellent review covering concepts, structure and ammonium ion binding of crown compounds is available [121]. For the highly dynamic motion of 18-crown-6 in complexation/decomplexation processes [122,123] and an interesting closer view on the binding of ammonium ions to 18-crown-6 and its competition with potassium ions [124] we refer the reader to the articles of Schalley and Kimura.

In the following we discuss recent examples of ammonium ion binding compounds which contain crown ether substructures but are more complex in structure than the parent compounds.

2.2. Ammonium ion binding by more complex crown ethers

An ammonium ionophore with better sodium selectivity than the natural antibiotic nonactin was developed based on a 19-membered crown compound (**11**) (Figure 8). Increased selectivity for ammonium ions over smaller and larger cations [125] was achieved by the introduction of decalino subunits which prevent a folding of the receptor to coordinate smaller cations and add bulkiness to block larger cations from entering the cavity. This compound was found to exhibit a high ammonium ion selectivity over K^+, similar to nonactin, and over Na^+ [log $K_{NH4+,\ K+} = -1.0$ (nonactin −1.0), log $K_{NH4+,\ Na+} = -3.5$ (nonactin −2.6) [126]] in an ion selective electrode (ISE). It had an almost Nernstian response (58.1 mV/decade) in the range 5×10^{-6}–10^{-1} M ammonium ion activity, reflecting a similar detection limit as nonactin.

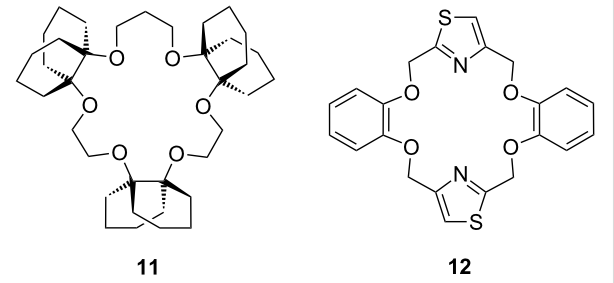

Figure 8: A 19-crown-6-ether with decalino blocking groups (**11**) and a thiazole-dibenzo-18-crown-6-ether (**12**).

Similarly, Kim et al. investigated the use of a thiazole containing dibenzo-18-crown-6 derivative (**12**) as an ammonium ionophore (Figure 8) in an ISE sensor and reported a strongly enhanced selectivity for ammonium ions over sodium ions, and a slightly higher selectivity vs. potassium ions in comparison to nonactin [127] [log $K_{NH4+,\ K+} = -1.3$ (nonactin −1.0), log $K_{NH4+,\ Na+} = -3.9$ (nonactin −2.6) [126]]. This ionophore exhibited a similar detection limit of ~3×10^{-6} M compared to nonactin (1×10^{-6} M) [128] in an ISE sensor format. This design was primarily based on size-fit factors. In addition, the aromatic units increase rigidity and the thiazoles provide hydrogen bonding sites.

Campayo et al. examined acyclic compounds containing the 1,3-bis(6-oxopyridazin-1-yl)propane and the corresponding heteroaromatic macrocycles containing pyridine units [129] (Figure 9). The cyclic receptor **13** is a most effective carrier of ammonium ions (v = 57 μM h^{-1}) and exhibits an excellent selectivity for NH_4^+ in relation to three metal cations investigated (NH_4^+/Na^+ = 9.2, NH_4^+/K^+ = 9.5, NH_4^+/Ca^{2+} = 11.8). The acyclic intermediate **14** shows efficient carrier properties for NH_4^+ ions and excellent selectivity in NH_4^+ transport in relation to K^+ (NH_4^+/K^+ = 73), which was almost seven times higher than that for nonactin [126]. An impressive selectivity in relation to Ca^{2+} (NH_4^+/Ca^{2+} = 146) was also observed. The formation of a pseudocavity by intramolecular hydrogen bonding in **14** and contribution to the binding of the host's oxyimino part were suggested by molecular modeling of the ammonium complex.

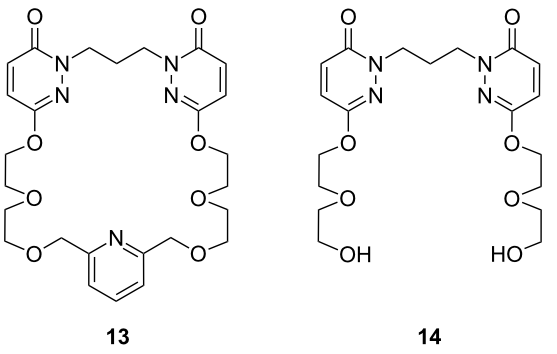

Figure 9: 1,3-Bis(6-oxopyridazin-1-yl)propane derivatives **13** and **14** by Campayo et al.

In ammonium ions, where hydrogen atoms arereplaced by organic residues, the substituent will influence the binding. The co-ordination of primary ammonium ions salts with varying steric demand was investigated. The sensing ability of fluorescently labelled 1,10-diaza-18-crown-6 (**16**) was compared to the analogous monoaza-18-crown-6 coumarin sensor (**15**) [130]. The co-ordination experiments were monitored both by fluorescence and ^1H NMR spectroscopy in $CH_2Cl_2/CDCl_3/CD_3OD$ 90/9/1 v/v/v %. According to the NMR titrations, sensor **15** shows the highest affinity, two orders of magnitude greater than that of **16a** (Table 3). The stoichiometry of the complexes with *n*-butylammonium perchlorate was established as 1:1 in all cases. For ammonium salts of increased steric demand, the binding values generally decrease.

The 18-crown-6 based PET sensors output was linked to the changes in the sensors' conformational dynamics on complexation (Figure 10). The fluorescence enhancements upon guest addition of the diaza compounds **16** (140 to 170 fold) were

Table 3: Binding constants of **15** and **16**.

Perchlorate of	log K_{ass} (**15**)	log K_{ass} (**16a**)	log K_{ass} (**16b**)
n-butylamine	6.0	3.5	4.5
tert-butylamine	4.6	2.8	4.5
neopentylamine	5.2	2.8	5.1

three to four times higher than that of the monoaza receptor **15** (only 40 fold increase). The changes in the conformational mobility of these sensors induced by guest binding have a profound effect on their signaling.

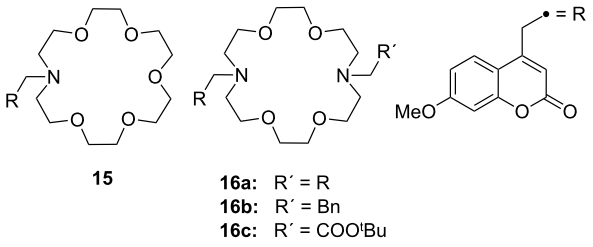

Figure 10: Fluorescent azacrown-PET-sensors based on coumarin.

2.3. Enantioselective recognition of chiral ammonium ions by crown ethers

Chiral ammonium salts are found in many biologically active molecules. The enantioselective discrimination of such molecules is of interest as the biological properties of enantiomers may differ [131]. Since Cram et al. synthesized BINAP-crown ethers, which were the first enantioselective receptors for primary organoammonium salts [132] leading to a novel separation technique [133], a great number of attempts have been made to distinguish chiral ammonium ions by chiral crown ethers [134]. Amino acids and their derivatives are of particular interest [131]. Chiral macrocyclic ethers and their derivatives are typical receptors for enantioselective recognition of primary organoammonium salts [135-144]. Recent examples will be discussed.

Pyridino crown receptors were extensively studied for this purpose by Huszthy et al. [145] and Izatt, Bradshaw and co-workers [131,146]: An achiral (**17**) and a chiral pyridine-based macrobicyclic cleft (**18**) were prepared [147] and compared to pyridine-18-crown-6 without the additional podand bridge (**19**) [148] (Figure 11). Compound **17** formed complexes in $CH_3OH/CHCl_3$ (1:1, v/v) with primary ammonium salts with binding strengths around 10^3 M^{-1} as evidenced by a significant change in the ^1H NMR spectrum. The strong intermolecular binding observed is attributed to the 3-point hydrogen bonding

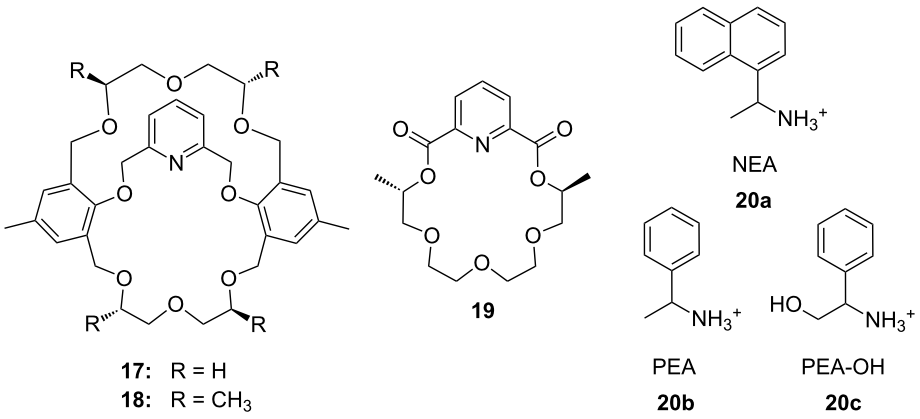

Figure 11: Two different pyridino-cryptands (**17** and **18**) compared to a pyridino-crown (**19**); chiral ammonium ions as guests (**20a–c**).

of the ammonium hydrogen atoms to the pyridine nitrogen atom and two of the oxygen atoms within the ring [149]. Binding strengths for **18** are slightly higher than for **17**. Compared to (*S,S*)-**19**, macrobicyclic (*S,S,S,S*)-**18** shows an improved stereoselective recognition towards NEA (1-naphthyl-ethyl ammonium salt, **20a**) in its three-dimensional cavity. A large difference in stabilities between the complexes of (*R*)- and (*S*)-NEA with (*S,S,S,S*)-**18** ($\Delta\log K_{ass} = 0.85$) is observed in a 2:8 (v/v) $EtOH/C_2H_4Cl_2$ solvent mixture, while the $\Delta\log K_{ass}$ value for (*R*)- and (*S*)-NEA interactions with (*S,S*)-**19** is 0.46 in the same solvent mixture. This high degree of enantiomeric recognition was attributed to an increase in molecular rigidity by introducing a second macrocyclic ring in the monocyclic pyridino crown ligand. Positive values of entropy changes for **18**-NEA interactions, as compared to **19**-NEA interactions (which show negative values of entropy changes) suggest a smaller conformational change of ligand **18** during complexation.

Pyridino crown systems proved to be advantageous for enantiodiscrimination in the extensive studies of Izatt and Bradshaw. Other groups employed the principle for the preparation of other chiral receptors (Figure 12): A series of enantiomerically pure chiral pyridino-18-crown-6 ligands were prepared by Samu et al. [150] and their ability to act as enantioselective hosts for primary ammonium salts was demonstrated with the two enantiomers of NEA [151]. The equilibrium constants were measured in a $CD_3OD/CDCl_3$ mixture by NMR spectroscopy. The best example (*R,R*)-**21** (R = ^{t}Bu) shows a four times higher log K_{ass} for the *S*-enantiomer over the *R*-enantiomer of the guest, being more selective as the former examples, but a weaker binder ($\log K_{ass} < 10^3\ M^{-1}$).

Structurally similar acridino-18-crown-6 ligands like **22** were studied by the same group and the association process between

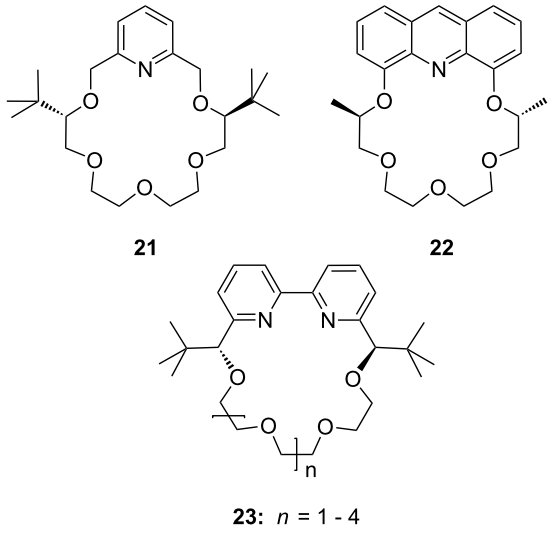

Figure 12: Pyridino-18-crown-6 ligand (**21**), a similar acridino-18-crown-6 ligand (**22**) and a structurally related bispyridyl (bpy)-18-crown-6 receptor **23**.

ligands and organic ammonium ions monitored by changes in their photophysical properties in acetonitrile [152]. With the enantiomerically pure (*R,R*)-ligand good binding and enantiodiscrimination in favor of the *S*-enantiomers of PEA (**20b**) [150] ($K_{ass} = 2.3 \times 10^6\ M^{-1}$) and NEA ($K_{ass} = 1.7 \times 10^6\ M^{-1}$) over the corresponding *R*-enantiomers ($K_{ass} = 4.4 \times 10^5\ M^{-1}$ and $K_{ass} = 3.4 \times 10^5\ M^{-1}$, respectively) was observed.

This optically active dimethylacridino-18-crown-6 ether (*R,R*)-**22** showed higher enantioselectivity towards NEA (**20a**) and PEA (**20b**) than its comparable pyridino analogue (*S,S*)-**21** (R = Me instead of ^{t}Bu) [152]. The higher enantioselectivity was rationalized by the stronger π–π-interaction of the extended π-system of the acridine unit and the more rigid conformation of

host molecule. An interesting application was demonstrated by Lakatos: Molecule **22** was attached to a silica gel surface to produce a stationary phase for enantioseparation of racemic protonated primary arylalkyl amines [153].

Comparable enantioselectivities with a stronger co-ordinating ligand can be achieved using a crown ether bearing a bispyridyl (bpy) unit in the ring (**23**). A series of these C_2-symmetric 2,2-bipyridine-containing crown macrocycles have been developed by Lee et al. [154] who studied their enantiomeric recognition properties towards a number of amino acid derivatives and chiral organic ammonium salts using UV–vis and NMR methods. The macrocycles were found to be strong chelating agents for primary organic ammonium salts with binding affinities K_{ass} up to 4.8×10^5 M^{-1} in CH_2Cl_2 with 0.25% CH_3OH. The bpy-crown macrocycle with $n = 1$, reflecting the pseudo 18-crown-6 type structure, exhibited the best properties and the highest enantioselectivity towards the *S*-enantiomer of phenylglycine methyl ester hydrochloride with a *K*(*S*) to *K*(*R*) ratio of 2.1 ($\Delta\Delta G_0 = -1.84$ kJ mol^{-1}). The Job's plot analysis supported the 1:1 stoichiometry of the host–guest complex. An analysis of the structure–binding relationship showed that the aromatic subunit and the ester group of the ammonium guests are both important for achieving high enantioselectivity.

The enantiomeric recognition of a different pyridino crown type ligand bearing aminoalcohol subunits on the exterior (Figure 13) were investigated by UV titration in chloroform [155]. The hosts formed very stable 1:1 complexes with α-phenylethylamine hydrochloride (**20b**) and α-cyclohexylethylamine hydrochloride (**25**) with relatively similar binding constants (10^4 M^{-1}) as calculated by a modified Benesi–Hildebrand equation. A preference for enantiomers with an (*S*) absolute configuration for both amine salts was found: Host **24a** bearing isobutyl groups shows an enantiomer recognition factor of 2.0 and 5.0 (K_S/K_R), which corresponds to approximately 33% and 67% *ee* for **20b** and **25**, respectively. For the host bearing a phenyl residue (**24b**) similar factors of 2.1 and 5.0 (K_S/K_R) corresponding to approximately 36% and 67% *ee* for **20b** and **25**, were observed. With the benzyl substituted moiety (**24c**) a far weaker discrimination was found. Hydrogen bonding of the alcohols combined with π–π staking, π–charge interaction and steric complementarity were assumed to be responsible for the enantioselective recognition.

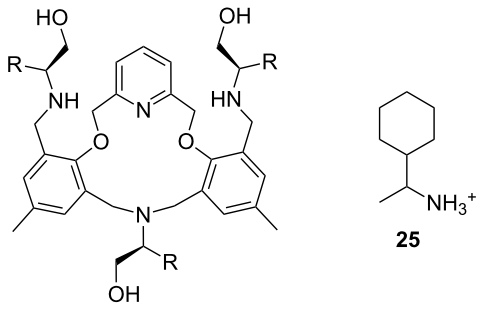

Figure 13: Ciral pyridine-azacrown ether receptors **24**.

Even better enantioselectivities than with pyridino crowns were observed with chiral azacrown compounds (Figure 14), but the binding constants were for comparable cases approximately one order of magnitude lower. Togrul et al. [156] and Turgut et al. [157] examined several chiral monoaza-15-crown-5 ethers based on chiral aminoalcohols and investigated the effect of the substituent at the stereogenic centre on the enantioselectivity. The benzocrown derivative of *S*-leucinol and the 15-crown-5 prepared from (*R*)-(−)-2-amino-1-butanol were found to be the most effective examples [158]. Both molecules show enantioselectivity towards (*R*)-**20b** perchlorate compared to (*S*)-**20b** perchlorate [151]: The aggregate was for **26b** 4.76 times more stable for the *R*-enantiomer than with the *S*-form ($\Delta\Delta G_0 = -1.73$ kJ mol^{-1}; $K_{ass,R} = 9.8 \times 10^4$ dm^3 mol^{-1}, $K_{ass,S} = 2.2 \times 10^4$ dm^3 mol^{-1}). In the case of **26a** they observed a ratio of $K_R/K_S = 4.46$ ($\Delta\Delta G_0 = -3.7$ kJ mol^{-1}; $K_{ass,R} = 9.5 \times 10^3$ dm^3 mol^{-1}, $K_{ass,S} = 4.8 \times 10^3$ dm^3 mol^{-1}).

Enantiomeric recognition of chiral primary ammonium perchlorate salts was investigated with analogous chiral mono

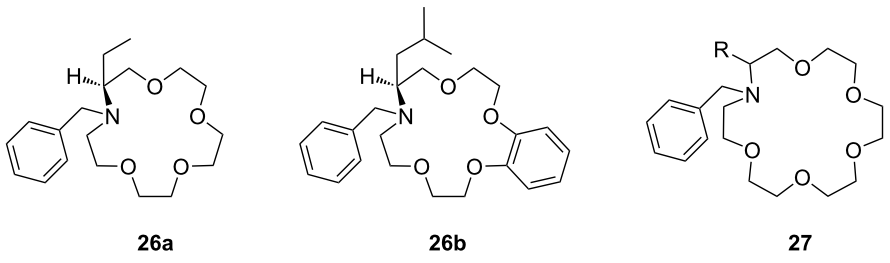

26a **26b** **27**

Figure 14: Chiral 15-crown-5 receptors **26** and an analogue 18-crown-6 ligand **27** derived from amino alcohols.

aza-18-crown-6 derivatives such as **27** [159]. For the isobutyl compound (**27**, R = ^{i}Bu), the host exhibited the highest binding constant and the best enantiomeric selectivity ability towards 1-phenylethylammonium perchlorate isomers (**20b**): The complex with the *R*-isomer ($K_a = 3.3 \times 10^4$ dm^3 mol^{-1}) was 2.5 times more stable than the one with the *S*-configuration ($K_a = 1.3 \times 10^4$ dm^3 mol^{-1}) [158].

Turgut et al. investiged the corresponding C_2-symmetric chiral diaza-18-crown-6 ethers **28a** and **28b** derived from chiral (*R*)-(−)-2-amino-1-butanol [160] (Figure 15). The association constants, measured by UV–vis spectroscopy in methanol/chloroform solvent mixture, revealed for *S*-, *R*-Ala-OMe hydrochloride the highest value for both macrocycles ($K_a = 1.5 \times 10^4$ dm^3 mol^{-1}) as calculated by a modified Benesi–Hildebrand equation, but without pronounced chiral discrimination. The highest enantioselectivity was observed in the case of Trp-OMe hydrochloride ($K_R/K_S = 12.5$) with a binding strength in the same order of magnitude as observed for the alanine ester. This was the highest factor reported to date for such systems. The authors reasoned that steric and π–π-interactions with the crowns phenyl substituents are the decisive factor for the enantioselective recognition.

Recently, Turgut et al. reported a comparable series of C_2-symmetric chiral aza crown ether macrocycles (**29**) based on (*S*)-3-phenyloxy-1,2-propanediol and (*S*)-1-methyl-1,2-propanediol for the enantiomeric recognition of amino acid ester derivatives [161]. The four similar macrocycles have been shown to be complexing agents for primary organic ammonium salts by ^{1}H NMR titration. The best example, the depicted host **29**, exhibited enantioselective bonding toward the *R*-enantiomer of phenylalanine methyl ester hydrochloride with K_R/K_S of 6.87 in $CDCl_3$ with 0.25% CD_3OD. The binding constants were far lower as in the former examples.

Related macrocycles **30** with diamide-diester groups derived from dimethyloxalate and amino alcohols (Figure 16) also showed a considerable binding affinity and enantiomeric discrimination of aromatic amine salts [162]. The binding properties were evaluated by ^{1}H NMR titration in acetonitrile. For the (*R,R*)- and (*S,S*)-configurated host with a phenyl residue, the highest differences in the K_{ass} values were observed: (*R*)-NEA and (*S*)-NEA (**20a**) [151] to (*S,S*)-**30** and (*R,R*)-**30** (R = Ph) show ratios of $K_S/K_R = 5.55$ and $K_R/K_S = 3.65$, respectively. A general tendency for the host to include the guests with the same absolute configuration was found. The amide and ester groups ensure a high rigidity of the host. The highest binding constant of 7.8×10^3 M^{-1} was found for the complex of phenyl substituted (*R,R*)-**30** with the *R*-enantiomer of the guest.

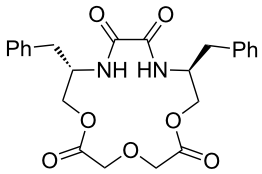

30

Figure 16: Macrocycles with diamide-diester groups (**30**).

Chiral side arms derived from phenethylamine attached to diaza-18-crown-6 ethers **31** (Figure 17) effectively enable the molecular recognition of aromatic amino acid potassium and sodium salts [163] as shown in the selectivity order Phe > Thr > Ala. The ability of the crown ethers to co-ordinate to the salts was investigated using UV–vis titration in a solution of acetonitrile/water (50:1). The highest affinities of 4×10^4 M^{-1} were obtained with the monoaromatic ring system **31a** for the potassium salt of *S*-Phe. The cavity of the macrocycle plays an important role in recognition: A dibenzo substitution on the diazacrown ether may close the cavity due to steric hindrance of the arene units on the ring and the resulting π–π-interaction between the two aromatic moieties on the ring. However, π–stacking interactions between the aromatic moiety and aromatic part of the amino acid contributes to the overall binding strength of the receptor.

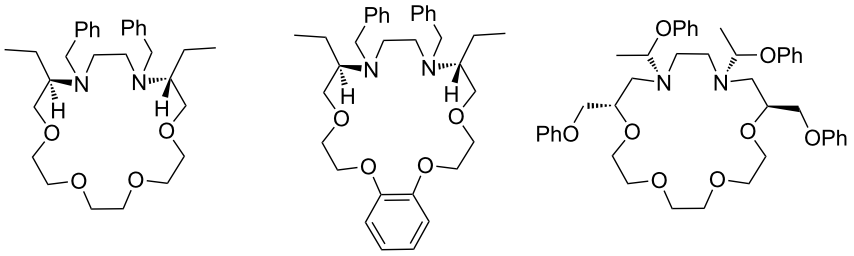

28a **28b** **29**

Figure 15: C_2-symmetric chiral 18-crown-6 amino alcohol derivatives **28** and related macrocycles.

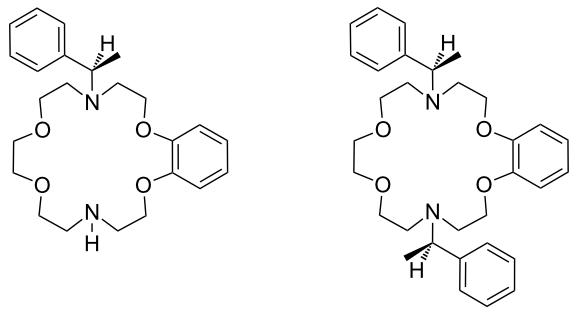

31a 31b

Figure 17: C_2-symmetric chiral aza-18-crown-6 ethers (**31**) with phenethylamine residues.

In transport experiments, chiral lariat ethers (Figure 18) show an increased flux of amino acids or their carboxylate salts and enantiomeric discrimination (Table 4): With preference for the *R*-enantiomers, the benzo- and naphtho-18-crown-6 **33a** and **33b** generally revealed a larger flux of the aromatic amino acids or their salts than hosts **32a** and **32b** [164]. This was attributed to a strong π–π stacking interaction. The highest flux values and enantiomeric selectivities were obtained for the *R*-enantiomers of tyrosine and its potassium salt. The more pronounced enantioselectivity of tyrosine may be explained by hydrogen bonding and the favorable π–π interaction between the hosts' side arm and the aromatic moiety of guests. The higher enantioselectivity of potassium salts in comparison to other salts was explained by apical-π or a sandwich-type supramolecular complex due to the larger size of the ion.

The approach to introduce chirality for a similar function by the introduction of C-pivot podand arms (Figure 19), resulting in stereogenic centres, was presented by Colera et al. [165]. The properties of the compounds were evaluated with two different chiral alkylammonium picrates, (+)-(*S*)- and (−)-(*R*)-**35** (AmI) and (+)-(*R*)- and (−)-(*S*)-**20b** (AmII) in acetonitrile. The ligands (*R,R*)-**34b** and (*R,R*)-**34a** showed enantioselective binding: (*R,R*)-**34b** favored (*R*)-AmI over (*S*)-AmI and (*R*)-AmII over (*S*)-AmII by a Δlog K_{ass} of 2.06 and 3.23, respectively. Similar results were observed with (*R,R*)-**34a** with Δlog K_{ass} = 2.64 and 2.43 for AmI and AmII. These results indicated that the presence of the phenyl rings in ligand (*R,R*)-**34b** not only gives rise to higher complexation constants with (*R*)-AmII than with (*R*)-AmI (log K_{ass} = 5.42 and = 4.61, respectively) but also increases the enantioselective recognition. In addition, racemic aqueous solutions of the ammonium salts have been enriched in the *R*-enantiomer after extraction experiments, with the best results obtained for (±)-AmII with an *ee* of 33%.

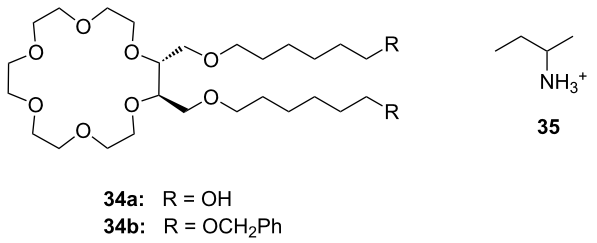

34a: R = OH
34b: R = OCH_2Ph

35

Figure 19: Chiral lariat crown ether **34**.

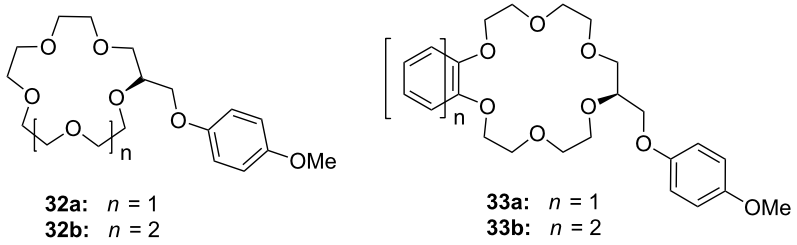

32a: *n* = 1
32b: *n* = 2

33a: *n* = 1
33b: *n* = 2

Figure 18: Chiral C-pivot *p*-methoxy-phenoxy-lariat ethers.

Table 4: Fluxes and enantiomeric selection behavior of substance class **32** and **33**.

	32a		**32b**		**33a**		**33b**	
	f_{72}×10^8 (mol m^{-2} s^{-1})	α_T	f_{72}×10^8 (mol m^{-2} s^{-1})	α_T	f_{72}×10^8 (mol m^{-2} s^{-1})	α_T	f_{72}×10^8 (mol m^{-2} s^{-1})	α_T
S-Tyr	3.05	13.7	11.01	3.5	7.96	4.9	2.56	15.5
R-Tyr	41.87		38.04		38.73		39.81	
S-Tyr K^+	4.62	8.3	10.81	3.5	7.18	5.2	2.75	14.1
R-Tyr K^+	38.34		37.65		37.45		38.83	

It is difficult to compare the results of the previous examples since their properties were investigated in different solvent mixtures and by different methods. However, this underlines the versatility of the systems published: For different conditions and separation problems several approaches are available.

A general trend is observable: 18-crown-6-systems reveal higher binding constants then 15-crown-5-systems, due to the better size fit of the guest ion. Aromatic substituents lead to better recognition and enantiomeric excess (up to 70%) with aromatic guests such as NEA (**20a**) or phenylglycinol (**20c**). For tryptophan (**81b**) the best results were achieved with selection factors of one enantiomer over the other up to 13 fold, corresponding to over 90% *ee*. This is explained by π–π-interactions.

Besides chiral substituents on the crown ether ring, chiral groups in the ring can be employed for enantioselection of guest ions: Stoddart determined the stability of complexes of D-mannitol based crown ethers with ammonium cations by NMR spectroscopy [166]. In another example fructopyrano-crown ethers with different ring sizes were employed [167].

The chiral azacoronands **36a** and **36b** based on sucrose (Figure 20) display high enantioselectivity in the complexation of phenylethylammonium chlorides [168]. The stability constants of these receptors in acetone towards ammonium cations (NMR titration of NH_4SCN) were 560 M^{-1} for **36a** and 230 M^{-1} for **36b** [169]. In NMR titration experiments in chloroform the receptors showed the preferential complexation of the (*S*)-ammonium salt with the highest value (K_{ass} = 1244 M^{-1}) for the complex of compound **36a** with α-phenylethylammonium chloride. The complex with the (*R*)-amine was of lower affinity (K_a = 837 M^{-1}, K_S/K_R = 1.84). Although the stability constants of **36b** with the (*S*)-amine were lower than for **36a** (K_{ass} = 945 M^{-1}), it has interesting complexing abilities: The macrocycle did not complex the (*R*)-enantiomer of α-phenylethylamine. In all cases a Job's plot confirmed a 1:1 stoichiometry of the aggregates.

The use of cyclodextrin type structures in chiral discrimination is well documented [170-173]. In a recent example (Figure 21), Shizuma and Sawada demonstrated a high degree of chiral discrimination between amino acid ester salts with a permethylated fructooligosaccharide (pentasaccharide) by an induced-fitting chiral recognition mechanism with amino acid ester salts [174]: ValOPr***i*** gave $I_R/I_{S\text{-}Dn}$ = 0.14 corresponding to $\Delta\Delta G_{enan}$ = 1.2 kcal mol^{-1} with *S*-selectivity and PheOPr***i*** led to $I_R/I_{S\text{-}Dn}$ = 0.18 corresponding to $\Delta\Delta G_{enan}$ = 1.0 kcal mol^{-1}, also with *S*-selectivity. It was assumed that a pseudo-18-crown-6-ring structure surrounding the ammonium ion was formed by the acyclic methylated pentasaccharide in the complexation. The

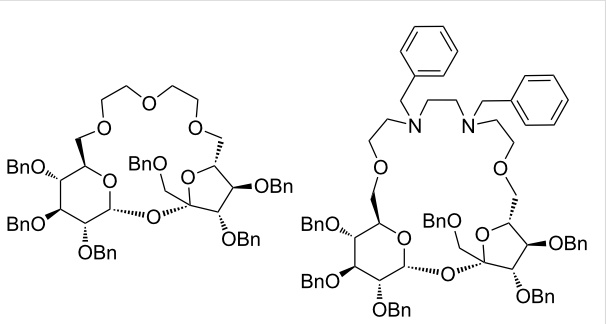

36a **36b**

Figure 20: Sucrose-based chiral crown ether receptors **36**.

chiral discrimination was ascribed to the steric effect of the fructofuranose rings of the pentasaccharide and the substituent of a given amino acid ester salt (complexation-induced selectivity). The binding ability of compound **44** in solution ($CHCl_3$) was determined by UV–vis spectrometry using a picrate anion probe. This is one of the rare examples of podands used for enantioselective recognition.

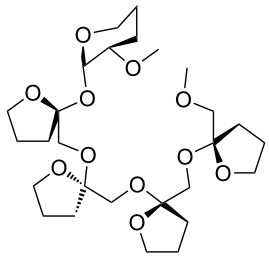

37

Figure 21: Permethylated fructooligosaccharide **37** showing induced-fit chiral recognition.

The pioneering work on this topic was carried out in the 1970s by Cram et al. [135] who studied the chiral recognition ability of binaphtol based chiral macrocycles using the picrate salt extraction method [175].

Many examples of chiral receptors have been reported, which exhibit chiral recognition towards cations derived from phenylethylamine. The biphenanthryl-18-crown-6 derivative **38** presented by Yamamoto et al. [176] (Figure 22) displayed one of the highest enantioselectivities towards one enantiomer of phenylethylamine hydrochloride as was demonstrated by liquid/liquid extraction experiments [the respective *ee* values are 42% (*R*) and 45% (*S*)].

Fuji et al. [177] have developed the related chiral lariat crown ether **39** (Figure 23). Its phenolic hydroxyl group converts basic

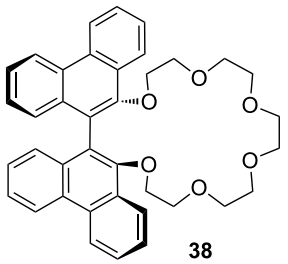

38

Figure 22: Biphenanthryl-18-crown-6 derivative **38**.

amines into ammonium ions, which are bound more tightly. A salt bridge between the ammonium and the phenolate ions supports the binding process. From UV and NMR titration experiments, the authors derive binding constants for hexylamine of 14 M^{-1} in THF and >10^5 M^{-1} in DMSO. This is surprising, because an increased ability of the solvent to act as a hydrogen bond acceptor typically leads to decreased binding constants. A significant contribution of the phenolate-ammonium salt bridge or from π–cation interactions is likely. The best enantioselective binding of chiral ammonium ions was observed using phenylglycinol: The *R*-enantiomer (K_{ass} = 30 M^{-1}) was bound preferentially over the *S*-enantiomer (K_{ass} = 9 M^{-1}) by a factor of 3.2 in a methanol/acetonitrile solvent mixture.

The authors expanded their approach with two similar binaphthyl crown recognition systems containing phenylboronic acid **40a** and 2,4-dinitrophenylurea **40b** as lariat parts [178] (Figure 23). Host **40a** had 30% extraction efficiency for γ-aminobutyric acid (GABA) in solid–liquid extraction in DMSO, but showed only much lower selectivities for α-amino acids: Boc-*R*-Lys-OH (18.5%), Boc-*S*-Lys-OH (14.1%) and H-*R*-Asp-NH_2 (8.2%), H-*S*-Asp-NH_2 (4.3%). The chromogenic host **40b** discriminated amino acids by their length. After extraction, the color of the solvent changed from colorless to yellow due to increased absorbance around 460 nm. The extent of the color change correlates with the affinity for the guest amino acid. ω-Aminohexanoic acid produced the most significant change. Although the color change is visible to the naked eye, the maximum amount extracted (3%) was small.

Homochiral phenolic crown ethers with "aryl chiral barriers" (Figure 24) were investigated and published in 1998 by the group of Naemura [179]. This system displayed, on investigation by UV–vis spectroscopy in chloroform, a good enantiodiscrimination ability in favor of (*R*)-phenylalaninol with an $\Delta_{R\text{-}S}\Delta G$ = 6.4 kJ mol^{-1}. In succession, Steensma et al. investigated thermodynamic data and conditions for chiral separation of amines and amino alcohols [180]. The azophenolic crown ether was a versatile and a highly enantioselective host for their chiral separation by reactive extraction. Transport from a basic aqueous solution of the racemic mixture in CH_2Cl_2 and toluene was followed by UV–vis titration. Compound **41** showed the highest affinity for phenylglycinol (**42b**) with association constants of K_{ass} = 1.5 × 10^5 M^{-1} in CH_2Cl_2 and K_{ass} = 8.0 × 10^4 M^{-1} in toluene with a 10 fold higher binding constant to the *R*-enantiomer. In addition, norephedrine (**42c**) and 2-amino-

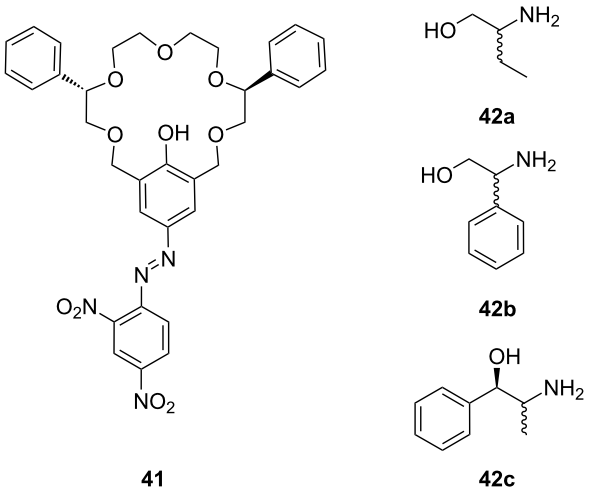

41 **42a** **42b** **42c**

Figure 24: Chiral phenolic crown ether **41** with "aryl chiral barriers" and guest amines.

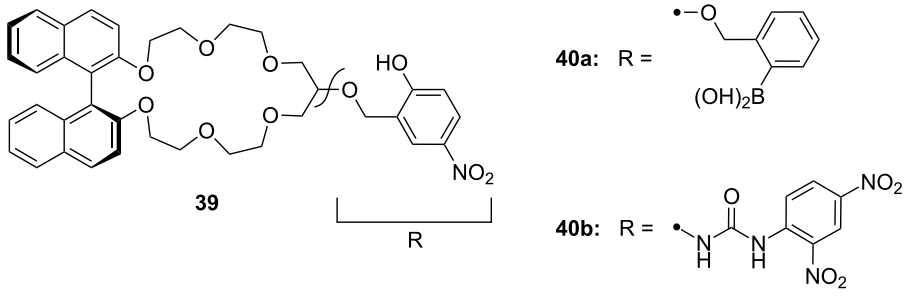

39

Figure 23: Chiral lariat crown ethers derived from binol by Fuji et al.

butanol (**42a**) could be separated in an acceptable ratio. The extractant could be reused for further chiral separations without loss of activity or selectivity. Ammonium ion binding by chiral azophenol crowns and of diamines by bisazophenol crown ethers has been summarized in a special review [181].

2.4. Di- and tritopic crown ether receptors for the recognition of bis- and tris-ammonium ions

Fuji et al. investigated a ditopic receptor **43** to distinguish between the length of α,ω-diamines (Figure 25). The receptor consists of a meso-ternaphthalene backbone and two crown ether rings [182]. Receptor **43** preferably binds and transfers the di-picrate of 1,9-diaminononane and 1,10-diaminodecane from an aqueous solution to $CHCl_3$.

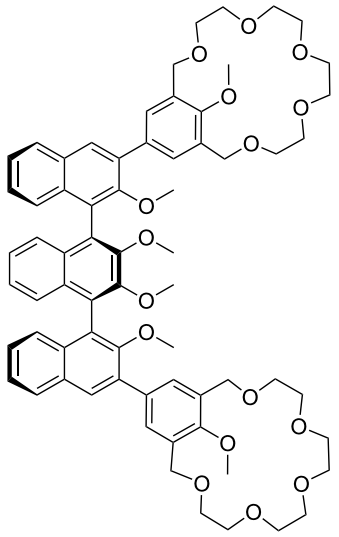

43

Figure 25: Chiral bis-crown receptor **43** with a meso-ternaphthalene backbone.

The group also reported a colorimetric approach for recognition of such guests (Figure 26), a phenolphthalein core substituted with two crown ether moieties [183]. On amine binding, the phenolic hydroxyl groups are deprotonated, which leads to lactone ring opening and the formation of a colored quinone conjugated carboxylate structure. The chemosensor discriminated terminal diamines by length: 1,8-diaminooctane (K_{ass} = 1270 M^{-1}) and 1,9-diaminononane (K_{ass} = 2020 M^{-1}) showed the highest binding constants in methanol. Diamines with an alkyl chain length shorter than five carbons were not bound.

Investigation of the stoichiometry of the aggregate formation led to a value of 1.2 to 1.3, because one diamine is bound by the two crown ethers and a second diamine is recruited as the ammonium counter ion of the carboxylate. Addition of an excess of *N*-ethylpiperidine as base established the expected stoichiometry of the aggregate as 1:1. Control experiments with *N*-ethylpiperidine and phenolphthalein without crown ether moieties confirmed the ammonium ion crown ether interaction as being essential for the color response. Unprotected dipeptides showed an affinity to compound **44** if amino groups were present within a suitable distance, for example, as found in dipeptides with a C-terminal Lys. Lys-Lys (K_{ass} = 1020 M^{-1}) and Gly-Lys (K_{ass} = 930 M^{-1}) showed the highest affinity constants in methanol/water 10:1 [184].

The same host (**44**) is able to signal the length of a linear triamine in a similar manner. Triamines **45a**–**45c** and spermidine (**45e**) (Figure 27) developed a bright purple color by forming complexes with the host in a 1:1 ratio with the inner imino group capturing the carboxylate after lactone ring opening. The color develops over a limited temperature range and therefore can be also used as a visible index of temperature. The association constants (K_{ass}) as well as molar absorption coefficients (ε) were determined by UV–vis titration. For

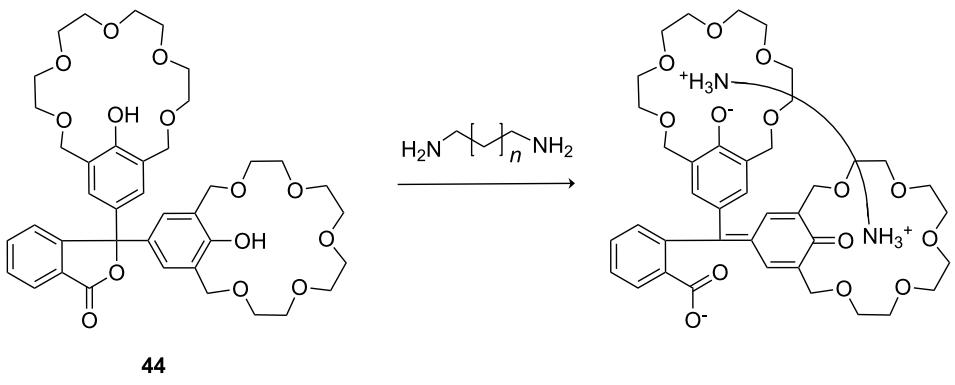

44

Figure 26: Chromogenic pH-dependent bis-crown chemosensor **44** for diamines.

triamine **45c** thermodynamic parameters ΔH = −127.4 ± 6.3 kJ mol^{-1} and ΔS = −362.8 ± 21.3 J mol^{-1} K^{-1} were obtained, and temperature dependent measurement of the association constants were measured (K_{ass} = 14870 ± 880 M^{-1}, ε = 5100 ± 30 at 15 °C; K_{ass} = 2270 ± 30 M^{-1}, ε = 5080 ± 20 at 25 °C; K_{ass} = 1090 ± 10 M^{-1}, ε = 4980 ± 10 at 30 °C). Both K_{ass} and ε reach maximum values with triamine **45c**.

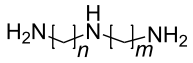

45a: $n = m = 3$
45b: $n = m = 4$
45c: $n = m = 5$
45d: $n = m = 6$
45e: $n = 3$; $m = 4$

Figure 27: Triamine guests for binding to receptor **44**.

Based on this phenolphthalein skeleton, the host was later further developed for use in visual enantiomeric discrimination [185] (Figure 28). Various types of chiral host molecules were examined for their enantioselective color effect in complexation with chiral amino acid derivatives in methanol solution. The methyl substituted compound (*S*,*S*,*S*,*S*)-**46a** showed a particularly prominent selectivity for the alanine amide derivatives with 1,5-pentane diamine and 1,6-hexane diamine: A combination of methyl substituted host (*S*,*S*,*S*,*S*)-**46a** with the *R*-enantiomers developed a purple color, whereas no color development was observed with *S*-enantiomers. When Ala-1,6-hexane diamines with different optical purities were added to the host **46a** solution, a linear relationship was observed between the absorbance (λ_{max} = 574 nm) and the *ee* of the added guest. The phenyl substituted compound (*S*,*S*,*S*,*S*)-**46b** showed an even more intensive color change induced by a wide range of (*S*)-α-amino alcohols compared to the corresponding (*R*)-α-amino alcohols. The function, mechanisms and applicability of phenolphthalein crown systems have been recently summarized by Tsubaki [186].

Ditopic receptors can consist of two or more crown ether amino acids. The group of Voyer reported crown ether based receptors for diamino and diammonium alkanes [187]. They used crown ether amino acid (CEAA) **19** (Figure 29), which was incorporated twice into an oligo Ala peptide chain.

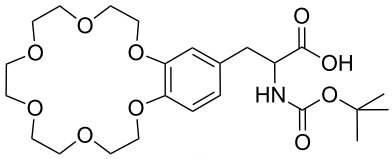

47

Figure 29: Crown ether amino acid **47**.

The receptor structure was modified by varying of the number of Ala residues between the crown ether amino acids from one to three: Boc-Ala-Ala-CEAA-(Ala)$_{1\text{-}3}$-CEAA-Ala-^{n}Pr. 1,9-Diaminononane was found to be the diamine with highest affinity for all three sequences among all tested diaminoalkanes from C_2 to C_9. The binding constants were derived from picrate extraction [188] from water into chloroform with 2 × 10^{10} M^{-1} as the highest binding constant. However, binding constants determined by extraction methods may have larger errors [189] and the binding process includes a phase boundary transition. Therefore, binding constants cannot be compared to other systems investigated in homogeneous solutions. Surprisingly, despite the difference in crown ether spacer length in the Voyer's and Fuji's systems, both preferentially bind 1,9-diaminononane. To match the distance of the phenolphthalein system, the CEAA units must be connected directly. This indicates that the actual binding conformation of the bis-crown ether-diammonium ion aggregates may be more complex under

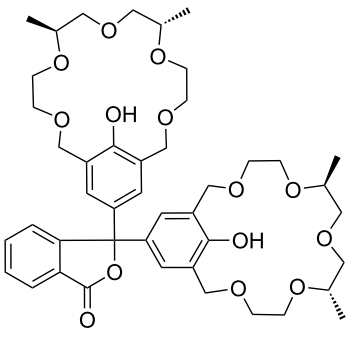

46a

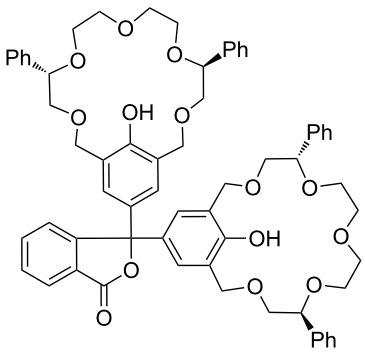

46b

Figure 28: Chiral bis-crown phenolphthalein chemosensors **46**.

the experimental conditions. Recently, they reported the application of a similar peptide forming an α-helical amphiphilic peptide nanostructure with cytolytic activity. A potential use of these peptide nanostructures is as pro-drugs that may be activated by a specific proteolytic enzyme to target selectively and destroy undesirable cells [190].

Kim et al. reported two bis(azacrown)anthracene derivatives **48a** and **48b** (Figure 30) for the recognition and detection of alkyldiammonium ions in ethanol or in a chloroform/methanol mixture (9:1) based on the PET principle [191]. The fluorescence of the anthracene function is quenched by the free electron pairs of the nitrogen atoms. When hydrogen bonds are formed by both nitrogen atoms to the bis-ammonium guests, the photoinduced electron transfer (PET) is inhibited and the system shows an enhanced fluorescence. The binding was dependent on the chain length between the two cations, displaying a maximum stability in the case of the protonated 1,3-diaminopropane. for the bis(aza-15-crown-5) chemosensor **48a** the following binding constants were observed: K_{ass} = 4412 M^{-1} for n = 3; K_{ass} = 272 M^{-1} for n = 4; K_{ass} = 35 M^{-1} for n = 5; K_{ass} = 98 M^{-1} for n = 6. Compound **48b** showed a similar selectivity towards the guests.

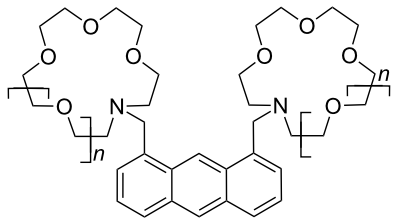

48a: n = 1
48b: n = 2

Figure 30: Luminescent receptor **48** for bis-alkylammonium guests.

König et al. combined both principles. They investigated luminescent crown ether amino acid (CEAA) dipeptide (**49b**) (Figure 31) which showed high affinity for ammonium ions with the binding processes signalled by an increase in their emission [192]. In contrast to Voyer's system, the crown ether moieties are the central part of the CEAA enabling the synthesis of linear receptors. Both crown ether parts in the ditopic receptor bound independently to mono-ammonium guests with similar affinities than monomeric CEAAs. A bis-ammonium guest, such as lysine methyl ester, was co-operatively bound with a higher affinity (log K_{ass} = 4.3 for the phthalimide containing part and log K_{ass} = 4.7 for the phthalate ester containing part in methanol). The binding affinity increased more than 100 fold in comparison to a single receptor CEAA. The affinity of the bis-CEAA to bis-ammonium ions is distance dependent, which made it possible to distinguish between isomeric small peptides containing a lysine residue in different positions. Peptides with *N*-terminal lysine showed the highest affinity to **49b**. The binding events of the crown ether groups can be monitored independently by changes of their specific emission properties.

The approach was extended to linear tris-CEAA receptors (**50**) for di-lysine peptides [193] (Figure 32). The additional chromophore leads to a stronger emission, which becomes visible to the naked eye, but the extension from bis- to tris-crown ethers does not lead to an increase of ammonium binding affinities as demonstrated by emission titration. Compared to **49b**, comparable binding constants for di-lysine-guests in methanol (log K_{ass}

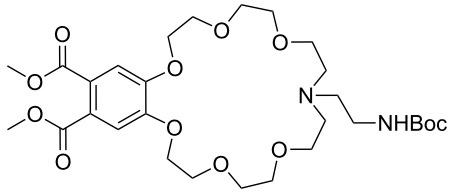

49a

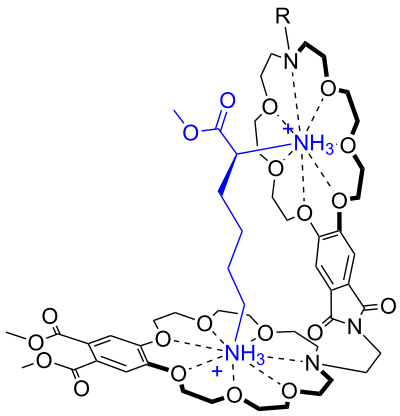

49b - Lys-OMe

Figure 31: Luminescent CEAA (**49a**), a bis-CEAA receptor for amino acids (**49b**) and the structure of lysine binding.

= 4.5) and in buffered aqueous solution (log K_{ass} = 2.5) are achieved with **50**. The flexible structure of the extended crown ethers and their peptidic guest molecules is a likely rational for the observation: the limited pre-organization of the extended receptor binding sites prohibits an additive or co-operative action of the intermolecular interactions, and illustrates the importance of well balanced entropy and enthalpy contributions in the design of synthetic receptors.

More unusual, but demonstrating the wide scope of ammonium ion recognition with crown ethers, are systems which utilize guest self assembly for enhancement of binding strength. The assembly of the C_{60}–ammonium cation **51b** with the oligophenylenevinylene derivative bearing two crown ether moieties **51a** (Figure 33) led to the co-operative formation of the 2:1 complex as a result of intramolecular fullerene-fullerene interactions [194]. High stability constants in dichloromethane (log K_1 = 5.6 by luminescence titration and log K_2 = 6.5 by UV absorption) were reported, but due to the small spectral changes upon binding, the binding constants obtained had high errors. The observation was also supported by electrospray mass spectrometry. The co-operative recognition process could be shown by fluorescence quenching experiments: The stability of the supramolecular *syn*-complex is significantly higher than that of its corresponding anti-complex. The combination of several weak interactions such as π–π-stacking and hydrophobic associations between the two C_{60} units was proposed to explain the stronger co-ordination and its ability to self-aggregate.

With larger crown ethers (24-crown-8 and above) secondary amines or pyridylium ions can also be recognized. Such an approach for ditopic crown receptors with enhanced guest selectivity was presented by Chen [195]. A triptycene-based macrotricyclic host **52** containing two dibenzo-[24]-crown-8 moieties (Figure 34) selectively forms stable 1:1 or 1:2 complexes with different functionalized paraquat derivatives

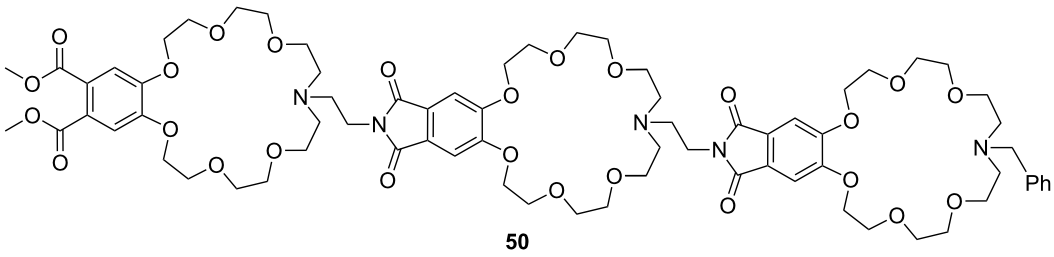

50

Figure 32: Luminescent CEAA tripeptide for binding small peptides.

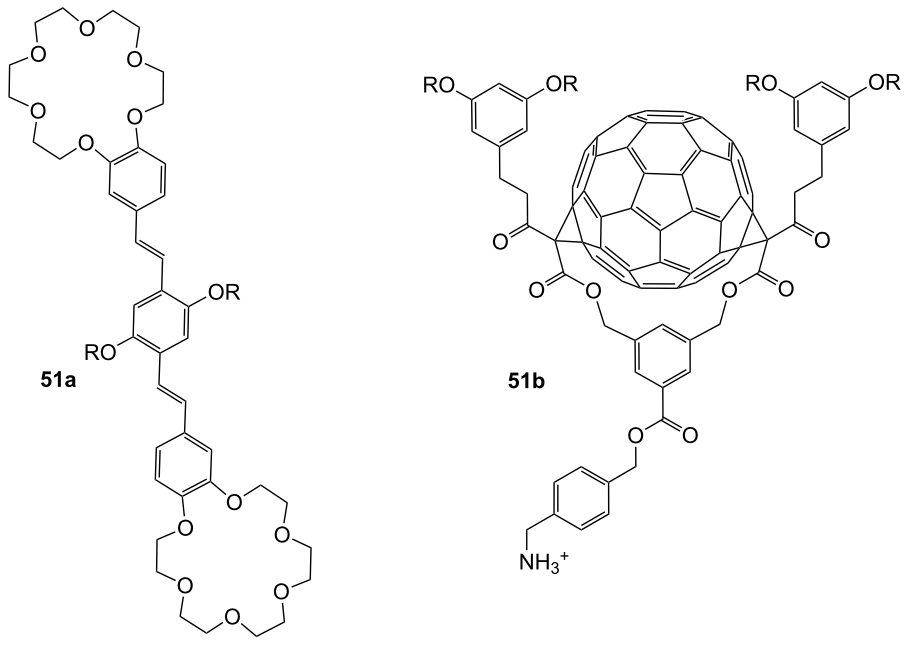

51a **51b**

Figure 33: Bis crown ether **51a** self assembles co-operatively with C_{60}-ammonium ion **51b**.

and secondary ammonium salts (K_{ass} ~ 10^3–10^4 M^{-1} in acetonitrile/chloroform). These guest-dependent complexation modes have been confirmed by 2D NMR experiments and X-ray crystallographic analysis. Alkyl substituted paraquat derivatives thread the lateral crown cavities of the host to form 1:1 complexes in chloroform/acetonitrile 1:1 (2–4 × 10^3 M^{-1}) [196]. The host forms a 1:2 complex with two 9-anthracylmethylbenzylammonium salts (R = 9-anthracyl) in the same solvent (K_1 = 8.0 × 10^3 M^{-1} and K_2 = 1.2 × 10^3 M^{-1}), in which the two 9-anthracyl groups were selectively positioned outside the central cavity. The competing complexation of the host and two different guests, the hexyl-substituted paraquat derivative and a dibenzylammonium salt, can be controlled by the addition of acid or base.

Paraquat and its derivatives are widely used in crown ether rotaxanes and several recent examples of crown ether [197-202] or cryptand [203-205] complexes with paraquat have been described. Such complexes are not within the scope of this review and the interested reader is referred to the literature cited above.

2.5. Crown ether ammonium ion receptors with appended binding sites for other functionalities than ammonium

Crown ether receptors with appended moieties for the binding of different functionalities in addition to the ammonium ion have been reported. The combination of the luminescent ammonium-binding crown ether (**49a**) with a pendant copper imido diacetic acid complex (Figure 35) with an imidazole-co-ordinating site led to receptor **53a**, which co-ordinates peptides bearing both functional groups with high affinity in buffered aqueous solution [206]. An increase in emission intensity, visible to the naked eye, signals the guest binding: The response is triggered by the ammonium ion binding to the crown ether unit, which is in water only possible intramolecularly within the assembly. Compound **53** does not respond to the presence of an ammonium group, even in large excess. In the case of His-Lys-OMe a 1:1 complex with a molar binding constant of log K_{ass} = 4.2 is observed. The receptor was applied for the selective detection of small peptides containing *N*-terminal histidine or histidine (**81e**) among all other natural α-amino acids at physiological conditions.

In succession, the combination of a copper(II)-NTA complex with the benzocrown ether led to a receptor (**53b**) (Figure 35) that preferably binds to specific histidine-glycine peptide sequences under physiological conditions [207]. Nearly micromolar affinities were observed for Gly-Gly-His (log K_{ass} = 5.8) and Gly-His-Gly (log K_{ass} = 5.8) by emission titration in HEPES-buffered (pH 7.5) aqueous solution. In tetrapeptides, the recognition motif R′-xxx-HGG was identified, in which the *N*-terminal amino acid residue may vary (R′-xxx = Leu, Ala, Gly, Gln). Only the *N*-terminal amino group triggered an emission signal; the ammonium moiety of a lysine side chain did not.

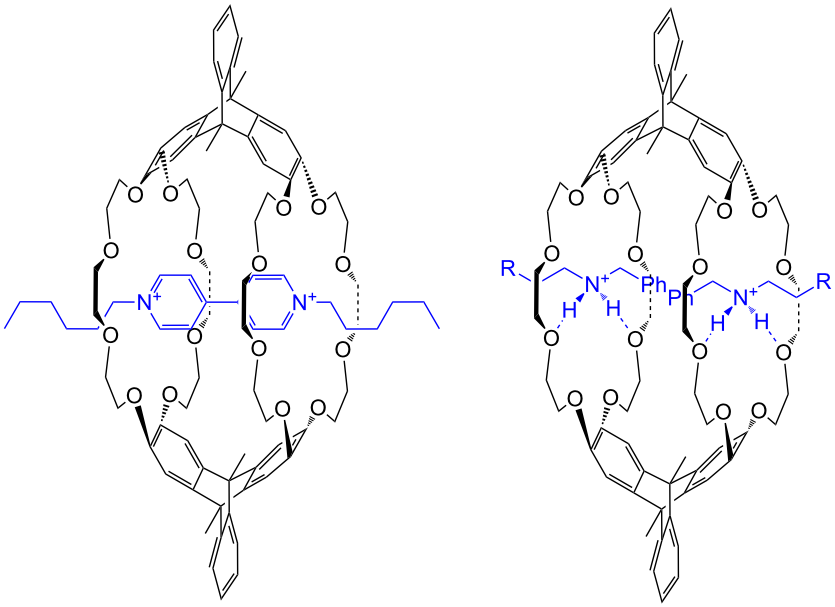

Figure 34: Triptycene-based macrotricyclic dibenzo-[24]-crown-8 ether host **52** and guests.

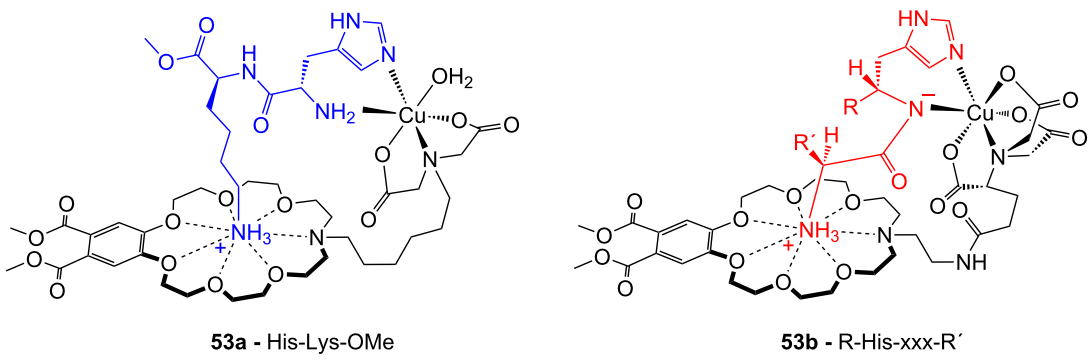

Figure 35: Copper imido diacetic acid azacrown receptor **53a** and the suggested His-Lys binding motif; a copper imido triacetic acid azacrown receptor **53b** and the target binding area (R = COO^-, $CONHCH_2COO^-$, $CONHCH_2COOCH_3$, $CONHCH_2CONHCH_2CONH_2$; R′ = H, CH_3,CH_2-$CH(CH_3)_2$, $CH_2CH_2CONH_2$).

Besides metal complexes, which will be discussed in detail in a later chapter, urea, thiourea and charged binding sites such as quaternary ammonium ions or guanidines are often employed as second anchoring functionalities for amino acids.

Receptor **54** binds to zwitterionic amino acids via a combination of urea-carboxylate and crown ether-ammonium hydrogen bonding (Figure 36), and thus efficiently transports them across a $CHCl_3$ liquid membrane [208]. The binding properties of **54** were also examined by solid-liquid and liquid-liquid extraction experiments. The amounts of amino acids extracted into the chloroform phase were determined by the ^1H NMR. In comparison to similar compounds devoid of one of these functional groups, receptor **54** efficiently extracted amino acids with non-polar side chains such as Phe, Ile, Leu, and Trp into $CHCl_3$. The overall transport efficiencies (Phe > Trp > Ile > Leu > Val >> Ala > Ser >> Asp, His) were consistent with the extraction results (Phe > Ile > Leu > Val > Ala >> Ser, Asp, His, Tyr). No preference for aromatic amino acids over aliphatic amino acids was observed in extraction and transport experiments; no binding constants were however, reported.

A recent example by Costero et al. employed a comparable heteroditopic ligand in the solid-liquid extraction of ω-amino acids into DMSO solutions (Figure 36). The prepared ligand contained thiourea or amide groups for anion recognition [209]. Compound **55** was found to be an efficient solid-liquid extractant for lysine (**81c**) as well as 4-aminobutanoic, 5-aminopentanoic and 6-aminohexanoic acids, with the highest value recorded for 4-aminobutanoic acid (GABA). The simultaneous complexation of the anionic and cationic moieties by the ligand gave rise to extraction values much higher than those obtained with equimolar mixtures of the corresponding monotopic ligands. The introduction of a *para*-nitro group in the phenylthiourea made the extraction process much faster.

The molecular recognition of *S*-amino acids such as asparagine, glutamine, lysine (**81c**) and arginine (**81d**) with crown pyrylium ions **56a** to **56c** (Figure 37) as receptors was examined by Moghimi et al. [210,211]. Their receptors use a two point binding of the guest: Ion pairing for the two oppositely charged carboxylate anion and pyrylium cation, and hydrogen bonding between crown ethers and the amino acid terminal NH's. The

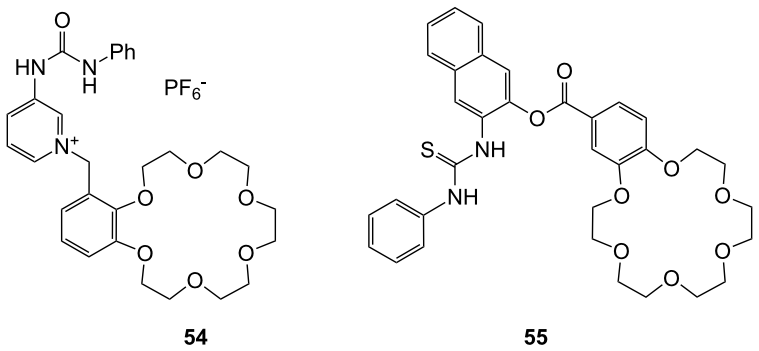

Figure 36: Urea (**54**) and thiourea (**55**) benzo crown receptor for transport and extraction of amino acids.

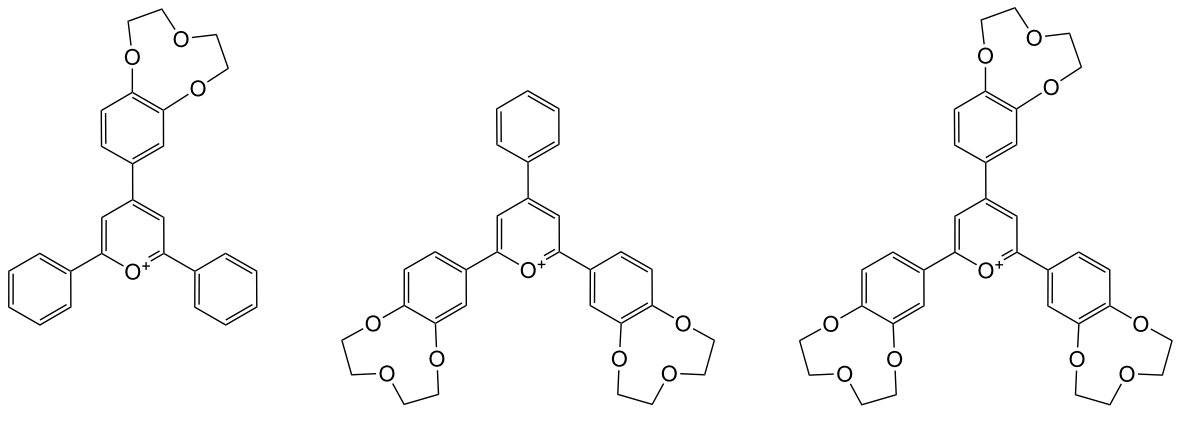

56a **56b** **56c**

Figure 37: Crown pyryliums ion receptors **56** for amino acids.

terminal NH_2 to COOH distance of *S*-asparagine is best matched when the crowns are located in the *ortho*-position of the receptors, **56b** (K_{ass} = 1290 ± 60 M^{-1}) and **56c** (K_{ass} = 1740 ± 90 M^{-1}). The distance in *S*-asparagine and *S*-glutamine is not long enough for interaction with **56a**. The binding properties were evaluated by fluorimetric titration in methanol.

A different receptor type **57** for zwitterionic amino acids was described by Barboiu et al. [212]. Simultaneous complexation of the ammonium moiety of the amino acid by the benzo-18-crown-6 cavity and of the sodium ion in the benzo-15-crown-5 cavity (Figure 38) induces charge interactions of the carboxylate moiety with Na^+-15-crown-5 and π–π-stacking interactions between the aromatic ring of phenylalanine (**81a**) and the aromatic moieties of **57**. The membrane transport mechanism of phenylalanine (**81a**) through a bulk liquid membrane was achieved and monitored as a function of the co-transported alkali cation.

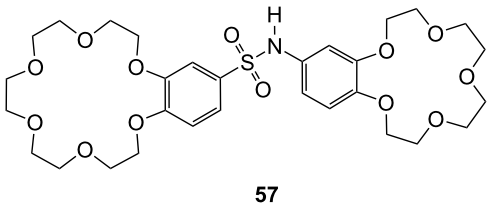

57

Figure 38: Ditopic sulfonamide bridged crown ether receptor **57**.

Schneider and Hossain [213] investigated the crown ether **58** (structurally related to the Voyer compound **47**) for peptide binding in water (Figure 39). Here, a peralkylated ammonium group interacts with the peptides carboxylate, whilst the primary ammonium ion is bound by the benzo crown ether. The bridging amine can be functionalized by a luminescent dansyl group as in **58b** to allow facile optical detection of the binding event and supplies additional hydrophobic interactions to aromatic peptide side chains. Several di- and tripeptides were tested with compound **58a**: Triglycine showed the highest binding affinity in water (K_{ass} = 200 M^{-1}) and methanol (K_{ass} = 13000 M^{-1}) as determined by NMR titration. Fluorescence titrations with **58b** revealed the effect of hydrophobic or π–stacking interactions of the dansyl group. Tripeptides bearing an amino acid with aromatic side chain functionality, such as Trp, showed a significant increased affinity (K_{ass} = 2150 M^{-1} for Gly-Trp-Gly) to **58b** in water compared to triglycine (K_{ass} = 210 M^{-1}).

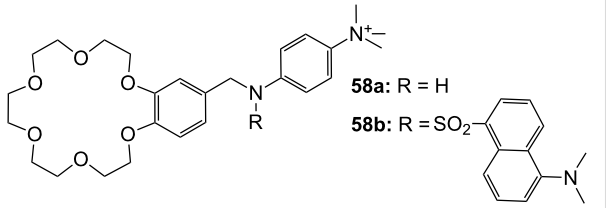

Figure 39: Luminescent peptide receptor **58**.

Cooper and James prepared mono-aza-18-crown-6 ether **59** with a boronic acid binding site [214] (Figure 40). The additional interaction of boronic acid has been used to create a photoinduced electron transfer (PET) sensory system for saccharides. Binding studies were carried out in 33.2% (w/w) ethanol–water buffer, showing selective fluorescent enhancement with D-glucosamine hydrochloride (log K_{ass} = 3.31) at pH 7.18. In this medium, compound **59** showed no increase with D-glucose. For a fluorescent output both a diol and the ammonium group must be present in the guest. The increase in

stability can be attributed to co-operative binding by the boronic acid and azacrown ether.

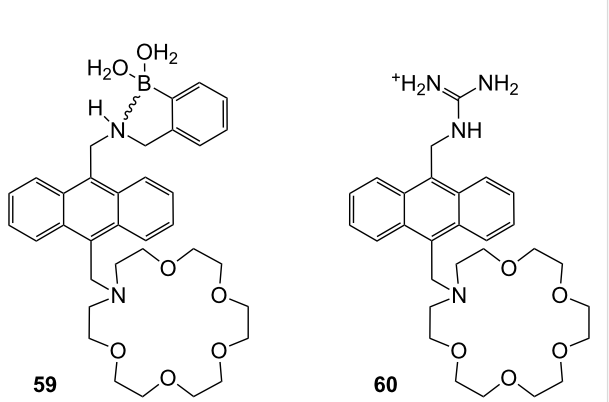

Figure 40: Luminescent receptor **59** for the detection of D-glucosamine hydrochloride in water/ethanol and luminescent receptor **60** for ω-amino acids.

Guanidines are well known binders for oxoanions such as carboxylates [215]. A molecule similar to **59** was introduced for the recognition of amino acids by de Silva et al. [216] (Figure 40): Chemosensor **60** is capable of recognizing the distance between the two functional groups in methanol/water (3:2) at pH 9.5. Co-ordination of the carboxyl group to the guanidinium moiety of the receptor has a strong effect on the fluorescence output of the system. As in the former example, upon binding of the ammonium functionality in the crown ether the quenching by the PET of the nitrogen atom's free electron pair disappears and an enhancement in the fluorescence of the anthracene is observed. 5-Aminopentanoic acid binds with K_{ass} = 84 M^{-1}, while 3-aminopropanoic acid binds with only K_{ass} = 17 M^{-1}. A limitation of the compound is its similar response to simple amines, e.g. propylamine (K_{ass} = 79 M^{-1}).

Suzuki et al. employed a similar approach for sensing amino acids in receptor **61**, which is based on tri-aza-18-crown-6 [217] (Figure 41). The ammonium-ion binding crown ether is substituted by two guanidinium groups interacting with carboxylates, and the luminescent anthracene moiety. Upon ammonium ion binding the quenching of the anthracene emission by PET is intercepted leading to an emission increase. The authors did not report binding constants, but described glycine, lysine (**81c**) and GABA (γ-aminobutyric acid) as preferred guests. The emission intensity increased upon addition of GABA to compound **61** in methanol/water 1:2 by a factor of 2.2.

A ditopic receptor **62** for the effective binding of zwitterionic GABA (γ-aminobutyric acid) was investigated by Schmidtchen [218] who combined triaza-18-crown-6 with a positively

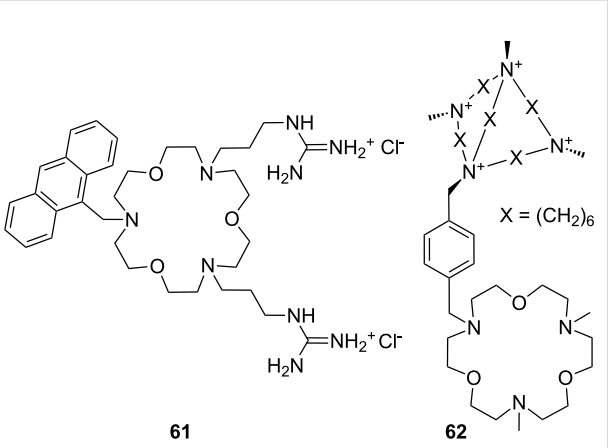

Figure 41: Guanidinium azacrown receptor **61** for simple amino acids and ditopic receptor **62** with crown ether and polyammonium macrocycle for GABA binding.

charged polyammonium macrocycle for the construction of the synthetic receptor (Figure 41).

The same group described synthetic receptor **63** with bicyclic guanidinium and azacrown ether binding sites for amino acid zwitterions [219] (Figure 42). The chiral bicyclic guanidinium salt acts as strong anchor for the carboxylate and the triaza-crown ether binds the ammonium ion. The hydrophobic silyl ether provides additional interactions and facilitates the transfer of hydrophilic amino acid zwitterions into an organic phase. Quantification of the extraction process by radiometry revealed a 1:1 stoichiometry and suggests the zwitterion as the species undergoing phase transfer. Small hydrophilic (Ser, Gly), but no charged amino acids were extracted. Some enantioselectivity was observed in the transfer of phenylalanine (**81a**, 40% *ee*). In the case of **63** the order of decreasing extractability was Phe > Leu > Trp > Gly, Ser.

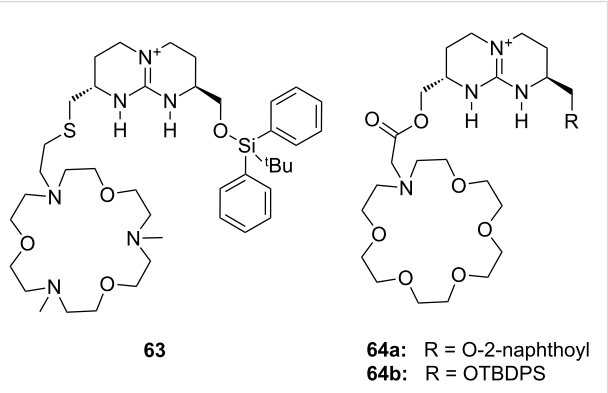

Figure 42: Chiral bicyclic guanidinium azacrown receptor **63** and similar receptor **64** for the enantioselective transport of simple amino acids into organic phases.

Comparable artificial carriers based on this bicyclic chiral guanidinium scaffold (Figure 42) attached to crown ethers (**64**) or lasalocid A were able to reach up to 80% enantiomeric excess in transport experiments for the separation mixtures of amino acid enantiomers under neutral conditions. Such chiral selectors for underivatized amino acids have been prepared, usually as the (*S*,*S*)-compounds, and evaluated by de Mendoza et al. [220]. Crown ethers were shown to be superior to lasalocid derivatives and amides were found to be better carriers than esters, though less enantioselective for transport across the bulk model membranes. Receptor **64a** proved to be the best "chiral selector", followed by **64b**.

CEAA **65** with appended guanidinium ions or quaternary ammonium side chains (Figure 43), as in **66**, were tested for amino acid recognition in aqueous methanol [221]. By following the binding events by fluorescence and UV–vis spectroscopy in methanol/water 9:1 (v/v), compound **65** showed selectivity for γ-aminobutyric acid (K_a = 1300 M^{-1}) over ε-aminohexanoic acid, β-alanine and lysine (**81c**) at pH = 6.5. Compound **66** revealed a pronounced selectivity for $(Gly)_3$ (K_a = 600 M^{-1}) over $(Gly)_2$, γ-aminobutyric acid and ε-aminohexanoic acid at pH 7.4. A 1:1 stoichiometry was always observed. Both receptors did not bind other amino acids.

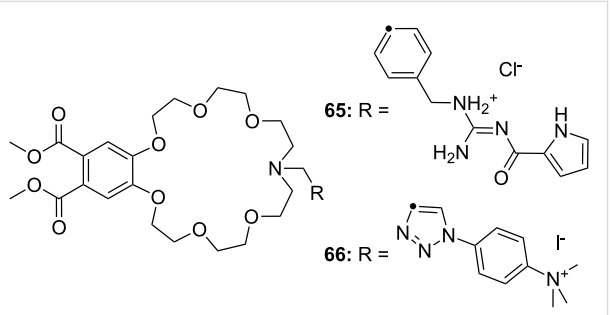

Figure 43: Receptors for zwitterionic species based on luminescent CEAAs.

The last examples presented in this chapter combine crown ether ammonium recognition with moieties for co-ordination or inclusion of non-polar side chains. Extended π-systems such as porphyrins, developing hydrophobic or stacking interactions, or carbohydrates and cyclodextrins, binding alkyl- and aryl chains by hydrophobic or van-der-Waals interactions, are discussed.

Cyclodextrins (**136**) [222,223], cyclic oligosaccharides of six (α), seven (β) or eight (γ) α-1→4 linked D-glucose units, can include non-polar guests such as alkyl chains or aromatic moieties in their hydrophobic interior mainly by van-der-Waals and hydrophobic interactions. Entropic effects play an important role: Complex formation leads to the release of high-energy water molecules from the cavity of cyclodextrins and is therefore entropically favorable. The selectivity depends principally on the steric fit, similar to the crown ethers.

Combinations of a diaza-18-crown-6-ether with α-cyclodextrin- (**67a**, **68**) and celobiosyl- (**67b**) residues (Figure 44) bind efficiently *S*-arginine (**81d**), *S*-lysine (**81c**) and the anticancer agent

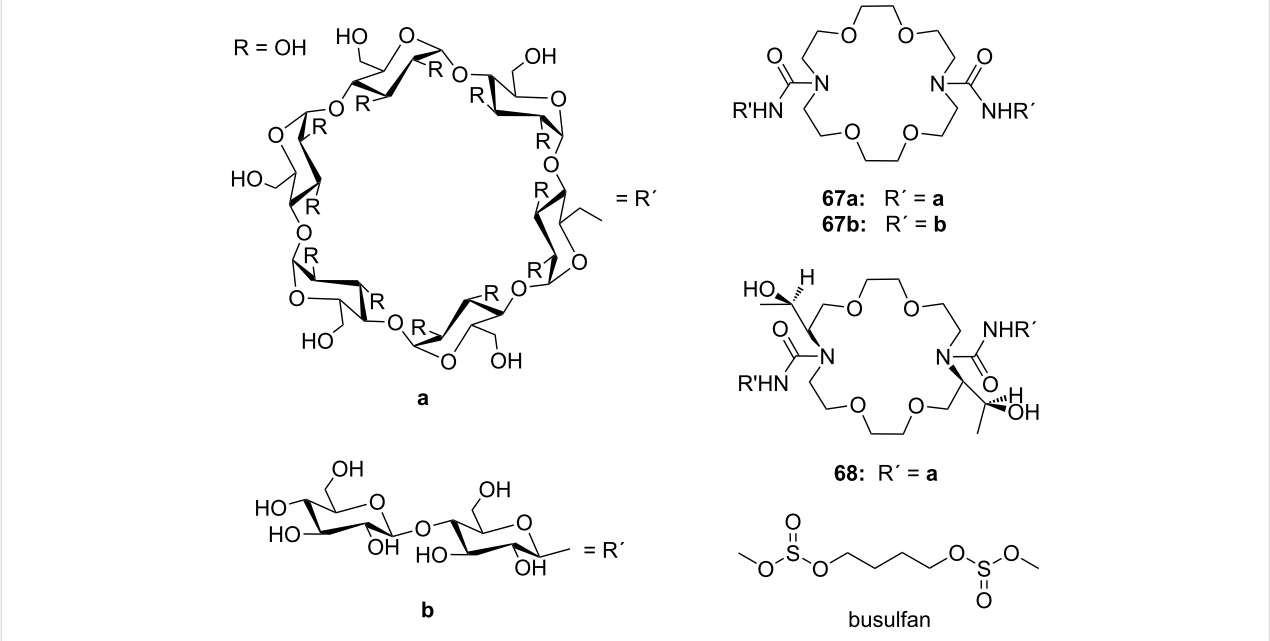

Figure 44: 1,10-Azacrown ethers with sugar podand arms and the anticancer agent busulfan.

busulfan [224]. The Job's plots indicate 1:1 stoichiometries in all the complexes. Complexation constants (K_{ass}) of ca. 4000 M^{-1} were estimated for [*S*-arginine/**68**], 5500 M^{-1} for [*S*-lysine/**68**], and 6000 M^{-1} for [*S*-arginine/**67b**] and 4500 M^{-1} for the [*S*-lysine/**67b**]. No significant differences between *S* and *R* series could be observed. Busulfan bound to all three ligands with the highest association constant of 1600 M^{-1} for **68** [225]. 2D NMR results clearly established that a similar mode of complexation is involved for both the amino acids and the anticancer agent: They are not embedded in the cyclodextrins cavity, but hydrogen bonded across the azacrown macrocycle to the urea functions.

Another combination of crown ethers and sugars as ditopic receptors was described by Suzuki et al. who used a β-cyclodextrin derivative modified with benzo-18-crown-6 moiety (Figure 45) for the recognition of tryptophan (**81b**) in zwitterionic form in water [226]. The molecular recognition ability of **69** was improved by the co-operation of hydrophobic binding by the cyclodextrin cavity and the ammonium cation binding by the benzocrown moiety (188 M^{-1} vs. 31 M^{-1} for single side interaction). 2D ROESY experiments confirmed that the ammonium cation of Trp is located at the secondary hydroxy side of the cyclodextrin cavity and is recognized by the benzo-18-crown-6 moiety.

The association constant of ammonium ions with 18-crown-6 was reported to be 10–17 M^{-1} in water [106]. The β-cyclodextrin **70** functionalized with diaza-18-crown-6 at its primary face (Figure 45) showed a 7–10 fold enhanced binding affinity for aromatic ammonium ions in aqueous media compared to unmodified β-cyclodextrin [227]. Compared to **69**, this receptor reveals a binding constant in the same order of magnitude for an aromatic amine guest e.g. Trp. The point of attachment of the crown ether does not significantly alter the ammonium binding ability.

A crown-appended permethylated α-cyclodextrin azophenol **71a** (Figure 46) showed a significant, distinguishable color change, observable with the naked eye, for primary and secondary amines. No change was evident in the case of tertiary amines, which is a similar analytic distinction as in the Hinsberg test [228]. The system was investigated by UV–vis spectrophotometry in chloroform. Association constants with primary amines were found to range from log K_{ass} = 4.2 to 4.8 and from log K_{ass} = 2.0 to 2.3 for secondary amines. The selective complexation is explained by H-bonding between the ammonium ion and oxygen atoms of the 18-crown-6 [229]. The

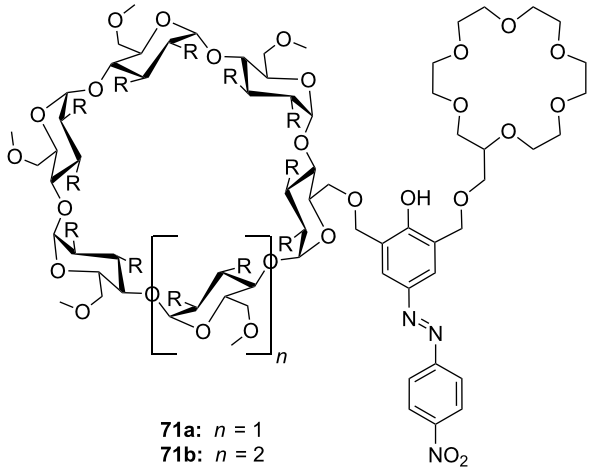

Figure 46: Receptors for colorimetric detection of primary and secondary ammonium ions.

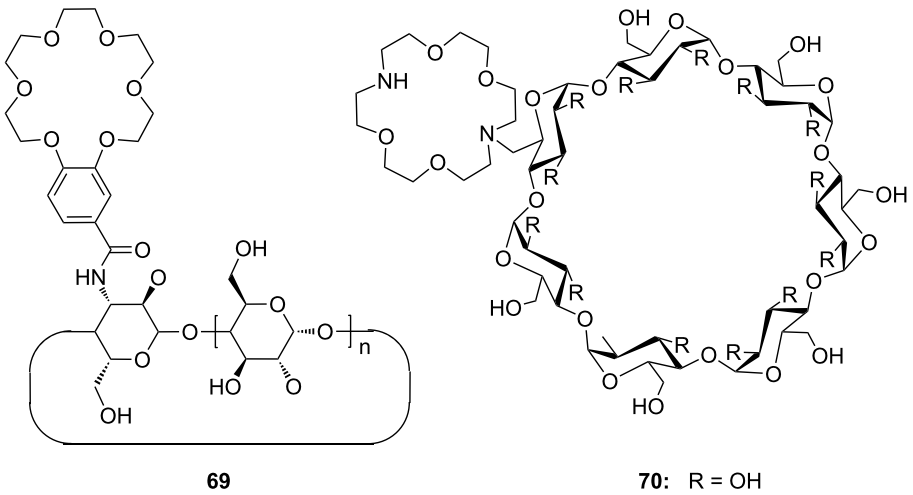

Figure 45: Benzo-18-crown-6 modified β-cyclodextrin **69** and β-cyclodextrin functionalized with diaza-18-crown-6 at primary face (**70**).

hydrophobic interaction between the cyclodextrin and the lipophilic tail of the amine in combination with the acidity of the host molecule (pK_a = 5.6) assist the binding.

The studies were expanded by the related 18-crown-6 azophenol dye with permethylated β-cyclodextrin **71b** [230] (Figure 46). The binding of various amines was investigated by UV–vis spectrophotometry in chloroform. As before, the addition of primary and secondary amines shifted the absorbance maximum differently, from 380 nm (yellow) to 580 nm (violet) and 530 nm (pink), respectively with no change observable with tertiary amines. The log K_{ass} values are, compared to compound **71a**, generally 5 to 10% higher (4.25–4.95 for primary, 2.10–2.48 for secondary amines). The selectivity was calculated to be 60–720. Receptors which lack the crown ether moiety, changed from yellow (380 nm) to pink (500 nm) upon addition of amines, but with no selectivity and binding constants being one order of magnitude lower. NMR spectroscopy indicated the formation of 1:1 complexes and the inclusion of the alkyl chain in the cyclodextrin by a strong shift of the CH_2-protons. In a competition experiment, *n*-propylamine was added to the chloroform solution of **71b** containing 2000 equiv of triethylamine. A small amount of *n*-propylamine was already known to result in a marked increase in absorption intensity, whilst in the case of the tertiary amine no spectral changes were observed.

The formation of efficient H-bond interactions of the ammonium ion to the oxygen atoms of the crown ether and their number, the hydrophobic interaction between the cyclodextrins and the lipophilic tail of the amine as well as the acidity of the host molecule determine the selectivity and binding strengths of these ditopic receptors.

The following examples involve crown ether–porphyrin conjugates. In these examples the ammonium ion binding takes place at the crown ether moiety. Ammonium ion binding using porphyrin based binding sites will be discussed later in this survey.

Schneider et al. described a water-soluble host compound with three pyridinium units and one spacer-connected benzocrown ether unit in the meso-positions of porphyrin and its Zn(II) or Cu(II) complexes [231] (Figure 47). They investigated the complexation constants of unprotected di-, tri- and tetrapeptides with the metal-free and the metalated hosts in water. Metalation led to small changes of the selectivities towards different peptides compared to the apo-derivative, with complexation constants in water of 10^5 M^{-1} to 10^6 M^{-1}. One complex containing the tripeptide Gly-Gly-Phe was analyzed in detail by COSY, HSQC, HMBC, and NOESY NMR experiments and clearly indicated complexation of the ammonium ion in the crown and π–π-stacking interactions of the phenyl of Phe with the porphyrin. Peptides containing aromatic side chains were always bound better than the corresponding simple oligoglycines. The titration curves showed isosbestic points, in line with the expected 1:1 complexes, which were supported by very good nonlinear least-squares fits to a 1:1 model.

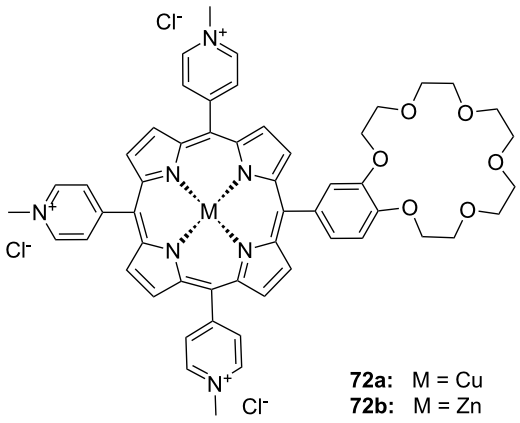

Figure 47: Porphyrine-crown-receptors **72**.

Nierengarten et al. investigated the ability of a methanofullerene derivative with an ammonium subunit to form an aggregate with a porphyrin–crown ether conjugate (Figure 48) by NMR, UV–vis, electrospray mass spectrometry and luminescence experiments [232]. In addition to the ammonium–crown ether recognition, they found intramolecular stacking of the fullerene moiety to the porphyrin subunit. Due to this additional recognition element, the association constant for the aggregate was increased by two orders of magnitude when compared to the K_{ass} values found for the complexation of **74** with the crown ether (2100 M^{-1} in $CDCl_3$). The value is consistent with association constants reported for associates resulting from ammonium–crown ether interactions [233].

The broad variability of crown ethers allows manifold adaption for specific tasks: A variety of crown ether receptors for co-operative recognition of ammonium moieties in diamines, for transport and effective enantioselective recognition of amino acids, as esters or in zwitterionic form have been described. Crown ethers have been widely used for the recognition of primary organoammonium compounds as found in amino acids, neurotransmitters such as GABA and other biological important molecules like dopamine (**2**).

3. Calixarenes, resorcinarenes and cavitands

Calixarenes are versatile host molecules for ammonium ions with unique structure and complexation properties. In this chapter we discuss approaches for ammonium ion recognition

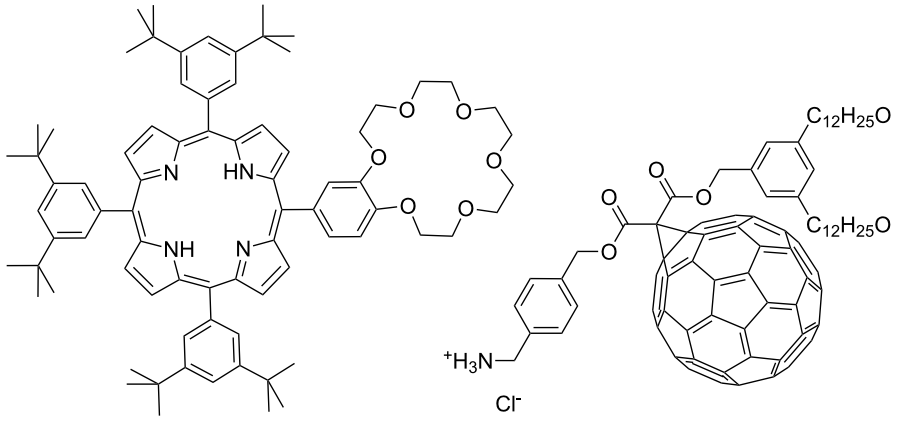

73 **74**

Figure 48: Porphyrin-crown ether conjugate **73** and fullerene-ammonium ion guest **74**.

with calixarenes and related molecules. We will start our survey with simpler substitution patterns and proceed with more complex substituted calixarenes for enantiodiscrimination, for colorimetric assays and capped structures. Resorcinarenes and deeper cavities, ditopic receptors, and capsules are also included.

3.1. Basic examples with simpler substitution pattern

Calixarenes and resorcinarenes (**75)** (Figure 49) belong to the most versatile building blocks in supramolecular chemistry. Several books and reviews covering their synthesis, structural properties and applications have been published [234-236]. A variety of methods for the synthesis and functionalization of the macrocycles has been developed [237,238]. Likewise, the synthesis and application of resorcinarenes and O-alkylated derivatives have been comprehensively summarized [239]. Calixarenes, e.g., **75a** resemble a vase like (chalice) shape but are not completely rigid. They may form many conformational isomers by the rotation of the phenol units through the annulus, thus affording a large number of unique cavities of different size and shape. Homooxocalix[4]arenes (example **75b**, Figure 49) and their methyl esters are more recently studied examples [240]. Together with the structurally related resorcin[*n*]arenes (example **75c**) and calixpyrroles, calixarenes are used in a variety of applications, such as chromo- and fluorophores [241,242] for metal ion binding in solution [243,244], anion complexation [245-248] and binding of neutral guests [249], as potentiometric sensors [250-252] in ion selective electrodes [253-255] or as molecular switches [256]. The aromatic cavity of calixarenes is an excellent model for the investigation of cation–π-interactions [11,257-259].

A calix[4]arene includes ammonium ions in its pre-organized cone cavity via electrostatic attraction between the positive charge of the guest and the electron rich faces of the aromatic rings ("cation–π-interaction") (Figure 50) [260-262]. The inclusion of alkyl ammonium ions in the cavity of calixarenes is

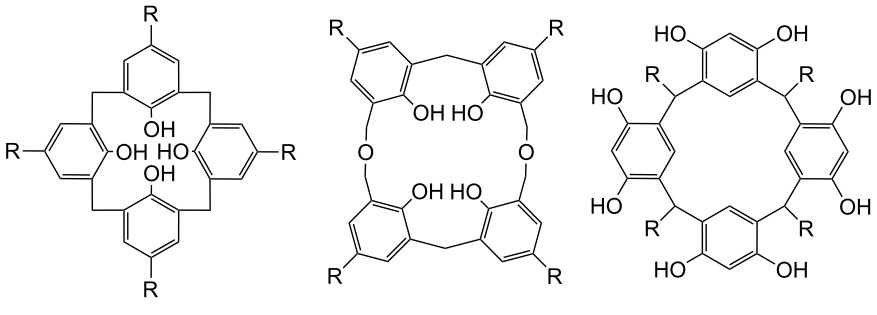

75a **75b** **75c**

Figure 49: Calix[4]arene (**75a**), homooxocalix[4]arene (**75b**) and resorcin[4]arene (**75c**) compared (R = H, alkyl chain).

therefore reflected in a high field shift of the host signals in the ^{1}H NMR spectrum. Based on the magnitude of the shifts of the different host signals, conclusions can be drawn on the preferred orientation of the guest in the cavity [263].

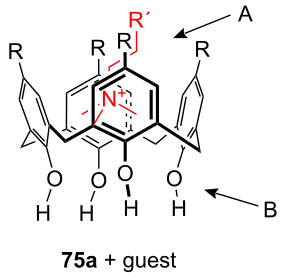

Figure 50: Calix[4]arene and ammonium ion guest (R = H, alkyl, OAcyl etc.), possible binding sites; A: co-ordination of cationic or neutral guests (cation–π-interaction), B: binding site for cationic guests (ion–dipole-interaction or H-bonding).

Gutsche et al. reported the complexation of aliphatic amines by alkylcalix[4]arene with a binding strength in the order of 10^4 M^{-1} in acetonitrile [264,265]. The contribution of cation–π-interactions to the binding was demonstrated for several examples of complexes with quaternary ammonium [266,267] or tetraalkylammonium [261,268,269] salts in organic media. Proton transfer from OH-groups of the calixarene to the amine, followed by association and inclusion is a different binding situation: The guest is co-ordinated by a tripodal H-bonding [265,266,270,271]. The complexation behavior seems to be mainly determined by the conformational mobility of the calix. Control of the conformational properties of these macrocycles is crucial for their applications in supramolecular chemistry.

Typical guests (Figure 51) in studies with calixarenes and resorcinarenes utilizing the explained modes of interaction are the physiologically relevant quaternary ammonium compounds choline (**76**), acetylcholine (**3**), carnithine (**77a**) and acetylcarnithine (**77b**), as well as the salts of the aromatic amines 2-phenethylamine (**78a**), dopamine (**2**), ephedrine (**79a**), norephedrine (**79b**), adrenaline (**80a**) and noradrenaline (**80b**).

Additionally, amino acids and their derivatives are also bound by calixarenes, especially aromatic amino acids such as phenylalanine (**81a**) or tryptophan (**81b**) or the basic representatives, for example, lysine (**81c**), arginine (**81d**) and histidine (**81e**) (Figure 51), and peptides containing these residues. Similar to larger crown ethers (24-crown-8 and larger) or cyclodextrins, calixarenes may also be threaded to form rotaxane like structures. A common guest for this is paraquat. The reader is referred to the literature covering this topic [272-275]. We discuss now some recent examples in ammonium ion recognition with the calixarene class of receptors and focus on the

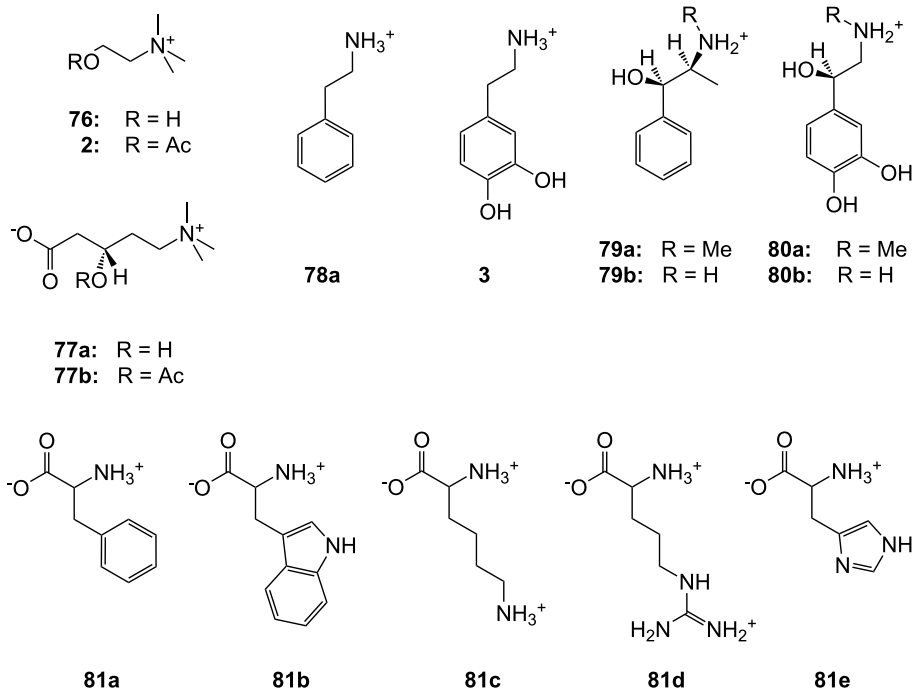

Figure 51: Typical guests for studies with calixarenes and related molecules.

recognition of these ammonium targets e.g. *N*-terminal peptide recognition, preferably in water and/or under neutral conditions. The binding of metal ions is not covered and has been already reviewed [243]. For detailed thermodynamic data we recommend the articles of Izatt et al. [146] and Namor et al. [276]. Recognition of biochemical targets was recently covered comprehensively by Ludwig [277]. Biros and Rebek have summarized the application of water soluble resorcinarenes for the recognition of ammonium ions in their recent review [278].

In the simplest case, only one side of the calixarene skeleton is substituted. For example, *p-tert*-butylcalix[5]arene **82** modified at the lower rim [279] (Figure 52) was investigated in $CDCl_3$/CD_3OD (9/1). The binding affinities of isomeric butylammonium picrate salts show high log K_{ass} values with the *n*-$BuNH_3^+$ ion ranging from 4.63 to 6.47, while other branched cations, such as *tert*-$BuNH_3^+$ give significantly lower values. The stability of the complexes generally decreased in the order: **82d** > **82a** > **82b** > **82c** for one given isomer, with the highest selectivity of calix[5]arenes **82a** and **82d** towards *n*-$BuNH_3^+$ ion. The presence of *tert*-butyl substituents on the upper rim is essential to force the molecule into a regular C_{5v} cone conformation and ensure selective inclusion of R-NH_3^+-ions. Receptors **82a** and **82d** formed 1:1 inclusion complexes only with Na-Ac-Lys-OMe hydrochloride and Lys-Gly-OMe dihydrochloride. In the latter the ε-butylenammonium group was recognized by the cavity and complexed in the presence of an unprotected α-ammonium group. The methyl ester hydrochlorides of the neurotransmitter γ-aminobutyric acid (GABA) and the related plasmin inhibitor ε-aminocaproic acid (ε-Ahx) [280] were also strongly included with degrees of complexation up to 80%.

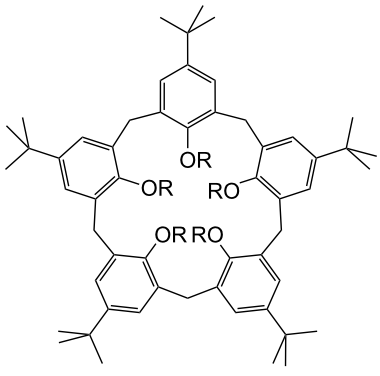

82a: R = $(CH_2)_3CH(CH_3)_2$
82b: R = $(CH_2)_2OCH(CH_3)_2$
82c: R = $CH_2COOCH(CH_3)_2$
82d: R = $CH_2COOC(CH_3)_3$

Figure 52: Lower rim modified *p-tert*-butylcalix[5]arenes **82**.

Similar to the unsubstituted calixarenes such examples are only poorly soluble in water and polar substituents are required to increase water solubility. Several examples of water soluble calixarenes bearing phosphonate [281], amino acid [282] or neutral groups [283] at the upper rim have been reported already in the 1990s. Arduini et al. reported the first example of a water soluble calix[4]arene in the fixed cone conformation (Figure 53). It carries four carboxylate groups at the lower rim but shows no inclusion of neutral molecules in water [284].

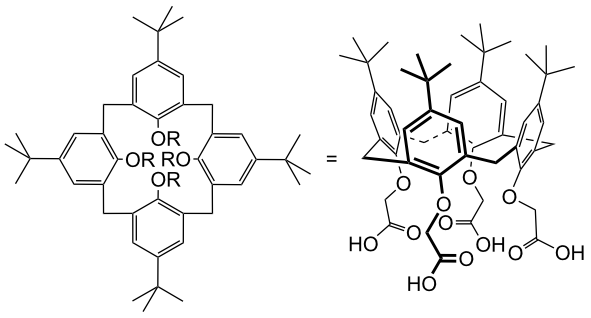

83: R = CH_2COOH

Figure 53: The first example of a water soluble calixarene.

Sulfonated calix[*n*]arenes (**84**, *n* = 4, 6, 8) [266] (Figure 54) have good water solubility. They complex trimethylanilinium cations (K_{ass} for *n* = 4 is 5600 M^{-1}) and adamantlytrimethylammonium cations (K_{ass} for *n* = 4 is 21000 M^{-1}) in water [285,286]. Studies by Gokel and Kaifer on the inclusion of ferrocene derivatives in water showed that calix[6]arene hexasulfonate (**84b**) is a good receptor for the complexation of a bulky trimethylammonium ion with a association constant of K_{ass} = 10930 M^{-1} [287].

Later, the investigated scope was expanded to the corresponding calix[5]arene (**84d**). The inclusion of tetramethylammonium and ditopic trimethylammonium cations was studied at neutral pH by ^1H NMR and compared to the homologous tetrasulfonatocalix[4]arene (**84a**) [288]. The more flexible host exhibits a more efficient and selective complexation of ditopic methylammonium ions compared to the more pre-organized calix[4]arene receptors (**84a**). This is a rare case of molecular recognition by induced fit enhancing affinity and selectivity.

Utilizing the outstanding complexation properties of calixarenes for quaternary ammonium ions, the binding of acetylcholine (**3**) has attracted much interest due to its biological importance as a neurotransmitter. It has been shown, that the cationic ammonium group of acetylcholine (**3**) binds to the aromatic cavity of calixarenes through cation–π-interactions

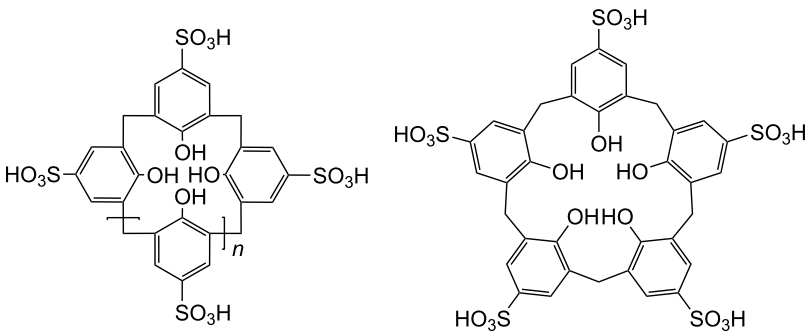

Figure 54: Sulfonated water soluble calix[*n*]arenes that bind ammonium ions.

(see also later examples of **75c**, **115c**, **116, 117, 118** and **126a/c**).

Compound **84b** was used to sense the presence of acetylcholine (**3**) in neutral aqueous or water/methanol solution. The sulfonatocalix[6]arene binds acetylcholine (**3**) in preference to primary and secondary amines, and allows the use of the pyrene indicator **85** in a displacement assay (Figure 55). Upon displacement of the fluorescent pyrene cation by **3**, the binding event is signalled by the increased fluorescence intensity of **85** in solution [289].

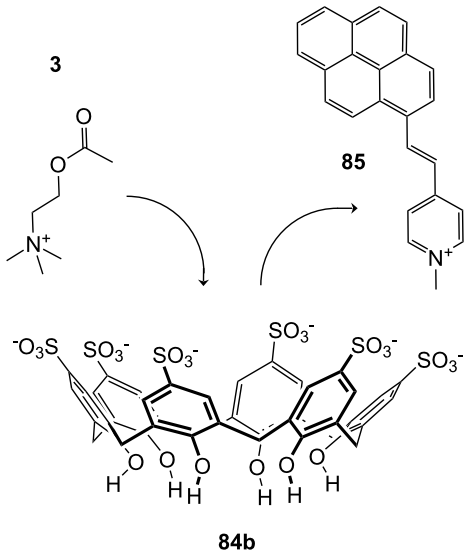

Figure 55: Displacement assay for acetylcholine (**3**) with a sulfonatocalix[6]arene (**84b**).

The affinity of the *p*-sulfonatocalix[*n*]arenes (**84**) (*n* = 4, 6, and 8) towards amino acids was also extensively investigated by ^{1}H NMR [290-292], microcalorimetry [293] and HPLC-methods [294].

The *p*-sulfonatocalix[4]arenes formed 1:1 complexes more strongly with basic amino acids with K_{ass} values for Arg and Lys of 1520 and 740 M^{-1}, respectively (phosphate buffer at pH 8), than with aliphatic or aromatic amino acids: Val, Leu, Phe, His, Trp, with K_{ass} values between 16 M^{-1} and 63 M^{-1} (phosphate buffer at pD 7.3) [292,295].

The basic amino acids arginine (**81d**) and lysine (**81c**) show strong electrostatic binding to calix[4]arene sulphonate at pH 5 (Figure 56). For higher calixarenes, only weak interactions at the faces of the flattened macrocycles occur. This binding is in contrast to the inhibition of protein–protein interactions by the calixarenes where the calix[6]arene and calix[8]arene sulfonates show much stronger effects [291].

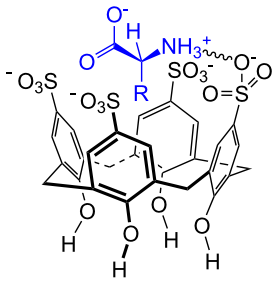

Figure 56: Amino acid inclusion in *p*-sulfonatocalix[4]arene (**84a**).

Their application as glycosylaminoglycan (GAG) mimicry [296] was demonstrated by the binding thermodynamics towards certain di- and tripeptides bearing lysine (**81c**) or arginine residues in aqueous buffer at pH 8.0 [296]. Due to their key role in these peptide sequences present in GAG recognition

sites, arginine (**81d**) and lysine (**81c**) were also used as guests in the titration microcalorimetry and NMR studies. The simple amino acids were bound with $K_{ass} = 10^3$ dm^3 mol^{-1}. With the corresponding dipeptides there was a of 3 to 4 fold increase in binding, with the tripeptide of 5 to 8 fold increase was observed in comparison to Arg or Lys, respectively. More interaction sites were involved in their binding. Mixed Arg-Lys-peptides were bound more strongly and were sequence independent. The selectivity order (Arg > Lys > other amino acids) was retained in the peptides and was governed by hydrophobic interactions between the calixarene cavity and the aliphatic or aromatic guest moiety. The apolar part of the peptide inserts into the cavity.

Ungaro et al. introduced sulfonate groups instead of the bulky *tert*-butyl groups in **83** [297], resulting in more flexible hosts [*n* = 1; X = H (**83**) and SO_3H (**86a**); R = CH_2COO^-] (Figure 57). From compound **83** to **86a** a significant increase in log K_{ass} values for the binding of organic ammonium ions was observed: 1.7 and 3.3 for benzyl-NMe_3^+ or 1.7 and 3.4 for *p*-nitrobenzyl-NMe_3^+, respectively [298]. The inclusions were enthalpically driven and disfavored for entropy reasons.

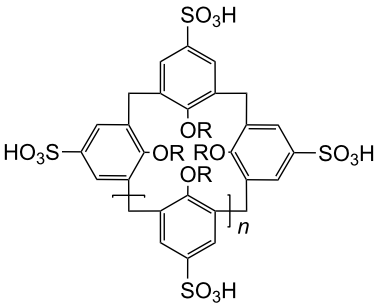

86a: *n* = 1; R = CH_2COOH
86b: *n* = 2; R = CH_2COOH
86c: *n* = 3; R = CH_2COOH

Figure 57: Calixarene receptor family **86** with upper and lower rim functionalization.

Calix[5]arenepentasulfonates (**86b**) bind trimethylammonium ions in water (pD 7.3) with association constants between 4.0 × 10^3 and 1.3 × 10^5 M^{-1}. The alkylammonium group is completely immersed in the cavity [288]. The corresponding calix[6]arene (**86c**) binds a variety of amino acids in water. The highest binding affinities were found for aspartic acid, arginine (**81d**) and tryptophan (**81b**, $K_{ass} = 4.1 \times 10^3$ M^{-1}, 3.6×10^3 M^{-1} and 2.5×10^3 M^{-1}, respectively). Coleman et al. investigated a similar calix[6]arene with one carboxyl group at the lower rim (Figure 58) in amino acid recognition in water [299]. The selectivity changed in favor of asparagine (log K_{ass} = 3.82 for **87a** and 3.61 for **87b**). These most stable complexes resulted from the double H-bonding, which is known from carboxylate dimers. Similar contributions could be observed for arginine (**81d**) and lysine (**81c**). Additional π–π-interactions stabilized the complexes with aromatic amino acids; the hydroxy or thiol groups in cysteine and serine showed no effect on the complex stability. In summary, the 1:1 complex stability follows the following order: acidic > aromatic ~ basic > aliphatic ~ polar amino acids. The more polar compound **86b** binds non-polar guests weaker.

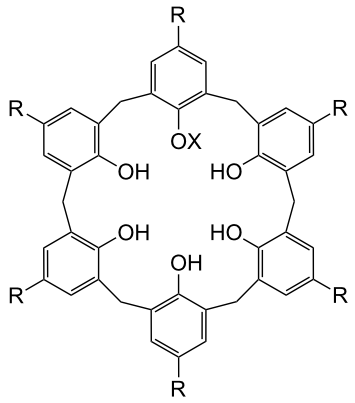

Figure 58: Calix[6]arenes **87** with one carboxylic acid functionality.

Consequently, da Silva and Coleman studied complexing properties of *p*-sulfonatocalix[*n*]arenes (*n* = 4, 6, 8) mono-functionalized at a phenolic oxygen (Figure 59) towards 11 amino acids by means of ^{1}H NMR spectroscopy in unbuffered aqueous sodium hydroxide solution (pH 8.0) and compared them to the unsubstituted parent calixarenes [300]. In general, the receptors follow the trends discussed above: Arg and Lys, and sometimes His are bound more strongly than Gly, Ala, Leu, Pro, Phe and Trp. Receptors with acid functionality (**88a**, **89a** and **90a**) often show higher binding values for the basic amino acids. Especially noteworthy is the enhanced complexing ability for aspartic acid with K_{ass} values ranging from 2200 (**88b**) to 2500 M^{-1} (**90b**) for the amide functionalization, 2800 (**88a**) to 3200 M^{-1} (**90a**) for the acid functionality and, not surprisingly observing the highest values of 5600 M^{-1} (**88c**) to 5400 M^{-1} (**90c**) for the amine substitution pattern. Ser bound strongly to **88a** with K_{ass} = 3555 M^{-1} attributed to its additional hydrogen bonding site and the optimal fit.

The formation of complexes between derivatized cyclotetrachromotropylene host (**91**) (Figure 60) and Ala, Asp and Lys in aqueous solution at pD 1.0 was also investigated [301]. For tetraalkylammonium ions, the hosts reveal the same stability trend as has been reported for the 1:1 complexes of *p*-sulfon-

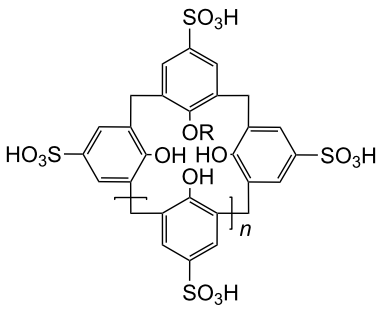

88a: n = 1; R = CH_2COOH
88b: n = 1; R = CH_2CONH_2
88c: n = 1; R = $CH_2CH_2NH_2$

89a: n = 3; R = CH_2COOH
89b: n = 3; R = CH_2CONH_2
89c: n = 3; R = $CH_2CH_2NH_2$

90a: n = 5; R = CH_2COOH
90b: n = 5; R = CH_2CONH_2
90c: n = 5; R = $CH_2CH_2NH_2$

Figure 59: Sulfonated calix[*n*]arenes with mono-substitution at the lower rim systematically studied on their response to amino acids.

atocalix[4]arene (**84a**). The K_{ass} values, reaching 2.7 × 10^4 M^{-1} for the complexation of Et_4N^+ in D_2O, are in the same order of magnitude as for **84a**. A similar behavior is observed for amino acids. The basic representative lysine (**81c**) is bound best in a 1:1 complex with the host with a K_{ass} value of 2.0 × 10^3 M^{-1}. The binding values for aspartic acid and alanine were substantially smaller (250 M^{-1} and 70 M^{-1}, respectively).

The non-covalent phosphate–ammonium interaction not only plays a key role in living systems for many critical molecular recognition processes, it can also inspire the design of water-soluble artificial receptors.

The influence of phosphonic acids groups instead of sulfonate groups at the upper rim of calix[4]arenes has also been investigated. Witt et al. researched the complexation properties of water-soluble calix[4]arenes based cavitands (Figure 61) with (1*R*,2*S*)-(−)-ephedrine (**79a**), (1*R*,2*S*)-(−)-norephedrine (**79b**), (*R*)-(−)-noradrenaline hydrochloride (**80b**) and 2-phenylethylamine hydrochloride (**78a**) in phosphate buffer at pD 7.3 [302]. The host molecules were intended to mimic the adrenergic receptor. The participation of the calixarene hydrophobic cavity was confirmed and the structural requirements for the binding of the ammonium ion guests were investigated. The host compounds were able to form 1:1 complexes with an association constant K_{ass} of up to 145 M^{-1} (2-phenylethylamine hydrochloride (**78**)–(**92b**)). The aggregate stoichiometry was confirmed by a Job's plot. For ammonium type guest, a stronger interaction is observed when phosphonic acids groups are attached at the upper rim (K_{ass} for **92b** > **92a**).

A similar receptor for amino acids was studied by Zielenkiewicz et al. who investigated the thermodynamics of distally substituted bis(dihydroxyphosphorylhydroxymethyl)-calix[4]arene at the upper rim of racemic **93** (Figure 61) in the binding of several amino acids [303,304] and dipeptides [305] in methanol by isothermal titration calorimetry, NMR and UV–vis spectroscopy. Free amino acids as well as dipeptides gave strong 1:1 complexes. The complex stability correlates with the hydrophobicity of the amino acid residues and decreases with decreasing hydrophobicity: Ile > Leu > Val > Ala > Gly with log K_{ass} = 4.23 for Ile and 3.84 for Gly. Neutral aliphatic and aromatic amino acids were better bound than basic ones. The stability constants for dipeptides were in a similar range of 25000–45000 M^{-1}, enthalpy changes in the range of −10.5 to −5.9 kJ mol^{-1} and −26.5 to −25.3 kJ mol^{-1} in the estimated Gibbs free energy, respectively. The complexation phenomenon was found to be driven by electrostatic interac-

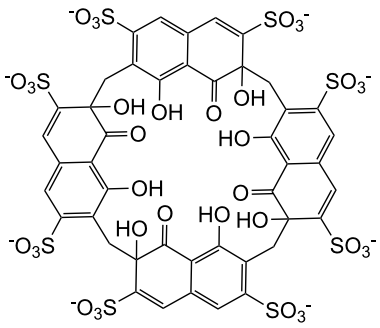

91

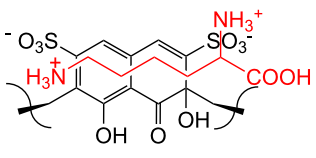

91 + lysine

Figure 60: Cyclotetrachromotropylene host (**91**) and its binding to lysine (**81c**).

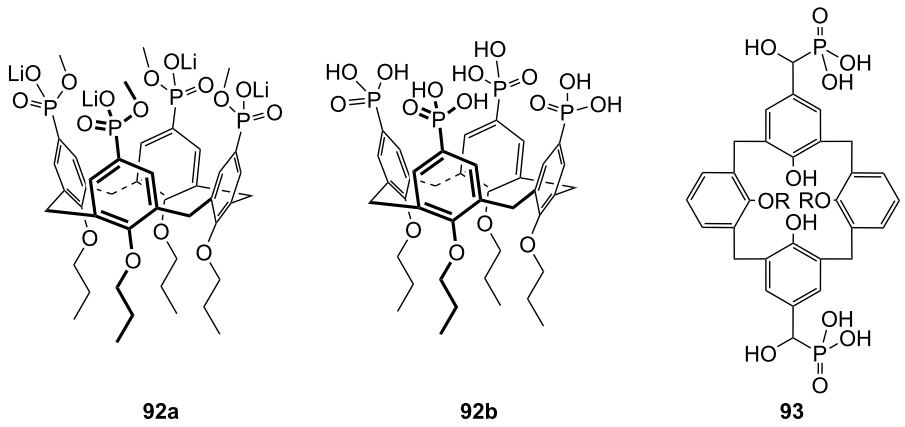

Figure 61: Calixarenes **92** and **93** with phosphonic acids groups.

tions between the protonated *N*-terminal amino group of the guest and the calixarene phosphoryl groups.

Water soluble calix[4]arenes with one, two or four dihydroxyphosphoryl groups at the lower rim can form salts with (1*S*,2*R*)-(+)-ephedrine and 2-phenylethylamine hydrochloride [306]. The salts of these inherently chiral calixarene phosphoric acids with the chiral amines are easily separated into diastereomeric forms.

Based on the results of the former investigations, studies with **92b** were extended to amino acid derivatives and also compared to a series of calix[4]arene phosphonic acids [307]. The influence of the calixarenes conformation flexibility and its hydrophobic cavity shape dependent on the lower rim substitution pattern on the complexation process was monitored by ^{1}H NMR spectroscopy in deuterated phosphate buffer at pD 7.3. Receptor **92b** did not show any remarkable selectivity towards the investigated amino acids methyl esters (K_{ass} = 10^2 M^{-1}). Only mixed 1:2 and 2:1 (host–guest) complexes were observed for compound **92b**. By contrast, compounds **94** (Figure 62) showed selectivity for basic amino acid methyl esters, i.e. Lys-OMe (K_{ass} (**94b**) = 170 M^{-1}, K_{ass} (**94a**) = 600 M^{-1}), Arg-OMe (K_{ass} (**94b**) = 120 M^{-1}, K_{ass} (**94a**) = 600 M^{-1}), and His-OMe (K_{ass} (**94b**) = 30 M^{-1}, K_{ass} (**94a**) = 200 M^{-1}) forming 1:1 complexes. More H-bonding sites increase the binding strength. Modification of the lower rim of the calix[4]arene skeleton by bridging ligands lowered the complexation ability of the more rigid molecule **93b** although its binding selectivity was preserved.

Calixarene tetraphosphonate (**92c**) (Figure 63) was described as specific receptor for basic amino acids, with preference for arginine (**81d**). Binding constants in methanol ranged from 7.9 × 10^2 M^{-1} for Ac-Lys-OMe (Lys, K_{ass} = 3 × 10^3 M^{-1}) to 1.9 × 10^4 M^{-1} for Ts-Arg-OMe (Arg, K_{ass} = 7.9 × 10^2 M^{-1}).

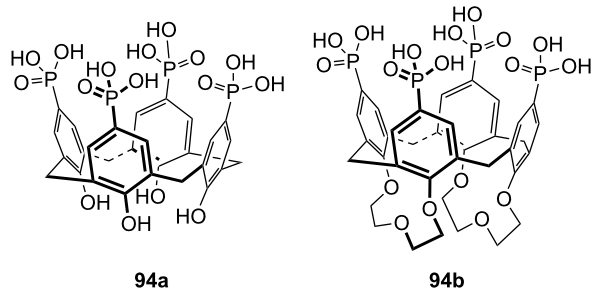

Figure 62: Calix[4]arene tetraphosphonic acid (**94a**) and a double bridged analogue (**94b**).

Consequently, this host molecule was used in lipid monolayers for recognition of peptides and basic protein surfaces in buffered aqueous solution [308,309] (HEPES), and the binding events monitored with the aid of a Langmuir film balance. Histone H1 and Cytochrome C were recognized in the range of 10^{-8} mol/L guest concentration [306].

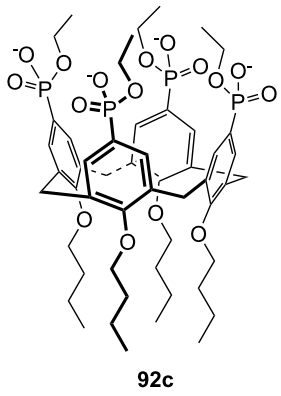

Figure 63: Calix[4]arene tetraphosphonic acid ester (**92c**) for surface recognition experiments.

Similar calix[4]arenes with α-aminophosphonic acid fragments at the upper or lower rim were described and their remarkable selectivity as carriers for zwitterionic aromatic amino acids in membrane transport reported [310].

By introducing these H-donor and H-acceptor groups in the host skeleton, it was shown that a calix[4]arene molecule binds hydrophilic amino acid zwitterions in its polar cavity: Two aminophosphonate groups at the lower rim (Figure 64) lead to selective transport of His over Phe, Tyr and Trp, while upper rim modification changes the selectivity towards Phe. In the later case the substituents can participate in complexation and recognize the aromatic side chains of amino acids. The selectivity of membrane transport for phenylalanine (**81a**) was enhanced 40 times over tryptophan (**81b**) (fluxes ratio for **95a** −7.3, for **95b** −4.9).

In addition, phosphorylated calixarenes have been used to bind uracils (K_{ass} up to 5.43×10^4 M^{-1}) in aqueous solvent mixtures [311-313]. Together with the examples **92** and **94**, a whole series of phosphonate substituted calixarenes for amino acids binding has been reported, which have proved to be more versatile than the *p*-sulfonatocalix[*n*]arenes and applicable at pH values closer to those found under physiological conditions. The binding constants for amino acids in water are of the same order of magnitude for both functionalizations, where comparable. The preference for basic amino acids is evident.

3.2. More complex calixarenes: optical readout, enantiodiscrimination, bridges and caps

Calixarenes have been modified to exhibit special properties such as optical readout by chromophoric groups, enabling quick and easy monitoring of guest binding, or by groups supplying chirality for enantiodiscrimination. In addition, the cavity has been expanded or rigidified by bridges or even caps to improve binding properties. Often no sharp dividing line can be drawn between these concepts. We present now the current approaches, where we try to keep the direction, starting with optical readout systems, followed by calixarenes for chiral recognition and then go on to more complex systems ending with capped moieties with additional functionalities.

Bridging of calixarenes and resorcinarenes with ethyleneglycol chains leads to calixcrowns and resorcinarene crowns, or even calixcryptands [314]. The synthesis, structure and fundamental properties of such systems have been reviewed [315]. We will point out their application in ammonium ion recognition in comparison to other calixarenes with selected examples. Related systems carry ether bridges in the calixarene ring (Figure 65). Such homocalixarenes are structurally similar to crown ethers (**4**) and can bind primary ammonium ions [316-320].

Two typical examples have been described by Chen et al. (**95**) [321] and Masci et al. (**96**) [322] (Figure 65). Compounds **95** show selectively binding ability towards linear primary alkylammonium ions from *n*-$BuNH_3^+$ to *n*-hexyl-NH_3^+ with the formation of 1:1 complexes in $CDCl_3/CD_3CN$ and K_{ass} = 600 M^{-1}. Compound **96a** binds the tetramethylammonium ion with K_{ass} = 280 M^{-1} in $CDCl_3$.

Homocalix[3]arene **97a**, reported by Tsubaki et al., consists of an 18-membered ring and six oxygen atoms available for cation co-ordination [323]. In addition, the molecule contains a Reichardts dye E_T1 (**97b**) type pyridinium phenolate moiety (Figure 66), which becomes deprotonated upon ammonium ion binding. The resulting betaine structure shows long wavelength charge transfer absorption observable in the visible spectrum. Only compound **97a**, and not the dye E_T1 (**97b**) itself, showed a color change upon addition of amines or an alkaline earth acetate. This confirms a binding process and excludes a simple deprotonation reaction as the origin of the color change. Due to

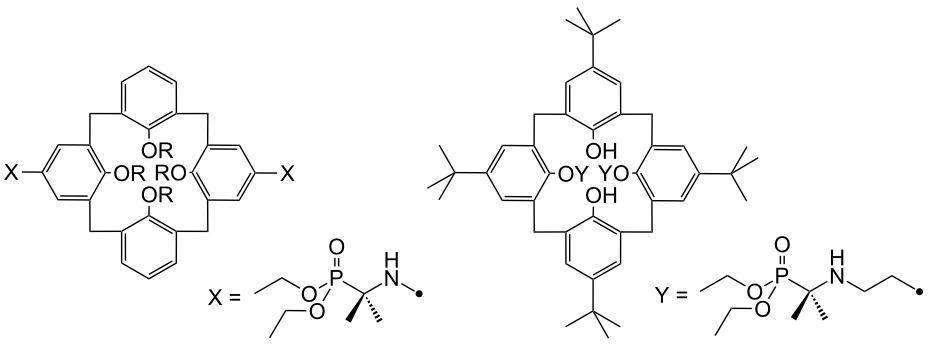

94a **94b**

Figure 64: Calixarene receptors **95** with α-aminophosphonate groups.

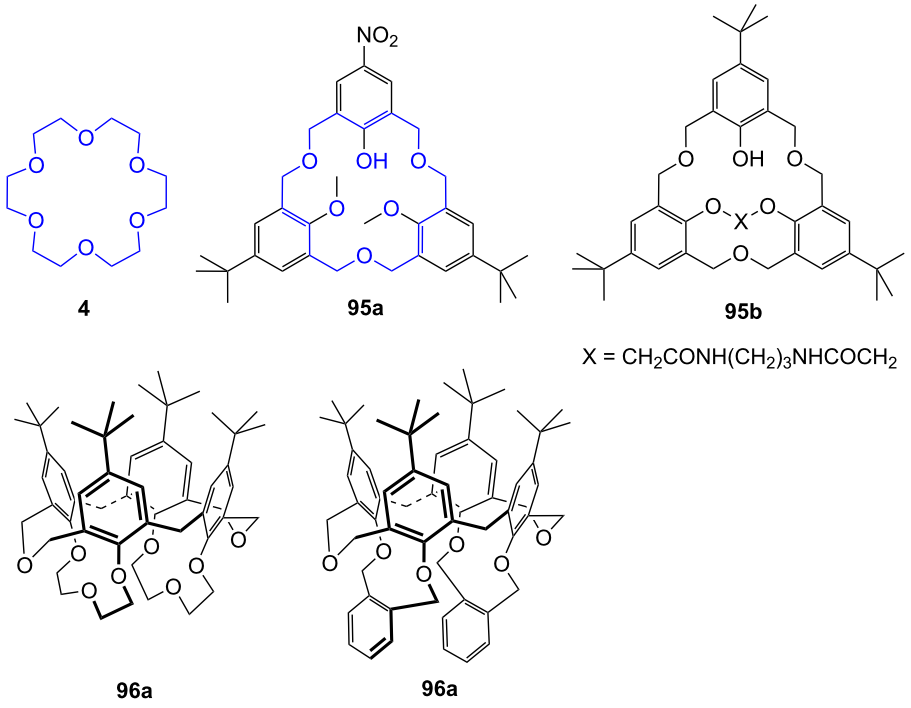

4 95a 95b 96a 96a

Figure 65: A bridged homocalix[3]arene **95** and a distally bridged homocalix[4]crown **96**.

steric reasons, primary amines are preferentially bound over secondary and tertiary amines. *N*-Butylamine showed a binding constant of 135 M^{-1} in DMSO.

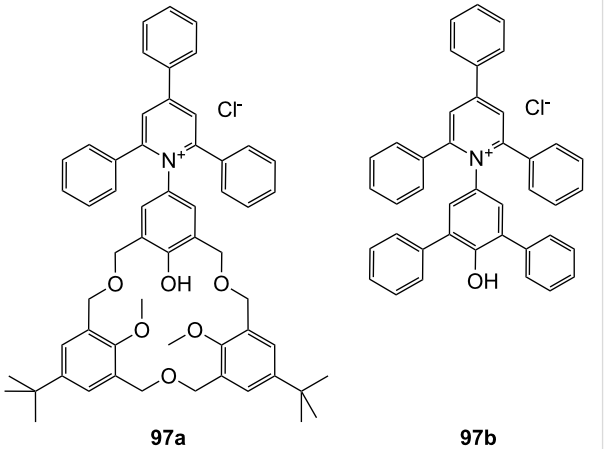

97a **97b**

Figure 66: Homocalix[3]arene ammonium ion receptor **97a** and the Reichardt's dye (**97b**) for colorimetric assays.

Diazo-bridges in calix[4]arenes also allow distinguishing the binding of amines and diamines (or triamines) by color changes, caused by host–guest proton transfer [324]. Bisazobiphenyl-bridged chromogenic calix[4]arenes **98** (Figure 67) were employed as reagents for the visual discrimination of aliphatic and aromatic amines [325]. Various amines were added to **98** in DMSO resulting in distinct color changes. For instance, *tert*-butyl amine induced bathochromic shift of the absorption of 84 nm, whilst the addition of aromatic amines did not induce any color change or shift in the absorption maxima. The yellow color was restored upon acidification of a solution of the **98**-*tert*-butylamine complex. This indicated that the color change could be attributed to the ionization of hydroxyl groups of **98**. Conductometric titration gave further evidence: On addition of the guest, the conductivity continuously increased until it reached a plateau at equimolar concentration of amine.

In an earlier publication, Arduini et al. introduced short diethylene glycol bridges into calix[4]arene. The resulting derivative was successfully used for the cation–π-complexation study of methylammonium and tetramethylammonium ions [326]. When a crown ether moiety bridges a calix[4]arene at the lower rim it prefers primary ammonium ions over the isomeric derivatives (*n*-butyl >> *tert*-butyl) for steric reasons [327]; a similar selectivity was observed if two parallel crown-3 moieties at the lower rim are introduced in *p*-phenylcalix[4]arene [326] and the same order of preference was noted (i.e. *n*- >> *s*- > *tert*-butylamines) if two carboxymethoxy groups at the lower rim of a calix[4]arene are bridged by a crown-3 group [328].

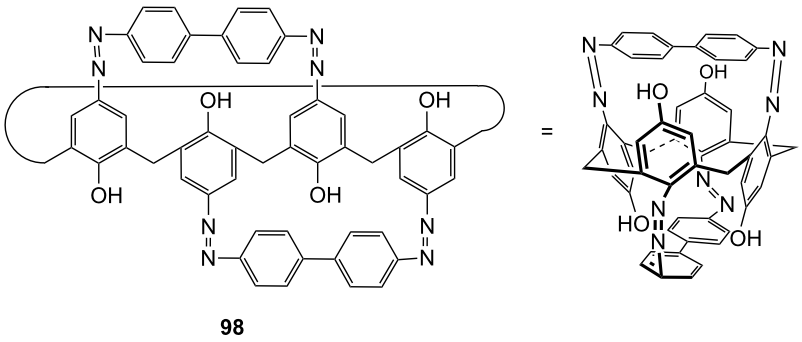

98

Figure 67: Chromogenic diazo-bridged calix[4]arene **98**.

The parent calix[4]arene was used by Huang to develop an amine receptor with optical readout. The dinitrated calix[4]arene is bridged by oligoethyleneglycol chains of different length (Figure 68) by the alkylation of the phenolic hydroxyl groups of the non-substituted arenes [329].

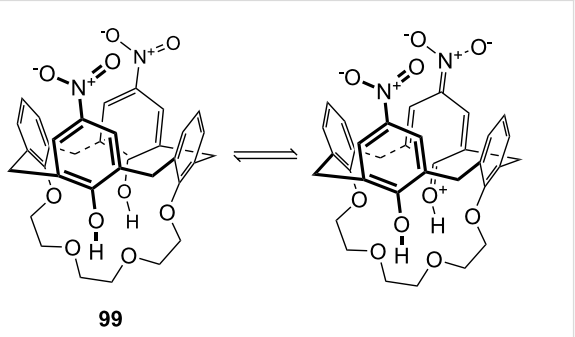

99

Figure 68: Calixarene receptor **99** by Huang et al.

As in the previous examples, the binding of the amine by the resulting phenolate ion is crucial for the development of the color. Because of two phenols being deprotonable per calixarene, it is not surprising that the authors identified a 1:2 receptor to amine stoichiometry. For this class of receptors a clear preference for binding of primary amines over branched, secondary and tertiary guests was observed. For the depicted receptor they found the best binding properties with *n*-butylamine (K = 326 M^{-1}) in chloroform.

Enantioselective analysis and separation of amino acids was addressed using chiral calixarene type macrocycles: A pseudo-C_2-symmetrical homooxacalix[3]arene discriminates between chiral amino acids [138], whilst chiral calix[4]crown ethers were used for the binding of alkylammonium ions [330]. Amino acid esters were separated in liquid membrane transport experiments with an efficiency dependent on their hydrophobicity, with preference to *S*-Phe- and *S*-Trp- ester showing the highest flux [331].

A calix[5]arene related to **82** for attempted enantiodiscrimination was reported by Parisi et al. [332]. Replacing the *tert*-butyl group (**100a**) by a urea functionality (**100b** and **100c**) on the upper rim (Figure 69) significantly improved the binding constants towards ammonium guests.

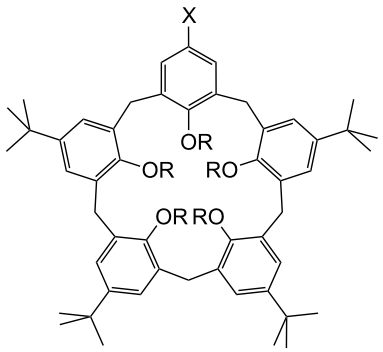

100a: X = ^{t}Bu
100b: X = (*R*)-PhMeCHNHC(O)NH
100c: X = (*S*)-PhMeCHNHC(O)NH

R = $(CH_2)_3CH(CH_3)_2$

Figure 69: Calixarenes **100** reported by Parisi et al.

The free rotation around the aromatic-*N*-(urea)-bond allows the urea unit to act as a hydrogen bond acceptor to bind ammonium ions and as a hydrogen bond donor for carboxylate binding. However, a comparison of the binding constants shows that carboxylate ions are bound more tightly. This is indicated by the difference between the binding of 1,5-diaminopentane dihydrochloride (DAP × 2 HCl, **101a**) and 5-aminopentanoic

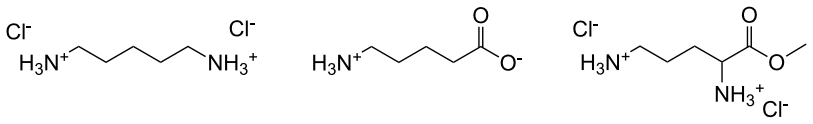

101a **101b** **101c**

Figure 70: Guest molecules for inclusion in calixarenes **100**: DAP × 2 HCl (**101a**), APA (**101b**) and Lys-OMe × 2 HCl (**101c**).

Table 5: Binding constants of different guest molecules (**101**) with receptors **100** (NMR titration in $C_2D_2Cl_4/CD_3OD$ 2/1).

Receptor	**101a**	**101b**	**101c**
100a	300 M^{-1}	1070 M^{-1}	43 M^{-1}
100b	12820 M^{-1}	16140 M^{-1}	2240 M^{-1}
100c	11860 M^{-1}	16850 M^{-1}	2190 M^{-1}

acid (APA, **101b**) (Figure 70, Table 5). The chirality of the receptors **100b** and **100c** did not lead to any enantiodifferentiation of chiral guest molecules.

The inclusion properties of the chiral cone peptidocalix[4]arenes **102** with different conformation flexibility (Figure 71) towards aliphatic and aromatic amino acids and their methyl esters were investigated in D_2O (pD 7.3, phosphate buffer) [333]. The authors compared the recognition properties towards α-amino acids and aromatic quaternary ammonium cations of **102c**, and the more rigid water soluble peptidocalix[4]arene **103** by ^1H NMR titration experiments. The complexation occurred exclusively through the interaction of the calixarene cavity with the apolar groups of the guests [334].

Rigid receptor **103** with two di(ethylene glycol) units introduced in proximal positions at the lower rim of the calix[4]arene skeleton (Figure 71) was much more efficient than the flexible analogue in all complexation processes. Aromatic molecules were better bound than aliphatic ones with the highest association constants values K_{ass} = 110 and 620 M^{-1} for *S*-Trp and *S*-Trp-OMe, respectively [335]. The magnitude of log K_{ass} decreased with decreasing hydrophilicity (log K_{ass} in brackets): *R*-Trp-OMe, *S*-Trp-OMe (2.8) > *R*-Phe-OMe, *S*-PhGly-OMe, *S*-Phe-OMe (2.6) > *S*-Leu-OMe (2.5) > *S*-Val-OMe (2.3) > *S*-Tyr-OMe (2.2) > *S*-Ala-OMe, *S*-Trp (2.0) > *S*-Phe (1.8) > *S*-Tyr, *S*-Leu (<1.3) > Ala, Val, Gly. A similar behavior was noted on examining the pH dependence of the association constant between **103** and *S*-Phe-OMe: pH = 6.0 (K = 710 M^{-1}), pH = 7.3 (K = 400 M^{-1}) and pH = 8.0 (K = 220 M^{-1}), corresponding to the decrease in the percentage of the protonated guest species. The hydrazides of these "*N*-linked-peptido-calixarenes" were able to extract complementary amino acids and dipeptides such as acetyl-*R*-alanine and acetyl-*R*-alanyl-*R*-alanine.

Introduction of chirality by the insertation of an amino acid into the ring of the calixarene moiety potentially enables enantiodis-

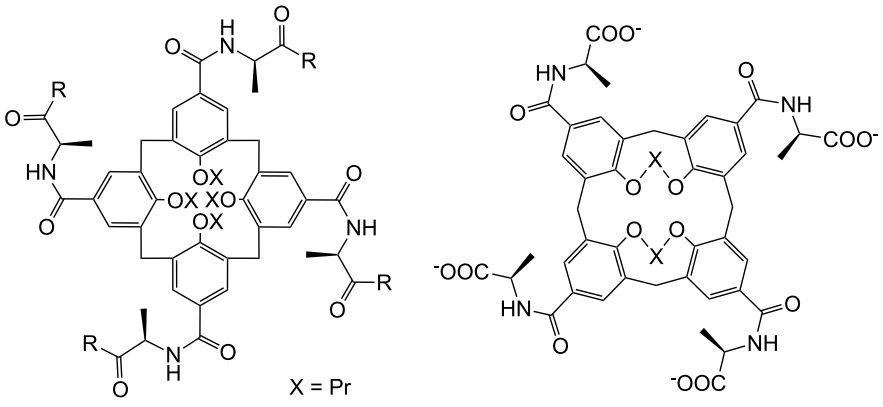

102a: R = OMe
102b: R = $NHNH_2$
102c: R = OH

X = $(CH_2)_2O(CH_2)_2$

103

Figure 71: Different *N*-linked peptido-calixarenes open and with glycol chain bridges.

crimination properties by the formation of diastereomeric complexes with racemic ammonium ions [336].

For the visual discrimination between enantiomers, Kubo et al. synthesized a receptor (**104**) which undergoes a color change upon the binding of chiral substrates [337] (Figure 72). Upon binding of the enantiomers, two different bathochromic spectral shifts of the two chromophores attached to the binding cavity were observed, with significant optical response only for one enantiomer. The best strongest binding occurred with (*R*)-phenylalaninol salt in ethanol K_{ass} = 159 ± 16 dm^3 mol^{-1}. The formation of a 1:1 complex was confirmed by mass spectroscopy. Other amino acids enantiomers, such as the those from phenylglycine, were distinguishable with the system.

Diamond et al. synthesized compound **105** to obtain a sensor (Figure 73) which discriminates enantiomers by hydrogen bonding interactions [338,339]. Without directly observable optical readout option, the fluorescence quenching of the receptor's emission was investigated in chloroform (λ_{ex} 274 nm). Compound **105** shows some selectivity for (*R*)-1-phenylethylamine and also discriminates between the enantiomers of phenylglycinol in methanol.

p-*tert*-Butylcalix[6]arenes were modified with chiral amino alcohols (Figure 74) to achieve enantioselective binding of amino acids and amino alcohols [340]. The extraction properties of the two homochiral receptors **106a** and **106b** for some amino acid methyl esters and amino alcohols were studied by liquid–liquid extraction. The results show that these derivatives were excellent extractants for all the amino acids and amino alcohols, but only a weak or no chiral discrimination of the guests was found. Table 6 shows some selected results.

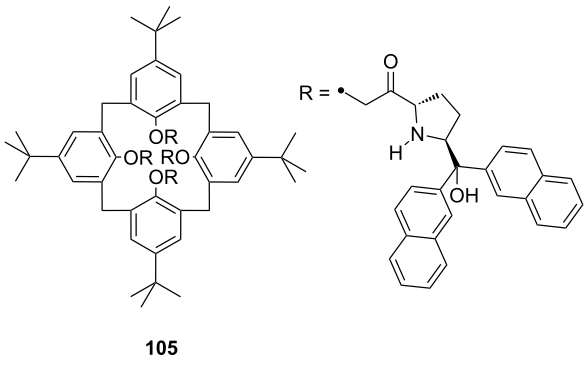

105

Figure 73: A chiral ammonium-ion receptor **105** based on the calix[4]arene skeleton.

The inclusion of quaternary ammonium cations in the cavity of calixarenes with more enclosing substituents, has been extensively studied over the years in the gas phase, in solution and in the solid state [341,342]. The next step is to close the cavity from one side, to bridge or cap the moiety. Bridging of the upper rim of a calixarene may lead to altered selectivity and higher binding constants due to the pre-organized and fixed cavity.

A triply bridged capped C_3-symmetric hexahomotrioxacalix[3]arene **107** (Figure 75) exhibited high affinity (K_{ass} = 7.6 × 10^4 M^{-1}) for the *n*-butylammonium ion [343]. The association constant of receptor **107** with the picrate salt was determined in CH_2Cl_2/THF (99:1, v/v) by the Benesi–Hildebrand equation and exhibited a very well-defined linear shape for a 1:1 interaction.

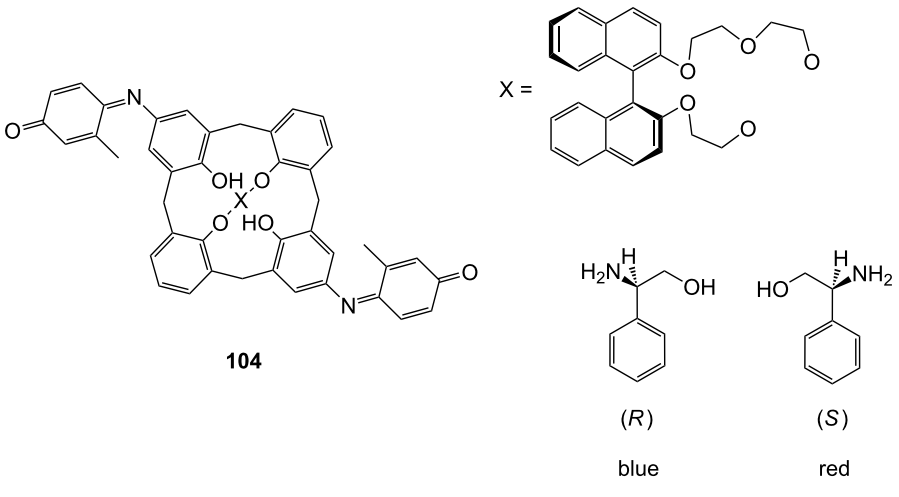

104

Figure 72: (S)-1,1′-Bi-2-naphthol calixarene derivative **104** published by Kubo et al.

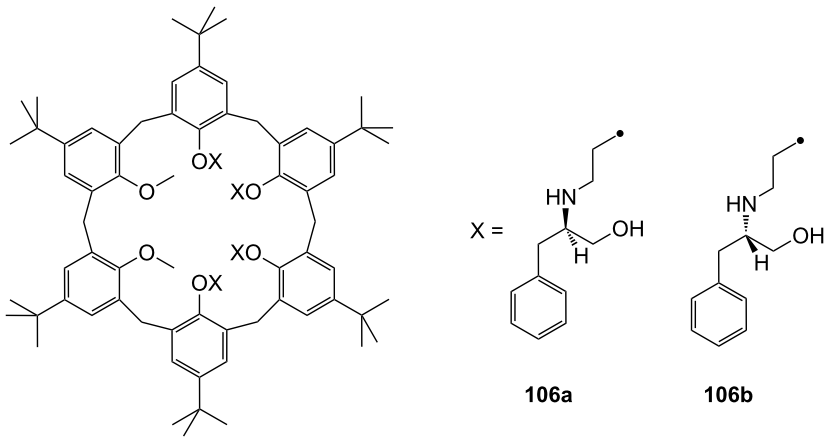

Figure 74: *R*-/*S*-phenylalaninol functionalized calix[6]arenes **106a** and **106b**.

Table 6: Extraction abilities in % of receptors **106a** and **106b**.[a]

Receptor	106a	106b
S-Ala-OMe	91.4	84.3
R-Ala-OMe	89.1	89.6
S-Phe-OMe	90.3	87.2
S-Phe-OMe	90.7	82.5
R-Trp-OMe	87.5	85.4
S-Trp-OMe	93.2	89.8
R-phenylglycinol	92.3	83.5
S-phenylglycinol	72.5	87.6

[a]Extraction for 1 h from water with 2.0×10^{-5} M ammonium picrate to CH_2Cl_2; 25 °C

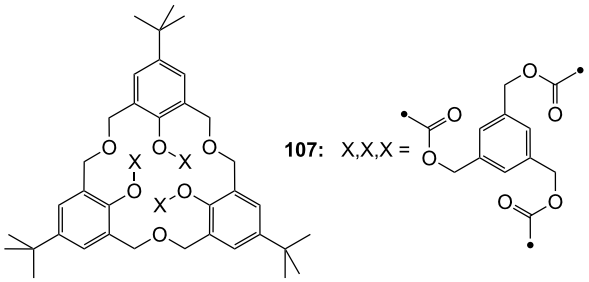

Figure 75: Capped homocalix[3]arene ammonium ion receptor **107**.

A three point connected thioether bridge led to a rigid calix[6]arene moiety (**108**) with C_3 symmetry [344] (Figure 76). This pre-organization enabled better cation–π-interactions with the derivative **108** resulting in a 10–20 fold enhanced association constant for trimethylanilinium iodide (CD_2Cl_2, K_{ass} = 10^2 dm^3mol^{-1}) compared to the reference compound hexamethoxy-*tert*-butylcalix[6]arene.

Compound **109** held rigidly in the cone conformation (Figure 76) displayed an exceptionally high affinity for small ammonium ions forming *endo*-complexes [345]. Extraction and competitive binding experiments gave values that were, at that time, the highest ever obtained with a calixarene-type host. The best affinity was observed for ethylammonium picrate (K_{ass} = 3.3×10^4 M^{-1}) with a more than 100 fold stronger association constant than butylammonium- and secondary ammonium ions. Quaternary ammonium ions were not complexed in chloroform. With the aid of X-ray diffraction, the authors identified the origin of the strong inclusion as contributions of hydrogen bonding to both, the aza cap and one phenolic unit of the calixarene, and to cationic as well as to CH–π-interactions between the ammonium ion and the aromatic walls of the host compound.

A C_{3v}-symmetrical calix[6]cryptand with a P,N-crypto cap was prepared leading to a pre-organized well-defined hydrophobic cavity open at the large rim (Figure 77). The free base of **110a** is able to complex cationic ammonium guests. ^{1}H NMR studies showed that the methoxy substituents point towards the inside of the cavity.

Reinaud et al. provided another example of synergistic combination of a polyaza and a calix[6]arene structure: Calix[6]tmpa **111** [346] (Figure 78). The compound behaved as a single proton sponge and appeared reluctant to undergo polyprotonation, unlike classical tris(2-pyridylmethyl)amine (tmpa) derivatives.

Calix[6]tmpa **111** and its sodium and protonated species display conformational properties that differ from the properties previously observed for other calix[6]-azacryptands: ^{1}H NMR studies indicated that the ligand, as well as its complexes, adopt

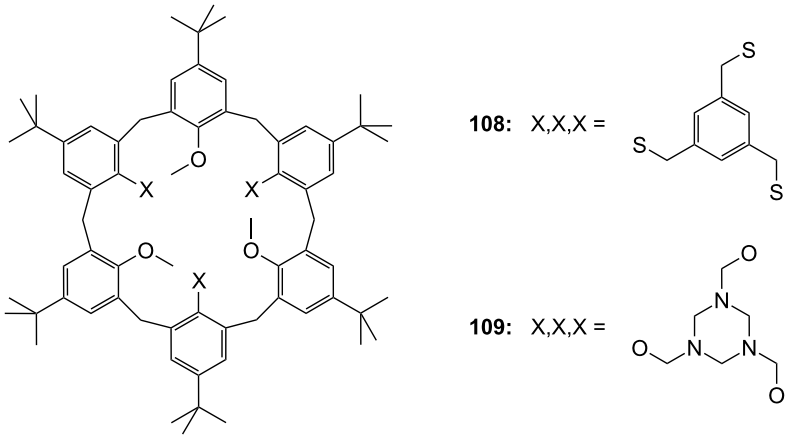

Figure 76: Two C_3 symmetric capped calix[6]arenes **108** and **109**.

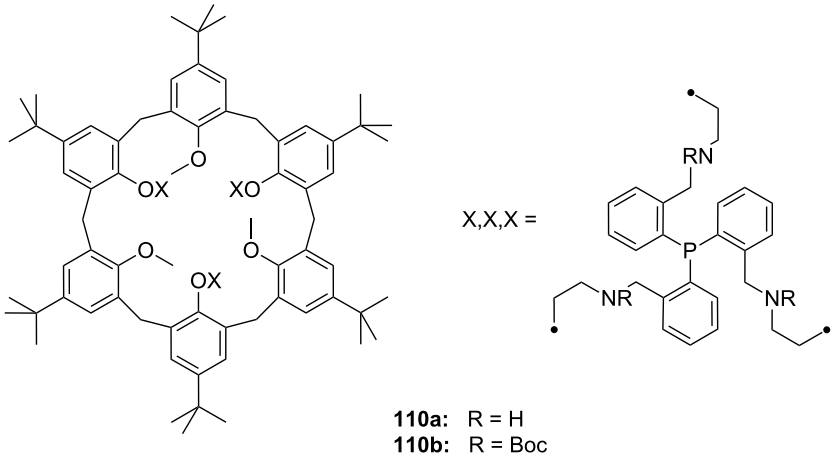

Figure 77: Phosphorous-containing rigidified calix[6]arene **110**.

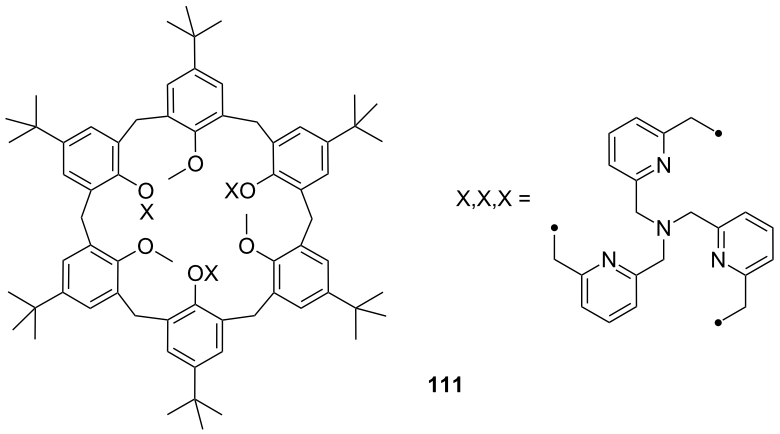

Figure 78: Calix[6]azacryptand **111**.

a flattened cone conformation probably due to the high steric constraint from the tmpa cap.

The monoprotonated derivative behaved as a good receptor for amines, leading to inclusion complexes, and as a good host for ammonium ions. Interestingly, it strongly binds sodium ions and neutral guest molecules, such as ureas, amides, or alcohols, co-operatively. Since it preferentially includes cyclic ureas, amides, or alcohols rather than primary amines, the group found the first example of a funnel complex binding an alkali-metal cation, comparable with related Zn^{2+} funnel complexes [347]. It displayed five fold selectivity in favor of propylammonium hydrochloride over the corresponding ethyl- and two fold selectivity over the butyl–guest in chloroform.

Even larger structures, based on this trimethoxy-calix[6]arene scaffold triple-bridged with a cyclotriveratrylen or connected to dimers via alkyl bridges, were applied for ammonium ion pair inclusion [348].

The use of such ditopic receptors and capped calixarenes with enhanced strength by ion-pair recognition has been an emerging field. In succession of the presented examples, a second generation of the hosts has been introduced [349]. These heteroditopic receptors (Figure 79) can bind ammonium ions or organic ion pair salts with a positive co-operativity [350]. The host–guest properties of receptors **112a** and **112b** toward the picrate and chloride salts of propylammonium ion were studied by ^{1}H NMR spectroscopy and compared to **109**. No distinct binding constants were reported, but addition of 1 equiv of $PrNH_3^+Pic^-$ to $CDCl_3$ solutions of **112a** or **112b** led to the quantitative formation of the corresponding endocomplexes [**112a**·$PrNH_3^+$], Pic^- and [**112b**·$PrNH_3^+$], Pic^-. With XCl, in comparison with [**109**·$PrNH_3^+$], Cl^-, a much larger amount of [**112b**·$PrNH_3^+$], Cl^- was produced with less than 1 equiv of $PrNH_3Cl$. This highlights that the simultaneous binding of the anion by the urea groups of the ditopic receptor **112b** enhances the endocomplexation of the ammonium ion and consequently a much larger binding constant should be observed compared to the first generation molecule **109**.

3.3. Resorcinarenes and deeper cavities

Resorcin[4]arene (**75c**) is a macrocycle with eight hydroxy groups at the upper rim, which form intramolecular H-bonds (Figure 80). Their interior is much smaller than that of cucurbituril. Resorcinarenes are versatile compounds for molecular

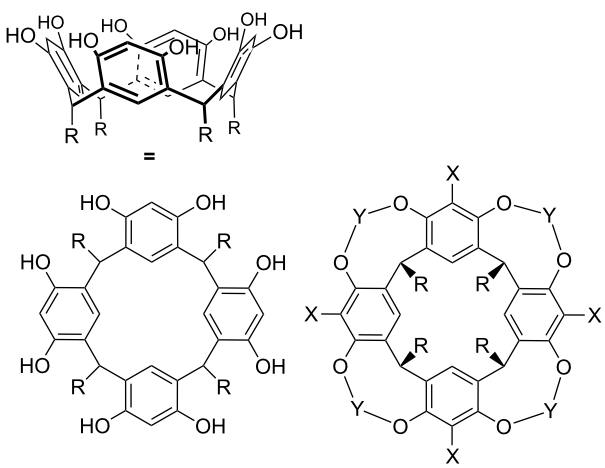

Figure 80: Resorcin[4]arene (**75c**) and the cavitands (**113**).

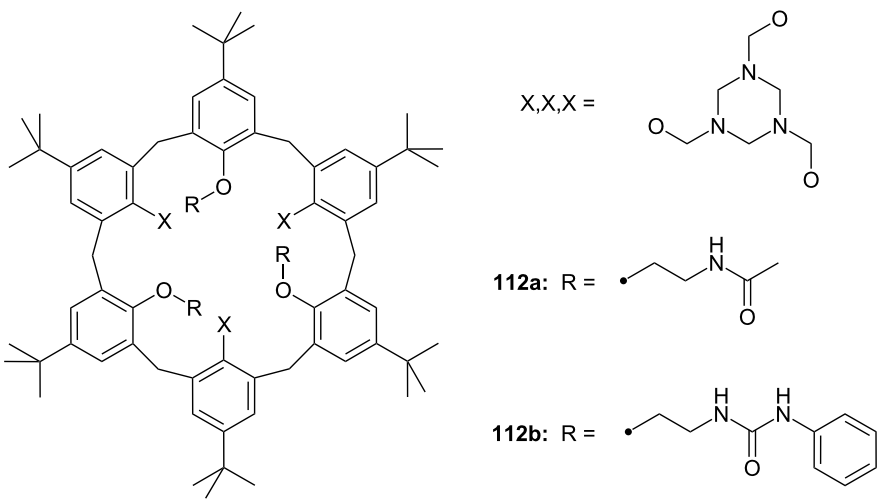

Figure 79: Further substituted calix[6]azacryptands **112**.

recognition [351-353] and like calixarenes, they include guest molecules in the bowl-shaped cavity (cation–π-interaction).

The monomeric resorcinarene (**75c**) and its simple derivatives show recognition properties, but their shallow curvatures cannot provide sufficient surface contacts for selecting between targets. Nevertheless, they bind ammonium ions, choline (**76**), acetylcholine (**3**), and carnitine (**77a**) in protic solvents [354-357]. Larger guests such as DABCO can also be included [358,359]. Significant interactions to the ammonium ion can also occur via hydrogen bonds to the phenolic OH-groups. In unsubstituted resorcinarenes, these are preferably formed intramolecularily involving two neighboring OH groups of the host. For example, in dilute aqueous sodium hydroxide solution (pH 12–13) the tetraanionic structure, in which one hydroxyl group per aromatic moiety is deprotonated and stabilized by a strong intramolecular hydrogen bond, can bind tetralkylammonium ions in the 10^4–10^5 M^{-1} range [360].

Similar to *p*-sulfonatocalix[*n*]arenes (**84**) tetrasulfonatomethylcalix[4]resorcinarene (Figure 81) forms complexes with amino acids in D_2O (pD 7.2, phosphate buffer) [361]. The K_{ass} values for these complexes, estimated from ^1H NMR experiments, decrease in the order Lys > Arg > Pro > Trp > Phe (with a maximum log K_{ass} of 3 for basic amino acids). No interactions with Asp, Asn, Thr, Leu, Met were observed.

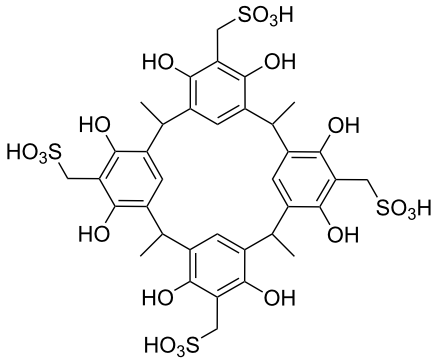

114

Figure 81: Tetrasulfonatomethylcalix[4]resorcinarene (**114**).

Only recently, the complexation properties of pyrogallo[4]arenes (**115c**) towards quaternary ammonium salts were compared with two resorcin[4]arenes (**115a**/**b**) [362] (Figure 82). The stability constants (*K*), standard free energy (ΔG_o), enthalpy (ΔH_o) and entropy changes (ΔS_o) for the complexation of pyrogallol[4]arenes with ammonium cations were determined in ethanol by isothermal titration calorimetry. The binding strengths were in the order of 10^3–10^4 M^{-1} and generally 2 to 7 fold higher compared to the corresponding simple resorcinarenes. In the best example, diethyldimethylammonium and triethylmethylammonium ions were included in **115c** with K_{ass} = 6900 M^{-1} and 7500 M^{-1}, respectively. The trends observed in the thermodynamic parameters for 1:1 and/or 1:2 host–guest complexations correspond to the systematic structural changes of the guest molecules. Molecular modeling calculations confirmed the results.

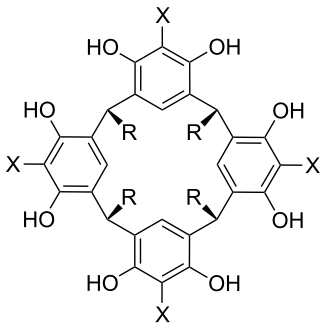

115a: X = H, R = $CH_2CH(CH_3)_2$
115b: X = CH_3, R = $CH_2CH(CH_3)_2$
115c: X = OH, R = $CH_2CH(CH_3)_2$

116: X = OH, R = $(CH_2)_{10}CH_3$

Figure 82: Resorcin[4]arenes (**115a/b**) and pyrogallo[4]arenes (**115c, 116**).

Similar pyrrogallol[4]arenes carrying long alkyl chains (**116**) were applied as amphiphilic receptors in an aqueous micelle system and their interaction with dopamine (**2**) and acetylcholine (**3**) studied by NMR methods [363].

The inclusion of acetylcholine (**3**) in resorcinarene (**75c**) via multiple cation–π-interactions was proved by crystallography [355]. Not surprisingly, resorcinarenes were also employed in a fluorescent displacement assay (Figure 83) for acetylcholine (**3**). Similar to Shinkai's study with *p*-sulfonatocalix[6]arene (**84b**), a tetracyanoresorcin[4]arene (**117**) in comparison to the parent compound **75c** (R = Et) was used as complex with indicator **85** [364]. The binding constants observed for acetylcholine (**3**) were 2 to 2.5 fold higher for the tetracyanoresorcin[4]arene (**117**). This was attributed to the larger contact area and a more suitable pK_a value of the resorcinarene in consequence to the strong electron withdrawing effect of the cyano groups. With increasing pH, acetylcholine (**3**) was bound more strongly by the receptors, with a K_{ass} of up to 10^6 in phosphate buffer at pH 8.

A mono-bridged resorcinarene host for acetylcholine (**3**) with tetramethoxy resorcinarene mono-crown-5 (**118**) was reported

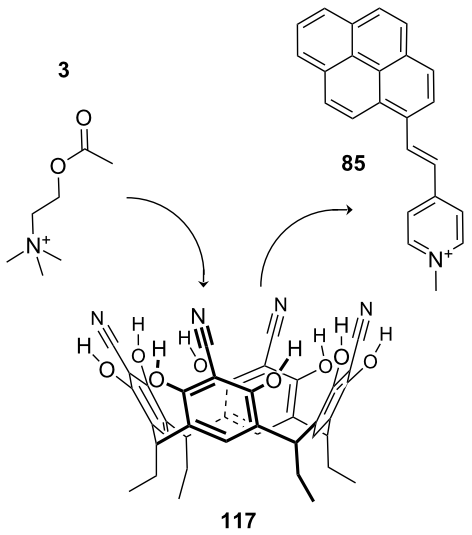

Figure 83: Displacement assay for acetylcholine (**3**) with tetracyanoresorcin[4]arene (**117**).

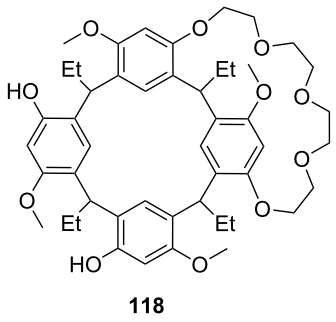

Figure 84: Tetramethoxy resorcinarene mono-crown-5 (**118**).

[365] (Figure 84). The dual nature of the cavity formed between the crown bridge at one end and the two hydroxyl groups at the other offers a better fit to acetylcholine (**3**) compared to the smaller tetramethylammonium cation. Acetylcholine (**3**) is able to interact with both the crown ether moiety and the free hydroxyl groups of receptor **118** simultaneously: the quaternary trimethylammonium group binds to the crown moiety through cation–O and cation–π-interactions, whereas hydrogen bonding interactions prevail between the acetate group and the hydroxyl part of the cavity. The binding of acetylcholine (**3**) to **118** was investigated by an ^{1}H NMR titration technique in $CDCl_3$ and showed 1:1 host–guest complex formation. The titration data indicated a stability constant of 150 M^{-1}, which is 10–10^3 orders smaller compared to the values found with acetylcholine complexes of resorcinarenes (**75c** and **117**), pyrogallolarenes (**115c** and **116**) or deep-cavitands (**126a/c**).

Following such a bridging approach, even deeper cavities (**113**) can be formed based on the structurally related resorcinarenes such as **75c** (Figure 80). By covalent bridging of the OH groups of two neighboring aromatic subunits by aromatic moieties, a resorcinarene can be made more rigid and the cavity formed can enclose guest molecules completely.

One way of achieving this is the use of phosphonate-cavitands [366]. Following a similar principle as in the acetylcholine (**3**) displacement assays (**84b** or **117** + **85**) mentioned above, Prodi et al. reported a suitable protocol for the reversible complexation of methylammonium and methylpyridinium salts with the phosphonate cavitand **119** [367] (Figure 85). The K_{ass} values measured for the *N*-methyl complexes exceeded 10^7 M^{-1} in dichloromethane. As displaceable guest they used compound **120**, consisting of a methylpyridinium unit as recognition moiety connected to a pyrene probe via a diester. In this molecule the cation–dipole interactions and CH_3–π-interactions

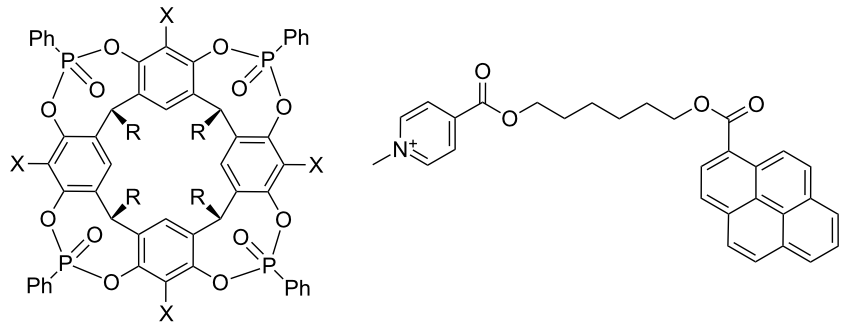

Figure 85: Components of a resorcinarene based displacement assay for ammonium ions.

of the acidic +N–CH_3 group with the π-basic cavity could be assisted in a synergistic manner by two simultaneous hydrogen bonds to the phosphonate groups. In the case of protonated secondary amines such as *N*-methyl-butylamine, a K_{ass} = 7.8 × 10^6 M^{-1} was determined for **119a**.

As a different approach of cavity deepening, Botta, Speranza and colleagues presented both enantiomers of the two chiral basket resorcin[4]arenes **121a** and **121b** rigidified and doublespanned with 1,2-diaminocyclohexane and 1,2-diphenylethylenediamine bridges, respectively, in a flattened cone conformation [368] (Figure 86). Binding constants were not reported, but in several ESI-experiments the proton bonded diastereomeric complexes with amino acid guests exhibited a pronounced selectivity towards the enantiomers of tyrosine methyl ester and amphetamine. An additional kinetic study on the base-induced displacement of the guest revealed that the *S*-Tyr-OMe and *R*-amphetamine enantiomer was displaced faster from the heterochiral complex than from the homochiral one.

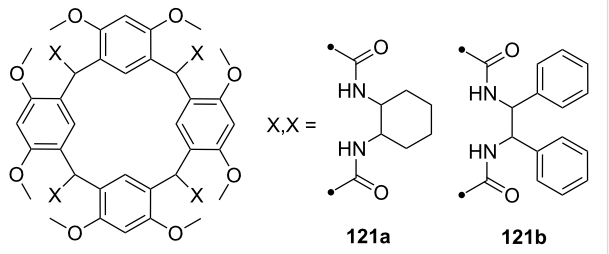

Figure 86: Chiral basket resorcin[4]arenas **121**.

Cavitands [369] and carcerands [370] are additional examples of resorcin[4]arene based supramolecular host systems. Ideally, a synthetic receptor should provide a congruent surface and chemical complementarity to the target molecule. Cavitands (**113**) with (hetero-) arene linker between the resorcin[*n*]arene oxygen atoms, thus adding three or four walls to the resorcinarene skeleton, form a larger and deeper cavity than the according alkyl or glycol chain bridged homologues [279,371-373]. This not only increases the cavitand's space but also increases the curvature. Non-functionalized resorcin[4]arenes are dominated by hydrogen bonding as driving force for complex formation and aggregation. For the latter cases, the resorcinol hydroxyl groups are functionalized and, therefore, π-interaction and electron donation become more important in their binding processes. Larger guests can be included, more surface capacitating cation–π-interaction is available and a stronger solvent shielding effect can be achieved. Thus, their binding properties and selectivities can be enhanced [374].

Two examples (Figure 87) of this were recently studied by Rebek et al. as a different concept for the molecular recognition of choline (**76**) and carnitine (**77a**). They enhanced the affinity and the selectivity by a better complementarity of size and shape instead of optimizing charge/charge attractions [374]. Specific cation–π attractions between the positive charge of the guest and the electron-rich aromatic surfaces of the host result in the formation of complexes with highly kinetic and thermodynamic stability. *R*-Carnitine (**77a**) is complexed with an association constant of 15000 ± 3000 M^{-1} reflecting the fact that its carboxyl and hydroxyl functions are well-positioned for hydrogen bonding to the amino groups at the rim of the host. Both choline hydrochloride (**76**) with 12000 ± 2400 M^{-1} and

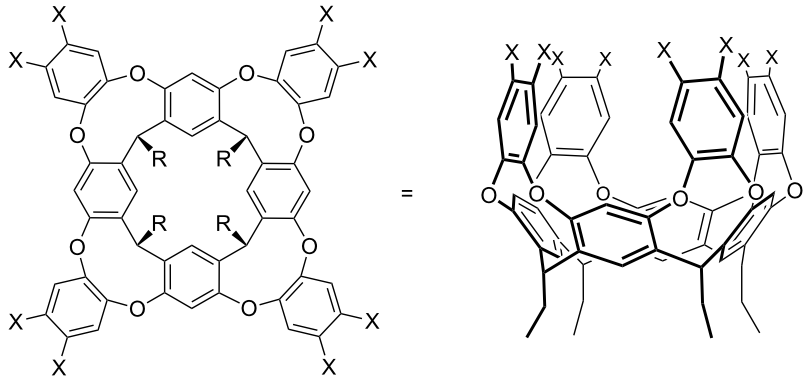

122a R = Et, X = NO_2
122b R = Et, X = NH_2
122c R = $C_{11}H_{23}$, X = NHC(O)Alk

Figure 87: Resorcinarenes with deeper cavitand structure (**122**).

also tetramethylammonium chloride in DMSO with 22000 ± 4000 M^{-1} are bound tightly by **119a**. The molecule can be seen as a further development of the calixarene tetrasulfonate of Shinkai et al., which also had a very good affinity for choline (**76**) in water (log K_{ass} = 4.7), but was less selective.

A comparable receptor molecule **123** (Figure 88) in a vase-like conformation was employed as supramolecular fluorescent sensor system for choline (**76**). The selectivity of the hybrid cavitand resorcin[4]arene receptor is explained by its enforced scoop-shaped cavity and multiple cation–π-interactions. Deprotonation in alkaline aqueous media afforded a negatively charged receptor which interacted more strongly by means of charge–charge attraction. NMR titration gave the stability constant of 0.1 × 10^2 M^{-1} for **123** in DMSO with the tetramethylammonium chloride complex. The tetraethylammonium chloride was bound with a similar affinity, whilst the larger tetrapropylammonium chloride showed a sharp decrease in affinity. Choline (**76**) chloride was bound in pure DMSO with a K_{ass} of 80 M^{-1}. In alkaline media (0.01 M KOH/DMSO) the stability constants for the complexes of tetramethylammonium-chloride and choline (**76**) hydrochloride were determined as 0.2 × 10^3 and 0.1 × 10^3 M^{-1}, respectively. In dipolar aprotic solvents such as DMSO, the ammonium salt is recognized as a close contact ion pair. Consequently, the chloride may also interact with the receptor [375]. In protic solvents, such as methanol, **123** is a neutral species capable of forming thermodynamically stable complexes exclusively by cation–π and CH–π-interactions with ammonium cations which are complementary in size and shape.

Rebek et al. reported a similar water-stabilized, deep cavitand (Figure 89) recognizing various amines and ammonium guests of different shapes. The absence of a fourth wall allows the binding of bulky ammonium groups [376]. In D_2O saturated chloroform, **124a** strongly includes 1-aminoadamantane (K_{ass} = 1 × 10^3 M^{-1}) and carnitine (**77a**, K_{ass} = 2 × 10^3 M^{-1}) as measured by NMR titration methodology. Choline (**76**, K_{ass} = 4 × 10^2 M^{-1}) and carnitine (**77a**), which are poorly soluble in water-saturated chloroform, were taken up forming 1:1 complexes, but acetylcholine (**3**) was not. Such guests with small hydrophobic regions are accommodated with the trimethylammonium group positioned deep inside the cavity. The hydroxyl and carboxylate functions can then provide

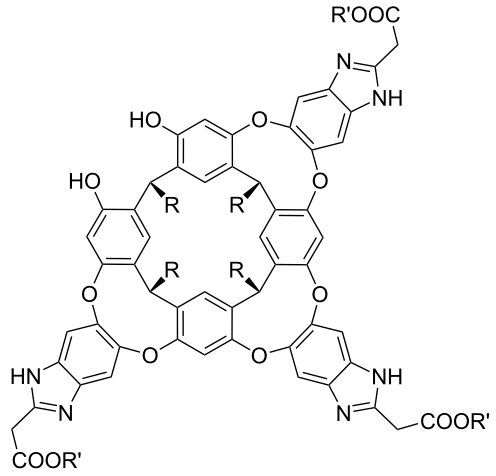

124a: R = $C_{10}H_{20}CH_3$, R´ = Et
124b: R = Et, R´ = Et
125: R = Et, R´ = Na

Figure 89: Water-stabilized deep cavitands with partially structure (**124**, **125**).

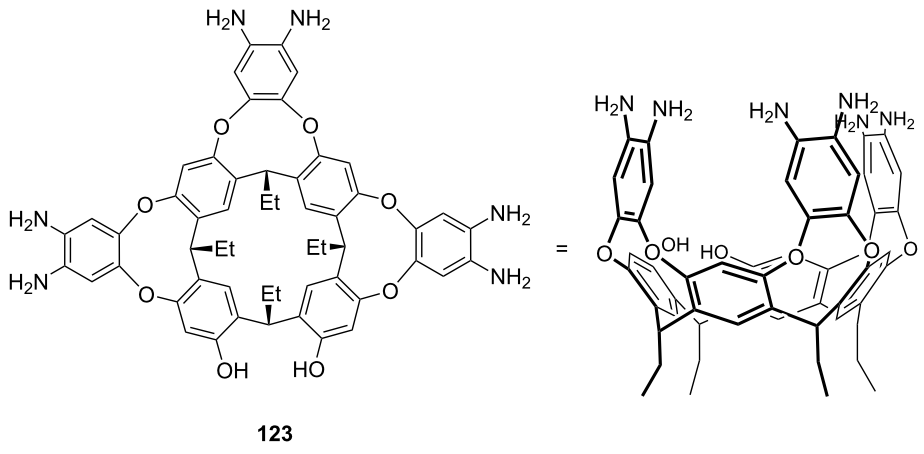

123

Figure 88: Resorcinarene with partially open deeper cavitand structure (**123**).

hydrogen bonding interactions with the groups at the rim. The ester group of acetylcholine (**3**) appears unable to reach such binding sites. Cavitand **125** exists as dimer or larger, kinetically unstable aggregates. With an excess of 1-adamantanol the aggregates break up and providing a sharp NMR-spectrum of a 1:1 complex. Other guests are not included or disassemble the aggregates.

Molecules of the cavitand family **126** (Figure 90) are all effective phase transfer catalysts which transport a hydrophobic guest, for example, an adamantyl residue from dichloromethane into water. If the reaction product is water soluble, it is easily released [377]. Compound **126a** forms stable 1:1 complexes with a variety of guests in water: (*S*)-nicotinium, chinuclidinium (both with $K_{ass} > 10^4$ M^{-1}), *R*-carnitine (**77**, 1.5×10^2 M^{-1}), choline (**76**, 2.6×10^4 M^{-1}) and acetylcholine (**3**, 1.5×10^4 M^{-1}) [378,379]. Compound **126b** shows a folded vase conformation in water and encloses cyclohexane and cycloheptane effectively ($K_{ass} > 10^4$ M^{-1}) [380]. Cavitand **126c** can distinguish between several substituted adamantyl residues [381].

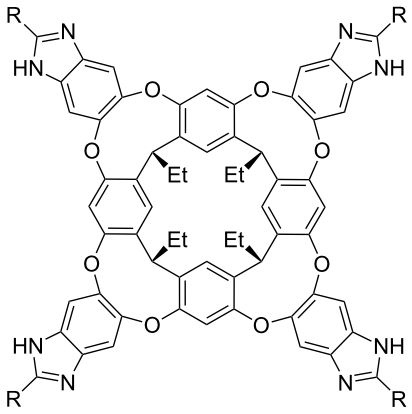

Figure 90: Charged cavitands **126** for tetralkylammonium ions.

Studies of **126c** with choline (**76**), acetylcholine (**3**) and carnithine (**77a**) were later extended. Binding mode and properties of these guest complexes were studied by NMR and calorimetry in water at pH 7.8 [382]. It was found, that **126c** preferably binds choline (**76**, 2.6×10^4 M^{-1}) over acetylcholine (**3**, 1.5×10^4 M^{-1}). The binding of carnithine is in comparison negligibly small (1.5×10^2 M^{-1}). The guest is inserted with its tetramethylammonium substituent deep in the cavity with the other end pointing to the carboxylic acid groups at the upper rim of the host.

3.4. Larger structures, capsules and ditopic binders

Enhancing the binding strength and the selectivity can also be achieved by adding more binding sites. Comparable to a hemicarcerand [85,383], two calixes can be connected by a suitable spacer to obtain a ditopic binder for ammonium ions (Figure 91). Using only one connection point makes the molecule sufficiently flexible to bind a bis-ammonium guest. Some recent examples of calixarenes following this concept have been published.

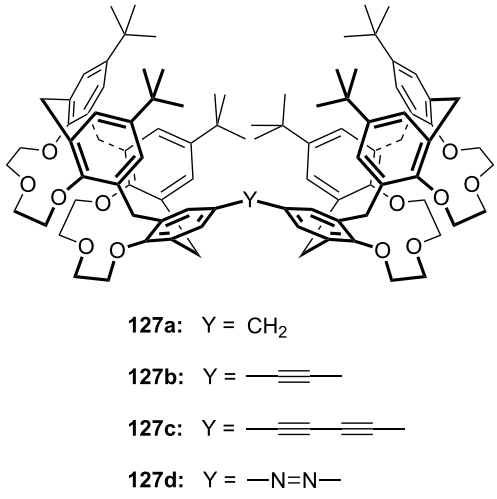

Figure 91: Ditopic calix[4]arene receptor **127** capped with glycol chains.

The binding abilities of a head-to-head linked bis-calix[4]arene-bis(crown-3) (**127**) fixed in the rigid cone conformation with bridges of different nature and length was described [384]. Tetraalkylammonium and *N*-methylpyridinium cations different in size and shape were investigated by ^{1}H NMR spectroscopy in $CDCl_3$ solution and in the more polar $CDCl_3/CD_3CN$ solvent mixture. As a result a substantial decrease in the K_{ass} values was observed: association constants were generally almost an order of magnitude lower for all guests, due to CD_3CN competing for the binding sites in the host. The double calixarenes have been found to exhibit efficiencies much higher than that of the corresponding reference cavitand calix[4]arene-bis(crown-3). The bridge present in these double calix[4]arenes dictated the orientation and distance between the two rigid caps and thus determine the efficiency and selectivity of binding. The two rigid caps could adapt in response to a potential guest and possibly co-operate in binding by forming a capsule.

Another ditopic receptor was described by the Parisis group [385]. It was developed for the binding of linear, long-chain α,ω-alkanediyldiammonium dichloride salts, combining the

co-operative action of two converging calix[5]arene cavities in the encapsulation of the dication with the ability of the two ureido functions (Figure 92) to bind the relevant counter anions. Binding properties as well as the host–guest architectures, were investigated by a combination of ^{1}H NMR spectroscopy in $(CDCl_2)_2/CD_3OD$ (2:1 v/v) and electrospray mass spectrometry (ESI-MS). Addition of the guest salts to a solution of **128** caused the formation of very strong inclusion complexes, whose host–guest stoichiometries (1:1 and/or 2:1) and geometries were dependent on the length of the diammonium ion and the [host]/[guest] ratio. The use of non-protic solvents showed a beneficial effect of the ureido functions by loosening the ion-paired salt and the association of the anion by formation of six-membered chelate rings with halide or picrate anions and eight-membered chelate rings with carboxylate anions. Table 7 shows the binding constants for long chain diammonium ions.

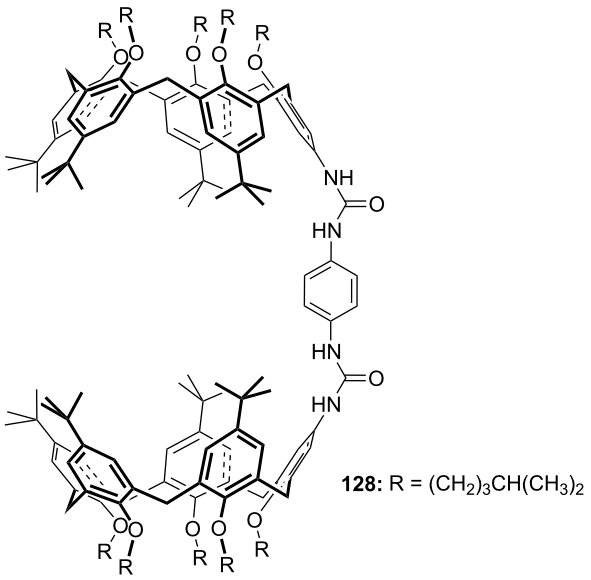

Figure 92: A calix[5]arene dimer for diammonium salt recognition.

Biological molecules often possess ionic moieties as well as functional groups capable of forming hydrogen bonding interactions within the same molecule. It is quite appealing to consider ditopic cavities as binding sites based on this principle. Even larger structures can be assembled by complementary recognition of receptor parts to each other [386] – a more specialized case of recognition involving self assembly [387].

In the following example the authors used the receptor structure **92c** and appropriate ammonium counterparts, for example **129a**, to form supramolecular assemblies [388] (Figure 93). From NMR titration, the stability constants K_{ass} of the assembly **92c** and **129a** was $(7.0 \pm 2.5) \times 10^5$ M^{-1} in methanol, whilst for **92c** with **129b** the K_{ass} was $(1.0 \pm 0.4) \times 10^4$ M^{-1} in methanol/water 4:1.

Table 7: Binding constants of different guests with the ditopic receptor **128**.

$H_3N^+(CH_2)_nNH_3^+ \times 2\ Cl^-$	K_{ass} [M^{-1}][a]
n = 8	212
n = 10	163
n = 12	2400
n = 16	2600

[a]NMR titration in $CDCl_3$/DMSO 3/2; 1:1 complexes; errors < 15%.

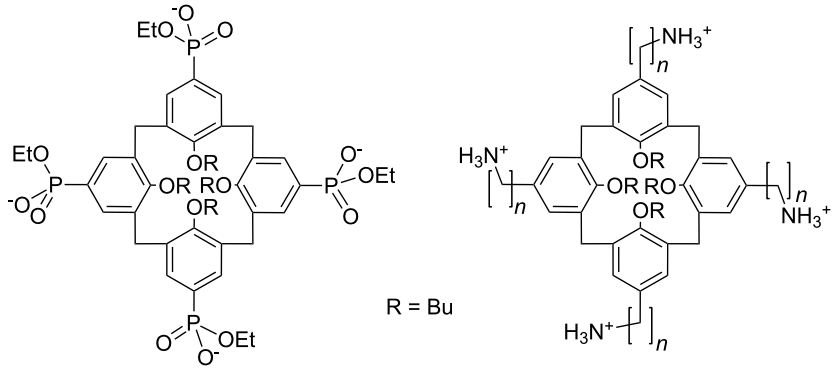

92c **129a:** n = 0 **129b:** n = 1

Figure 93: Calixarene parts **92c** and **129** for the formation molecular capsules.

Zadmard et al. studied these capsules formed in polar solvents by two cone calix[*n*]arenes in greater detail (*n* = 4 and 6). The first was substituted at the upper rim by phosphonic ethyl ester lithium salt groups (**92c** and its calix[6]arene analogue), while the second consisted of ammonium cations (**129a** and its calix[6]arene analogue) [389] (Figure 93). Inclusion of Phe, aniline, tetramethylammonium salts and other organic molecules into the capsule cavity in methanol was investigated [390]. Since the capsules were far more stable than the complex with the guest molecule, 10^5 vs. 10^3 M^{-1} in methanol-d_4, the authors concluded that a guest molecule was included inside the anionic half-sphere after opening the capsule.

Resorcinarene can also form dimers by a self assembling process, in which the cavity is filled [391]. For instance, the tetramethylammonium cation can be included (Figure 94). This was nicely evidenced by mass spectroscopy and by examining several crystal structures of smaller tetraalkylammonium cations with unsubstituted resorcinarenes such as **75c** with different alkyl chain lengths. Competitive mass spectrometric studies clearly indicated the preference for the tetramethylammonium cation over the tetraethylammonium cation and especially, the tetrabutylammonium cation. The two resorcinarene units are held together mediated by hydrogen-bonded networks via solvent molecules of methanol and water [392].

A tetralkylammonium ion (R = propyl to hexyl), together with one to three chloroform molecules can also be complexed and included in a capsule surrounded by six resorcinarenes stabilized by H-bonds [393].

Expanding the studies, Cohen et al. demonstrated a pH dependent inclusion of quaternary ammonium salts in a hexameric structure such as **130** (Figure 95) in $CDCl_3$ by NMR studies [394].

These selected, recent examples give an impression of the possibilities for ammonium recognition with calixarenes and resorcinarenes utilizing self assembly. A discussion of all options possible is beyond the scope of this review. The reader is referred to the appropriate literature [395-397]. Larger capsules for the inclusion of a variety of guests were recently described by the Rebek group [398].

The advantages of calixarenes as hosts for ammonium ion binding in comparison with other synthetic macrocycles is obvious: good accessibility, the possibility of tuning shape and size of the inner cavity and the introduction of various functional groups to address nearly any ammonium ion guest selectivity. Calixarenes are often used for the synthesis of more complicated and elaborated structures, to enclose or strongly complex larger guests with high selectivities and outstanding binding strengths.

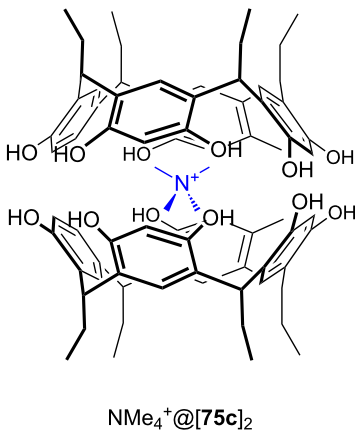

NMe_4^+@[**75c**]$_2$

Figure 94: Encapsulation of a quaternary ammonium cation by two resorcin[4]arene molecules (NMe_4^+@[**75c**]$_2$ × Cl^- × 6MeOH × H_2O; for clarity, solvent molecules and counterions have been omitted).

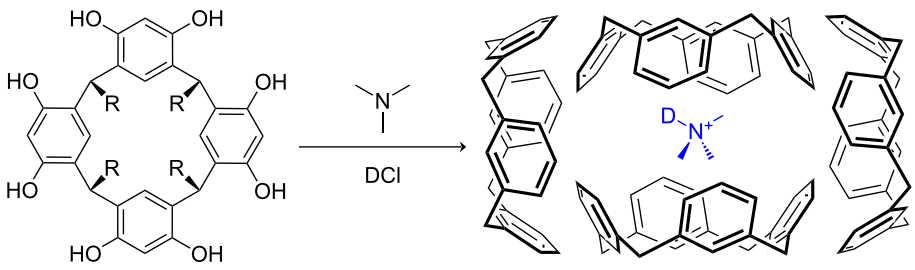

130: R = $(CH_2)_{10}CH_3$

Figure 95: Encapsulation of a quaternary ammonium cation by six resorcin[4]arene molecules (NMe_3D^+@[**130**]$_6$ × Cl^-; solvent molecules, substituents and counterions are omitted for clarity; the last two resorcinarene calixes are arranged behind and in front of the scheme's plane).

Calixarenes often achieve selectivities in cation binding which are superior to crown ethers due to the guest inclusion being controlled by steric factors and various interactive forces of host and guest. Some calixarene-based artificial receptors show remarkable selectivities for amine isomer recognition. Especially noteworthy is their ability to complex strongly with quaternary ammonium ions, which outperforms nearly every other receptor class, except the cucurbiturils (see "4. Cucurbiturils and related structures"). This was applied in assays for such important biomolecules as acetylcholine (**3**).

A considerable number of synthetic receptors based on a calixarene framework for amino acids derivatives has been designed and studied in organic media, but only a few examples have been reported in aqueous solution. Calixarenes are able to select precisely basic or aromatic amino acids in aqueous solution. Because of this property, they can be applied even as enzyme mimetics.

4. Cucurbiturils and related structures

Behrend's polymer was reported over a century ago as a by-product of aminal type polymers [399] however, the structure of the material was only fully characterized in 1981. Because of the resemblance of the barrel-shaped molecule to a pumpkin, the investigators gave the macrocyclic methylene-bridged glyconuril oligomers the name cucurbiturils, derived from the Latin name of the plant family (cucurbitacae). All have a hydrophobic cavity and two identical carbonyl-laced portals ("occuli") in common and are readily prepared by the condensation of glyconuril with formaldehyde.

Cucurbit[6]uril (CB[6], **131**), a macrocycle comprising six glycoluril units connected by 12 methylene bridges (Figure 96), is the oldest and most frequenly encountered member of the host family cucurbit[*n*]uril (CB[*n*], *n* = 5–11) [400-404].

Crystalline complexes incorporating various metal salts and some dyes were observed and consequently cucurbiturils were investigated as receptors by Mock and Shih [405]. Alkylammonium ions were the first organic guests to be reported for CB[6] (**131a**) [406]. Mock [407], Buschmann and co-workers [408,409], and Kim et al. [410] further investigated the molecular-recognition properties. Cucurbiturils bind their guests by hydrogen-bonding or ion-dipole interactions in combination with the hydrophobic effect of the cavity. The rigidity of the structure enables selective recognition of hydrophobic residues or cations. The selectivity strongly depends on the inner size of the cavity and possible guest orientations therein, as in cyclodextrins and calixarenes: *para*-methylbenzylamine is bound, while the *ortho*- and *meta*-isomers are not [411]. Isaacs et al. published a crystal structure of the cucurbit[6]uril *p*-xylylenediammonium inclusion complex. The ammonium cations are symmetrically located in the centre of a ring formed by the carbonyl oxygens. The benzene ring is rotationally disordered in the cavity between two orientations [412].

The upper and the lower regions of the cucurbituril – the occuli – bear at least six urea carbonyl groups, representing an area of negative charge accumulation, co-ordinating to cationic species such as alkanediamines. The high specificity for ammonium ions is explained mainly by this electrostatic ion-dipole attraction assisted by hydrogen bonding. Proper alignment of the bound ammonium ions with the host carbonyl dipoles is critical: In the homologous series of *n*-alkane amines a clear trend in stability of the complexes was observed, reaching the maximum for *n*-butylamine: *n* = 1 < 2 < 3 < 4 > 5 > 6 > 7. α,ω-Alkane-

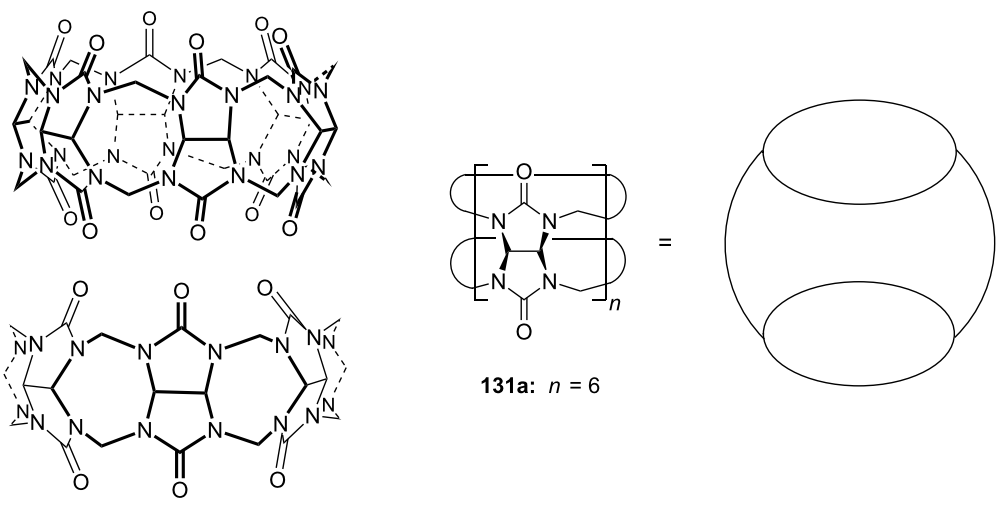

Figure 96: Structure and schematic of cucurbit[6]uril (CB[6], **131a**).

diammonium ions (H_3N^+–$(CH_2)_n$–NH_3^+) are bound by CB[6] (**131a**) with a preference for an alkyl chain length of n = 5 or 6. Substituents fitting the size of the cavity are bound with the highest strength and affinity; longer chains protrude into the second oculus of the cucurbituril, interfering with the carbonyl dipoles and their solvation sphere [413,414].

In contrast to the moderate to good water soluble related host molecules with a comparable cavity size, the cyclodextrins (**136**) [55,223,415,416], the poor solubility of CB[6] (**131a**) in common solvents and water makes it difficult to study its host–guest chemistry in solution.

During the 1990s it was discovered that CB[6] is readily soluble in aqueous solutions containing alkali or alkaline earth metal ions. Since then, such aqueous solutions have often been employed for studies on complexation properties of CB[6] (**131a**) [417,418]. Mock and Shih examined its binding affinity towards a variety of aliphatic ammonium ions in 50% (v/v) aqueous formic acid and determined binding constants (K) of around 10^3–10^4 M^{-1} for n-alkylammonium ions and 10^4–10^5 M^{-1} for α,ω-alkanediammonium ions from NMR and/or UV spectroscopy measurements [413]. Typical binding constants for ammonium guests, e.g. simple amines, diamines and aromatic amines range from 10^1 to 10^7 M^{-1} in H_2O/HCOOH mixture [419]. In aqueous salt solutions, for example, 50 mM sodium chloride solution, even higher values for α,ω-alkanediammonium ions (up to 1.5×10^9 M^{-1} for H_3N^+–$(CH_2)_5$–NH_3^+, cadaverin) have been reported [420].

Not only simple amines, but also many amino acids and amino alcohols have been employed as guests. Buschmann and co-workers first studied the complex formation between cucurbituril and some aliphatic amino acids by means of calorimetric titrations in aqueous formic acid (50% v/v) or aqueous solution for comparison of the interaction of cucurbituril with some aliphatic amino alcohols and aliphatic amino compounds: The complex formation of amino acids was found to be favored by enthalpic and entropic contributions. The situation changes completely in the case of amino alcohols. Reaction enthalpies and entropies are influenced by the number of methylene groups: 3-aminopropanol formed the most stable complex. With an increasing number of methylene groups the stability of the complexes decreased, which is attributed to entropic factors [421].

Paraquat and its derivatives are typical guests for cucurbit[n]urils [422-427]. Amino azabenzenes are bound with binding strengths in the range of 10^3–10^6 M^{-1} [428]. Many homologues from cucurbit[5]uril to cucurbit[10]uril, as well as derivatives, congeners and analogues are available, even exceeding the cavity size span of the cyclodextrin family. Their chemistry has been discussed in several books [429-431] and reviews [420,432-436]. In the following part, some recent examples of the molecular recognition of ammonium ions will be discussed.

Various cucurbit[n]uril derivatives have been synthesized by introducing alkyl groups at the equator of the molecules to improve their solubility in water and other commonly used organic solvents [437-440]. Different reactive functional groups have been introduced directly onto the surface of the cucurbit[n]urils to improve their solubility, and for further modification [411,441,442].

Such a water soluble example was reported with cyclohexanocucurbit[6]uril (CB × [6], **132**) (Figure 97). Complexation properties with various organic mono- and diammonium ions were studied by isothermal titration calorimetry and ^{1}H NMR spectroscopy [443]. X-ray crystal structures of α,ω-alkanediammonium ions (H_3N^+–$(CH_2)_n$–NH_3^+, n = 4–8) and spermine (**133**) complexes with **132** revealed that the aliphatic chains of the guest molecules were in an extended or partially bent conformation in the cavity, depending on their length. The hexamethylene chain conformation is twisted to allow strong ion–dipole interactions between both ammonium groups and the carbonyl groups at the portals. This increases the hydrophobic interactions between the alkyl part of the guest and the inner wall of the host, which results in the largest enthalpic gain and a preference for this guest among all α,ω-alkanediammonium

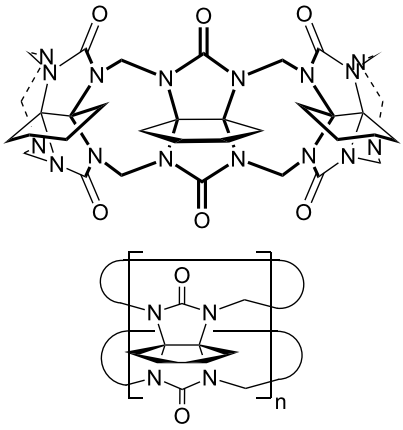

132: n = 6

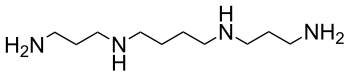

133

Figure 97: Cyclohexanocucurbit[6]uril (CB′[6], **132**) and the guest molecule spermine (**133**).

ions. The selectivities match with those of **131a.** The cavity dimensions are essentially the same as in CB[6] (**131a**). The binding affinities of CB′[6] (**132**) towards *n*-alkylammonium ions (10^4–10^8 M^{-1}) and α,ω-alkanediammonium ions (10^7–10^{10} M^{-1}) in water are 3–5 and 2–3 orders of magnitude higher than those of CB[6] in 50% formic acid [407,416,417] and in 0.05 m NaCl solution [420], respectively. This was attributed mainly to the larger enthalpic gain upon complex formation in the absence of interfering ions, such as protons and Na^+. In particular, the binding constant of spermine to CB × [6] was found to be 3.4×10^{12} M^{-1}, which is the highest binding constant ever reported for CB[6] or its derivatives.

Cucurbit[*n*]urils strongly bind amino acids. A crystal structure of the inclusion complex of *S*-glutamate (*S*-Glu) in α,α,δ,δ-tetramethylcucurbit[6]uril (**134**) (Figure 98), captured by a host in a 1:1 host:guest ratio, gives more insight [444]. The protonated amino moiety is located at the portal of the host whilst the side chain carboxyl anion moiety is included in the cavity of **134**. A combination of hydrogen bonding and ion–dipole interactions of the ammonium group and the portal carbonyls of the host were seen as the driving force for the complex formation. In addition, the carboxyl moiety of the amino acid located at the portal of the host could interact with the portal carbonyl of the host through hydrogen bonding.

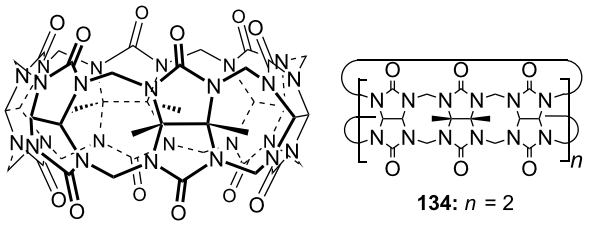

Figure 98: α,α,δ,δ-Tetramethylcucurbit[6]uril (**134**).

Unsubstituted cucurbiturils are not fluorescent. Issacs and co-workers described the incorporation of a fluorescent (bis)-phthalhydrazide in cucurbit[6]uril (Figure 99), which made the system accessible to monitoring by fluorescence spectroscopy [442]. This analogue (**135**) shows good molecular recognition properties for a variety of guests in aqueous sodium acetate buffer at pH 4.74: Association constants for α,ω-alkanediammonium ions (H_3N^+–$(CH_2)_n$–NH_3^+, n = 6 to 12) increase with the length of the alkane chain. The maximum binding strength was observed for n = 10 and 11 with 2.3×10^4 M^{-1}. Aromatic ammonium targets were complexed even stronger due to the additional π–π-interactions. The best examples were benzidine with an association constant of 4.6×10^6 M^{-1}, nile red [445] with 8.2×10^6 M^{-1} and the similar dye nile blue chloride with 1.1×10^6 M^{-1}. The authors argue, that increasing the surface area for π–π-interactions by increasing the size of the π-system of the guest as well as increasing the co-planarity of the guest molecule significantly increases the association constant. Biologically relevant guests such as amino acids and nucleobases were bound in the cavity of **135** with K_{ass} values ranging from 10^3 to 10^6 M^{-1}. Similarly, good affinities to aromatic amino acids as a result of π–π-stacking and ion-dipole interactions were observed: For *S*-phenylalanine (**81a**), *S*-tyrosine and *S*-tryptophan (**81b**) association constants of 4.2×10^4, 5.7×10^4 and 3.2×10^6 M^{-1}, respectively were determined. Due to the larger size of the indole ring compared to that of the monocyclic systems, tryptophan (**81b**) was bound more tightly.

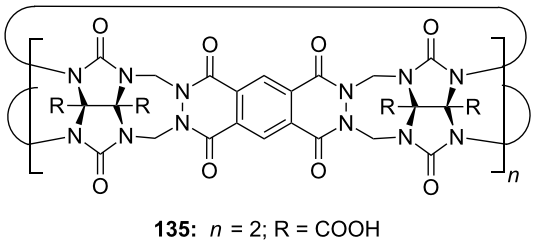

Figure 99: Structure of the cucurbituril-phthalhydrazide analogue **135**.

A dual-response colorimetric sensor array based on supramolecular host–guest complexation in cyclodextrins (α-, β- and γ-cyclodextrin, **136**) and cucurbit[*n*]urils (CB, n = 5–8, **131**) was used for the identification of amines in water [446] (Figure 100). The displacement of colored or fluorescent dyes such as methylene blue (**137a**), pyronine (**137b**) and acridine orange (**137c**) led to discrimination among primary, secondary, tertiary, aliphatic, aromatic, linear and branched amines by color change or by the increase in fluorescence. The combination of the images obtained from visible and UV light identified each of the 14 analytes investigated. The selectivity of the sensor array is based on the analyte's interaction with the host–guest complex, which involves the combination of a large number of parameters, including hydrophilicity–hydrophobicity, coulombic effects, dipolar interactions and hydrogen bonding.

Nau and co-workers introduced a general supramolecular assay principle in which amino acid decarboxylase activity can be continuously monitored by measuring changes in fluorescence, which results from the competition of the enzymatic product and the dye for forming a complex with a cucurbit[*n*]uril macrocycle [447].

The combination of cucurbit[6]uril (**131a**) and the 3-amino-9-ethylcarbazole dye **138a** leads to a suitable displacement assay

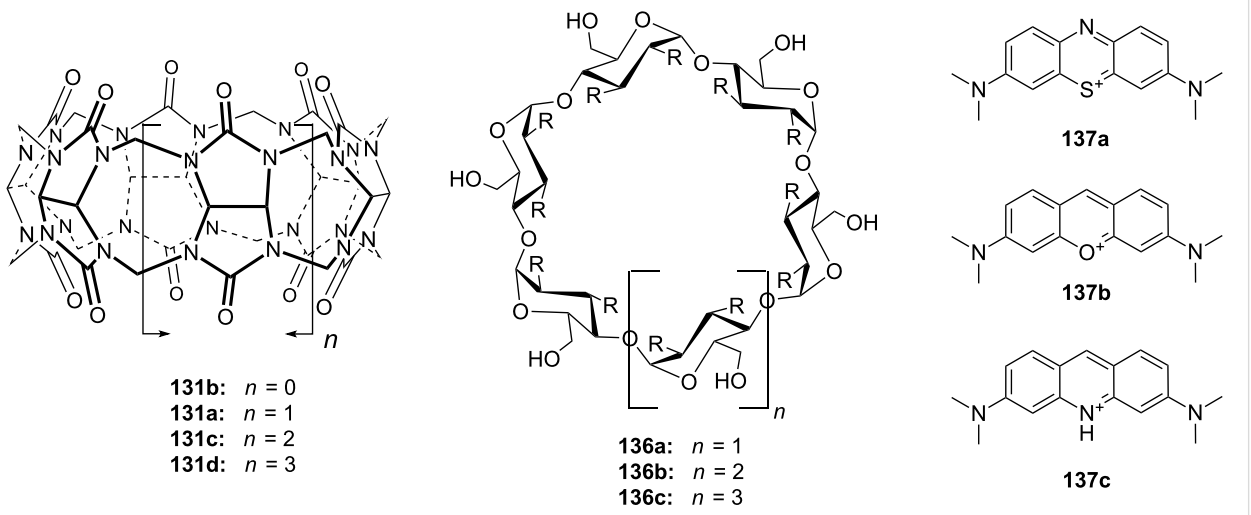

Figure 100: Organic cavities for the displacement assay for amine differentiation.

(Figure 101) for monitoring the enzymatic activity of lysine decarboxylase in aqueous buffer at pH 7 [448]. Due to a complexation-induced pK_a shift, a large dual fluorescence response (100-fold increase at 375 nm and 9-fold decrease at 458 nm) accompanied by a color change upon supramolecular encapsulation in cucurbit[6]uril (**131a**) is observed. The enzymatic decarboxylation of lysine (**81c**) converts the amino acid *S*-lysine (**81c**) into cadaverine (**139a**), which competes very efficiently (K_{ass} = 9.5 × 10^9 M^{-1} in 10 mM NH_4OAc buffer) and so fully reverts the fluorescence changes originally caused by the addition of the macrocycle. The binding constant of the substrate lysine (**81c**) is too low to displace the more strongly bound fluorescent dye (K_{ass} = 2.22 × 10^7 M^{-1}) and causes no effect.

This principle was employed in a similar manner with cucurbit[7]uril (**131c**) and the fluorescent dye Dapoxyl (**138b**) (Figure 101). It forms a strong inclusion complex with **131c** (K_{ass} = (2.0 ± 0.2) × 10^4 M^{-1}) in ammonium acetate buffer at pH 6, which shows up to 200 times higher emission intensity (λ_{em} = 380 nm) than the free dye [449]. Addition of amino acids has little effect on the fluorescence intensity of the CB7-Dapoxyl reporter pair. Addition of low-micromolar concentrations of amines lead to a steep decrease in fluorescence as a result of competitive binding. This allows real-time monitoring of enzymatic activity by a switch-off fluorescence response in 10 mM NH_4OAc buffer at pH 6.0.

As demonstrated by simple titration experiments, the substrates lysine (**81c**), arginine (**81d**), histidine (**81e**) and ornithine have low affinity to **131c**, and cannot interfere with the formation of the strongly fluorescent complex (K_{ass} < 10^3 M^{-1}). Decarboxylation produces the corresponding amines cadaverine (**139a**), agmatine (**139c**), histamine (**1**) or putrescine (**139b**), so increases the net positive charge and thereby the affinity of the competitor by removal of the carboxylate group. These guests exist in their ammonium ion forms near neutral pH and thus have a very high affinity for **131c** (K_{ass} < 4.3 × 10^4 M^{-1}). This tandem assay principle has millimolar sensitivity.

The versatile approach was extended to aromatic guests and applied for enantiodiscrimination, respectively resolution [450]. Similar observations were published: The amino acids histidine (**81e**), tyrosine and tryptophan (**81b**) bind to the reporter pair **131c**/**138b** with approx. 1000 M^{-1}, the diamines in contrast with 10^4 to 10^6 M^{-1} affinity in 10 mM NH_4OAc buffer solutions (pH 6.0) and, therefore, displace the dye from the complex.

Time-dependent fluorescence response monitoring of *S*-lysine decarboxylation with varying *S*-lysine enantiomeric excess allowed accurate determination of optical purity of the amino acid over a wide range of *ee* (64–99.98%) by different kinetic fluorescence decay traces with a 2.4 nmol limiting sensitivity. Only the *S*-enantiomer is accepted by the enzyme as a substrate and is converted to the product that is responsible for the observed fluorescence signal. No response and no conversion by the enzyme are observed with the *R*-enantiomer.

Recently, Isaacs et al. demonstrated the chiral recognition of some amino acids inside a novel chiral cucurbituril: nor-seco-cucurbituril (±)-bis-ns-CB[6] (**140**, Figure 102), which demonstrates enantio- and diastereoselective recognition inside its cavity [451].

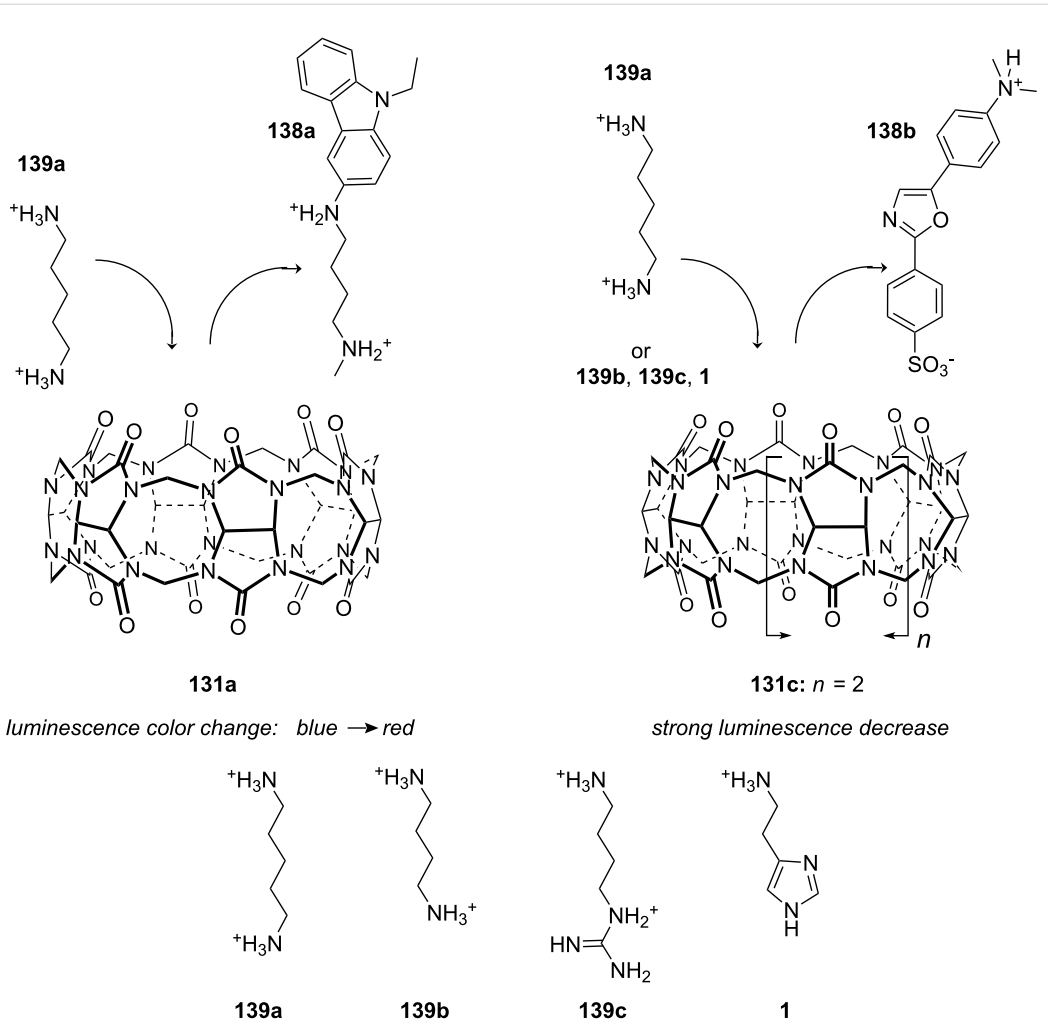

Figure 101: Displacement assay methodology for diammonium- and related guests involving cucurbiturils and some guests.

The K_{ass} values for **140** towards diammonium guests were measured by UV–vis spectroscopic titration and ^{1}H NMR spectroscopy competition experiments in water with association values mainly in the range of 10^3 to 10^4 M^{-1}. The affinity of (±)-bis-ns-CB[6] toward 1,6-diaminohexane in its protonated form was even higher (1.3×10^5 M^{-1}). Conversely, this affinity is 3400-fold lower than found with CB[6] (**131a**), which presumably arises from differences in the strength of ion–dipole interactions, the degree of aqueous solvation of the C=O portals, or both.

Host **140** undergoes diastereoselective complexation (up to 88:12) with chiral amines including amino acids and amino alcohols as well as with meso-diamine **141e**. In the ^{1}H NMR spectra recorded for a mixture of (±)-bis-ns-CB[6] and excess of the guest (−)-**78b**, a 72:28 ratio of the diastereomer was found. Toward amino acids **81f** (77:23) and **81a** (88:12) and amino alcohol **81g** (76:24) minimal higher values were observed. Interestingly, (±)-bis-ns-CB[6] is even able to distinguish between the enantiotopic groups of meso-compound **78c** (74:26).

A combination of achiral host cucurbiturils and chiral inductor can also serve as a supramolecular chiral host (Figure 103). A chiral guest added to the solution of cucurbit[6]uril-based complexes with enantiopure amines can replace one of the originally bound amines achieving an enantiodifferentiation by accommodating two different chiral guests inside a self assembled achiral capsule. In this way significant enantiomeric and diastereomeric discrimination by incorporating a strong chiral binder is possible [452]. Comprehensive studies on the chiral recognition of guests were performed: Dissolving cucurbit[6]uril (CB[6]) in an aqueous solution of an enantiopure organic amine, such as (*R*)- or (*S*)-2-methylpiperazine (MP) or (*R*,*R*)- or (*S*,*S*)-*trans*-1,2-diaminocyclohexane (DC), led to the formation of the respective enantiopure complex, i.e.,

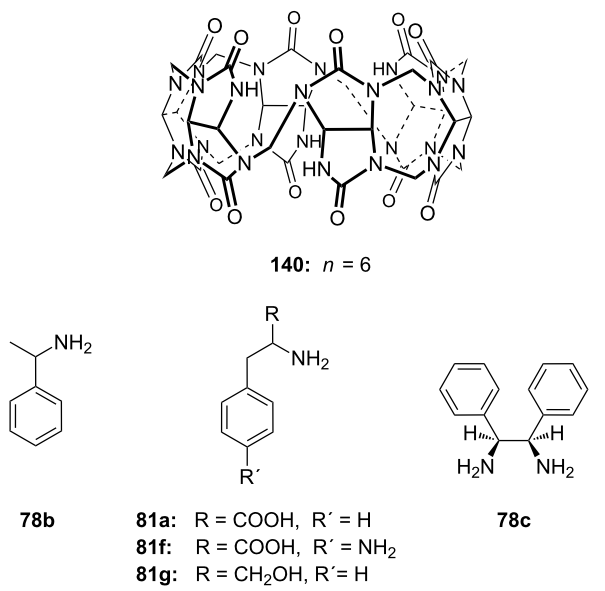

Figure 102: Nor-seco-Cucurbituril (±)-bis-ns-CB[6] (**140**) and guest molecules.

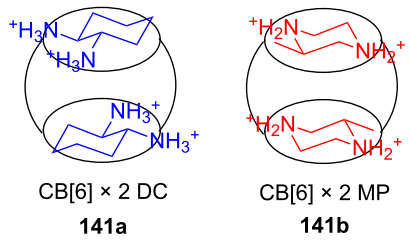

Figure 103: The cucurbit[6]uril based complexes **141** for chiral discrimination.

(*R*;*R*)- or (*S*;*S*)-[CB-[6] × 2MP]$^{4+}$ (**141b**) or (*R*,*R*;*R*,*R*)- or (*S*,*S*;*S*,*S*)-[CB[6] × 2DC]$^{4+}$ (**141a**). (*S*)-2-Methylbutylamine could be discriminated by these assemblies with up to 95% *ee* by formation of diastereomeric (*S*;*R*)- and (*S*;*S*)-[CB[6] × MP × MB]$^{3+}$ ternary complexes. (*S*)-MB controls the degree of chiral supramolecular assembling of (*R*)-MP or (*S*)-MP with cucurbit[6]uril:

[CB[6] × 2((*R*)-MP)]$^{4+}$ + (*S*)-MB^{+} → [CB[6] × (*R*)-MP × ((*S*)-MB)]$^{3+}$ + (*R*)-MP^{2+}

with a K_{ass} of 15000 ± 3000 M^{-1} for this process

[CB[6] × 2((*S*)-MP)]$^{4+}$ + (*S*)-MB^{+} → [CB[6] × (*S*)-MP × ((*S*)-MB)]$^{3+}$ + (*S*)-MP^{2+}

with a K_{ass} of 800 ± 100 M^{-1} for this process.

The authors also found cucurbit[7]uril (**131c**) binding the diastereomeric dipeptide *S*-Phe-*S*-Leu-NH_3^+ up to eight times tighter than *S*-Phe-*R*-Leu-NH_3^+ with its larger cavity. The discrimination of dipeptides was not possible with the previously discussed system.

The cavity size of cucurbit[7]uril enables the molecule to bind ferrocenyl and adamantyl substituted amines strongly as 1:1 complexes: Rimantadin, an amino adamantyl derivative, which is used as an anti-viral drug, is included in aqueous buffer at pD 4.74 with an association constant of around 4.2 × 10^{12} M^{-1} [453].

The molecular host cucurbit[7]uril (**131c**) forms an extremely stable inclusion complex with the dicationic ferrocene derivative bis(trimethylammoniumethyl)ferrocene (**142c**) in aqueous solution [454] (Figure 104). The equilibrium association constant for this host–guest pair is 3 × 10^{15} M^{-1}, equivalent to that exhibited by the avidin–biotin pair.

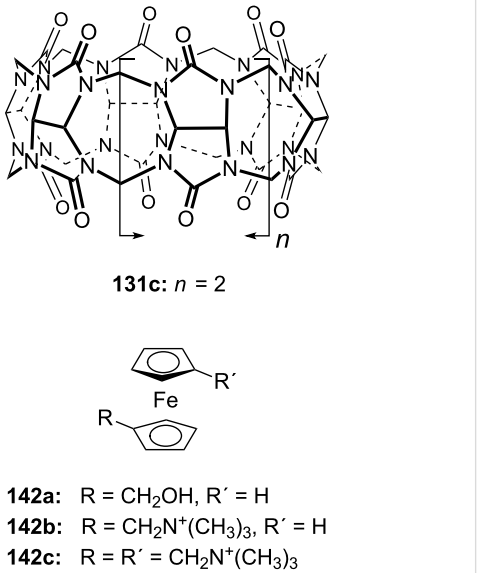

Figure 104: Cucurbit[7]uril (**131c**) and its ferrocene guests (**142**) opposed.

The large association strength has been determined from serial competitive ITC binding studies (Table 8). Two different series, also giving K_{ass} values for other interesting ammonium guests, were pursued. All amines were protonated under the conditions of the study.

The values for **142a** and **142b** are (3.2 ± 0.5) × 10^9 M^{-1} and (4.1 ± 1.0) × 10^{12} M^{-1}, respectively. A significant loss in the complex stability by a factor of 1400 in the K_{ass} value is observed upon oxidation of the ferrocene centre of **142c**,

Table 8: Two series of binding constants for different guests to CB[7] (**131c**).

Guest	Competitor	K_{ass}/M^{-1}
S-Phe (**81a**)	none	$(1.8 \pm 0.2) \times 10^6$
1,6-hexanediamine	*S*-Phe (**81a**)	$(2.1 \pm 0.4) \times 10^9$
aminocyclohexane	1,6-hexanediamine	$(1.3 \pm 0.4) \times 10^{11}$
142c	aminocyclohexane	$(3.0 \pm 1.0) \times 10^{15}$
cyclopentanone	none	$(4.2 \pm 0.3) \times 10^5$
spermine (**133**)	cyclopentanone	$(4.8 \pm 0.6) \times 10^8$
N,N′-bis(aminoethyl)-1,6-hexanediamine	spermine (**133**)	$(1.7 \pm 0.4) \times 10^{11}$
142c	*N,N*′-bis(aminoethyl)-1,6-hexanediamine	$(3.3 \pm 1.0) \times 10^{15}$

enabling a switching process of complexation/decomplexation dependent on the competitor.

The extremely large affinities of the complexes surveyed are due to a large enthalpic gain, originating from the tight fit of the ferrocene core to the rigid CB[7] cavity achieving optimal van der Waals contacts, critically assisted by the entropic gain arising from the extensive host desolvation, and largely uncompensated by losses in configurational entropy. The crystal structure of the complex shows the complete inclusion of the ferrocenyl residue in the CB[7] cavity and the almost ideal positioning of each of the trimethylammonium groups maximizing ion–dipole interactions with the carbonyl rims on each of the host portals. The ferrocene core of the guest fills 55% of the host cavity volume, approximately equal to the optimal filling fraction proposed [455].

Quaternary cations such as NMe_4^+, NEt_4^+, PMe_4^+, and PEt_4^+ are encapsulated within the cavity of CB[7] (**131c**) (Figure 104), with $K_{ass} = (1.2 \pm 0.4) \times 10^5$, $(1.0 \pm 0.2) \times 10^6$, $(2.2 \pm 0.4) \times 10^6$, and $(1.3 \pm 0.3) \times 10^5$ M^{-1}, respectively [456].

Consistent with these values, acetylcholine (**3**) and other cationic cholines ($R_3NCH_2CH_2OR'^+$), their phosphonium analogues ($R_3PCH_2CH_2OR'^+$) (R_3 = Me_3, Et_3, or Me_2Bz, or R_3N = quinuclidinium, and R′ = H, $COCH_3$, $CO(CH_2)_2CH_3$, or PO_3H) and (±)-carnithine (**77a**) form stable 1:1 host–guest complexes with cucurbit[7]uril (**131c**) in aqueous solution (K_{ass} in the order of magnitude 10^5–10^6 M^{-1}) [457]. The complexation behavior has been investigated using ^1H and ^{31}P NMR spectroscopy and ESI mass spectrometry. This study is one rare example, where molecular recognition of cholines in aqueous solution is achieved with a neutral host without aromatic walls for cation–π-interactions. The acetyl-substituent is included in the cavity and the quaternary ammonium ion is co-ordinated by the carbonyl functions of **131c**. In the case of phosphonium groups, these substituents are generally included in the cavity additionally stabilized by van der Waals contacts. The acetyl substituent sits on the outside of the cavity (Figure 105).

The cucurbit[7]uril (**131c**) host molecule forms also very stable host–guest complexes with the local anaesthetics procaine (**144a**, $K_{ass} = (3.5 \pm 0.7) \times 10^4$ dm^3 mol^{-1}), tetracaine (**144b**,

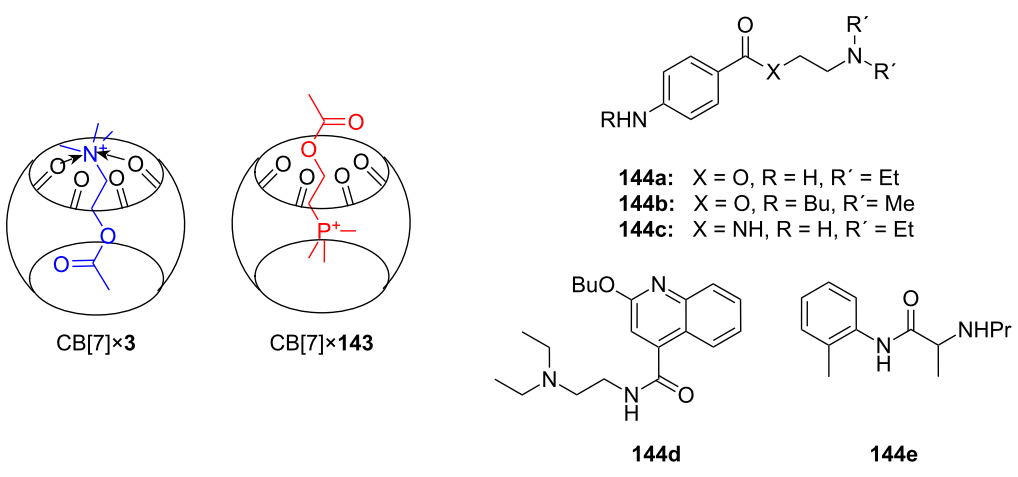

Figure 105: Cucurbit[7]uril (**131c**) guest inclusion and representative guests.

K_{ass} = (1.5 ± 0.4) × 10^4 dm^3 mol^{-1}), procainamide (**144c**, K_{ass} = (7.8 ± 1.6) × 10^4 dm^3mol^{-1}), dibucaine (**144d**, K_{ass} = (1.8 ± 0.4) × 10^5 dm^3 mol^{-1}) and prilocaine (**144e**, K_{ass} = (2.6 ± 0.6) × 10^4 dm^3 mol^{-1}) in aqueous solution (pD = 4.75) (Figure 105) as observed by NMR studies [458]. The stability constants are 2–3 orders of magnitude higher than the values reported for binding by the comparably sized β-cyclodextrin (**136b**) host molecule. The protonated forms are bound more strongly in acidic solution. Upon protonation the cucurbit[7]uril sits around the aromatic unit of **144a**–**144c**, in the deprotonated case it includes the alkylated amine centre.

Similarly, "bolaform" guests with two cationic end groups, such as succinylcholine chloride (**145**) and α,ω-bis(trialkylammonium)alkane dications (or their phosphonium analogues) form strong host–guest complexes and [2]pseudorotaxanes with cucurbit[7]uril [459]. An analogous dimeric guest series to the amines discussed previously containing NMe_3^+, NEt_3^+, quinuclidinium (**146g**), PMe_3^+ and PEt_3^+ endgroups, was studied in aqueous solution by ^1H and ^{31}P NMR spectroscopy, as well as ESI mass spectrometry [460].

The formation of 1:1 aggregates is assigned to a [2]pseudorotaxane structure with the NMe_3^+ and NEt_3^+ end groups outside the cavity near the carbonyl oxygens on the portal and the guest molecule located in the hydrophobic cavity (Figure 106). The 1:1 host–guest stability constants range from 8 × 10^6 (guest **145**) to 3 × 10^{10} M^{-1} (guest **146b**) and are dependent on the nature of the end group and the length and hydrophobicity of the central linker. The stability constants for the 1:1 complexes with guests with the same decamethylene linker follows the order **146c** > **146e** > **146f** > **146d**, indicating that for threads with the same alkyl chain length, the stability constant is related to charge diffusion on the peralkylonium end group. Changing the end groups from NMe_3^+ to NEt_3^+ (**146c** to **146d**) or PMe_3^+ to PEt_3^+ (**146e** to **146f**) results in a lowering of K_{ass} value by one order of magnitude as the less polar triethyl-substituted groups have weaker ion-dipole interactions with the polar portals of CB[7] than the methyl analogues.

With the exceptions of the shorter $[(CH_3)_3N(CH_2)_nN(CH_3)_3]^{2+}$ (n = 6, 8) dications, the addition of a second CB[7] results in the translocation of the first CB[7], such that the hydrophobic

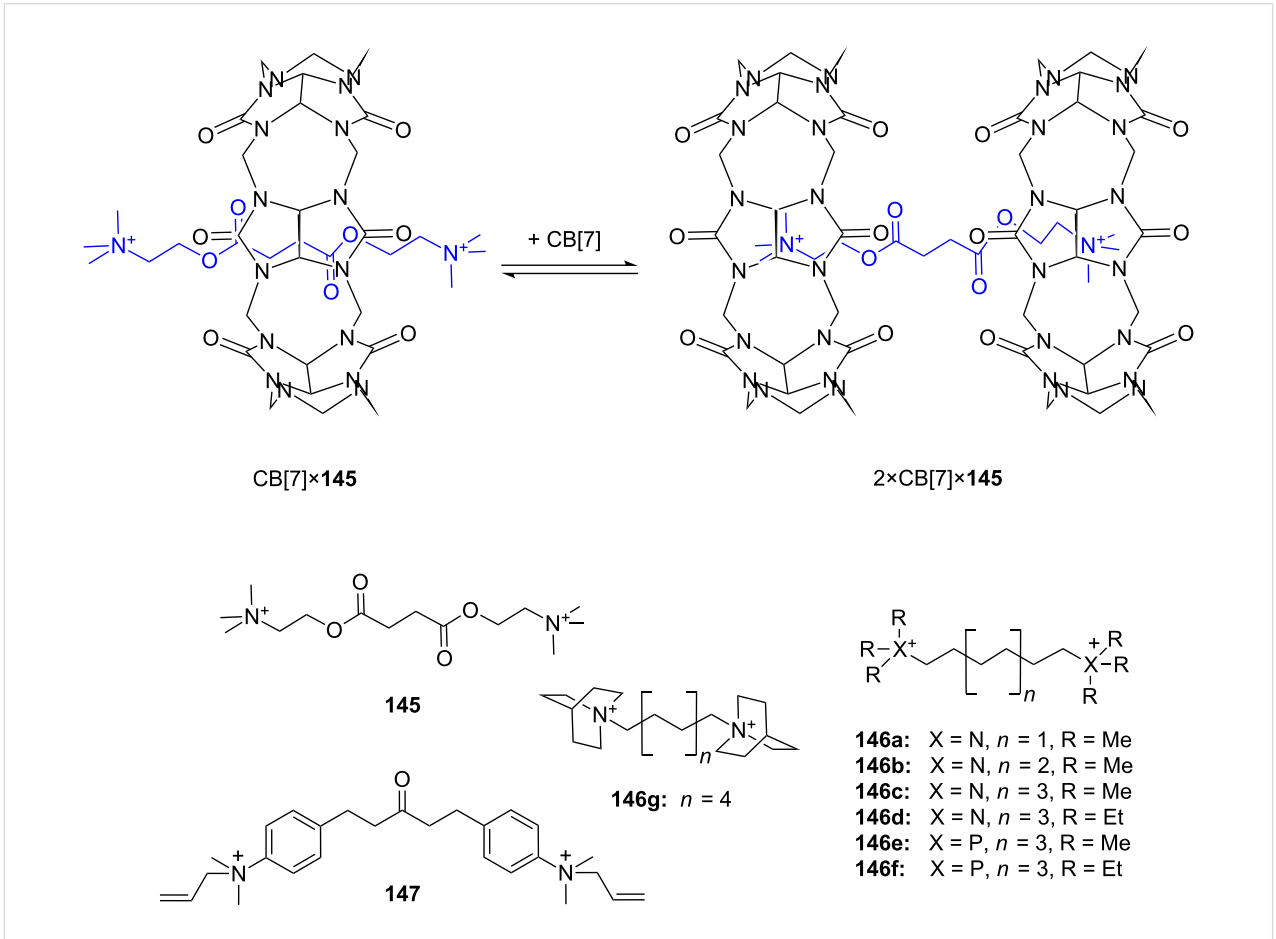

Figure 106: Cucurbit[7]uril (**131c**) binding to succinylcholine (**145**) and different bis-ammonium and bis-phosphonium guests.

$-NR_3^+$ and $-PR_3^+$ end groups (R = Me or Et) are encapsulated in the cavities, while the central linker extends through the CB[7] portals (Figure 106). The magnitude of the stability constants for the 2:1 complexes closely follows the trend observed previously for CB[7] binding with the NR_4^+ and PR_4^+ cations.

The vast majority of host–guest complexes of CB[7] (**131c**) with cationic guests, such as paraquat [461,462], assemble with the cationic part of the guest located outside of the cavity, adjacent to the oxygens of the portal carbonyls. The remaining hydrophobic region of the guest is positioned inside the cavity.

Mohanty and co-workers have found that the fluorescent dye thioflavin T, used extensively to probe the presence of amyloid fibrils, forms 1:1 and 2:1 host–guest complexes with cucurbit[7]uril (**131c**), with binding constants in the order of magnitude of 10^5 and 10^3 M^{-1}, respectively [463].

By enlarging the host by one glyconuril unit to cucurbit[8]uril (**131d**) (Figure 107) a cavity comparable in size with γ-cyclodextrin (**136c**) results, which is in the position to capture and include even other macrocycles like cyclene (**6**) or cyclam (**7**) and their complexes with transition metals [464].

Kim and co-workers report that **131d** can bind to aromatic guests, such as tryptophan (**81b**), tyrosine, and dopamine (**2**) as observed by the resulting changes in visible color and in their NMR spectra [433,465].

In the crystal structures of the inclusion complexes of *S*-tyrosine (*S*-Tyr), *S*-histidine (**81e**, *S*-His), *S*-leucine (*S*-Leu) in cucurbit[8]uril (**131d**) a 1:2 host:guest ratio was found [444]. It is common, that the ammonium moiety is always located at the portal of the host, co-ordinated by hydrogen bonding and ion–dipole interaction with the carbonyl groups of the host. The host can include not only the stacked aromatic moieties, but also the alkyl moieties of the amino acids.

Consistent with these observations, cucurbit[8]uril (**131d**) is known to form 1:1:1 heteroternary complexes with paraquat (**148**) and a second aromatic guest (Figure 107): Urbach et al. describe the molecular recognition of amino acids by cucurbit[8]uril and its complex with 1,1′-dimethyl-4,4′-bipyridinium (paraquat, **148**). A comprehensive examination of the 20 genetically encoded amino acids was carried out by ^1H NMR spectroscopy and isothermal titration calorimetry in aqueous solution [466]. The amino acid to host stoichiometry is controlled by the presence (1:1) or absence (2:1) of paraquat (**148**). Both **131d** and the complex **149** bind measurably to only tryptophan (**81b**), phenylalanine (**81a**) and tyrosine. For the 1:1 complexes with the cucurbit[8]uril-paraquat-assembly (**149**) a selectivity of Trp (**81b**, $K_{ass} = 4.3 \times 10^4$ M^{-1}) with 8-fold and 19-fold specificity over Phe (**81a**, $K_{ass} = 5.3 \times 10^3$ M^{-1}) and Tyr ($K_{ass} = 2.2 \times 10^3$ M^{-1}), respectively, was found. The binding strengths for the 2:1 complexes of cucurbit[8]uril reach 10^8 M^{-1} (Trp, $K_{ass} = 6.9 \times 10^7$ M^{-1} and Phe, $K_{ass} = 1.1 \times 10^8$ M^{-1}).

The interaction of the host system with tryptophan (**81b**) was investigated in greater detail by using a combination of isothermal titration calorimetry, mass spectrometry, UV–visible, fluorescence, and ^1H NMR spectroscopy methods [467], with the finding that the selectivity is mediated by the electrostatic charge in aqueous solution.

The ITC data showed that **149** binds Trp guests with ammonium group like Trp-OMe and tryptamine ($K_{ass} \sim 5 \times 10^4$ M^{-1}) with approximately 20-fold selectivity over guests lacking this functionality, such as *N*-acetyl-Trp ($K_{ass} = 2–3 \times 10^3$ M^{-1}). For the binding of Trp (**81b**) and its derivatives, a 1:1 binding stoichiometry was observed in all experiments.

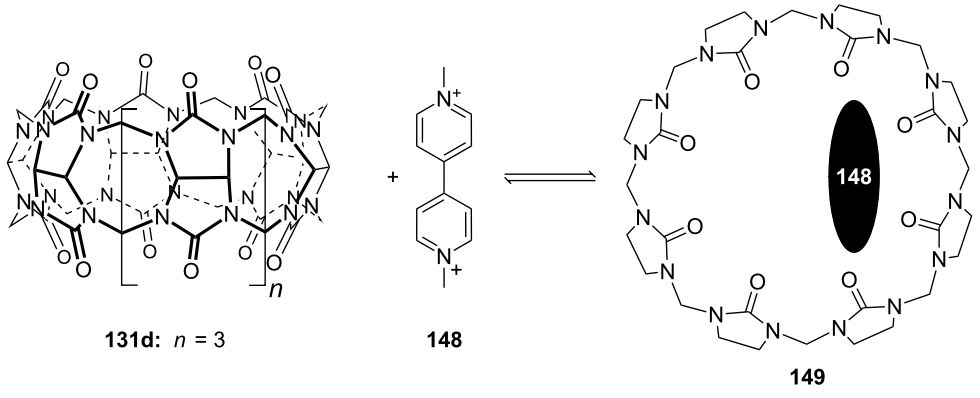

131d: *n* = 3 **148** **149**

Figure 107: Paraquat-cucurbit[8]uril complex **149**.

N-Terminal tryptophan residues are bound with higher affinity than C-terminal or internal tryptophan residues. The complex binds Trp-Gly-Gly with high affinity (K_{ass} = 1.3 × 10^5 M^{-1}, log K_{ass} = 5.1), with 6-fold specificity over Gly-Trp-Gly (log K_{ass} = 4.3), and with 40-fold specificity over Gly-Gly-Trp (log K_{ass} = 3.5).

In addition, cucurbit[8]uril (**131d**) was reported to be a remarkably synthetic host for selective recognition and non-covalent dimerization of *N*-terminal aromatic peptides in aqueous solution [468]. Cucurbiturils are known to recognize *N*-terminal tryptophan over internal and C-terminal sequence isomers. Tripeptides of the sequence X-Gly-Gly, Gly-X-Gly, and Gly-Gly-X with X being Trp, Phe, Tyr and His were studied. Compound **131d** selectively binds and dimerizes Trp-Gly-Gly and Phe-Gly-Gly with high affinity (ternary complex association constant in the range of 10^9–10^{11} M^{-1}), the binding constants for the other 10 peptides were too small to be measured by ITC. Both peptides are bound in a stepwise manner, the latter with positive co-operativity. The crystal structures revealed the structural basis for selective recognition as the inclusion of the hydrophobic aromatic side chain and chelation of the proximal *N*-terminal ammonium group by carbonyl oxygens on the cucurbituril. In view of application the authors pointed out the potential study of dimer-mediated biochemical processes and the potential use for the separation of peptides and proteins.

Nolte and Escuder published a series of cucurbituril related molecules, amino acid appended diphenylglycouril-based chiral molecular receptors (**150**) [469] (Figure 108). The binding of several biologically relevant guests with aromatic moieties was studied with UV–vis spectroscopy in competition experiments with 4-(4-nitrophenylazo)resorcinol ("Magneson") and 2-(4-hydroxyphenylazo)benzoic acid (HABA) in water at pH 8 and 4.5, respectively. Compound **150b** forms thin tubules in chloroform and vesicles in water, with the possibility of surrounding the guest. Aggregates of the chiral host **150b** bind catecholamines and aromatic amino acids in water and are able to discriminate between their enantiomers. The calculated binding constants were moderate to high and a remarkable enantioselectivity for the corresponding enantiomers of *R*-tyrosine (1.6 × 10^4 M^{-1} vs. 2 × 10^3 M^{-1}), *S*-phenylalanine (**81a**, 2.6 × 10^4 M^{-1} vs. 1.2 × 10^4 M^{-1}) and *R*-tryptophan (**81b**, 5.6 × 10^4 M^{-1} vs. 1.7 × 10^4 M^{-1}) was observed.

The rigid structure and capability of forming stable complexes with a wide range of molecules and ions, mediated by ammonium ion co-ordination in combination with inclusion of the side chains make cucurbit[*n*]urils very attractive not only as a synthetic receptor. As previously stated, self assembly systems is outwith the scope of this review, but it has to be

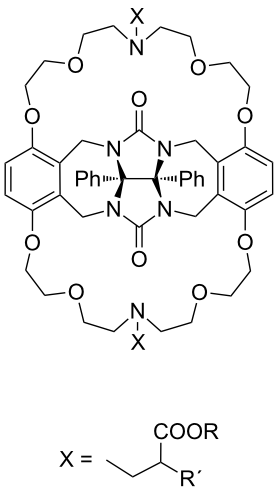

150a: R = H, R´= NHBoc, *n* = 1
150b: R = H, R´= NHBoc, *n* = 4
150c: R = $C_{16}H_{33}NH$, R´= NH_3^+, *n* = 1
150d: R = $C_{16}H_{33}NH$, R´= NH_3^+, *n* = 4

Figure 108: Gluconuril-based ammonium receptors **150**.

mentioned since nearly as many papers as published for molecular recognition with cucurbit[*n*]urils are found using the macrocycles as building blocks for the construction of supramolecular architectures, often relying on the interaction with an ammonium species. The interested reader is referred to the large body of recent literature [470-485].

In summary, cucurbiturils and their derivatives are valuable and versatile hosts for ammonium and diammonium guests, as well as amino acids and peptides, reaching the highest binding constants of all presented receptor families in highly competitive media (up to 10^{10} to 10^{12} M^{-1}). Generally, the ammonium guests are co-ordinated by the carbonyl groups of the host by electrostatic ion–dipole attraction assisted by hydrogen bonding. The non-polar part of the guest is included in the cavity. The binding is governed by hydrophobic effects and van der Waals contacts. The entropic gain upon binding additionally supports the high association constants found with cucurbiturils. Similar facts are also relevant to quaternary ammonium species, which are bound by the same interactions. Notably, cucurbit[*n*]urils are one example, where these guests are not bound by cation–π-interactions. Here the area of negative charge accumulation, represented by the carbonyl groups, co-ordinates cationic species strongly. For a more comprehensive discussion of the binding properties of the cucurbit[*n*]uril family, we recommend the recent review article by Issacs et al. [436], thermodynamic aspects of the binding process are discussed in detail in recent overviews [429,432].

5. Molecular clefts, tweezers, trigonal ligands, phosphonates and cyclophane structures as receptors for ammonium ions

Typical host structures for ammonium guests are macrocyclic, like calixarenes, cyclodextrins or cucurbiturils with polar functionalities organized in a circular manner. However, many suitable synthetic receptors fall in a second category: Non-cyclic compounds, with more open structures. These hosts have pockets or cavities into which a guest can fit, but is not completely encapsulated. These clefts, clips and tweezers are discussed in the following section together with tripods and suitably functionalized cyclophanes. In the topic of ammonium ion recognition, it is difficult to draw a dividing line, as both concepts – clefts and cyclophanes – function similarly or were developed in parallel for similar purposes. We will first discuss clefts, clips and tweezers, then tripods and related systems, and finally cyclophanes with ionic functionalities.

Vitally important biochemical processes involving ammonium ions rest upon the specific interactions supported by negatively charged substituents such as carbonates, sulfates, or phosphates. As demonstrated with several examples before, these charged groups contribute significantly to the substrate binding. For clefts, tweezers and cyclophane structures such substituents are of key importance to complement the ammonium ion binding by ionic and hydrogen bond interactions. In the cavities the guests can be bound utilising non-covalent bonding interactions such as hydrophobic forces, van der Waals or dispersion forces, π-stacking, hydrogen bonding, as well as metal co-ordination and electrostatic effects.

Clefts (Figure 109) have a certain degree of flexibility, provided that the open cavity is large enough and the geometry is optimal to accommodate the desired guest molecule. Clefts organize polar functionality with hydrogen bonding or ionic co-ordination capabilities at precise distances and orientations. This conformational fixation is achieved by covalent and non-covalent constraints. Generally, acylic clefts, clips and tweezers must position functional groups on a rigid molecular scaffold, often of concave shape, to focus these inwards, to assure the desired conformation, and to prevent the collapse of the binding pocket. As in macrocycles, proper pre-organization can significantly augment binding strengths.

Molecular tweezers (Figure 109) are different examples of molecular clefts. Molecular tweezers or molecular clips can be understood as non-cyclic macrocyclic molecular complexes with open cavities bearing two “arms” that bind the guest molecule between them [486]. For ammonium ion recognition they divide into two different subtypes: Either they are characterized by convergent functional groups directed towards each

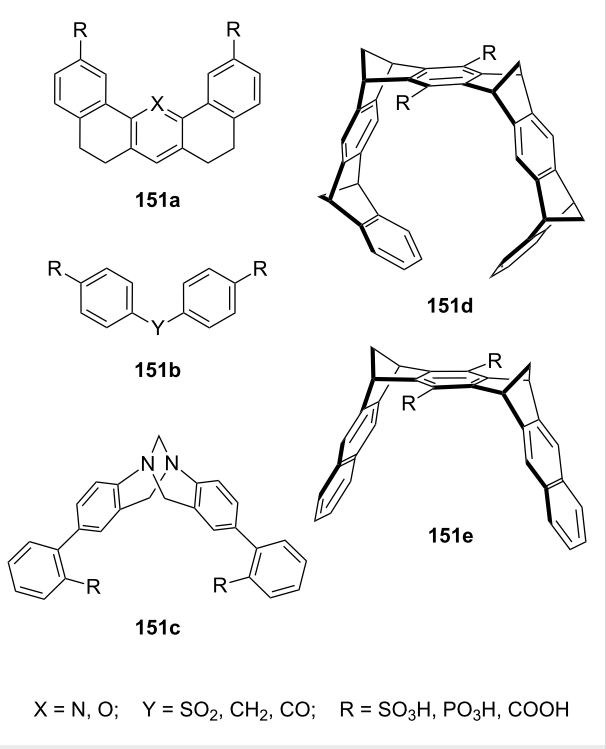

Figure 109: Examples of clefts (**151a**), tweezers (**151b, 151c, 151d**) and clips (**151e**).

other, mounted on a rigid backbone with a certain degree of freedom – the space between the functional groups provides the cleft into which a guest can bind – or the cavity of this kind of receptors is made up of two sidewalls connected to each other by a central spacer unit, which can be either flexible or rigid. The second type contains two aromatic surfaces which “pinch” aryl or more rarely an non-polar guest between them and uses an additional ionic functionality to complement the ammonium part. Molecules like Kagan’s ether or Tröger’s base (see **151c**) are employed in many examples to give the tweezer a bent shape. The synthesis and properties of such often chiral molecular clefts and tweezers have been reviewed [487].

Tweezers and similar molecules “wrapping around” their targets, namely cyclophanes and cavitands, benefit to a large extent from selective co-ordination and inclusion by charged groups. Quaternary ammonium ions can be additionally co-ordinated by the cation–π-interaction to the aromatic surfaces.

Molecular tweezers were originally developed by Whitlock [488,489] and Zimmerman [490-494]. These formed sandwich complexes with aromatic guests by π–π-interactions. Hydrophobic interactions also play a significant role in their tight binding to aromatic (bis-phenol)carboxylates in water. The tweezers constructed by Zimmerman were more rigid and

showed high association constants with guests such as polynitroaromatics and 9-alkylated adenines in chloroform.

Further contributions and examples representing the different types of such molecules with open cavities were published by the groups of Vögtle [495], Rebek [496], Nolte [497], Harmata [498,499,518], Chen [500], Klärner [486,501-503] and Schrader (see the discussed example, Figure 112). Cations and some alkyl or a variety of aromatic guests, especially electron deficient aromatic systems [501,504-507] can be co-ordinated by dispersive forces such as π–π, CH–π- and cation–π-interaction. The introduction of polar functionality enables the binding of guests by additional interactions, for example, 1,3-dihydroxybenzene [497] by H-bonding or nucleosides [508-512] by ionic interactions. Similarly, ammonium ions, diamines [513,514] or chiral guests [515] can be recognized by appropriate functional groups arranged on these scaffolds.

Clips, tweezers [486,516], related V-shaped molecules [517] and their chiral analogs (e.g. Figure 109, **151c**) [518,519] have been reviewed. In the following we will discuss recent examples based on these backbones for inclusion of quaternary ammonium compounds, or, when suitably substituted, for ammonium ion recognition.

5.1. Clefts for different ammonium targets

The ability to bind the guest by π–π-interactions and thehydrophobic effect is extended by the possibility of hydrogen bonding to the guest molecule with a receptor family developed by Rebek et al. on the basis of Kemp's triacid (**152a**) (Figure 110). Due to the convergent carboxyl groups on the cyclohexane ring, condensation of the acid with aromatic amines – one to three aromatic rings are arranged in a linear manner – yields receptors such as **152b**, in which two carboxyl groups are pre-orientated in a convergent, optimal arrangement for the substrate binding. Rotation around the C–N bond can be prevented by a methyl group in *ortho*-position of the aromatic amine.

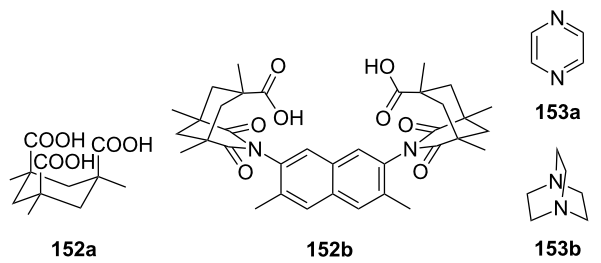

Figure 110: Kemp's triacid (**152a**), on example of Rebek's receptors (**152b**) and guests.

The largest receptor binds diamines, such as pyrazine (**153a**) or DABCO (**153b**) (Figure 110), in chloroform by salt formation. Dicarboxylic acids are linked by hydrogen bonds, similar to those found in carboxcylic acid dimers. On binding amino acids, a carboxyl group of the receptor co-ordinates to the carboxyl group of the substrate. In addition, salt formation occurs between the other carboxyl group of the receptor and the amino group of the guest [520,521]. Receptor **154** (Figure 111) is able to complex ammonium ions with its carboxylate group; the pyridinium cation binds in addition. The extended π-system allows for π-stacking [522].

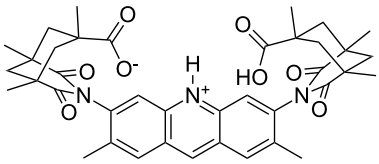

154

Figure 111: Amino acid receptor (**154**) by Rebek et al.

The authors identified a binding preference for phenylalanine (**81a**), tyrosine and tryptophan (**81b**) by extraction experiments (water/chloroform) with unprotected amino acids. Leucine, isoleucine and valine were, however, not transported into the organic phase. Thus, the π-stacking interaction seems to result in a decisive contribution to the complex stabilization here. Phenylglycine, due to its geometry, is also not in the position to participate in π-stacking in addition to the molecular bonds of the charged parts. The mode of binding and the interactions were investigated in detail by a theoretical study and verify the results and conclusions [523].

Because of the frequent occurance of basic amino acids (Lys, Arg, His) in biological processes, the molecular recognition of these amino acids by synthetic receptor molecules is of special interest [524-527]. Bell et al. described three receptors for guanidinium and ammonium guests [528]. These highly pre-organized clefts, bearing two carboxylate groups on a hexagonal lattice design with defined planar arrays of hydrogen-bonding groups, differ in the number of nitrogen atoms contained in their cavity (Figure 112). Complexation studies were conducted in methanol by ^{1}H NMR titration for several guanidinium and ammonium ion guests. Compound **155a** bound most guests very strongly (K_{ass} > 100 000 M^{-1}) and was selective for arginine (**81d**) more than 3-fold versus lysine (**81c**, K_{ass} = 29 000 M^{-1}). Surprisingly, the affinity for *N*-acetyl-*S*-lysine and propylammonium chloride was also found to be very high (K_{ass} = 10^5 M^{-1}). Interesting for ammonium ion recognition is receptor **155b**, which bound

lysine (**81c**) better than **155a**. In general, it tends to have higher affinity towards alkylammonium guests than to alkylguanidinium salts. It displayed a preference for binding primary alkylammonium guests, including *S*-lysine (**81c**), *N*-acetyl-*S*-lysine, 6-aminocaproic acid and 1-propylamine (K_{ass} = 10^5 M^{-1}). Among guanidinium guests, only arginine (**81d**) bound with very high affinity to **155b**. The complex of **155b** with *N*-methylguanidinium had a significantly lower stability (K_{ass} = 3900 M^{-1}). This selectivity was explained in terms of energies of cavity solvation: The larger cavity of **155a** is more highly solvated prior to binding than the smaller cavity of **155b**. The compact ammonium ion with its higher charge density was expected to form stronger attractive electrostatic interactions. In contrast, the alkylguanidinium ion was able to form more H-bonds with the planar receptor **155a**.

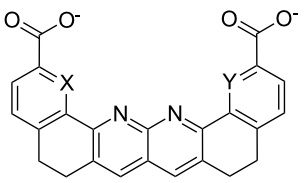

155a: X = Y = N
155b: X = N, Y = CH
155c: X = Y = CH

Figure 112: Hexagonal lattice designed hosts by Bell et al.

The amidinium ion is closely related to the ammonium and the guanidinium ion. The amidinium functionality plays an important role in drugs targeting binding pockets for the arginine side chain. In contrast to the spherical ammonium ion, the amidinium group has to be surrounded in a half-moon-like array by at least four hydrogen bond acceptors, which are ideally pre-oriented for maximum electrostatic as well as hydrogen bond interactions for efficient binding. This was demonstrated by Bell et al., who developed a concave, highly pre-organized receptor molecule based on annulated pyridines (**156**) which binds benzamidine (**157**, R = Ph) (Figure 113) very efficiently in 10% methanolic dichloromethane (K_{ass} ~ 10^7 M^{-1}) [529].

The efforts of the group concerning the binding of ureas, amines and guanidines by the hexagonal lattice design receptors have been nicely summarized in an overview [530].

5.2. Clips and tweezers

The interaction of carboxylates with a variety of functional groups, receptors for amino acids and nucleotides has been explained in detail in the literature [531,532], and detailed

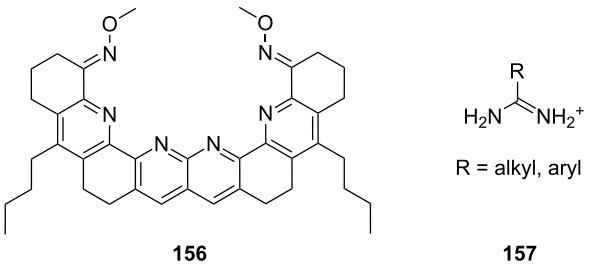

156 **157**

Figure 113: Bell's amidinium receptor (**156**) and the amidinium ion (**157**).

binding data for oxoanions to ammonium and guanidinium groups has been published [533].

Sulfonate groups were widely used with success for the recognition of ammonium ions in calixarenes (see chapter 4), but are of less importance for ammonium recognition with tweezers and clefts. The ammonium – phosphonate binding is by far more widely used as interaction.

The P=O double bond system features strong hydrogen bond acceptor property and weak Brønsted basicity in combination with a high dipole moment. Additional co-operative hydrogen bonds render even simple bisphosphonates highly selective [534].

Many biologically important classes of organic cations like mono- and disaccharides, amino alcohols, arginine derivatives and guanidines are bound in polar media.

Phosphonic acids (Figure 114), phosphonates and their mono esters are especially employed for cation recognition. Simple representatives such as benzyl phosphonic (**158a**), *meta*- and *para*-xylene diphosphonic (**158b/c**) and mesitylene triphosphonic acid (**158d**) have shown their ability to complex selectively potassium and ammonium cations [535]. Ammonium ions were bound two to three times better than potassium in capillary electrophoresis experiments in protic media.

In 1996 Schrader introduced a new class of artificial receptor for alkylammonium ions, i.e., xylene bisphosphonates such as **159** [536] (Figure 115). The host molecules, designed to imitate the natural adrenergetic receptor [537,538], are selective for 1,2- and 1,3-amino alcohols. In their 1:1 chelate-binding mode an almost ideal array of short, linear hydrogen bonds with the ammonium ion is created pointing towards one of the phosphonate moieties. Formation of an additional co-operative hydrogen bond between the second phosphonate anion and the hydroxyl groups provides maximum electrostatic and hydrogen-bond interactions. Biologically important amino alcohols such

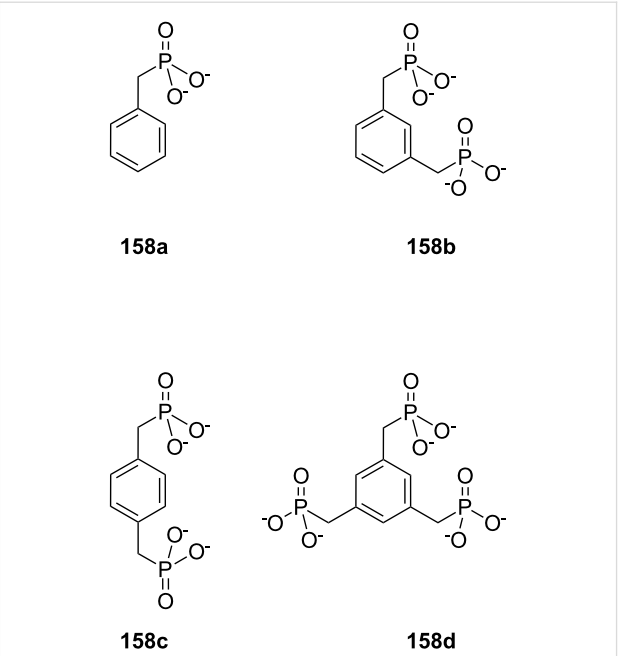

Figure 114: Aromatic phosphonic acids.

as glucosamine, 1-aminosorbitol, ephedrine, and the β-blocker propranolol were bound in DMSO with K_{ass} values of between 60 000 and 130 000 M^{-1}. Secondary amines are complexed at least as strongly as primary amines; amino alcohols were bound much stronger than their simple amine counterparts. The association constants for some of the amino alcohols with 60 000 M^{-1} is five times higher than the average estimate for simple amines of 12 000 M^{-1}. In addition, adrenaline model compounds were recognized by phosphonates which allow lateral recognition of the substrate by extended aromatic ester groups by π–π-interactions (**160a** and **160b)** [539] (Figure 115). Only a moderate binding of adrenaline to **159** was observed and rationalized by intermolecular competition of the catechol OH groups.

The recognition with *para*-xylene-bisphosphonates was shown with several examples of ammonium [540,541] and guanidinium [528,542] cations by Schrader et al. Similarly, the group demonstrated the recognition of the amidinium ion with the simple *m*-xylene bisphosphonate **159**.

A bifurcated hydrogen bond complex is typical for the classical amidinium binding pattern with carboxylates or phosphonates [543] with values for the association constant usually in the range of $K_{ass} \sim 10^3$ M^{-1} in solvents such as DMSO [544]. This binding constant could be also observed for the 2:1 complex with **159**. Interestingly, when a 1:1 stoichiometry is ensured by performing dilution experiments with a surplus of **157** with respect to the amidinium ion, a far stronger co-ordination is observed in DMSO: Each amino group is bound by a phosphonate moiety of the tweezer ligand. All association constants lie two orders of magnitude higher than the classical amidinium-phosph(on)ate complexes (10^5 M^{-1} vs. 10^3 M^{-1}). The association constants for various substituted benzamidines correlate with the electronic character of the substituents. The electron rich *p*-methoxybenzamidine is bound with $K_{ass} = 7.6 \times 10^4$ M^{-1}, acetamidine and benzamidine with ~10^5 M^{-1}, and the electron deficient *m*-nitrobenzamidine even with $K_{ass} = 2.5 \times 10^5$ M^{-1}.

Combination of a boronic ester as recognition motif with the xylene bisphosphonate unit **159** and an appropriate spacer (Figure 116) permitted recognition of neurotransmitters [545]. For noradrenalin (**80b**) in 100 mM phosphate at pH 7.0 a strong association was found (K_{ass} = 190, 340 and 690 M^{-1} for **161a**, **161b** and **161c**, respectively). It was possible to evaluate the association constants for a number of catecholamines such as adrenaline (**80a**) and noradrenaline (**80b**) highlighting the importance of both the aminoalcohol and catechol motifs within the guest. Receptor **161c** as the best example bound adrenaline (**80a**, K_{ass} = 550 M^{-1}), 3,4-dihydroxyphenethylamine (K_{ass} = 590 M^{-1}), dopamine (**2**, K_{ass} = 630 M^{-1}) and noradrenaline (**80b**, K_{ass} = 690 M^{-1}) with about 2-fold selectivity over catechol (**162**, K_{ass} = 350 M^{-1}). The receptor was then developed into a color sensor by employing the colored dye alizarin complexone in an indicator displacement assay. On binding to the receptors, the color of the dye changed from deep red to orange, permitting an association constant of K_{ass} = 1700 M^{-1} to be determined by ^{1}H NMR titrations. Upon addition of catecholamines, displacement of the indicator and recovery of the original color were observed. Binding constants similar to those obtained by NMR spectroscopy were obtained

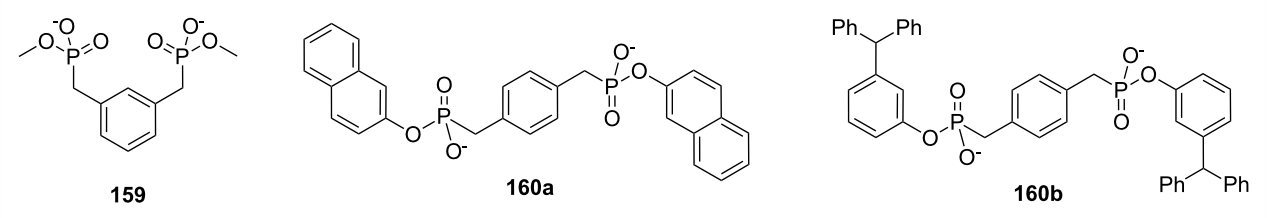

Figure 115: Xylene phosphonates **159** and **160a/b** for recognition of amines and amino alcohols.

by UV spectroscopy in water. Finally, a calibration curve for the receptor-indicator complex in the presence of varying concentrations of noradrenaline was constructed, which allowed an exact quantitative determination of the concentration of catecholamines even in complex mixtures and urine samples. On changing from water to a 3:1 mixture of methanol/water (HEPES buffer, pH 7.0), the K_{ass} value for alizarin complexone increased to 7000 M^{-1}. A rise in noradrenaline binding could not be confirmed. All catecholamines were bound in the range of 300–400 M^{-1}, catechol somewhat less tightly with 200 M^{-1} and simple amines such as phenylethylamine were not bound at all. Adrenaline was bound 2–3 times stronger than catechol.

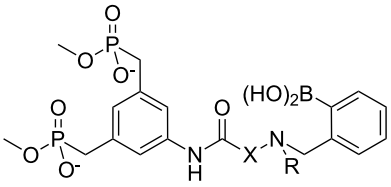

161a: X = C_6H_4-CH_2 R = H
161b: X = $(CH_2)_3$ R = H
161c: X = $(CH_2)_3$ R = Me

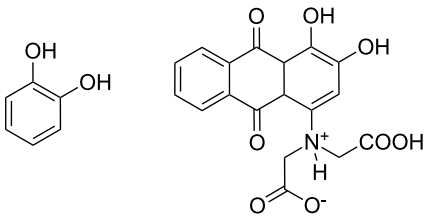

162 **163**

Figure 116: Bisphosphonate recognition motif **161** for a colorimetric assay with alizarin complexone (**163**) for catechols (**162**).

Klärner and Schrader introduced tweezers and clips based on an electron-rich torus-shaped cavity adorned with two peripheral anionic phosphonate and phosphate groups (Figure 117) capable of ammonium ion and amino acid recognition in water. These molecular tweezers were synthesized via repetitive Diels–Alder reactions and combine the binding properties of a non-polar aromatic cavity with the bisphosphonates. In addition, the bisphosphonate units lead to the desired solubility in polar protic solvents such as methanol and water. In water, the π–π and cation–π-interaction are coupled with the hydrophobic effect, and these are much more pronounced than in aprotic solvents and thus lead to higher binding constants. The phosphonates are fully deprotonated due to their pK_a value of 1.8 in neutral aqueous solution. Upon inclusion of a guest in the cavity, they can grab it like a pair of pincers and build ionic hydrogen bonds to the ammonium ion to support the binding.

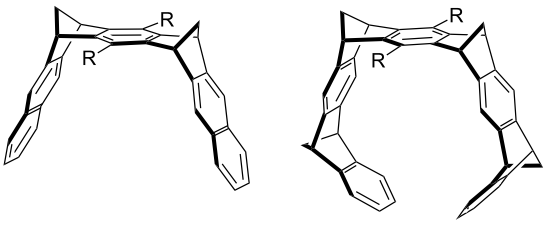

164a: R= O-P(O)(CH_3)OH
164b: R= O-P(O)(CH_3)O^-·N^+(^{n}Bu)$_4$
164c: R= OP(O)(OLi)$_2$

165a: R= O-P(O)(CH_3)O^-·Li^+

Figure 117: Bisphosphonate/phosphate clip **164** and bisphosphonate cleft **165**.

The phosphonate substituted clip **164b** [546] selectively binds *N*-alkylpyridinium salts such as *N*-methylnicotinamide iodide (**166b,** NMNA) and NAD^+ (**166c**) (Figure 118) in methanol and in aqueous solution. Further studies pointed to a significant contribution of the hydrophobic effect to the host–guest interaction in aqueous solution [547]. The binding constants in water are significantly higher, than those observed in methanol: for example, **166a** bound with K_{ass} = 9400 or 600 M^{-1} and **166b** with K_{ass} = 68000 or 16700 M^{-1} in water and methanol, respectively.

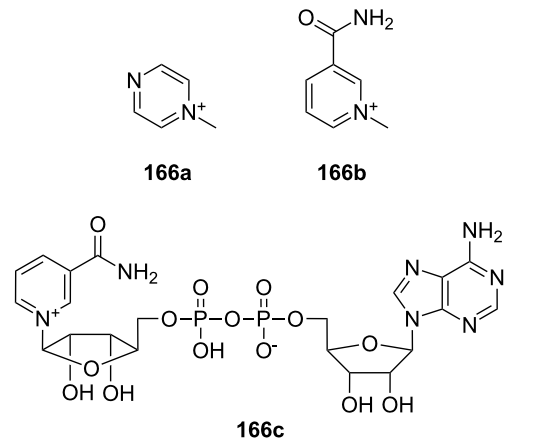

166a **166b**

166c

Figure 118: *N*-Methylpyrazine **166a**, *N*-methylnicotinamide iodide (**166b**) and NAD^+ (**166c**).

In the complex with NAD^+ (**166c**, K_{ass} = 6500 M^{-1}), one of the most important redox coenzymes in nature, a dynamic equilibrium is observed in aqueous solution. The protons of the subunits, the nicotinamide as well as the adenine moiety, are shifted upfield in the ^{1}H NMR spectrum indicating that either the nicotinamide or the adenine subunit are included inside the cavit. Equilibration is rapid on the NMR time scale. A Monte Carlo conformer search, leading to the energy-minimized double-sandwich structures supported the experimental result.

Water-soluble molecular clips substituted with phosphate groups (**164c**) (Figure 117) were also investigated regarding their binding properties. Despite the similarity between the phosphonate and phosphate functional groups, the supramolecular properties of both clips are different from each other. The phosphate clip lithium salt **164c** shows self-aggregation in aqueous solution while there is no evidence of this phenomenon for the phosphonate clip dilithium salt **164a** [548]. Additionally, the binding properties of these clips in phosphate buffer solution (pH = 7.2) change dramatically from one clip to another (Table 9) as well as with the pH values of the solution. For the most guest molecules, the phosphate clip **164c** shows association constants between two and ten times larger than those of the phosphonate clip **164a**.

Table 9: Comparison of association constants (M^{-1}) of biological relevant molecules with the phosphonate and phosphate clips in phosphate buffered aqueous solution (pH = 7.2).

Guest	Phosphonate clip **164b** K_{ass} [M^{-1}]	Phosphate clip **164c** K_{ass} [M^{-1}]
nicotinamide mononucleotide	550	1120
adenosine	1115	1400
cytidine	1070	9685
N-methylnicotinamide iodide (**166b**)	11270	35000
caffeine	9550	42700
NAD^+ (**166c**)	4200	5630

N-Alkylated pyridinium salts are also strongly bound in the tweezer **165a**. Only *para*-substituted compounds are strongly bound, other substitution patterns do not lead to an effective inclusion in the downward shielded cavity.

In contrast to the bisphosphonate clip, the bisphosphonate tweezer also binds primary and secondary ammonium cations. The binding correlated with the steric requirements of substituents. The bulkier the substituent, the lower is the binding constant. Primary ammonium cations (K_{ass} up to 800–900 M^{-1} in aqueous solution) are bound more strongly than their secondary analoges. Dopamine (**2**) is bound with millimolar strength in water. Interestingly, the basic amino acids arginine (**81d**) and lysine (**81c**) are significantly better bound (up to 23000 M^{-1} for Ts-Lys-OMe in aqueous phosphate buffer) compared to 900 M^{-1} for simple amines.

The molecular cleft (**165a**) displayed comparable and also exceptionally high affinity for lysine (**81c**, K_{ass} = 5000 M^{-1} in neutral phosphate buffer) [549]. Selectivity for arginine (**81d**) and lysine (**81c**) is achieved by threading the whole amino acid side chain through the cavity and subsequent locking by formation of a phosphonate-ammonium/guanidinium salt bridge, reflecting a pseudorotaxane-like geometry. Thus the aggregate can be stabilized by strong electrostatic and dispersive interactions, supported by the hydrophobic effect.

The basic amino acids were effectively bound in small signaling peptides (Lys or Arg rich). These experiments confirmed the selectivity. When two lysine residues separated by other amino acids are present in the peptide, both can be individually bound by one bisphosphonate tweezer in a 2:1-complex. With two lysine residues close together, the formation of a cluster with the bisphosphonates was preferred in a water/methanol mixture. In this case it is apparently more favorable to build hydrogen bonds from the ammonium cations to the bisphosphonates, rather than trapping the lysine side chains in the cavity. This artificial lysine binder shows a one order of magnitude increased affinity compared to all other receptor molecules that have been designed for this purpose. Only Bell's molecule (**155c**) was later identified as a selective lysine binder (K_{ass} > 10^5 M^{-1} in methanol). The binding mode and strength seem to be largely governed by steric effects: bulky substituents close to the ammonium functionality prevent an effective inclusion, while a slim ethylammonium environment allows complete insertion into the host interior.

The two corresponding water-soluble host molecules with phosphate substituents (Figure 119) designed for cofactor and amino acid recognition are able to inhibit the enzymatic activity of alcohol dehydrogenase (ADH) in vitro [550]. As previously noted, clip **164c** binds strongly to NAD^+ (**166c**) and tweezer **165a** shows high affinity to lysine (Ac-Lys-OMe, K_{ass} = 5000 M^{-1}) in aqueous buffer. Clip **164c** pulls out NAD^+ (**166c**) from the Rossman fold and thereby depletes the cofactor level below a critical threshold. An excess of this molecule led to irreversible denaturation. Tweezer **165b** with its high lysine preference decorates the whole enzyme surface, especially the cofactor entrance site. While the absolute enzymatic activity

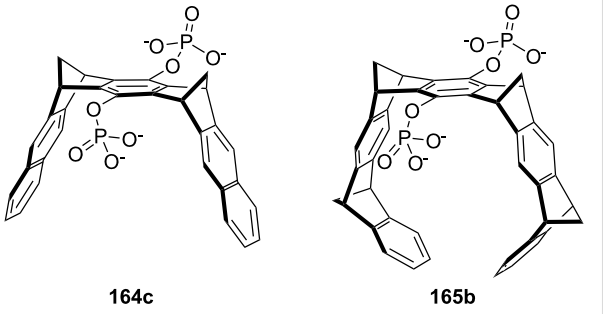

Figure 119: Bisphosphate cavitands.

was not influenced at all, 0.6 equiv of tweezer was sufficient for total enzyme shut down. Addition of lysine (**81c**) could switch on the enzyme function again in a totally reversible manner. Lineweaver-Burk plots indicated a competitive mechanism for the clip, with respect to both substrate and cofactor, while the tweezer clearly follows a non-competitive mechanism.

In 2000 a macrocyclic receptor molecule, which binds arginine (**81d**) and lysine (**81c**) in a stereoselective fashion was reported [551]. The chiral bisphosphonate **167** (Figure 120) binds ammonium and guanidinium ions by hydrogen and salt bridges. The mechanism of enantioselective recognition relies on two simultaneous cation–phosphonate interactions. The amino acid is in close contact to the surface of the chiral tether in **167** and one enantiomer is bound preferentially. The overall binding constants were only in the range of 10^4 M^{-1} in DMSO.

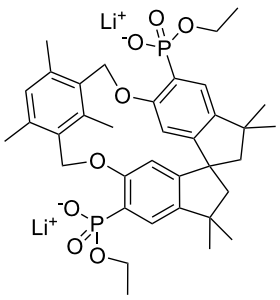

167

Figure 120: Bisphosphonate **167** of Schrader and Finocchiaro.

In examining the binding properties by NMR titration in DMSO, the authors found out that for short diammonium guests such as *S*-histidine (**81e**), and *S*-ornithine (both as dihydrochlorides) a 1:2 (receptor: guest) stoichiometry is present, but there is no chiral discrimination. However, the complexes for lysine (**81c**, K_{ass} = 2.1 × 10^4 M^{-1}) and arginine (**81d**, K_{ass} = 9.4 × 10^3 M^{-1}) have a 1:1 molar ratio and a distinction between the enantiomers is possible. The distance between the two ammonium groups in a guest molecule must obviously be large enough to bind to both phosphonates of the receptor. The enantiomeric excess was determined to be 17% for arginine (**81d**) and 33% for lysine (**81c**).

An artificial receptor molecule **168** with high noradrenalin specificity uses highly pre-organized stiff elements and connections (Figure 121) for a more favorable complexation entropy and improved desolvation of the included guest [552]. NMR titrations with neurotransmitters and related guests in d_4-methanol revealed low micromolar affinity to *rac*-adrenaline (**80a**, 260 M^{-1}), dopamine (**2**, 340 M^{-1}) and aromatic amino acid esters (~200 M^{-1}). Other amino acids, catechol (**162**) and phenylethylamine (**78a**) gave no response. Job's plot analysis confirmed a 1:1 complex stoichiometry. The rigid phenazine moiety in receptor **168** strongly improves the affinity for the desired guest (K_{ass} = 1800 M^{-1}). The effective 1:1 complex formation between (**168**) and noradrenaline (**80b**) could also be monitored by ESI-MS, producing clean mass spectra with host and aggregate ion peaks, exclusively.

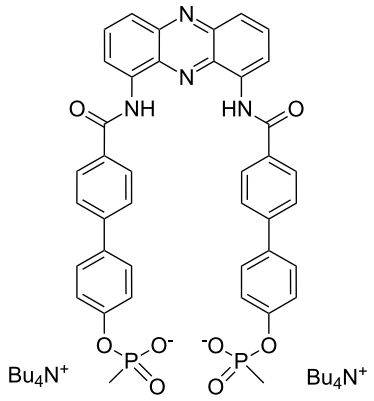

168

Figure 121: Tweezer 168 for noradrenaline (**80b**).

Due to the highly amphiphilic structure of **168**, the receptor molecule was incorporated in a stearic acid monolayer at the air/water interface. In the Langmuir film balance, substantial shifts were produced upon subinjection of the various analytes into the aqueous sub-phase (10^{-4} M) reflecting the interaction with the embedded receptor molecule (no effects were produced with stearic acid alone). By far the largest shift is obtained from noradrenaline (**80b**), followed by much smaller shifts from adrenaline (**80a**) and dopamine (**2**).

5.3. Tripodal receptors

Tripodal ligands are C_3 symmetrical molecules related to tweezers, with three side chains on a rigid platform (Figure 122). Several of these artificial receptors have C_{3v} symmetry [553-557]. In ammonium ion recognition with tripods, the flexible arms form three hydrogen bonds to acidic protons of the guest amine RNH_3^+.

The binding can benefit from this additional co-ordination site. Even more, recognition of biologically important guests often necessitates a receptor that can make multiple non-covalent contacts. This concept was nicely demonstrated with receptor **169** utilizing the threefold ammonium sulfonate/sulfate contact

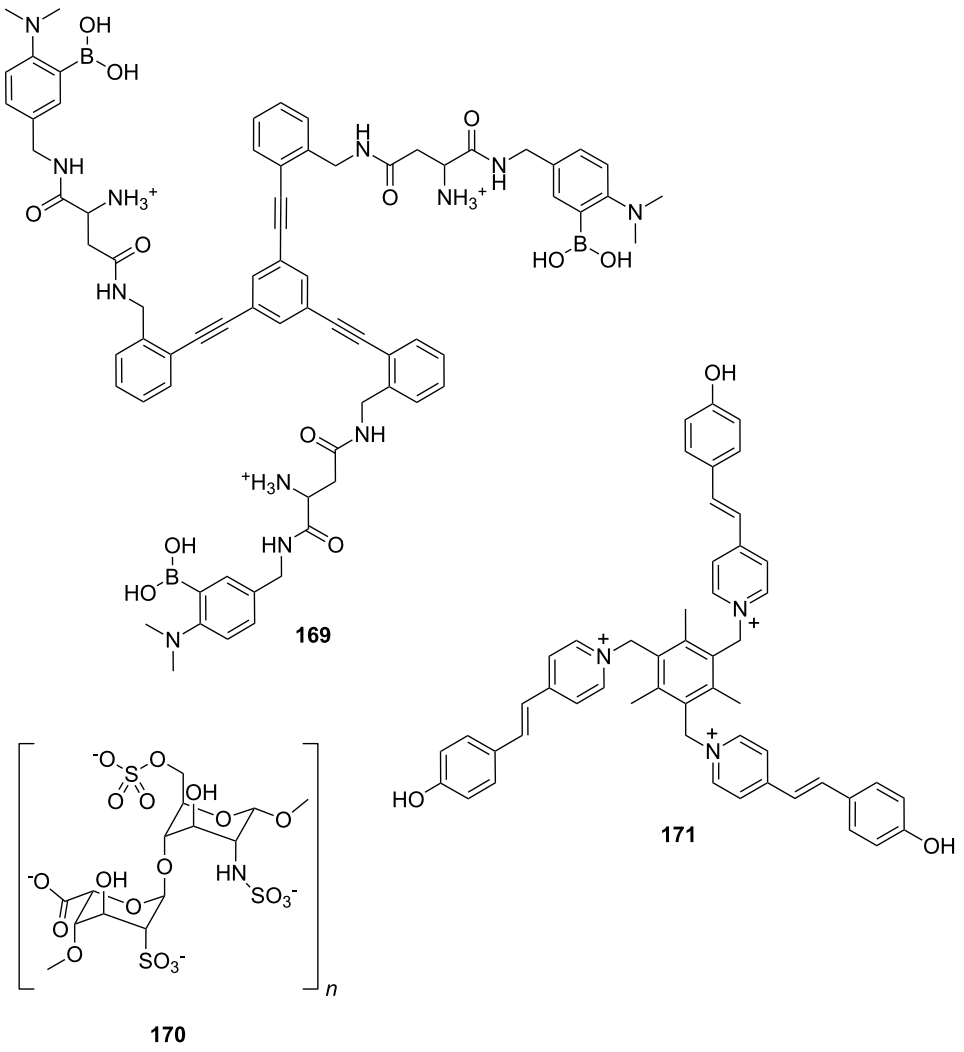

Figure 122: Different tripods and heparin (**170**).

to recognize heparin (**170**) [558] and bind it strongly with K_{ass} = 1.4 × 10^8 M^{-1} in 10 mM HEPES buffer [559].

Such a three-point co-ordinating cavity can better exclude solvent influences and enables recognition in strongly competitive solvent mixtures. For example, colorimetric discrimination between certain ω-aminoacids (H_3N^+–$(CH_2)_{n-1}$COOH) was achieved by the use of a chromogenic tripodal receptor functionalized with stilbazolium dyes (**171**) in mixed DMSO–water 90:10 v/v solutions [560]. UV-experiments revealed a preference for n = 4–6 (λ = 560 nm).

Quaternary ammonium ions can be co-ordinated entirely utilizing, for example, an additional cation–π-interaction with the third arm. The group of Ballester introduced squaramido rings as binding units in abiotic tripodal receptors (Figure 123), thus utilizing multiple O to C–H interactions [561]. This led to efficient receptors for tetraalkylammonium compounds such as choline (**76**), acetylcholine (**3**) and related ammonium salts. Association constants in the range 10^3 to 10^4 M^{-1} were determined by a ^{1}H NMR titration using a 1:1 model (**172e** vs. choline (**76**) hydroiodide in $CDCl_3$: K_{ass} = 14509 ± 1403 M^{-1}). The formation of intracavity complexes was supported by intermolecular cross peaks in 2D ROESY experiments. Complexation studies carried out in 10% MeOD-d_4/$CDCl_3$ mixtures gave association constants that were roughly 20–25 times weaker than in $CDCl_3$ alone, but the formation of the corresponding complexes was still evident.

The interaction with aromatic π-electron clouds plays an important role in the interaction of the synthetic NH_4^+ receptor (**173**) by Kim [128]. The cage like molecule (Figure 124) binds ammonium ions in addition by multiple hydrogen bonds and by cation–π-interactions.

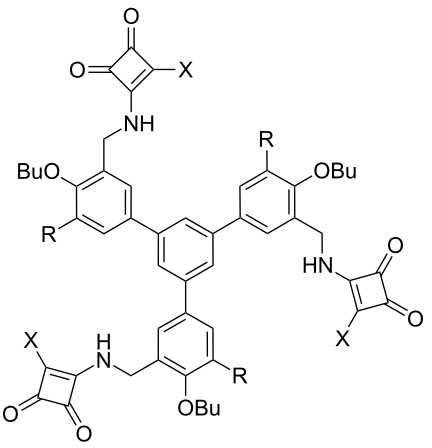

172a: R = H, X = Et_2N
172b: R = Pr, X = BnNH
172c: R = Pr, X = $HO(CH_2)_5NH$
172d: R = Pr, X = *p*-$Me_2NC_4H_6NH$
172e: R = Pr, X = *p*-$Me_2NC_4H_6$
172f: R = H, X = OEt
172g: R = Pr, X = OEt

Figure 123: Squaramide based receptors **172**.

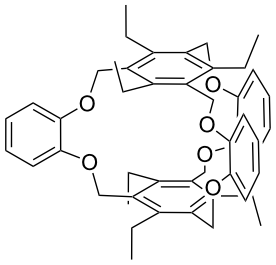

173

Figure 124: Cage like NH_4^+ receptor **173** of Kim et al.

The cavity has been calculated to be optimal for ammonium ions, but too large for lithium- and sodium ions. When used in ion selective electrodes, **173** showed a slightly higher detection limit (3.2×10^{-6} M) as the natural ammonium sensor nonactin (1.5×10^{-6} M) and an increased ammonium/potassium selectivity coefficient of log K $(NH_4^+)/(K^+) = -0.97$ (Nonactin: log K $(NH_4^+)/(K^+) = -0.88$). The binding constant of the ammonium ion determined by extraction experiments [188] was 3.3×10^7 M^{-1}.

Chin and co-workers synthesized 1,3,5-tri(3,5-dimethylpyrazol-1-ylmethyl)-2,4,6-triethylbenzene (Figure 125) in which the three pyrazole groups provide hydrogen-bonding sites [562]. In comparison to **173**, receptor **174a** shows an increased ammonium selectivity (log K $(NH_4^+)/(K^+) = -2.6$), but the binding constant, determined by extraction experiments [189], was lower ($K_{ass} = 1.4 \times 10^6$ M^{-1}). An ion selective electrode (ISE) incorporating this molecule showed improved ammonium ion over potassium ion selectivity as compared to nonactin (log K $(NH_4^+)/(K^+) = -2.6$), again illustrating the importance of hydrogen bonding and symmetry. This ionophore is pre-organized into the required tetrahedral geometry for complexing ammonium ions through hydrogen bonding involving the imine nitrogen atoms. The ethyl and methyl groups provide steric interactions to force the receptor into the desired geometry and to block the ligands from binding potassium ions. Despite its high selectivity for ammonium, the limit of detection for this ionophore is two orders of magnitude higher than for nonactin, and therefore, it is not sufficiently sensitive for some applications.

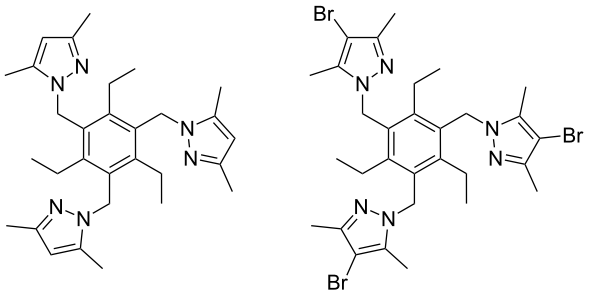

174a **174b**

Figure 125: Ammonium receptors **174** of Chin et al.

To lower the binding of water and thus increase the sensitivity of the receptor, electron withdrawing groups – bromine atoms – were introduced in the pyrazole rings of the receptor (**174b**) [563] (Figure 125). This modification did indeed lead to a far lower detection limit (2.5×10^{-5} M) for ammonium ions in an ISE, comparable to nonactin (2.2×10^{-5} M). The ammonium versus potassium selectivity of this receptor was strongly enhanced compared to the unbrominated heterocycle (log $K_{NH4+/K+} = -2.3$, nonactin log $K_{NH4+/K+} = -1.3$).

The further development of this structural motif, carried out by Ahn et al., led to an exchange of the weakly basic pyrazole ($pK_a \approx 2.5$) with the 2-oxazoline (Figure 126) of slightly higher basicity ($pK_a \approx 5$) [564].

The binding constants of the molecules **175a** – **d** towards ammonium and potassium ions were investigated by picrate extraction experiments [189] and were compared to the natural ammonium binder nonactin (Table 10).

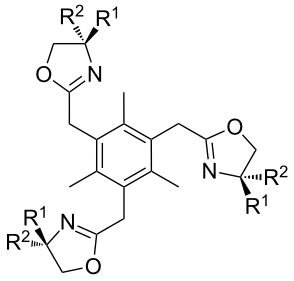

175a: R^1=R^2=H
175b: R^1=Me, R^2=H
175c: R^1=H, R^2=*i*Pr
175d: R^1=R^2=Me

176: R^1=H, R^2=Ph

Figure 126: 2-Oxazolin-based ammonium receptors **175a–d** and **176** by Ahn et al.

Due to these structural changes, the authors succeeded in further improving the binding constants (K_{ass} (**174**, NH_4^+) = 1.4 × 10^6, K_{ass} (**175b**, NH_4^+) = 2.5 × 10^7 M^{-1}) and enhancing the NH_4^+/K^+ selectivity from 398 to 437. Another advantage of oxazoline compared to the pyrazole substituents is the possibility of introducing chirality into the receptor. Ahn et al. have studied the binding of enantiomerically pure **176** towards a variety of guest molecules [565]. An increase in discrimination of the enantiomers of racemic molecules is represented by the presence of a hydrogen bridge acceptor in γ- or β-position to the ammonium ion. The authors rationalized this to the existence of a "bifurcated" H-bridge, which restricts the free rotation of the β-substituent. From ITC titration experiments in acetonitrile, the binding constants for the *R*- and *S*-enantiomers of **177a** were found to be 3.0 × 10^4 M^{-1} or 9.2 × 10^3 M^{-1}, respectively. The enantioselectivity of the extraction is 63:37 in favor of the *R*-enantiomer. The best selectivity found for **177b** (Figure 127) was 83:17, but only an extraction of <5% was possible due to the increased water solubility of **177b**.

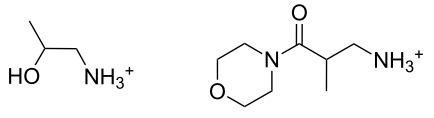

177a **177b**

Figure 127: Racemic guest molecules **177**.

Theoretical studies indicated such trisoxazolines are alternatives to azacrowns for binding and sensing of ammonium and alkylammonium ions [565-567]. The importance of the C_3 symmetry in chiral recognition has been pointed out [555]. Apart from Kubiks cyclo-hexapeptide (**233**) and the example **176** from Ahn et al. previously noted, there are only a few examples of enantioselective receptors for chiral ammonium ions with C_3 symmetry [554,568-571].

This receptor type is built by coupling the chiral binding arms to the achiral backbone in such a way that they can organize themselves around a potential guest in a predetermined arrangement. To obtain sufficient stereoinduction, the chiral elements and the donor groups have to be arranged close to each other. An alternative design of three-armed, C_3 symmetric receptors for enantiomeric discrimination is the use of chiral scaffolds to which achiral binding arms can be coupled. Here, the scaffold not only serves as a spacer but also pre-organizes the conformation of the binding arms, thus leading to an enantioselective discrimination of chiral guests.

Only recently Schnopp and Haberhauer described C_3 symmetric, imidazole-containing, macrocyclic peptides with different binding arms (Figure 128) that bind α-chiral primary organoammonium ions with up to 30,000 M^{-1} [572]. The binding constants and the selectivity ratios were estimated by standard ^{1}H NMR titration techniques in $CDCl_3$. The chirality of the backbone [573] and the selection of adequate receptor arms make these systems highly selective enantiodiscriminators. The receptors **178b** and **178c** showed opposite selectivities toward those organoammonium ions bound most strongly. With the isoquinoline receptor **178c**, it was possible to generate a C_3 symmetric receptor with a good selectivity ratio of 87:13 for (*R*)-PEA (**20b**). The obtained binding constants were 4500 M^{-1} for (*S*)-PEA and 30,000 M^{-1} for (*R*)-PEA (**20b**).

Titrations of (*R*)-PAM (**179a**) and (*S*)-PAM with **178b** resulted in values for K_{ass} of 16,000 M^{-1} and 1900 M^{-1}, respectively, thus reaching the high selectivity ratio of 90:10 [574]. A possible explanation for the enantioselectivity was deduced from the conformation of the complexes: They calculated the molecular structures of the energetically preferred conformers

Table 10: Binding constants and selectivity constants of the receptors **175a–d**.

	175a	**175b**	**175c**	**175d**	*Nonactin*
K_{ass} (NH_4^+) [M^{-1}]	5.1 × 10^6	2.5 × 10^7	9.4 × 10^6	3.9 × 10^6	2.0 × 10^8
K_{ass} (K^+) [M^{-1}]	3.0 × 10^4	5.7 × 10^4	2.4 × 10^4	5.7 × 10^4	6.7 × 10^7
K_{ass} (NH_4^+)/K_{ass} (K^+)	173	437	393	68	3

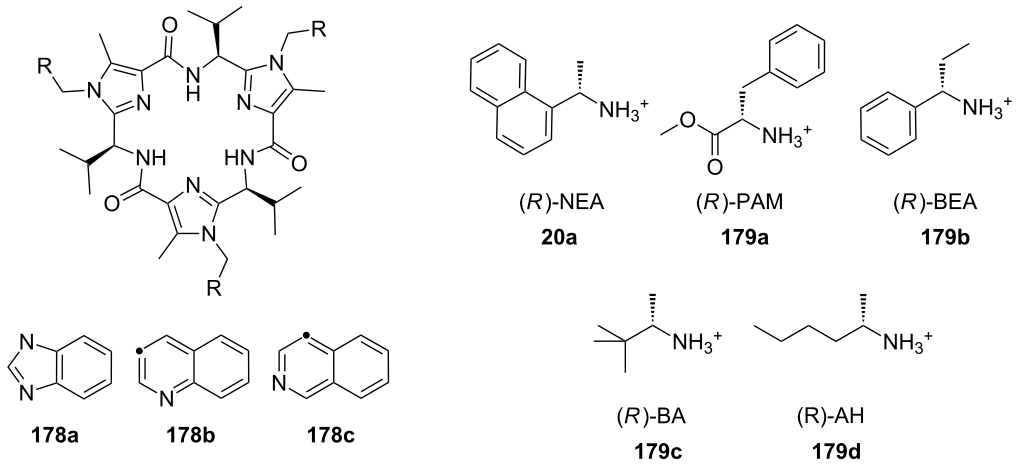

Figure 128: Tripods based on a imidazole containing macrocycle (**178**) and the guest molecules employed in the study (**20a**, **179a–d**).

of **178c** × (*R*)-PEA and **178c** × (*S*)-PEA by density functional theory (DFT) reproducing their observations in the theoretical model by finding a less favored conformation and higher steric repulsion for the complex with (*S*)-PEA.

The enantiopure C_3 symmetric *syn*-benzotriborneol **180** (Figure 129) revealed the capability to act as host for ammonium ions, and in particular, the efficient chiral recognition of the two enantiomers of (1-phenylethyl)ammonium chloride [575]. The rigid C_3 symmetric structure of triol **180** bearing three hydroxy groups on the concave side of the molecule, led to two fold better complexation capabilities of the triol *syn*-**180** with (−)-(1-phenylethyl)ammonium chloride ($K_{ass\ 1:1}$ = 230 M^{-1}, $K_{ass\ 1:2}$ = 2380 M^{-1}) with respect to the (+)-enantiomer ($K_{ass\ 1:1}$ = 120 M^{-1}, $K_{ass\ 1:2}$ = 1220 M^{-1}). The complexes were characterized in deuteriochloroform by means of ^{1}H NMR titrations. The Job's plots showed the clear formation of the 1:2 complex between the triol and the ammonium salt. The NMR titration experiments clearly showed that two different processes take place. The process that takes place at low concentrations is the complexation of the first ion pair whilst at high concentrations binding of a second ion pair for the reformation of the dimer present in solution occurs.

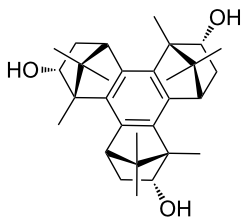

180

Figure 129: Ammonium ion receptor **180**.

5.4. Cyclophane structures for binding ammonium ions

Cyclophanes are well pre-organized macrocycles with several aromatic subunits [258], which usually have a large hydrophobic cavity capable of inclusion of neutral or positively charged guest molecules. Their binding properties and their solubility can be varied within a wide scope by introducing appropriate substituents.

Neutral aromatic guest molecules bind to cyclophanes over dispersive and π–π-interactions. In the complexation of organic cations the cation–π-interaction gives crucial contributions. Dougherty and co-workers [576-579] and the group of H. J. Schneider [580,581] proved cyclophane hosts to be suitable for recognition of quaternary ammonium salts: the positive charge of the guest interacts with attractive cation–π-interactions provided by the electron-rich surfaces of their aromatic rings. This fact was also verified by a theoretical study [582]. Such a charge-assisted NH–π-interaction was confirmed only recently [583].

Quaternary ammonium guests such as acetylcholine (**3**) and tetramethylammonium salts (TMA) are strongly bound mainly by cation–π-interaction [261,584-591]. Paraquat and its derivatives are also strongly included, also assisted by π–π-interaction [205,592].

Of equal importance to the properties of these cavities are their peripheral solubilising groups. Water-soluble derivatives especially have a great importance in the host–guest chemistry of cyclophanes. Water soluble cyclophanes are a well known class of receptors providing hydrophobic cavities of definite shape and size for inclusion complexes with various organic compounds in aqueous solution [593-595]. The hydrophobic effect

critically assists the co-ordination to ammonium compounds by strong inclusion of the non-polar part of the guest in the cavity [580,596] and plays an important role in the complex formation in general, i.e. the release of guest molecules from the solvation shell around host and guest [597]. In addition, competitive interactions of the H-bond donor water are reduced by the apolar shielding. The synthesis [598-601] and interactions [602] of cyclophanes with typical guest molecules have been described in numerous publications.

A series of oxa[3.*n*]paracyclophanes (Figure 130) was investigated with respect to their binding properties towards quaternary ammonium ions, namely tetramethylammonium and acetylcholine (**3**) with different counter ions in $CDCl_3$ by ^1H NMR titrations [603].

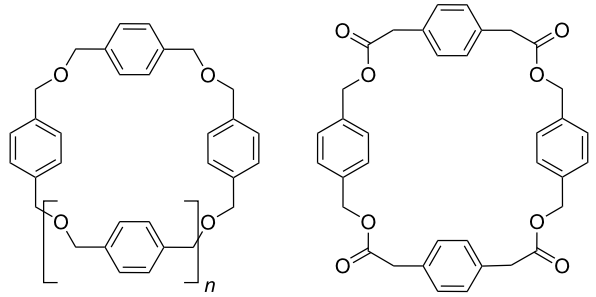

181a: *n* = 1
181b: *n* = 2
181c: *n* = 3
181d: *n* = 4
181e: *n* = 5

182

Figure 130: Tetraoxa[3.3.3.3]paracyclophanes **181** and a cyclophanic tetraester (**182**).

Association of **181a** with tetramethylammonium picrate (K_{ass} = 460 M^{-1}) was compared to the parent tetraester **182**, the corresponding cyclophanic tetraamine, the open-chain counterpart of **181a**, and its cyclo-oligomers from the pentamer (**181b**) to the octamer (**181e**). Binding enhancements ranging from 15-fold (with respect to the tetraester and the tetraamine) to over 80-fold (with respect to the open-chain tetraether) were observed. With the appropriate choice of the anion, i.e., with a poorly inhibiting counterion ($Me_2SnCl_3^-$), the association constant for tetramethylammonium is raised to the order of 10^3 M^{-1}, with a binding increase of over 400-fold with respect to the tetraester. Acetylcholine (**3**) was bound by **181a** with 440 M^{-1} (counterion $Me_2SnCl_3^-$) or 360 M^{-1} (picrate salt).

Many attempts have been made to create synthetic receptor molecules for catecholamines. Most of these are monotopic: for example, dopamine selectivity has been achieved with a pyrazole containing podand [604], a homocalix[3]arene triether [605], or with a sol–gel process [606].

Boronic acids have been used in ditopic receptors for molecular recognition of the catechol ring, as shown in the example above (**161**), by the systems of Glass et al. (**247**) and with related systems in literature [607,608]. In an alternative design, the catechol has been bound by a symmetric hydrophobic cavity with peripheral carboxylate groups for dopamine (**2**) recognition [609].

A cationic chiral cyclophane (Figure 131) was synthesized and studied as a host for chiral and racemic π-donor molecules. The cyclophane host **183** has a rigid binding cavity flanked by (*S*)-(valine-leucine-alanine) and *N,N*′-dibenzyl-4,4′-bipyridinium subunits, which allow for hydrogen-bonding and π-stacking interactions with included aromatic guest molecules [610].

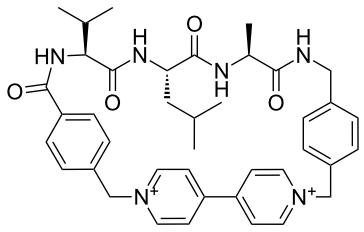

183

Figure 131: Peptidic bridged paraquat-cyclophane.

^1H NMR binding titrations were performed with several different pharmaceutically interesting guest molecules including β-blockers, NSAIDs, and amino acids and amino acid derivatives. The host–guest complexation constants were generally small for neutral and cationic guests (0–39 M^{-1} at 20 °C in water/acetone mixtures). However, an enantioselectivity ratio of 13 was found for dopamine (**2**), a strongly π-donating cationic guest. (*R*)-Dopamine showed the strongest association in 1:1 water/acetone (39 M^{-1}).

Two-dimensional NOESY ^1H NMR spectra confirm that (*R*)-dopamine binds inside the cavity of the host and that there is no measurable interaction of the cavity with (*S*)-dopamine under the same conditions.

All of these artificial host molecules are not biomimetic and not selective for catechol-amino alcohols. Schrader et al. studied the natural surroundings of such guest and published several approaches based on the imitation of the natural receptors.

In order to imitate the natural binding site, an artificial biomimetic adrenaline host should be able to provide – at least after an induced-fit process – a microenvironment with a shape complementary to the geometrical form of its guest. A high number of van der Waals contacts would help desolvation in water and lead to a strong hydrophobic attraction.

A shape-selective adrenaline-inspired host was investigated [611] (Figure 132). A number of closely related biogenic amines and amino alcohols were examined in a 1:1 mixture of water and methanol by NMR to check the selectivity of the new host molecule.

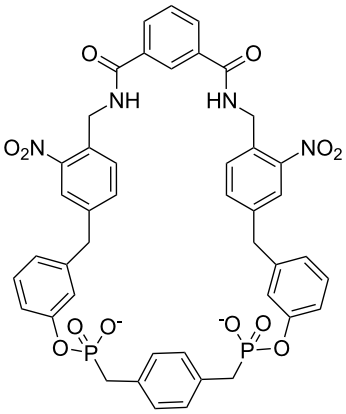

184

Figure 132: Shape-selective noradrenaline host.

Adrenaline (**80a**, K_{ass} = 153 M^{-1}), noradrenaline (**80b**, K_{ass} = 215 M^{-1}) and dopamine (**2**, K_{ass} = 246 M^{-1}) were stronger bound than 2-phenylethylamine (**78a**, 102 M^{-1}) and ethanolamine (54 M^{-1}). The binding constant for dopamine (**2**) in water is three orders of magnitude lower than that of the natural example (10^5 M^{-1}).

The small K_{ass} value of ethanolamine, which is half an order of magnitude below that of noradrenaline (**80b**), shows that the receptor molecule clearly recognizes the hormone's catechol ring. This is supported by the decrease in binding energy when the phenolic hydroxyl groups are missing from the guest structure (**78a**, 2-phenylethylamine).

All the effects discussed above confirm that the macrocyclic host **184** recognizes adrenaline derivatives in mixtures of water and methanol (1:1) by multiple non-covalent interactions including electrostatic attraction, hydrogen bonds, π-stacking, and hydrophobic forces.

The nitro-arene groups in the macrocyclic receptor molecule can undergo double π-stacking interactions with the catechol ring of adrenaline without producing any significant ring strain in the receptor molecule, whilst the isophthalic amide group is ideally pre-oriented to form hydrogen bonds to the phenolic OH groups.

Schrader et al. introduced a similar system **185** for the detection of adrenaline and related biologically important amines [612] (Figure 133). Various amines, such as ethanolamine and propranolol bind to the receptor in methanol with low selectivity. The values of the binding affinities vary between 700 and 1600 M^{-1}. However, the insertion of **185** into a monolayer of stearic acid at the air-water interface leads to selective noradrenaline (**80b**) binding (10^5 M^{-1}). The binding is monitored by changes in the pressure dependent surface area diagrams with the Langmuir film balance. The drastic change in comparison to solution is explained by the forced inclusion of the guests in the cavity of the receptor on the surface, and the formation of new hydrogen bonds between the NH of **185** and the phenolic oxygen of the noradrenaline. Other catecholamines do not show this effect.

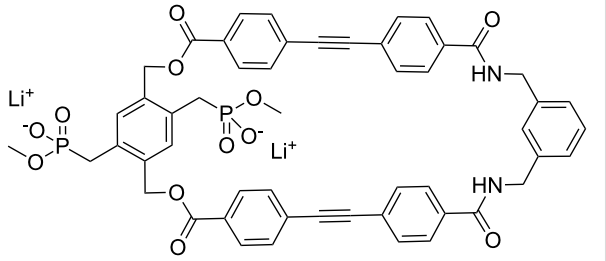

185

Figure 133: Receptor **185** for binding of noradrenaline on surface layers from Schrader et al.

A slight variation of the receptor, the introduction of a second bisphosphonate moiety (Figure 134), resulted in high affinity towards catecholamines in water, especially for structures with extended aromatic π-faces as found in many β-blockers (up to 7 × 10^3 M^{-1} for each single complexation step or 5 × 10^7 M^{-1} for both steps). Job's plot analyses showed a 2:1-stoichiometry, NMR titrations revealed no co-operativity in any case. For ease of comparison, the authors always used 1:1 association constants for each single binding step and varied the solvent polarity from pure methanol to methanol/water (1:1) to pure water. Here, the recognition profited from the amphiphilic structural design [613] and even more from the extensive self-association by the aromatic π-planes. Affinity and selectivity towards adrenergic receptor substrates was greatly enhanced if the receptor molecule **186** was transferred from water into a

lipid monolayer. Above the critical micelle concentration of 3 × 10^4 M, the host formed micelles that produce a favorable microenvironment for hydrophobic attraction of the ammonium alcohol by the phosphonate anions, combined with hydrophobic contributions between the aromatic moieties. Ionic hydrogen bonds with the polar OH or NH groups of the guest enforced the non-covalent interactions, and finally led to increased specificity. Especially β-blockers with minute structural changes can be easily distinguished from each other. A remarkable dependence of the 1:1 binding constant was revealed for noradrenaline. The binding amounts to 4000 M^{-1} in MeOD, fell to ~700 M^{-1} in MeOD/D_2O (1:1), but increased to 1200 M^{-1} in water.

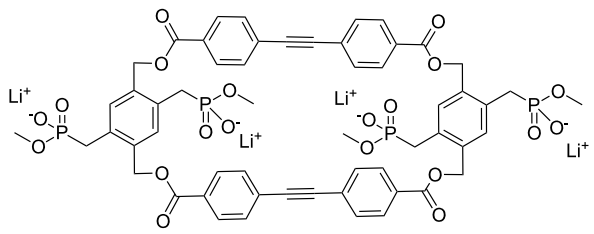

186

Figure 134: Tetraphosphonate receptor for binding of noradrenaline.

For further and more detailed discussion of the interesting topic of recognition of catecholamines with artificial receptors in aqueous solution, we refer the reader to a recent overview [614].

Bell's receptors **155** (Figure 112) can bind free arginine (**81d**) with a K_{ass} value of 900 M^{-1}, another binds lysine derivatives with a millimolar binding strength. The tetrasulfonate calixarene hosts (**84**) reach 1500 M^{-1} in borate buffer (see chapter 4); in calixarenes **92**, the phosphonate groups are responsible for the major contribution to binding and selectivity. Following these examples and the survey of molecules given above, this shows that by adding more phosphonate groups to a rigid scaffold, binding strength and selectivity are increased. Indeed, by virtually "dimerizing" clefts, cyclic moieties like cyclophanes result, which have suitable cavities and substitution patterns for a selective artificial ammonium ion receptor. These molecules bind strongly to bis-ammonium guests in even more polar solvents.

The further development of receptor **167** led to the tetraphosphonate (**187**) [615] (Figure 135). By doubling the number of phosphonate groups binding increases, so that the receptor can be used in water. X-ray analysis and molecular modeling revealed that the host adopts a favorable open conformation [616]. Typical stoichiometries with diammonium amino acids are 1:2; only lysine (**81c**) forms a 1:1 complex. Table 11 summarizes the results.

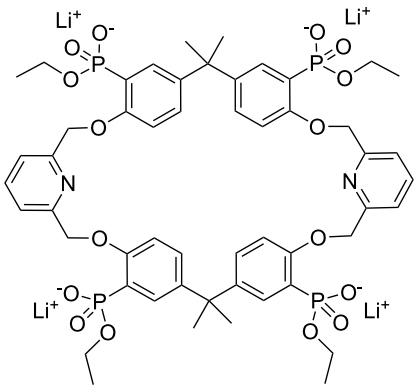

187

Figure 135: Tetraphosphonate **187** of Schrader and Finocchiaro.

Table 11: Binding constants for the complexes of **187** with different amino acids.

Amino acid (dihydrochlorides)	K_{ass} [M^{-1}] (methanol)	K_{ass} [M^{-1}] (water)	Receptor: guest stoichiometry
His	29000	650	1:2
Orn	9500	221	1:2
Arg	8800	165	1:2
Lys	21000	1200	1:1

In methanol all amino acids are bound strongly in a double chelate binding mode. The exceptionally good binding of histidine (**81e**) is explained by a chelate complex, which includes both imidazole nitrogen atoms in addition to the amino acids ammonium functionality. From methanol to water, the stoichiometry of all complexes is retained, but a 20–50 fold drop is observed in the association constants of the four investigated amino acids attributed to the competition of the water molecules. Lysine (**81c**) is complexed 5–7 times more strongly than ornithine and arginine (**81d**) and even twice as strongly as histidine (**81e**). The contribution of hydrogen bonds in water is negligible, while electrostatic interactions represent the major attractive force. It is known, that in this respect the hard ammonium ion with its high charge density is superior to the softer guanidinium and also the imidazolium ion, where the positive charge is delocalized across several atoms [617]. The electrostatic attraction exerted by the second ammonium functionality of lysine (**81c**) is stronger than that of arginine's guanidinium ion and even histidine's imidazolium ion. In addition, lysine (**81c**) is in the position to undergo a four-point inter-

action in its complex with **187** which is stronger than the two-point interaction in the related assemblies with ornithine and arginine (**81d**).

Charged clefts have previously been discussed. A similar class, quite related to the hosts presented in this chapter are cavitands or macrocycle bearing phosphate and phosphonate groups. The negative charged phosphorus derivatives are closely comparable to the carboxylate residues mentioned above. In combination with cavitands structures and/or molecular clefts e.g. tweezer backbones, they are employed with great benefits for ammonium ion recognition.

Extensive hydrophobic interactions with a self-associated or self-organized microenvironment and utilising a combination of van der Waals interactions and substantial electrostatic contributions for locking of the guest are responsible for the observed high efficiency and specificity found in clefts and cavitands. Often electrostatic interactions contribute most to the stabilization energy in the complexes. In larger cavities the loss of one hydrogen bond can be overcompensated by, e.g., hydrophobic interactions. Optimized host structures implementing elements of much higher rigidity can achieve more effective pre-organization and desolvation.

In summary, C_{3v} symmetric tripods, tweezer ligands and pre-organized molecular clefts reach selectivities and affinities in ammonium ion binding which compete with naturally occurring recognition motifs such as nonactin or valinomycin [618].

6. Porphyrins and other metal complexes for ammonium ion recognition

In this part of the review we will discuss ammonium ion recognition involving metal complexes. Metal complexes are important binding sites for amines, but have even more extensively been used for amino acid recognition. In fact, the following examples typically involve simultaneous binding of ammonium and carboxylate ions. Discussion of amino acid zwitterion binding by metal complexes has been added to supplement our survey, although ammonium ion recognition is only part of the binding process.

6.1. Porphyrins

Porphyrins and their metal complexes play a fundamental role in a variety of biological processes, for example, the chlorophylls as photoreaction centres in photosynthesis, haemoglobin as the oxygen carrier in blood and myoglobin for oxygen storage in muscles, cytochromes in electron-transfer processes in respiration or as important prosthetic groups and coenzymes as found in vitamin B12 [619]. They have been employed as electroactive materials for molecular electronics [620], effective photosensitizers [621] for photodynamic therapy or as supramolecular building blocks for energy conversion devices [622] and dye sensitized solar cells [623]. The synthesis and properties of porphyrins and related compounds, such as porphycenes or texaphyrins, have been extensively reviewed in several books and articles [619,624,625].

Porphyrins have been widely used for the recognition of various guest molecules [626-629]. Two reviews on their general properties and recognition scope have been published [630,631]. Articles on the related porphyrinoid [632,633], and chiral multifunctional porphyrins [634] have been reviewed. We will focus in the following section on examples of porphyrin based receptors for amines or ammonium ion recognition.

Zinc porphyrin receptors bearing 12 ester groups in the meso phenyl groups [635] and the corresponding water soluble potassium carboxylates [636] (Figure 136) are selective receptors for amines, amino acid esters and oligopeptides as demonstrated by UV–vis experiments in dichloromethane and buffered aqueous medium. Using small substituents as in **188a** or the unsubstituted parent compound, butyl ammonium chloride or phenethylamine hydrochloride (up to 52700 M^{-1} in dichloromethane) bind with highest affinity. The ester groups of **188a** assist the binding of aromatic *R*-amino esters (K_{ass} = 8000–23000 M^{-1}) in this medium and inhibited the binding of bulky aliphatic *R*-amino esters (K_{ass} of 460 M^{-1} for Leu-OMe). This indicated that CH–π-type interactions and steric repulsions control the selectivity. The corresponding salts **189** showed a good selectivity for binding of hydrophobic guests: **189c** binds Trp-OMe or pyridine in water with binding constants of 7000–8000 M^{-1}. These anionic zinc porphyrins bind histamine (**1**) and a histidine-containing oligopeptide even more tightly. The highest binding strength for histamine was found for **189a, 189b** and **189c** in pH 8 buffer with binding constants of 157000,

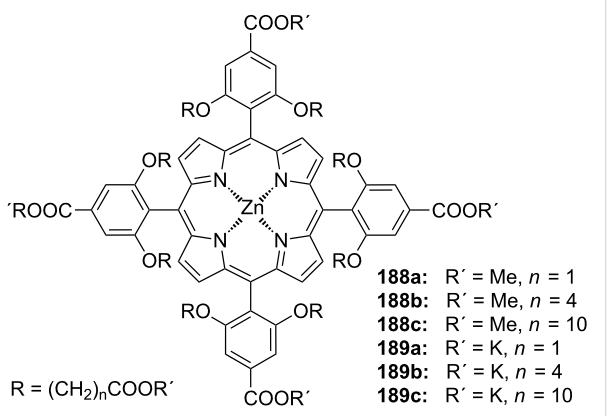

Figure 136: Zinc-Porphyrin ammonium-ion receptors **188** and **189** of Mizutani et al.

31000, and 18200 M^{-1}, respectively. Co-ordination of the imidazole to the zinc centre and a significant electrostatic interaction between the ammonium group of histamine and the carboxylate groups of receptor stabilizes these complexes. In a series of amino acid esters, receptor **189a** co-ordinated best to the cationic Arg-OMe, with an enthalpically driven binding of 11000 M^{-1}. Strong dependence of the binding affinity on ionic strength and pH revealed that electrostatic interactions between charged functional groups are an important driving force for recognition of hydrophilic guest molecules in water. Comparisons of binding affinity between hydrophilic receptor **189a** and hydrophobic receptor **189c** revealed that the hydrophobic binding pocket of **189c** enhanced the affinity in water towards hydrophobic guests. A lower affinity of the receptors in methanol-water than in water indicated that water plays a significant role in binding energetics.

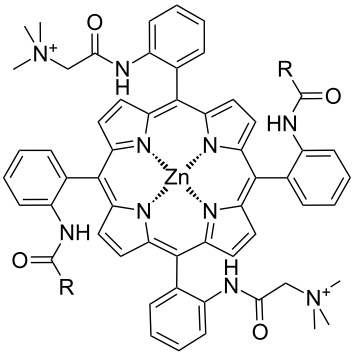

190a: R = Ph
190b: R = ^{t}Bu

Figure 137: Zinc porphyrin receptor **190**.

Imai et al. also employed highly charged water-soluble zinc porphyrins (Figure 137). With an ammonium group and a phenyl or tertiary butyl group above each porphyrin plane, they recognize amino carboxylates in aqueous solution [637]. Binding constants were determined spectrophotometrically in aqueous carbonate buffer at pH = 10.4 and revealed the maximum binding strength for *rac*-tryptophan (**81b**) with 1000 M^{-1} for **190a** and 830 M^{-1} for **190b**. The authors suggest a three point recognition for amino carboxylates by co-operative co-ordinative, coulombic, and hydrophobic interactions.

The binding of amino acids to water-soluble zinc porphyrins in basic aqueous solution was spectrophotometrically analyzed with similar receptors (**191**) [638] (Figure 138). The amino acids were bound to the porphyrins through the co-ordination of the N atom with the central zinc ion. Additional stabilization of the aggregate comes from coulombic interactions between the $–COO^–$ anion of the amino acids and the $–N^+(CH_3)_3$ cation of the porphyrin substituents, and the hydrophobic interactions between the porphyrin plane and the hydrophobic substituents of the amino acids. In the study, the binding of amino acids (10^2 M^{-1}) is apparently stronger than that of aminoethanol (10 M^{-1}), due to additively co-operated coulombic interaction between the cation substituent(s) of porphyrins and the carboxylate anion of amino acids. This explanation is supported by the fact that the K_{ass} values increase as the number of possible coulombic interactions increases: the K_{ass} values for amino acids for **191a** and **191b** are approximately two times larger than those for **191c**, and the binding of *S*-Asp ($K_{ass,191a}$ = 780 M^{-1} and $K_{ass,191b}$ = 770 M^{-1}) and *S*-Glu ($K_{ass,191a}$ = 390 M^{-1} and $K_{ass,2}$ = 540 M^{-1}) is enhanced compared to that of Gly ($K_{ass,191a}$ = 110 M^{-1} and $K_{ass,191b}$ = 150 M^{-1}). Co-ordination of the aromatic amino acids Phe ($K_{ass,191a}$ = 320 M^{-1} and

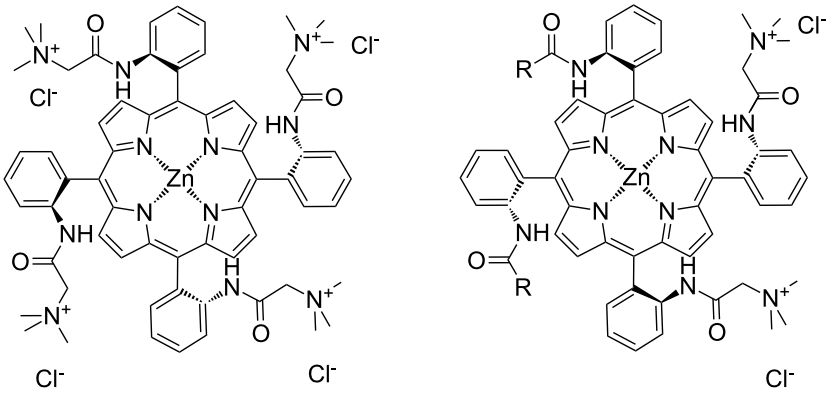

191a

191b: R = $CH_2N(CH_3)_3^+$ Cl^-
191c: R = ^{t}Bu

Figure 138: Zinc porphyrin receptors **191** capable of amino acid binding.

$K_{ass,191b}$ = 180 M^{-1}) and Trp ($K_{ass,191a}$ = 1300 M^{-1} and $K_{ass,191b}$ = 770 M^{-1}) is strengthened by hydrophobic interactions between the phenyl or indole group of the amino acids and the porphyrin plane, which is also supported by observations of the relevant peak shifts by ^{1}H NMR in Na_2CO_3 buffered D_2O.

The coulombic interactions between dipeptides and porphyrins are comparable to those between amino acids and porphyrins. The K_{ass} values of Gly-*S*-Phe ($K_{ass,191a}$ = 200 M^{-1} and $K_{ass,191b}$ = 340 M^{-1} and $K_{ass,191c}$ = 240 M^{-1}) and Gly-*S*-Trp ($K_{ass,191a}$ = 770 M^{-1} and $K_{ass,191b}$ = 1100 M^{-1} and $K_{ass,191c}$ = 780 M^{-1}) are larger than those of Gly-Gly (K_{ass} ~ 100 M^{-1}), indicating that the interactions between these dipeptides and the porphyrins are similar to those between *S*-Phe and *S*-Trp and porphyrins.

The molecular recognition of amino acid esters in $CHCl_3$ was investigated by UV–vis titration with *S*-tyrosine- [639] and *S*-threonine [640] substituted chiral zinc porphyrins (**192**). The association constants of the molecular recognition reactions were all $K_R > K_S$ and followed the order of *K*(PheOMe) > *K*(LeuOMe) > *K*(ValOMe) > *K*(AlaOMe) in host **192a** and *K*(ThrOMe) > *K*(LeuOMe) > *K*(ValOMe) > *K*(AlaOMe) > *K*(PheOMe) in host **192b**. All the results are summarized in Table 12.

A significant contribution of π–π-interaction can be observed for the binding of phenylalanine (**81a**) to receptor **192a**, as is also evident by comparison to the second system with a threonine side chain (**192b**) (Figure 139). Here the binding constant for the aromatic amino acid is the lowest in the series.

Circular dichroism spectra were used to explain chiral molecular recognition. It was found that chiral recognition arose mainly from the chiral matching between host and guest. The enthalpy–entropy compensation relationship revealed a significant conformational change during the process of chiral recognition. The induced CD spectra of the complexes exhibited characteristic Cotton effects. The authors proposed that the induced CD spectrum was caused by the coupling between the electric transition moment (the π–π*-transition) of the carbonyl group in Boc-*S*-Tyr side chain and that of the porphyrin. The molecular recognition process of this host–guest system was confirmed by quantum chemical methods. The result was a structure where the *R*-enantiomer was more tightly bound with a better steric fit to the host than its enantiomer. By comparison minimal energy conformations, it was evident that host *R*-AlaOCH$_3$ has lower energy than host *S*-Ala-OCH$_3$, indicating that the former was more stable than the latter.

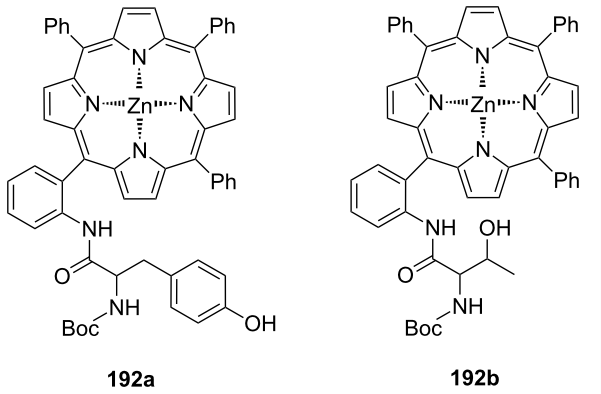

Figure 139: Zinc-porphyrins with amino acid side chains for stereoinduction.

Porphyrin dimer- or tweezer-systems have been successfully used to determine the stereochemistry of chiral amines [641,642], alcohols [643,644] and carboxylic acids [645-647].

The principle advantage of the porphyrin tweezer system resides with the non-covalent binding of the chiral guest and the

Table 12: Binding constants and enantiomeric distinction factors of chiral porphyrin-amino-acid dipeptide receptors in chloroform at 20 °C.

Guest	K_{ass} [M^{-1}], **192a**	K_R/K_S	K_{ass} [M^{-1}], **192b**	K_R/K_S
S-Ala-OMe	320	1.4	155.2 ± 12	3.1
R-Ala-OMe	450		488.6 ± 20	
S-Val-OMe	621	1.2	175.2 ± 10	2.9
R-Val-OMe	713		502.2 ± 15	
S-Leu-OMe	1030	1.2	179.8 ± 13	4.9
R-Leu-OMe	1290		881.5 ± 22	
S-Phe-OMe	679	2.2	420.7 ± 10	1.1
R-Phe-OMe	1490		442.3 ± 10	
S-Thr-OMe	n.d.	n.d.	537.6 ± 15	2.6
R-Thr-OMe	n.d.		1391.3 ± 25	

stereoinduction by the two asymmetrically linked metal-co-ordination centres.

Crossley and his co-workers have reported a bis-zinc(II)-bis-porphyrin Tröger's base analogue (**193**) (Figure 140) as a host molecule for diamines [648] and for the chiral recognition of histidine and lysine esters [649]. The X-ray crystal structure of the analogous palladium bis(tetraphenylporphyrinato) complex reveals a concave chiral cavity with two metal ion binding sites suitable for ditopic interactions with guest molecules.

Several α,ω-diamines (H_2N–$(CH_2)_n$–NH_2) are strongly co-ordinated with a certain preference for n = 2–4 and K_{ass} ~ 2 × 10^8 M^{-1} as measured by spectrophotometric titrations in toluene. With increasing chain length, the affinity starts to decrease with K_{ass} ~ 6.1 × 10^7 M^{-1} and K_{ass} ~ 3.7 × 10^7 M^{-1} for 1,5-diaminopentane and 1,6-diaminohexane, respectively. Monoamines, such as hexylamine are less strongly bound (K_{ass} ~ 5.1 × 10^4 M^{-1}).

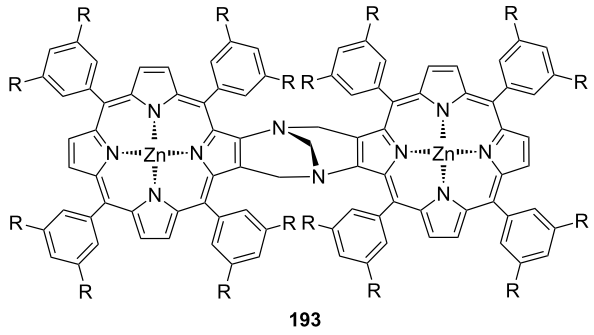

Figure 140: Bis-zinc-bis-porphyrin based on Tröger's base **193**.

The tweezer can be resolved on a small scale by chromatography on a silica – *S*-histidine benzyl ester support [650]. Resolution of the bisporphyrin Tröger's base analogue **193** affords homochiral clefts that tightly bind histidine esters with 80–86% *ee* and lysine benzyl ester with 48% *ee*. The histidine esters are bound in fixed conformations that can be readily detected by ^{1}H NMR spectroscopy as a result of the large dispersion of proton resonances by the ring currents of the two porphyrins. The binding constants are in the same order of magnitude as observed previously for diamines.

A zinc porphyrin dimer (**194**) linked by the chiral 1,1′-binaphthyl derivative (Figure 141) shows a size specific interaction with α,ω-diamines (H_2N–$(CH_2)_n$–NH_2) [651]: The zinc complex binds α,ω-diamines H_2N–$(CH_2)_n$–NH_2 (n = 6, 8, 10, 12; K_{ass} = 5 × 10^5–2 × 10^6 M^{-1} in CH_2Cl_2) with preference for n = 6 and 8. Shorter guests such as ethylenediamine or monoamines such as *n*-butylamine gave binding constants (K_{ass} ~ 3 × 10^3 M^{-1}) comparable to the co-ordination of alkylamine guests to the corresponding zinc porphyrin monomer (K_{ass} = 2.2 × 10^3 M^{-1}). These complexes gave characteristic CD spectra due to exciton coupling of the two zinc porphyrins. Their

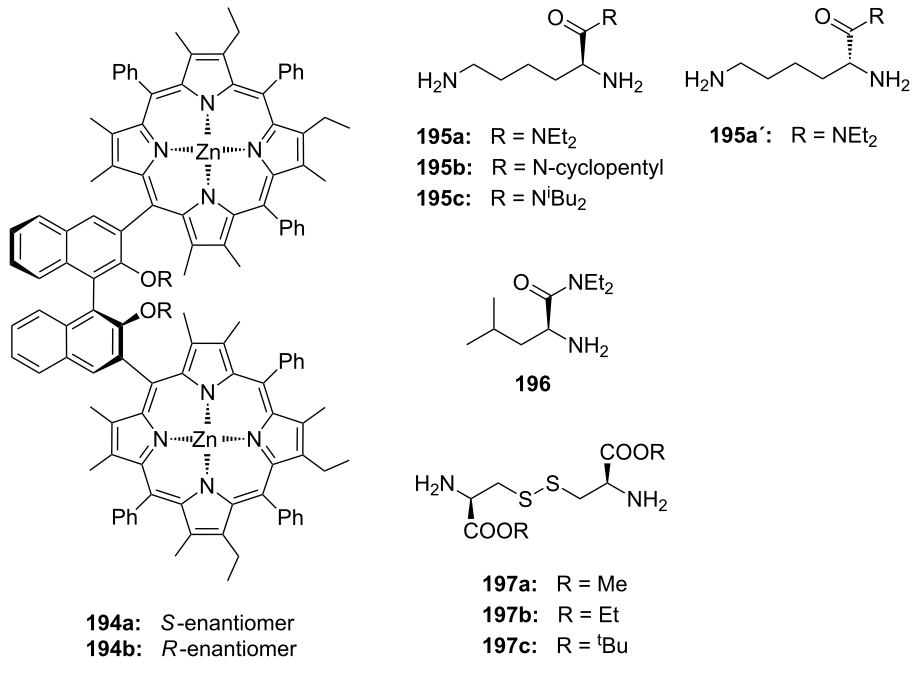

Figure 141: BINAP-zinc-prophyrin derivative **194** and it's guests.

intensity depends on the length of diamine. The CD spectrum in the complex reflects the angle and flexibility of the chiral twist between two zinc porphyrin units.

The chiral zinc porphyrin dimer linked by (*R*)-2,2′-dimethoxy-1,1′-binaphthyl (**194**) (Figure 141) not only tightly binds diamines via a zinc–nitrogen co-ordinated ditopic interaction, it displays a prominent enantioselectivity for several lysine derivatives (Table 13) [652]. The enantioselectivity obtained is one of the best for chiral zinc-porphyrin recognition systems. In particular, the D/L selectivity is determined to be 11–12 for lysine derivatives, as also demonstrated by CD-spectroscopy.

Table 13: Binding constants and enantiomeric distinction factors for chiral porphyrin-dimers **194** in dichloromethane.

Host	Guest	K_{ass} [M^{-1}]	K_S/K_R
(*S*)-**194**	**195a**	160000	12
(*R*)-**194**	**195a**	13000	
(*S*)-**194**	**195a′**	14000	11
(*R*)-**194**	**195′**	150000	
(*S*)-**194**	**195b**	120000	8.6
(*R*)-**194**	**195b**	14000	
(*S*)-**194**	**195c**	120000	11
(*R*)-**194**	**195c**	11000	
(*S*)-**194**	**196**[a]	1200	1.2
(*R*)-**194**	**196**[a]	980	

[a]for 1:1 complex formation.

Two different achiral hosts (Figure 142) were investigated for their binding properties to the same guests in the course of the study. Titration in dichloromethane monitored by UV–vis titration demonstrated a 1:1 complexation between the zinc-porphyrin dimers and the amino acid derivatives **195** and **197**. Compared to **198a** (K_{ass} for **195** = 1–8 × 10^5 M^{-1}, K_{ass} for **197** = 1–4 × 10^5 M^{-1}), the zinc porphyrin dimer **198b** has higher affinity for cysteine derivatives. The binding constants of **198b** for **197a** and **197b** were determined to be 1.7 and 2.4 × 10^6 M^{-1}, respectively. The length of both amine-guests almost fits the Zn-to-Zn distance, leading to the strongest binding, consistent with the former study of **194** versus diamines. The other values range from 3 to 5 × 10^5 M^{-1}. The achiral zinc porphyrin dimers linked by a biphenyl unit exhibit a significantly induced CD in the Soret region in the presence of chiral diamines such as lysine amides and cysteine diesters, indicating that the chirality of the amino acid derivatives can be monitored by complexation to the achiral zinc-porphyrin dimer.

Kubo et al. developed a bis-porphyrinic system coupled with biphenyl-20-crown-6 as an allosteric spacer [653,654]. The

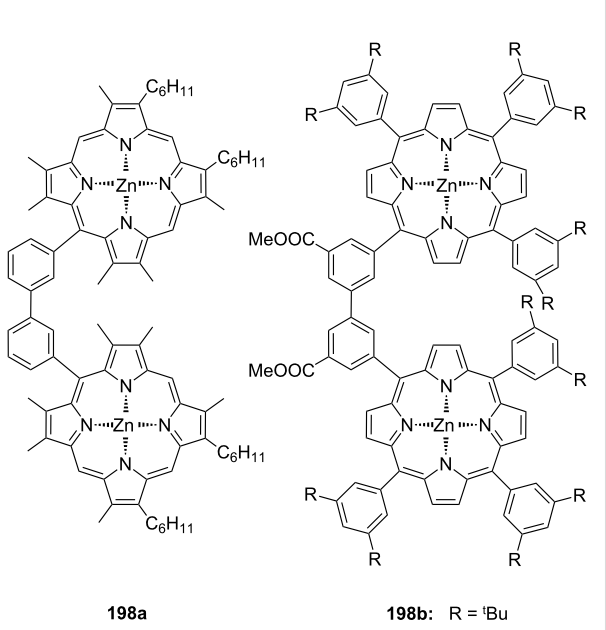

Figure 142: Bisaryl-linked-zinc-porphyrin receptors.

biphenyl unit is connected by a rigid spacer to the two porphyrins and bridged with a crown-ether (Figure 143). The porphyrin centre-to-centre distance can be switched by Ba^{2+} ion complexation in the crown-ether cavity. In its concave conformer, **199** can bind a diamine guest, such as 1,4-bis(3-aminopropyl)piperazine (**200a**). UV–vis titration in CH_2Cl_2/CH_3CN 9:1 confirmed 1:1 complex formation and a binding constant (K_{ass}) of 7.9 × 10^5 M^{-1}. In addition, the chiral bis-amino guest Tröger's base **200b** was used to probe an anti-cooperative binding event. Due to the axial chirality, **199** existed as two chiral atropisomers that rapidly interconvert at room temperature as evidenced by CD measurement. The binding of the chiral base transferred its chirality to the host upon complexation.

Another example from the same group also demonstrated this for the chiral induction with a crown-ether bis-zinc-porphyrin combination (**201**) (Figure 144). Upon complexation of a chiral sodium carboxylate by the flexible dibenzo-30-crown-10 ether, the topology was changed into a tweezers-like structure [655] and gave a ditopic chiral guest binding site. Circular dichroism (CD) spectroscopy revealed a chiral screw conformation, which interacted with various chiral diamines, for example, *N*,*N*-dimethylcyclohexane-1,2-diamine.

This chiral induction by a ditopic bound guest was employed to determine the absolute configurations of diamines, amino acids and amino alcohols by exciton-coupled circular dichroism (ECCD).

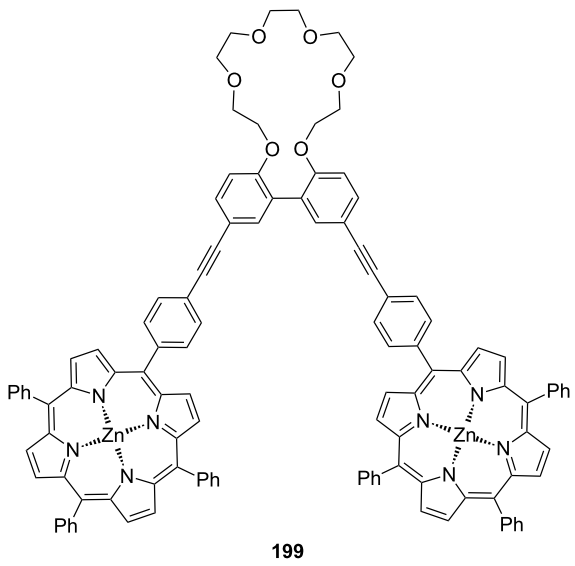

Figure 143: Bis-zinc-porphyrin **199** for diamine recognition and guests.

The achiral chromophoric host porphyrin tweezer **202a** [641] or its electron deficient fluorinated analogue **202b** [656] (Figure 145) both bind to an acyclic chiral diamine through nitrogen/zinc co-ordination to form a macrocyclic host guest complex with a CD spectrum, that reflects the absolute configuration of the diamine. The exhibited exciton-coupled bisignate CD spectra reveal predictable signs based on the substituents at the chiral centre. The absolute stereochemical determination of both *threo* and *erythro* systems without the need for chemical derivatization is thus possible.

This method can be extended to amino acids and amino alcohols after simple chemical modifications. With the fluorinated system **202b**, the absolute configurations of *erythro* and *threo* diols could be also effectively determined. Binding of diols to the porphyrin tweezer system is greatly enhanced by increasing the Lewis acidity of the metalloporphyrin by the strong electron withdrawing effect of the fluorine substituents.

The binding constants to amino- and hydroxy-functionalities were determined for the monoesters (**203**) by UV–vis titration. For isopropanol as the guest K_{ass} = 2140 and 50 M^{-1} and for isopropylamine K_{ass} = 473000 and 11400 M^{-1} are observed for the fluorinated porphyrin **203b** and the triphenyl substituted compound **203a**, respectively.

A [3]rotaxane and its copper complex (**204**) have recently been presented as a binding concept [657] (Figure 146). The properties of the system were investigated by UV spectroscopy in toluene. The complexes were also investigated and assigned by NMR DOSY experiments. In these two states of the [3]rotaxane, free and complexed with copper, the two zinc(II)

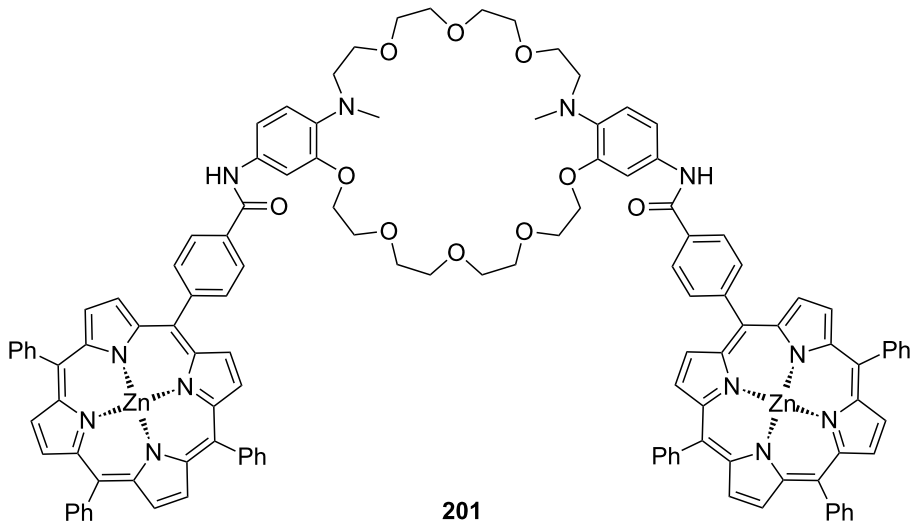

Figure 144: Bis-zinc-porphyrin crown ether **201**.

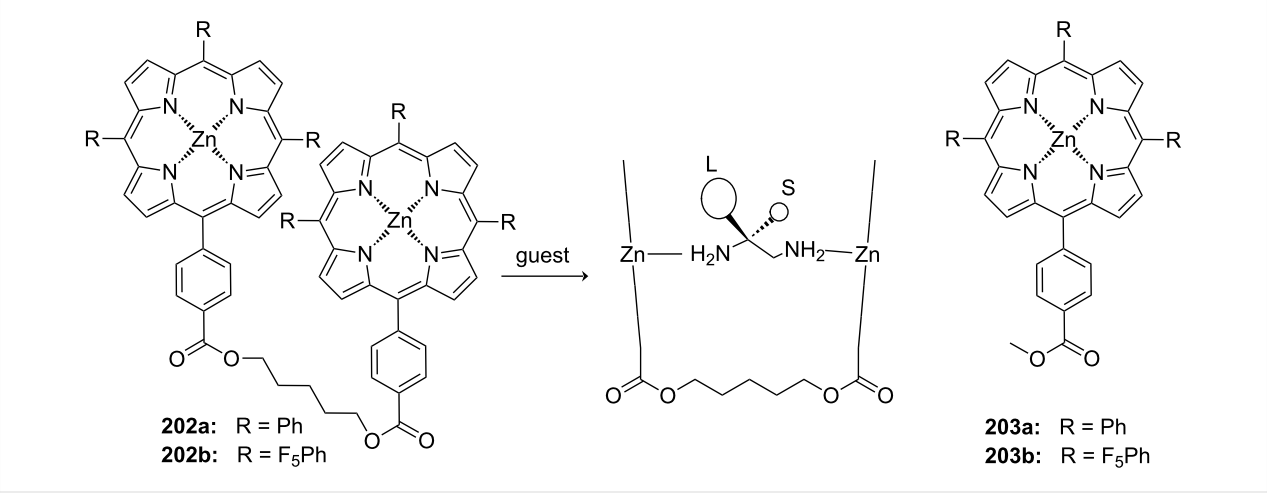

Figure 145: Bis-zinc-porphyrin **202** for stereodiscrimination (L = large substituent; S = small substituent).

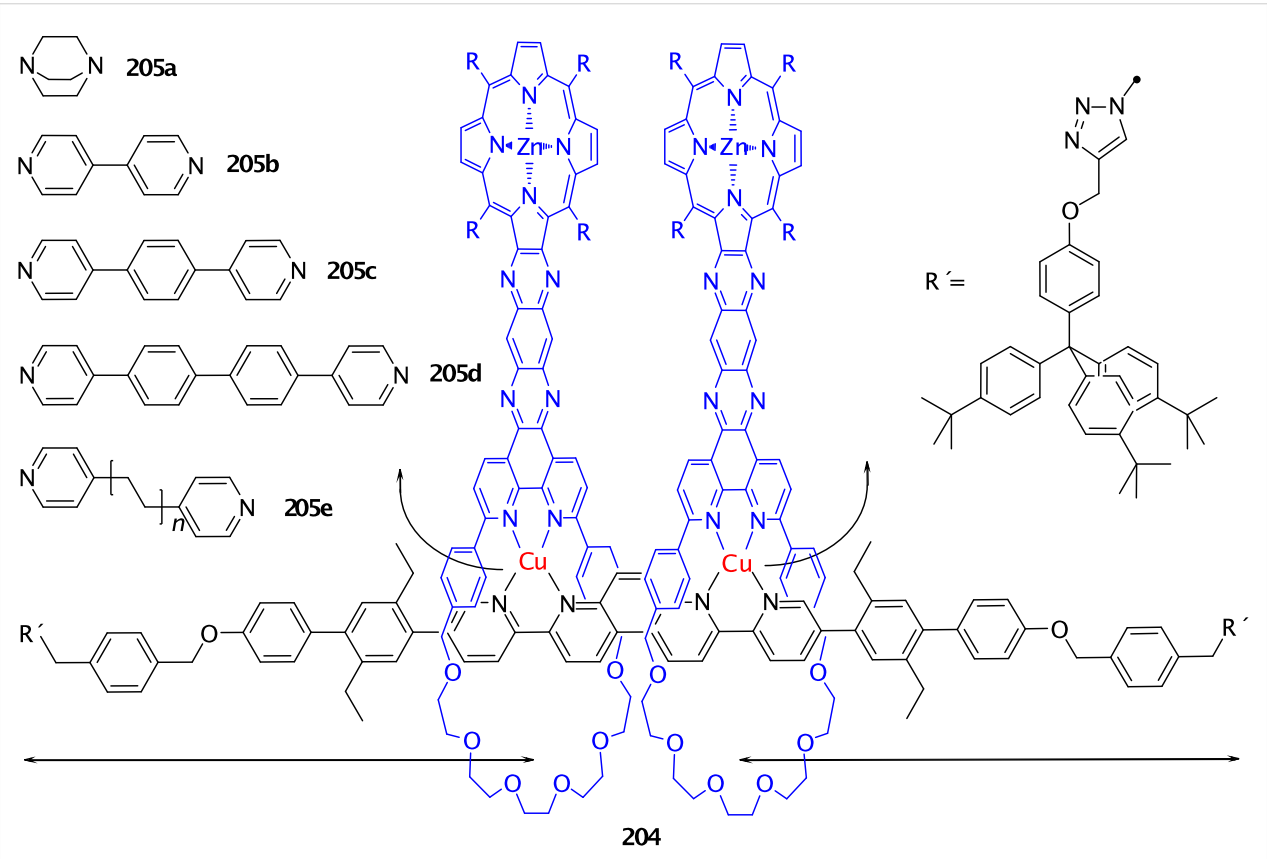

Figure 146: Bis-zinc-porphyrin[3]rotaxane and its copper complex and guests.

porphyrins attached to the rings can bind different ditopic guests bearing pyridyl groups or amines as terminal functions.

Removal of the two Cu(I) cations releases the two rings which are now free to move along and around the thread. The metal-free [3]rotaxane is a new type of receptor by which guests of very different sizes can be trapped between the two mobile porphyrins since they can move over an 80 Å plane-to-plane distance on the thread. It is both a strong and highly adaptable receptor with high stability constants for the host/guest complexes, log K_{ass} being in the range of 6.3 to 7.5 for guests between 2.8 and 18 Å.

In the copper-complexed [3]rotaxane, the rings are fixed by co-ordinative bonds to the rod and the distance between the porphyrins is therefore controlled to a certain extent, leading to destabilization of the host/guest complex with long guests, due to distortions on both the guest and the porphyrin rings. The copper-complexed [3]rotaxane is a good receptor for small guests with preference for **205c** (log K_{ass} = 7.5) due to an entropic gain for this pre-organized molecule compared to the free [3]rotaxane.

6.2. Other metal complex centres

Due to their strong complexing ability, many other co-ordinatively unsaturated metal complexes, can be employed as suitable potential binding sites for synthetic receptors, especially for molecular recognition in protic solvents [658]. Non-covalent forces are weakened in this medium with high dielectric constant, since a large number of solvent molecules interfere. The selection of the ligands is defined by the ability of their corresponding transition metal complexes to reversibly and tightly bind Lewis basic guest molecules in competing solvents, such as water. Amino acids are strongly bound by their side chains or in a bidentate complex bridging the metal. Complexes of cyclene, cyclam and related structures are widely used. The recognition with aza macrocycle complexes was recently reviewed [659].

Amino acids can be targeted by co-operative chelation between the carboxylate and the amine: The co-ordination of metal ions through the amino and carboxyl groups gives five-membered metallocycles [660]. Bipyridines (bpy) or nitrilotriacetic acid (NTA) are widely used as ligands. A typical example are [Cu(NTA)]-complexes, which co-ordinate amino acids [661,662]. Binding affinities have been determined for a variety of amino acids in aqueous medium (Table 14). The co-ordination of His to [Cu(NTA)] is a special case, containing mixtures of species in which His is co-ordinated either as an anion or in its zwitterionic form [663].

Table 14: Binding constants of amino acid guests to Cu[NTA].

Amino acid	log K_{ass}[a]
Gly	5.44
Ala	5.42
Phe	4.99
Leu	5.35
Val	5.10
β-Ala	4.56
His	4.16 (monodentate) 5.73 (bidentate)

[a]Standard deviation <0.01; at 25 °C.

Bis-dien bis-copper complexes of ligand **206** (Figure 147) bind imidazole as bridging ligand between two Cu(II) ions with the simultaneous extrusion of a proton as demonstrated by Fabbrizzi et al. [664]. A binding constant of log K_{ass} = 4.7 was derived by pH titration. For histamine a binding of log K_{ass} = 4.3 was obtained and for *S*-His the value of log K_{ass} was 5.5. The 1:1 complex stoichiometry was verified by spectrophotometric titrations. Later the same group reported a luminescent sensor for histidine (**81e**) based on a tridentate Zn(II)-tren complex [665].

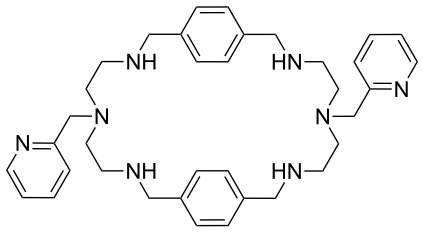

206

Figure 147: Dien-bipyridyl ligand **206** for co-ordination of two metal atoms.

The dichloro-cobalt-complex **207** (Figure 148) was reacted with glycine, *S*-alanine, *R*-alanine, *S*-phenylalanine and *R*-phenylalanine (**81a**), *S*-tryptophan and *R*-tryptophan (**81b**) [666]. Alanine forms a five-membered ring upon chelation to the metal complex. Deuteration experiments monitored by NMR showed that α-hydrogens of the three co-ordinated *R*-amino acids exchanged rapidly with little or no observable epimerization. In contrast, the α-hydrogens of the three *S*-amino acids exchanged slowly with concomitant epimerization. It was not possible to fully deuterate the *S*-amino acid complexes due to competing decomposition reactions. Thus, the *R*-enantiomer of the receptor binds the *R*-enantiomers of the amino acids more tightly and converts the *S*-enantiomers to the *R*-enantiomers.

The X-ray crystallographic and ^{1}H NMR data underlined that co-ordination of alanine takes place with unprecedented regio-

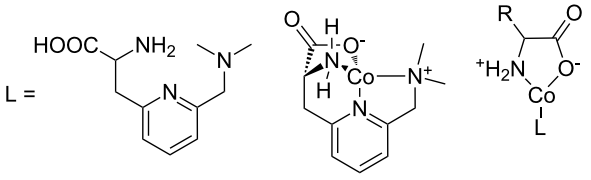

207

Figure 148: The ligand and corresponding tetradentate co-complex **207** serving as enantioselective receptor for amino acids.

specicity and stereospecicity. The regiospecicity is controlled by electrostatic effects while the stereospecicity is controlled by steric effects in a highly predictive manner. This approach thus provides detailed structural insights into general separation of bidentate α-H-amino acids into *R*- and *S*-forms with a single chiral metal complex.

Bis(oxazolines) are widely employed in asymmetric catalysis, for example, in cyclopropanations. Besides this they are also valuable receptor moieties [667]: The enantioselective recognition of amino acids has been studied with C_2 symmetric chiral pyridine bis(oxazoline)–copper(II) complex **208** (Figure 149) at physiological pH by UV–vis titration and revealed a strong binding with a submillimolar dissociation constant in aqueous solution. Moderate selectivity of up to 2:1 between *R*- and *S*-amino acids was achieved with best affinities of the *R*-host to *R*-amino acids.

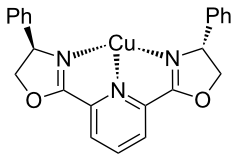

208

Figure 149: Bis(oxazoline)–copper(II) complex **208** for the recognition of amino acids in aqueous solution.

Zinc–salophen complexes have also attracted much attention as receptors. Their well known capability to accept one axially co-ordinated donor species, along with their photophysical properties [668-670], make them suitable candidates for the development of amine receptors [671].

Zinc–salophen compounds incorporating 2,3-diaminonaphthalene (**209a**) and 9,10-diaminophenantrene (**209b**) (Figure 150) moieties show unprecedented selectivities of quinuclidine (**210d**) vs. triethylamine (**210b**) higher than 10^5 as investigated by UV–vis and fluorescence spectroscopy in chloroform solution [672]. The binding to the zinc–salophen compounds to tertiary amines is influenced by steric effects. The binding constants for quinuclidine (**210d**) were all larger than 10^6 M^{-1}, for triethylamine (**210b**) values of ~50 M^{-1} and smaller were recorded. Dimethylethylamine (**210c**) has an affinity of 1500 to 1900 M^{-1}, while diisopropylethylamine (**210a**) gave a negligible response. The axial co-ordination of tertiary amines is in general stronger for zinc-salophen compounds than for zinc-porphyrins. X-ray diffraction showed that in the solid state compound **209a** is dimeric, but its 1:1 quinuclidine complex is monomeric. Strong indications were obtained that both free receptors and their amine adducts are monomeric in dilute chloroform solution.

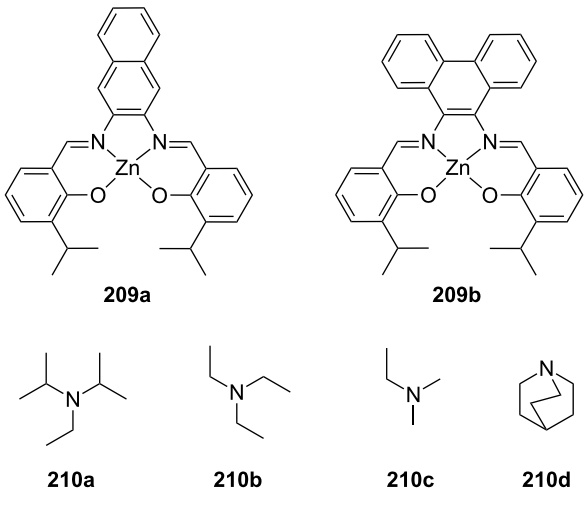

Figure 150: Zinc-salen-complexes **209** for the recognition tertiary amines.

A "ditopic binder" recognizing ammonium ions with its side chains in water was described with a water soluble zinc-salophen complex **211** [673] (Figure 151). Its binding to carboxylate anions in water is very strong ($K_{ass} > 10^6$ M^{-1}). Amino acids are bound with associations constants ranging from $K_{ass} = 3800$ M^{-1} for glycine to $K_{ass} < 5$ M^{-1} for tryptophan (**81b**) were found from UV–vis spectrophotometric titrations. The general trend shows a gradual decrease in binding strength with increasing steric hindrance. The K_S/K_R ratio of 9.6 observed for phenylalanine (**81a**, 2500 M^{-1} and 260 M^{-1}, respectively) is among the highest values found for the chiral recognition of amino acids in water [674,675]. These findings led to the conclusion that amino acids are bound via zinc-carboxylate co-ordination and hydrogen bonding between the ammonium group and two oxygen atoms of one of the D-glucose moieties. This was supported by structures of the 1-glycine complex calculated at the semiempirical level (PM3).

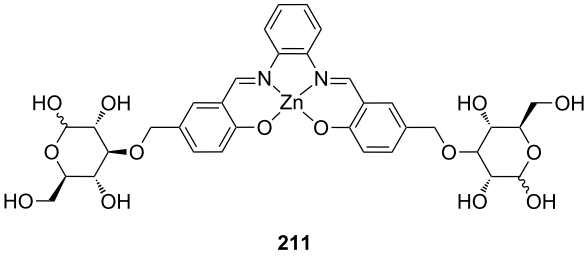

211

Figure 151: Bis(oxazoline)–copper(II) **211** for the recognition of amino acids in aqueous solution.

A new fluorescence macrocyclic receptor **212** based on the Zn(II)-complex of a C_2 terpyridine and a crown ether (Figure 152) has been developed for molecular recognition of zwitterionic amino acids in water/DMF solution with strong binding to *S*-aspartate (K_{ass} = 4.5 × 10^4 M^{-1}) and *R*-cysteine (K_{ass} = 2.5 × 10^4 M^{-1}) [676]. The Zn(II)-tpy subunit co-ordinates with the carboxylate group of the zwitterionic amino acids, and functions as a chromophore (λ_{max} = 348 nm) for the fluorescence sensing in aqueous solutions. The crown ether subunit binds the ammonium group of the zwitterionic amino acids. Without the crown ether subunit the binding to *S*-aspartate was about 90 times smaller, no significant change in fluorescence was observed for other amino acids. The binding properties of receptor **212** to different *S*-amino acids were studied by UV and fluorimetric titration methods. In all cases a 1:1 stoichiometry was observed and the equilibrium binding constant K_{ass} was estimated using the Benesi–Hildebrand equation. The binding affinity of receptor **212** to *S*-amino acids is highly dependent on the co-ordinating abilities of the side-chain chelating groups towards the Zn(II) metal (carboxylate > thiol >> amide >hydroxylammonium). *S*-Aspartate and *S*-cysteine showed the highest level of affinity to receptor **212**, which is about 4–14 times higher than *S*-asparagine and *S*-serine. *S*-Aspartate exhibited a much stronger binding (18 to 79 times greater) than the amino acids bearing an alkyl or aryl side-chain, and about 180 times higher than the cationic substrate (*S*-ornithine). The rigid C_2 symmetric chiral groups in the Zn(II)-tpy subunit lead to enantioselectivity towards *R*-amino acids with K_R/K_S up to 3.0 in the case of phenylglycine.

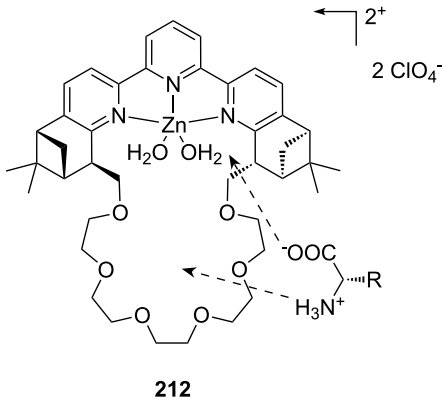

212

Figure 152: Zn(II)-complex of a C_2 terpyridine crown ether.

Indicator displacement assays are a popular method for converting a synthetic receptor into optical chemosensors. Amino acids are one substance class, which can be targeted by such colorimetric, fluorescent, and metal containing assays. Many examples along with their biological counterparts have been highlighted [677].

Anslyn et al. targeted the neurotransmitters aspartate and glutamate in a pyrocatechol violet displacement assay (Figure 153) in a water/methanol mixture (1:1; buffered with 10 mM HEPES at pH 7.4) [678]. The zinc complex was perfectly stable under these conditions. The highest affinity was found for aspartate (K_{ass} = 1.5 × 10^5 M^{-1}) with a seven fold stronger recognition over succinate, or glutamate, and by a factor of near 15 over the hydrophobic amino acids. The affinity of **213** is dominated by the interaction with Zn(II). In the case of aspartate the appended guanidinium groups also contributed to the binding. In addition, it was also observed that the use of metals in receptors can lead to larger color changes in indicator displacement assays. A shift in absorbance of the bound indicator that cannot be achieved with receptors which simply rely on hydrogen bonding and ion pairing for perturbing the ionization state was given as reason for this observation.

They also reported a comparable colorimetric technique for *ee* determination of non-derivatized *R*-amino acid samples in H_2O/MeOH solutions based on a displacement assay with pyrocatechol violet (Figure 154). This instance a copper complex was

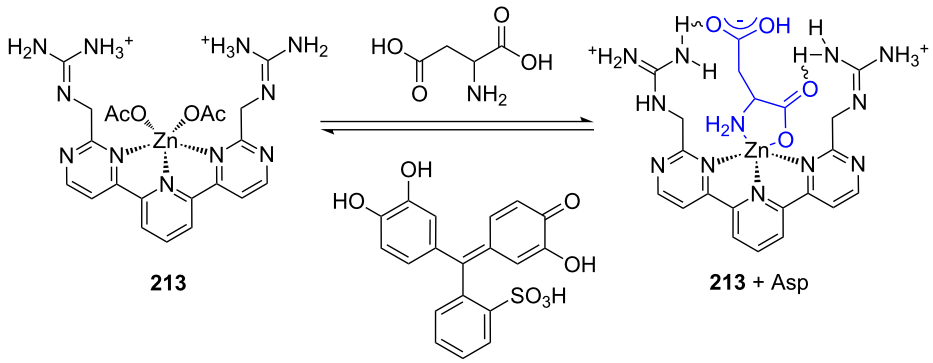

213 **213** + Asp

Figure 153: Displacement assay and receptor for aspartate over glutamate.

used for the competitive metal co-ordination [679]. The ability of (*S*,*S*)-**214** to differentiate enantioselectively four of the hydrophobic *R*-amino acids was shown by UV–vis spectroscopy. Titration of *R*-amino acids in (*S*,*S*)-**214** resulted in a decrease of the Cu(II) absorbance. These experiments were carried out in the presence of a 10-fold excess of ligand (*S*,*S*)-**214** to discourage dissociation of (*S*,*S*)-**214**, and avoid the creation of 2:1 complexes. Valine and tryptophan (**81b**) gave the best values for their 1:1 complexes. *R*-Val and *S*-Val bound with association constants of 5.2×10^5 M^{-1} and 2.0×10^5 M^{-1}, respectively, resulting in an enantioselectivity $K_R/K_S = 2.6$. For *R*-Trp and *S*-Trp the values were 1.1×10^6 M^{-1} and 5.0×10^5 M^{-1}, giving a discrimination of $K_R/K_S = 2.2$. Overall, the data showed a consistent preference for *R*-amino acids by about a factor of 2 to 2.6.

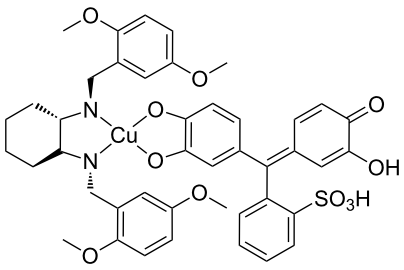

214

Figure 154: Chiral complex **214** for a colorimetric displacement assay for amino acids.

The insertion of strong co-ordination centres into peptides enables the construction of selective molecular receptors with complementary frameworks suitable for differentiation of amino acids and small peptides. A metal-centred receptor **215** consisting of a rigid backbone region and variable tripeptide arms [680] (Figure 155) for the recognition of tripeptides has been reported. The receptor is selective by co-operative interactions of the peptidic arms for *S*-xxx-*S*-Lys-*S*-Lys, with xxx = *S*-His, *R*-Cys, and *S*-Met with association constants near 10^6 M^{-1}. The binding studies in a water/methanol solution (1:1; buffered with 100 mM HEPES at pH 7.4) by UV–vis titration indicated from the association constants of the protected peptides, that amino acids were bound through their amino terminus. *N*-Terminal metal-chelating amino acids appended to basic amino acids bound with enhanced affinities via metal-chelating and ion pairing. *N*-Terminal His with two appended Lys showed the maximum binding with a value of 10^6 M^{-1}. The increase in affinity by a factor of near 10–30 over *R*-Cys-*S*-Lys-*S*-Lys and *S*-Met-*S*-Lys-*S*-Lys with $K_{ass} = 3.0 \times 10^5$ and 10^5 M^{-1}, respectively, was contributed to by the ion-pairing interactions possible with the guest peptide residues. In contrast, the His-, Cys-, and Met-Gly-Gly analogues affinities dropped approximately 100 fold.

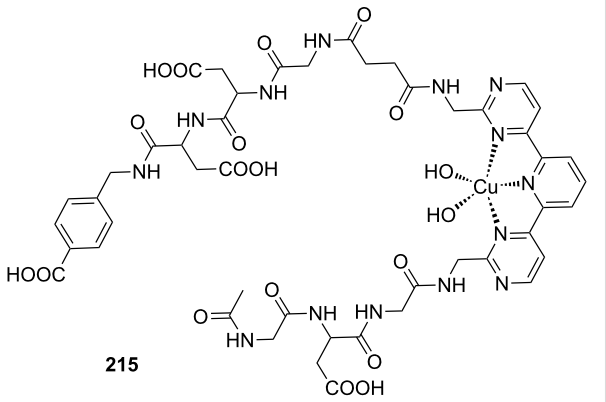

215

Figure 155: Metal complex receptor **215** with tripeptide side arms.

Recognition of amino acids [681] and peptides [682] can be performed by a displacement assay with the rhodium sandwich complex **216** and an azo dye such as **217** (Figure 156). The aggregate distinguishes peptides with His and Met residues in position 1 or 2 at the *N*-terminus from other peptide sequences. The association constant of His-Ala, His-Gly-Gly, Leu-His-Leu or Gly-Met-Gly to **216** with values around 10^{10} M^{-1} exceed the binding strength of the dye **217** by three orders of magnitude. Peptides such as Val-Phe or Lys-Tyr compete so weakly with the dye that recognition of the former noted peptides in aqueous solution is possible even in the presence of a 100 fold excess of them. A colorimetric assay for the 20 natural amino acids in water was developed with this system [682].

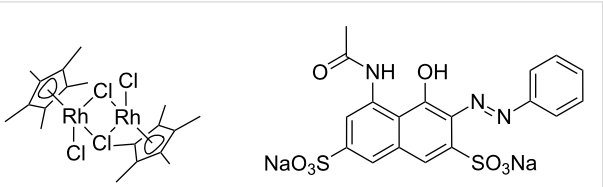

216 **217**

Figure 156: A sandwich complex **216** and its displaceable dye **217**.

A recent example uses lanthanide complexes as receptors for the recognition of unprotected amino acids. Lipophilic lanthanide complexes of fluorinated diketonate ligands **218** to **220** (Figure 157) were shown by extraction experiments to bind unprotected phenylalanine (**81a**), leucine, and other amino acids under neutral conditions [683]. All tris(diketonates) formed 1:1 complexes with amino acids. The observations were verified by NMR and CD spectroscopic studies, which also suggested that the metal complexes bound the amino acid guests at two points.

Their extraction, transport, and chiral recognition behaviors were significantly controlled by a combination of central lanthanide cation and co-ordinating ligand: The chiral ytterbium complex **219d** offered good enantioselectivity in the extraction of unprotected amino acids (Ph-Gly; 49% *ee*), and the related praseodymium complex **219a** provided efficient membrane transport (Phe; 62%). For receptors **218** the order of extraction from DCM to water was determined as Phe > Trp > Leu > Ph-Gly with a maximum value of 52%. Compounds **219b** and **219b** extracted Ph-Gly, Phe and Trp up to 62% under the same conditions. Complex **219b** especially exhibited excellent extraction ability for amino acids due to the effect of the electronegative fluorinated moieties [684-686] of the ligand that increase the Lewis acidity of the lanthanide tris(diketonate). This led to strong co-ordination of the carboxylate anion of the amino acid guest. In addition, fluorinated ligands enhanced the solubility of lanthanide tris(diketonates) and their ternary complexes with amino acids in the organic media [687].

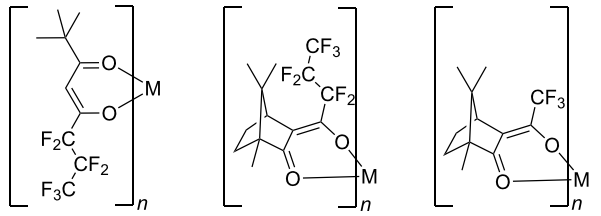

218a: M = Pr
218b: M = Eu
218c: M = Dy
218d: M = Yb

219a: M = Pr
219b: M = Eu
219c: M = Er
219d: M = Yb

220a: M = Eu
220b: M = Er

n = 3

Figure 157: Lanthanide complexes **218**–**220** for amino acid recognition.

Metal complexes of porphyrins, bisoxazolines, tripyridines, salens and many other ligands are valuable binding sites for amines and amino acids. By co-ordinative bonds they are able to form stable aggregates even in highly competitive media, such as water. Thus, they enable the recognition of targets such as amino acids and peptides in this challenging surrounding. Bidentate co-ordination of the guest allows enantiodiscrimination.

7. Other concepts: natural ionophores, (cyclo)peptidic hosts, reactive systems and more

A variety of less frequently applied concepts for ammonium ion binding have been reported in the literature, which cannot be allocated to one of the former sections: natural ionophores, their derivatives and related molecules, peptidic- and cyclopeptidic structures, and reactive groups. We discuss selected examples of these concepts in the following part.

7.1. Natural ionophores

The best known naturally occurring macrocycles with ammonium ion affinity are the nonactins (**221**), valinomycin (**222**) [618] or the natural antibiotic vancomycin (**223**) [688] (Figure 158). Vancomycin (**223**) recognizes the Lys-*R*-Ala-*R*-Ala sequence and inhibits linking of these building blocks in the bacteria cell walls, thus causing cell death by osmotic overpressure [5]. For a considerable time it has been used as a reserve antibiotic, a so called “last line of defence”, because little resistance was observed [688] which is no longer the case.

Valinomycin (**222**) is a cyclodeca-depsipeptide consisting of *S*-valine, *R*-valine, *S*-lactate and *R*-hydroxyisovalerate with the repetitive structure (*S*-Lac-*S*-Val-*R*-Hiv-*R*-Val-)$_3$, forming a ring of 36 atoms, with alternating amide and ester bonds. Similar to the interaction of crown ethers with cations, valinomycin guest binding is based on ion-dipole interactions between the oxygen atoms positioned along the ring and the guest [689]. The molecule is pre-organized through hydrogen bonding of its amide carbonyl groups to form a pocket with six ester carbonyl oxygens available for electrostatic stabilization of potassium ions through octahedral complexation [690]. Ammonium ions are bound in the same way. The selective transport of potassium ions by valinomycin through the cell membrane causes cells death by breakdown of the membrane potential [691,692]. The binding strength for potassium ions in aqueous media is 10^6 M^{-1} [693-696].

Investigations of the ammonium ion complex of valinomycin in methanol by capillary electrophoresis gave an apparent stability constant of log K_{NH4+} of 1.52 ± 0.22 [618,697], which is in good agreement with the earlier determined value of log K_{ass} = 1.67 obtained from spectrophotometric measurements [698]. In comparison to the ammonium ion binding ability of 18-crown-6 (**4**) in the same solvent obtained by conductivity measurements (log K_{ass} = 4.1) [699], the value is two orders of magnitude lower.

The binding properties and association constants (K_{ass}) of synthetic crown ethers with different cavity size and substituents and the natural ionophores valinomycin and nonactin versus deferriferrioxamine B, $CH_3(CH_2)_4NH_3^+$, NH_4^+, K^+, and Mg^{2+} in water saturated chloroform were reported (Table 15) [700].

These values were later confirmed by a mass spectrometric study [702]. Evaluation of the cation complexation by ^1H or ^{13}C NMR methods, in solution or solid-state, has been reported for thel ionophores: valinomycin [703-706], nonactin and tetranactin [707], and cereulide [708]. Potassium ions cause significant interference in ammonium ion detection because the

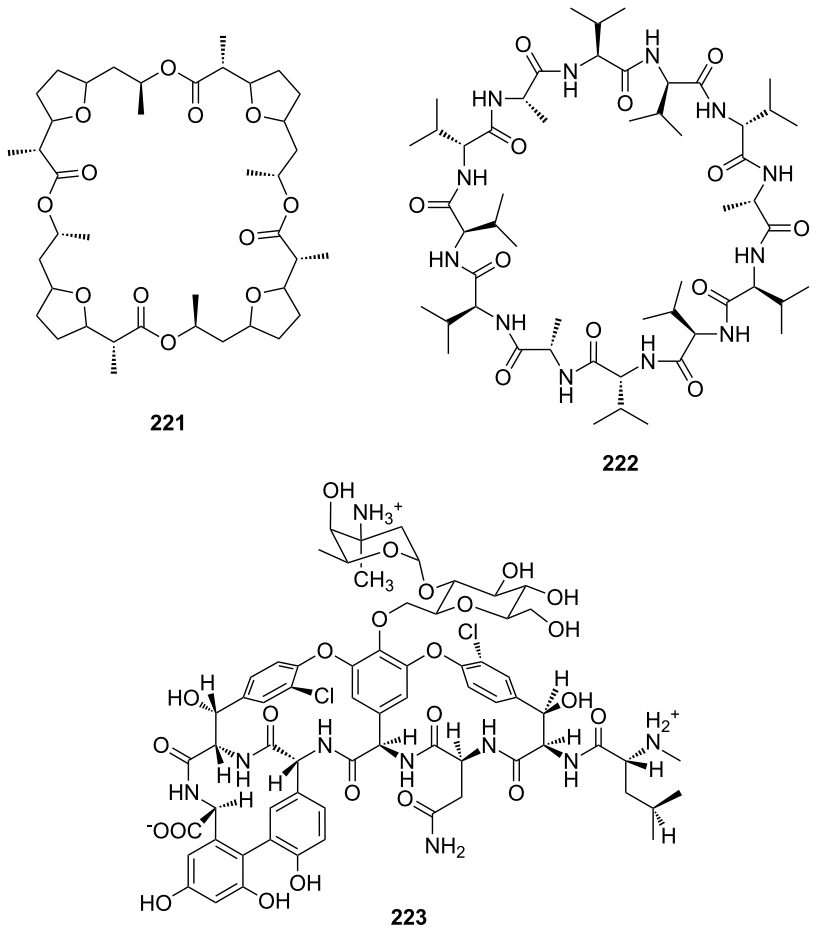

Figure 158: Nonactin (**221**), valinomycin (**222**) and vancomycin (**223**).

Table 15: Binding values of natural ionophores compared to a 18-crown-6-derivative in chloroform.

Host	log K_{ass} (guest perchlorate salt)		
	Potassium	Ammonium	*n*-butylammonium
cis-dicyclohexano-18-crown-6[a]	8.23	7.69	6.16
valinomycin (**222**)	8.99	7.15	4.20
nonactin (**221**)	7.18	7.66	5.19

[a]= Reference [701].

potassium ion is similar in size to the ammonium ion (1.33 Å) [118].

In contrast to valinomycin, nonactin is selective for ammonium ions over potassium ions. It exceeds crown ethers in selectivity and shows excellent selectivity in NH_4^+ transport relative to K^+ ($NH_4^+/K^+ \sim 14$) [126]. In ion transfer reactions of the ammonium, potassium, and sodium ions with the ionophores dibenzo-18-crown-6, nonactin (**221**) and valinomycin (**222**) investigated at a water/1,2-dichloroethane interface, nonactin was found to be the most selective towards the ammonium ion, with a calculated association constant of 14.1 [709]. It is therefore widely employed in ion selective electrodes since it is superior to many artificial ionophores [$\log K_{NH4+,\ K+} = -1.0$, $\log K_{NH4+,\ Na+} = -2.6$] [126] and exhibits a detection limit for ammonium ions of 10^{-6} M [128]. Often it serves as a reference compound for the development of new ionophores for ISEs.

Nonactin (**221**) (Figure 158) is a naturally occurring ionophore, a highly symmetric meso compound with flexible conformation,

when no ion is present [710]. The unbound conformation is relaxed and almost planar, possesses strong intramolecular non-bonding dipoles and lacks hydrogen bonding interactions [711]. It adopts a puckered conformation when bound to ammonium ions, pre-organized with the ion bound, leading to a good overlap of the oxygens which stabilize the charged ammonium hydrogens [712,713].

Monensin esters (Figure 159) are sodium ionophores, but synthetic analogs bind primary ammonium ions selectively and offer chiral recognition ability comparable to that of Cram's binaphthyl crown ether. As demonstrated by experiments in an ion selective electrode in buffered aqueous solution and by NMR studies in chloroform, enantioselective complexation is found for chiral phenethylamine and naphthylamine salts, as well as for some amino acid esters. (*R*)-1-(l-Naphthyl)ethylammonium acetate is bound with three fold selectivity over the corresponding *S*-enantiomer by (*S*)-**224b** [714].

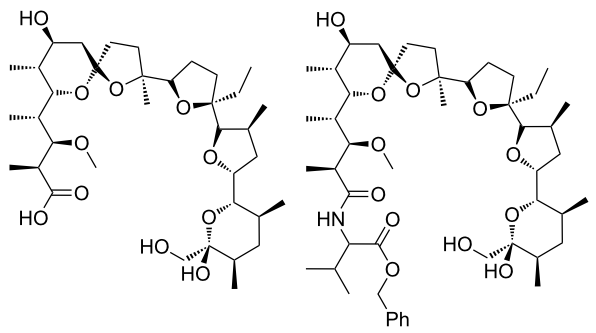

Figure 159: Monesin (**224a**) and a chiral analogue for enantiodiscrimination of ammonium guests (**224b**).

A variety of natural polycyclic antibiotics bear a structural resemblance to podants and they reveal often stunning selectivities and binding properties. Podands form complexes of lower stability than their corresponding macrocyclic counterparts. In the case of pentaglyme dimethylether (**225**) versus 18-crown-6 (**4**) (Figure 160), the macrocyclic ether binds the *tert*-butylammonium ion 10^4 times more tightly [100]. The enormous difference in binding results from the macrocyclic effect. In structures such as the monesins (**224a**) and lasalocid A (**228**) this is overcome by the pre-organizing effect of the furan and pyran rings leading to a half-moon like array, as well as the possibility to build manifold contacts to the guest.

This effect can be nicely seen in the artificial systems presented by Still et al. Chiral podand analogs (**226b**) of 18-crown-6 (Figure 160), conformationally locked, reveal ionophoric properties closely related to the macrocycle. These host molecules have a cation-binding site with six oxygens with the same geometrical arrangement as found in the crystal structure of potassium 18-crown-6 [715].

The conformationally homogeneous podand receptor (**226a**) even binds proline-derived dipeptidic substrates (**227**) enantioselectively and diastereoselectively [716]. A closely related enantiomerically pure, C_2 symmetric tetracyclic podand forms well-defined complexes with chiral ammonium salts. With derivatives of α-phenethylammonium hexafluorophosphate as guests, binding enantioselectivity up to 60% *ee* is achieved [136].

Lasalocid A (**228**, Figure 161) binds by its OH groups and ether oxygens, and can compete with the macrocycles. It is a widely employed ionophore antibiotic that can effectively complex ammonium ions in a similar manner to crown ethers. As a drug

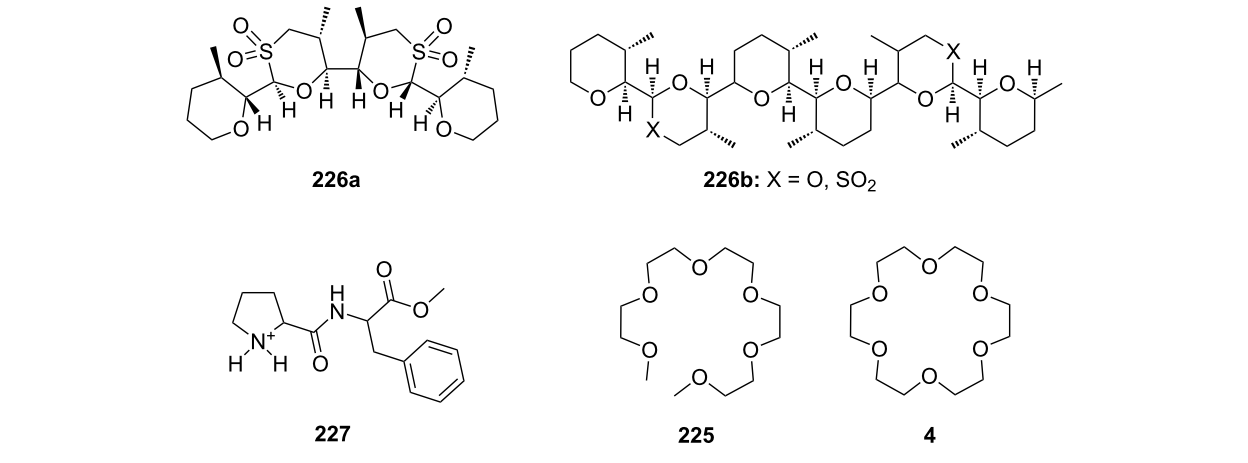

Figure 160: Chiral podands (**226**) compared to pentaglyme-dimethylether (**225**) and 18-crown-6 (**4**).

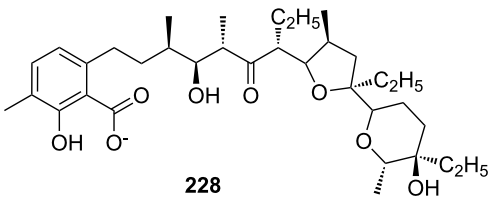

Figure 161: Lasalocid A (**228**).

it is used as its sodium salt. The mechanism of lasalocid activity is clearly attributed to its ionophoric properties where especially the influx of Na^+ in the cell of Gram-positive and anaerobic bacteria causes swelling, vacuolization and finally cell death [717].

Lasalocid A can form strong complexes with biogenic amines such as dopamine (**2**), norepinephrine, 2-aminoheptane, as well as tyramine and transport them across biological membranes [718-724]. The crystal structure of a protonated amine with lasalocid shows all protons of NH_3^+ hydrogen bonded. The complex is stabilized, in addition, by some intramolecular hydrogen bonds [725]. In the gas, liquid and solid states lasalocid forms a very stable 1:1 complex with allylamine with its structure comparable in all states examined. Due to these interactions the outside of the complex is hydrophobic enabling ammonium transport across the biological membranes.

Sessler et al. reported sapphyrin ± lasalocid conjugates (**230**) which feature binding sites for both carboxylate anion complexation and ammonium group recognition (Figure 162) as efficient and selective carriers for aromatic amino acids [726]. In through-membrane model transport experiments, carrier **229** showed selectivity for phenylalanine (**81a**) over tryptophan (**81b**). Tyrosine is not transported to any significant extent. In general *S*-amino acids were transported with greater efficiency than the corresponding *R*-enantiomers by this particular carrier. The high level of amino acid carrier capability displayed by receptor **229** in dichloromethane solutions correlates well with the results of equilibrium binding studies carried out using visible-spectroscopic titrations.

By comparison two second generation sapphyrin ± lasalocid conjugates **230** were reported as carriers for the transport of Phe, Trp, and Tyr. A clear difference was observed between the free acid and the ester of **230**. The former did not affect amino acid transport, which was explained by receptor inactivation by self assembly. Depending on the chirality of the phenylalanine appendage (**230a** or **230b**) used, either *S*- or *R*-enantiomers of amino acid substrates were transported faster.

Coporphyrin I (CP, **231**, Figure 163) was employed as a host molecule [727]. As a tetraanion it binds electrostatically to the terminal ammonium groups of diammonium cations and interacts simultaneously with the hydrocarbon chain by its hydrophobic π-plane. Aliphatic diamines [$H_2N–(CH_2)_n–NH_2$, n = 2–8] were studied by spectrophotometry, fluorimetry and ^1H NMR spectroscopy in the pH range 7–10 and ionic strengths 0.01–0.1 M in water. The dominant factor for binding was assigned to the ion-pair interaction. Diprotonated diammonium cations induced dimerization of CP by forming 1:1 complexes with CP, which undergo much stronger self-aggregation than

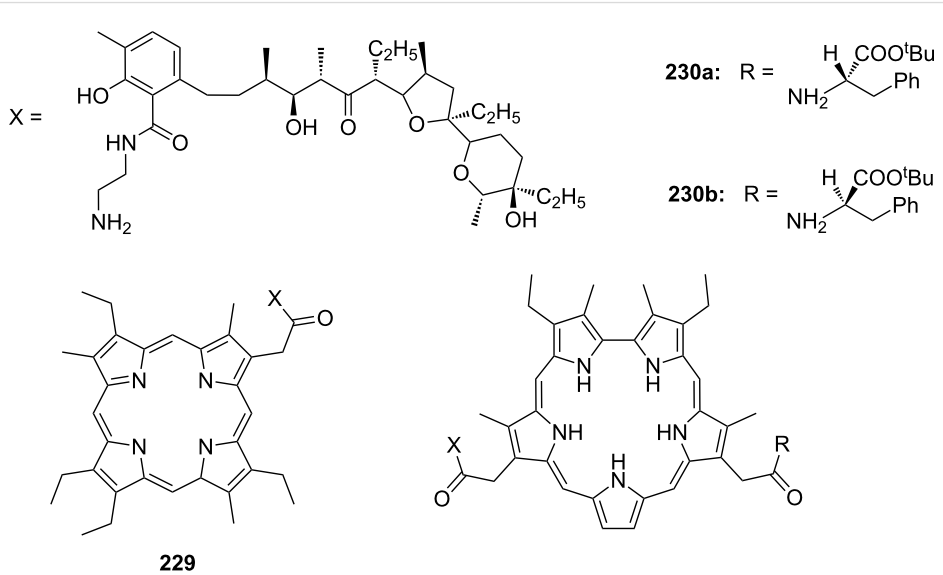

Figure 162: Lasalocid derivatives (**230**) of Sessler et al.

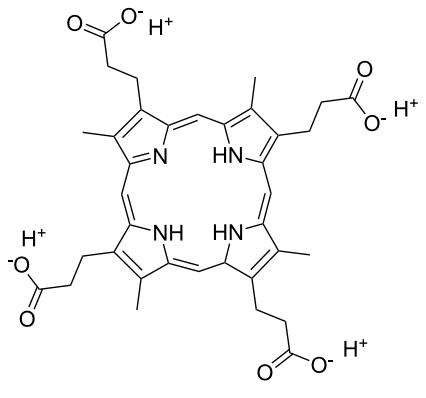

231

Figure 163: The Coporphyrin I tetraanion (**231**).

free CP tetraanions. Increasing the number of methylene units connecting the ammonium groups, leads to an increase of the binding constants for the complex formation with monomeric CP (K_S), but the dimerization constants of the resulting complexes were found to decrease. Even at I = 0.1 M the association is still fairly strong with log K_{ass} = 3. In the series of H_3N^+–$(CH_2)_n$–NH_3^+ cations, the log K_{ass} decreases with the increasing length of the guest by 0.1–0.3 units per methylene group.

7.2. Peptidic- and cyclopeptidic ammonium hosts

Cyclic peptides are known to bind and transport metal cations in biological systems [728]. Their ease of synthesis and potential for flexible sequence modification make them good candidates for new ionophores [729].

Cyclic peptides platform structures with convergently oriented groups for ion recognition have been highlighted [730]. A review of peptide cyclization and cyclopeptides has only recently appeared [731]. Many examples for the synthesis of cyclic and bicyclic peptides can be found in the literature [732-740]. Kubik et al. published a comprehensive review about cyclopeptides as macrocyclic hosts [741]. Several cyclic peptide systems have been synthesized for ammonium complexation. We now present some representative, recent examples.

The RGD sequence is a key recognition element found in many proteins that interact with integrins on cell surfaces [742]. The combination of an integrin-binding RGD-cyclopeptide with a hexadecalysine DNA binding domain leads to peptidic minivectors for efficient gene transport [743]. The recognition of the ammonium residues by the DNA is crucial for this process.

The two tetrapeptide sequences Trp-Aib-Gly-Leu-NH-Ar (Aib: α-aminoisobutyric acid, 2-amino-2-methylpropanoic acid, Ar = phenyl or 3,5-dimethylphenyl) (Figure 164) bind ammonium ions by their aromatic moieties. The turn structure induced by the amino acid sequence leads to a sandwich complex of the guest between both π-systems as confirmed by 2D NMR ROESY experiments [744]. The peptide **232** bound several quaternary ammonium salts in $CDCl_3$ with the highest binding constants for benzyltrimethylammonium chloride and *N*-butylpyridinium chloride with association constants of 580 M^{-1} and 1000 M^{-1}, respectively.

The chiral recognition of guest compounds by the tetrapeptides (X-Trp-Aib-Gly-Leu-NH-Ar) was also observed. The binding constants and the enantioselectivities of *N*-terminal free

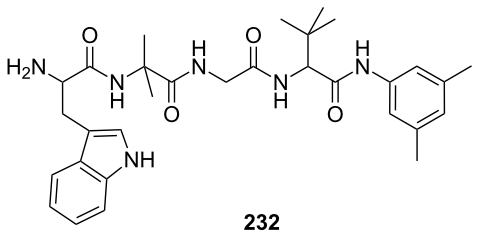

232

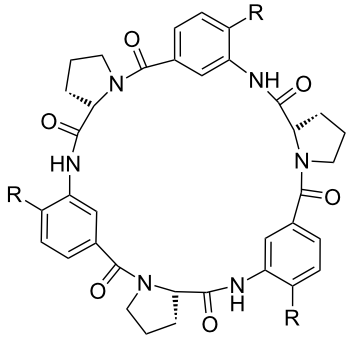

233a: R = CH_3 **233d:** R = H
233b: R = Cl **233e:** R = OCH_3
233c: R = CH_2OCH_3 **233f:** R = $COOCH_3$

Figure 164: Linear and cyclic peptides for ammonium ion recognition.

peptides were larger than those of peptides, which have a benzyloxycarbonyl group at the *N*-terminus [745].

Kubik et al. constructed a cyclic peptide composed of *S*-proline and three amino benzoic acids in an alternating sequence (Figure 164) that was able to bind ammonium ions with stability constants between 11000 and 42000 M^{-1} in chloroform. The series of cyclic hexapeptides contains different 4-substituted 3-aminobenzoic acid units (R = CH_3, Cl, CH_2OCH_3, OCH_3, $COOCH_3$) [746]. The authors demonstrated that cyclic peptides **233** bind a variety of ammonium iodide salts with positive co-operativity in $CDCl_3$. The cation complex stabilities depend on the substituents and can cover a wide range from K_{ass} = 140 M^{-1} for R = CH_3 to K_{ass} = 10800 M^{-1} for R = $COOCH_3$ (K_{ass} = 1260 M^{-1} for R = H) with *n*-butyltrimethylammonium picrate, for example. The peptide was found to adopt a conformation analogous to the cone conformation of a calixarene. Cations were bound by cation–π interactions, while the iodide counter ion co-ordinates via peptidic NH hydrogen bonds.

In a second study it was shown, that these cyclic peptides show enantiodiscrimination properties [747]. The best two examples, **233e** and **233f**, distinguish the two enantiomers of *N*,*N*,*N*-trimethyl-1-phenylethyl ammonium picrate in 0.1% DMSO–$CDCl_3$ with K_R/K_S = 1.5. NMR titrations revealed binding constants (K_{ass}) with the quaternary ammonium ion of 1550 M^{-1} for the *R*- and 1030 M^{-1} for the *S*-enantiomer binding to **233e** or 4550 M^{-1} for the *R*- and 3050 M^{-1} for the *S*-enantiomer binding to **233f** in 1:1 complexes.

The corresponding cyclic tetrapeptides composed of alternating *S*-proline and 3-aminobenzoic acid subunits possess a significantly smaller cation affinity than the hexapeptides [748]. Derivatives with suitable substituents on the aromatic subunits can be used as tweezer-type receptors.

As illustrated by the discussed examples and demonstrated by several further publications [749-751], cyclic peptides, depsipeptides and many natural ionophores selectively bind ammonium cations. Therefore, such structures can be utilized for the electrochemical analyses of such ions. The group of McGimpsey presented two approaches using cyclopeptides for ammonium ion detection in an ion selective electrode.

A cyclic depsipeptide **234**, consisting of alternating amide and ester groups which is in effect half of the valinomycin structure (Figure 165), was employed as ammonium ionophore. Unlike valinomycin, this depsipeptide is too rigid to fold upon itself and therefore provides a cavity appropriately sized for ammonium ions, but not the octahedral binding geometry required by potassium ions (ionic radii: 1.43 and 1.33 Å, respectively) [752]. ISE sensors with this ionophore exhibited similar selectivity for ammonium over potassium and sodium ions compared to nonactin-based sensors (**221**) [126]. The ion selectivity follows the order of $NH_4^+ > K^+ > Na^+$, Ca^{2+}, Mg^{2+}, Li^+. The energy minimized structures showed the ammonium cation located within the pocket and able to hydrogen bond to at least five of the carbonyl groups. In contrast, the potassium cation adopts a position that is shifted to one side well above the plane of the disk-like structure of **234** reflecting an unfavorable binding site for potassium.

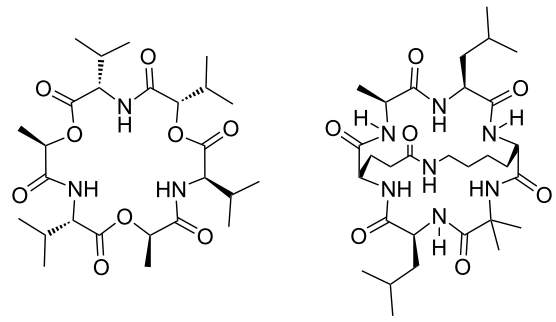

Figure 165: Cyclic and bicyclic depsipeptides for ammonium ion recognition.

These cyclic peptides are still too flexible to bind substrates in a well-defined cavity [753], leading to lowered selectivity as sensor components. The addition of a second ring yielding bicyclic peptides was thought to increase cation binding selectivity by increasing rigidity.

The bicyclic peptide **235**, cyclo (*S*-Glu1 – *R*-Leu2 –Aib3 – *S*-Lys4 – *R*-Leu5 – *R*-Ala6)-cyclo-(1γ–4ε) (Figure 165) was introduced [754], to provide an ammonium ion complexation site in a tetrahedral geometry. The bicyclic ammonium ionophore **235** was designed for optimal size-fit/pre-organization, binding geometry and ISE membrane compatibility. A semi-rigid framework with a cavity appropriately sized for ammonium ions (ionic radius 1.43 Å) is necessary to impart high selectivity over interfering cations of other sizes [125].

The bicyclic molecule provides hydrogen bonding opportunities for the ammonium ion, primarily through the amide carbonyl groups, but also potentially through the amide nitrogen atoms. NMR measurements in $CDCl_3/CD_3OD$ (1:1) indicate that four of the carbonyl groups are oriented towards the internal side of the cavity thus donating electron density upon complexation of ammonium ions. The compound shows higher selectivity for ammonium over potassium and sodium ions as

determined by the downfield shifts in the carbonyl ^{13}C NMR signals upon complexation.

7.3. Miscellaneous concepts

Cyclodextrins were one of the first molecular receptors described to bind organic molecules and are widely used for inclusion of non-polar guests; in some cases they have been used for the recognition of quaternary ammonium ions [55,755-758]. Only recently an extensive thermodynamic study on the inclusion of quaternary ammonium surfactants was published [759].

The formation of inclusion complexes between α-cyclodextrin (**136a**) and the local anesthetic 2-(diethylamino)ethyl-*p*-aminobenzoate (novocaine, **236**) (Figure 166) was investigated in aqueous solution using steady-state fluorescence-, UV–vis spectroscopy and electrical conductivity measurements [760]. In addition, both the nitrosation reaction of the primary amine group in mild acid medium and the hydrolysis of the ester function in an alkaline medium have been studied. The inclusion complex formation between neutral or protonated novocaine and **136a** with a 1:1 stoichiometry was observed. However, the binding constants depend on the nature of guest and host: high affinities with an inclusion constant K_{ass} = 1500 mol^{-1} dm^3 are observed under conditions where the novocaine and the cyclodextrin are neutral molecules.

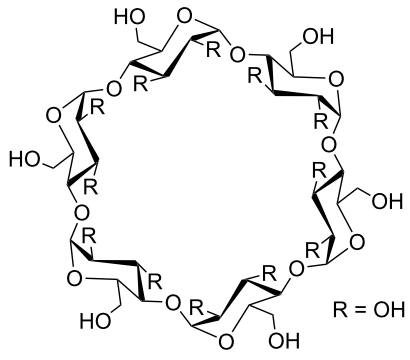

136a

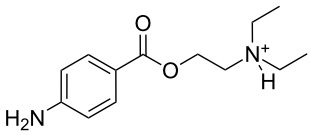

236

Figure 166: α-Cyclodextrin (**136a**) and novocaine (**236**).

The results obtained in this study showed that van der Waals interactions and hydrophobic interactions constitute the major driving forces for cyclodextrin complexation provided that the size and the conformation of the guest are complementary to the host cavity.

A completely different molecule has been shown to interact with various chiral amines and amino alcohols in organic solvents: the fluorescent helical diol **237** (Figure 167), reported by Reetz and Sostmann [761]. The authors suggest that the hydroxy moieties of **237** form hydrogen bonds with the amino group of the analyte, and no proton transfer is involved. Chiral discrimination was detected by differences in the fluorescence quenching observed upon binding to an amine. This chemosensor binds amines with modest stability constants.

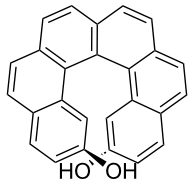

237

Figure 167: Helical diol receptor **237** by Reetz and Sostmann.

Oda et al. further developed Cram's spherands **238a** [17,762,763] to produce a better ammonium binder. They described a cyclophane (cyclic[6]metaphenylacetylene) [764] with six methoxy groups inside the cavity with acetylene units as spacers (**238b**) in a nearly planar carbon framework (Figure 168) as observed in the molecule's crystal structure. The six methoxy groups point up and down, alternately. The cavity size is appreciably larger than the size of a caesium ion (3.4 Å). No measurable complexation with alkali metal ions in solvent extraction experiments (chloroform/aq picrate salts) was found. Compound **238b** exhibits good ionophoric selectivity for the ammonium ion in spite of its smaller size (2.86 Å) compared with a caesium ion. A plot by Shono's method shows a straight line with a slope of approximately unity suggesting the formation of a 1:1 complex between **238b** and the ammonium ion in solution. The association constant obtained for the ammonium ion (log K_{ass} = 7.84) is smaller than that 18-crown-6 (log K_{ass} = 9.38), but larger than Cram's cavitand **238a** (log K_{ass} = 6.59).

Raymond et al. reported a tetrahedral supramolecular, chiral assembly of four gallium atoms bridged by *N,N*′-bis(2,3-dihydroxybenzoyl)-1,5-diaminonaphthalene units for binding cationic guests. This cage can recognize and include monoprotonated amines in aqueous solution [765]. This allows monitoring inversion at the nitrogen atom and H-bond formation in a variety of diamines [766].

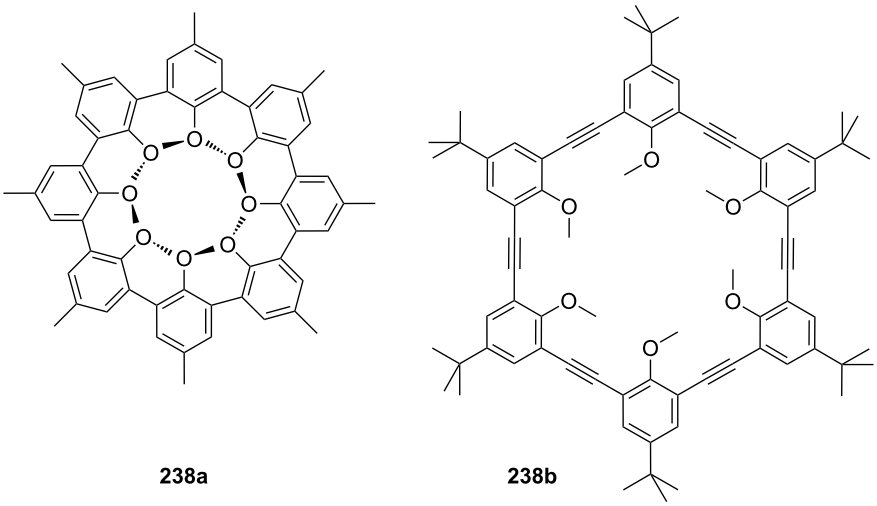

238a **238b**

Figure 168: Ammonium binding spherand by Cram et al. (**238a**) and the cyclic[6]metaphenylacetylene **238b** in comparison.

Based on the Kemp's triacid, compound **239** (Figure 169) was developed for combined backbone and functional group recognition of peptides [767]. One molecule binds the ammonium ion side chain, as demonstrated with Ac-Orn-Ala-OMe (K_{ass} = 2400 M^{-1}). A control experiment with *n*-propylammonium acetate gave a value of 490 M^{-1} for the salt bridge alone. Ornithine is bound with a 9:1 selectivity compared to all other amino acids employed in the dipeptide studied. All binding values were obtained by NMR titrations in chloroform; Job's plot analysis confirmed a 1:1 stoichiometry.

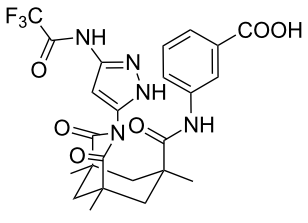

239

Figure 169: Receptor for peptide backbone and ammonium binding (**239**).

The demethylated naphthol reported by Lambert et al. binds by co-ordination via H-bonds and also via the amide nitrogen [768]. The authors chose a variation of the molecule [769,770] of Jiang et al. (Figure 170), which was able to bind a variety of anions (**240**). This group used the commercially available dye naphthol AS-BI, which was developed for the cytochemical detection of alkaline phosphatase [771]. Aliphatic amines are detected through binding with 7-bromo-3-hydroxy-*N*-(2-hydroxyphenyl)naphthalene 2-carboxamide and the fluorescence of the resulting complex.

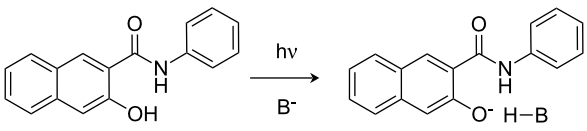

240 **240a**

Figure 170: Anion sensor principle with 3-hydroxy-2-naphthanilide of Jiang et al.

The demethylated derivative 7-bromo-3-hydroxy-*N*-(2-hydroxyphenyl)naphthalene 2-carboxamide (**241,** Figure 171, colorless in the ground state, λ_{max} = 335 nm), emits upon excited-state complexation at 525 nm. Proton transfer is enabled by the enhanced acidity of the OH group on the naphthalene on photoexcitation. Recognition of the amine by the chemosensor **241** therefore occurs via proton transfer of the naphthalenic OH proton to the amine and is facilitated by the presence of the phenol group. Amine basicity is the primary parameter for detection and consequently poorly basic aromatic and conjugated amines such as pyridine and aniline are not detected, but almost all aliphatic amines are. Hydrogen bonding within the complex allows further differentiation of aliphatic amines in the following order of binding strength: diamines > secondary amines > primary amines > tertiary amines > aromatic amines, heterocycles. Table 16 gives an overview of the binding strengths.

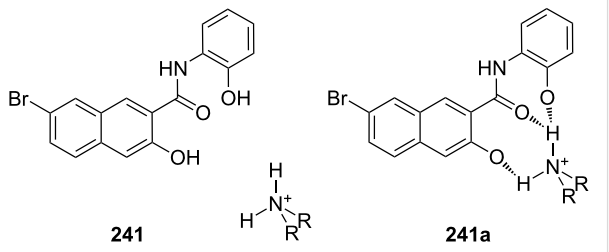

Figure 171: 7-bromo-3-hydroxy-*N*-(2-hydroxyphenyl)naphthalene 2-carboxamide (**241**) and its amine binding.

Table 16: Binding constants for **241** in acetonitrile.

Amine	K_{eq} (**241**) [M^{-1}]
1-propylamine	80000
1-butylamine	92000
benzylamine	7000
histamine	35000
diethylamine, diisopropylamine	150000
4-(dimethylamino)-pyridine	6900
triethylamine	28000
Diamine	**K_{eq} (241) [M^{-1}]**
1,2-diaminoethane, 1,4-diaminobutane	160000
1,3-diaminopropane, piperidine	180000
1,5-diaminopentane, 1,7-diaminoheptane	290000
1,8-diaminooctane	310000

Although non-covalent interactions are generally weak compared to covalent bonds, biomolecules achieve strong intermolecular binding forces by using several non-covalent interactions simultaneously. In a similar fashion, naturally occurring gallate-type catechins [772] stabilize complexes with quaternary ammonium ions by using dual non-covalent interactions [773].

Binding studies between the major catechins of green tea (Figure 172) and tetramethylammonium chloride (TMAC) [298] or benzyltrimethylammonium chloride (BMAC) were carried out by means of standard ^{1}H NMR titration experiments in acetonitrile-d_3/chloroform-d (1:1). The gallate-type catechins (for example **242**) had much higher binding ability (1300–2300 M^{-1}) than the non-gallate-type catechins (200–400 M^{-1}, for example **243**). This was attributed to the "biting effect" by the galloyl group and the B-ring. Compound **242** has the best binding ability of K_{ass} = 2300 M^{-1} towards BMAC.

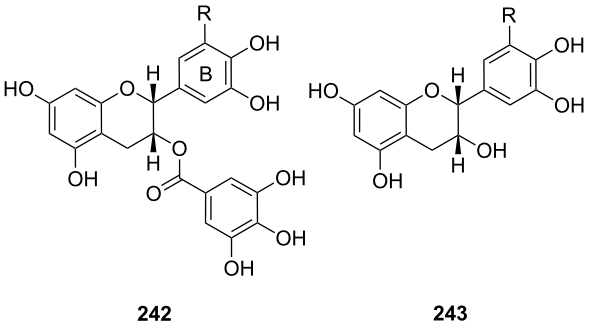

Figure 172: Naturally occurring catechins with affinity to quaternary ammonium ions.

Fuji et al. published a system for optical distinction of enantiomers of amino acids [774]. The authors used the thermo- and photochromic, colorless spiropyran **244**. On treatment with UV light the colored merocyanine is formed (Figure 173): The zwitterionic species **244a** binds to amino acids by ionic and hydrogen-bond interactions. This complex formation in turn stabilizes the colored merocyanine state and so the bleaching observed under dark conditions is slowed down.

Due to the binaphthyl system diastereomeric complexes arise with chiral amino acids, which are distinguished by their decoloration rates (Table 17). The best stabilization of **244a** was achieved with ammonium acetate ($t^{1/2}$ = 122 min).

Table 17: Dependency of the decoloring rate of **244a** in the presence of different *R*- and *S*-amino acids and ammonium acetate.

Guest	$t_{1/2}$ (*R*, *S*) [min]
none	13.3
alanine	24.1, 23.4
valine	32.5, 28.1
tryptophan	20.2, 17.0
phenylalanine	30.4, 26.8
ammonium acetate	122

7.4. Recognition by covalent bond formation

The ammonium ion is always in equilibrium with it's corresponding amine. Thus, the possibility of nucleophilic attack can be used for recognition, simply binding the guest as imine or aminal. Such concepts are now presented in the last part of this review.

A covalent approach for the detection of ammonium ions was applied by Glass et al. Their coumarin derivative **245** forms

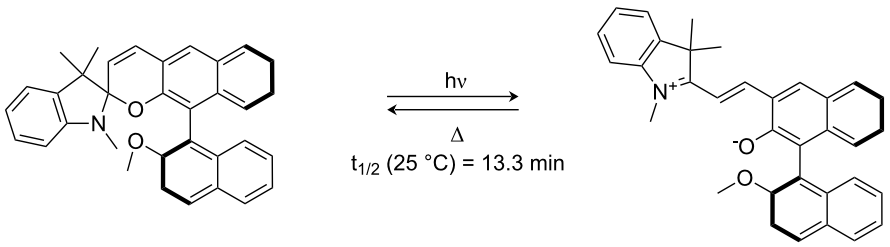

244 244a

Figure 173: Spiropyran (**244**) and merocyanine form (**244a**) of the amino acid receptors of Fuji et al.

iminium salts with ammonium ions (**245a**) [775] (Figure 174). The iminium formation can be monitored by UV spectroscopy using the resulting redshift of the long wavelength absorption band of approximately 440 nm to approximately 480 nm, as well as by a substantial (up to 45-fold) increase in the fluorescence intensity. As the main reason for the spectroscopic changes, the authors considered, the electronic effects caused by the formation of a hydrogen bond between the iminium hydrogen and the lactone carbonyl oxygen. The measurements were conducted under physiological conditions. Similar receptors based on hydrogen bond interaction show usually no affinity under these conditions. So, the equilibrium constants, e.g. for lysine (**81c**) K_{eq} = 6.5 M^{-1} for the retention of amino acids are certainly noteworthy.

Later the group reported a dopamine (**2**) receptor based on the same principle: A boronic acid-containing coumarin aldehyde was designed (**246**) [776] (Figure 175). The sensor binds to catecholamines such as dopamine (**2**) and norepinephrine by forming an iminium ion with the amine as well as a boronate ester with the catechol. It acts as an effective colorimetric sensor for dopamine (**2**, K_{ass} = 3400 M^{-1}, $\Delta\lambda_{max}$ = 30 nm) and norepinephrine (K_{ass} = 6500 M^{-1}, $\Delta\lambda_{max}$ = 24 nm) with excellent selectively over epinephrine (K_{ass} = 5000 M^{-1}, $\Delta\lambda_{max}$ = 0 nm), amino acids, and glucose (K_{ass} = 5–7 M^{-1}). The sensor responds differentially to catechol amines over simple amines, giving a fluorescence decrease in response to catechol-containing compounds (40–60% decrease) and a fluorescence increase with other amines (up to 50 fold for tyramine). The fluorescence quenching effect was found to be directly related to the catechol group. The electron-rich catechol is likely acting as a photoinduced electron transfer (PET) quencher of the coumarin under these conditions.

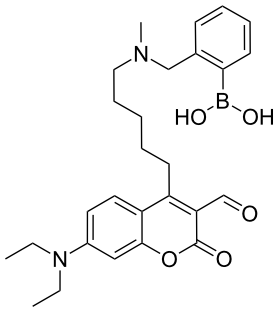

246

Figure 175: Coumarin aldehyde appended with boronic acid.

Other valuable binders for dopamine (**2**) have of course been described: Cyclophanes have been quite useful for selective dopamine recognition [777], including a recent example that displays shape-selective recognition with only non-covalent interactions [778]. For more examples the reader is referred to section six of this review.

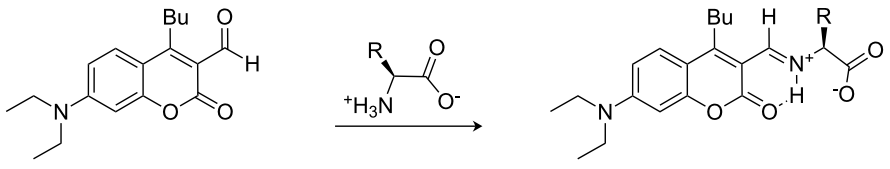

245 245a

Figure 174: Coumarin aldehyde (**245**) and its iminium species with amino acid bound (**245a**) by Glass et al.

A series of ditopic receptors (**247**) for diamines using dimers of a quinolone aldehyde chromophore (Figure 176) was explored by a combination of NMR, absorption and fluorescence spectroscopy [779]. It was shown that the dimeric sensors bound the diamine guests by formation of a bis-iminium ion, which produced large changes in the fluorescence of the quinolone core. Spectroscopic analysis was carried out in a 1:1 methanol–buffer solution system. The absorption spectra showed trends similar to those observed with the coumarin analogs in which a large red shift in absorption maximum was observed upon addition of diamines to the sensors. Diaminopropane was the best guest for all systems, with the highest binding to **247g** with a binding constant of 6700 M^{-1} which was 3–4 fold stronger compared to diamino-butane/pentane and 2.5 fold compared to ornithine/lysine (**81c**) with a maximum fluorescence increase at saturation (I_{sat}/I_0) of 6.6-fold. It bound lysine (**81c**) with 2800 M^{-1} and a fluorescence increase of 30 fold. The second best binder was **247d**. A shift in absorbance up to 28 nm was observed, consistent with a shift from aldehyde to iminium ion forms. The red shift in absorption has been attributed to the hydrogen bond between the formed iminium ion and the carbonyl group of the chromophore. By exciting the chromophore at 495 nm, a large increase in fluorescence was observed upon titration with the diamine: Up to 160 fold better binding for diamines compared to butylamine. The mode of binding and the 1:1 stoichiometry were confirmed by NMR experiments in chloroform.

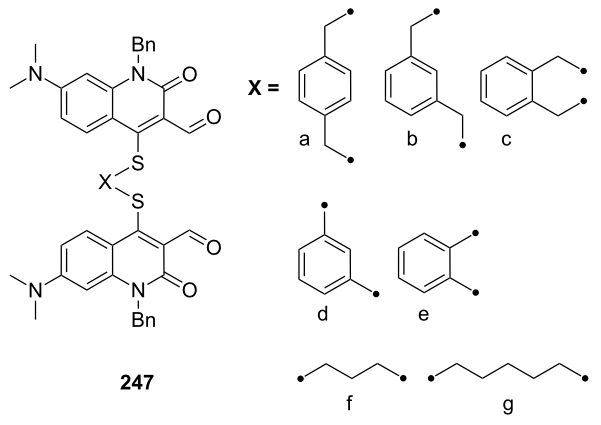

Figure 176: Quinolone aldehyde dimers by Glass et al.

Reversible covalent binding of an amino, e.g. forming a hemiaminal, has been realized in two chemosensor dyes with either one or two trifluoroacetophenone recognition moieties (Figure 177). As amines 1-propylamine, diethylamine, triethylamine, and aliphatic diamines of different chain length were used [780]. Their conversion into a hemiaminal or a zwitterion leads to a change in the electron delocalization within the dye molecule and subsequently to a shift in absorbance to shorter wavelengths. Comparing the interaction of **248a** and **248b** with amines in homogenous solution it was found, that for their reaction with diamines the K_{eq} values are significantly increased. The highest value was observed for 1,2-diaminoethane and the lowest for 1,4-diaminobutane. Table 18 compares the results.

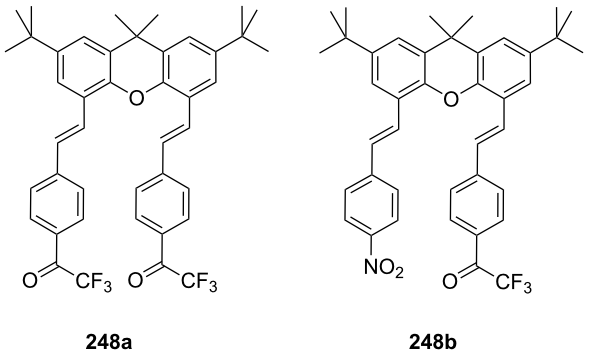

Figure 177: Chromogenic ammonium ion receptors with trifluoroacetophenone recognition motifs.

Table 18: Binding constants of amines to compounds **248a** and **248b** in ethyl acetate.

Amine	K_{eq} (**249a**) [M^{-1}]	K_{eq} (**249b**) [M^{-1}]
1-propylamine	195	210
1,2-diaminoethane	30000	5000
1,3-diaminopropane	26000	3500
1,4-diaminobutane	13000	700

The response and sensitivity towards monoamines was comparable, because only one functional group in **248a** can react with amines. The dyes embedded in thin layers of plasticized PVC (Figure 178) showed clear changes in absorbance on exposure to aliphatic amines.

Similarly, the chromogenic functional dye **249** (Figure 178) shows a significant color change in the presence of amines in organic solvents, with high sensitivity [781]. The cross-linked polymer sensor membranes allow a fast and reversible chemical reaction with solutions of primary aliphatic amines in most organic solvents. The equilibrium constants varied, depending on the solvent and analyte molecule, the sensor layers typically exhibited equilibrium constants of 100 M^{-1} for *n*-butylamine in chloroform, 1300 M^{-1} for 1,4-diaminobutane and 20,000 M^{-1} for tris(2-aminoethyl)amine in toluene. A change in selectivity due to the size or polarity of the analyte could not be observed.

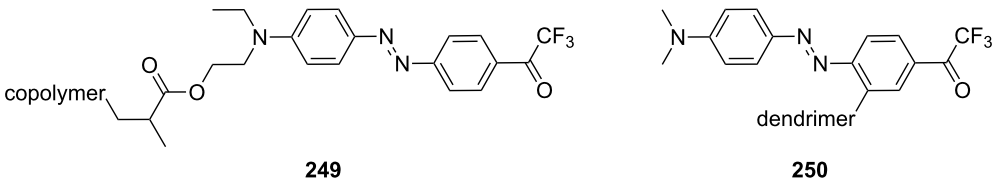

Figure 178: Chromogenic ammonium ion receptor with trifluoroacetophenone recognition motif bound on different matrices.

The reaction rate of the membranes with secondary and tertiary amines as well as with alcohols is slower than the rate with primary aliphatic amines, which gave the opportunity to distinguish ammonium guests by structure.

Zimmerman et al. have prepared receptors for diamines by incorporating trifluoromethyl ketones into a dendrimer (**250**) with success [782-784]. Such receptors showed, for example, selectivity for α,ω-diamines (H_3N^+–$(CH_2)_n$–NH_3^+) versus aromatic and cycloaliphatic diamine, amines, amino alcohols and diols. Complexation studies in THF by visible spectroscopy and NMR afforded an apparent association constant (K_{ass}) of 2.7×10^4 M^{-1} for $n = 3$ that was ca. 200-fold higher than that for *n*-butylamine (140 M^{-1}). The association constant for $n = 4$ was even 10–20% higher. Longer and shorter diamines bound less strongly [785].

Conclusion

We have presented various approaches for the detection and binding of ammonium ions and amino acids ranging from metal-complexing agents or reactive molecules via different inclusion compounds to weakly co-ordinating systems, such as crown ethers. A large number of molecular receptors of varying sizes, shapes and functionalities have been discussed in their interaction with the guests.

The synthetic hosts require complementarity to the ammonium guests in size, shape, and molecular interactions [786]. Typical interactions observed in the complexes of primary and secondary ammonium cations are ionic and dipolar interactions, dispersive forces such as van der Waals or hydrogen bonds. Cation–π- and ionic-interactions, often assisted by the hydrophobic effect and dispersive forces determine the binding of quaternary ammonium ions.

Binding an organic ammonium ion in solution three aspects have to be considered:

An organic ammonium ion never exists as a sole cation, an anion is always associated with it. Depending on the polarity and hydrogen donor/acceptor abilities of the solvent, the association strength is different [787]. The strength of the electrostatic interaction in solution, despite the solvation [788,789] of host and guest, influences the binding to an artificial receptor. Strongly co-ordinating counterions such as chloride generally lead to weaker binding constants upon recognition of the associated cation as compared to when large, soft and weakly co-ordinating counterions such as iodide (tetrafluoroborate, hexafluorophosphate or perchlorate) are employed [790-792].

The binding of primary, secondary and tertiary ammonium ions to the most receptor structures relies on H-bonding to a large extent. The complex stability depends on the number of H-bonds possible between host and guest [793], but also on the acidity of the ammonium ion. The more acidic an ammonium ion is, the stronger are the H-bonds with a particular donor site. For instance, primary, secondary and tertiary ammonium ions have pK_b-values between three and four and therefore stabilize a complex to a larger extent compared to an anilinium ion with a pK_b-value of nine to ten.

The third fact of importance is the steric bulk present in the guest (and the host). The better an ammonium ion can be placed in the recognition motif and the less interference is present in the complex, the stronger the association (assuming no additional co-ordination of the substituents can take place).

The many different examples reported in literature show that crown ethers are one of the most versatile classes of synthetic receptors for the recognition of ammonium ions. Crown ethers recognize ammonium-ions typically by hydrogen-bond interactions. Therefore only ammonium ions of primary and secondary amines are typical guests and quaternary ammonium ions are not bound. The crown-ether ammonium ion recognition motif has been extended to multitopic receptors allowing an analytical discrimination of diamines of different length, combined with anion recognition for the binding of amino acids. Many examples of transport and effective enantioselective recognition of amino acids, as esters or in zwitterionic form have been described. Crown ether amino acid building blocks for synthetic receptors were developed by Voyer [187] (Figure 29) and König [192,193] (Figure 31 and Figure 32). Such systems allow

the easy assembly of larger structures such as membrane channel mimics, which are of fundamental interest in medicine and biochemistry [794,795].

Substituted calixarenes can bind primary and secondary ammonium ions by ion–ion-, ion–dipole- and H-bond-interactions, and quaternary ammonium guests by ion–ion-, cation–π- and hydrophobic interactions. The molecular geometry of calixarenes is adjustable via their conformation, allowing a fine tuning of their selectivity for shape and size of the guest. This is not possible to the same extent with crown ethers. In addition, calixarenes often achieve binding selectivities exceeding those achieved with crown ethers due to guest inclusion being controlled by steric factors and various interactive forces of host and guest. Therefore, they can show remarkable selectivities in the discrimination of ammonium ion isomers. Especially noteworthy is their ability to complex strongly with quaternary ammonium ions.

Molecular tweezers and clips (Figure 109) serve as selective receptors for electron-deficient aromatic and aliphatic substrates. Cavity or clefts affect the thermodynamic stability and the binding kinetics; addition of side arms may enhance lipophilicity (long alkyl chains) or encourage interaction with some external entity, which makes these systems especially interesting for ammonium binding. Assisted by the hydrophobic effect of the cavity, van der Waals interactions and substantial electrostatic contributions for locking of the guest are responsible for the observed high efficiency and specificity found in clefts and cavitands. Water-soluble clips form stable complexes with *N*-alkylpyridinium, phenethylammonium ions, catechols and basic amino acids, which are often more stable in aqueous solution than in methanol due to a positive contribution of the hydrophobic effect to the receptor-substrate binding processes. C_{3v} symmetric tripods, tweezer ligands and preorganized molecular clefts reach ammonium ion binding selectivities that compete with naturally occurring recognition systems such as nonactin or valinomycin [618].

Cucurbiturils often reveal remarkably high affinity for alkanediammonium ions, size, shape, and functional group selectivity as a consequence of ion–dipole and hydrophobic interactions and have the highest binding constants of all presented receptor families in aqueous media (up to 10^{10} to 10^{12} M^{-1}). Generally, ammonium guests are co-ordinated by the carbonyl groups of the moieties by electrostatic ion–dipole attraction assisted by hydrogen bonding. The non-polar part of the guest is included in the cavity. The binding is governed by hydrophobic effects and van der Waals contacts. The entropic gain upon binding additionally supports the high association constants found with cucurbiturils. Together with cyclodextrins, a wide range of host cavities for ammonium ions with different shape, solubility, and chemical functionality is available.

Lewis-acidic metal centres in combination with carboxylate, trimethylammonium or H-bond donors bind guests with a high degree of selectivity and affinity. Amines and amino acids are preferred guests. Ionic interactions in combination with hydrogen bonds and the hydrophobic effect are the main contributions for their complex stabilization. The strong co-ordination of the metal centre allows guest binding even in competitive media like water.

Porphyrins in particular provide a useful framework for artificial receptors. The conjugated system facilitates the detection of interactions by UV–vis, fluorescence or circular dichroism measurements. It also provides a planar structure for the design of well-defined binding pockets with recognition groups attached in several distinct positions. The types of interactions utilized in these receptors include hydrophobic interaction, hydrogen bonding and, in most cases, co-ordinative bonds, taking advantage of the Lewis acidity of a metal, typically zinc [796]. Dimer structures based on metal-porphyrins allow for the enantiodiscrimination of diamines, amino acids, peptides and amino alcohols.

The rules how synthetic receptors interact with ammonium ion guests become clearer, which paves the way for a rational design of biomimetic devices, non-covalent synthesis and responsive host–guest systems. The study of synthetic ammonium ion receptors has certainly contributed to a better understanding of intermolecular interactions in various fields including drug design, DNA processing, enzyme interactions or approaches for the inhibition of protein–protein interactions [797,798]. Applications of ammonium ion recognition may be envisaged in many areas: Drug design, photo switching, separation, or motion and transport [799,800], self assembly in solution, and in the solid state.

References

1. Braman, S. S. *N. Engl. Reg. Allergy Proc.* **1987,** *8,* 116–120. doi:10.2500/108854187778994446
2. Idzko, M.; la Sala, A.; Ferrari, D. *J. Allergy Clin. Immunol.* **2002,** *109,* 839–846. doi:10.1067/mai.2002.124044
3. Yanai, K.; Tashiro, M. *Pharmacol. Ther.* **2007,** *113,* 1–15. doi:10.1016/j.pharmthera.2006.06.008
4. Ito, C. *Drug News Perspect.* **2004,** *17,* 383–387. doi:10.1358/dnp.2004.17.6.829029
5. Hubbard, B. K.; Walsh, C. T. *Angew. Chem., Int. Ed.* **2003,** *42,* 730–765. doi:10.1002/anie.200390202
6. Gingrich, J. A.; Caron, M. G. *Annu. Rev. Neurosci.* **1993,** *16,* 299–321. doi:10.1146/annurev.ne.16.030193.001503
7. Wolfbeis, O. S.; Li, H. *Biosens. Bioelectron.* **1993,** *8,* 161–166. doi:10.1016/0956-5663(93)85028-M

8. Jeffrey, G. A. *An Introduction to Hydrogen Bonding;* Oxford University Press: Oxford, U.K., 1997.
9. Rüdiger, V.; Schneider, H.-J.; Solov'ev, V. P.; Kazachenko, V. P.; Raevsky, O. A. *Eur. J. Org. Chem.* **1999,** 1847–1856. doi:10.1002/(SICI)1099-0690(199908)1999:8<1847::AID-EJOC1847>3.0.CO;2-Q
10. Hibbert, F.; Emsley, J. *Adv. Phys. Org. Chem.* **1990,** *26,* 255–379. doi:10.1016/S0065-3160(08)60047-7
11. Ma, J. C.; Dougherty, D. A. *Chem. Rev.* **1997,** *97,* 1303–1324. doi:10.1021/cr9603744
12. Sunner, J.; Nishizawa, K.; Kebarle, P. *J. Phys. Chem.* **1981,** *85,* 1814–1820. doi:10.1021/j150613a011
13. Sussman, J. L.; Harel, M.; Frolow, F.; Oefner, C.; Goldman, A.; Toker, L.; Silman, I. *Science* **1991,** *253,* 872–879. doi:10.1126/science.1678899
14. Burley, S. K.; Petsko, G. A. *Adv. Prot. Chem.* **1988,** *39,* 125–189. doi:10.1016/S0065-3233(08)60376-9
15. Eblinger, F.; Schneider, H.-J. *Angew. Chem., Int. Ed.* **1998,** *37,* 826–829. doi:10.1002/(SICI)1521-3773(19980403)37:6<826::AID-ANIE826>3.0.CO;2-Z
16. Hossain, M. A.; Schneider, H.-J. *Chem.–Eur. J.* **1999,** *5,* 1284–1290. doi:10.1002/(SICI)1521-3765(19990401)5:4<1284::AID-CHEM1284>3.0.CO;2-6
17. Cram, D. J. *Angew. Chem., Int. Ed. Engl.* **1986,** *25,* 1039–1057. doi:10.1002/anie.198610393
18. Gellman, S. H. *Chem. Rev.* **1997,** *97,* 1231–1232. doi:10.1021/cr970328j
19. Gale, P. A. *Philos. Trans. R. Soc. London, Ser. A* **2000,** *358,* 431–453. doi:10.1098/rsta.2000.0540
20. Southall, N. T.; Dill, K. A.; Haymet, A. D. J. *J. Phys. Chem. B* **2002,** *106,* 521–533. doi:10.1021/jp015514e
21. Smithrud, D. B.; Sanford, E. M.; Chao, I.; Ferguson, S. B.; Carcanague, D. R.; Evansek, J. D.; Houk, K. N.; Diederich, F. *Pure Appl. Chem.* **1990,** *62,* 2227–2236. doi:10.1351/pac199062122227
22. Blokzijl, W.; Engberts, B. F. N. *Angew. Chem., Int. Ed. Engl.* **1993,** *32,* 1545–1579. doi:10.1002/anie.199315451
23. Hoeben, F. J. M.; Jonkheijm, P.; Meijer, E. W.; Schenning, A. P. H. J. *Chem. Rev.* **2005,** *105,* 1491–1546. doi:10.1021/cr030070z
24. Hunter, Ch. A. *Angew. Chem., Int. Ed. Engl.* **1993,** *32,* 1584–1586. doi:10.1002/anie.199315841
25. Cram, D. J.; Trueblood, K. N. In *Concept, Structure, and Binding in Complexation, Host–Guest Complex Chemistry 1;* Vögtle, F., Ed.; Springer: Berlin, 1981; pp 43–106. Chapter 2.
26. Schneider, H.-J. *Angew. Chem., Int. Ed.* **2009,** *48,* 3924–3977. doi:10.1002/anie.200802947
27. Anslyn, E. V.; Dougherty, D. A. *Modern Physical Organic Chemistry;* University Science Books: Sausalito, CA, USA, 2006; pp 162–168.
28. Cram, D. J. *Science* **1988,** *240,* 760–767. doi:10.1126/science.3283937
29. Cram, D. J.; Cram, J. M. *Science* **1974,** *183,* 803–809. doi:10.1126/science.183.4127.803
30. Shinkai, S.; Ikeda, M.; Sugasaki, A.; Takeuchi, M. *Acc. Chem. Res.* **2001,** *34,* 494–503. doi:10.1021/ar000177y
31. Ercolani, G. *J. Am. Chem. Soc.* **2003,** *125,* 16097–16103. doi:10.1021/ja038396c
32. Hunter, C. A.; Anderson, H. L. *Angew. Chem., Int. Ed.* **2009,** *48,* 7488–7499. doi:10.1002/anie.200902490
33. Lindoy, L. F. *The Chemistry of Macrocyclic Ligand Complexes;* Cambridge University Press: New York & Melbourne, USA & Australia, 1989. doi:10.1017/CBO9780511564376
34. Cram, D. J. *Science* **1983,** *219,* 1177–1183. doi:10.1126/science.219.4589.1177
35. Lehn, J.-M. *Supramolecular Chemistry – Concepts and Perspectives;* Wiley-VCH: New York, USA, 1995.
36. Oshovsky, G. V.; Reinhoudt, D. N.; Verboom, W. *Angew. Chem., Int. Ed.* **2007,** *46,* 2366–2393. doi:10.1002/anie.200602815
37. Gill, V. M. S.; Oliveria, N. C. *J. Chem. Educ.* **1990,** *67,* 473–478. doi:10.1021/ed067p473
38. Macomber, R. S. *J. Chem. Educ.* **1992,** *69,* 375–378. doi:10.1021/ed069p375
39. Connors, K. A. *Binding Constants;* Wiley: New York, USA, 1987.
40. Horvath, G.; Huszthy, P.; Szarvas, S.; Szokan, G.; Redd, J. T.; Bradshaw, J. S.; Izatt, R. M. *Ind. Eng. Chem. Res.* **2000,** *39,* 3576–3581. doi:10.1021/ie000272a
41. Helgeson, R. C.; Koga, K.; Timko, J. M.; Cram, D. J. *J. Am. Chem. Soc.* **1973,** *95,* 3021–3023. doi:10.1021/ja00790a052
42. Gasparrini, F.; Misiti, D.; Villani, C.; Borchardt, A.; Burger, M. T.; Still, W. C. *J. Org. Chem.* **1995,** *60,* 4314–4315. doi:10.1021/jo00119a003
43. Ryoo, J. J.; Song, Y.-A.; Jeong, Y. H.; Hyun, M. H.; Park, J. H.; Lee, W. *Bull. Korean Chem. Soc.* **2006,** *27,* 637–641.
44. Kim, I. W.; Kwon, S. H.; McNeff, C. V.; Carr, P. W.; Jang, M. D.; Park, J. H. *Bull. Korean Chem. Soc.* **2006,** *27,* 589–592.
45. Chao, Y.; Cram, D. J. *J. Am. Chem. Soc.* **1976,** *98,* 1015–1017. doi:10.1021/ja00420a026
46. Talma, A. G.; Jouin, P.; De Vries, J. G.; Troostwijk, C. B.; Buning, G. H. W.; Waninge, J. K.; Visscher, J.; Kellogg, R. M. *J. Am. Chem. Soc.* **1985,** *107,* 3981–3997. doi:10.1021/ja00299a038
47. Breslow, R.; Czarnik, A. W.; Lauer, M.; Leppkes, R.; Winkler, J.; Zimmerman, S. *J. Am. Chem. Soc.* **1986,** *108,* 1969–1979. doi:10.1021/ja00268a040
48. Choi, S. H.; Huh, K. M.; Ooya, T.; Yui, N. *J. Am. Chem. Soc.* **2003,** *125,* 6350–6351. doi:10.1021/ja034149x
49. Bae, Y.; Fukushima, S.; Harda, A.; Kataoka, K. *Angew. Chem., Int. Ed.* **2003,** *42,* 4640–4643. doi:10.1002/anie.200250653
50. Tsukanov, A. V.; Dubonosov, A. D.; Bren, V. A.; Minkin, V. I. *Chem. Heterocycl. Compd.* **2008,** *44,* 899–923. doi:10.1007/s10593-008-0132-3
51. Kirkovits, G. J.; Shriver, J. A.; Gale, P. A.; Sessler, J. L. *J. Inclusion Phenom. Macrocyclic Chem.* **2001,** *41,* 69–75. doi:10.1023/A:1014468126351
52. Cametti, M.; Nissinen, M.; Cort, A. D.; Mandolini, L.; Rissanen, K. *J. Am. Chem. Soc.* **2007,** *129,* 3641–3648. doi:10.1021/ja068561z And literature given therein.
53. Mahoney, J. M.; Davis, J. P.; Beatty, A. M.; Smith, B. D. *J. Org. Chem.* **2003,** *68,* 9819–9820. doi:10.1021/jo035270p And literature citations therein.
54. Gutsche, C. D. *Calixarenes: An Introduction; Monographs in Supramolecular Chemistry,* 2nd ed.; Royal Society of Chemistry: Cambridge, U.K., 2008.
55. Rekharsky, M. V.; Inoue, Y. *Chem. Rev.* **1998,** *98,* 1875–1918. doi:10.1021/cr970015o
56. Steffen, A.; Apostolakis, J. *Chem. Cent. J.* **2007,** *1,* No. 29. doi:10.1186/1752-153X-1-29

57. Buschmann, H. J.; Schollmeyer, E.; Mutihac, L. *Thermochim. Acta* **2003,** *399,* 203–208. doi:10.1016/S0040-6031(02)00462-8
58. Crowley, J. D.; Goldup, S. M.; Lee, A.-L.; Leigh, D. A.; McBurney, R. T. *Chem. Soc. Rev.* **2009,** *38,* 1530–1541. doi:10.1039/b804243h
59. Xu, X.-N.; Wang, L.; Wang, G.-T.; Lin, J.-B.; Li, G.-Y.; Jiang, X.-K.; Li, Z.-T. *Chem.–Eur. J.* **2009,** *15,* 5763–5774. doi:10.1002/chem.200900309
60. Chang, T.; Heiss, A. M.; Cantrill, S. J.; Fyfe, M. C. T.; Pease, A. R.; Rowan, S. J.; Stoddart, J. F.; Williams, D. J. *Org. Lett.* **2000,** *2,* 2943–2946. doi:10.1021/ol006187g
61. Chang, T.; Heiss, A. M.; Cantrill, S. J.; Fyfe, M. C. T.; Pease, A. R.; Rowan, S. J.; Stoddart, J. F.; Williams, D. J.; White, A. J. P. *Org. Lett.* **2000,** *2,* 2947–2950. doi:10.1021/ol0061889
62. Huang, F.; Slebodnick, C.; Ratliff, A. E.; Gibson, H. W. *Tetrahedron Lett.* **2005,** *46,* 6019–6022. doi:10.1016/j.tetlet.2005.07.011
63. Harada, A.; Hashidzume, A.; Yamaguchi, H.; Takashima, Y. *Chem. Rev.* **2009,** *109,* 5974–6023. doi:10.1021/cr9000622
64. Huang, F.; Jones, J. W.; Slebodnick, C.; Gibson, H. W. *J. Am. Chem. Soc.* **2003,** *125,* 14458–14464. doi:10.1021/ja036606f
65. Niu, Z.; Gibson, H. W. *Chem. Rev.* **2009,** *109,* 6024–6046. doi:10.1021/cr900002h
66. Raymo, F. M.; Stoddart, J. F. *Pure Appl. Chem.* **1996,** *68,* 313–322. doi:10.1351/pac199668020313
67. Wu, J.; Fang, F.; Lu, W.-Y.; Hou, J.-L.; Li, C.; Wu, Z.-Q.; Jiang, X.-K.; Li, Z.-T.; Yu, Y.-H. *J. Org. Chem.* **2007,** *72,* 2897–2905. doi:10.1021/jo062523g
68. Cantrill, S. J.; Chichak, K. S.; Peters, A. J.; Stoddart, J. F. *Acc. Chem. Res.* **2005,** *38,* 1–9. doi:10.1021/ar040226x
69. Steed, J. W.; Atwood, J. L. In *Comprehensive Supramolecular Chemistry;* Gokel, G. W., Ed.; Pergamon: Oxford, U.K., 1996; Vol. 1, pp 213–243.
70. Collet, A. *Tetrahedron* **1987,** *43,* 5725–5759. doi:10.1016/S0040-4020(01)87780-2
71. Collet, A.; Dutasta, J.-P.; Lozach, B.; Canceill, J. *Top. Curr. Chem.* **1993,** *165,* 103–129. doi:10.1007/BFb0111282
72. Brotin, T.; Dutasta, J.-P. *Chem. Rev.* **2009,** *109,* 88–130. doi:10.1021/cr0680437
73. Ushakov, E. N.; Alfimov, M. V.; Gromov, S. P. *Russ. Chem. Rev.* **2008,** *77,* 39–58. doi:10.1070/RC2008v077n01ABEH003757
74. Shigeyuki, O.; Hironori, A.; Michinori, T.; Takehiko, Y. *Nippon Kagakkai Koen Yokoshu* **2003,** *83,* 658–667.
75. Tokunaga, Y.; Nakamura, T.; Yoshioka, M.; Shimomura, Y. *Tetrahedron Lett.* **2006,** *47,* 5901–5904. doi:10.1016/j.tetlet.2006.06.062
76. Northrop, B. H.; Zheng, Y.-R.; Chi, K.-W.; Stang, P. J. *Acc. Chem. Res.* **2009,** *42,* 1554–1563. doi:10.1021/ar900077c
77. Lehn, J.-M. *Chem. Soc. Rev.* **2007,** *36,* 151–160. doi:10.1039/b616752g
    And literature therein.
78. Faul, C. F. J.; Krattiger, P.; Smarsly, B. M.; Wennemers, H. *J. Mater. Chem.* **2008,** *18,* 2962–2967. doi:10.1039/b802690d
79. Cazacu, A.; Tong, C.; van der Lee, A.; Fyles, T. M.; Barboiu, M. *J. Am. Chem. Soc.* **2006,** *128,* 9541–9548. doi:10.1021/ja061861w
80. Reczek, J. J.; Kennedy, A. A.; Halbert, B. T.; Urbach, A. R. *J. Am. Chem. Soc.* **2009,** *131,* 2408–2415. doi:10.1021/ja808936y
81. Gnichwitz, J.-F.; Wielopolski, M.; Hartnagel, K.; Hartnagel, U.; Guldi, D. M.; Hirsch, A. *J. Am. Chem. Soc.* **2008,** *130,* 8491–8501. doi:10.1021/ja8018065
82. Philp, D.; Stoddart, J. F. *Angew. Chem., Int. Ed. Engl.* **1996,** *35,* 1155–1196. doi:10.1002/anie.199611541
83. Ihm, C.; Paek, K. *Tetrahedron Lett.* **2007,** *48,* 3263–3266. doi:10.1016/j.tetlet.2007.03.005
84. Badjic, J. D.; Balzani, V.; Credi, A.; Lowe, J. N.; Silvi, S.; Stoddart, J. F. *Chem.–Eur. J.* **2004,** *10,* 1926–1935. doi:10.1002/chem.200305687
85. Jasat, A.; Sherman, J. C. *Chem. Rev.* **1999,** *99,* 931–967. doi:10.1021/cr960048o
86. Sherman, J. C. *Chem. Commun.* **2003,** 1617–1623. doi:10.1039/b208553b
    And literature therein.
87. Sherman, J. C. *Tetrahedron* **1995,** *51,* 3395–3422. doi:10.1016/0040-4020(94)01072-8
88. Chiari, M.; Cretich, M.; Damin, F.; Di Carlo, G.; Oldani, C. *J. Chromatogr., B* **2008,** *866,* 89–103. doi:10.1016/j.jchromb.2008.01.006
89. Danielsson, B. *Adv. Biochem. Eng./Biotechnol.* **2008,** *109,* 97–122. doi:10.1007/10_2007_088
90. Nguyen, T. H.; Ansell, R. J. *Org. Biomol. Chem.* **2009,** *7,* 1211–1220. doi:10.1039/b816733h
91. Che, Y.; Zang, L. *Chem. Commun.* **2009,** 5106–5108. doi:10.1039/b913138h
92. Huang, F.; Nagvekar, D. S.; Slebodnick, C.; Gibson, H. W. *J. Am. Chem. Soc.* **2005,** *127,* 484–485. doi:10.1021/ja0438516
93. Ali, S. R.; Parajuli, R. R.; Balogun, Y.; Ma, Y.; He, H. *Sensors* **2008,** *8,* 8423–8452. doi:10.3390/s8128423
94. Stoddart, J. F. *Chem. Soc. Rev.* **2009,** *38,* 1802–1820. doi:10.1039/b819333a
95. Arduini, A.; Demuru, D.; Pochini, A.; Secchi, A. *Chem. Commun.* **2005,** *5,* 645–647. doi:10.1039/b411883a
96. Oesch, U.; Ammann, D.; Simon, W. *Clin. Chem.* **1986,** *32,* 1448–1459.
97. Pedersen, C. J. *Angew. Chem., Int. Ed. Engl.* **1988,** *27,* 1021–1027. doi:10.1002/anie.198810211
98. Pedersen, C. J. *J. Am. Chem. Soc.* **1967,** *89,* 7017–7036. doi:10.1021/ja01002a035
99. Cram, D. J. *Angew. Chem., Int. Ed. Engl.* **1988,** *27,* 1009–1020. doi:10.1002/anie.198810093
100. Timko, J. M.; Moore, S. S.; Walba, D. M.; Hiberty, P. C.; Cram, D. J. *J. Am. Chem. Soc.* **1977,** *99,* 4207–4219. doi:10.1021/ja00455a001
101. The binding strength decreases in the order prim. > sec. > tert. ammonium ion. It depends on the number of H-bonds that can be formed with the guest [see [794]].
102. Macrocyclic and macrobicyclic host compounds bind cations stronger (“macrocyclic or macrobicyclic effect”). Enthalpic and entropic effects contribute to this effect; the entropic “price” has been already paid during synthesis. The binding sites are oriented towards the guest molecule. The open chain analog podands would have to reorganize for binding first. Since this is associated with unfavorable entropy change complexes of podands are orders of magnitude less stable than those of coronands. Therefore simple podands are only of minor significance in modern recognition chemistry of ammonium ions.
103. Pedersen, C. J.; Frensdorff, H. K. *Angew. Chem., Int. Ed. Engl.* **1972,** *11,* 16–26. doi:10.1002/anie.197200161
104. Buschmann, H.-J.; Mutihac, R.-C.; Schollmeyer, E. *J. Solution Chem.* **2009,** *38,* 209–217. doi:10.1007/s10953-008-9358-z
105. Maleknia, S.; Brodbelt, J. *J. Am. Chem. Soc.* **1993,** *115,* 2837–2843. doi:10.1021/ja00060a034

106. Gokel, G. W. *Monographs in Supramolecular Chemistry: Crown Ethers and Cryptands;* Royal Society of Chemisty: Cambridge, U.K., 1991.
107. Czekalla, M.; Stephan, H.; Habermann, B.; Trepte, J.; Gloe, K.; Schmidtchen, F. P. *Thermochim. Acta* **1998,** *313,* 137–144. doi:10.1016/S0040-6031(98)00254-8
108. Cantrill, S. J.; Fulton, D. A.; Heiss, A. M.; Pease, A. R.; Stoddart, J. F.; White, A. J. P.; Williams, D. J. *Chem.–Eur. J.* **2000,** *6,* 2274–2287. doi:10.1002/1521-3765(20000616)6:12<2274::AID-CHEM2274>3.0.CO;2-2
109. Christensen, J. J.; Hill, J. O.; Izatt, R. M. *Science* **1971,** *174,* 459–467. doi:10.1126/science.174.4008.459
110. Geduhn, J.; Walenzyk, T.; König, B. *Curr. Org. Synth.* **2007,** *4,* 390–412. doi:10.2174/157017907782408770
111. Dietrich, B.; Kintzinger, J. P.; Lehn, J. M.; Metz, B.; Zahidi, A. *J. Phys. Chem.* **1987,** *91,* 6600–6606. doi:10.1021/j100311a009
112. Chekhlov, A. N. *J. Struct. Chem.* **2002,** *43,* 881–885. doi:10.1023/A:1022854130582
113. Chekhlov, A. N. *J. Struct. Chem.* **2003,** *44,* 335–339. doi:10.1023/A:1025583715549
114. Gokel, G. W.; Schall, O. F. In *Comprehensive Supramolecular Chemistry;* Gokel, G. W., Ed.; Pergamon Press: New York, USA, 1996; Vol. 1, pp 97–152.
115. Lehn, J.-M. *Angew. Chem., Int. Ed. Engl.* **1988,** *27,* 89–112. doi:10.1002/anie.198800891
116. Dietrich, B. In *Comprehensive Supramolecular Chemistry;* Gokel, G. W., Ed.; Pergamon Press: New York, USA, 1996; Vol. 1, pp 153–212.
117. de Namor, A. F. D.; Ritt, M. C.; Lewis, D. F. V.; Schwing-Weill, M. J.; Neu, F. A. *Pure Appl. Chem.* **1991,** *63,* 1435–1439. doi:10.1351/pac199163101435
118. Graf, E.; Kintzinger, J. P.; Lehn, J.-M.; LeMoigne, J. *J. Am. Chem. Soc.* **1982,** *104,* 1672–1678. doi:10.1021/ja00370a037
119. Bradshaw, J. S.; Izatt, R. M.; Bordunov, A. V.; Zhu, C. Y.; Hathaway, J. K. In *Comprehensive Supramolecular Chemistry;* Gokel, G. W., Ed.; Pergamon Press: New York, USA, 1996; Vol. 1, pp 35–95.
120. Gokel, G. W.; Abel, E. In *Comprehensive Supramolecular Chemistry;* Gokel, G. W., Ed.; Pergamon Press: New York, USA, 1996; Vol. 1, pp 511–535.
121. Cram, D. J.; Trueblood, K. N. *Top. Curr. Chem.* **1981,** *98,* 43–106. doi:10.1007/BFb0111246
122. Weimann, D. P.; Winkler, H. D. F.; Falenski, J. A.; Koksch, B.; Schalley, C. A. *Nat. Chem.* **2009,** *1,* 573–577. doi:10.1038/nchem.352
123. Winkler, H. D. F.; Weimann, D. P.; Springer, A.; Schalley, C. A. *Angew. Chem., Int. Ed.* **2009,** *48,* 7246–7250. doi:10.1002/anie.200902437
124. Kado, S.; Kimura, K. *J. Am. Chem. Soc.* **2003,** *125,* 4560–4564. doi:10.1021/ja029397s
125. Suzuki, K.; Siswanta, D.; Otsuka, T.; Amano, T.; Ikeda, T.; Hisamoto, H.; Yoshihara, R.; Ohba, S. *Anal. Chem.* **2000,** *72,* 2200–2205. doi:10.1021/ac9911241
126. Bülhman, P.; Prestch, E.; Bakker, E. *Chem. Rev.* **1998,** *98,* 1593–1687. doi:10.1021/cr970113+
127. Kim, H. S.; Park, H. J.; Oh, H. J.; Koh, Y. K.; Choi, J. H.; Lee, D. H.; Cha, G. S.; Nam, H. *Anal. Chem.* **2000,** *72,* 4683–4688. doi:10.1021/ac000177b
128. Jon, S. Y.; Kim, J.; Kim, M.; Park, S. H.; Jeon, W. S.; Heo, J.; Kim, K. *Angew. Chem., Int. Ed.* **2001,** *40,* 2116–2119. doi:10.1002/1521-3773(20010601)40:11<2116::AID-ANIE2116>3.0.CO;2-M
129. Campayo, L.; Pardo, M.; Jaúregui, A. C. O.; Yunta, M. J. R.; Cano, C.; Gomez-Contreras, F.; Navarrob, P.; Sanz, A. M. *Tetrahedron* **2004,** *60,* 979–986. doi:10.1016/j.tet.2003.11.040
130. Nagy, K.; Béni, S.; Szakacs, Z.; Bényei, A. C.; Noszál, B.; Kele, P.; Kotschy, A. *Tetrahedron* **2008,** *64,* 6191–6195. doi:10.1016/j.tet.2008.05.006
131. Zhang, X. X.; Bradshaw, J. S.; Izatt, R. M. *Chem. Rev.* **1997,** *97,* 3313–3361. doi:10.1021/cr960144p
132. Kyba, E. B.; Koga, K.; Sousa, L. R.; Siegel, M. G.; Cram, D. J. *J. Am. Chem. Soc.* **1973,** *95,* 2692–2693. doi:10.1021/ja00789a051
133. Dotsevi, G.; Sogah, D. G. Y.; Cram, D. J. *J. Am. Chem. Soc.* **1975,** *97,* 1259–1261. doi:10.1021/ja00838a059
134. Stoddart, J. F. In *Chiral Crown Ethers – Topics in Stereochemistry;* Eliel, E. L.; Wilen, S. H., Eds.; Wiley: New York, USA, 1988; Vol. 17.
135. Kyba, E. P.; Timko, J. M.; Kaplan, L. J.; De Jong, F.; Gokel, G. W.; Cram, D. J. *J. Am. Chem. Soc.* **1978,** *100,* 4555–4568. doi:10.1021/ja00482a040
136. Wang, X.; Erickson, S. D.; Iimori, T.; Still, W. C. *J. Am. Chem. Soc.* **1992,** *114,* 4128–4137. doi:10.1021/ja00037a014
137. Cram, D. J.; Cram, J. M. *Acc. Chem. Res.* **1978,** *11,* 8–14. doi:10.1021/ar50121a002
138. Lingenfelter, D. S.; Helgeson, R. C.; Cram, D. J. *J. Org. Chem.* **1981,** *46,* 393–406. doi:10.1021/jo00315a033
139. Davidson, R. B.; Bradshaw, J. S.; Jones, B. A.; Dalley, N. K.; Christensen, J. J.; Izatt, R. M.; Morin, F. G.; Grant, D. M. *J. Org. Chem.* **1984,** *49,* 353–357. doi:10.1021/jo00176a026
140. Stoddart, J. F. *Top. Stereochem.* **1987,** *17,* 207–288. doi:10.1002/9780470147269.ch3
141. Bradshaw, J. S.; Huszthy, P.; McDaniel, C. W.; Zhu, C. Y.; Dalley, N. K.; Izatt, R. M.; Lifson, S. *J. Org. Chem.* **1990,** *55,* 3129–3137. doi:10.1021/jo00297a031
142. Huszthy, P.; Bradshaw, J. S.; Zhu, C. Y.; Izatt, R. M.; Lifson, S. *J. Org. Chem.* **1991,** *56,* 3330–3336. doi:10.1021/jo00010a028
143. Armstrong, A.; Still, W. C. *J. Org. Chem.* **1992,** *57,* 4580–4582. doi:10.1021/jo00043a010
144. Araki, K.; Inada, K.; Shinkai, S. *Angew. Chem., Int. Ed. Engl.* **1996,** *35,* 72–74. doi:10.1002/anie.199600721
145. Huszthy, P.; Tóth, T. *Per. Pol. Chem. Eng.* **2007,** *51,* 45–51. doi:10.3311/pp.ch.2007-2.07
146. Izatt, R. M.; Pawlak, K.; Bradshaw, J. S. *Chem. Rev.* **1995,** *95,* 2529–2586. doi:10.1021/cr00039a010
147. Hellier, P. C.; Bradshaw, J. S.; Young, J. J.; Zhang, X. X.; Izatt, R. M. *J. Org. Chem.* **1996,** *61,* 7270–7275. doi:10.1021/jo960890u
148. Izatt, R. M.; Wang, T.-M.; Hathaway, J. K.; Zhang, X. X.; Curtis, J. C.; Bradshaw, J. S.; Zhu, C.-Y.; Huszthy, P. *J. Inclusion Phenom. Mol. Recognit. Chem.* **1994,** *17,* 157–175. doi:10.1007/BF00711856
149. Izatt, R. M.; Zhu, C.-Y.; Dalley, N. K.; Curtis, J. C.; Kou, X.; Bradshaw, J. S. *J. Phys. Org. Chem.* **1992,** *5,* 656. doi:10.1002/poc.610051007
150. Samu, E.; Huszthy, P.; Horváth, G.; Szöllosy, A.; Neszmélyi, A. *Tetrahedron: Asymmetry* **1999,** *10,* 3615–3626. doi:10.1016/S0957-4166(99)00381-X
151. NEA; NapEtHClO$_4$: (1-napthyl)ethylamine perchlorate salt; PEA; PhEtHClO$_4$: (1-phenyl)ethylamine perchlorate salt.

152. Prodi, L.; Bolletta, F.; Montalti, M.; Zaccheroni, N.; Huszthy, P.; Samu, E.; Vermes, B. *New J. Chem.* **2000,** *24,* 781–785. doi:10.1039/b004600k
153. Lakatos, S.; Fetter, J.; Bertha, F.; Huszthy, P.; Tóth, T.; Farkas, V.; Orosz, G.; Hollósi, M. *Tetrahedron* **2008,** *64,* 1012–1022. doi:10.1016/j.tet.2007.09.056
154. Lee, C.-S.; Teng, P.-F.; Wong, W.-L.; Kwonga, H.-L.; Chan, A. S. C. *Tetrahedron* **2005,** *61,* 7924–7930. doi:10.1016/j.tet.2005.06.014
155. Ozer, H.; Kocakaya, S. O.; Akgun, A.; Hosgören, H.; Togrul, M. *Tetrahedron: Asymmetry* **2009,** *20,* 1541–1546. doi:10.1016/j.tetasy.2009.06.010
156. Togrul, M.; Turgut, Y.; Hosgören, H. *Chirality* **2004,** *16,* 351–355. doi:10.1002/chir.20047
157. Turgut, Y.; Sahin, E.; Togrul, M.; Hosgören, H. *Tetrahedron: Asymmetry* **2004,** *15,* 1583–1588. doi:10.1016/j.tetasy.2004.03.035
158. Binding constants (*K*) with the enantiomers of the organic ammonium salts were determined by a titration UV–vis method in $CHCl_3$. In all cases the authors observed values supporting a linear relationship, supporting a 1:1 complex formation. The association constants of the supramolecular systems formed were calculated according to the Benesi–Hildebrand equation.
159. Karakaplan, M.; Turgut, Y.; Aral, T.; Hosgören, H. *J. Inclusion Phenom. Macrocyclic Chem.* **2006,** *54,* 315–319. doi:10.1007/s10847-005-9011-z
160. Turgut, Y.; Demirel, N.; Hosgören, H. *J. Inclusion Phenom. Macrocyclic Chem.* **2006,** *54,* 29–33. doi:10.1007/s10847-005-3125-1
161. Turgut, Y.; Aral, T.; Hosgören, H. *Tetrahedron: Asymmetry* **2009,** *20,* 2293–2298. doi:10.1016/j.tetasy.2009.09.010
162. Sunkur, M.; Baris, D.; Hosgoren, H.; Togrul, M. *J. Org. Chem.* **2008,** *73,* 2570–2575. doi:10.1021/jo702210c
163. Demirel, N.; Bulut, Y. *Tetrahedron: Asymmetry* **2003,** *14,* 2633–2637. doi:10.1016/S0957-4166(03)00594-9
164. Aydın, I.; Aral, T.; Karakaplan, M.; Hosgören, H. *Tetrahedron: Asymmetry* **2009,** *20,* 179–183. doi:10.1016/j.tetasy.2009.01.005
165. Colera, M.; Costero, A. M.; Gavin, P.; Gil, S. *Tetrahedron: Asymmetry* **2005,** *16,* 2673–2679. doi:10.1016/j.tetasy.2005.06.039
166. Curtis, W. D.; Laidler, D. A.; Stoddart, J. F.; Jones, G. H. *J. Chem. Soc., Perkin Trans. 1* **1977,** 1756–1769. doi:10.1039/P19770001756
167. Ellinghaus, R.; Schröder, G. *Liebigs Ann. Chem.* **1985,** *2,* 418–420. doi:10.1002/jlac.198519850218
And literature therein.
168. Lewandowski, B.; Jarosz, S. *Chem. Commun.* **2008,** 6399–6401. doi:10.1039/b816476b
169. Jarosz, S.; Lewandowski, B. *Carbohydr. Res.* **2008,** *343,* 965–969. doi:10.1016/j.carres.2008.01.016
170. Szejtli, J.; Osa, T. In *Comprehensive Supramolecular Chemistry;* Szejtli, J.; Osa, T., Eds.; Pergamon: Oxford, U.K., 1996; Vol. 3, pp 185–204.
171. Szente, L. In *Comprehensive Supramolecular Chemistry;* Szejtli, J.; Osa, T., Eds.; Pergamon: Oxford, U.K., 1996; Vol. 3, pp 253–278.
172. Snopek, J.; Smolkova-Keulemansova, E.; Cserhati, T.; Stalcup, A. M.; Gahm, K. H. In *Comprehensive Supramolecular Chemistry;* Szejtli, J.; Osa, T., Eds.; Pergamon: Oxford, U.K., 1996; Vol. 3, pp 515–572.
173. Harada, A.; Zsadan, B. In *Comprehensive Supramolecular Chemistry;* Szejtli, J.; Osa, T., Eds.; Pergamon: Oxford, U.K., 1996; Vol. 3, pp 573–586.
174. Shizuma, M.; Adachi, H.; Kawamura, M.; Takai, Y.; Takeda, T.; Sawada, M. *J. Chem. Soc., Perkin Trans. 2* **2001,** 592–601. doi:10.1039/b007478k
175. Kyba, E. B.; Koga, K.; Sousa, L. R.; Siegel, M. G.; Cram, D. J. *J. Am. Chem. Soc.* **1973,** *95,* 2692–2693. doi:10.1021/ja00789a051
176. Yamamoto, K.; Fukushima, H.; Okamoto, Y.; Hatada, K.; Nakazaki, M. *J. Chem. Soc., Chem. Commun.* **1984,** 1111–1113. doi:10.1039/C39840001111
177. Tsubaki, K.; Tanaka, H.; Kinoshita, T.; Fuji, K. *Tetrahedron* **2002,** *58,* 1679–1684. doi:10.1016/S0040-4020(02)00074-1
178. Tsubaki, K.; Tanaka, H.; Morikawa, H.; Fuji, K. *Tetrahedron* **2003,** *59,* 3195–3199. doi:10.1016/S0040-4020(03)00478-2
179. Naemura, K.; Nishioka, K.; Ogasahara, K.; Nishikawa, Y.; Hirose, K.; Tobe, Y. *Tetrahedron: Asymmetry* **1998,** *9,* 563–574. doi:10.1016/S0957-4166(97)00638-1
180. Steensma, M.; Kuipers, N. J. M.; de Haan, A. B.; Kwant, G. *J. Chem. Technol. Biotechnol.* **2006,** *81,* 588–597. doi:10.1002/jctb.1434
181. Misumi, S. *Pure Appl. Chem.* **1990,** *62,* 493–498. doi:10.1351/pac199062030493
182. Tsubaki, K.; Tanaka, H.; Furuta, T.; Kinoshita, T.; Fuji, K. *Tetrahedron Lett.* **2000,** *41,* 6089–6093. doi:10.1016/S0040-4039(00)01018-2
183. Fuji, K.; Tsubaki, K.; Tanaka, K.; Hayashi, N.; Otsubo, T.; Kinoshita, T. *J. Am. Chem. Soc.* **1999,** *121,* 3807–3808. doi:10.1021/ja9836444
184. Tsubaki, K.; Kusumoto, T.; Hayashi, N.; Nuruzzaman, M.; Fuji, K. *Org. Lett.* **2002,** *4,* 2313–2316. doi:10.1021/ol026191n
185. Tsubaki, K.; Tanima, D.; Nuruzzaman, M.; Kusumoto, T.; Fuji, K.; Kawabata, T. *J. Org. Chem.* **2005,** *70,* 4609–4616. doi:10.1021/jo050387u
186. Tsubaki, K. *J. Inclusion Phenom. Macrocyclic Chem.* **2008,** *61,* 217–225. doi:10.1007/s10847-008-9419-3
187. Voyer, N.; Deschenes, D.; Bernier, J.; Roby, J. *J. Chem. Soc., Chem. Commun.* **1992,** 664–668. doi:10.1039/C39920000664
188. Lein, G. M.; Cram, D. J. *J. Am. Chem. Soc.* **1985,** *107,* 448–455. doi:10.1021/ja00288a029
189. Schneider, H.-J.; Yatsimirsky, A. *Principles and Methods in Supramolecular Chemistry;* John Wiley & Sons Ltd.: Chichester, U. K., 2000.
190. Boudreault, P.-L.; Voyer, N. *Org. Biomol. Chem.* **2007,** *5,* 1459–1465. doi:10.1039/b702076g
191. Kim, S. K.; Bang, M. Y.; Lee, S.-H.; Nakamura, K.; Cho, S.-W.; Yoon, J. *J. Inclusion Phenom. Macrocyclic Chem.* **2002,** *43,* 71–75. doi:10.1023/A:1020454519360
192. Mandl, C. P.; König, B. *J. Org. Chem.* **2005,** *70,* 670–674. doi:10.1021/jo048105y
193. Späth, A.; König, B. *Tetrahedron* **2009,** *65,* 690–695. doi:10.1016/j.tet.2008.10.086
194. Elhabiri, M.; Trabolsi, A.; Cardinali, F.; Hahn, U.; Albrecht-Gary, A.-M.; Nierengarten, J.-F. *Chem.–Eur. J.* **2005,** *11,* 4793–4798. doi:10.1002/chem.200500246
195. Zhao, J.-M.; Zong, Q.-S.; Han, T.; Xiang, J.-F.; Chen, C.-F. *J. Org. Chem.* **2008,** *73,* 6800–6806. doi:10.1021/jo801170t
196. Paraquat derivatives containing two-hydroxyethyl or γ-hydroxypropyl groups form 1:2 complexes, in which two guests threaded the central cavity of the host. Other functional paraquat derivatives containing terminal hydroxyl, methoxyl, 9-anthracylmethyl, and amide groups were included in the cavity of the host to form 1:1 complexes.

197. Badjic, J. D.; Balzani, V.; Credi, A.; Silvi, S.; Stoddart, J. F. *Science* **2004,** *303,* 1845–1849. doi:10.1126/science.1094791
198. Badjic, J. D.; Cantrill, S.; Stoddart, J. F. *J. Am. Chem. Soc.* **2004,** *126,* 2288–2289. doi:10.1021/ja0395285
199. Huang, F.; Fronczek, F. R.; Gibson, H. W. *Chem. Commun.* **2003,** 1480–1481. doi:10.1039/b302682e
200. Long, B.; Nikitin, K.; Fitzmaurice, D. *J. Am. Chem. Soc.* **2003,** *125,* 15490–15498. doi:10.1021/ja037592g
201. Han, T.; Chen, C.-F. *Org. Lett.* **2006,** *8,* 1069–1072. doi:10.1021/ol053008s
202. Peng, X.-X.; Lu, H.-Y.; Han, T.; Chen, C.-F. *Org. Lett.* **2007,** *9,* 895–898. doi:10.1021/ol070017n
203. Huang, F.; Gibson, H. W.; Bryant, W. S.; Nagvekar, D. S.; Fronczek, F. R. *J. Am. Chem. Soc.* **2003,** *125,* 9367–9371. doi:10.1021/ja034968h
204. Huang, F.; Switek, K. A.; Zakharov, L. N.; Fronczek, F. R.; Slebodnick, C.; Lam, M.; Golen, J. A.; Bryant, W. S.; Mason, P. E.; Rheingold, A. L.; Ashraf-Khorassani, M.; Gibson, H. W. *J. Org. Chem.* **2005,** *70,* 3231–3241. doi:10.1021/jo050187i
205. Zhang, J.; Huang, F.; Li, N.; Wang, H.; Gibson, H. W.; Gantzel, P.; Rheingold, A. L. *J. Org. Chem.* **2007,** *72,* 8935–8938. doi:10.1021/jo701653q
206. Kruppa, M.; Mandl, Ch. P.; Miltschitzky, S.; König, B. *J. Am. Chem. Soc.* **2005,** *127,* 3362–3365. doi:10.1021/ja043930h
207. Stadlbauer, S.; Riechers, A.; Späth, A.; König, B. *Chem.–Eur. J.* **2008,** *14,* 2536–2541. doi:10.1002/chem.200701442
208. Jeong, K.-S.; Park, T.-Y. *Bull. Korean Chem. Soc.* **1999,** *20,* 129–131.
209. Costero, A. M.; Rodriguez-Muniz, G. M.; Gil, S.; Peransi, S.; Gavina, P. *Tetrahedron* **2008,** *64,* 110–116. doi:10.1016/j.tet.2007.10.066
210. Moghimi, A.; Rastegar, F. R.; Ghandi, M.; Taghizadeh, M.; Yari, A.; Shamsipur, M.; Yap, G. P. A.; Rahbarnoohi, H. *J. Org. Chem.* **2002,** *67,* 2065–2074. doi:10.1021/jo010869f
211. Moghimi, A.; Maddah, B.; Yari, A.; Shamsipur, M.; Boostani, M.; Rastegar, M. F.; Ghaderi, A. R. *J. Mol. Struct.* **2005,** *752,* 68–77. doi:10.1016/j.molstruc.2005.05.043
212. Mihai, D.; Barboiu, D.; Hovnanian, N. D.; Lucab, C.; Cop, L. *Tetrahedron* **1999,** *55,* 9221–9232. doi:10.1016/S0040-4020(99)00478-0
213. Hossain, M. A.; Schneider, H.-J. *J. Am. Chem. Soc.* **1998,** *120,* 11208–11209. doi:10.1021/ja982435g
214. Cooper, Ch. R.; James, T. D. *Chem. Commun.* **1997,** 1419–1420. doi:10.1039/a703300a
215. Suhs, T.; König, B. *Mini-Rev. Org. Chem.* **2006,** *3,* 315–331. doi:10.2174/157019306778742841
216. de Silva, A. P.; Gunaratne, H. Q. N.; McVeigh, C.; Maguire, G. E. M.; Maxwell, P. R. S.; O'Hanlon, E. *Chem. Commun.* **1996,** 2191–2192. doi:10.1039/cc9960002191
217. Sasaki, S.-i.; Hashizume, A.; Citterio, D.; Fuji, E.; Suzuki, K. *Tetrahedron Lett.* **2002,** *43,* 7243–7245. doi:10.1016/S0040-4039(02)01618-0
218. Schmidtchen, F. P. *J. Org. Chem.* **1986,** *51,* 5161–5168. doi:10.1021/jo00376a021
219. Metzger, A.; Gloe, K.; Stephan, H.; Schmidtchen, F. P. *J. Org. Chem.* **1996,** *61,* 2051–2055. doi:10.1021/jo951436d
220. Breccia, P.; van Gool, M.; Pérez-Fernandez, R.; Martín-Santamari, S.; Gago, F.; Prados, P.; de Mendoza, J. *J. Am. Chem. Soc.* **2003,** *125,* 8270–8284. doi:10.1021/ja026860s
221. Späth, A.; König, B. *Tetrahedron* **2010,** *66,* 1859–1873. doi:10.1016/j.tet.2010.01.028
222. Wenz, G. *Angew. Chem., Int. Ed.* **1994,** *33,* 803–822. doi:10.1002/anie.199408031
223. Special issue: Cyclodextrine chemistry. *Chem. Rev.* **1998,** *98,* 1741–2076.
224. Porwanski, S.; Dumarcay-Charbonnier, F.; Menuel, S.; Joly, J.-P.; Bulach, V.; Marsura, A. *Tetrahedron* **2009,** *65,* 6196–6203. doi:10.1016/j.tet.2009.05.057
225. Menuel, S.; Joly, J.-P.; Courcot, B.; Elyseè, J.; Ghermani, N. E.; Marsura, A. *Tetrahedron* **2007,** *63,* 1706–1714. doi:10.1016/j.tet.2006.10.070
226. Suzuki, I.; Obata, K.; Anzai, J.-i.; Ikeda, H.; Ueno, A. *J. Chem. Soc., Perkin Trans. 2* **2000,** 1705–1710. doi:10.1039/b002195o
227. Park, J. W.; Lee, S. Y.; Park, K. K. *Chem. Lett.* **2000,** *29,* 594–595. doi:10.1246/cl.2000.594
228. Hinsberg, O. *Chem. Ber.* **1890,** *23,* 2962–2965.
229. Jung, J. H.; Lee, S. J.; Kim, J. S.; Lee, W. S.; Sakata, Y.; Kaneda, T. *Org. Lett.* **2006,** *8,* 3009–3012. doi:10.1021/ol060923k
230. Jung, J. H.; Lee, H. Y.; Jung, S. H.; Lee, S. J.; Sakata, Y.; Kaneda, T. *Tetrahedron* **2008,** *64,* 6705–6710. doi:10.1016/j.tet.2008.05.013
231. Sirish, M.; Chertkov, V. A.; Schneider, H.-J. *Chem.–Eur. J.* **2002,** *8,* 1181–1188. doi:10.1002/1521-3765(20020301)8:5<1181::AID-CHEM1181>3.0.CO;2-U
232. Solladié, N.; Walther, M. E.; Herschbach, H.; Leize, E.; van Dorsselaer, A.; Figueira Duartec, T. M.; Nierengarten, J.-F. *Tetrahedron* **2006,** *62,* 1979–1987. doi:10.1016/j.tet.2005.07.120
233. Lehn, J.-M. *Supramolecular Chemistry, Concepts and Perspectives;* Wiley-VCH: Weinheim, Germany, 1995.
234. *Calixarenes: A Versatile Class of Macrocyclic Compounds;* Vicens, J.; Böhmer, V., Eds.; Topics in Inclusion Science, Vol. 3; Kluwer Academic Publishers: Dortrecht, The Netherlands, 1991.
235. Schneider, H.-J., Ed. *Frontiers in Supramolecular Chemistry;* Verlag Chemie: Weinheim, Germany, 1991.
236. Böhmer, V. *Angew. Chem.* **1995,** *107,* 785–818. doi:10.1002/ange.19951070704
237. Pochini, A.; Ungaro, R. In *Comprehensive Supramolecular Chemistry;* Vögtle, F., Ed.; Pergamon Press: New York, USA, 1996; Vol. 2, pp 103–142.
And literature citations herein.
238. Coquiere, D.; Marrot, J.; Reinaud, O. *Org. Lett.* **2007,** *9,* 3271–3274. doi:10.1021/ol071208t
And literature citations herein.
239. Moore, D.; Matthews, S. E. *J. Inclusion Phenom. Macrocyclic Chem.* **2009,** *65,* 137–155. doi:10.1007/s10847-009-9623-9
240. Masci, B.; Mortera, S. L.; Persiani, D.; Thuery, P. *J. Org. Chem.* **2006,** *71,* 504–511. doi:10.1021/jo051922t
241. Rydberg, J.; Musikas, C.; Choppin, G. R., Eds. *Principles and Practices of Solvent Extraction;* Marcel Dekker: New York, USA, 1992; p 357.
242. *Supramolecular Technology;* Reinhoudt, D. N., Ed.; Comprehensive Supramolecular Chemistry, Vol. 10; Pergamon Press: Oxford, U.K., 1996.
243. Ikeda, A.; Shinkai, S. *Chem. Rev.* **1997,** *97,* 1713–1734. doi:10.1021/cr960385x
244. Yordanov, A. T.; Roundhill, D. M. *Coord. Chem. Rev.* **1998,** *170,* 93–124. doi:10.1016/S0010-8545(97)00074-X
245. Beer, P. D. *J. Chem. Soc., Chem. Commun.* **1996,** 689–696. doi:10.1039/cc9960000689

246. Atwood, J. L.; Holman, K. T.; Steed, J. W. *J. Chem. Soc., Chem. Commun.* **1996,** 1401–1407. doi:10.1039/cc9960001401
247. Stibor, I.; Hafeed, D. S. M.; Lhotak, P.; Hodacova, J.; Koca, J.; Cajan, M. *Gazz. Chim. Ital.* **1997,** *127,* 673–685.
248. Gale, P. A.; Sessler, J. L.; Král, V. *J. Chem. Soc., Chem. Commun.* **1998,** 1–8. doi:10.1039/a706280j
249. Darbost, U.; Zeng, X.; Giorgi, M.; Jabin, I. *J. Org. Chem.* **2005,** *70,* 10552–10560. doi:10.1021/jo051886y
250. Diamond, D. *J. Inclusion Phenom. Mol. Recognit. Chem.* **1994,** *19,* 149–166. doi:10.1007/BF00708980
251. *Molecular Recognition: Receptors for Cationic Guests;* Gokel, G. W., Ed.; Comprehensive Supramolecular Chemistry, Vol. 1; Pergamon Press: Oxford, U.K., 1996; pp 605–634.
252. Diamond, D.; McKervey, M. A. *Chem. Soc. Rev.* **1996,** *25,* 15–24. doi:10.1039/cs9962500015
253. Giannetto, M.; Mori, G.; Notti, A.; Pappalardo, S.; Parisi, M. F. *Anal. Chem.* **1998,** *70,* 4631–4635. doi:10.1021/ac9803840
254. Shvedene, N. V.; Nemilova, M. Y.; Zatonskaya, V. L.; Pletnev, I. V.; Baulin, V. E.; Lyubitov, I. E.; Shvyadas, V. K. *J. Anal. Chem.* **1995,** *50,* 402–408.
255. Shvedene, N. V.; Nemilova, M. Y.; Kovalev, V. V.; Shokova, E. A.; Pletnev, I. V. *Sens. Actuators, B* **1995,** 372–379. doi:10.1016/0925-4005(94)01620-W
256. Rydberg, J.; Cox, M.; Musikas, C.; Choppin, G. R., Eds. *Solvent Extraction Principles and Practice,* 2nd ed.; Marcel Dekker: New York, 2004.
257. Castellano, R. K.; Diederich, F.; Meyer, E. A. *Angew. Chem., Int. Ed.* **2003,** *42,* 1210–1250. doi:10.1002/anie.200390319
258. Gokel, G. W.; Barbour, L. J.; Ferdani, R.; Hu, J. *Acc. Chem. Res.* **2002,** *35,* 878–886. doi:10.1021/ar000093p
259. Gokel, G. W.; DeWalland, S. L.; Meadows, E. S. *Eur. J. Org. Chem.* **2000,** *17,* 2967–2978. doi:10.1002/1099-0690(200009)2000:17<2967::AID-EJOC2967>3.0.CO;2-O
260. Araki, K.; Shimizu, H.; Shinkai, S. *Chem. Lett.* **1993,** *22,* 205–208. doi:10.1246/cl.1993.205
261. Atwood, L.; Szumna, A. *J. Supramol. Chem.* **2002,** *2,* 479–482. doi:10.1016/S1472-7862(03)00068-6
262. Hong, J.; Song, J.; Ham, S. *Tetrahedron Lett.* **2007,** *48,* 1327–1330. doi:10.1016/j.tetlet.2006.12.127
263. Pappalardo, S.; Parisi, M. F. *J. Org. Chem.* **1996,** *61,* 8724–8725. doi:10.1021/jo9615108
264. Bauer, L. J.; Gutsche, C. D. *J. Am. Chem. Soc.* **1985,** *107,* 6063–6069. doi:10.1021/ja00307a040
265. Gutsche, C. D.; Iqbal, M.; Alam, I. *J. Am. Chem. Soc.* **1987,** *109,* 4314–4320. doi:10.1021/ja00248a029
266. Shinkai, S. *Tetrahedron* **1993,** *49,* 8933–8969. doi:10.1016/S0040-4020(01)91215-3
267. Arnecke, R.; Böhmer, V.; Cacciapaglia, R.; Dalla Cort, A.; Mandolini, L. *Tetrahedron* **1997,** *53,* 4901–4908. doi:10.1016/S0040-4020(97)00185-3
268. Casnati, A.; Jacopozzi, P.; Pochini, A.; Ugozzoli, F.; Cacciapaglia, R.; Mandolini, L.; Ungaro, R. *Tetrahedron* **1995,** *51,* 591–598. doi:10.1016/0040-4020(94)00918-K
269. Iwamoto, K.; Ikeda, A.; Araki, K.; Harada, T.; Shinkai, S. *Tetrahedron* **1993,** *49,* 9937–9946. doi:10.1016/S0040-4020(01)80191-5
270. Görmar, G.; Seiffarth, K.; Schulz, M.; Chachimbombo, C. L. *J. Prakt. Chem.* **1991,** *333,* 475–479. doi:10.1002/prac.19913330314
271. Thuéry, P.; Asfari, Z.; Nierlich, M.; Vicens, J. *Acta Crystallogr., Sect. C: Cryst. Struct. Commun.* **2002,** *C58,* O223–O225. doi:10.1107/S0108270102003220
272. Arduini, A.; Ferdani, R.; Pochini, A.; Secchi, A.; Ugozzoli, F. *Angew. Chem., Int. Ed.* **2000,** *39,* 3453–3456. doi:10.1002/1521-3773(20001002)39:19<3453::AID-ANIE3453>3.0.CO;2-I
273. Arduini, A.; Calzavacca, F.; Pochini, A.; Secchi, A. *Chem.–Eur. J.* **2003,** *9,* 793–799. doi:10.1002/chem.200390089
274. Credi, A.; Dumas, S.; Silvi, S.; Venturi, M.; Arduini, A.; Pochini, A.; Secchi, A. *J. Org. Chem.* **2004,** *69,* 5881–5887. doi:10.1021/jo0494127
275. Arduini, A.; Ciesa, F.; Fragassi, M.; Pochini, A.; Secchi, A. *Angew. Chem., Int. Ed.* **2005,** *44,* 278–281. doi:10.1002/anie.200461336
276. de Namor, A. F. D.; Cleverley, R. M.; Zapata-Ormachea, M. L. *Chem. Rev.* **1998,** *98,* 2495–2525. doi:10.1021/cr970095w
277. Ludwig, R. *Microchim. Acta* **2005,** *152,* 1–19. doi:10.1007/s00604-005-0422-8
278. Biros, S. M.; Rebek, J., Jr. *Chem. Soc. Rev.* **2007,** *36,* 93–104. doi:10.1039/b508530f
279. Arnaud-Neu, F.; Fuangswasdi, S.; Notti, A.; Pappalardo, S.; Parisi, M. F. *Angew. Chem., Int. Ed.* **1998,** *37,* 112–114. doi:10.1002/(SICI)1521-3773(19980202)37:1/2<112::AID-ANIE112>3.0.CO;2-O
280. Steffen, L. W.; Steffen, B. W. *Clin. Chem.* **1976,** *22,* 381–383.
281. Shinkai, S. Functionalized Calixarenes: New applications. In *Calixarenes: A versatile class of macrocyclic compounds;* Vicens, J.; Böhmer, V., Eds.; Topics in Inclusion Science, Vol. 3; Kluwer Academic Publishers: Dordrecht, The Netherlands, 1991; pp 173–198.
282. Nagasaki, T.; Tajiri, Y.; Shinkai, S. *Recl. Trav. Chim. Pays-Bas* **1993,** *112,* 407–411.
283. Shinkai, S.; Kawabata, H.; Matsuda, T.; Kawaguchi, H.; Manabe, O. *Bull. Chem. Soc. Jpn.* **1990,** *63,* 1272–1274. doi:10.1246/bcsj.63.1272
284. Arduini, A.; Pochini, A.; Reverberi, S.; Ungaro, R. *J. Chem. Soc., Chem. Commun.* **1984,** 981–982. doi:10.1039/C39840000981
285. Shinkai, S.; Araki, K.; Matsuda, T.; Manabe, O. *Bull. Chem. Soc. Jpn.* **1989,** *62,* 3856–3862. doi:10.1246/bcsj.62.3856
286. Shinkai, S.; Araki, K.; Manabe, O. *J. Am. Chem. Soc.* **1988,** *110,* 7214–7215. doi:10.1021/ja00229a046
287. Zhang, L.; Macias, A.; Lu, T.; Gordon, J. L.; Gokel, G. W.; Kaifer, A. E. *J. Chem. Soc., Chem. Commun.* **1993,** 1017–1019. doi:10.1039/C39930001017
288. Arena, G.; Gentile, S.; Gulino, F. G.; Sciotto, D.; Sgarlata, C. *Tetrahedron Lett.* **2004,** *45,* 7091–7094. doi:10.1016/j.tetlet.2004.07.108
289. Koh, K. N.; Araki, K.; Ikeda, A.; Otsuka, H.; Shinkai, S. *J. Am. Chem. Soc.* **1996,** *118,* 755–758. doi:10.1021/ja951488k
290. Douteau-Guevel, N.; Coleman, A. W.; Morel, J.-P.; Morel-Desrosiers, N. *J. Phys. Org. Chem.* **1998,** *11,* 693–696. doi:10.1002/(SICI)1099-1395(1998100)11:10<693::AID-POC18>3.0.CO;2-8
291. Arena, G.; Contino, A.; Gulio, F. G.; Magri, A.; Sansone, F.; Sciotto, D.; Ungaro, R. *Tetrahedron Lett.* **1999,** *40,* 1597–1600. doi:10.1016/S0040-4039(98)02654-9
292. Arena, G.; Casnati, A.; Contino, A.; Magri, A.; Sansone, F.; Sciotto, D.; Ungaro, R. *Org. Biomol. Chem.* **2006,** *4,* 243–249. doi:10.1039/b514896k

293. Douteau-Guevel, N.; Coleman, A. W.; Morel, J.-P.; Morel-Desrosiers, N. *J. Chem. Soc., Perkin Trans. 2* **1999,** 629–633. doi:10.1039/a806855k
294. Kalchenko, O. I.; Perret, F.; Morel-Desrosiers, N.; Coleman, A. W. *J. Chem. Soc., Perkin Trans. 2* **2001,** 258–263. doi:10.1039/b005497f
295. Douteau-Guével, N.; Perret, F.; Coleman, A. W.; Morel, J.-P.; Morel-Desrosiers, N. *J. Chem. Soc., Perkin Trans. 2* **2002,** 524–532. doi:10.1039/b109553f
296. Interaction with GAG receptor sequences can lead to modulation of lysyloxidase activity and antithrombotic effects.
297. Arena, G.; Casnati, A.; Contino, A.; Lombardo, G. G.; Sciotti, D.; Ungaro, R. *Chem.–Eur. J.* **1999,** *5,* 738–744. doi:10.1002/(SICI)1521-3765(19990201)5:2<738::AID-CHEM738>3.0.CO;2-6
298. TMA = tetramethylammonium, BTMA = benzyltrimethylammonium, BTMAN = nitrobenzyltrimethylammonium, TMAC = tetramethylammonium chloride, BMAC = benzyltrimethylammonium chloride.
299. Kalchenko, O. I.; Da Silva, E.; Coleman, A. W. *J. Inclusion Phenom. Macrocyclic Chem.* **2002,** *43,* 305–310. doi:10.1023/A:1021203505307
300. Da Silva, E.; Coleman, A. W. *Tetrahedron* **2003,** *59,* 7357–7364. doi:10.1016/S0040-4020(03)01137-2
301. Poh, B.-L.; Teem, Ch. M. *Tetrahedron* **2005,** *61,* 5123–5129. doi:10.1016/j.tet.2005.03.032
302. Witt, D.; Dziemidowicz, J.; Rachon, J. *Heteroat. Chem.* **2004,** *15,* 155–162. doi:10.1002/hc.10229
303. Zielenkiewicz, W.; Marcinowicz, A.; Poznanski, J.; Cherenok, S.; Kalchenko, V. *J. Inclusion Phenom. Macrocyclic Chem.* **2006,** *55,* 11–19. doi:10.1007/s10847-005-9012-y
304. Zielenkiewicz, W.; Marcinowicz, A.; Poznanski, J.; Cherenok, S.; Kalchenko, V. *J. Mol. Liq.* **2005,** *121,* 8–14. doi:10.1016/j.molliq.2004.08.031
305. Zielenkiewicz, W.; Marcinowicz, A.; Poznanski, J.; Cherenok, S.; Kalchenko, V. *Supramol. Chem.* **2006,** *18,* 167–176. doi:10.1080/10610270500484738
306. Tairov, M. A.; Vysotsky, M. O.; Kalchenko, O. I.; Pirozhenko, V. V.; Kalchenko, V. I. *J. Chem. Soc., Perkin Trans. 1* **2002,** 1405–1411. doi:10.1039/b110691k
307. Dziemidowicz, J.; Witt, D.; Rachon, J. *J. Inclusion Phenom. Macrocyclic Chem.* **2008,** *61,* 381–391. doi:10.1007/s10847-008-9434-4
308. Zadmard, R.; Schrader, T. *J. Am. Chem. Soc.* **2005,** *127,* 904–915. doi:10.1021/ja045785d
309. Kolusheva, S.; Zadmard, R.; Schrader, T.; Jelinek, R. *J. Am. Chem. Soc.* **2006,** *128,* 13592–13598. doi:10.1021/ja064957z
310. Antipin, I. S.; Stoikov, I.; Pinkhassik, E. M.; Fitseva, N. A.; Stibor, I.; Konovalov, A. *Tetrahedron Lett.* **1997,** *38,* 5865–5868. doi:10.1016/S0040-4039(97)01305-1
311. Cherenok, S.; Vovk, A.; Muravyova, I.; Shivanyuk, A.; Kukhar, V.; Lipkowski, J.; Kalchenko, V. *Org. Lett.* **2006,** *8,* 549–552. doi:10.1021/ol052469a
312. Cherenok, S.; Vovk, A.; Kalchenko, V.; Kukhar, V. P.; Muzychka, O. V.; Lozynsky, M. O. *Org. Biomol. Chem.* **2004,** *2,* 3162–3166. doi:10.1039/b409526j
313. Kalchenko, O.; Marcinowicz, A.; Poznanski, J.; Cherenok, S.; Solovyov, A.; Zielenkiewicz, W.; Kalchenko, V. *J. Phys. Org. Chem.* **2005,** *18,* 578–585. doi:10.1002/poc.902
If a calix[4]arene carries dihydroxyphosphoryl groups at the lower rim it is a potent enzyme inhibitor.
314. Pulpoka, B.; Asfari, Z.; Vicens, J. *Tetrahedron Lett.* **1996,** *37,* 8747–8750. doi:10.1016/S0040-4039(96)02018-7
315. Salorinne, K.; Nissinen, M. *J. Inclusion Phenom. Macrocyclic Chem.* **2008,** *61,* 11–27. doi:10.1007/s10847-008-9411-y
316. Takeshita, M.; Inokuchi, F.; Shinkai, S. *Tetrahedron Lett.* **1995,** *36,* 3341–3344. doi:10.1016/0040-4039(95)00536-L
317. Araki, K.; Inada, K.; Otsuka, H.; Shinkai, S. *Tetrahedron* **1993,** *49,* 9465–9478. doi:10.1016/S0040-4020(01)80216-7
318. Takeshita, M.; Shinkai, S. *Chem. Lett.* **1994,** *23,* 1349–1352. doi:10.1246/cl.1994.1349
319. Takeshita, M.; Shinkai, S. *Chem. Lett.* **1994,** *23,* 125–128. doi:10.1246/cl.1994.125
320. Tsubaki, K.; Otsubo, T.; Tanaka, K.; Fuji, K. *J. Org. Chem.* **1998,** *63,* 3260–3265. doi:10.1021/jo971945a
321. Liu, S.-L.; Gong, S.-L.; Chen, Y.-Y. *Chin. J. Chem.* **2005,** *23,* 1651–1654. doi:10.1002/cjoc.200591651
322. De Iasi, G.; Masci, B. *Tetrahedron Lett.* **1993,** *34,* 6635–6638. doi:10.1016/0040-4039(93)88124-2
323. Tsubaki, K.; Morimoto, T.; Otsubo, T.; Fuji, K. *Org. Lett.* **2002,** *4,* 2301–2304. doi:10.1021/ol026019j
324. Mohindra Chawla, H.; Srinivas, K. *J. Chem. Soc., Chem. Commun.* **1994,** 2593–2594. doi:10.1039/c39940002593
325. Mohindra Chawla, H.; Srinivas, K. *J. Org. Chem.* **1996,** *61,* 8464–8467. doi:10.1021/jo950808f
326. Arduini, A.; McGregor, W. M.; Paganuzzi, D.; Pochini, A.; Secchi, A.; Ugozzoli, F.; Ungaro, R. *J. Chem. Soc., Perkin Trans. 2* **1996,** 839–846. doi:10.1039/p29960000839
327. Jung, Y. E.; Song, B. M.; Chang, S.-K. *J. Chem. Soc., Perkin Trans. 2* **1995,** 2031–2034. doi:10.1039/p29950002031
328. Zheng, Q.-Y.; Chen, C.-F.; Huang, Z.-T. *Tetrahedron* **1997,** *53,* 10345–10356. doi:10.1016/S0040-4020(97)00653-4
329. Zheng, Q.-Y.; Chen, C.-F.; Huang, Z.-T. *J. Inclusion Phenom. Macrocyclic Chem.* **2003,** *45,* 27–34. doi:10.1023/A:1023018512104
And literature herein.
330. Pappalardo, S.; Parisi, M. F. *Tetrahedron Lett.* **1996,** *37,* 1493–1496. doi:10.1016/0040-4039(96)00047-0
331. Chang, S.-K.; Hwang, H.-S.; Son, H.; Youk, J.; Kang, Y. S. *J. Chem. Soc., Chem. Commun.* **1991,** *4,* 217–218. doi:10.1039/C39910000217
332. Ballistreri, F. P.; Notti, A.; Pappalardo, S.; Parisi, M. F.; Pisagatti, I. *Org. Lett.* **2003,** *5,* 1071–1074. doi:10.1021/ol034093b
333. Sansone, F.; Barboso, S.; Casnati, A.; Fabbi, M.; Pochini, A.; Ungaro, R. *Eur. J. Org. Chem.* **1998,** *5,* 897–905. doi:10.1002/(SICI)1099-0690(199805)1998:5<897::AID-EJOC897>3.0.CO;2-K
334. Sansone, F.; Barboso, S.; Casnati, A.; Sciotto, D.; Ungaro, R. *Tetrahedron Lett.* **1999,** *40,* 4741–4744. doi:10.1016/S0040-4039(99)00838-2
335. Casnati, A.; Sansone, F.; Ungaro, R. *Acc. Chem. Res.* **2003,** *36,* 246–254. doi:10.1021/ar0200798
336. Ito, K.; Noike, M.; Kida, A.; Ohba, Y. *J. Org. Chem.* **2002,** *67,* 7519–7522. doi:10.1021/jo020300u
337. Kubo, Y.; Maeda, S.; Tokita, S.; Kubo, M. *Nature* **1996,** *382,* 522–524. doi:10.1038/382522a0
338. Grady, T.; Harris, S. J.; Smyth, M. R.; Diamond, D.; Hailey, P. *Anal. Chem.* **1996,** *68,* 3775–3782. doi:10.1021/ac960383c
339. Grady, T.; Joyce, T.; Smyth, M. R.; Harris, S. J.; Diamond, D. *Anal. Commun.* **1998,** *35,* 123–125. doi:10.1039/a802025f

340. Erdemir, S.; Tabakci, M.; Yilmaz, M. *Tetrahedron: Asymmetry* **2006,** *17,* 1258–1263. doi:10.1016/j.tetasy.2006.04.013
341. Arduini, A.; Giorgi, G.; Pochini, A.; Secchi, A.; Ugozzoli, F. *J. Org. Chem.* **2001,** *66,* 8302–8308. doi:10.1021/jo016035e
342. Harrowfield, J. M.; Ricmond, W. R.; Sobolev, A. N. *J. Inclusion Phenom. Mol. Recognit. Chem.* **1994,** *19,* 257–276. doi:10.1007/BF00708986
343. Yamato, T.; Zhang, F.; Tsuzuki, H.; Miura, Y. *Eur. J. Org. Chem.* **2001,** 1069–1075. doi:10.1002/1099-0690(200103)2001:6<1069::AID-EJOC1069>3.0.CO;2-R
344. Takeshita, M.; Nishio, S.; Shinkai, S. *J. Org. Chem.* **1994,** *59,* 4032–4034. doi:10.1021/jo00094a003
345. Darbost, U.; Giorgi, M.; Reinaud, O.; Jabin, I. *J. Org. Chem.* **2004,** *69,* 4879–4884. doi:10.1021/jo035859o
346. Zeng, X.; Coquire, D.; Alenda, A.; Garrier, E.; Prang, T.; Li, Y.; Reinaud, O.; Jabin, I. *Chem.–Eur. J.* **2006,** *12,* 6393–6402. doi:10.1002/chem.200600278
347. Sénéque, O.; Rager, M.-N.; Giorgi, M.; Reinaud, O. *J. Am. Chem. Soc.* **2000,** *122,* 6183–6189. doi:10.1021/ja000185+
348. Le Gac, S.; Jabin, I. *Chem.–Eur. J.* **2008,** *14,* 548–557. doi:10.1002/chem.200701051
349. Le Gac, S.; Ménand, M.; Jabin, I. *Org. Lett.* **2008,** *10,* 5195–5198. doi:10.1021/ol8021726
350. Sessler, J. L.; Gale, A. P.; Cho, W.-S. *Anion Receptor Chemistry;* Royal Society of Chemistry: Cambridge, U.K., 2006; pp 259–293. doi:10.1039/9781847552471-00259
For a review on receptors for ion pairs.
351. Szumna, A. *Org. Biomol. Chem.* **2007,** *5,* 1358–1368. doi:10.1039/b701451a
352. Hayashida, O.; Ito, J.; Matsumoto, S.; Hamachi, I. *Org. Biomol. Chem.* **2005,** *3,* 654–660. doi:10.1039/b418880b
353. Saito, S.; Nuckolls, C.; Rebek, J., Jr. *J. Am. Chem. Soc.* **2000,** *122,* 9628–9630. doi:10.1021/ja002220i
354. Murayama, K.; Aoki, K. *Chem. Commun.* **1997,** 119–120. doi:10.1039/a607131g
355. Lehn, J.-M.; Meric, R.; Vigneron, J.-P.; Cesario, M.; Guilhem, J.; Pascard, C.; Asfari, Z.; Vicens, J. *Supramol. Chem.* **1995,** *5,* 97–103. doi:10.1080/10610279508029480
356. Atwood, J. L.; Barbour, L. J.; Junk, P. C.; Orr, W. *Supramol. Chem.* **1995,** *5,* 105–108. doi:10.1080/10610279508029481
357. Schneider, H.-J.; Schneider, U. *J. Org. Chem.* **1987,** *52,* 1613–1615. doi:10.1021/jo00384a046
358. Mansikkamäki, H.; Schalley, C. A.; Nissinen, M.; Rissanen, K. *New J. Chem.* **2005,** *29,* 116–127. doi:10.1039/b415401k
359. Mansikkamäki, H.; Nissinen, M.; Rissanen, K. *Chem. Commun.* **2002,** 1902–1903. doi:10.1039/b204937f
360. Schneider, H.-J.; Güttes, D.; Schneider, U. *Angew. Chem., Int. Ed. Engl.* **1986,** *25,* 647–649. doi:10.1002/anie.198606471
361. Kazakova, E. Kh.; Ziganshina, A. U.; Muslinkina, L. A.; Morozova, J. E.; Makarova, N. A.; Mustafina, A. R.; Habicher, W. D. *J. Inclusion Phenom. Macrocyclic Chem.* **2002,** *43,* 65–69. doi:10.1023/A:1020404220640
362. Schnatwinkel, B.; Rekharsky, M. V.; Brodbeck, R.; Borovkov, V. V.; Inoue, Y.; Mattay, J. *Tetrahedron* **2009,** *65,* 2711–2715. doi:10.1016/j.tet.2009.01.066
363. Demura, M.; Yoshida, T.; Hirokawa, T.; Kumaki, Y.; Aizawa, T.; Nitta, K.; Bitter, I.; Tóth, K. *Bioorg. Med. Chem. Lett.* **2005,** *15,* 1367–1370. doi:10.1016/j.bmcl.2005.01.012
364. Tan, S.-D.; Chen, W.-H.; Satake, A.; Wang, B.; Xu, Z.-L.; Kobuke, Y. *Org. Biomol. Chem.* **2004,** *2,* 2719–2721. doi:10.1039/b410296g
365. Salorinne, K.; Tero, T.-R.; Riikonen, K.; Nissinen, M. *Org. Biomol. Chem.* **2009,** *7,* 4211–4217. doi:10.1039/b911389d
366. Melegari, M.; Suman, M.; Pirondini, L.; Moiani, D.; Massera, C.; Ugozzoli, F.; Kalenius, E.; Vainiotalo, P.; Mulatier, J.-C.; Dutasta, J.-P.; Dalcanale, E. *Chem.–Eur. J.* **2008,** *14,* 5772–5779. doi:10.1002/chem.200800327
367. Biavardi, E.; Battistini, G.; Montalti, M.; Yebeutchou, R. M.; Prodi, L.; Dalcanale, E. *Chem. Commun.* **2008,** 1638–1640. doi:10.1039/b801729h
368. Botta, B.; D'Acquarica, I.; Nevola, L.; Sacco, F.; Lopez, Z. V.; Zappia, G.; Fraschetti, C.; Speranza, M.; Tafi, A.; Caporuscio, F.; Letzel, M. C.; Mattay, J. *Eur. J. Org. Chem.* **2007,** 5995–6002. doi:10.1002/ejoc.200700829
369. Moran, J. R.; Karbach, S.; Cram, D. J. *J. Am. Chem. Soc.* **1982,** *104,* 5826–5828. doi:10.1021/ja00385a064
370. Sherman, J. C.; Knobler, C. C.; Cram, D. J. *J. Am. Chem. Soc.* **1991,** *113,* 2194–2204. doi:10.1021/ja00006a043
371. Dalcanale, E.; Soncini, P.; Bacchilega, G.; Ugozzoli, F. *J. Chem. Soc., Chem. Commun.* **1989,** 500–502. doi:10.1039/C39890000500
372. Tunstad, L. M.; Tucker, J. A.; Dalcanale, E.; Weiser, J.; Bryant, J. A.; Sherman, J. C.; Helgeson, R. C.; Knobler, C. B.; Cram, D. J. *J. Org. Chem.* **1989,** *54,* 1305–1312. doi:10.1021/jo00267a015
373. Rudkevich, D. M.; Rebek, J., Jr. *Eur. J. Org. Chem.* **1999,** 1991–2005. doi:10.1002/(SICI)1099-0690(199909)1999:9<1991::AID-EJOC1991>3.0.CO;2-5
374. Ballester, P.; Shivanyuk, A.; Rafai Far, A.; Rebek, J., Jr. *J. Am. Chem. Soc.* **2002,** *124,* 14014–14016. doi:10.1021/ja0282689
375. Ballester, P.; Sarmentero, M. A. *Org. Lett.* **2006,** *8,* 3477–3480. doi:10.1021/ol061097i
376. Lledó, A.; Hooley, R. J.; Rebek, J., Jr. *Org. Lett.* **2008,** *10,* 3669–3671. doi:10.1021/ol801228b
377. Hooley, R. J.; Biros, S. M.; Rebek, J., Jr. *Angew. Chem.* **2006,** *118,* 3597–3599. doi:10.1002/ange.200600405
378. Trembleau, L.; Rebek, J., Jr. *Science* **2003,** *301,* 1219–1220. doi:10.1126/science.1086644
379. Biros, S. M.; Ullrich, E. C.; Hof, F.; Trembleau, L.; Rebek, J., Jr. *J. Am. Chem. Soc.* **2004,** *126,* 2870–2876. doi:10.1021/ja038823m
380. Hooley, R. J.; van Anda, H. J.; Rebek, J., Jr. *J. Am. Chem. Soc.* **2006,** *128,* 3894–3895. doi:10.1021/ja058727g
381. Haas, C. H.; Biros, S. M.; Rebek, J., Jr. *Chem. Commun.* **2005,** 6044–6045. doi:10.1039/b513408k
382. Hof, F.; Trembleau, L.; Ullrich, E. C.; Rebek, J., Jr. *Angew. Chem., Int. Ed.* **2003,** *42,* 3150–3153. doi:10.1002/anie.200351174
383. Warmuth, R.; Yoon, J. *Acc. Chem. Res.* **2001,** *34,* 95–105. doi:10.1021/ar980082k
384. Arduini, A.; Pochini, A.; Secchi, A. *Eur. J. Org. Chem.* **2000,** 2325–2334. doi:10.1002/1099-0690(200006)2000:12<2325::AID-EJOC2325>3.0.CO;2-E
385. Garozzo, D.; Gattuso, G.; Notti, A.; Pappalardo, A.; Pappalardo, S.; Parisi, M. F.; Perez, M.; Pisagatti, I. *Angew. Chem., Int. Ed.* **2005,** *44,* 4892–4896. doi:10.1002/anie.200500985
386. The principle is widely employed in enzymes e.g. the barrel structures of glutaminase enzymes assembled from the HisF and HisG part.
387. Rebek, J., Jr. *Angew. Chem., Int. Ed.* **2005,** *44,* 2068–2078. doi:10.1002/anie.200462839

388. Zadmard, R.; Kraft, A.; Schrader, T.; Linne, U. *Chem.–Eur. J.* **2004,** *10,* 4233–4239. doi:10.1002/chem.200400034
389. Zadmard, R.; Schrader, T.; Grawe, T.; Kraft, A. *Org. Lett.* **2002,** *4,* 1687–1690. doi:10.1021/ol0257631
390. Zadmard, R.; Junkers, M.; Schrader, T.; Grawe, T.; Kraft, A. *J. Org. Chem.* **2003,** *68,* 6511–6521. doi:10.1021/jo034592q
391. Rose, K. N.; Barbour, L. J.; Orr, G. W.; Atwood, J. L. *Chem. Commun.* **1998,** 407–408. doi:10.1039/a707802a
392. Mansikkamäki, H.; Nissinen, M.; Schalley, C. A.; Rissanen, K. *New J. Chem.* **2003,** *27,* 88–97. doi:10.1039/b207875a
393. Yamanaka, M.; Shivanyuk, A.; Rebek, J., Jr. *J. Am. Chem. Soc.* **2004,** *126,* 2939–2943. doi:10.1021/ja037035u
394. Avram, L.; Cohen, Y. *J. Am. Chem. Soc.* **2003,** *125,* 16180–16181. doi:10.1021/ja0377394
395. Conn, M. M.; Rebek, J., Jr. *Chem. Rev.* **1997,** *97,* 1647–1668. doi:10.1021/cr9603800
396. Rebek, J., Jr. *Chem. Commun.* **2000,** 637–643. doi:10.1039/a910339m
397. Hof, F.; Craig, S. L.; Nuckolls, C.; Rebek, J., Jr. *Angew. Chem., Int. Ed.* **2002,** *41,* 1488–1508. doi:10.1002/1521-3773(20020503)41:9<1488::AID-ANIE1488>3.0.CO;2-G
And literature in these citations.
398. Ajami, D.; Rebek, J., Jr. *Proc. Natl. Acad. Sci. U. S. A.* **2007,** *104,* 16000–16003. doi:10.1073/pnas.0707759104
399. Behrend, R.; Meyer, E.; Rusche, F. *Liebigs Ann. Chem.* **1905,** *339,* 1–37. doi:10.1002/jlac.19053390102
400. Kim, J.; Jung, I.-S.; Kim, S.-Y.; Lee, E.; Kang, J.-K.; Sakamoto, S.; Yamaguchi, K.; Kim, K. *J. Am. Chem. Soc.* **2000,** *122,* 540–541. doi:10.1021/ja993376p
401. Day, A.; Arnold, A. P.; Blanch, R. J.; Snushall, B. *J. Org. Chem.* **2001,** *66,* 8094–8100. doi:10.1021/jo015897c
402. Liu, S.; Zavalij, P. Y.; Isaacs, L. *J. Am. Chem. Soc.* **2005,** *127,* 16798–16799. doi:10.1021/ja056287n
403. Lee, J. W.; Han, S. C.; Kim, J. H.; Ko, Y. H.; Kim, K. *Bull. Korean Chem. Soc.* **2007,** *28,* 1837–1840.
404. Jeon, Y. J.; Ko, Y. H.; Kim, K. *Bull. Korean Chem. Soc.* **2008,** *29,* 2043–2046.
405. Freeman, W. A.; Mock, W. L.; Shih, N. Y. *J. Am. Chem. Soc.* **1981,** *103,* 7367–7368. doi:10.1021/ja00414a070
406. Mock, W. L.; Shih, N. Y. *J. Org. Chem.* **1986,** *51,* 4440–4446. doi:10.1021/jo00373a018
407. Mock, W. L. Cucurbituril. In *Supramolecular Chemistry II – Host Design and Molecular Recognition;* Weber, E., Ed.; Topics in Current Chemistry, Vol. 175; Springer: Berlin/Heidelberg, 1995; pp 1–24. doi:10.1007/3-540-58800-0_16
408. Buschmann, H. J.; Cleve, E.; Schollmeyer, E. *Inorg. Chim. Acta* **1992,** *193,* 93–97. doi:10.1016/S0020-1693(00)83800-1
409. Hoffmann, R.; Knoche, W.; Fenn, C.; Buschmann, H.-J. *J. Chem. Soc., Faraday Trans.* **1994,** *90,* 1507–1511. doi:10.1039/ft9949001507
410. Jon, S. Y.; Selvapalam, N.; Oh, D. H.; Kang, J.-K.; Kim, S.-Y.; Jeon, Y. J.; Lee, J. W.; Kim, K. *J. Am. Chem. Soc.* **2003,** *125,* 10186–10187. doi:10.1021/ja036536c
411. Freeman, W. A. *Acta Crystallogr., Sect. B* **1984,** *40,* 382–387. doi:10.1107/S0108768184002354
412. Huang, W.-H.; Zavalij, P. Y.; Isaacs, L. *Acta Crystallogr., Sect. E* **2008,** *64,* o1321–o1322. doi:10.1107/S1600536808018412
413. Mock, W. L.; Shih, N.-Y. *J. Am. Chem. Soc.* **1988,** *110,* 4706–4710. doi:10.1021/ja00222a031
414. Mock, W. L.; Shih, N.-Y. *J. Am. Chem. Soc.* **1989,** *111,* 2697–2699. doi:10.1021/ja00189a053
415. Connors, K. A. *Chem. Rev.* **1997,** *97,* 1325–1358. doi:10.1021/cr960371r
416. Szejtli, J. *Chem. Rev.* **1998,** *98,* 1743–1754. doi:10.1021/cr970022c
417. Jeon, Y. M.; Kim, J.; Whang, D.; Kim, K. *J. Am. Chem. Soc.* **1996,** *118,* 9790–9791. doi:10.1021/ja962071x
418. Whang, D.; Heo, J.; Park, J. H.; Kim, K. *Angew. Chem., Int. Ed.* **1998,** *37,* 78–80. doi:10.1002/(SICI)1521-3773(19980202)37:1/2<78::AID-ANIE78>3.0.CO;2-9
419. Cucurbiturils are dissolving appreciably in acidic solution. A mixture of formic acid and water has established as standard solvent for studies on them.
420. Rekharsky, M. V.; Ko, Y. H.; Selvapalam, N.; Kim, K.; Inoue, Y. *Supramol. Chem.* **2007,** *19,* 39–46. doi:10.1080/10610270600915292
421. Buschmann, H. J.; Jansen, K.; Schollmeyer, E. *Thermochim. Acta* **1998,** *317,* 95–98. doi:10.1016/S0040-6031(98)00377-3
422. Ko, Y. H.; Kim, E.; Hwang, I.; Kim, K. *Chem. Commun.* **2007,** 1305–1315. doi:10.1039/b615103e
And references cited therein.
423. Kwangyul, M.; Grindstaff, J.; Sobransingh, D.; Kaifer, A. E. *Angew. Chem., Int. Ed.* **2004,** *43,* 5496–5499. doi:10.1002/anie.200460179
424. Kwangyul, M.; Kaifer, A. E. *Org. Lett.* **2004,** *6,* 185–188. doi:10.1021/ol035967x
425. Liu, Y.; Li, X.-Y.; Zhang, H.-Y.; Li, C.-J.; Ding, F. *J. Org. Chem.* **2007,** *72,* 3640–3645. doi:10.1021/jo0624288
426. Ma, X.; Wang, Q.; Qu, D.; Xu, Y.; Ji, F.; Tian, H. *Adv. Funct. Mater.* **2007,** *17,* 829–837. doi:10.1002/adfm.200600981
427. Sindelar, V.; Silvi, S.; Parker, S. E.; Sobransingh, D.; Kaifer, A. E. *Adv. Funct. Mater.* **2007,** *17,* 694–701. doi:10.1002/adfm.200600969
428. Neugebauer, R.; Knoche, W. J. *J. Chem. Soc., Perkin Trans. 2* **1998,** 529–534. doi:10.1039/a708015h
429. Mock, W. L. Cucurbituril. In *Molecular Recognition: Receptors for molecular Guests;* Vögtle, F., Ed.; Comprehensive Supramolecular Chemistry, Vol. 2; Pergamon: Oxford, U.K., 1996; pp 477–493.
430. Kim, K.; Kim, H.-J. In *Encyclopedia of Supramolecular Chemistry;* Atwood, J. L.; Steed, J. W., Eds.; Marcel Dekker: New York, 2004; pp 390–397.
431. Huang, W.-H.; Liu, S.; Isaacs, L. Cucurbit[n]urils. In *Modern Supramolecular Chemistry;* Diederich, F.; Stang, P. J.; Tykwinski, R. R., Eds.; Wiley-VCH: New York, USA, 2008; pp 113–142. doi:10.1002/9783527621484.ch4
432. Kim, K. *Chem. Soc. Rev.* **2002,** *31,* 96–107. doi:10.1039/a900939f
433. Kim, K.; Selvapalam, N.; Oh, D.-H. *J. Inclusion Phenom. Macrocyclic Chem.* **2004,** *50,* 31–36. doi:10.1007/s10847-004-8835-7
434. Kim, K.; Selvapalam, N.; Ko, Y. H.; Park, K. M.; Kim, D.; Kim, J. *Chem. Soc. Rev.* **2007,** *36,* 267–279. doi:10.1039/b603088m
435. Lee, J. W.; Samal, S.; Selvapalam, N.; Kim, H.-J.; Kim, K. *Acc. Chem. Res.* **2003,** *36,* 621–630. doi:10.1021/ar020254k
436. Lagona, J.; Chakrabarti, S.; Mukhopadhyay, P.; Isaacs, L. *Angew. Chem., Int. Ed.* **2005,** *44,* 4844–4870. doi:10.1002/anie.200460675
437. Zhao, J. Z.; Kim, H. J.; Oh, J.; Kim, S. Y.; Lee, J.; Sakamoto, W. S.; Yamaguchi, K.; Kim, K. *Angew. Chem., Int. Ed.* **2001,** *40,* 4233–4235. doi:10.1002/1521-3773(20011119)40:22<4233::AID-ANIE4233>3.0.CO;2-D

438. Isobe, H.; Sato, S.; Nakamura, E. *Org. Lett.* **2002,** *4,* 1287–1292. doi:10.1021/ol025749o
439. Day, A. I.; Arnold, A. P.; Blanch, R. J. *Molecules* **2003,** *8,* 74–84. doi:10.3390/80100074
440. Zhao, Y. J.; Xue, S. F.; Zhu, Q. J.; Tao, Z.; Zhang, J. X.; Wei, Z. B.; Long, L. S.; Hu, M. L.; Xiao, H. P.; Day, A. I. *Chin. Sci. Bull.* **2004,** *49,* 1111–1116.
441. Lagona, J.; Fettinger, J. C.; Issacs, L. *J. Org. Chem.* **2005,** *70,* 10381–10392. doi:10.1021/jo051655r
442. Lagona, J.; Wagner, B. D.; Isaacs, L. *J. Org. Chem.* **2006,** *71,* 1181–1190. doi:10.1021/jo052294i
443. Kim, Y.; Kim, H.; Ko, Y. H.; Selvapalam, N.; Rekharsky, M. V.; Inoue, Y.; Kim, K. *Chem.–Eur. J.* **2009,** *15,* 6143–6151. doi:10.1002/chem.200900305
444. Yi, J.-M.; Zhang, Y.-Q.; Cong, H.; Xue, S.-F.; Tao, Z. *J. Mol. Struct.* **2009,** *933,* 112–117. doi:10.1016/j.molstruc.2009.06.006
445. Wagner, B. D.; Boland, P. G.; Lagona, J.; Isaacs, L. *J. Phys. Chem. B* **2005,** *109,* 7686–7691. doi:10.1021/jp044369c
446. Montes-Navajas, P.; Baumes, L. A.; Corma, A.; Garcia, H. *Tetrahedron Lett.* **2009,** *50,* 2301–2304. doi:10.1016/j.tetlet.2009.02.189
447. Hennig, A.; Bakirci, H.; Nau, W. M. *Nat. Methods* **2007,** *4,* 629–632. doi:10.1038/nmeth1064
448. Praetorius, A.; Bailey, D. M.; Schwarzlose, T.; Nau, W. M. *Org. Lett.* **2008,** *10,* 4089–4092. doi:10.1021/ol8016275
449. Koner, A. L.; Nau, W. M. *Supramol. Chem.* **2007,** *19,* 55–66. doi:10.1080/10610270600910749
450. Bailey, D. M.; Hennig, A.; Uzunova, V. D.; Nau, W. M. *Chem.–Eur. J.* **2008,** *14,* 6069–6077. doi:10.1002/chem.200800463
451. Huang, W. H.; Zavalij, P. Y.; Isaacs, L. *Angew. Chem., Int. Ed.* **2007,** *46,* 7425–7427. doi:10.1002/anie.200702189
452. Rekharsky, M. V.; Yamamura, H.; Inoue, C.; Kawai, M.; Osaka, I.; Arakawa, R.; Shiba, K.; Sato, A.; Ko, Y. H.; Selvapalam, N.; Kim, K.; Inoue, Y. *J. Am. Chem. Soc.* **2006,** *128,* 14871–14880. doi:10.1021/ja063323p
453. Liu, S. M.; Ruspic, C.; Mukhopadhyay, P.; Chakrabarti, S.; Zavalij, P. J.; Isaacs, L. *J. Am. Chem. Soc.* **2005,** *127,* 15959–15967. doi:10.1021/ja055013x
454. Rekharsky, M. V.; Mori, T.; Yang, C.; Ko, Y. H.; Selvapalam, N.; Kim, H.; Sobransingh, D.; Kaifer, A. E.; Liu, S.; Isaacs, L.; Chen, W.; Moghaddam, S.; Gilson, M. K.; Kim, K.; Inoue, Y. *Proc. Natl. Acad. Sci. U. S. A.* **2007,** *104,* 20737–20742. doi:10.1073/pnas.0706407105
455. Mecozzi, S.; Rebek, J., Jr. *Chem.–Eur. J.* **1998,** *4,* 1016–1022. doi:10.1002/(SICI)1521-3765(19980615)4:6<1016::AID-CHEM1016>3.0.CO;2-B
456. St-Jacques, A. D.; Wyman, I. W.; Macartney, D. H. *Chem. Commun.* **2008,** 4936–4938. doi:10.1039/b811823j
457. Wyman, I. W.; Macartney, D. H. *Org. Biomol. Chem.* **2010,** *8,* 253–260. doi:10.1039/b917610a
458. Wyman, I. W.; Macartney, D. H. *Org. Biomol. Chem.* **2010,** *8,* 247–252. doi:10.1039/b915694a
459. These molecules are potent acetylcholine esterase inhibitors and depolarizing muscle relaxants.
460. Wyman, I. W.; Macartney, D. H. *J. Org. Chem.* **2009,** *74,* 8031–8038. doi:10.1021/jo901861e
461. Kim, H.-J.; Jeon, W. S.; Ko, Y. H.; Kim, K. *Proc. Natl. Acad. Sci. U. S. A.* **2002,** *99,* 5007–5011. doi:10.1073/pnas.062656699
462. Ong, W.; Gomez-Kaifer, M.; Kaifer, A. E. *Org. Lett.* **2002,** *4,* 1791–1793. doi:10.1021/ol025869w
463. Choudhury, S. D.; Mohanty, J.; Upadhyaya, H. P.; Bhasikuttan, A. C.; Pal, H. *J. Phys. Chem. B* **2009,** *113,* 1891–1898. doi:10.1021/jp8103062
464. Kim, S. Y.; Jung, I. S.; Lee, E.; Kim, J.; Sakamoto, S.; Yamaguchi, K.; Kim, K. *Angew. Chem., Int. Ed.* **2001,** *40,* 2119–2121. doi:10.1002/1521-3773(20010601)40:11<2119::AID-ANIE2119>3.0.CO;2-4
465. Kim, K.; Kim, J.; Jung, I.-S.; Kim, S.-Y.; Lee, E.; Kang, J.-K. Cucurbituril derivatives, their preparation methods and uses. U.S. Patent 6,365,734, April 2, 2002.
466. Rajgariah, P.; Urbach, A. R. *J. Inclusion Phenom. Macrocyclic Chem.* **2008,** *62,* 251–254. doi:10.1007/s10847-008-9464-y
467. Bush, M. E.; Bouley, N. D.; Urbach, A. R. *J. Am. Chem. Soc.* **2005,** *127,* 14511–14517. doi:10.1021/ja0548440
468. Heitmann, L. M.; Taylor, A. B.; Hart, P. J.; Urbach, A. R. *J. Am. Chem. Soc.* **2006,** *128,* 12574–12781. doi:10.1021/ja064323s
469. Escuder, B.; Rowan, A. E.; Feiters, M. C.; Nolte, R. J. M. *Tetrahedron* **2004,** *60,* 291–300. doi:10.1016/j.tet.2003.11.019
470. Roh, S.-G.; Park, K.-M.; Park, G.-J.; Sakamoto, S.; Yamaguchi, K.; Kim, K. *Angew. Chem., Int. Ed.* **1999,** *38,* 637–641. doi:10.1002/(SICI)1521-3773(19990301)38:5<637::AID-ANIE637>3.0.CO;2-4
471. Lee, E.; Heo, J.; Kim, K. *Angew. Chem., Int. Ed.* **2000,** *39,* 2699–2701. doi:10.1002/1521-3773(20000804)39:15<2699::AID-ANIE2699>3.0.CO;2-Z
472. Isobe, H.; Tomita, N.; Lee, J. W.; Kim, H.-J.; Kim, K.; Nakamura, E. *Angew. Chem., Int. Ed.* **2000,** *39,* 4257–4260. doi:10.1002/1521-3773(20001201)39:23<4257::AID-ANIE4257>3.0.CO;2-6
473. Buschmann, H.-J.; Wego, A.; Schollmeyer, E.; Döpp, D. *Supramol. Chem.* **2000,** *11,* 225–231. doi:10.1080/10610270008049132
474. Lee, E.; Kim, J.; Heo, J.; Whang, D.; Kim, K. *Angew. Chem., Int. Ed.* **2001,** *40,* 399–402. doi:10.1002/1521-3773(20010119)40:2<399::AID-ANIE399>3.0.CO;2-W
475. Lee, J. W.; Ko, Y. H.; Park, S.-H.; Yamaguchi, K.; Kim, K. *Angew. Chem., Int. Ed.* **2001,** *40,* 746–749. doi:10.1002/1521-3773(20010216)40:4<746::AID-ANIE7460>3.0.CO;2-P
476. Kim, H.-J.; Heo, J.; Jeon, W. S.; Lee, E.; Kim, J.; Sakamoto, S.; Yamaguchi, K.; Kim, K. *Angew. Chem., Int. Ed.* **2001,** *40,* 1526–1529. doi:10.1002/1521-3773(20010417)40:8<1526::AID-ANIE1526>3.0.CO;2-T
477. Park, K.-M.; Kim, S.-Y.; Heo, J.; Whang, D.; Sakamoto, S.; Yamaguchi, K.; Kim, K. *J. Am. Chem. Soc.* **2002,** *124,* 2140–2147. doi:10.1021/ja011654q
478. Park, K.-M.; Whang, D.; Lee, E.; Heo, J.; Kim, K. *Chem.–Eur. J.* **2002,** *8,* 498–508. doi:10.1002/1521-3765(20020118)8:2<498::AID-CHEM498>3.0.CO;2-M
479. Lim, Y.-B.; Kim, T.; Lee, J. W.; Kim, S.-M.; Kim, H.-J.; Kim, K.; Park, J.-S. *Bioconjugate Chem.* **2002,** *13,* 1181–1185. doi:10.1021/bc025581r
480. Lee, J. W.; Choi, S. W.; Ko, Y. H.; Kim, S.-Y.; Kim, K. *Bull. Korean Chem. Soc.* **2002,** *23,* 1347–1350.

481. Park, K.-M.; Lee, E.; Roh, S.-G.; Kim, J.; Kim, K. *Bull. Korean Chem. Soc.* **2004,** *25,* 1711–1713.
482. Kim, S.-Y.; Lee, J. W.; Han, S. C.; Kim, K. *Bull. Korean Chem. Soc.* **2005,** *26,* 1265–1268.
483. Rekharsky, M. V.; Yamamura, H.; Kawai, M.; Osaka, I.; Arakawa, R.; Sato, A.; Ko, Y. H.; Selvapalam, N.; Kim, K.; Inoue, Y. *Org. Lett.* **2006,** *8,* 815–818. doi:10.1021/ol0528742
484. Yang, C.; Ko, Y. H.; Selvapalam, N.; Origane, Y.; Mori, T.; Wada, T.; Kim, K.; Inoue, Y. *Org. Lett.* **2007,** *9,* 4789–4792. doi:10.1021/ol702142j
485. Liu, Y.; Ke, C.-F.; Zhang, H.-Y.; Wu, W.-J.; Shi, J. *J. Org. Chem.* **2007,** *72,* 280–283. doi:10.1021/jo0617159
486. Klärner, F.-G.; Kahlert, B. *Acc. Chem. Res.* **2003,** *36,* 919–932. doi:10.1021/ar0200448
487. Turner, J. J.; Harding, M. M. *Supramol. Chem.* **2005,** *17,* 369–375. doi:10.1080/10610270500073796
488. Chen, C.-W.; Whitlock, H. W. *J. Am. Chem. Soc.* **1978,** *100,* 4921–4922. doi:10.1021/ja00483a063
489. Whitlock, B. J.; Whitlock, H. W. *J. Am. Chem. Soc.* **1990,** *112,* 3910–3915. doi:10.1021/ja00166a027
490. Zimmerman, S. C. *Top. Curr. Chem.* **1993,** *165,* 71–102. doi:10.1007/BFb0111281
491. Zimmerman, S. C.; VanZyl, C. M. *J. Am. Chem. Soc.* **1987,** *109,* 7894–7896. doi:10.1021/ja00259a055
492. Zimmerman, S. C.; VanZyl, C. M.; Hamilton, G. S. *J. Am. Chem. Soc.* **1989,** *111,* 1373–1381. doi:10.1021/ja00186a035
493. Zimmerman, S. C.; Zeng, Z.; Wu, W.; Reichert, D. E. *J. Am. Chem. Soc.* **1991,** *113,* 183–196. doi:10.1021/ja00001a027
494. Zimmerman, S. C.; Wu, W.; Zeng, Z. *J. Am. Chem. Soc.* **1991,** *113,* 196–201. doi:10.1021/ja00001a028
495. Güther, R.; Nieger, M.; Vögtle, F. *Angew. Chem., Int. Ed. Engl.* **1993,** *32,* 601–603. doi:10.1002/anie.199306011
496. Rebek, J., Jr. *Science* **1987,** *235,* 1478–1484. doi:10.1126/science.3823899
497. Sijbesma, R. P.; Nolte, R. J. M. *Top. Curr. Chem.* **1995,** *175,* 26–56. doi:10.1007/3-540-58800-0_17
498. Harmata, M.; Murray, T. *J. Org. Chem.* **1989,** *54,* 3761–3763. doi:10.1021/jo00277a001
499. Harmata, M.; Barnes, C. L. *J. Am. Chem. Soc.* **1990,** *112,* 5655–5657. doi:10.1021/ja00170a049
500. Zhu, X.-Z.; Chen, C.-F. *J. Org. Chem.* **2005,** *70,* 917–924. doi:10.1021/jo0483015
501. Klärner, F.-G.; Benkhoff, J.; Boese, R.; Burkert, U.; Kamieth, M.; Naatz, U. *Angew. Chem., Int. Ed. Engl.* **1996,** *35,* 1130–1133. doi:10.1002/anie.199611301
502. Klärner, F.-G.; Panitzky, J.; Bläser, D.; Boese, R. *Tetrahedron* **2001,** *57,* 3673–3697. doi:10.1016/S0040-4020(01)00230-7
503. Klärner, F.-G.; Kahlert, B.; Boese, R.; Bläser, D.; Juris, A.; Marchioni, F. *Chem.–Eur. J.* **2005,** *11,* 3363–3374. doi:10.1002/chem.200401257
504. Marchioni, F.; Juris, A.; Lobert, M.; Seelbach, U. P.; Kahlert, B.; Klärner, F.-G. *New J. Chem.* **2005,** *29,* 780–784. doi:10.1039/b501880c
505. Kamieth, M.; Klärner, F.-G. *J. Prakt. Chem.* **1999,** *34,* 245–251. doi:10.1002/(SICI)1521-3897(199904)341:3<245::AID-PRAC245>3.0.CO;2-J
506. Klärner, F.-G.; Burkert, U.; Kamieth, M.; Boese, R.; Benet-Buchholz, J. *Chem.–Eur. J.* **1999,** *5,* 1700–1707. doi:10.1002/(SICI)1521-3765(19990604)5:6<1700::AID-CHEM1700>3.0.CO;2-9
507. Kamieth, M.; Klärner, F.-G.; Diederich, F. *Angew. Chem., Int. Ed.* **1998,** *37,* 3303–3306. doi:10.1002/(SICI)1521-3773(19981217)37:23<3303::AID-ANIE3303>3.0.CO;2-T
508. Zimmerman, S. C.; Wu, W. *J. Am. Chem. Soc.* **1989,** *111,* 8054–8055. doi:10.1021/ja00202a077
509. Rowan, A. E.; Elemans, J. A. A. W.; Nolte, R. J. M. *Acc. Chem. Res.* **1999,** *32,* 995–1006. doi:10.1021/ar9702684
510. Elemans, J. A. A. W.; Rowan, A. E.; Nolte, R. J. M. *Ind. Eng. Chem. Res.* **2000,** *39,* 3419–3428. doi:10.1021/ie000079g
511. Reek, J. N. H.; Elemans, J. A. A. W.; de Gelder, R.; Beurskens, P. T.; Rowan, A. E.; Nolte, R. J. M. *Tetrahedron* **2003,** *59,* 175–185. doi:10.1016/S0040-4020(02)01480-1
512. Reek, J. N. H.; Priem, A. H.; Engelkamp, H.; Rowan, A. E.; Elemans, J. A. A. W.; Nolte, R. J. M. *J. Am. Chem. Soc.* **1997,** *119,* 9956–9964. doi:10.1021/ja970805f
513. Gokel, G. W.; Medina, J. C.; Chensheng, L. *Synlett* **1991,** 677–678. doi:10.1055/s-1991-21985
514. Medina, J. C.; Chensheng, L.; Bott, S. G.; Atwood, J. L.; Gokel, G. W. *J. Am. Chem. Soc.* **1991,** *113,* 366–368. doi:10.1021/ja00001a057
515. Rebek, J., Jr.; Askew, B.; Ballester, P.; Doa, M. J. *J. Am. Chem. Soc.* **1987,** *109,* 4119–4120. doi:10.1021/ja00247a051
516. Lobert, M.; Bandmann, H.; Burkert, U.; Buchele, U. P.; Podsadlowski, V.; Klärner, F.-G. *Chem.–Eur. J.* **2006,** *12,* 1629–1641. doi:10.1002/chem.200500902
517. Bishop, R. Supramolecular Host–Guest Chemistry of Heterocyclic V-Shaped Molecules. In *Heterocyclic Supramolecules II;* Gupta, R. R., Ed.; Topics in Heterocyclic Chemistry, Vol. 18; Springer: Berlin, 2009; pp 37–74. doi:10.1007/7081_2008_9
518. Harmata, M. *Acc. Chem. Res.* **2004,** *37,* 862–873. doi:10.1021/ar030164v
And references given therein.
519. Fukuhara, G.; Madenci, S.; Polkowska, J.; Bastkowski, F.; Klärner, F.-G.; Origane, Y.; Kaneda, M.; Mori, T.; Wada, T.; Inoue, Y. *Chem.–Eur. J.* **2007,** *13,* 2473–2479. doi:10.1002/chem.200601585
520. Rebek, J., Jr. *Top. Curr. Chem.* **1988,** *149,* 189–210. doi:10.1007/3-540-19338-3_4
521. Rebek, J., Jr. *Angew. Chem., Int. Ed. Engl.* **1990,** *29,* 245–255. doi:10.1002/anie.199002451
522. Rebek, J., Jr.; Nemeth, D. *J. Am. Chem. Soc.* **1985,** *107,* 6738–6739. doi:10.1021/ja00309a068
523. Lipkowitz, K. B.; Zegarra, R. *J. Comput. Chem.* **1989,** *10,* 595–602. doi:10.1002/jcc.540100502
524. Lehn, J.-M.; Vierling, P.; Hayward, R. C. *J. Chem. Soc., Chem. Commun.* **1979,** 296–298. doi:10.1039/C39790000296
The first receptor molecules for arginine derivatives.
525. Eliseev, A. V.; Nelen, M. I. *J. Am. Chem. Soc.* **1997,** *119,* 1147–1148. doi:10.1021/ja961893r
526. Hamilton, A. D.; Lehn, J.-M.; Sessler, J. L. *J. Am. Chem. Soc.* **1986,** *108,* 5158–5167. doi:10.1021/ja00277a021
Artificial receptor molecules for α,ω-diammonium ions.
527. Schrader, T. *Chem.–Eur. J.* **1997,** *3,* 1537–1541. doi:10.1002/chem.19970030923
528. Bell, T. W.; Khasanov, A. B.; Drew, M. G. B. *J. Am. Chem. Soc.* **2002,** *124,* 14092–14103. doi:10.1021/ja0273694
529. Bell, T. W.; Santora, V. J. *J. Am. Chem. Soc.* **1992,** *114,* 8300–8302. doi:10.1021/ja00047a057
530. Bell, T. W.; Hext, N. M.; Khasanov, A. B. *Pure Appl. Chem.* **1998,** *70,* 2371–2377. doi:10.1351/pac199870122371

531. Seel, C.; Galán, A.; de Mendoza, J. *Top. Curr. Chem.* **1995,** *175,* 101–132. doi:10.1007/3-540-58800-0_19
532. Berg, J. M. *Biochemistry,* 6th ed.; Freeman & Worth Publishing Group: Bedford, N.Y., 2006.
533. Springs, B.; Haake, P. *Bioorg. Chem.* **1977,** *6,* 181–190. doi:10.1016/0045-2068(77)90019-0
534. Schrader, T. *J. Inclusion Phenom. Macrocyclic Chem.* **1999,** *34,* 119–131. doi:10.1023/A:1008086624845
535. Morin, C. J.; Carli, M.; Mofaddel, N.; Al Rifa, R.; Jaffres, P. A.; Villemin, D.; Desbene, P. L. *Chromatographia* **2005,** *62,* 139–143. doi:10.1365/s10337-005-0594-8
536. Schrader, T. *Angew. Chem., Int. Ed. Engl.* **1996,** *35,* 2649–2651. doi:10.1002/anie.199626491
537. Iisma, T. P.; Biden, T. J.; Shine, J. *G Protein-Coupled Receptors;* Springer: Heidelberg, Germany, 1995.
The adrenergic receptor family possesses enormous importance for the living organism. Its G-protein-coupled signal transduction influences a broad range of vital body functions from respiration to blood pressure.
538. Trumpp-Kallmeyer, S.; Hoflack, J.; Bruinvels, A.; Hibert, M. *J. Med. Chem.* **1992,** *35,* 3448–3462. doi:10.1021/jm00097a002
In the natural β-adrenergic receptor the binding site is formed by a cyclic array of seven membrane-spanning α-helices which supply a rather hydrophobic surrounding for the adrenaline guest.
539. Schrader, T. *J. Org. Chem.* **1998,** *63,* 264–272. doi:10.1021/jo971297v
540. Schrader, T. *J. Am. Chem. Soc.* **1998,** *120,* 11816–11817. doi:10.1021/ja982067g
541. Herm, M.; Schrader, T. *Chem.–Eur. J.* **2000,** *6,* 47–53. doi:10.1002/(SICI)1521-3765(20000103)6:1<47::AID-CHEM47>3.0.CO;2-I
542. Schrader, T. *Tetrahedron Lett.* **1998,** *39,* 517–520. doi:10.1016/S0040-4039(97)10672-4
543. Kirby, J. P.; Roberts, J. A.; Nocera, D. G. *J. Am. Chem. Soc.* **1997,** *119,* 9230–9236. doi:10.1021/ja970176+
And literature cited herein.
544. Schneider, H.-J.; Kramer, R.; Simova, S.; Schneider, U. *J. Am. Chem. Soc.* **1988,** *110,* 6442–6448. doi:10.1021/ja00227a025
And literature cited therein.
545. Maue, M.; Schrader, T. *Angew. Chem., Int. Ed.* **2005,** *44,* 2265–2270. doi:10.1002/anie.200462702
546. Jasper, C.; Schrader, T.; Panitzky, J.; Klärner, F.-G. *Angew. Chem., Int. Ed.* **2002,** *41,* 1355–1358. doi:10.1002/1521-3773(20020415)41:8<1355::AID-ANIE1355>3.0.CO;2-6
547. Fokkens, M.; Jasper, C.; Schrader, T.; Koziol, F.; Ochsenfeld, C.; Polkowska, J.; Lobert, M.; Kahlert, B.; Klärner, F.-G. *Chem.–Eur. J.* **2005,** *11,* 477–494. doi:10.1002/chem.200400603
548. Klärner, F.-G.; Kahlert, B.; Nellesen, A.; Zienau, J.; Ochsenfeld, C.; Schrader, T. *J. Am. Chem. Soc.* **2006,** *128,* 4831–4841. doi:10.1021/ja058410g
549. Fokkens, M.; Schrader, T.; Klärner, F.-G. *J. Am. Chem. Soc.* **2005,** *127,* 14415–14421. doi:10.1021/ja052806a
550. Talbiersky, P.; Bastkowski, F.; Klärner, F.-G.; Schrader, T. *J. Am. Chem. Soc.* **2008,** *130,* 9824–9828. doi:10.1021/ja801441j
551. Werner, M.; Finochiaro, P.; Failla, S.; Consiglio, G. *Org. Lett.* **2000,** *2,* 605–608. doi:10.1021/ol991355u
552. Molt, O.; Rübeling, D.; Schrader, T. *J. Am. Chem. Soc.* **2003,** *125,* 12086–12087. doi:10.1021/ja035212l
553. Kim, S.-G.; Ahn, K. H. *Chem.–Eur. J.* **2000,** *6,* 3399–3403. doi:10.1002/1521-3765(20000915)6:18<3399::AID-CHEM3399>3.0.CO;2-M
554. Kim, S.-G.; Kim, K.-H.; Jung, J.; Shin, S. K.; Ahn, K. H. *J. Am. Chem. Soc.* **2002,** *124,* 591–595. doi:10.1021/ja0119696
555. Moberg, C. *Angew. Chem., Int. Ed.* **1998,** *37,* 248–268. doi:10.1002/(SICI)1521-3773(19980216)37:3<248::AID-ANIE248>3.0.CO;2-5
556. Gibson, S. E.; Castaldi, M. P. *Angew. Chem., Int. Ed.* **2006,** *45,* 4718–4720. doi:10.1002/anie.200600776
557. Moberg, C. *Angew. Chem., Int. Ed.* **2006,** *45,* 4721–4723. doi:10.1002/anie.200601214
558. Heparin is a heterogenous mixture of chain lengths consisting of repeating copolymers of 1-4-linked iduronic and glucosamine residues in a semi random order. It binds to its natural substrate thrombin III through the numerous sulfate and carboxylate residues in the main chain, which give it the highest anionic charge to mass ratio of any biopolymer.
559. Wright, A. T.; Zhong, Z.; Anslyn, E. V. *Angew. Chem., Int. Ed.* **2005,** *44,* 5679–5682. doi:10.1002/anie.200501437
560. García-Acostaa, B.; Martínez-Máñez, R.; Ros-Lisa, J. V.; Sancenón, F.; Soto, J. *Tetrahedron Lett.* **2008,** *49,* 1997–2001. doi:10.1016/j.tetlet.2008.01.076
561. Tomas, S.; Prohens, R.; Vega, M.; Rotger, M. C.; Deya, P. M.; Ballester, P.; Costa, A. *J. Org. Chem.* **1996,** *61,* 9394–9401. doi:10.1021/jo9614147
562. Chin, J.; Walsdorff, C.; Stranix, B.; Oh, J.; Chung, H. J.; Park, S.-M.; Kim, K. *Angew. Chem., Int. Ed.* **1999,** *38,* 2756–2759. doi:10.1002/(SICI)1521-3773(19990917)38:18<2756::AID-ANIE2756>3.0.CO;2-6
563. Chin, J.; Oh, J.; Jon, S. Y.; Park, S. H.; Walsdorff, Ch.; Stranix, B.; Ghoussoub, A.; Lee, S. J.; Chung, H. J.; Park, S.-M.; Kim, K. *J. Am. Chem. Soc.* **2002,** *124,* 5374–5379. doi:10.1021/ja0174175
564. Ahn, K. H.; Kim, S.-G.; Jung, J.; Kim, K.-H.; Kim, J.; Chin, J.; Kim, K. *Chem. Lett.* **2000,** 170–171. doi:10.1246/cl.2000.170
565. Kim, S.-G.; Kim, K.-H.; Kim, Y. K.; Shin, S. K.; Ahn, K. H. *J. Am. Chem. Soc.* **2003,** *125,* 13819–13824. doi:10.1021/ja037031p
566. Ahn, K. H.; Ku, H.-Y.; Kim, Y.; Kim, S.-G.; Kim, Y. K.; Son, H. S.; Ku, J. K. *Org. Lett.* **2003,** *5,* 1419–1422. doi:10.1021/ol034041m
567. Kim, J.; Kim, S.-G.; Seong, H. R.; Ahn, K. H. *J. Org. Chem.* **2005,** *70,* 7227–7231. doi:10.1021/jo050872p
568. De Jong, F.; Siegel, M. G.; Cram, D. J. *J. Chem. Soc., Chem. Commun.* **1975,** 551–553. doi:10.1039/C39750000551
569. Löhr, H. G.; Vögtle, F. *Acc. Chem. Res.* **1985,** *18,* 65–72. doi:10.1021/ar00111a001
570. Hong, J. I.; Namgoong, S. K.; Bernardi, A.; Still, W. C. *J. Am. Chem. Soc.* **1991,** *113,* 5111–5112. doi:10.1021/ja00013a084
571. Pieters, R. J.; Diederich, F. *Chem. Commun.* **1996,** 2255–2256. doi:10.1039/cc9960002255
572. Schnopp, M.; Haberhauer, G. *Eur. J. Org. Chem.* **2009,** 4458–4467. doi:10.1002/ejoc.200900510
573. Haberhauer, G.; Oeser, T.; Rominger, F. *Chem.–Eur. J.* **2005,** *11,* 6718–6726. doi:10.1002/chem.200500224
574. According to the authors the values and the selectivity coefficients calculated for the complexation of the ammonium ions with quinoline receptor **178b** must be taken with caution as these values derived from rather small $\Delta\delta_{max}$ values.
575. Fabris, F.; Pellizzaro, L.; Zonta, C.; De Lucchi, O. *Eur. J. Org. Chem.* **2007,** 283–291. doi:10.1002/ejoc.200600673

576. Dougherty, D. A. *Science* **1996,** *271,* 163–168. doi:10.1126/science.271.5246.163
577. McCurdy, A.; Jimenez, L.; Stauffer, D. A.; Dougherty, D. A. *J. Am. Chem. Soc.* **1992,** *114,* 10314–10321. doi:10.1021/ja00052a031
578. Shepodd, T. J.; Petti, M. A.; Dougherty, D. A. *J. Am. Chem. Soc.* **1988,** *110,* 1983–1985. doi:10.1021/ja00214a063
579. Petti, A.; Shepodd, T. J.; Barrans, R. E., Jr.; Dougherty, D. A. *J. Am. Chem. Soc.* **1988,** *110,* 6825–6840. doi:10.1021/ja00228a036
580. Schneider, H.-J.; Blatter, T.; Zimmermann, P. *Angew. Chem., Int. Ed. Engl.* **1990,** *29,* 1161–1162. doi:10.1002/anie.199011611
581. Schneider, J.; Ruf, D. *Angew. Chem., Int. Ed.* **1990,** *29,* 1159–1160. doi:10.1002/anie.199011591
582. Chipot, C.; Maigret, B.; Pearlman, D. A.; Kollman, P. A. *J. Am. Chem. Soc.* **1996,** *118,* 2998–3005. doi:10.1021/ja950302e
583. Ilioudis, C. A.; Bearpark, M. J.; Steed, J. W. *New J. Chem.* **2005,** *29,* 64–67. doi:10.1039/b415532g
584. Roelens, S.; Torriti, R. *Supramol. Chem.* **1999,** *10,* 225–232. doi:10.1080/10610279908559289
585. Roelens, S.; Torriti, R. *J. Am. Chem. Soc.* **1998,** *120,* 12443–12452. doi:10.1021/ja981338k
586. Bartoli, S.; Roelens, S. *J. Am. Chem. Soc.* **2002,** *124,* 8307–8315. doi:10.1021/ja025884w
587. Stauffer, D. A.; Dougherty, D. A. *Tetrahedron Lett.* **1988,** *29,* 6039–6042. doi:10.1016/S0040-4039(00)82259-5
588. Kearney, P.; Mizoue, L. S.; Kumpf, R. A.; Forman, J. E.; McCurdy, A.; Dougherty, D. A. *J. Am. Chem. Soc.* **1993,** *115,* 9907–9919. doi:10.1021/ja00075a006
589. Collet, A.; Dutasta, J.-P.; Lozach, B. *Bull. Soc. Chim. Belg.* **1990,** *99,* 617–632.
590. Garel, L.; Lozach, B.; Dutasta, J.-P.; Collet, A. *J. Am. Chem. Soc.* **1993,** *115,* 11652–11653. doi:10.1021/ja00077a096
591. Masci, B. *Tetrahedron* **1995,** *51,* 5459–5464. doi:10.1016/0040-4020(95)00207-O
592. Gibson, H. W.; Wang, H.; Slebodnick, C.; Merola, J.; Kassel, W. S.; Rheingold, A. L. *J. Org. Chem.* **2007,** *72,* 3381–3393. doi:10.1021/jo070030l
593. Koga, K.; Odashima, K. *J. Inclusion Phenom. Macrocyclic Chem.* **1989,** *7,* 53–60. doi:10.1007/BF01112782
594. Tabushi, I.; Yamamura, K. *Top. Curr. Chem.* **1983,** *113,* 145–182. doi:10.1007/3-540-12397-0
595. Meric, R.; Lehn, J.-M.; Vigneron, J.-P. *Bull. Soc. Chim. Fr.* **1994,** *131,* 579–583.
596. Schneider, H. J.; Kramer, R.; Theis, I.; Zhou, M.-Q. *J. Chem. Soc., Chem. Commun.* **1990,** 276. doi:10.1039/C39900000276
597. Diederich, F. *Cyclophanes;* Royal Society of Chemistry: Cambridge, 1991.
598. Organic Syntheses, 1973, Coll. Vol. 5, 883; 1962, Ann. Vol. 42, 83.
599. Tobe, Y.; Ueda, K.; Kaneda, T.; Kakiuchi, K.; Odaira, Y.; Kai, Y.; Kasai, N. *J. Am. Chem. Soc.* **1987,** *109,* 1136–1144. doi:10.1021/ja00238a024
600. Kane, V. V.; Wolf, A. D.; Jones, M., Jr. *J. Am. Chem. Soc.* **1974,** *96,* 2643–2644. doi:10.1021/ja00815a070
601. Wei, C.; Mo, K.-F.; Chan, T.-L. *J. Org. Chem.* **2003,** *68,* 2948–2951. doi:10.1021/jo0267044
602. Pascal, R. A., Jr. *Eur. J. Org. Chem.* **2004,** 3763–3771. doi:10.1002/ejoc.200400183
603. Sarri, P.; Venturi, F.; Cuda, F.; Roelens, S. *J. Org. Chem.* **2004,** *69,* 3654–3661. doi:10.1021/jo049899j
604. Rodríguez-Franco, M. I.; San Lorenzo, P.; Martínez, A.; Navarro, P. *Tetrahedron* **1999,** *55,* 2763–2772. doi:10.1016/S0040-4020(99)00047-2
605. Odashima, K.; Yagi, K.; Tohda, K.; Umezawa, Y. *Bioorg. Med. Chem. Lett.* **1999,** *9,* 2375–2378. doi:10.1016/S0960-894X(99)00395-9
606. Makote, R.; Collinson, M. M. *Chem. Mater.* **1998,** *10,* 2440. doi:10.1021/cm9801136
607. Paugam, M.-F.; Valencia, L. S.; Boggess, B.; Smith, B. D. *J. Am. Chem. Soc.* **1994,** *116,* 11203–11204. doi:10.1021/ja00103a064
608. Paugam, M.-F.; Bien, J. T.; Smith, B. D.; Christoffels, A. J.; de Jong, F.; Reinhoudt, D. N. *J. Am. Chem. Soc.* **1996,** *118,* 9820–9825. doi:10.1021/ja9615076
609. Inoue, M. B.; Velazquez, E. F.; Inoue, M.; Fernando, Q. *J. Chem. Soc., Perkin Trans. 2* **1997,** 2113–2118. doi:10.1039/a700242d
610. Gavin, J. A.; Garcia, M. E.; Benesi, A. J.; Mallouk, T. E. *J. Org. Chem.* **1998,** *63,* 7663–7669. doi:10.1021/jo980352c
611. Herm, M.; Molt, O.; Schrader, T. *Angew. Chem., Int. Ed.* **2001,** *40,* 3148–3151. doi:10.1002/1521-3773(20010903)40:17<3148::AID-ANIE3148>3.0.CO;2-S
612. Molt, O.; Schrader, T. *Angew. Chem., Int. Ed.* **2003,** *42,* 5509–5513. doi:10.1002/anie.200352186
613. Molt, O.; Rübeling, D.; Schäfer, G.; Schrader, T. *Chem.–Eur. J.* **2004,** *10,* 4225–4232. doi:10.1002/chem.200400100
614. Chui, J. K. W.; Fyles, T. *Supramol. Chem.* **2008,** *20,* 397–405. doi:10.1080/10610270701278269
615. Grawe, T.; Schrader, T.; Finocchiaro, P.; Consiglio, G.; Failla, S. *Org. Lett.* **2001,** *3,* 1597–1600. doi:10.1021/ol015668c
616. Consiglio, G. A.; Failla, S.; Finocchiaro, P.; Visi, M.; Hardcastle, K. I. *Supramol. Chem.* **2000,** *11,* 177–184. doi:10.1080/10610270008049127
617. Grawe, T.; Schrader, T.; Gurrath, M.; Kraft, A.; Osterod, F. *Org. Lett.* **2000,** *2,* 29–32. doi:10.1021/ol9910924
618. Ehala, S.; Kašička, V.; Makrlík, E. *Electrophoresis* **2008,** *29,* 652–657. doi:10.1002/elps.200700583
619. Chambron, J.-C.; Heitz, V.; Sauvage, J.-P. In *The Porphyrin Handbook;* Kadish, K. M.; Smith, K. M.; Guilard, R., Eds.; Academic Press: New York, USA, 2000; Vol. 4.
620. Kim, D.; Osuka, A. *J. Phys. Chem. A* **2003,** *107,* 8791–8816. doi:10.1021/jp030490s
621. Sternberg, E. D.; Dolphin, D.; Brückner, C. *Tetrahedron* **1998,** *54,* 4151–4202. doi:10.1016/S0040-4020(98)00015-5
622. Camerel, F.; Gilles, U.; Barberá, J.; Ziessel, R. *Chem.–Eur. J.* **2007,** *13,* 2189–2200. doi:10.1002/chem.200601475
623. Campbell, W. M.; Jolley, K. W.; Wagner, P.; Walsh, P. J.; Gordon, K. C.; Schmidt-Mende, L.; Nazeeruddin, M. K.; Wang, Q.; Grätzel, M.; Officer, D. L. *J. Phys. Chem. C* **2007,** *111,* 11760–11762. doi:10.1021/jp0750598
624. Sessler, J. L.; Weghorn, S. J. *Expanded, Contracted & Isomeric Porphyrins;* Elsevier Science: Oxford, U. K., 1997.
625. Kobuke, Y. *J. Porphyrins Phthalocyanines* **2004,** *8,* 156–174. doi:10.1142/S1088424604000155
626. Antonisse, M. M. G.; Reinhoudt, D. N. *Chem. Commun.* **1998,** 443–448. doi:10.1039/a707529d

627. Mamardashvili, G. M.; Storonkina, O. E.; Mamardashvili, N. Zh. *Russ. J. Gen. Chem.* **2004,** *74,* 1446–1450. doi:10.1007/s11176-005-0029-0
628. Ruan, W.-J.; Zhao, X.-J.; Wang, S.-J.; Zhang, Y.-H.; Zhang, Z.-H.; Nan, J.; Zhu, Z.-A.; Wang, J.-G.; Ma, Y. *Chin. J. Chem.* **2005,** *23,* 1381–1386. doi:10.1002/cjoc.200591381
629. Satake, A.; Kobuke, Y. *Tetrahedron* **2005,** *61,* 13–41. doi:10.1016/j.tet.2004.10.073
630. Even, P.; Boitrel, B. *Coord. Chem. Rev.* **2006,** *250,* 519–541. doi:10.1016/j.ccr.2005.09.003
631. Jasat, A.; Dolphin, D. *Chem. Rev.* **1997,** *97,* 2267–2340. doi:10.1021/cr950078b
632. Sessler, J. L.; Král, V.; Hoehner, M. C.; Chin, K. O. A.; Davila, R. M. *Pure Appl. Chem.* **1996,** *68,* 1291–1295. doi:10.1351/pac199668061291
633. Vogel, E. *Pure Appl. Chem.* **1996,** *68,* 1355–1360. doi:10.1351/pac199668071355
634. Ogoshi, H.; Mizutani, T. *Acc. Chem. Res.* **1998,** *31,* 81–89. doi:10.1021/ar9603165
635. Mizutani, T.; Wada, K.; Kitagawa, S. *J. Org. Chem.* **2000,** *65,* 6097–6106. doi:10.1021/jo000557x
636. Mizutani, T.; Yagi, S.; Morinaga, T.; Nomura, T.; Takagishi, T.; Kitagawa, S.; Ogoshi, H. *J. Am. Chem. Soc.* **1999,** *121,* 754–759. doi:10.1021/ja9830849
637. Imai, H.; Misawa, K.; Munakata, H.; Uemori, Y. *Chem. Lett.* **2001,** 688–689. doi:10.1246/cl.2001.688
638. Imai, H.; Misawa, K.; Munakata, H.; Uemori, Y. *Chem. Pharm. Bull.* **2008,** *56,* 1470–1472. doi:10.1248/cpb.56.1470
639. Wang, S.-J.; Ruan, W.-J.; Zhao, X.-J.; Luo, D.-B.; Zhu, Z.-A. *Chin. J. Chem.* **2005,** *23,* 44–49. doi:10.1002/cjoc.200590010
640. Ruan, W.-J.; Zhao, X.-J.; Wang, S.-J.; Zhang, Y.-H.; Zhang, Z.-H.; Nan, J.; Zhu, Z.-A.; Wang, J.-G.; Ma, Y. *Chin. J. Chem.* **2005,** *23,* 1381–1386. doi:10.1002/cjoc.200591381
641. Huang, X.; Rickman, B. H.; Borhan, B.; Berova, N.; Nakanishi, K. *J. Am. Chem. Soc.* **1998,** *120,* 6185–6186. doi:10.1021/ja973539e
642. Huang, X. F.; Fujioka, N.; Pescitelli, G.; Koehn, F. E.; Williamson, R. T.; Nakanishi, K.; Berova, N. *J. Am. Chem. Soc.* **2002,** *124,* 10320–10335. doi:10.1021/ja020520p
643. Lintuluoto, J. M.; Borovkov, V. V.; Inoue, Y. *J. Am. Chem. Soc.* **2002,** *124,* 13676–13677. doi:10.1021/ja0267270
644. Kurtán, T.; Nesnas, N.; Li, Y.-Q.; Huang, X.; Nakanishi, K.; Berova, N. *J. Am. Chem. Soc.* **2001,** *123,* 5962–5973. doi:10.1021/ja010249w
645. Proni, G.; Pescitelli, G.; Huang, X.; Quraishi, N. Q.; Nakanishi, K.; Berova, N. *Chem. Commun.* **2002,** 1590–1591. doi:10.1039/b204554k
646. Yang, Q.; Olmsted, C.; Borhan, B. *Org. Lett.* **2002,** *4,* 3423–3426. doi:10.1021/ol026527t
647. Proni, G.; Pescitelli, G.; Huang, X.; Nakanishi, K.; Berova, N. *J. Am. Chem. Soc.* **2003,** *125,* 12914–12927. doi:10.1021/ja036294g
648. Crossley, M. J.; Hambley, T. W.; Mackay, L. G.; Try, A. C.; Walton, R. *J. Chem. Soc., Chem. Commun.* **1995,** 1077–1079.
649. Crossley, M. J.; Mackay, L. G.; Try, A. C. *J. Chem. Soc., Chem. Commun.* **1995,** 1925–1927.
650. Allen, P. R.; Reek, J. N. H.; Try, A. C.; Crossley, M. J. *Tetrahedron: Asymmetry* **1997,** *8,* 1161–1164. doi:10.1016/S0957-4166(97)00116-X
651. Hayashi, T.; Nonoguchi, M.; Aya, T.; Ogoshi, H. *Tetrahedron Lett.* **1997,** *38,* 1603–1606. doi:10.1016/S0040-4039(97)00123-8
652. Hayashi, T.; Aya, T.; Nonoguchi, M.; Mizutani, T.; Hisaeda, Y.; Kitagawa, S.; Ogoshi, H. *Tetrahedron* **2002,** *58,* 2803–2811. doi:10.1016/S0040-4020(02)00166-7
653. Kubo, Y.; Murai, Y.; Yamanaka, J.-I.; Tokita, S.; Ishimaru, Y. *Tetrahedron Lett.* **1999,** *40,* 6019–6023. doi:10.1016/S0040-4039(99)01187-9
654. Kubo, Y.; Ohno, T.; Yamanaka, J.-I.; Tokita, S.; Iida, T.; Ishimaru, Y. *J. Am. Chem. Soc.* **2001,** *123,* 12700–12701. doi:10.1021/ja0113448
655. Kubo, Y.; Ishii, Y.; Yoshizawa, T.; Tokita, S. *Chem. Commun.* **2004,** 1394–1395. doi:10.1039/b403684k
656. Li, X.; Tanasova, M.; Vasileiou, C.; Borhan, B. *J. Am. Chem. Soc.* **2008,** *130,* 1885–1893. doi:10.1021/ja0752639
657. Collin, J.-P.; Frey, J.; Heitz, V.; Sauvage, J.-P.; Tock, C.; Allouche, L. *J. Am. Chem. Soc.* **2009,** *131,* 5609–5620. doi:10.1021/ja900565p
658. Kruppa, M.; König, B. *Chem. Rev.* **2006,** *106,* 3520–3560. doi:10.1021/cr010206y
659. Geduhn, J.; Walenzyk, T.; König, B. *Curr. Org. Synth.* **2007,** *4,* 390–412. doi:10.2174/157017907782408770
660. Laurie, S. H. In *Comprehensive Coordination Chemistry;* Wilkinson, G.; Gillard, R. D.; McCleverty, J. A., Eds.; Pergamon Press: New York, 1987; Vol. 2, p 739.
661. Newlin, D. E.; Pellack, M. A.; Nakon, R. *J. Am. Chem. Soc.* **1977,** *99,* 1078–1082. doi:10.1021/ja00446a017
662. Dembowski, J. S.; Kurtz, D. C.; Nakon, R. *Inorg. Chim. Acta* **1988,** *152,* 209–210. doi:10.1016/S0020-1693(00)91469-5
663. Perrin, D. D.; Sharma, V. S. *J. Chem. Soc. A* **1967,** 724–728. doi:10.1039/j19670000724
664. Fabbrizzi, L.; Pallavicini, P.; Parodi, L.; Perotti, A.; Taglietti, A. *Chem. Commun.* **1995,** 2439–2449.
665. Fabbrizzi, L.; Francese, G.; Licchelli, M.; Perotti, A.; Taglietti, A. *Chem. Commun.* **1997,** 581–582. doi:10.1039/a608531h
666. Chin, J.; Lee, S. S.; Lee, K. J.; Park, S.; Kim, D. H. *Nature* **1999,** *401,* 254–257. doi:10.1038/45751
667. Kim, H.-J.; Asif, R.; Chung, D. S.; Hong, J.-I. *Tetrahedron Lett.* **2003,** *44,* 4335–4338. doi:10.1016/S0040-4039(03)00937-7
668. La Deda, M.; Ghedini, M.; Aiello, I.; Grisolia, A. *Chem. Lett.* **2004,** *33,* 1060–1061. doi:10.1246/cl.2004.1060
669. Cozzi, P. G.; Dolci, L. S.; Garelli, A.; Montalti, M.; Prodi, L.; Zaccheroni, N. *New J. Chem.* **2003,** 692–697. doi:10.1039/b209396k
670. Splan, K. E.; Massari, A. M.; Morris, G. A.; Sun, S.-S.; Reina, E.; Nguyen, S. T.; Hupp, J. T. *Eur. J. Inorg. Chem.* **2003,** 2348–2351. doi:10.1002/ejic.200200665
671. Ma, C. T. L.; MacLachlan, M. J. *Angew. Chem., Int. Ed.* **2005,** *44,* 4178–4182. doi:10.1002/anie.200500058
672. Ercolani, G. *Struct. Bonding* **2006,** *121,* 167–215. doi:10.1007/430_019
673. Cort, A. D.; de Bernardin, P.; Schiaffino, A. *Chirality* **2009,** *21,* 104–109. doi:10.1002/chir.20614
674. Imai, H.; Munakata, H.; Uemori, Y.; Sakura, N. *Inorg. Chem.* **2004,** *43,* 1211–1213. doi:10.1021/ic0302837
675. Pagliari, S.; Corradini, R.; Galaverna, G.; Sforza, S.; Dossena, A.; Montalti, M.; Prodi, L.; Zaccheroni, N.; Marchelli, R. *Chem.–Eur. J.* **2004,** *10,* 2749–2758. doi:10.1002/chem.200305448
676. Kwong, H.-L.; Wong, W.-L.; Lee, C.-S.; Yeung, C.-T.; Teng, P.-F. *Inorg. Chem. Commun.* **2009,** *12,* 815–818. doi:10.1016/j.inoche.2009.06.013
677. Nguyen, B. T.; Anslyn, E. V. *Coord. Chem. Rev.* **2006,** *250,* 3118–3127. doi:10.1016/j.ccr.2006.04.009
678. Aït-Haddou, H.; Wiskur, S. L.; Lynch, V. M.; Anslyn, E. V. *J. Am. Chem. Soc.* **2001,** *123,* 11296–11297. doi:10.1021/ja011905v
679. Folmer-Andersen, J. F.; Lynch, V. M.; Anslyn, E. V. *J. Am. Chem. Soc.* **2005,** *127,* 7986–7987. doi:10.1021/ja052029e

680. Wright, A. T.; Anslyn, E. V. *Org. Lett.* **2004,** *6,* 1341–1344. doi:10.1021/ol036441f
681. Buryak, A.; Severin, K. *Angew. Chem.* **2004,** *116,* 4875–4878. doi:10.1002/ange.200460808
682. Buryak, A.; Severin, K. *J. Am. Chem. Soc.* **2005,** *127,* 3700–3701. doi:10.1021/ja042363v
683. Tsukube, H.; Shinoda, S.; Uenishi, J.; Kanatani, T.; Itoh, H.; Shiode, M.; Iwachido, T.; Yonemitsu, O. *Inorg. Chem.* **1998,** *37,* 1585–1591. doi:10.1021/ic970103r
684. Bednarski, M.; Danishefsky, S. *J. Am. Chem. Soc.* **1983,** *105,* 3716–3717. doi:10.1021/ja00349a064
685. Ziegler, F. E.; Sobolov, S. B. *J. Am. Chem. Soc.* **1990,** *112,* 2749–2758. doi:10.1021/ja00163a043
686. Mikami, K.; Terada, M.; Nakai, T. *J. Org. Chem.* **1991,** *56,* 5456–5459. doi:10.1021/jo00018a049
687. Tsukube, H.; Shinoda, S. *Chem. Rev.* **2002,** *102,* 2389–2403. doi:10.1021/cr010450p
688. Williams, D. H.; Bardsley, B. *Angew. Chem., Int. Ed.* **1999,** *38,* 1173–1193.
689. Pletnev, V. Z.; Tsygannik, I. N.; Fonarev, Y. D.; Mikhailova, I. Y.; Kulikov, Y. V.; Ivanov, V. T.; Langs, D. A.; Duax, W. L. *Bioorg. Khim.* **1995,** *21,* 828–833.
690. Pullman, A. *Chem. Rev.* **1991,** *91,* 793–812. doi:10.1021/cr00005a008
691. Cammann, K. *Top. Curr. Chem.* **1985,** *128,* 219–258.
692. Rose, L.; Jenkins, A. *Bioelectrochemistry* **2007,** *70,* 387–393. doi:10.1016/j.bioelechem.2006.05.009
693. Gennis, R. B. *Biomembranes: Molecular Structure and Function;* SpringerVerlag: New York, USA, 1989.
694. Berg, J. M.; Tymoczko, J. L.; Stryer, L. *Biochemistry;* Freeman: New York, USA, 2003. Chapter 13.
695. Ovchinnikov, Y. A. *Eur. J. Biochem.* **1979,** *94,* 321–336. doi:10.1111/j.1432-1033.1979.tb12898.x
696. Pressman, B. C. *Annu. Rev. Biochem.* **1976,** *45,* 501–530. doi:10.1146/annurev.bi.45.070176.002441
697. Dybal, J.; Ehala, S.; Kašička, V.; Makrlík, E. *Biopolymers* **2008,** *89,* 1055–1060. doi:10.1002/bip.21034
698. Izatt, R. M.; Bradshaw, J. S.; Nielsen, S. A.; Lamb, J. D.; Christensen, J. J.; Sen, D. *Chem. Rev.* **1985,** *85,* 271–339. doi:10.1021/cr00068a003
699. Izatt, R. M.; Pawlak, K.; Bradshaw, J. S.; Bruening, R. L. *Chem. Rev.* **1991,** *91,* 1721–1785. doi:10.1021/cr00008a003
700. Batinić-Haberle, I.; Spasojević, I.; Crumbliss, A. L. *Inorg. Chem.* **1996,** *35,* 2352–2359. doi:10.1021/ic951414+
701. Spasojević, I.; Batinić-Haberle, I.; Choo, P. L.; Crumbliss, A. L. *J. Am. Chem. Soc.* **1994,** *116,* 5714–5721. doi:10.1021/ja00092a023
702. Tristani, E. M.; Dubay, G. R.; Crumbliss, A. L. *J. Inclusion Phenom. Macrocyclic Chem.* **2009,** *64,* 57–65. doi:10.1007/s10847-009-9536-7
703. Bystrov, V. F.; Ivanov, V. T.; Koz'min, S. A.; Mikhaleva, I. I.; Khalilulina, K. K.; Ovchinnikov, Y. A.; Fedin, E. I.; Petrovskii, P. V. *FEBS Lett.* **1972,** *21,* 34–38. doi:10.1016/0014-5793(72)80156-X
704. Bystrov, V. F.; Gavrilov, Y. D.; Ivanov, V. T.; Ovchinnikov, Y. A. *Eur. J. Biochem.* **1977,** *78,* 63–68. doi:10.1111/j.1432-1033.1977.tb11714.x
705. Ohnishi, M.; Fedarko, M.-C.; Baldeschwieler, J. D.; Johnson, L. F. *Biochem. Biophys. Res. Commun.* **1972,** *46,* 312–320. doi:10.1016/0006-291X(72)90664-X
706. Patel, D. J. *Biochemistry* **1973,** *12,* 496–501. doi:10.1021/bi00727a021
707. Tabeta, R.; Saito, H. *Biochemistry* **1985,** *24,* 7696–7702. doi:10.1021/bi00347a029
708. Pitchayawasin, S.; Kuse, M.; Koga, K.; Isobe, M.; Agata, N.; Ohta, M. *Bioorg. Med. Chem. Lett.* **2003,** *13,* 3507–3517. doi:10.1016/S0960-894X(03)00731-5
709. Osborne, M. D.; Girault, H. H. *Electroanalysis* **1995,** *7,* 425–434. doi:10.1002/elan.1140070505
710. Marrone, T. J.; Merz, K. M., Jr. *J. Am. Chem. Soc.* **1992,** *114,* 7542–7549. doi:10.1021/ja00045a030
711. Dobler, M. *Helv. Chim. Acta* **1972,** *55,* 1371–1384. doi:10.1002/hlca.19720550504
712. Neuport-Laves, K.; Dobler, M. *Helv. Chim. Acta* **1976,** *59,* 614–623. doi:10.1002/hlca.19760590225
713. Prestegard, J. H.; Chan, S. I. *Biochemistry* **1969,** *8,* 3921–3927. doi:10.1021/bi00838a007
714. Maruyama, K.; Sohmiya, H.; Tsukube, H. *Tetrahedron* **1992,** *48,* 805–818. doi:10.1016/S0040-4020(01)88185-0
715. Li, G.; Still, C. W. *Tetrahedron Lett.* **1993,** *34,* 919–922. doi:10.1016/S0040-4039(00)77454-5
716. Li, G.; Still, C. W. *Bioorg. Med. Chem. Lett.* **1992,** *2,* 731–734. doi:10.1016/S0960-894X(00)80401-1
717. Pressman, B. C. *Annu. Rev. Biochem.* **1976,** *45,* 501–530. doi:10.1146/annurev.bi.45.070176.002441
718. Kinsel, J. F.; Melnik, E. I.; Lindenbaum, S.; Sternson, L. A.; Ovchinnikov, Y. A. *Int. J. Pharm.* **1982,** *12,* 97–99. doi:10.1016/0378-5173(82)90110-7
719. Kinsel, J. F.; Melnik, E. I.; Lindenbaum, S.; Sternson, L. A.; Ovchinnikov, Y. A. *Biochim. Biophys. Acta, Biomembr.* **1982,** *684,* 233–240. doi:10.1016/0005-2736(82)90011-6
720. Kinsel, J. F.; Melnik, E. I.; Sternson, L. A.; Lindenbaum, S.; Ovchinnikov, Y. A. *Biochim. Biophys. Acta* **1982,** *692,* 377–384. doi:10.1016/0005-2736(82)90387-X
721. Gueco, R. C. R.; Everett, G. W. *Tetrahedron* **1985,** *41,* 4437–4442. doi:10.1016/S0040-4020(01)82337-1
722. Tsukube, H.; Sohmiya, H. *J. Org. Chem.* **1991,** *56,* 875–878. doi:10.1021/jo00002a075
723. Chia, P. S. K.; Lindoy, L. F.; Walker, G. W.; Everett, G. W. *J. Am. Chem. Soc.* **1991,** *113,* 2533–2537. doi:10.1021/ja00007a030
724. Khutorsky, V. E. *Biophys. Chem.* **1997,** *69,* 161–166. doi:10.1016/S0301-4622(97)00086-0
725. Huczyński, A.; Janczak, J.; Rutkowski, J.; Łowicki, D.; Pietruczuk, A.; Stefańska, J.; Brzezinski, B.; Bartl, F. *J. Mol. Struct.* **2009,** *936,* 92–98. doi:10.1016/j.molstruc.2009.07.021
726. Sessler, J. L.; Andrievsky, A. *Chem.–Eur. J.* **1998,** *4,* 159–167. doi:10.1002/(SICI)1521-3765(199801)4:1<159::AID-CHEM159>3.0.CO;2-N
727. Flores-Villalobos, A.; Morales-Rojas, H.; Escalante-Tovar, S.; Yatsimirsky, A. K. *J. Phys. Org. Chem.* **2002,** *15,* 83–93. doi:10.1002/poc.454
728. Cusack, R. M.; Grøndahl, L.; Abbenante, G.; Fairlie, D. P.; Gahan, L. R.; Hanson, G. R.; Hambley, T. W. *J. Chem. Soc., Perkin Trans. 2* **2000,** 323–326. doi:10.1039/a906090a
729. Crusi, E.; Giralt, E.; Andreu, D. *Pept. Res.* **1995,** *8,* 62–69.
730. Singh, Y.; Dolphin, G. T.; Razkin, J.; Dumy, P. *ChemBioChem* **2006,** *7,* 1298–1314. doi:10.1002/cbic.200600078
731. Davies, J. S. *J. Pept. Sci.* **2003,** *9,* 471–501. doi:10.1002/psc.491

732. Bonomo, R. P.; Impellizzeri, G.; Pappalardo, G.; Purrello, R.; Rizzarelli, E.; Tabbi, G. *J. Chem. Soc., Dalton Trans.* **1998,** 3851–3857.
733. Isied, S. S.; Kuehn, C. G.; Lyon, J. M.; Merrifield, R. B. *J. Am. Chem. Soc.* **1982,** *104,* 2632–2634. doi:10.1021/ja00373a049
734. Gisin, B. F.; Merrifield, R. B.; Tosteson, D. C. *J. Am. Chem. Soc.* **1969,** *91,* 2691–2695. doi:10.1021/ja01038a047
735. Kubik, S. *J. Am. Chem. Soc.* **1999,** *121,* 5846–5855. doi:10.1021/ja983970j
736. Kurome, T.; Inami, K.; Inoue, T.; Ikai, K.; Takesako, K.; Kato, I.; Shiba, T. *Tetrahedron* **1996,** *52,* 4327–4346. doi:10.1016/0040-4020(96)00132-9
737. Oliva, R.; Falcigno, L.; D'Auria, G.; Saviano, M.; Paolillo, L.; Ansanelli, G.; Zanotti, G. *Biopolymers* **2000,** *53,* 581–595. doi:10.1002/(SICI)1097-0282(200006)53:7<581::AID-BIP5>3.0.CO;2-C
738. Ösapay, G.; Profit, A.; Taylor, J. *Tetrahedron Lett.* **1990,** *31,* 6121–6124.
739. Tolle, J. C.; Staples, M. A.; Blout, E. R. *J. Am. Chem. Soc.* **1982,** *104,* 6883–6884. doi:10.1021/ja00388a114
740. Zanotti, G.; Birr, C.; Wieland, T. *Int. J. Pept. Protein Res.* **1978,** *12,* 204–216.
741. Kubik, S. Cyclopeptides as macrocyclic host molecules for charged guest. In *Highlights in Bioorganic Chemistry – Methods and Applications;* Schmuck, C.; Wennemers, H., Eds.; Wiley-VCH: Weinheim, Germany, 2004; pp 124–137. doi:10.1002/3527603727.ch2b
742. Hynes, R. O. *Cell* **1992,** *69,* 11–25. doi:10.1016/0092-8674(92)90115-S
743. Cooper, R. G.; Harbottle, R. P.; Schneider, H.; Coutelle, C.; Miller, A. D. *Angew. Chem., Int. Ed.* **1999,** *111,* 2128–2132. doi:10.1002/(SICI)1521-3757(19990712)111:13/14<2128::AID-ANGE2128>3.0.CO;2-H
744. Yanagihara, R.; Katoh, M.; Hanyuu, M.; Miyazawa, T.; Yamada, T. *J. Chem. Soc., Perkin Trans. 2* **2000,** 551–556. doi:10.1039/a906439g
745. Hanyu, M.; Yanagihara, R.; Miyazawa, T.; Yamada, T. *Pept. Sci.* **2002,** *2001,* 373–376.
746. Kubik, S.; Goddard, R. *Eur. J. Org. Chem.* **2001,** 311–322. doi:10.1002/1099-0690(200101)2001:2<311::AID-EJOC311>3.0.CO;2-M
And literature therein.
747. Heinrichs, G.; Vial, L.; Lacour, J.; Kubik, S. *Chem. Commun.* **2003,** 1252–1253. doi:10.1039/b302092d
748. Pohl, S.; Goddard, R.; Kubik, S. *Tetrahedron Lett.* **2001,** *42,* 7555–7558. doi:10.1016/S0040-4039(01)01505-2
749. Ghadiri, M. R.; Granja, J. R.; Milligan, R. A.; McRee, D. E.; Khazanovich, N. *Nature* **1993,** *366,* 324–327. doi:10.1038/366324a0
750. Granja, J. R.; Ghadiri, M. R. *J. Am. Chem. Soc.* **1994,** *116,* 10785–10786. doi:10.1021/ja00102a054
751. Hartgerink, J. D.; Granja, J. R.; Milligan, R. A.; Ghadiri, M. R. *J. Am. Chem. Soc.* **1996,** *118,* 43–50. doi:10.1021/ja953070s
752. Benco, J. S.; Nienaber, H. A.; McGimpsey, W. G. *Anal. Chem.* **2003,** *75,* 152–156. doi:10.1021/ac0257851
753. Kubik, S.; Goddard, R. *J. Org. Chem.* **1999,** *64,* 9475–9486. doi:10.1021/jo991087d
754. McGimpsey, W. G.; Soto, E.; Driscoll, P. F.; Nowak, C.; Benco, J. S.; Cooper, Ch. G. F.; Lambert, C. R. *Magn. Reson. Chem.* **2008,** *46,* 955–961. doi:10.1002/mrc.2287
755. Connors, K. A. In *Comprehensive Supramolecular Chemistry;* Szejtli, J.; Osa, T., Eds.; Pergamon: New York, USA, 1996; Vol. 3, p 205.
756. Breslow, R.; Greenspoon, N.; Guo, T.; Zarzycki, R. *J. Am. Chem. Soc.* **1989,** *111,* 8296–8297. doi:10.1021/ja00203a050
757. Jiang, T.; Lawrence, D. S. *J. Am. Chem. Soc.* **1995,** *117,* 1857–1858. doi:10.1021/ja00111a035
758. Venema, F.; Nelissen, H. F. M.; Berthault, P.; Birlirakis, N.; Rowan, A. E.; Feiters, M. C.; Nolte, R. J. M. *Chem.–Eur. J.* **1998,** *4,* 2237–2250. doi:10.1002/(SICI)1521-3765(19981102)4:11<2237::AID-CHEM2237>3.0.CO;2-4
759. Qu, X. K.; Zhu, L. Y.; Li, L.; Wei, X.-L.; Liu, F.; Sun, D.-Z. *J. Solution Chem.* **2007,** *36,* 643–650. doi:10.1007/s10953-007-9132-7
760. Iglesias, E. *J. Org. Chem.* **2006,** *71,* 4383–4392. doi:10.1021/jo052666n
761. Reetz, M. T.; Sostmann, S. *Tetrahedron* **2001,** *57,* 2515–2520. doi:10.1016/S0040-4020(01)00077-1
762. Cram, D. J.; Kaneda, T.; Helgeson, R. C.; Brown, S. B.; Knobler, C. B.; Maverick, E.; Trueblood, K. N. *J. Am. Chem. Soc.* **1985,** *107,* 3645–3657. doi:10.1021/ja00298a040
763. Cram, D. J.; Carmack, R. A.; de Grandpre, M. P.; Lein, G. M.; Goldberg, I.; Knobler, C. B.; Maverick, E. F.; Trueblood, K. N. *J. Am. Chem. Soc.* **1987,** *109,* 7068–7072. doi:10.1021/ja00257a027
And references therein.
764. Hosokawa, Y.; Kawase, T.; Oda, M. *Chem. Commun.* **2001,** 1948–1949. doi:10.1039/b104325k
765. Pluth, M. D.; Bergman, R. G.; Raymond, K. N. *J. Am. Chem. Soc.* **2007,** *129,* 11459–11467. doi:10.1021/ja072654e
766. Pluth, M. D.; Bergman, R. G.; Raymond, K. N. *J. Am. Chem. Soc.* **2008,** *130,* 6362–6366. doi:10.1021/ja076691h
767. Wehner, M.; Schrader, T. *Angew. Chem., Int. Ed.* **2002,** *41,* 1751–1754. doi:10.1002/1521-3773(20020517)41:10<1751::AID-ANIE1751>3.0.CO;2-#
768. Lu, G.; Grossman, J. E.; Lambert, J. B. *J. Org. Chem.* **2006,** *71,* 1769–1776. doi:10.1021/jo0518405
769. Zhang, X.; Guo, L.; Wu, F.-Y.; Jiang, Y.-B. *Org. Lett.* **2003,** *5,* 2667–2670. doi:10.1021/ol034846u
770. Tolbert, L. M.; Solntsev, K. M. *Acc. Chem. Res.* **2002,** *35,* 19–27. doi:10.1021/ar990109f
771. Guilbault, G. G.; Vaughan, A.; Hackney, D. *Anal. Chem.* **1971,** *43,* 721–724. doi:10.1021/ac60301a001
772. Catechins are a class of polyphenols found in the leaves and buds of the tea plant (Camellia sinensis). They have recently been discovered to have various physiologically modulating effects such as anti-carcinogenic, anti-metastatic, anti-oxidative, anti-hypertensive, anti-hypercholesterolemic, or anti-bacterial.
773. Hayashi, N.; Ujihara, T. *Tetrahedron* **2007,** *63,* 9802–9809. doi:10.1016/j.tet.2007.07.003
774. Tsubaki, K.; Mukoyoshi, K.; Morikawa, H.; Kinoshita, T.; Fuji, K. *Chirality* **2002,** *14,* 713–715. doi:10.1002/chir.10111
775. Feuster, E. K.; Glass, T. E. *J. Am. Chem. Soc.* **2003,** *125,* 16174–16175. doi:10.1021/ja036434m
776. Secor, K. E.; Glass, T. E. *Org. Lett.* **2004,** *6,* 3727–3730. doi:10.1021/ol048625f
777. Inoue, M. B.; Velazquez, E. F.; Inoue, M.; Fernando, Q. J. *J. Chem. Soc., Perkin Trans. 2* **1997,** 2113–2118. doi:10.1039/a700242d

778. Herm, M.; Molt, O.; Schrader, T. *Chem.–Eur. J.* **2002,** *8,* 1485–1499. doi:10.1002/1521-3765(20020315)8:6<1485::AID-CHEM1485>3.0.CO;2-H
779. Secor, K.; Plante, J.; Avetta, C.; Glass, T. *J. Mater. Chem.* **2005,** *15,* 4073–4077. doi:10.1039/b503269e
780. Reinert, S.; Mohr, G. J. *Chem. Commun.* **2008,** 2272–2274. doi:10.1039/b717796h
781. Gräfe, A.; Haupt, K.; Mohr, G. J. *Anal. Chim. Acta* **2006,** *565,* 42–47. doi:10.1016/j.aca.2006.02.034
782. Mohr, G. J.; Demuth, C.; Spichiger-Keller, U. E. *Anal. Chem.* **1998,** *70,* 3868–3873. doi:10.1021/ac980279q
783. Mertz, E.; Beil, J. B.; Zimmerman, S. C. *Org. Lett.* **2003,** *5,* 3127–3130. doi:10.1021/ol0351605
784. Mertz, E.; Elmer, S. L.; Balija, A. M.; Zimmerman, S. C. *Tetrahedron* **2004,** *60,* 11191–11204. doi:10.1016/j.tet.2004.08.100
785. Mertz, E.; Zimmerman, S. C. *J. Am. Chem. Soc.* **2003,** *125,* 3424–3425. doi:10.1021/ja0294515
786. Ammonium ionophores, need a rigid framework with a cavity appropriately sized for ammonium ion (ionic radius 1.43 Å) to impart high selectivity over interfering cations of other sizes. The complexation is thermodynamically more favorable when the ionophore is conformationally pre-organized into the correct binding geometry in order to minimize the entropic cost of cation binding. The ammonium ionophore should exhibit a spatial distribution of lone-pair electrons for effective hydrogen bonding with the tetrahedral ammonium ion.
787. Marcus, Y.; Hefter, G. *Chem. Rev.* **2006,** *106,* 4585–4621. doi:10.1021/cr040087x
An excellent review summarises all important facts on ion pairs like hydration, activity, ionic strength and energetic considerations.
788. Fraenkel, G.; Kim, J. P. *J. Am. Chem. Soc.* **1966,** *88,* 4203–4211. doi:10.1021/ja00970a018
And literature therein.
789. Leung, D. H.; Bergman, R. G.; Raymond, K. N. *J. Am. Chem. Soc.* **2008,** *130,* 2798–2805. doi:10.1021/ja075975z
In water solvent reorganization has to be considered as important factor for encapsulation.
790. Okada, T.; Usui, T. *J. Chem. Soc., Faraday Trans.* **1996,** *92,* 4977–4981. doi:10.1039/ft9969204977
Demonstrated with crown ethers.
791. Gevorkyan, A. A.; Arakelyan, A. S.; Esayan, V. A.; Petrosyan, K. A.; Torosyan, G. O. *Russ. J. Gen. Chem.* **2001,** *71,* 1327–1328. doi:10.1023/A:1013214204817
And literature cited therein for association in quaternary ammonium salts.
792. Arduini, A.; Giorgi, G.; Pochini, A.; Secchi, A.; Ugozzoli, F. *J. Org. Chem.* **2001,** *66,* 8302–8308. doi:10.1021/jo016035e
Observed with Calixarenes.
793. Izatt, R. M.; Lamb, J. D.; Izatt, N. E.; Rossiter, B. E., Jr.; Christensen, J. J.; Haymore, B. L. *J. Am. Chem. Soc.* **1979,** *101,* 6273–6276. doi:10.1021/ja00515a019
794. Biron, E.; Voyer, N.; Meillon, J.-C.; Cormier, M.-E.; Auger, M. *Biopolymers* **2001,** *55,* 364–372. doi:10.1002/1097-0282(2000)55:5<364::AID-BIP1010>3.0.CO;2-Z
795. Voyer, N.; Robitaille, M. *J. Am. Chem. Soc.* **1995,** *117,* 6599–6600. doi:10.1021/ja00129a027
796. Chambron, J.-C.; Heitz, V.; Sauvage, J.-P. In *The Porphyrin Handbook;* Kadish, K. M.; Smith, K. M.; Guilard, R., Eds.; Academic Press: New York, USA, 2000; Vol. 6, pp 1–42.
797. Yin, H.; Lee, G.-I.; Sedey, K. A.; Kutzki, O.; Park, H. S.; Orner, B. P.; Ernst, J. T.; Wang, H.-G.; Sebti, S. M.; Hamilton, A. D. *J. Am. Chem. Soc.* **2005,** *127,* 10191–10196. doi:10.1021/ja050122x
798. Yin, H.; Lee, G.-I.; Park, H. S.; Payne, G. A.; Rodriguez, J. M.; Sebti, S. M.; Hamilton, A. D. *Angew. Chem., Int. Ed.* **2005,** *44,* 2704–2707. doi:10.1002/anie.200462316
799. van Delden, R. A.; ter Wiel, M. K. J.; Pollard, M. M.; Vicario, J.; Koumura, N.; Feringa, B. L. *Nature* **2005,** *437,* 1337–1340. doi:10.1038/nature04127
800. Fletcher, S. P.; Dumur, F.; Pollard, M. M.; Feringa, B. L. *Science* **2005,** *310,* 80–82. doi:10.1126/science.1117090

License and Terms

Beilstein Journal of Organic Chemistry

Anion receptors containing thiazine-1,1-dioxide heterocycles as hydrogen bond donors

Hong-Bo Wang, James A. Wisner* and Michael C. Jennings

Full Research Paper

Open Access

Address:
Department of Chemistry, University of Western Ontario, 1151 Richmond St., London, Ontario N6A 5B7, Canada

Email:
James A. Wisner* - jwisner@uwo.ca

* Corresponding author

Keywords:
anions; hydrogen bonds; receptors; sulfonamides; supramolecular chemistry

Beilstein J. Org. Chem. **2010,** *6,* No. 50.
doi:10.3762/bjoc.6.50

Received: 18 February 2010
Accepted: 22 April 2010
Published: 19 May 2010

Guest Editor: C. A. Schalley

Abstract

The synthesis, X-ray crystal structures and anion recognition properties of two receptors containing thiazine-1,1-dioxide heterocycles as hydrogen bond donating subunits are reported. The newly synthesized receptors display much different anion selectivities in acetone-d_6 than *N*,*N*′-diphenyl-1,3-disulfonamidobenzene that was used as a comparison. The selectivity exhibited by one of the new receptors for chloride anions can be attributed to greater steric demand in the cleft formed, in part, by its terminal phenyl rings; an effect that is absent in the comparison receptor.

Introduction

The synthesis of neutral hosts and study of their anion recognition properties is an area of research that has grown in interest over the past several years owing to the potential use of such receptors in environmental, biomedical and materials applications [1,2]. The basic design methodology for these hosts has largely focused on the use of nitrogen-based hydrogen bond donor groups such as amides [3,4], ureas [5], pyrroles/indoles/carbazoles [6,7] and sulfonamides [8-23] to complex the anionic targets in a topologically complementary fashion. Sulfonamides are an interesting case as the hydrogen bond donor is often significantly more acidic (pK_a approx. 11 for simple *N*-phenylaryl sulfonamides such as **3** (see below)) than that presented by other groups typically incorporated in these frameworks. The greater acidity of such a subunit can be an advantage by providing greater potential hydrogen bond donor strength with anionic guests. Alternatively, the possibility of deprotonation in some specific systems by basic anions such as carboxylates or fluoride can be employed as an indicator for these species. Regardless, the incorporation of sulfonamide functional groups has typically been realized synthetically by sulfonylation of an amine to form a sulfonamide product. This approach is somewhat limited, from a design perspective, in that the majority of examples to date consist of sulfonamides derived from a few commercially available starting materials such as benzenesulfonyl, toluenesulfonyl, dansyl, and benzenedisulfonyl chlorides [8-23]. We have recently investigated

thiazine-1,1-dioxide heterocycles (Figure 1A) as hydrogen bond donor groups in the formation of double helical complexes [24]. The parent heterocycle can be viewed as a cyclic, vinylogous sulfonamide that presents a different spatial, conformational and electronic relationship between the sulfonyl and NH subunits than that of a typical sulfonamide function (Figure 1B). It is a simple matter to access many such derivatives with this framework using straightforward synthetic methods and inexpensive materials and reagents. Herein, we describe an illustrative synthesis of two anion hosts incorporating these heterocycles and compare their binding affinities with some common anionic guests to that of an analogous benzene disulfonamide anion receptor.

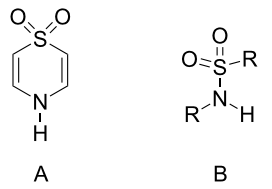

Figure 1: Structures of thiazine-1,1-dioxide heterocycle (A) and sulfonamide function (B).

Results and Discussion

The two receptor structures **1** and **2** (Figure 2) were chosen with the intent of evaluating their efficacy in comparison to the known anion host *N*,*N*′-diphenyl-1,3-disulfonamidobenzene **3** (Figure 2) [21]. Originally investigated for anion recognition by Crabtree and coworkers, **3** was considered a representative comparator given the similar stereochemical arrangement of the two NH donors and the 1,3-benzenediyl spacer. The incorporation of a pyridyl spacer in **2** was chosen to examine the possible effect the ring nitrogen atom might have on the preorganization and anion recognition properties of the resulting host in comparison to **1**. It is well known that structurally related 2,6-dicarboxamidopyridine containing hosts have markedly different properties compared to their analogous isophthalamide derivatives in these regards as well [25,26]. It is an indication of the potential versatility of the synthetic method described here that the elusive 2,6-disulfonamidopyridine host **4** (Figure 2) that would provide a more direct comparison to **2** is at present unknown and likely synthesized only with some difficulty.

The syntheses of receptors **1** and **2** are summarized in Scheme 1. α,α′-Dibromo-1,3-diacetylbenzene (**5**) and α,α′-dibromo-2,6-diacetylpyridine (**6**) are both simply generated by bromination of the corresponding diacylarenes. The reaction of either dibromide with α-mercaptoacetophenone in the presence of 2,6-lutidine yields dithioether intermediates **7** and **8**. Oxidation of these dithioethers to the disulfones **9** and **10** with urea-hydrogen peroxide (UHP) and trifluoroacetic anhydride (TFAA) in acetonitrile at room temperature proceeds in high yields. The final products **1** and **2** were obtained by the cyclization and dehydration of these intermediate disulfones with ammonium acetate in refluxing glacial acetic acid. Overall, the yields of receptors **1** and **2** are 62% and 72% respectively, from the dibromides. The simplicity and mild nature of these transformations make them easily applicable to the derivatization of most α-bromoacyl functional groups should one desire the installation of this subunit in a potential host.

The solid-state structures of both newly synthesized receptors were confirmed by X-ray diffraction analysis of single crystals grown by the slow diffusion of isopropyl ether into concentrated DMSO solutions of each (Figure 3). Unfortunately, attempts to co-crystallize the receptors with anionic guests in a number of organic solvents were unsuccessful. The conformations of the receptors in the solid state are surprisingly different given the similarity in molecular structure; the two receptors differ only in the replacement of an aryl CH in **1** for N in **2**. The structure of **1** is in an extended, approximately *anti-anti* conformation [27] where each of the NH groups is hydrogen bonded to a different DMSO solvent molecule in the lattice (N···O = 2.821(3) and 2.770(3) Å). In contrast, **2** crystallizes in an approximately cleft-shaped *syn-syn* conformation where both NH groups are hydrogen bonded to a single DMSO solvent molecule (N···O = 2.971(2) and 2.950(3) Å). The difference

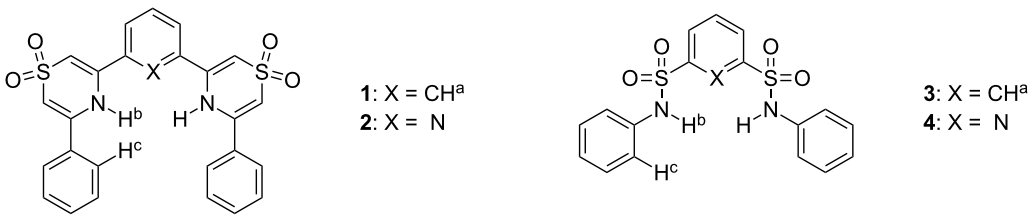

Figure 2: Structures of anion receptors **1**–**4**.

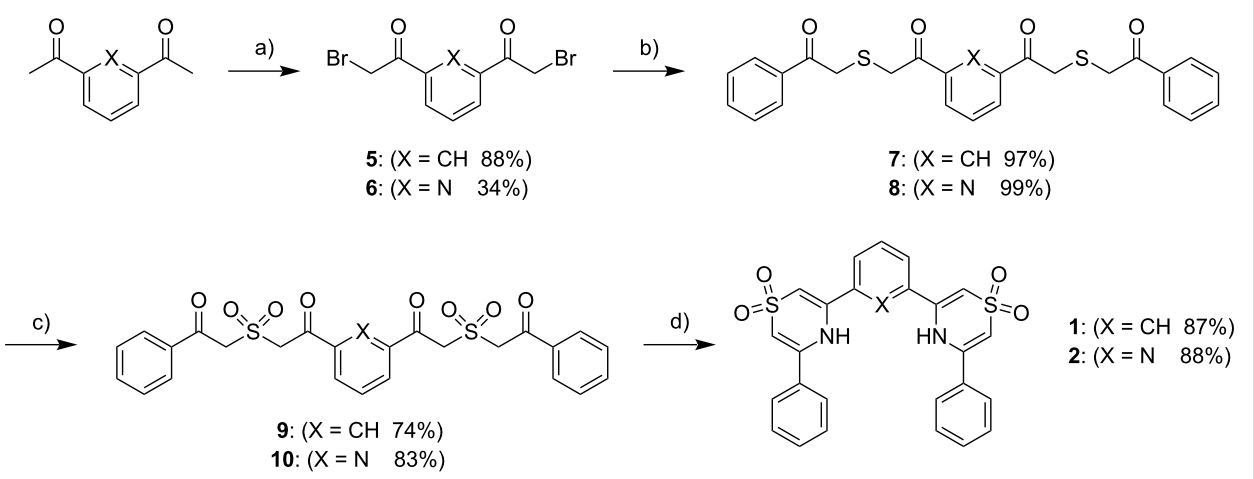

Scheme 1: Syntheses of **1** and **2**. Reaction conditions: (a) (X = CH) NBS, TsOH, CH_3CN, reflux or (X = N) Br_2, $AlCl_3$, Et_2O, 0 °C; (b) 2,6-lutidine, α-mercaptoacetophenone (2 equiv), CH_2Cl_2; (c) UHP/TFAA, CH_3CN; (d) NH_4OAc, AcOH, reflux.

may be rationalized by the presence of a weak intramolecular N-H···N hydrogen bond between the central pyridine ring and each of the two thiazine-1,1-dioxide rings in **2** that is necessarily absent in **1**. This conclusion is supported by the approximate 0.5 ppm chemical shift difference of the two receptor NH resonances in acetone-d_6 (**2** > **1**) and similar shift differences observed in analogous hosts that are even larger when measured in the less competitive solvent $CDCl_3$ [28].

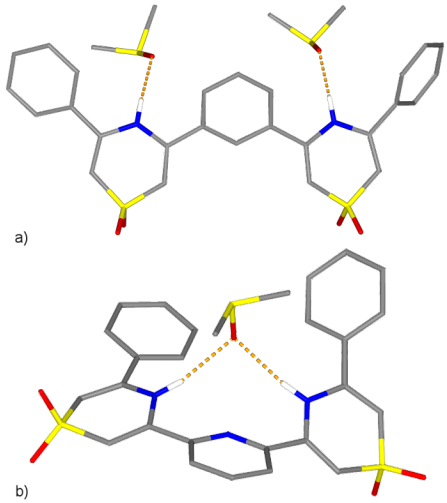

Figure 3: Stick representations of the X-ray crystal structures of (a) receptor **1** and (b) receptor **2**. Non-acidic hydrogen atoms omitted for clarity. Red = oxygen, blue = nitrogen, yellow = sulfur, grey = carbon. Hydrogen bonds denoted by dotted orange lines.

The three receptors were each titrated in acetone-d_6 with a number of TBA (tetrabutylammonium) salts of common anionic guests and the shifts of their ^{1}H NMR resonances were observed as a function of anion concentration. In the majority of cases the downfield shift of the NH protons of the receptors was used to determine the stability constants. However, the addition of less than a half an equivalent of either acetate or dihydrogen phosphate anions to any of the three receptors resulted in the disappearance of the receptor NH proton resonances in their NMR spectra. In these cases, either the upfield shift of a CH resonance on the thiazine-1,1-dioxide rings (**1** and **2**) or the downfield shift of the 2-CH proton on the central phenyl ring of the receptor (**3**) was used to determine the stability constants. Non-linear least squares fitting of the data using the program EQNMR [29] yielded the complex stability constants in all cases. All of the titrations were fit to a 1:1 (receptor:anion) binding model except for the titration of receptor **1** with TBA chloride. In this case the data fit a 1:1 binding model that included a much weaker 2:1 (receptor:anion) component. It should also be noted that the data from titration of **3** with acetate had a binding constant that was too large to be reliably fit by this method. The titration results are summarized in Table 1.

Receptor **1** exhibits a clear preference for a chloride anion guest over the other anions tested. Chloride is likely an excellent steric match to the cleft formed by the NH protons, the 2-CH proton of the central aryl ring and two of the *ortho*-protons of the terminal phenyl rings of **1** in a planar *syn-syn* binding conformation similar to that observed in the solid state structure of **2** with DMSO (Figure 1B). This conclusion is supported by the observation of significant downfield shifts of all three of these protons (Figure 2) in the ^{1}H NMR spectrum upon chloride complexation ($\Delta\delta_{max}$ = 0.15 (H^a), 1.91 (H^b), 0.17 (H^c) ppm). The progressively reduced affinity of **1** for bromide and iodide

Table 1: Stability constants (K_a) determined by ^{1}H NMR in acetone-d_6 solution at 298 K for receptors **1**–**3** with a variety of anionic guests.

Anion[a]	Receptor **1**	Receptor **2**	Receptor **3**
Cl^-	(2:1) 300 (1:1) 59000	300	4300
Br^-	380	83	740
I^-	53	—[b]	86
HSO_4^-	220	130	560
AcO^-	12500	480	$>10^5$
$H_2PO_4^-$	540	360	79000

[a]Added as their tetrabutylammonium salts. Errors are estimated to be <10%.
[b]No change was observed in the ^{1}H NMR of the receptor upon anion addition.

can be attributed both to their inability to fit into this idealized cleft conformation and their respectively decreasing efficacies as hydrogen bond acceptors. In fact, this observation is common to **1** and **2** and mirrors the behaviour of similar acyclic isophthalamide hosts studied previously by Crabtree and coworkers in CD_2Cl_2 [21]. Receptor **1** shows a preference for the complexation of chloride over acetate (5:1) and a distinct discrimination against the dihydrogen phosphate (>100:1 $Cl:H_2PO_4$) guest. Presumably, the larger size of the dihydrogen phosphate anion prevents complexation by **1** in a coplanar *syn-syn* conformation. The distortion of the receptor from a low energy coplanar binding geometry should reduce its affinity for such guests, despite their greater basicity. This supposition is supported in the case of dihydrogen phosphate by a very small $\Delta\delta_{max}$ for H^a observed when **1** is titrated with this anion (0.01 ppm) though $\Delta\delta_{max}$ of protons H^c remains significant (0.15 ppm) indicating their continued participation in the binding event. The titration of **1** with the less basic but similarly sized and shaped HSO_4^- anion displays an *upfield* shift of H^a ($\Delta\delta_{max}$ = −0.05 ppm) and a reduced downfield shift of H^c ($\Delta\delta_{max}$ = 0.07 ppm).

Replacement of the central phenyl ring spacer of **1** for pyridine in **2** results in a significant reduction of the association constants for all of the anions tested. This result was expected as a consequence of repulsion of anionic guests by the lone pair of the pyridine ring nitrogen atom upon binding in the cleft of the receptor. The other outcome of this replacement is a loss of any selectivity for chloride and, in fact, a slight preference by receptor **2** for acetate and dihydrogen phosphate.

The simple disulfonamide receptor **3** exhibits very different complexation behaviour than **1** and **2** with the anions investigated. Receptor **3** displays a strong preference for acetate and dihydrogen phosphate over all of the other anions investigated in this solvent. The binding constant for chloride is reduced by an order of magnitude but is still preferred over bromide even though the affinity of **3** for the latter guest has approximately doubled in comparison to receptor **1**. No change in the ^{1}H NMR spectrum of **3** is observed upon the addition of iodide. We believe that the differences in anion binding between these two receptors can be satisfactorily explained by the differences in their cleft geometries. The central three atoms (NH and CH^a) that define the binding cleft in both **1** and **3** circumscribe a very similar meridian. In fact, we manipulated the single crystal molecular structures of **1** and the 4,4′-di-*t*-butyl derivative of **3** [30] (available from the Cambridge Crystallographic Database #1003/6124) by rotating the two relevant dihedral angles to bring the NH groups into plane with their central aryl rings in an idealized *syn-syn* conformation. Measurement of these "closest approach" N···N distances in the two models yields values of 4.76 and 4.77 Å for **1** and the derivative of **3**, respectively; a difference of 0.01 Å. The terminal phenyl rings of **3** do not, however, occlude this central cleft like those of **1** and **2**. Rather, they form a divergent "V"-shaped geometry upon chelation of anionic species by the two NH groups of **3**, regardless of whether coplanarity is maintained with the central benzene ring. The *ortho*-protons of these terminal rings (H^c) are certainly too far away to contribute to the stability of the halide anion complexes that presumably form in this manner. The general result of this relaxation of the steric requirements for anion complexation by **3**, in comparison to **1**, is a marked increase in binding strength for all of the larger anions. Thus, the binding affinities of **3** for these larger anions follow the trend of their aqueous basicities (pK_a conj. acid): AcO^- (4.75), $H_2PO_4^-$ (2.12), HSO_4^- (−3), Br^- (−9), I^- (−10) [31].

Conclusions

We have presented a simple synthetic route for the incorporation of thiazine-1,1-dioxide heterocycles as hydrogen bond donating subunits in two new acyclic anion receptors. The two new receptors **1** and **2**, were titrated with a number of anions and displayed very different complexation behaviour to the known disulfonamide receptor **3** that was used as a comparison. The difference can be attributed to the differing steric demands of the terminal phenyl rings in the two different receptor geometries despite the similar character of their central binding clefts. The steric effect of these rings in receptor **1** generates significant selectivity by the receptor for chloride versus the other, larger anions studied. The replacement of the central 1,3-benzenediyl spacer in **1** for 2,6-pyridinediyl in **2** greatly reduces the affinity of the resulting receptor for all of the anions examined and eliminates any selectivity for chloride. The synthetic approach described here can be easily adapted to the synthesis of oligomeric analogues of these two receptors that we expect will display an even greater selectivity for chloride anions and operate in more competitive solvent environments.

Supporting Information

Details of synthetic procedures, characterization data for intermediates and final products, and binding isotherms for receptors **1** and **2** with TBA salts of anions.

Supporting Information File 1

Experimental details.
[http://www.beilstein-journals.org/bjoc/content/supplementary/1860-5397-6-50-S1.pdf]

Supporting Information File 2

X-ray crystal data for receptor **1**.
[http://www.beilstein-journals.org/bjoc/content/supplementary/1860-5397-6-50-S2.cif]

Supporting Information File 3

X-ray crystal data for receptor **2**.
[http://www.beilstein-journals.org/bjoc/content/supplementary/1860-5397-6-50-S3.cif]

Acknowledgements

We thank the Natural Sciences and Engineering Council of Canada and the Ontario Ministry of Research and Innovation for their generous financial support of this research.

References

1. Sessler, J. L.; Gale, P. A.; Cho, W.-S. *Anion Receptor Chemistry;* Royal Society of Chemistry: Cambridge, U.K., 2006.
2. Katayev, E. A.; Kolesnikov, G. V.; Sessler, J. L. *Chem. Soc. Rev.* **2009,** *38,* 1572–1586. doi:10.1039/b806468g
3. Kubik, S. *Chem. Soc. Rev.* **2009,** *38,* 585–605. doi:10.1039/b810531f
4. Kang, S. O.; Begum, R. A.; Bowman-James, K. *Angew. Chem., Int. Ed.* **2006,** *45,* 7882–7894. doi:10.1002/anie.200602006
5. Zhang, Z.; Schreiner, P. R. *Chem. Soc. Rev.* **2009,** *38,* 1187–1198. doi:10.1039/b801793j
6. Cho, W.-S.; Sessler, J. L. Artificial pyrrole-based anion receptors. In *Functional Synthetic Receptors;* Schrader, T.; Hamilton, A. D., Eds.; Wiley-VCH: Weinheim, Germany, 2005; pp 165–256. doi:10.1002/352760572X.ch4
7. Gale, P. A. *Chem. Commun.* **2008,** 4525–4540. doi:10.1039/b809508f
8. López, M. V.; Bermejo, M. R.; Vásquez, M. E.; Taglietti, A.; Zaragoza, G.; Pedrido, R.; Martínez-Calvo, M. *Org. Biomol. Chem.* **2010,** *8,* 357–362. doi:10.1039/b916040j
9. Warr, R. J.; Westra, A. N.; Bell, K. J.; Chartres, J.; Ellis, R.; Tong, C.; Simmance, T. G.; Gadzhieva, A.; Blake, A. J.; Tasker, P. A.; Schröder, M. *Chem.–Eur. J.* **2009,** *15,* 4836–4850. doi:10.1002/chem.200802377
10. Kakuchi, R.; Kodama, T.; Shimada, R.; Tago, Y.; Sakai, R.; Satoh, T.; Kakuchi, T. *Macromolecules* **2009,** *42,* 3892–3897. doi:10.1021/ma900409h
11. Caltagirone, C.; Bates, G. W.; Gale, P. A.; Light, M. A. *Chem. Commun.* **2008,** 61–63. doi:10.1039/b713431b
12. Berryman, O. B.; Johnson, C. A., II; Zakharov, L. N.; Haley, M. M.; Johnson, D. W. *Angew. Chem., Int. Ed.* **2008,** *47,* 117–120. doi:10.1002/anie.200703971
13. Shang, X. F.; Lin, H.; Lin, H. K. *J. Fluorine Chem.* **2007,** *128,* 530–534. doi:10.1016/j.jfluchem.2007.01.005
14. Wu, Y.; Peng, X.; Fan, J.; Gao, S.; Tian, M.; Zhao, J.; Sun, S. *J. Org. Chem.* **2007,** *72,* 62–70. doi:10.1021/jo061634c
15. Kavallieratos, K.; Sabucedo, A. J.; Pau, A. T.; Rodriguez, J. M. *J. Am. Soc. Mass Spectrom.* **2005,** *16,* 1377–1383. doi:10.1016/j.jasms.2005.04.008
16. Kondo, S.-I.; Suzuki, T.; Toyama, T.; Yano, Y. *Bull. Chem. Soc. Jpn.* **2005,** *78,* 1348–1350. doi:10.1246/bcsj.78.1348
17. Smith, B. D.; Lambert, T. N. *Chem. Commun.* **2003,** 2261–2268. doi:10.1039/b303359g
18. Kondo, S.-I.; Suzuki, T.; Yano, Y. *Tetrahedron Lett.* **2002,** *43,* 7059–7061. doi:10.1016/S0040-4039(02)01543-5
19. Kavallieratos, K.; Moyer, B. A. *Chem. Commun.* **2001,** 1620–1621. doi:10.1039/b102152b
20. Chrisstoffels, L. A. J.; de Jong, F.; Reinhoudt, D. N. *Chem.–Eur. J.* **2000,** *6,* 1376–1385. doi:10.1002/(SICI)1521-3765(20000417)6:8<1376::AID-CHEM1376>3.0.CO;2-I
21. Kavallieratos, K.; Bertao, C. M.; Crabtree, R. H. *J. Org. Chem.* **1999,** *64,* 1675–1683. doi:10.1021/jo982382l
22. Davis, A. P.; Perry, J. J.; Williams, R. P. *J. Am. Chem. Soc.* **1997,** *119,* 1793–1794. doi:10.1021/ja9629930
23. Morzherin, Y.; Rudkevich, D. M.; Verboom, W.; Reinhoudt, D. N. *J. Org. Chem.* **1993,** *58,* 7602–7605. doi:10.1021/jo00078a052
24. Li, J.; Wisner, J. A.; Jennings, M. C. *Org. Lett.* **2007,** *9,* 3267–3269. doi:10.1021/ol071171c
25. Brooks, S. J.; Garcia-Garrido, S. E.; Light, M. E.; Cole, P. A.; Gale, P. A. *Chem.–Eur. J.* **2007,** *13,* 3320–3329. doi:10.1002/chem.200601647
26. Schmuck, C.; Machon, U. *Chem.–Eur. J.* **2005,** *11,* 1109–1118. doi:10.1002/chem.200400652
27. Hunter, C. A.; Purvis, D. A. *Angew. Chem., Int. Ed. Engl.* **1992,** *31,* 792. doi:10.1002/anie.199207921
28. Wisner, J. A.; Li, J. unpublished results.
29. Hynes, M. J. *J. Chem. Soc., Dalton Trans.* **1993,** 311. doi:10.1039/DT9930000311
30. Eagle, C. T.; Kavallieratos, K.; Bryan, J. C. *J. Chem. Crystallogr.* **2002,** *32,* 165. doi:10.1023/A:1020283701925
31. Brownstein, S.; Stillman, A. E. *J. Phys. Chem.* **1959,** *63,* 2061–2062. doi:10.1021/j150582a022

Beilstein Journal of Organic Chemistry

RAFT polymers for protein recognition

Alan F. Tominey[1], Julia Liese[1], Sun Wei[2], Klaus Kowski[2], Thomas Schrader[*2] and Arno Kraft[*1]

Full Research Paper

Open Access

Address:
[1]Chemistry, School of Engineering & Physical Sciences, Heriot-Watt University, Riccarton, Edinburgh EH14 4AS, United Kingdom and [2]Universität Duisburg-Essen, Fachbereich Chemie, Institut für Organische Chemie, Universitätsstraße 5, 45117 Essen, Germany

Email:
Thomas Schrader[*] - Thomas.Schrader@uni-due.de; Arno Kraft[*] - A.Kraft@hw.ac.uk

* Corresponding author

Keywords:
electrostatic interactions; hydrophobic effect; isothermal calorimetry; protein recognition; RAFT polymers

Beilstein J. Org. Chem. **2010,** *6,* No. 66.
doi:10.3762/bjoc.6.66

Received: 02 February 2010
Accepted: 28 May 2010
Published: 17 June 2010

Guest Editor: C. A. Schalley

Abstract

A new family of linear polymers with pronounced affinity for arginine- and lysine-rich proteins has been created. To this end, *N*-isopropylacrylamide (NIPAM) was copolymerized in water with a binding monomer and a hydrophobic comonomer using a living radical polymerization (RAFT). The resulting copolymers were water-soluble and displayed narrow polydispersities. They formed tight complexes with basic proteins depending on the nature and amount of the binding monomer as well as on the choice of the added hydrophobic comonomer.

Introduction

The ability of biological receptors to bind strongly and specifically to a particular molecular target is an essential part of biological machinery. The best example is the immune system where antibodies are generated in response to minute amounts of foreign antigens. A continual challenge in nanoscale chemistry is to mimic the biological molecular recognition functions by synthetic chemistry with the aim of producing systems of lower complexity. When successful, this will enable the manufacturing of robust and specific synthetic receptors for a given protein target [1]. Proteins are a formidable challenge in this respect because they represent large macromolecules with a characteristic shape, size and highly complex functionalized surface. Artificial protein receptors are desired for protein enrichment and purification, sensing and diagnostics applications, as well as therapeutic uses involving interference with critical protein–protein interactions.

Multivalency represents the key to generate high-affinity materials for biomacromolecules with a sufficient number of binding sites for Coulomb attraction and hydrophobic interactions [2]. A statistical evaluation of crystal structures led to the discovery that hot spots in protein–protein contact areas are

enriched in aromatic amino acids and in arginine. These are often surrounded by energetically less important residues that most likely serve to occlude bulk solvent from the hot spot and lower the local dielectric constant [3,4].

With this principle in mind, several groups have designed relatively simple linear polymeric structures with branched ionic comonomers and thus achieved remarkable affinities and biological properties. In their elegant work, Kulkarni et al. reported the use of NIPAM-based copolymers for lysozyme recovery by affinity thermoprecipitation. These polymers contained multiple acetamido groups in a hydrophilic environment for maximum interaction with the catalytic cleft and achieved high affinities [5]. Rotello and Thayumanavan have described amphiphilic polymer scaffolds, which nonspecifically bound to chymotrypsin, inhibited its peptidase activity and modulated substrate specificity; very high ionic strengths again released the protein from the polymer [6,7].

Protein recognition by multifunctional polymeric hosts features two prominent advantages. On one hand, it simplifies the complex recognition interface to isolated 1:1 complexes between monomeric binding sites and single complementary amino acid residues, while simultaneously allowing for an extensive induced-fit process of the linear polymer on the protein surface – in other words they encourage polymer/protein self-assembly in order to maximize attractive noncovalent interactions.

A second major advantage of multivalent polymeric hosts is their rapid and efficient synthesis at low cost as well as the high proteolytic stabilities of most polymer backbones. They also pose fewer racemization problems which often accompany proteinogenic amino acids in peptidic environments.

In recent years, our group has developed water-soluble linear polymeric protein binders which contained one or more different binding monomers and displayed micromolar protein affinities [8], accompanied in a number of cases with promising protein selectivities [9]. These linear polymers were all prepared by free radical copolymerization in DMF followed by deprotection of the binding monomers in polymer-analogous transformations. Thus, a polymerized bisphosphonate tetramethyl ester was subjected to LiBr-assisted nucleophilic cleavage to furnish the free bisphosphonate dianion binding site. This procedure has two major drawbacks. First, if the functional groups on the polymer backbone become restricted in their accessability, the final deprotection step will suffer from low conversion rates. Second, the resulting material is polydisperse, rendering the characterization of the protein binding event problematic. Even with incorporated fluorescence labels, the overall emission intensity change resulting from protein addition will reflect only a virtual averaged value, because short and long chains will bind simultaneously, most likely with different affinities and stoichiometries. A quantitative description must inherently suffer from this averaging effect.

Results and Discussion

Reversible addition–fragmentation chain transfer (RAFT) polymerization [10] and atom-transfer radical polymerization (ATRP) have become extremely useful tools for the controlled synthesis of a wide range of polymers and could solve both problems by formation of monodisperse functionalized polymer chains of equal length, without the need for final polymer-analogous deprotection. So far, there have been no reports of the successful use of ATRP with acrylamides. In contrast, RAFT can be used in a variety of solvents and, most importantly, it is compatible with NIPAM [11,12]. For this reason, RAFT was chosen in this paper as the preferred method for controlled synthesis of linear polymers.

For initial screenings we selected a combination of anionic and hydrophobic binding monomers (Figure 1) that were well suited for simultaneous recognition of basic amino acids (Lys/Arg) as well as nonpolar residues (Val, Leu, Ile, Phe). NIPAM was chosen as the main comonomer because it forms polymers which are water-soluble at room temperature and even allow thermoprecipitation with a bound protein guest. NIPAM-based polymers are also reminiscent of peptides since both contain an amide group in the repeat unit. RAFT makes use of a chain transfer agent (CTA) for which we selected the water-soluble trithiocarbonate **8** [13,14] which efficiently caps the growing polymer chain, but can be completely removed from the final polymer by reaction with an excess of AIBN and selective polymer precipitation into hexane [11].

Three anionic comonomers suitable for binding lysine and arginine were chosen from earlier work with linear polymers and microgels [9,15,16]: Sodium methacrylate (**2**) (S), polymerizable tetrazolate **3** (T) and bisphosphonate **4** (B). These anionic comonomers were directly copolymerized with NIPAM and a hydrophobic acrylamide. The latter carried cyclohexyl (CH), benzyl (BN) or octyl (OC) moieties as hydrophobic residues. In the polymer designation code, the first letter indicates the anionic comonomer used (S, T or B), the subsequent number its mol % in the monomer mixture; the two-letter abbreviation (CH, BN or OC) stands for the hydrophobic comonomer used, again followed by the mol %; the balance to 100 mol % was made up by NIPAM. For example, S10CH10 means that this RAFT copolymer was made from sodium methacrylate (10 mol %), *N*-cyclohexylacrylamide (10 mol %), and NIPAM (80 mol %).

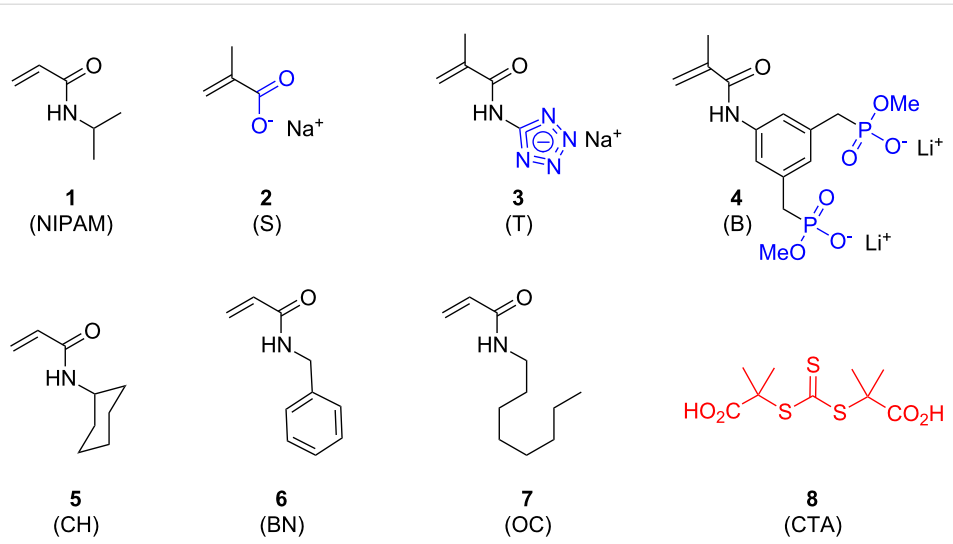

Figure 1: Structures of monomers **1**–**7** and chain transfer agent **8** used in the RAFT polymerizations.

RAFT polymerizations were carried out in methanol at 60 °C for 48 hours in the presence of CTA **8** and azo initiator V-50. The monomer concentration was 0.75 M, the molar ratio of [V-50]/[CTA] was 3, and the concentration of CTA and V-50 were adjusted to target polymers with a molecular weight of 3000, 7000 or 17000 g mol $^{-1}$ at full conversion. This is possible since the degree of polymerization under RAFT conditions is equal to the ratio between monomer and chain transfer reagent concentration. Conversion was almost 100%, and copolymers were isolated by precipitation in hexane. The absence of low-molecular weight impurities such as monomers was ascertained by ^{1}H NMR spectroscopy. Molecular weights were determined by gel-permeation chromatography (GPC) analysis of the copolymers. Narrow polydispersities (≤1.3) were observed for the shorter copolymers, although the highest molecular weights (targeted at 17000 g mol^{-1}) reached only experimental values of 11,000–12,000 g mol^{-1} and also produced slightly higher polydispersities (1.56). For comparison, some copolymers such as S20CH15 were also prepared with a molecular weight of ~3000 g mol^{-1}.

Titrations were first carried out by UV–vis spectroscopy with cytochrome C, a protein carrying a chromophore. Second derivative spectra were calculated using the Savitzky–Golay algorithm [17-19]. The second derivative is a useful method of refining the spectra to reveal subtle changes in the UV–vis absorption plot. The UV titration of a typical RAFT copolymer into a solution of cytochrome C in a phosphate buffer (pH 7, 0.15 M KCl) showed characteristic second derivative spectra, similar to those observed in the titrations of microgels into protein solutions [16]. Isosbestic points are clearly visible along with a bathochromic shift of the absorbance peak (Figure 2a). A dissociation constant of 1.6 × 10^{3} M^{-1} could be fitted to the binding isotherm when the second derivative values of the protein at 415 nm were plotted against the RAFT polymer concentration (Figure 2b). Cytochrome C already showed noticable and selective binding to microgels [16] containing 10 mol % sodium methacrylate and RAFT copolymers of similar composition. Unlike microgels whose molecular weight is very high (typically 10^{6}–10^{8} g mol^{-1}), cytochrome C possesses a relatively small molecular weight similar to the RAFT copolymers. As a result, the RAFT copolymers and cytochrome C favor 1:1 binding. The incorporation of a hydrophobic comonomer further improved binding. The maximum binding strength was observed for polymers containing 15 mol % of *N*-cyclohexylacrylamide and 20 mol % of sodium methacrylate (Table 1).

For an independent comparison, the same protein–polymer pairs were subsequently subjected to microcalorimetric titrations (Figure 3), which confirmed the major trends gained from spec-

Table 1: UV–vis titrations of cytochrome C with selected RAFT copolymers.

RAFT Copolymer[a]	Macroscopic K_a / M^{-1}	Polymer : Protein Stoichiometry
S10CH10	400	1:1
S10BN10	n.d.	n.d.
S10OC10	20	1:1
S10CH15	1600	1:1
S20CH15	>2000	n.d.

[a]S = sodium methacrylate, CH = *N*-cyclohexylacrylamide, BN = *N*-benzylacrylamide, OC = *N*-octylacrylamide.

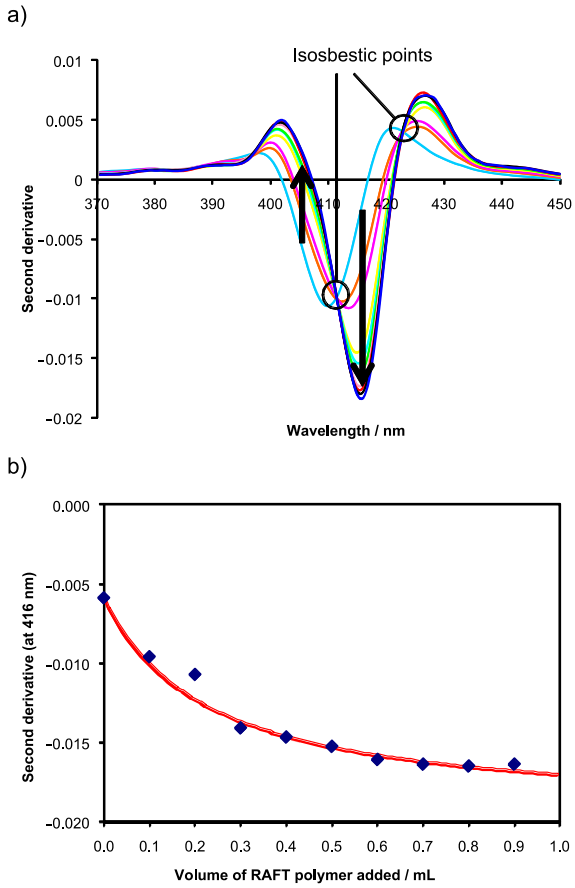

Figure 2: a) Second derivative UV–vis spectra [17-19] observed during a full titration of a stock solution of RAFT copolymer S10CH15 (6.3×10^{-3} mol L^{-1}) into a solution of cyt C (9.9×10^{-6} mol L^{-1}) in phosphate buffer at pH 7 and ionic strength of 0.15 mol L^{-1} KCl. The arrows indicate increasing amounts of RAFT copolymer added. b) Plot of second derivative values at 416 nm as a function of volume (in mL) of RAFT copolymer solution added. The filled diamonds are experimental values, whereas the drawn curve represents the calculated isotherm for a K_a of 1.6×10^3 M^{-1} assuming 1:1 binding [20].

troscopic detection but differed in several details (Table 2). Specifically, RAFT copolymers S10CH10, S10BN10, S10OC10, S10CH15 and S20CH15 were examined in their complex formation with cytochrome C (MW 14 kD, pI 9.2) and hemoglobin (MW 68 kD, pI 7.0). Negligible heat changes were observed for all titrations with sodium methacrylate-containing polymers, consistent with the small K_a values already determined by UV–vis titrations (20–1600 M^{-1}); obviously, the methacrylate anion is a weak binder for lysines and arginines on these protein surfaces. Moderate binding (3×10^4 M^{-1}) was only detected with S20CH15, which carries twice the amount of carboxylate groups. Association constants were initially calculated for each 1:1 complexation event of a single protein by the copolymer [20]. However, even with S20CH15, no binding was detectable with hemoglobin, confirming an interesting cytochrome C preference of all sodium methacrylate-carrying polymers, which also corresponded to previous results with microgels [16].

By contrast, tetrazolate copolymer T20CH15 and bisphosphonate copolymer B20CH15 showed large enthalpy changes and hence much higher K_a values (>10^6 M^{-1}) which were about two orders of magnitude higher than those achieved with sodium methacrylate copolymer S20CH15 (~10^4 M^{-1}). This is not surprising for the bisphosphonate, which carries twice the amount of negative charges. However, the monoanionic tetrazolate anion is very similar in acidity and hydrogen bond pattern to a carboxylate, so that similar affinities would have been expected. Most likely, the difference is explained by interactions with the π-face of the tetrazolate anion, which are not possible with a carboxylate.

In all cases, protein complexation by RAFT polymers was endothermic, i.e., entropy-driven. Hence, unspecific electrostatic attraction in combination with solvophobic forces contributed the most towards protein binding.

To quantify the contribution of nonpolar comonomers, hemoglobin was also titrated with pure tetrazolate and bisphosphonate copolymers. Intriguingly, K_a values dropped substantially by 1–2 orders of magnitude (see Table 1: T20 vs T20CH15). In other words, the random incorporation of cyclohexyl comonomers into the polymer was beneficial for the protein recognition event. Close inspection of thermodynamic data revealed that the entropy term was responsible for this increased affinity. We therefore tentatively explain the gain in free energy by an increased classical hydrophobic effect due to the presence of additional nonpolar cyclohexyl residues throughout the polymer chain.

For biological applications, it is desirable to keep the polymer size close to the size of the protein, so that specific 1:1 complexation is favored (Figure 4). In order to investigate this assumption, the sodium methacrylate polymer S20CH15 was titrated as a short oligomer (MW 3000 g mol^{-1}) and an average-size polymer (MW 12000 g mol^{-1}). Direct comparison produced a drastic difference: No binding could be detected for the short version, indicating that size matters and promotes multivalent or cooperative binding.

Finally, the protein series was extended to lysine-rich histone (pI 10), lysozyme (pI 9), proteinase K (pI 8) and bovine serum albumin or BSA (pI 6). Again, the strong binders B20CH15 and T20CH15 were examined concerning their affinities towards proteins of varying pI (Table 2). In direct comparison, the bisphosphonate seems to be superior to the tetrazolate. While B20CH15 stayed well below micromolar K_d values even with

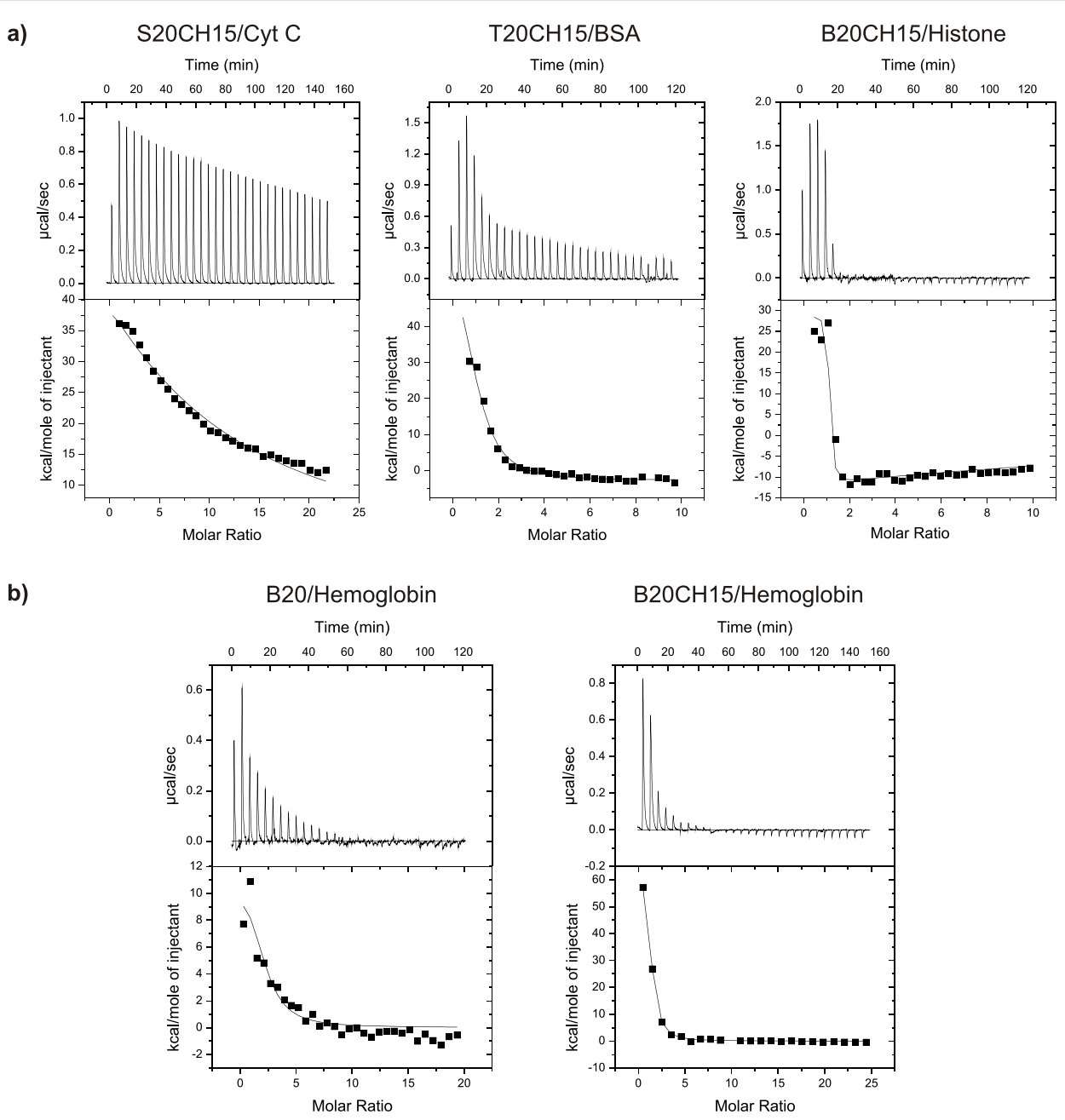

Figure 3: Isothermal calorimetric binding curves for selected polymer/protein host–guest pairs. a) Typical binding curves with representative proteins for the major polymers based on the three anionic binding sites. Note the marked affinity increase from sodium methacrylate over tetrazolate to bisphosphonate dianion. b) Binding curves of two bisphosphonate RAFT copolymers, one without and one with the hydrophobic *N*-cyclohexylacrylamide comonomer (15 mol %). The contribution of the nonpolar cyclohexyl monomer towards hemoglobin binding is evident from the steeper slope of the binding curve.

BSA, T20CH15 hardly ever reached the micromolar regime. Obviously, the bisphosphonate's high negative charge density is especially effective for protein surfaces with a high density of basic amino acids such as the DNA-binding histones or for those offering distinct clusters of cationic amino acid residues (e.g. BSA). Interestingly, although in most cases nonlinear regression converges with an assumed 1:1 complex stoichiometry, curve fitting is greatly improved with a sequential binding or 2-sites model [21]. In all these cases, the first polymer binds very tightly to the protein surface, but leaves significant room for a second polymer forming an – admittedly much weaker – 2:1 complex. Histone association with B20CH15 is an illustrative example. The first K_d value is 16 nM, followed by very weak binding at a second site with a

Table 2: Microcalorimetric protein titrations with RAFT polymers.

RAFT copolymer[a]	Protein[b]	Macroscopic K_a / M^{-1}	Polymer : protein	K_a per residue / M^{-1}	Monomer : protein	ΔG / kcal mol^{-1}	ΔH / kcal mol^{-1}	$T\Delta S$ / kcal mol^{-1}
S10CH10	Cyt C	NA	–	–	–	–	–	–
S10BN10	Cyt C	NA	–	–	–	–	–	–
S10OC10	Cyt C	NA	–	–	–	–	–	–
S10CH15	Cyt C	NA	–	–	–	–	–	
S10CH10	Hem	NA	–	–	–	–	–	–
S20CH15[b]	Cyt C	NA	–	–	–	–	–	–
S20CH15[c]	Cyt C	3×10^4	7:1	9×10^2	15:1	–	–	–
S20CH15[c]	Hem	NA	–	–	–	–	–	–
T20	Hem	~2×10^4	–	~9×10^3	–	–	–	–
T20CH15	His	$8 \times 10^5 \rightarrow 5 \times 10^3$	2 sites	2×10^4	–	–	–	–
	Lys	$8 \times 10^5 \rightarrow 5 \times 10^3$	2 sites	1×10^4	7:1	−5.5	+21.2	+26.7
	Prot K	$4 \times 10^5 \rightarrow 3 \times 10^3$	2 sites	3×10^3	13:1	−4.6	+17.7	+22.3
	Hem	4×10^6	3:1	1×10^4	78:1	−5.7	+4.2	+9.9
	BSA	$4 \times 10^5 \rightarrow 3 \times 10^3$	10:1	6×10^3	6:1	−5.2	+4.4	+9.6
B20	Hem	7×10^5	2:1	7×10^4	20:1	−6.6	+1.2	+7.8
B20CH15	His	$6 \times 10^7 \rightarrow 7 \times 10^2$	2 sites	2×10^5	18:1	−7.4	+2.4	+9.8
	Lys	$1 \times 10^6 \rightarrow 3 \times 10^3$	2:1	4×10^4	15:1	−6.3	+0.7	7.0
	Prot K	NA	–	–	–	–	–	–
	Hem	4×10^6	1:1	2×10^5	15:1	−7.2	+5.1	+12.3
	BSA	2×10^6	3:1	9×10^4	5:1	−6.7	+15.4	+22.1

[a]S = sodium methacrylate, T = tetrazolate **3**, B = bisphosphonate **4**, CH = *N*-cyclohexylacrylamide, BN = *N*-benzylacrylamide, OC = *N*-octylacrylamide.
[b]Cyt C = cytochrome C; Hem = hemoglobin; His = histone; Lys = lysozyme; Prot K = proteinase K; BSA = bovine serum albumin.
[c]MW ~3000 g mol^{-1}.
[d]MW ~17000 g mol^{-1}. NA indicates that no binding constant and thermodynamic data were obtained from microcalorimetry titrations, because heat changes were too small.

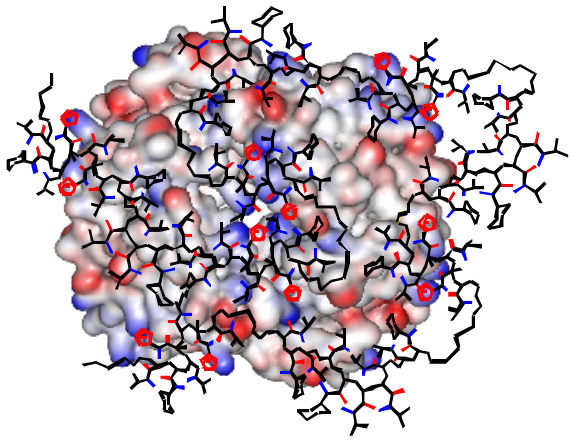

Figure 4: Graphical illustration of the potential binding mode on hemoglobin tetramer (represented as electrostatic potential surface, lysines = blue). The RAFT copolymer T20CH15 (tetrazole rings = red) undergoes an extensive induced fit procedure on the protein surface maximizing unspecific electrostatic and hydrophobic contacts. Some NIPAM sidechains were omitted for clarity.

K_d of 1 mM. With respect to varying pI values, both RAFT polymers display little selectivity: From lysozyme (pI > 9) down to BSA (pI < 6) protein affinities vary by less than one order of magnitude.

Conclusion

In summary, RAFT copolymerization of NIPAM with monomers containing anionic binding sites for basic amino acids led to polymers of low polydispersities which were effective protein binders in buffered aqueous solution, with tunable stoichiometries close to the ideal 1:1 ratio. Although molecular recognition is based on unspecific electrostatic attraction and hydrophobic forces, those proteins which feature a high density of positive charges on their surfaces are bound especially well by the bisphosphonate site, in some cases reaching micromolar or sub-micromolar K_d values. Copolymerization with *N*-cyclohexylacrylamide introduced additional nonpolar groups beneficial for protein binding, leading to a substantial entropy gain and significantly improving protein affinities. The best pair was a bisphosphonate-containing RAFT copolymer and lysine–rich histone (K_d = 16 nM). In the future, we intend

to investigate if it is possible to interrupt the nucleosome complex formation by noncovalent detachment of ds-DNA from its "own" histone proteins using histone-binding RAFT copolymers.

Supporting Information

Supporting Information File 1

Full experimental procedures, characterization details, microcalorimetry measurements, UV titration procedures and potentiometric titrations.
[http://www.beilstein-journals.org/bjoc/content/supplementary/1860-5397-6-66-S1.pdf]

Acknowledgements

We gratefully thank the School of Engineering and Physical Sciences at Heriot-Watt University for support and Dr Steven Rimmer (Sheffield University) for help with the aqueous GPC of the RAFT copolymers.

References

1. Schrader, T.; Hamilton, A., Eds. *Functional Synthetic Receptors;* Wiley-VCH: Weinheim, Germany, 2005.
2. Peczuh, M. W.; Hamilton, A. D. *Chem. Rev.* **2000,** *100,* 2479–2494. doi:10.1021/cr9900026
3. Bogan, A. A.; Thorn, K. S. *J. Mol. Biol.* **1998,** *280,* 1–9. doi:10.1006/jmbi.1998.1843
4. Larsen, T. A.; Olsen, A. J.; Goodsell, D. S. *Structure* **1998,** *6,* 421. doi:10.1016/S0969-2126(98)00044-6
5. Vaidya, A. A.; Lele, B. S.; Deshmukh, M. V.; Kulkarni, M. G. *Chem. Eng. Sci.* **2001,** *56,* 5681–5692. doi:10.1016/S0009-2509(01)00169-5
6. Sandanaraj, B. S.; Vutukuri, D. R.; Simard, J. M.; Klaikherd, A.; Hong, R.; Rotello, V. M.; Thayumanavan, S. *J. Am. Chem. Soc.* **2005,** *127,* 10693–10698. doi:10.1021/ja051947+
7. Sandanaraj, B. S.; Demont, R.; Aathimanikandan, S. V.; Savariar, E. N.; Thayumanavan, S. *J. Am. Chem. Soc.* **2006,** *128,* 10686–10687. doi:10.1021/ja063544v
8. Renner, C.; Piehler, J.; Schrader, T. *J. Am. Chem. Soc.* **2006,** *128,* 620–628. doi:10.1021/ja0560229
9. Koch, S.; Renner, C.; Xie, X.; Schrader, T. *Angew. Chem., Int. Ed.* **2006,** *45,* 6352–6355. doi:10.1002/anie.200601161
10. Barner-Kowollik, C.; Buback, M.; Charleux, B.; Coote, M. L.; Drache, M.; Fukuda, T.; Goto, A.; Klumperman, B.; Lowe, A. B.; McLeary, J. B.; Moad, G.; Monteiro, M. J.; Sanderson, R. D.; Tongue, M. P.; Vana, P. *J. Polym. Sci., Part A: Polym. Chem.* **2006,** *44,* 5809–5831. doi:10.1002/pola.21589
11. Convertine, A. J.; Lokitz, B. S.; Vasileva, Y.; Myrick, L. J.; Scales, C. W.; Lowe, A. B.; McCormick, C. L. *Macromolecules* **2006,** *39,* 1724–1730. doi:10.1021/ma0523419
12. Convertine, A. J.; Ayres, N.; Scales, C. W.; Lowe, A. B.; McCormick, C. L. *Biomacromolecules* **2004,** *5,* 1177–1180. doi:10.1021/bm049825h
13. Lai, J.; Filla, D.; Shea, R. *Macromolecules* **2002,** *35,* 6754–6756. doi:10.1021/ma020362m
14. Adewuyl, Y.; Carmichael, G. *Environ. Sci. Technol.* **1987,** *21,* 170–177. doi:10.1021/es00156a602
15. Tominey, A.; Andrew, D.; Oliphant, L.; Rosair, G. M.; Dupré, J.; Kraft, A. *Chem. Commun.* **2006,** 2492–2494. doi:10.1039/b604393c
16. Tominey, A.; Liese, J.; Ewen, D.; Kraft, A. *PMSE Prepr.* **2007,** *97,* 964–965.
17. Savitzky, A.; Golay, M. J. E. *Anal. Chem.* **1964,** *36,* 1627–1639. doi:10.1021/ac60214a047
18. Barak, P. *Anal. Chem.* **1995,** *67,* 2758–2762. doi:10.1021/ac00113a006
19. de Levie, R. *Advanced Excel for Scientific Data Analysis;* Oxford University Press: Oxford, U.K., 2004; pp 469–481.
20. Connors, K. A. *Binding constants;* Wiley: New York, 1987.
21. Stoichiometries in the "1 set of sites" fitting mode were indicated to be between 1 and 2. Indeed, curve fitting with only two assumed non-identical sites produced much better results than any other ratio.

License and Terms